Superconducting and mesoscopic structures (Preface)

[DOI: 10.1063/1.1789091]

It is remarkable that for 40 years the Josephson effect has maintained its position at the center of condensed matter physics. The reason probably lies in the very concept of weak coherent coupling between macroscopic quantum systems. It allows one to separate the effects of interaction, which creates the long-range order, from the correlation themselves, corresponding to this order. It provided the possibility to investigate the overlap of mutually exclusive (in the bulk) long-range orders. It gives the opportunity to look at the effects of finite size of the system. Josephson effect also gives a framework for the discussion and realization of macroscopic quantum phenomena (beyond the almost trivial fact that superconductors are macroscopic quantum objects). The last five years have seen the demonstration of macroscopic quantum resonant tunneling, quantum coherence, and quantum entanglement in Josephson structures. Josephson physics repaid the physics of bulk superconductivity by providing a means of investigation of unusual superconductors (e.g., demonstrating d-wave symmetry in high-T_c cuprates).

Brian D. Josephson discovered his remarkable effect in 1962. Josephson predicted that a zero voltage supercurrent could flow in a junction between two superconductors separated by a tunnel barrier. The magnitude of the Josephson current is related to the difference of the phases of the macroscopic wave functions (complex order parameters) of the superconductors forming the junction. P. W. Anderson and J. M. Rowell first observed this dc Josephson effect in 1963. If a dc voltage V is applied to the junction, an ac supercurrent with the frequency $2eV/\hbar$ appears between the superconductors. The first direct observation of the ac Josephson effect was made 40 years ago in Kharkov, Ukraine (I. K. Yanson, V. M. Svistunov, and I. M. Dmitrenko, Zh. Éksp. Teor. Fiz. **47**, 2091 (1964); **48**, 976 (1965) [Sov. Phys. JETP **20**, 1404 (1965); **21**, 650 (1965)]). Soon after Josephson's predictions for the tunnel junctions, it became clear that the effects are much more general and occur whenever two superconductors are weakly coupled. The physics of weak superconductivity (a term introduced by P. W. Anderson) became an area of a great interest for experimental and theoretical investigations. More than forty years after its discovery, the Josephson effect still attracts considerable attention and keeps providing us with exciting new physics and applications.

This issue is devoted to aspects of the physics of superconducting and mesoscopic structures. It represents reviews and original articles on the subject. The issue opens with papers by Yanson and Dmitrenko which review the initial steps in study of the ac Josephson effect in tunnel junctions and further experimental investigation of weakly coupled superconductors at the Institute for Low Temperature Physics and Engineering in Kharkov.

The Josephson effect arises in superconducting weak links—junctions of two weakly coupled superconductors (massive banks) S_1 and S_2. The coupling allows the exchange of electrons between the banks and establishes superconducting phase coherence in the system as a whole. The weakness of the coupling means that the superconducting order parameters of the banks are essentially the same as for disconnected superconductors, and they are characterized by the phases of the order parameters χ_1 and χ_2. The Josephson weak link can be considered as a ''mixer'' of the two superconducting macroscopic quantum states in the banks. The result of the mixing is a phase-dependent current-carrying state with current flowing from one bank to another. This current is determined (parameterized) by the phase difference $\varphi=\chi_2-\chi_1$ across the weak link. The specific form of the current–phase relation $I(\varphi)$ depends on the type of weak link.

A number of papers consider the coherent transport in Josephson weak links with coupling more complicated than just a tunneling barrier. In the paper by Kulik different types of superconducting weak links are reviewed, focusing on the origin of jumps in the current–phase relations. The author also discusses persistent currents in mesoscopic and nanoscopic Aharonov–Bohm structures. Novel effects in superconducting nanojunctions are studied theoretically in the paper by Zaikin. It is shown that interplay between quantum interference effects and Andreev reflection in S–N–S junctions with insulating barriers may qualitatively modify the Josephson current. Several papers included deal with spin effects in mesoscopic Josephson junctions. Shnirman *et al.* study the dynamics of a single spin embedded in the tunneling barrier between two superconductors. A new effect, ''Josephson nutation,'' is predicted. The paper by Krive *et al.* reviews the charge and spin effects in S–Luttinger liquid–S and S–quantum wire–S junctions.

The properties of the current carrying states in a weak link depend not only on the manner of coupling but also on the properties of the superconducting banks. The modern physics of superconductivity is essentially the physics of unconventional superconductivity.

The discovery of d-wave symmetry of the order parameter in high-temperature superconductors and of triplet superconductivity in compound Sr_2RuO_4 has caused a stream of theoretical and experimental research on unconventional superconductors. The sensitivity of the Josephson effect to the symmetry of the complex order parameter in the junction's banks stimulated numerous studies of Josephson weak links between unconventional superconductors. The current–phase relations for unconventional Josephson weak links are quite different from the conventional ones. For example, in grain-boundary junctions, depending on the angle of misorientation of d-wave order parameters in the banks, the current–phase relation is changed from a $\sin(\varphi)$-like curve to a $-\sin(2\varphi)$ dependence.

Clearly, this determines new features in the behavior of

such Josephson junctions in applied voltage or magnetic field. A considerable number of the papers included in this issue concern the study of unconventional Josephson weak links. One of the most striking manifestations of the unconventional order parameter symmetry is the appearance of spontaneous current flowing along the contact interface in addition to the Josephson current. The spontaneous current arises due to the breaking of the time-reversal symmetry (T) in the system. The study of T-breaking phenomena is not only of fundamental significance but also attracts interest from the standpoint of realization of qubits, basic units of quantum computers. The review by Kolesnichenko *et al.* focuses on spontaneous currents in junctions between d-wave and triplet superconductors. It also contains the review of superconducting qubit basics with emphasis on the properties of d-wave qubits. A theoretical paper by Tanaka *et al.* considers the impurity scattering effect on charge transport in high-T_c cuprate junctions. The results of experimental investigations of high-T_c grain boundary junctions and heterostructures are presented in the papers by Tafuri *et al.* Komissinski *et al.* and Timofeev *et al.* The specific features of ac Josephson effect in unconventional superconductors are reported in the theoretical paper by Kwon *et al.* Note that the problem of existence of the fractional ac Josephson effect in unconventional superconductors needs further theoretical and experimental investigations.

Mesoscopic structures consisting of several Josephson junctions are now being studied intensively from the point of view of qubit realization. A paper by Il'ichev *et al.* summarizes the results of implementation of advanced impedance measurement technique for characterization of interferometer-type superconducting qubits. In a theoretical paper by Ioffe *et al.* a new class of Josephson arrays is introduced. These arrays have nontrivial topology and exhibit novel quantum states at low temperatures. In the paper by Kuplevakhky, a detailed theory of Josephson vortices in layered superconductors is developed. The quantum dynamics of the order parameter and time-dependent BCS pairing is investigated in the framework of the Wigner distribution function by Amin *et al.*

A single issue cannot cover all aspects of the research. It gives the reader a brief overview of the current state of activities, which, we hope, will be useful and will stimulate further investigations in the field of superconducting and mesoscopic structures.

We greatly appreciate helpful discussions with all the contributors during the preparation of this issue.

A. N. Omelyanchouk

The ac Josephson effect: observation of electromagnetic radiation (Review)

I. K. Yanson*

B. Verkin Institute for Low Temperature Physics and Engineering of the National Academy of Sciences of Ukraine, 47 Lenin Ave., Kharkov 61103, Ukraine
(Submitted January 22, 2004)
Fiz. Nizk. Temp. **30**, 689–697 (July–August 2004)

An historical review of the discovery and the early period of research on the Josephson effect is given. Experiments on the tunneling effect in superconductors done in the 1960s at the Institute for Low Temperature Physics and Engineering of the National Academy of Sciences of Ukraine, Kharkov (ILTPE), which led to the observation of Josephson electromagnetic radiation are described in detail. The experimental data are illustrated by the original curves, and the dates they were taken are indicated. The physical mechanism for the generation of rf radiation in superconducting tunnel junctions is examined, and some of the more promising applications of the ac Josephson effect are briefly listed. © *2004 American Institute of Physics.* [DOI: 10.1063/1.1789911]

1. INTRODUCTION

In the first half of the year 1962 the young English theoretical physicist Brian Josephson, still a postgraduate student, calculated the tunneling current between two superconductors and found additional terms. According to Josephson, the barrier could be penetrated not only by ''normal'' electrons, i.e., current carriers whose motion in a metal meets with resistance and leads to heat release, but also, with a comparable probability, by ''superconducting'' electrons, which through their interaction with the crystal lattice are attracted to each other, forming so-called Cooper pairs with charge $2e$ (e is the elementary electric charge). The superconducting electrons, when moving in a metal with a velocity not exceeding a critical value, do not encounter resistance. The penetration of normal electrons through an insulating layer several nanometers thick finds a natural explanation in the framework of the quantum tunneling effect. The tunneling of Cooper pairs can loosely be called a ''double'' quantum effect, since it derives its existence from the wave nature of the whole ensemble of superconducting electrons as a whole, described by a single quantum wave function Ψ(r). Naturally, from the standpoint of quantum mechanics, if the phenomenon of superconductivity is not taken into account, the simultaneous tunneling of two electrons is proportional to the square of the coefficient of transparency of the potential barrier, which is ordinarily a negligibly small quantity. It is unusual that the transparency of the barrier for a Cooper pair is actually of the same order of magnitude as for a single normal electron.

In a brief communication published in one of the first issues of the newly launched journal *Physics Letters*[1] (6/8–7/1/1962)[1)] Josephson very briefly set forth the implications of his theoretical calculations. Besides the *dc* superconducting current flowing at *zero* voltage across the barrier, there should also exist an *ac* superconducting current that flows when a *dc* voltage is applied across the barrier. At a potential difference of 1 μV the frequency of the alternating current is 483.6 MHz. In fact, in order to be observable, the ac Josephson current must give rise to a small ac component of the potential difference across the barrier, which is responsible for some mechanism of dissipation of the oscillation energy. Josephson also pointed out the kinds of experiments that would most clearly manifest the unusual properties of the Cooper-pair tunneling current. For direct current this is the oscillatory dependence of the critical (i.e., maximum possible) supercurrent on the value of a weak magnetic field piercing the cross-sectional area of the tunnel junctions. This dependence is a consequence of the sensitivity of the phase $\chi(r)$ of the wave function $\Psi(r)=|\Psi(r)|e^{i\chi(r)}$ of the superconducting electrons to magnetic field, or more precisely, to the field of the vector potential $\mathbf{A}(r)$. Another experiment that would indicate the existence of an alternating supercurrent is the extremely unusual detection of external electromagnetic radiation in the microwave range by a Josephson tunnel structure. Since the frequency of the alternating current is proportional to the voltage across the tunnel junction, a small microwave component induced by an external field will lead to frequency modulation of the alternating current, and dc components will appear in the spectrum each time the dc voltage across the contact satisfies the relation

$$2eV=n\hbar\omega \quad (n=1,2,3,...). \tag{1}$$

Consequently, the current–voltage (I–V) characteristic will have vertical segments (steps) at which the current changes at a nearly constant voltage.

Relation (1) is easily interpreted from a physical standpoint. The Cooper pairs have a total spin equal to zero and therefore obey Bose–Einstein statistics. At temperatures far below the transition temperature of the metal to the superconducting state, as a result of Bose condensation almost all of the Cooper pairs occupy the same energy level, corresponding to the chemical potential of the conduction electrons. If a static voltage is applied between two superconductors in tunneling contact, their chemical potentials will differ by eV. Consequently, an elementary tunneling event of a Cooper pair having charge $2e$ in this case will be a process accompanied by the emission or absorption of one or several

quanta of energy $\hbar\omega$. It is easy to see that relation (1) is an expression of the energy conservation law in such an elementary process.

The events leading to the experimental discovery of the predicted effects developed rapidly. A half year after publication of Josephson's first paper[1] under the cautious title ''Possible new effects in superconductive tunneling,'' P. W. Anderson and J. M. Rowell published an experimental paper[4] (1/11–3/15/1963) under the similarly cautious title ''Probable observation of the Josephson superconducting tunneling effect,'' in which they presented certain facts that did not fit in with the existing (before Josephson) theory of the currents through a tunnel contact and which find a natural explanation in Josephson's theory of the dc supercurrent. The complete triumph of Josephson's ideas came in mid-1963, when Rowell reported the observation of an oscillatory dependence of the critical current[5] (7/24–9/1/1963), which gave direct proof of the existence of the dc supercurrent. In experiments with detection of external electromagnetic radiation[6] (6/13–7/15/1963) S. Shapiro observed the current steps predicted by Josephson, which could be regarded as convincing indirect proof of the existence of an alternating current. A summary of these successes was presented at the International Conference on Superconductivity at Colgate University (USA), August 26–29, 1963. There, in addition to the achievements already mentioned, M. D. Fiske presented a report[7] containing experimental confirmation of the predicted temperature dependence of the Josephson critical current and the observation of vertical current steps at finite voltages in the absence of external microwave radiation. In the same issue of the journal the famous English scientist A. B. Pippard, in a discussion section, made a guess (later brilliantly confirmed) that the mechanism for the onset of these steps is a consequence of the excitation of electromagnetic oscillations of a miniature strip resonator with open walls, formed by the tunnel junction. Pippard and Anderson can be regarded as the ''godfathers'' of the Josephson effect, since they were the ones with whom Josephson discussed his ideas and obtained from them complete mutual understanding and support. Besides, Anderson made a large contribution to the development and interpretation of the physical essence of the effects predicted by Josephson. In particular, in collaboration with A. N. Dayem, he first showed[8] (6/18–8/10/1964) that the Josephson effects are also observed in superconducting microbridges, thereby expanding the class of objects exhibiting ''weak superconductivity,'' i.e., structures in which these effects are manifested. Josephson himself had mentioned in his first report that the effects he was predicting could take place not only in metal–insulator–metal tunnel structures but also in the so-called S–N–S structures, i.e., two superconductors separated by a thin layer of normal metal.

2. START OF TUNNELING RESEARCH ON SUPERCONDUCTORS AT ILTPE

The first tunneling measurements of the energy gap in the spectrum of quasiparticle excitations of superconductors were done in 1960 by I. Giaever[9] in the USA.[2)] In that same year the Institute for Low Temperature Physics and Engineering of the National Academy of Sciences of Ukraine (ILTPE) was founded in Kharkov. Tunneling in superconductors was included in the plan of scientific research of this institute. However, since it was necessary to create the entire experimental base from ''zero,'' Giaever's results were not reproduced until early 1963. These were measurements of the I–V characteristics of thin-film tunnel structures of the type aluminum–(aluminum oxide)–(lead, tin, or indium). One of the first characteristics on which the energy gap of lead ($\Delta = 1.34$ MeV) was clearly revealed is shown in Fig. 1.

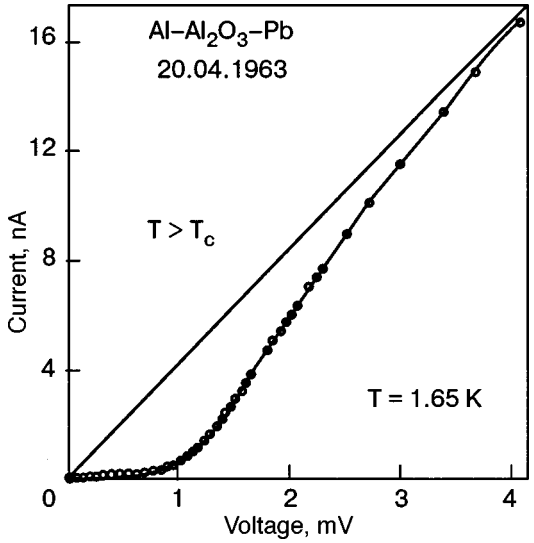

FIG. 1. Current–voltage characteristic of an Al–Al_2O_3–Pb junction.

By mid-1964 the technology of fabricating high-quality superconductor–insulator–superconductor tunnel structures had been developed,[10] making it possible to study the Josephson effects. In the very first paper[11] (7/30–12/1964) it was shown that the tin–oxide–tin structures we had fabricated had a thin and uniform potential barrier. The characteristic oscillatory dependence of the maximum Josephson current was obtained in a new experimental setup, in which an ''external'' magnetic field was created by an additional current flowing along one of the films. For tunnel junctions in which the width of the superconducting films is less than the so-called Josephson penetration depth of the magnetic field into the tunnel junction (which usually amounts to a few tenths of a millimeter), the dependence of the critical current on the field H_0 applied parallel to a film of width L conforms well to the relation

$$I_c(H_0) = I_0 \left| \frac{\sin(\pi\Phi/\Phi_0)}{(\pi\Phi/\Phi_0)} \right|, \tag{2}$$

where I_0 is the maximum dc Josephson current, $\Phi_0 = h/2e$ is the magnetic flux quantum in the superconductors, equal to 2×10^{-15} Wb, $\Phi = (d + 2\lambda_L)LH_0$ is the magnetic flux threading the tunnel junction, d is the thickness of the insulating layer (the oxide separating the superconducting films), and λ_L is the so-called London penetration depth of a static or not too high-frequency alternating magnetic field into the superconductor. Figure 2 shows the dependence of the Josephson critical current $I_c(H_0)$ on the magnetic field for the junction on which the electromagnetic radiation predicted by Josephson was first observed. In this case the dimensions of the junction exceeded the Josephson penetration depth. Con-

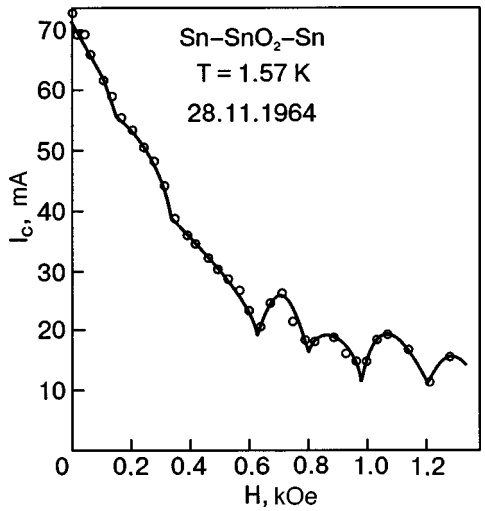

FIG. 2. Dependence of the critical current on an additional current along the film, expressed in terms of magnetic field strength in the tunnel junction.

sequently, the magnetic field penetrated nonuniformly into the junction, in the form of quantized lines or tubes of magnetic flux. This circumstance is responsible for the deviation of the observed dependence from formula (2). Nevertheless, the oscillatory dependence with a decaying envelope is clearly observed, indicating the uniformity of the insulating spacer and the absence of microshorts in the tunnel barrier.[11] At comparatively high magnetic fields the magnetic field distribution in the junction becomes close to uniform, and the field dependence of the critical current approaches formula (2).

The temperature dependence of the Josephson critical current was also confirmed, and the so-called ''subharmonic gap structure'' was observed.[11]

Of particular interest for the theme of this article is that the so-called stepped structure of the I–V characteristic at biases less than the threshold value (i.e., for eV less than the energy gap Δ) was observed in those measurements. A typical example of such structure is shown in Fig. 3, which shows the I–V characteristic of the junction on which the Josephson electromagnetic radiation was first observed. The dotted circle indicates the step on which the working point was set at the time of these experiments. One can sometimes observe unusual behavior at such steps: with increasing current the working point can jump not to higher but to lower voltage,[3)] a finding that cannot be explained by the possible destruction of some superconducting current paths connected in series. It was conjectured[11] that the stepped structure ''can probably be attributed to the excitation of the alternating supercurrent predicted by Josephson.'' Thus in mid-1964 our work had approximately reached the level that had been achieved abroad back in August of 1963.[4)]

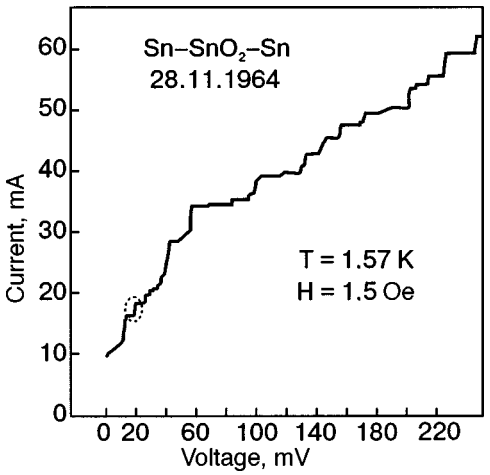

FIG. 3. Stepped structure of the I–V characteristic of the tunnel junction on which the Josephson electromagnetic radiation was first observed (note the step enclosed by the dotted circle).

3. OBSERVATION OF JOSEPHSON ELECTROMAGNETIC RADIATION

In spite of the fact that the mechanism producing the vertical segments on the I–V characteristics of tunnel junctions was unknown to us, there was no doubt in our minds that it involved the ac Josephson current. This could be proved by the direct observation of electromagnetic radiation accompanying the ac supercurrent. Registration of the radiation would be direct evidence of the tunneling of Cooper pairs with the emission of photons—one of the two fundamental quantum processes predicted by Josephson. Before that there existed only the indirect evidence mentioned above.[6,7]

It was known that the voltage should be related to the radiation frequency by the Josephson relation

$$\hbar\omega = 2eV. \tag{3}$$

In addition, it had been noted that the position of the steps on the voltage axis depended on the dimensions of the tunnel junction. The wider films are characterized by a shorter distance between adjacent steps. This made it possible to choose in an empirical way those films of a width such that the voltage at which any step corresponding to relation (3) would be observed at the frequency at which the radiation was detected. The height of the steps depended on the static magnetic field applied in the plane of the tunnel junction.

As a radiation receiver we used a P5-10 microwave radiometer for the 3-cm wavelength range. It had the advantage of a high threshold sensitivity ($\approx 10^{-16}$ W), self-calibration, and relatively compact size. It would later turn out that the choice of a receiving device with the highest threshold sensitivity was the key to the success of the whole experiment, since the power initially detected was very low (at a level of $\approx 10^{-14}$ W); Fig. 4.

The experiments were done as follows[12] (12/9/1964–3/1965). Films of such a width that a step was observed on the I–V characteristic at the required voltage (approximately 19.6 μV) were selected. From a number of tunnel structures, we selected those for which the critical current oscillated with a smoothly decaying envelope in a static magnetic field parallel to the films (like the dependence shown in Fig. 2). Satisfaction of this requirement attested to the presence of a thin and uniform oxide layer. After that a value of the magnetic field was chosen such that the required step would have maximum height. The sample was an 18×18 mm glass substrate (a microscope cover slip) on which two tin films with a width of around 1 mm and thickness of 10^{-4} mm had been deposited at right angles to each other in a high vacuum. The

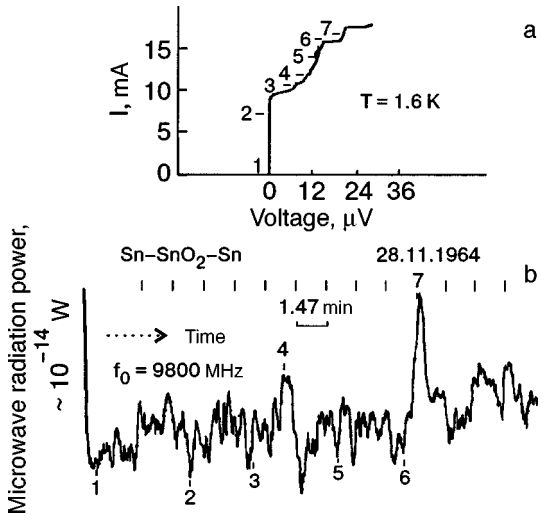

FIG. 4. Simultaneous recording of the I–V characteristic near a step (a) and the output signal of a microwave receiver with detection of the radiation (b).

first film had been covered by a thin insulating layer (2 nm thick) formed by oxidation in air or in oxygen. Thus the tunnel junction was the $\sim 1\times 1\times 10^{-4}$ mm region where these films overlapped. The remaining elements of the structure served for connection of the current and potential leads. The tunnel junction was held at liquid helium temperature in a standard 3-cm waveguide parallel to its wide wall and close to the short-circuiting plunger. The P5-10 receiver was mounted on the other end of the waveguide, away from the cryostat.

Figure 4 shows the initial part of the I–V characteristic (panel a) together with the output signal of the radiation detector (panel b), taken with a smooth variation of the current through the junction (and of the voltage across it). The step satisfying relation (3) for the frequency f_0 to which the receiver was tuned was placed in the region of marks 6 and 7. Marks 1–7 correspond to the same points in time in the graphs in Fig. 4a,b. The P5-10 receiver has a comparatively narrow passband (~ 1 MHz), and so the signal is observed only in the neighborhood of a certain point on the step. When the receiver is tuned to another (nearby) frequency, this point shifts on the step in accordance with relation (3). One can also notice a slight increase in the signal in the region of mark 4, which corresponds to relation (1) for $n=2$, i.e., a slight increase observed in the signal was due to the second harmonic of the Josephson radiation. The radiation power in the first experiments was very low ($\sim 10^{-14}$ W). This is because only a small fraction of the radiation generated leaked into the waveguide and could be detected. A large fraction of it was scattered inside the tunnel junction and converted to heat. In addition, in the first experiments the static magnetic field was directed along the axis of the waveguide and, hence the direction of propagation of the electromagnetic field generated by the wave of Josephson current was, strictly speaking, orthogonal to the axis. Nevertheless, because of the nonuniformity of the field near the edges of the junction, a significant amount of the electromagnetic energy was radiated along the waveguide axis and could therefore be detected. In the later experiments[13] the typical radiation power was $\approx 10^{-12}$ W and in certain cases could be increased to 10^{-9} W (Ref. 14) through better matching with the outer space. Although the power observed was extremely low, it was generated in a volume of the order of 10^{-6} cm^3, and so the specific microwave power was as high as 10 mW/cm^3, and it could be raised to $1-10$ W/cm^3. The main advantage of Josephson tunnel microwave generators is the ease with which they can be incorporated in integrated film microcircuits operating at low temperatures and, hence, having low noise.

Among the output devices of the P5-10 receiver is a loudspeaker, which served as an indicator of the noise signal in the band of sonic frequencies. Upon tuning to the working point of the I–V characteristic where the Josephson frequency relation is satisfied, there was usually a noticeable increase in the noise. Interestingly, on one occasion when the voltage across the junction reached a value satisfying the Josephson frequency relation (3), music was heard coming from the speaker instead of noise. It turned out that the intrinsic linewidth of the Josephson radiation is so narrow that the rf induction signal from a nearby radio translation station led to frequency modulation of the Josephson microwave radiation. After a double heterodyning in the P5-10 receiver, the signal of that radio station was reproduced in the loudspeaker.

Thus our work on the direct observation of the electromagnetic radiation helped forge a link in the compelling chain of discoveries due to Josephson's predictions.

Abroad, the main thrust of experimental research on the ac Josephson effect was toward explaining the mechanism of the indirect manifestations of the existence of the ac supercurrent. R. E. Eck, D. J. Scalapino, and B. N. Taylor[15] (5/18–7/6/1964) observed a broad resonance peak in the I–V characteristic of lead–oxide–lead tunnel junctions at biases less than half of the width of the energy gap of lead ($\Delta_{\mathrm{Pb}}=1.34$ meV). The position of this peak was proportional to the strength of the magnetic field applied in the plane of the junction. This peak arises as a result of the self-detection of the traveling electromagnetic wave excited by the traveling wave of ac Josephson current. Because of the large damping and structural inhomogeneities characteristic for lead tunnel junctions, reflection of electromagnetic waves from the boundaries of the junction were not observed. Somewhat later[16] those same authors observed and explained the stepped structure for lead junctions of better quality. The steps arise as a consequence of the self-detection of resonance types of electromagnetic oscillations generated by the ac Josephson current. An analogous explanation was given by D. D. Coon and M. D. Fiske[17] (10/5/1964–5/3/1965) for the stepped structure in the case of tin tunnel junctions. Unfortunately, the last two papers mentioned remained unknown to us for a long time, and we arrived at similar results independently [see Ref. 18 (5/18–7/1/1965) and Ref. 19 (6/12–8/1/1965)].

In parallel with the elucidation of the mechanism of generation of Josephson radiation, other researchers conducted experiments on its direct observation. For example, in Ref. 17 an attempt was undertaken to observe the radiation by means of transmission line expanding smoothly from ~ 1 nm (the distance between the film and the tunnel junction) to the

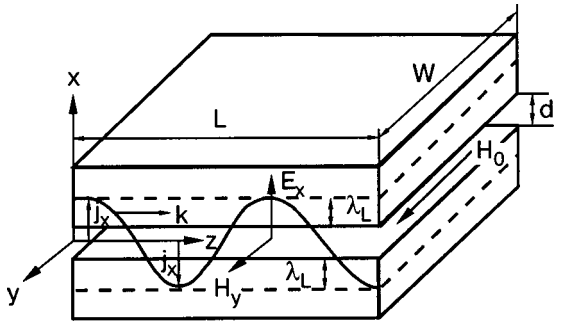

FIG. 5. Model of a tunnel junction and the electromagnetic fields and current in it.

macroscopic size of the coaxial cable or waveguide. No power was detected down to 10^{-12} W, even though one of the junctions gave a tunneling current of 30 mA at a voltage of $\sim 20\ \mu$V. We now know that the reason for the failure lay in the insufficient sensitivity of the radiation receiver, since the wave impedance mismatch of a tunnel junction (as a stripline) and a standard waveguide is large.

4. MECHANISM OF GENERATION OF ELECTROMAGNETIC RADIATION AT RESONANCE FREQUENCIES OF A TUNNEL JUNCTION

Two superconductors separated by a thin insulator layer can act as a stripline for the propagation of electromagnetic waves. These waves were considered by J. C. Swihart.[20] He showed that at a thickness of the insulating spacer much less than the penetration depth of magnetic field into the superconductor, electromagnetic waves are strongly slowed. The penetration depth of magnetic field into a superconductor is given by

$$\lambda_L = \left(\frac{mc^2}{4\pi n_s e^2} \right)^{1/2}.$$

Here e and m are the charge and mass of the electron, c is the speed of light, n_s is the density of superconducting electrons, which is of the same order of magnitude as the density of conduction electrons in a metal under the condition that the temperature is significantly below the critical temperature T_c of the transition to the superconducting state. For tin $T_c = 3.7$ K and $\lambda_L = 50$ nm. The thickness d of the insulator layer in a tunnel junction does not exceed 2 nm. Consequently, the electric and magnetic fields are separated in space. The first is concentrated in the insulating gap, while the second is mainly in the subsurface layers of the superconductor, occupying a total distance along the x axis of $\Lambda = 2\lambda_L + d \approx 100$ nm (Fig. 5).

The wave impedance of such a stripline is several orders of magnitude lower than that of free space, and electromagnetic waves are almost completely reflected from the edges of the tunnel junction as from the open end of a transmission line. Bounded on two sides, a tunnel junction is a strip resonator with resonance frequencies

$$\omega_n = \frac{\pi n}{L} c_0, \quad n = 1,2,3,...,$$

which are inversely proportional to the dimension L of the junction along which the standing electromagnetic wave is established. The phase velocity of the slowed electromagnetic wave is given by

$$c_0 = c \left(\frac{d}{\varepsilon_0 \Lambda} \right)^{1/2}$$

and for typical values of the parameters is about 20 times lower than c, the speed of light in free space. It follows immediately that a tunnel junction with dimensions somewhat large than 1 mm will resonate in the 3-cm wavelength range.

In analogy with how a density-modulated electron beam excites slow electromagnetic waves in microwave electronic devices, in a superconducting tunnel junction the wave of Josephson supercurrent density $j_x(z,t)$ excites resonance electromagnetic oscillations of the miniature microwave resonator made up of the crossed superconducting films (Fig. 5). The Josephson current flows along the x axis, i.e., between the superconducting films. Its time dependence is determined by the frequency (3). The dependence of the Josephson current density on the coordinates can be controlled by means of a static magnetic field H_0 applied in the plane of the junction. In the simplest case the rather weak coupling between the two superconductors (i.e., at a sufficiently low barrier transparency for the tunneling of Cooper pairs) this dependence is of a harmonic character for the z direction, which lies in the plane of the junction but perpendicular to the external magnetic field:

$$j = j_c \sin(\omega t - kz); \quad k = \frac{2e\Lambda H_0}{c}; \quad \omega = \frac{2eV}{\hbar}.$$

The phase velocity of the Josephson current density wave is given by

$$v_p = \frac{\omega}{k} = c \frac{V}{\Lambda H_0}$$

and it depends on both the voltage V across the junction and on the magnetic field H_0, which provides a means for controlling the phase velocity independently of the electromagnetic waves which are excited. The maximum interaction of a Josephson current density wave and an electromagnetic wave in a tunnel junction is brought about when the phase velocities of the field and current density are equal. This condition corresponds to the equality

$$V = \frac{c_0}{c} H_0,$$

which gives the value of the magnetic field at which the self-induced step on the current–voltage characteristic of a tunnel junction has its maximum height. This relation corresponds to equality of the wavelengths of the Josephson current density wave and electromagnetic wave. As the magnetic field H_0 is increased, the wavelength of the Josephson wave decreases, and a dephasing occurs between the current wave and the field excited. However, each time the current-density wave becomes an integer multiple of the field wave, the efficiency of interaction again increases. Therefore, the intensity of the generation on each type of oscillation and, along with it, the height of the corresponding step on the

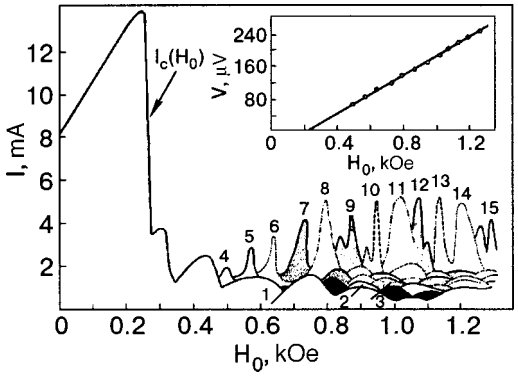

FIG. 6. Height of the characteristic steps on the I–V characteristic of a Josephson tunnel junction in an external magnetic field.

current–voltage characteristic, oscillates with increasing magnetic field, and the amplitude of those oscillations gradually decays.

Figure 6 shows how the height of the self-induced steps on the I–V characteristic of a $Sn–SnO_2–Sn$ Josephson tunnel junction depends on the external magnetic field. The number n of each step in the sequence is indicated near the corresponding principal maximum, the position of which on the voltage axis as a function of field is given in the inset to this figure. The deviation of the Josephson critical current (corresponding to $n=0$) from relation (2) is due to the fact that this junction, like that on which the radiation was first detected, has dimensions exceeding the Josephson penetration depth. The scheme for automatic registration of these curves works in such a way that the field dependence of each successive step can be determined provided that its position on the I–V curve is at a higher current than the one before it. Identical steps (except for $n=0$) correspond to the same sort of shading for an envelope rendered as a solid line or to the same shape of the envelope in the absence of shading. The complicated dependence that is observed is described well, on the whole, by the existing theory.

5. SOME PROMISING TOPICS FOR FURTHER RESEARCH AND APPLICATIONS OF THE AC JOSEPHSON EFFECT

Although the Josephson effects were discovered relatively long ago, research and development work on them is still intensively pursued. A whole region of low-temperature electronics involves the application of so-called SQUIDs—superconducting quantum interference devices, which are based on the very high sensitivity of the Josephson current to a static magnetic field. SQUIDs are used as sensors having a record sensitivity to the strength and gradient of an applied magnetic field and for amplifying and measuring small currents and voltages. They find application in geological prospecting for mineral resources and in medical diagnostics, where they are a basic element of devices such as the magnetocardiograph and magnetoencephalograph, and in other areas.

Josephson tunnel junctions as nonlinear elements can be used for the mixing of signals, frequency conversion, harmonic generation, and detection of electromagnetic radiation at frequencies up to the threshold frequency corresponding to the value of the energy gap in the spectrum of quasi-particle excitations. For superconductors such as lead and tin the latter lies in the far-infrared region of the spectrum, while for superconductors with higher critical temperatures (e.g., Nb_3Sn or the new high-temperature materials $YBa_2Cu_3O_{7-d}$ etc.) it lies in the infrared. Recently there has been increasing interest in the application of Josephson junctions as active microwave devices (heterodynes, mixers, and frequency converters) in thin-film integrated circuits. From a single tunnel junction one can extract a microwave power of up to 10^{-7} W, and from a system of coupled junctions, up to 1 μW. For this application barriers with higher transparency are used. Then the Josephson current exciting the resonance modes of a strip resonator propagate in the junction not in the form a traveling wave but as a soliton representing a quantum of magnetic flux which is multiply reflected from the edges of the junction. Such a soliton, which is also called a fluxon, is generated by the tunneling current itself, and in this case the external magnetic field is absent.

When speaking of the promising applications of the ac Josephson effect one must not fail to mention quantum voltage standards, which have long been used in a number of countries as primary government standards for the volt. Such devices are easily compared with each other, since they are checked by comparing the frequencies of the standard and of the device to be checked. Precision measurements of relation (1) have permitted refinement of the ratio of fundamental constants h/e and to eliminate any seeming contradiction between the predictions of quantum electrodynamics and experiment, which had arisen because of the use of a previous, inaccurate value of this ratio.[21]

*E-mail: yanson@ilt.kharkov.ua

[1)]This is how we shall indicate the dates of acceptance and publication for pioneering works. As recounted by P. W. Anderson,[2] in choosing the journal for publication it was decided not to send the first-claim report to the established American journal *Physical Review Letters* because of the importance and unusual nature of the results obtained and the fear that they would not be understood by the referees. As the further course of events would show,[3] even the two-time Nobel laureate John Bardeen did not agree with Josephson's conclusions at first.

[2)]In 1975 Giaever, Josephson, and L. Esaki, who had even earlier discovered the tunneling of electrons in highly doped semiconductors, were awarded the Nobel Prize.

[3)]It should be noted that the I–V characteristic is usually taken using a current source. Therefore the descending part of the I–V characteristic cannot be recorded directly but is manifested as hysteresis on recording in the forward and reverse directions.

[4)]The materials of the Colgate Conference on Superconductivity, published in the January 1964 issue of *Reviews of Modern Physics*, became known to the author only in the Fall of that year.

[1] B. D. Josephson, Phys. Lett. **1**, 251 (1962).
[2] P. W. Anderson, Phys. Today **23**(11), 23 (1970).
[3] J. Bardeen, Phys. Rev. Lett. **9**(4), 147 (1962).
[4] P. W. Anderson and J. M. Rowell, Phys. Rev. Lett. **10**, 230 (1963).
[5] J. M. Rowell, Phys. Rev. Lett. **11**, 200 (1963).
[6] S. Shapiro, Phys. Rev. Lett. **11**, 80 (1963).
[7] M. D. Fiske, Rev. Mod. Phys. **36**, 221 (1964).
[8] P. W. Anderson and A. H. Dayem, Phys. Rev. Lett. **13**, 195 (1964).
[9] I. Giaever, Phys. Rev. Lett. **5**, 148 (1960).
[10] I. O. Kulik and I. K. Yanson, *Josephson Effect in Superconducting Tunnel Structures*, Israel Program for Scientific Translations, Jerusalem (1972), Nauka, Moscow (1970).
[11] I. K. Yanson, V. M. Svistunov, and I. M. Dmitrenko, Zh. Éksp. Teor. Fiz. **47**, 2091 (1964) [Sov. Phys. JETP **20**, 1404 (1965)].

[12] I. K. Yanson, V. M. Svistunov, and I. M. Dmitrenko, Zh. Éksp. Teor. Fiz. **48**, 976 (1965) [Sov. Phys. JETP **21**, 650 (1965)].
[13] D. N. Langenberg, D. J. Scalapino, B. N. Taylor, and R. E. Eck, Phys. Rev. Lett. **15**, 294 (1965).
[14] I. M. Dmitrenko and I. K. Yanson, in *Proceedings of the Tenth International Conference on Low Temperature Physics (LT-10)* [in Russian], Moscow (1966), **IIA, p.** 228.
[15] R. E. Eck, D. J. Scalapino, and B. N. Taylor, Phys. Rev. Lett. **13**, 15 (1964).
[16] R. E. Eck, D. J. Scalapino, and B. N. Taylor, in *Low-Temperature Physics LT9: Proceedings of the IXth International Conference, 1964*, J. G. Daunt, D. O. Edwards, F. J. Milford, and M. Yaqub (eds.), Plenum Press, New York (1965), Part A, p. 415.
[17] D. D. Coon and M. D. Fiske, Phys. Rev. **138**, 744 (1965).
[18] I. M. Dmitrenko and I. K. Yanson, Zh. Éksp. Teor. Fiz. **49**, 1741 (1965) [Sov. Phys. JETP **22**, 1190 (1966)].
[19] I. O. Kulik, JETP Lett. **2**, 84 (1965).
[20] J. C. Swihart, J. Appl. Phys. **32**, 461 (1961).
[21] W. H. Parker, B. N. Taylor, and D. N. Langenberg, Phys. Rev. Lett. **18**, 287 (1967).

Translated by Steve Torstveit

Experimental studies of weakly coupled superconductors (Review)

I. M. Dmitrenko*

B. Verkin Institute for Low Temperature Physics and Engineering of the National Academy of Sciences of Ukraine, 47 Lenin Ave., Kharkov 61103, Ukraine

(Submitted January 29, 2004)
Fiz. Nizk. Temp. **30**, 698–704 (July–August 2004)

A review is given of the main experimental results obtained in research on weakly coupled superconductors after 1964 at the Institute for Low Temperature Physics and Engineering of the National Academy of Sciences of Ukraine, Kharkov (ILTPE). [DOI: 10.1063/1.1789912]

In the study of the phenomena of superconductivity there have been turning points that have opened up new fields of research. For example, such a role was played by Shubnikov's discovery of the ideal diamagnetism of superconductors, an effect which was later named after Meissner, who, following a visit to Kharkov, published his results somewhat earlier than Shubnikov.

The concept of superconductivity, which was developed phenomenologically by Fritz London in the years between 1934 and 1950 as a result of his attempt to explain the strangeness of the Meissner effect, was of fundamental importance.

The well-known quantum expression for the current, written with the aid of the wave functions of the carriers, can be reduced to the form

$$\mathbf{j}_s = \frac{e n_s}{m}\left(\hbar \nabla \varphi - \frac{e}{c}\mathbf{A}\right)$$

on the assumption that the square modulus of the wave function of the ''superfluid'' electron is equal to the density n_s of such electrons. The supercurrent j_s contains two terms: a paramagnetic part due to the gradients of the phase φ, and a diamagnetic part due to the vector potential $\mathbf{A}$.

A chief element of London's concept was the postulate of phase coherence of the wave functions of the superconducting electrons over macroscopic lengths and times. In this case the phase gradient vanished, and the direct coupling of the current and vector potential remained. Taking the curl of both sides of the equation gave the second London equation, which describes the Meissner effect.

London's concept implied a result no less strange than the Meissner effect—quantization of the magnetic flux in superconductors (F. London, *Superfluids* (1950)). But only after 11 years did ''the ice start to move:'' as we know, flux quantization was observed simultaneously in Europe and America.[1] The year before, Ivar Giaever had realized the tunnel effect in superconductors. A year later, Brian Josephson, a postgraduate student doing a theoretical study of the tunneling effect, predicted his famous Josephson effects.[2]

In 1960 the Institute for Low Temperature Physics and Engineering of the National Academy of Sciences of Ukraine (ILTPE), with a Department of Cryogenic Electronics, was founded in Kharkov. It soon became clear that superconductors were most promising in such a connection, and first attempt to use them was to create a detector of electromagnetic radiation based on a tunnel junction.

The first junctions were obtained in a temporary building (a bomb shelter under a residence) in conditions unsuitable for such studies. In 1964, now in the new building of the institute, I. K. Yanson obtained junctions of better quality on tin films and soon saw current at zero voltage (the dc Josephson effect).[3] It should be mentioned that in that paper reported the first observation of subharmonics of the gap on the current–voltage (I–V) characteristics of a $Sn–SnO_2–Sn$ junction. Good agreement with the theory was obtained for the dependence of the critical current on T and H. At the end of that year, with the aid of the most sensitive receiver in the 3-cm range then available (the P5-10) and a good understanding of the physics of the processes occurring in a tunnel junction, he successfully observed the radiation ($W \sim 10^{-14}$ W) generated in the ac Josephson effect in a direct experiment.[4]

A number of studies were subsequently done to study this radiation.[5] I. O. Kulik developed an electrodynamics of the Josephson tunnel junction,[6] and our experimental results were successfully interpreted in the framework of that theory.

We also studied the processes of aging of tunnel junctions,[7] which are accompanied by growth of the critical current and a lowering of the normal resistance. Although a tunnel junction is the limit of weak coupling of superconductors, with the growth of the critical current (coupling energy) we were able to observe in the spectrum of current steps on the I–V characteristic the subharmonic steps that are characteristic of the limit of strong coupling of superconductors, as studies of clamped point contacts would show.

The first weak link between superconductors that we studied was a tunnel junction. But such a link can also be created in contacts with direct conduction—point contacts, through a normal metal layer, etc.

Subsequent studies were done for delicate point contacts of the tip–plane type. Stable results in the presence of vibrations were obtained after a special mechanism was constructed (Fig. 1).[8] The mechanism permitted placement of the tips in the waveguide with an accuracy of 200–300 Å. This made it possible to made very smooth variations of R_N,

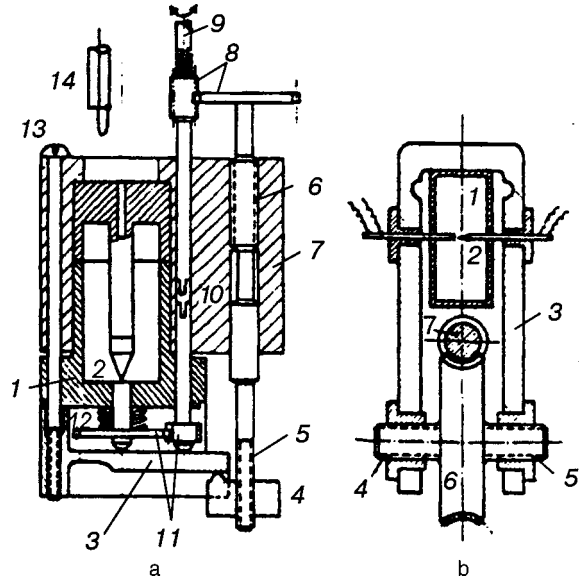

FIG. 1. Mechanisms for creating point contacts *2* in a resonator *1* (a) and in a waveguide *1* (b); *3*—elastic elements (flat spring and bracket); *5,6* (a) and *4,5* (b)—differential threads with a pitch difference of 0.05 mm. The gear set *11* and clutch *10* are used to rotate the center plate *12* to obtain a new contact.

the critical current, and, as it turned out, the coupling energy of the superconductors through the contact.

The earliest manifestations of the Josephson effect were observed on high-resistance contacts. Fluctuations first disrupt the current at zero voltage. The ac effect is more stable against fluctuations; it was first manifested in oscillations of the slope of the I–V characteristic, and at a fixed current it leads to the characteristic oscillations (Fig. 2).[9]

As the critical current increases, the spectral properties of the contacts (the spectrum of the steps on the I–V characteristic and the dependence of their height on the microwave radiation) change substantially.[10]

The Josephson relation

$$j(\varphi,t)=j_0\sin\varphi(t), \tag{1}$$

where j_0 is the maximum value of the dc Josephson current and φ is the phase difference, is well known. If $j(\varphi)$ has such a dependence and $\varphi(t)$ is a linear function, then everything is simple and beautiful: the spectrum of the steps is harmonic, and their height as a function of the microwave

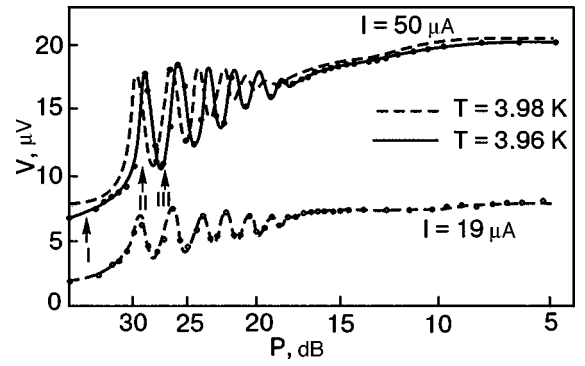

FIG. 2. Oscillations of the voltage across a superconducting point contact (data of a previous figure) for two fixed values of the current and with a change of the incident power.

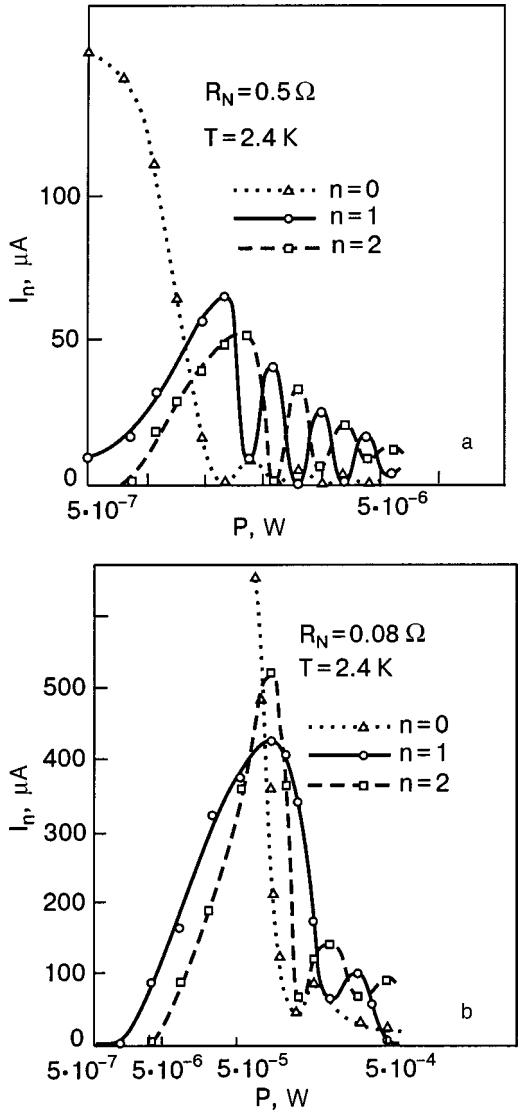

FIG. 3. Dependence of the zero current and step heights on the level of microwave power P delivered to superconducting point contacts: a high-resistance Ta–Ta contact (a); a contact between the same pair, enlarged by movement of the tip, the resistance decreasing to 0.08 Ω (b). The contact pair was placed in a standard 3-cm waveguide at a distance of a quarter wavelength from the short-circuiting plunger.

field varies as the modulus of the Bessel function of the corresponding order. But if the dependence $j(\varphi,t)$ differs from sinusoidal, then one must use the more general expression[10–12]

$$j(\varphi,t)=\sum_{n=1}^{\infty} j_n\sin n\varphi(t). \tag{2}$$

Even for a tunnel junction, as the transparency of the barrier increases the dependence $\varphi(t)$ deviates from linear,[13] and $j(\varphi)$ is not described by Eq. (1).[14] Research on the spectral properties of point contacts have led to the conclusion that value of the coupling energy is the key.[15] A nonsinusoidal dependence $j(\varphi)$ leads to the appearance of subharmonic steps, and a characteristic alternation of extrema of the Bessel function gives way in the strong-coupling limit to a single maximum (Fig. 3). By fitting Bessel functions one can approximate the dependence of the height of the step on the value of the microwave field (Fig. 4), having determined the

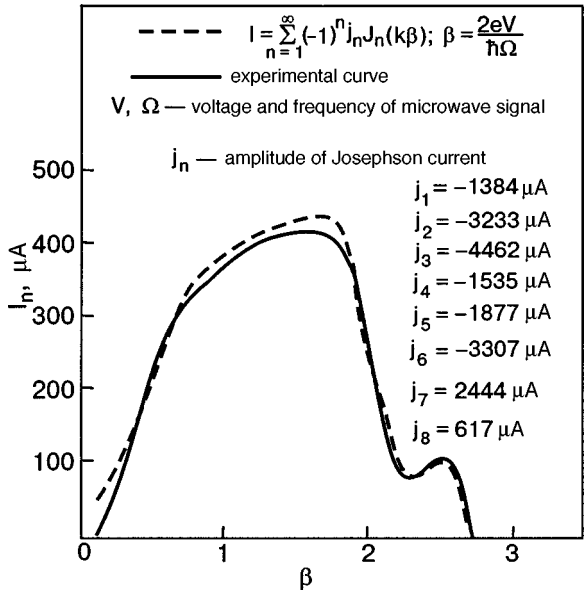

FIG. 4. Experimental and calculated curves of the height of the first current step versus the amplitude of the microwave field for a low-resistance Ta–Ta point contact. Approximation of the sum by eight Bessel functions.

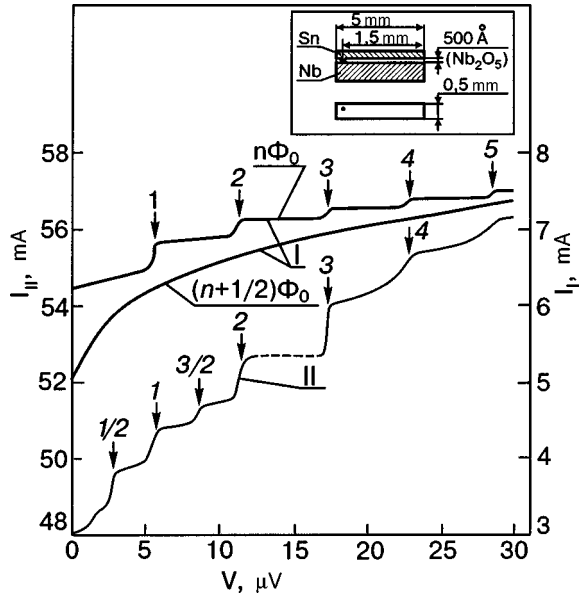

FIG. 5. I—current–voltage characteristic of a Nb–Sn contact with $R_N = 0.1\ \Omega$ and a system of harmonic characteristic steps. The contact is multiply connected, and therefore the I–V characteristics for $\Phi = n\Phi_0$ and $\Phi = (n+1/2)\Phi_0$ are substantially different. II—I–V characteristic of a Nb–Sn contact with $R_N = 0.01\ \Omega$ with subharmonic characteristic steps.

degree of deviation of the dependence $j(\varphi)$ from a sine and the effective number of elements of the series (2).

The inverse Josephson effect was studied on point contacts in Ref. 16; previously it had been observed only on tunnel junctions (the appearance of continuous and quantum dc voltages under the action of microwave radiation in the absence of a transport current).

Besides individual point contacts, we realized one-dimensional chains of point contacts between grains of niobium powder[17] and investigated interference effects in the joint action of microwave and magnetic fields on statistical systems of point contacts.[18]

On point contacts of the $S-N-S$ type we observed a new type of detection of microwave radiation in the absence of transport current through the contact, controlled by an external magnetic field.[19] The methods developed for making contacts of the point type[20] made it possible to study the characteristic steps on the I–V characteristics of contacts in various strip resonators.[21]

If more than one microcontact is placed in a strip system, it becomes possible to control the microwave generation by means of small magnetic fields. This opens up interesting possibilities in microwave and measurement technique.

It should be noted that a coherent lattice of contacts will generate the same frequency for any contact resistance R_N, since the ''banks'' are superconducting and the potential difference across all contacts is the same. And changing the flux by half a quantum rotates the phase of the microwave oscillations of adjacent contacts by π, i.e., it quenches the generation at the output.

Figure 5 is shown as an example. In contrast to the steps induced by an external microwave source, the position of the characteristic steps along the V axis changes with temperature as a result of the change in penetration depth and eigenfrequencies of the strip resonator.

Current-controlled Josephson contacts were proposed by us and studied in a crossed film geometry (Fig. 6).[22] A theoretical model for such control was developed in Ref. 23. Similar geometries have subsequently been investigated effectively in systems of multiterminal interferometers.[24]

Interesting weak links arise at phase-slip centers (PSCs) and the recently discovered and investigated phase-slip lines (PSLs).[25] PSLs arise in narrow superconducting channels, where the current and order parameter are uniform over the cross section, the magnetic field can be neglected, and Abrikosov vortices do not form. The current–voltage characteristics have the characteristic stepped form due to voltage steps. Such structures of the I–V characteristic have also been observed for wide films, where it is usually assumed that the resistive state is due to a dynamic mixed state (DMS) in which a flow of the vortices from the external field or the field of the current occurs at a current exceeding the vortex pinning strength.

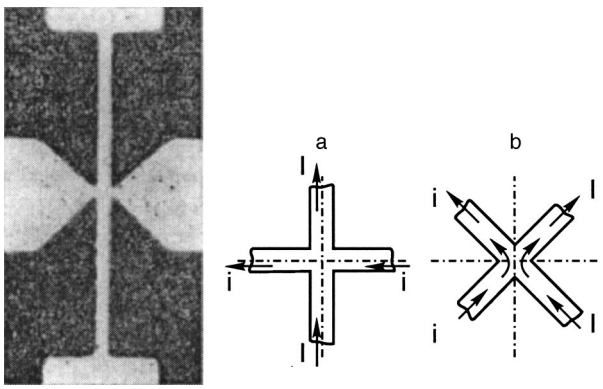

FIG. 6. Photograph of a cross-shaped thin-film structure. Magnification 1200×. Variants of the weak coupling in the cross-shaped sample (I is the transport current; i is the control current).

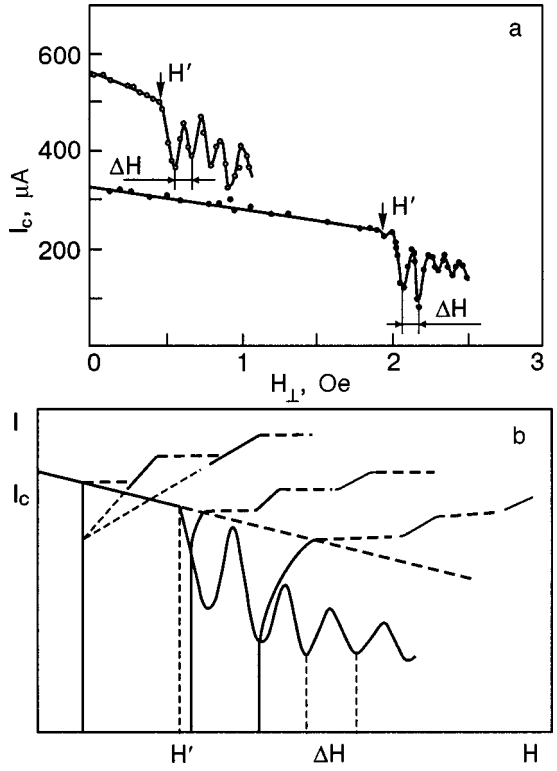

FIG. 7. $I_c(H_\perp)$ curves for two tin film samples: $w=3$ μm (●) and 5.4 μm (○) (a); schematic superpositoin of the initial parts of the I–V characteristics for $H<H'$ and $H>H'$ with the dependence for films of width $w<\lambda_\perp$ and $w>\lambda_\perp$ (b).[26,27]

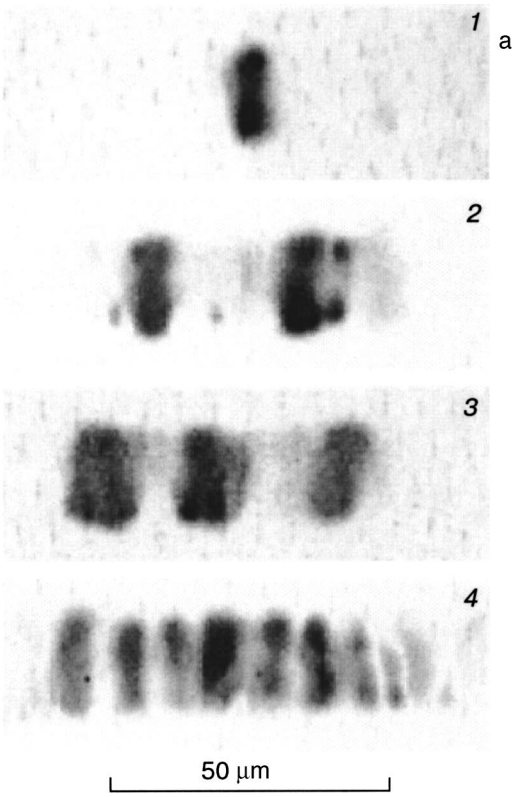

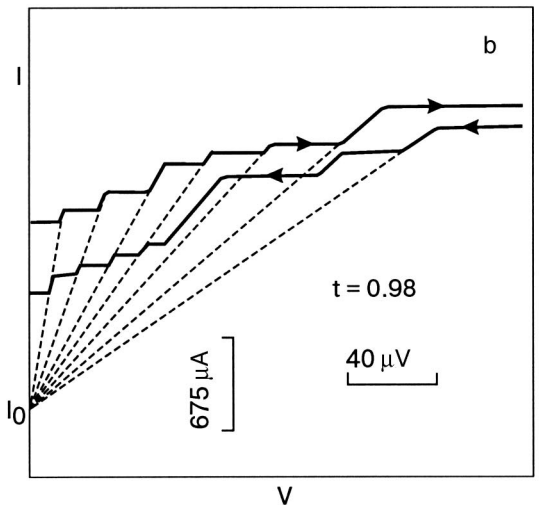

FIG. 8. Images of the voltage response of a uniform tin film as the transport current through the film is increased ($w>\lambda_\perp$). The dark regions are the locations of phase slip lines along the length of the film. The current increases for (*1*) to (*4*) (a). Stepped structure of the I–V characteristic of tin films shielded by a superconducting screen (b).

A fundamentally important result was obtained in studies of the dependence of the critical current of wide films on the value of a magnetic field perpendicular to the film (Fig. 7).[26] Besides the oscillations of the critical current itself at $H>H'$, at $H<H'$ the I–V characteristics have the same stepped character as a narrow channel, but, important, in the region of fields $H>H'$ where the vortices remain in place in the film, the I–V characteristic initially has the smooth, nonlinear form characteristic for a DMS, but then a new mechanism of resistivity, due to the formation not of PSCs but now (for the wide film) of PSLs, is turned on. This reflects, on the one hand, a more general case of resistivity of superconducting films (coexistence of two different mechanisms of resistivity of the films) and, on the other, confirms the existence of PSLs.

Interesting results on the dynamics of vortex motion in zones of charge imbalance (the neighborhoods of PSLs and the *SN* boundary) have been obtained on wide films.[27] Later A. G. Sivakov implemented a two-contact interferometer based on PSLs.[28]

PSLs were first observed visually with a low-temperature laser microscope at ILTPE (Fig. 8).

Research on quantum interference, which was started by S. I. Bondarenko, continued first on two-contact dc SQUIDs (more precisely, interferometers, since the SQUID is a device with electronics, a magnetic antenna, etc.). Later V. I. Shnyrkov began his studies of single-contact rf SQUIDs, which have proved to be fruitful and novel among the many papers on these superconducting devices.

Two-contact interferometers have been studied in a new resistive regime at currents larger than the critical. This, as has become clear, does not affect the fluxoid quantization or the interference.[29]

The rectifying properties of asymmetric interferometers were discovered[29] independently of the work of Ouboter at the Leiden laboratory.[30] An important role in interferometers is played by circulating fluxoidal current, equal to zero for integer numbers of quanta of the external magnetic field and reaching a maximum i_m at half-integer flux quanta $\Phi_e=(n+1/2)\Phi_0$; $i_m=\Phi_0/2L$, where L is the magnetic inductance of the circuit.

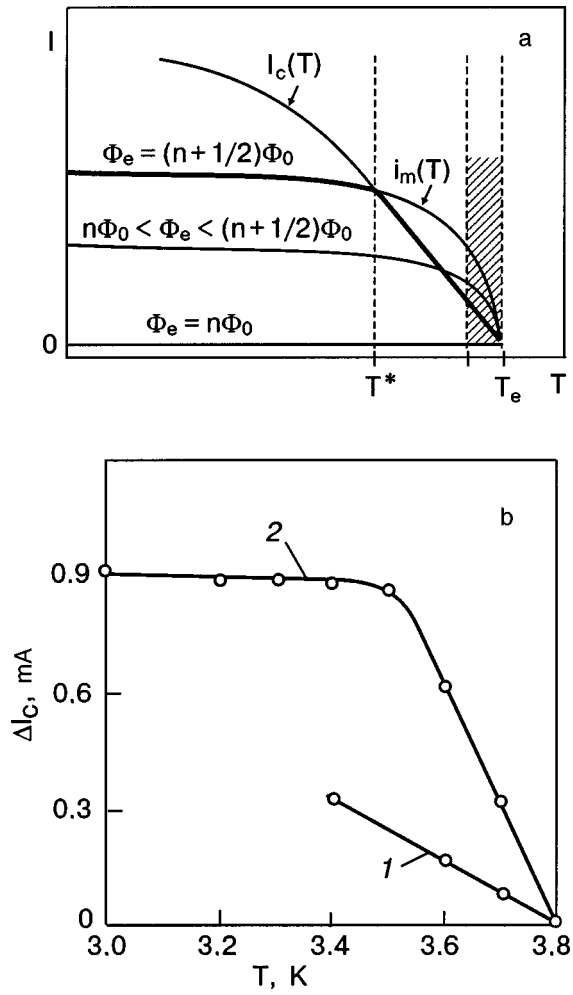

FIG. 9. Schematic illustration of the relationship between the critical current I_c and the maximum circulating current i_m with changing temperature of the superconducting quantum interferometer. The region ΔT in which the critical current is not observed because of the effect of fluctuations is shaded (a). The $\Delta I_c(T)$ curves. Curves *1* and *2* are recorded for different inductances of the quantizing circuit (b).

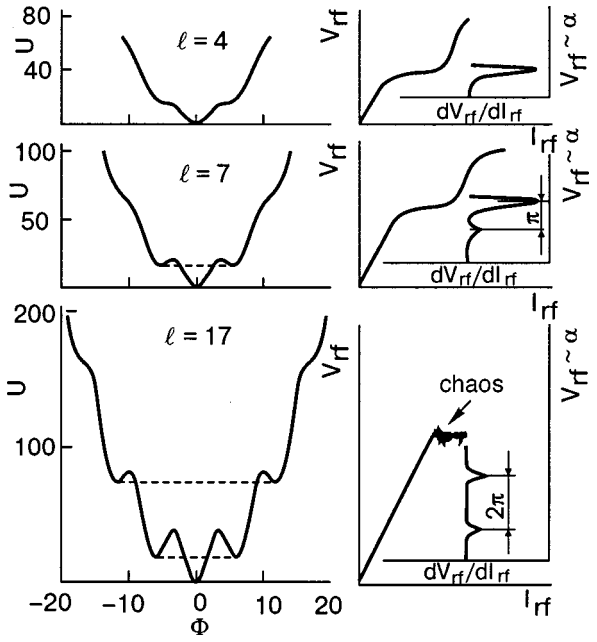

FIG. 10. Potential energy $U(\Phi)$ for $\Phi_e = 0$ and the experimental I–V characteristics with their derivatives; the dashed lines show the states corresponding to resonant tunneling of the macroscopic system.

When the kinetic inductance $L_{\rm kin} = mc(t/\sigma)/[e^2 n_s(T)]$ is taken into account, where t is the length and σ is the cross section of the weak link, the conditions of fluxoid quantization in the linear approximation has the form

$$\gamma L i_m + \Phi_e + L i_m = n\Phi_0,$$

where $\gamma = L_{\rm kin}/L$ and $i_m(T) = \Phi_0[1+\gamma(T)]^{-1}/2L$. With growth of γ the magnetic quantization becomes degenerate (see p. 178 of Ref. 21).

The properties of an interferometer depend substantially on the ratio of the critical current I_c to $i_m(T) \propto \lambda_L^{-2}(T) \propto (1 - t^4)$, where t is the reduced temperature. Near T_c this dependence is much steeper than $I_c(T) \propto \Delta T$ or $\Delta T^{2/3}$. What we have said is illustrated in Figure 9a (p. 199 of Ref. 21). For $T > T^*$ the critical current of the interferometer is nonzero on part of the oscillation period, and the amplitude ΔI_c of the oscillations of the critical current increases as $I_c(T)$. At $T = T^*$ the $I_c(T)$ curve bends over and goes practically to saturation (Fig. 9b). For $T < T^*$ the critical current $I_c(\Phi_e)$ does not reach zero at any Φ_e. Such behavior has been insufficiently studied, as has the question of the superposition of the circulating current, equilibrium current, and nonequilibrium transport current. It follows from experiments that the modulation depth $\Delta I_c(\Phi_e)$ is equal to $2i_m$. This is possible if the critical current of the contact decreases independently of the direction of the circulating current in relation to that of the transport current. In Ref. 29 this was interpreted in terms of a kinetic depairing and on the assumption of the existence of independent fluxes in the electron condensate.

These arguments can be valid only for the case when the transport current interacts with a stable fluxoid current, which cannot vary so long as fluxoid quantization holds.

If $i_m(\Phi_e)$ becomes greater than I_c, then in the interval of fluxes Φ_e near half-integer values of the quantum the flux $\Phi = \Phi_e$, the circulating current is equal to zero, and magnetic quantization gives way to kinetic quantization ($\gamma \gg 1$). The role of the kinetic inductance in fluxoid quantization was demonstrated back in 1964 in an experiment by T. K. Hunt and J. E. Mercereau.[31] Theoretically the I–V curves of superconducting interferometers were calculated in Ref. 32.

Many new results have been obtained on single-contact rf interferometers.[33–38] For example, V. I. Shnyrkov has studied the classical and then the quantum dynamics of rf SQUIDs, made a detailed study of the nonhysteretic regime, observed and studied, at temperatures around 1 K, the ''real quantum'' phenomena of macroscopic tunneling and macroscopic quantum interference of the quantum states of a SQUID which are degenerate in energy but lie on opposite branches of the $U(\Phi)$ parabola (Fig. 10), studied quantum noise, and observed for the first time on a SQUID the regime of stochastic oscillations—chaos.

It should be mentioned in closing that the normal resistance that determines the dissipation and damping and which is due to the presence of ''normal electrons'' increases exponentially with decreasing T in point contacts (contacts with direct conduction), just as in tunnel junctions.

*E-mail: dmitrenko@ilt.kharkov.ua

[1] R. Doll and M. Näbauer, Phys. Rev. Lett. **7**, 51 (1961); B. S. Deaver and W. M. Fairbank, *ibid.* **7**, 43 (1961).
[2] B. D. Josephson, Phys. Lett. **1**, 251 (1962).
[3] I. K. Yanson, V. M. Svistunov, and I. M. Dmitrenko, Zh. Éksp. Teor. Fiz. **47**, 2091 (1964) [Sov. Phys. JETP **20**, 1404 (1965)].
[4] I. K. Yanson, V. M. Svistunov, and I. M. Dmitrenko, Zh. Éksp. Teor. Fiz. **48**, 976 (1965) [Sov. Phys. JETP **21**, 650 (1965)].
[5] I. M. Dmitrenko, I. K. Yanson, and V. M. Svistunov, JETP Lett. **2**, 49, 112 (1965); Zh. Éksp. Teor. Fiz. **49**, 1741 (1965) [Sov. Phys. JETP **20**, 1190 (1966)].
[6] I. O. Kulik, JETP Lett. **2**, 84 (1965).
[7] I. M. Dmitrenko, I. I. Yurchenko, and A. S. Shul'man, Fizika Kondesirovannogo Sostoyaniya, issue **3**, 62 (1968); issue **8**, 160 (1970).
[8] L. E. Kolin'ko, T. P. Narbut, L. A. Bondarenko, S. I. Bondarenko, and I. M. Dmitrenko, Fizika Kondesirovannogo Sostoyaniya, issue **9**, 91 (1970).
[9] I. M. Dmitrenko, V. I. Karamushko, and L. K. Snegireva, Zh. Éksp. Teor. Fiz. **63**, 981 (1972) [Sov. Phys. JETP **36**, 514 (1973)].
[10] I. M. Dmitrenko, Yu. G. Bevza, and V. I. Karamushko, Phys. Status Solidi **17**, 59 (1973).
[11] I. M. Dmitrenko, Ukr. Fiz. Zh. (Russ. Ed.) **14**, 439 (1969); I. M. Dmitrenko and Yu. G. Bevza, Fizika Kondesirovannogo Sostoyaniya, issue **8**, 86 (1970).
[12] I. M. Dmitrenko, Yu. G. Bevza, and V. A. Mikhaĭlov, JETP Lett. **17**, 4 (1973).
[13] I. O. Kulik, Zh. Tekh. Fiz. **37**, 157 (1967) [Sov. Phys. Tech. Phys. **12**, 111 (1967)].
[14] V. P. Galaĭko, A. V. Svidzinskiĭ, and V. A. Slyusarev, Zh. Éksp. Teor. Fiz. **56**, 835 (1969) [Sov. Phys. JETP **29**, 454 (1969)].
[15] I. M. Dmitrenko and Yu. G. Bevza, Fizika Kondesirovannogo Sostoyaniya vyp. **3**, 70 (1968); I. M. Dmitrenko, Yu. G. Bevza, and V. I. Karamushko, Phys. Status Solidi A **17**, 59 (1973).
[16] I. M. Dmitrenko, Yu. G. Bevza, and V. A. Mikhaĭlov, Pis'ma Zh. Éksp. Teor. Fiz. **17**, 8 (1973)]; Yu. G. Bevza, V. A. Mikhaĭlov, É. A. Kel'man, and I. M. Dmitrenko, Fizika Kondesirovannogo Sostoyaniya, issue **29**, 13 (1973).
[17] I. I. Yurchenko, V. S. Kartavtsev, V. I. Matveev, and I. M. Dmitrenko, Zh. Tekh. Fiz. **43**, 2174 (1973).
[18] I. I. Yurchenko, V. S. Kartavtsev, V. I. Matveev, and I. M. Dmitrenko, Fiz. Tverd. Tela (Leningrad) **15**, 328 (1973) [Sov. Phys. Solid State **15**, 244 (1973)].
[19] Yu. G. Bevza, V. I. Karamushko, and I. M. Dmitrenko, Zh. Tekh. Fiz. **47**, 646 (1977).
[20] S. I. Bondarenko, I. M. Dmitrenko, and E. I. Balanov, Fiz. Tverd. Tela (Leningrad) **12**, 1417 (1970) [Sov. Phys. Solid State **12**, 1113 (1970)]; S. I. Bondarenko, E. I. Balanov, L. E. Kolin'ko, and T. P. Narbut, Prib. Tekh. Éksp., No. 1, 235 (1970); L. E. Kolin'ko, T. P. Narbut, L. A. Bondarenko, S. I. Bondarenko, and I. M. Dmitrenko, Fizika Kondesirovannogo Sostoyaniya, issue **9**, 91 (1970).
[21] I. M. Dmitrenko, Doctoral dissertation [in Russian], FTINT AN UkrSSR (1970).
[22] Yu. G. Bevza, G. G. Zach, V. I. Karamushko, and I. M. Dmitrenko, Pis'ma Zh. Tekh. Fiz. **2**, 367 (1976) [Sov. Tech. Phys. Lett. **2**, 140 (1976)]; Yu. G. Bevza, V. I. Karamushko, É. A. Kel'man, G. G. Tsakh, and I. M. Dmitrenko, Fiz. Nizk. Temp. **5**, 701 (1979) [Sov. J. Low Temp. Phys. **5**, 332 (1979)]; Yu. G. Bevza, V. I. Karamushko, and I. M. Dmitrenko, JETP Lett. **40**, 1 (1979).
[23] I. O. Kulik, A. N. Omel'yanchuk, and É. A. Kel'man, Fiz. Nizk. Temp. **3**, 1107 (1977) [Sov. J. Low Temp. Phys. **3**, 537 (1977)].
[24] R. de Bruyn Ouboter and A. N. Omeljanchuk, Superlattices Microstruct. **25**, 1005 (1999).
[25] I. M. Dmitrenko, Fiz. Nizk. Temp. **22**, 849 (1996) [Low Temp. Phys. **22**, 648 (1996)].
[26] L. E. Musienko and V. G. Volotskaya, Fiz. Nizk. Temp. **4**, 124 (1978) [Sov. J. Low Temp. Phys. **4**, 63 (1978)]; L. E. Musienko, Candidate's dissertation [in Russian], FTINT AN UkrSSR, Kharkov (1981).
[27] A. G. Sivakov and V. G. Volotskaya, Fiz. Nizk. Temp. **11**, 547 (1985) [Sov. J. Low Temp. Phys. **11**, 300 (1985)].
[28] A. G. Sivakov, A. M. Glukhov, A. N. Omelyanchouk, Y. Koval, P. Müller, and A. V. Ustinov, Phys. Rev. Lett. **91**, 267001 (2003).
[29] S. I. Bondarenko and I. M. Dmitrenko, Fizika Kondesirovannogo Sostoyaniya, issue **3**, 79 (1968).
[30] R. de Bruyn Ouboter *et al.*, Physica (Amsterdam) **32**, 1448 (1966); **37**, 114 (1967).
[31] T. K. Hunt and J. E. Mercereau, Phys. Rev. **135**, 944 (1964).
[32] Yu. G. Bevza and É. A. Kel'man, Zh. Tekh. Fiz. **49**, 2356 (1979) [Sov. Phys. Tech. Phys. **24**, 1315 (1979)].
[33] I. M. Dmitrenko, S. I. Bondarenko, and T. P. Narbut, Preprint [in Russian], FTINT AN UkrSSR, Kharkov (1969).
[34] I. M. Dmitrenko, G. M. Tsoi, V. I. Shnyrkov, and V. V. Kartsovnik, J. Low Temp. Phys. **49**, 713 (1982).
[35] I. M. Dmitrenko, G. M. Tsoi, and V. I. Shnyrkov, Fiz. Nizk. Temp. **8**, 660 (1982) [Sov. J. Low Temp. Phys. **8**, 330 (1982)].
[36] I. M. Dmitrenko, D. I. Konotop, G. M. Tsoĭ, and V. I. Shnyrkov, Fiz. Nizk. Temp. **9**, 375 (1983) [Sov. J. Low Temp. Phys. **9**, 340 (1983)].
[37] V. I. Shnyrkov, G. M. Tsoĭ, V. V. Kartsovnik, and S. S. Tinchev, Zh. Éksp. Teor. Fiz. **86**, 809 (1983) [Sov. Phys. JETP **59**, 472 (1983)].
[38] I. M. Dmitrenko, G. M. Tsoĭ, and V. I. Shnyrkov, Fiz. Nizk. Temp. **10**, 211 (1984) [Sov. J. Low Temp. Phys. **10**, 111 (1984)].

Translated by Steve Torstveit.

Spontaneous and persistent currents in superconductive and mesoscopic structures (Review)

I. O. Kulik*

Department of Physics, Bilkent University, Ankara 06533, Turkey; Physics Department, Stony Brook University, Stony Brook, New York 11794, USA; B. Verkin Institute for Low Temperature Physics and Engineering of the National Academy of Sciences of Ukraine, 47 Lenin Ave., Kharkov 61103, Ukraine

(Received February 4, 2004)
Fiz. Nizk. Temp. **30**, 705–713 (July–August 2004)

We briefly review aspects of superconductive persistent currents in Josephson junctions of the S/I/S, S/O/S and S/N/S types, focusing on the origin of jumps in the current versus phase dependences, and discuss in more detail the persistent and the ''spontaneous'' currents in Aharonov–Bohm mesoscopic and nanoscopic (macromolecular) structures. A fixed-number-of-electrons mesoscopic or macromolecular conducting ring is shown to be unstable against structural transformation removing spatial symmetry (in particular, azimuthal periodicity) of its electron–lattice Hamiltonian. In the case when the transformation is blocked by strong coupling to an external azimuthally symmetric environment, the system becomes bistable in its electronic configuration at a certain number of electrons. Under such a condition, the persistent current has a nonzero value even at an (almost) zero applied Aharonov–Bohm flux and results in very high magnetic susceptibility dM/dH at small nonzero fields, followed by an oscillatory dependence at larger fields. We tentatively assume that previously observed oscillatory magnetization in cyclic metallo-organic molecules by Gatteschi *et al.* can be attributed to persistent currents. If this proves correct, it may present an opportunity for (and, more generally, macromolecular cyclic structures may suggest the possibility of) engineering quantum computational tools based on the Aharonov–Bohm effect in ballistic nanostructures and macromolecular cyclic aggregates. © *2004 American Institute of Physics.*
[DOI: 10.1063/1.1789111]

1. SUPERCONDUCTIVE WEAK LINKS

Current can flow in a dissipationless manner under the control of an external parameter, the Josephson phase across a superconductive weak link[1,2] (Fig. 1a) or a phase difference along a mesoscopic normal-metallic loop[3–5] (Fig. 1b). In both cases, the phase is related to the magnetic flux piercing the loop. The flux can be considered as one created by a thin, infinitely long solenoid producing no magnetic field outside its interior (and therefore in a loop) but nevertheless affecting the quantum states of electrons in the loop. This nonlocal effect of magnetic flux on quantum states is known as the Aharonov–Bohm effect.[6] The phase shift φ due to magnetic flux $\Phi=\oint \mathbf{A}\cdot d\mathbf{l}$ is equal to

$$\varphi = 2\pi \frac{\Phi}{\Phi_0}, \tag{1}$$

where $\Phi_0=hc/e^*$ is the flux quantum. In the Josephson junction, φ is the phase of the pair wave function, and the effective charge e^* equals twice the charge of the electron, $e^*=2e$. In case of a normal-metal ring, e^* is a single-electron charge, e.

The current in a loop can be calculated as the derivative of the energy of the junction with respect to φ,

$$J = \frac{e^*}{\hbar}\frac{\partial \mathrm{E}}{\partial \varphi}. \tag{2}$$

Superconductive junction theory considers contact types S/I/S (tunnel junctions),[7] orifice-type contacts S/O/S,[8] and the superconductor–normal metal–superconductor contacts S/N/S.[9–11] The S/O/S and S/N/S contacts can include barriers at the interface between superconducting electrodes or inside the normal metal, respectively. The zero-temperature feature of the current–phase relation on which we will focus our attention is the existence of jumps at certain values of φ, in particular at $\varphi=\pi$ or $\varphi=0$. In the latter case (which is in effect a property of the Aharonov–Bohm weakly coupled loop considered in the next Section), the current assumes a nonzero value at zero flux. Jumps in $J(\varphi)$ in superconductive contacts are eliminated by the adjustment of the electronic system to the appropriate value of the gap parameter $\Delta(r)$. In the Aharonov–Bohm loop the adjustment will be achieved by the rearrangement of atoms in the loop (the Peierls or the Jahn–Teller effects, or more complex lattice transformation).

The Ambegaokar–Baratoff and Kulik–Omelyanchouk theories resulted in an interpolated current–phase relation suggested by Arnold[12] (see also the review[13])

$$J(\varphi) = \frac{\pi\Delta_0}{2eR_0}\frac{\sin\varphi}{\sqrt{r^2+t^2\cos^2(\varphi/2)}}, \tag{3}$$

where R_0 is the resistance of the junction in the normal state and r^2 and t^2 are the reflection and transmission probabilities (with $r^2+t^2=1$) in the normal state. Δ_0 is the order param-

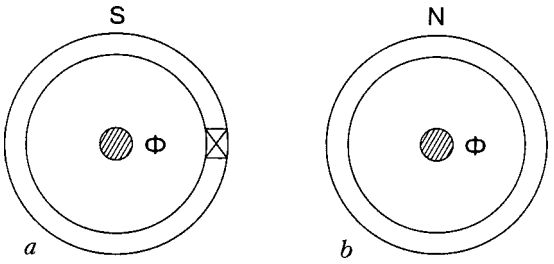

FIG. 1. Superconducting loop with a weak contact (crossed) (*a*). Normal-metal mesoscopic loop carrying current J (*b*).

eter of the superconductor (the BCS energy gap at $T=0$). At $t \ll 1$, formula (3) reduces to the Ambegaokar–Baratoff relation

$$J_{AB}=\frac{\pi\Delta_0}{2eR_0}\sin\varphi \tag{4}$$

whereas at $r=0$ (no barrier) it gives the Kulik–Omelyanchouk formula

$$J_{KO}=\frac{\pi\Delta_0}{eR_0}\sin(\varphi/2), \quad -\pi<\varphi<\pi \tag{5}$$

corresponding to twice as large a critical current at the same value of the contact resistence. The energy versus phase relation in the S/O/S structure with barriers is given by

$$E_{SOS}=-\frac{\pi\hbar\Delta_0}{2e^2R_0t^2}\sqrt{r^2+t^2\cos^2(\varphi/2)} \tag{6}$$

and is presented in Fig. 2. The S/N/S junction is represented by the $E(\varphi)$ dependence at $T=0$

$$E_{SNS}=-\frac{\hbar v_F}{6d}N_\perp t^2\left[1-\left(\frac{\varphi \bmod 2\pi}{\pi}\right)^2\right] \tag{7}$$

where v_F is the Fermi velocity of the metal and $N_\perp = Sk_F^2/4\pi$ is the number of perpendicular conducting channels in the normal bridge between superconductors of length d and cross section S. From the above expression, the current in the S/N/S structure at $T=0$ becomes

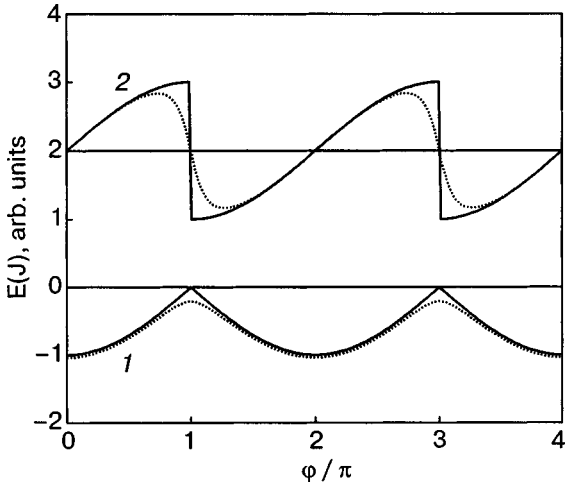

FIG. 2. Energy of the S/O/S contact versus phase at $T=0$ (*1*). Supercurrent versus phase (*2*). The solid curves correspond to $r=0$, the dotted curves to $r=0.2$. The $J(\varphi)$ curves are shifted upward arbitrarily for clarity.

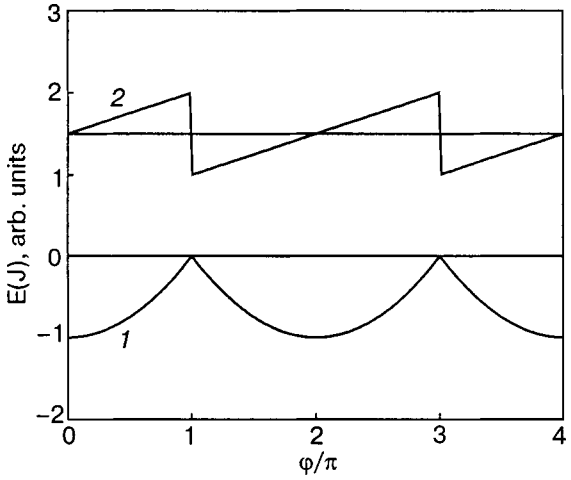

FIG. 3. Energy of the S/N/S contact versus phase at $T=0$ (*1*). Supercurrent versus phase (*2*). The $J(\varphi)$ curve is shifted upward arbitrarily for clarity.

$$J(\varphi)\approx\frac{2\hbar v_F}{3\pi eR_0d}\varphi, \quad -\pi<\varphi<\pi \tag{8}$$

and is presented in Fig. 3 together with the $E(\varphi)$ dependence.

2. PERSISTENT CURRENTS IN MESOSCOPIC SYSTEMS

Persistent currents (first discovered and termed nondecaying currents[4]) have been predicted for mesoscopic conducting loops[3–5] which do not show the effect of superconductivity. The current appears in the presence of magnetic field as a result of the Aharonov–Bohm effect.[6] As discussed in a review paper,[14] persistent currents are similar to the orbital currents in normal metals first considered by Teller[15] in his interpretation of Landau diamagnetism in metals,[16] but specific to the doubly connected geometry of the conductors (loops, hollow cylinders, etc.). Observations of persistent currents have been made in indirect[17,18] as well as in direct[19–21] experiments, showing single-flux-quantum $\Phi_0 = hc/e$ periodicity in the resistance of thin Nb wires[17] and networks of isolated Cu rings,[18] and in single-loop experiments on metals,[19] semiconductors,[20] and macromolecular metallo-organic compounds.[21] Contrary to the authors of Ref. 21 (an interpretation of magnetic oscillation[21] based on antiferromagnetic ordering of Fe ions in a ''ferric wheel'' $[Fe(OMe)_2(O_2CCH_2Cl)]_{10}$), we propose that the $6T$-periodic magnetization in this compound is due to Aharonov–Bohm persistent current flowing in the outer ring of O atoms while the inner ring of Fe atoms serves as a concentrator of magnetic field to the center of the ring. In Ref. 22 the $8T$-periodic variation of resistivity in molecular conducting cylinders (carbon nanotubes) was attributed to the Altshuler–Aronov–Spivak effect,[23] a companion effect to the classical Aharonov–Bohm mechanism but with a twice smaller periodicity in magnetic flux $\Delta\Phi = hc/2e$.

Aspects of the Aharonov–Bohm persistent currents in complex and correlated systems have been considered in various papers, in particular by studying the strong coupling[24–26] and localization[27,28] effects, thermodynamic–statistical properties,[29–31] polaron effects,[32,33] effects of strong magnetic field[34,35] and spin–orbit interaction,[36,37]

Peierls transition,[38–40] Wigner crystallization[41] and Coulomb blockade,[42] persistent current oscillation in hollow cylinders with toroidal geometry,[43] nonequilibrium and time-dependent effects,[44–48] weak links in the loop,[49] as well as the nontraditional phase effects (geometrical and Berry's phase, instantons, etc.)[50–53] summarized in recent reviews.[14,54–57] Further trends in the macromolecular persistent and spontaneous currents[58–60] include quantum computational[61] prospects of using Aharonov–Bohm loops as quantum bits (qubits) with the advantages of easier (radiation-free) manipulation of qubit states and increased decoherence times as compared to macroscopic "Schrödinger cat" structures (Josephson junctions). The smallest (three-site) persistent current ring displays a Λ-shaped energy configuration[59] with two degenerate ground states at external flux $\Phi_0 = hc/2e$. The spontaneous persistent current loop will achieve the degenerate state at zero field or, if the degeneracy is lifted by the electron–phonon coupling, at a reasonably low field.

Persistent current is a voltage-free nondecaying current which exists as a manifestation of the fact that the ground state of a doubly connected conductor in a magnetic field is a current-carrying one. This statement has been proved for ballistic loops[4] and for diffusive rings.[5] There is no fundamental difference between these two extremes. Counterintuitively, ballistic structure does not show infinite conductivity, as has sometimes been naively supposed; the dc resistance of the loop is infinite rather than zero when a dc electric field is applied to the system. In the case when a current is fed through the structure, no voltage appears provided that the magnitude of the current is smaller than a certain critical value. This applies to both elastic and inelastic scattering. The magnitude of the critical current of the ballistic ring smoothly matches the current of the diffusive ring when the mean free path l becomes large. In the dirty limit, $l \ll L$, where L is the ring circumference, the critical value of the supercurrent decreases proportionally to l/L according to Ref. 62, or to $(l/L)^{1/2}$ according to a numerical simulation.[14] The nondecaying current does not even require severe restriction on the so-called "phase breaking" electron mean free path. In fact, the normal-metal supercurrent is an analog of the "incoherent" Josephson effect,[63,64] in which the phase of the superconductor is considered as a classical variable. Stronger criteria (that the dephasing length is larger than the system size, and the analogous requirement in the time domain, that the "decoherence time" is larger than the characteristic time of observation) apply to persistent current rings as quantum computational tools mentioned above, which are the analogs of the macroscopic quantum tunneling.[65–67]

3. SPONTANEOUS PERSISTENT CURRENTS

Persistent current appears in a ballistic ring due to the Aharonov–Bohm field. The current, however, can also originate when the external field is zero—the "spontaneous" current. This situation has been noticed accidentally by various authors, in particular, in Refs. 68–70, but it has not seemed convincing due to the fixed-chemical-potential configuration, and it has been attributed to the effect of Peierls instability in the ring[40] (criticized in Refs. 71 and 72 in regard to the inaccuracy of the mean field approximation). In fact, the fixed-number-of-particles ring with an odd number of electrons displays a number of structural instabilities: the Peierls transformation[73] and the Jahn–Teller effect[74] are the best-known examples, and the (generally more complex) atomic rearrangement when the ground state proves degenerate in a symmetric configuration.

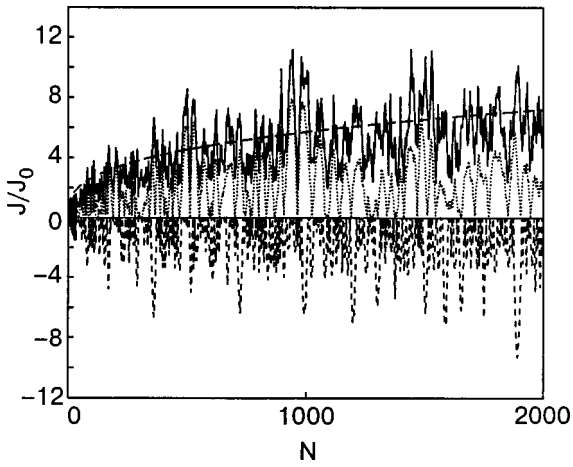

FIG. 4. Persistent current versus number of electrons in a ring with a ratio of cross-sectional dimensions $L:L_1:L_2 = 10:1:1$ (spinfull configuration). The upper curve is the maximum current in units of $J_0 = ev_F/L$ at given N, the dotted curve is the amplitude of the first harmonic of $J_{\text{pers}}(\Phi)$, and the curve at negative J is the spontaneous persistent current as defined below, also in units of J_0. The dashed curve is the square root of the number of perpendicular channels $N_\perp$ plotted against N.

In Fig. 4 we show the dependence of the maximal persistent current, as well as the spontaneous current, on the number of electrons in a ring which was modeled as a finite-length hollow cylinder with rectangular cross section $L_1 \times L_2$ containing a finite number of perpendicular electron channels $N_\perp = L_1 L_2 k_F^2/2\pi^2$. Note that the magnitude of the current in a ballistic ring is not ev_F/L, as is sometimes suggested (v_F is the Fermi velocity), but rather approaches a value $J_{\max} \sim (ev_f/L)N_\perp^{1/2}$ (see Ref. 4). The dependence $J_{\max}(N)$ at $T=0$ is irregular due to the addition of negative and positive currents from different electron eigenstates in longitudinal and transverse channels.

Figure 5 shows the bistability effect in a ring. While at

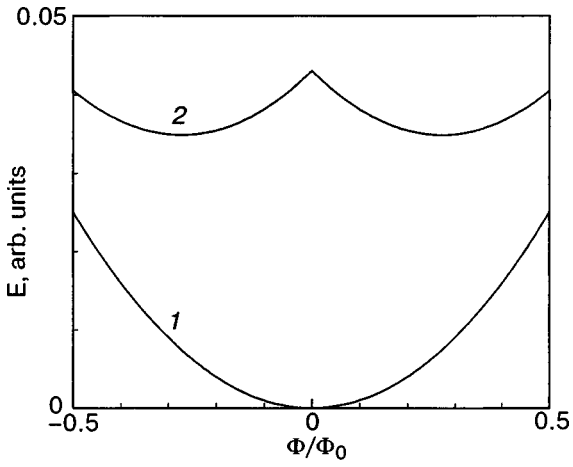

FIG. 5. Bistable configuration in a ring: Energy versus flux in a ring of 10 electrons (*1*) and 11 electrons (*2*). The second curve is shifted downward for convenience (but not rescaled).

an even number of electrons the electronic energy has a minimum at $\Phi=0$, it acquires a maximum when the number of electrons is odd. (The inductive energy, to be included below, will shift the position of the minima in curve *2* of Fig. 5 to the origin, so that a degenerate state will appear in the near vicinity of $\Phi=0$.)

The spontaneous current has the same order of magnitude as the maximal persistent current and represents an inseparable part of the Aharonov–Bohm effect. The structural transformation is investigated below in an exact way by considering the ring dynamics in the tight binding approximation. The ''lattice'' (the atomic configuration of the loop) can respond to the degenerate ground state by making an atomic readjustment similar to the Peierls transition (doubling of the lattice period in a one-dimensional atomic chain; see, e.g., Refs. 75 and 76), or a more complex atomic rearrangement.

In fact, such a possibility clearly shows up in the case of a 1D loop with the discrete quantum states (θ is the azimuthal angle)

$$\psi_n=\frac{1}{\sqrt{L}}\exp(in\theta) \tag{9}$$

corresponding to energies

$$\varepsilon_n=\frac{\hbar^2}{2mR^2}(n-f)^2, \tag{10}$$

where $n=0,\pm1,\pm2,\ldots$ and $f=\Phi/\Phi_0$ is the magnetic flux threading the loop in units of the flux quantum $\Phi_0=4\times10^{-7}$ G·cm^2.

As an example, the loop with 3 electrons has energy

$$E(f)=\varepsilon_0\left[f^2+\frac{1}{2}(\pm1-f)^2\right]+\frac{\mathcal{L}J_0^2}{2c^2}J^2(f) \tag{11}$$

corresponding to two spin-1/2 states with $n=0$ and one state with $n=1$ or $n=-1$. The last term in Eq. (11) is the magnetic inductive energy and $\mathcal{L}$ is the inductance (of the order of the ring circumference, in the units adopted). The current $J=-(e/h)\partial E/\partial f$ is equal to

$$J(f)=J_0(\pm1-3|f|), \quad J_0=e\varepsilon_0/h \tag{12}$$

and is nonzero at $f=0$ in either of the states $\pm$. The ratio of magnetic energy to kinetic energy is of order

$$\eta=\frac{\mathcal{L}J_0^2}{2c^2\varepsilon_0}\simeq\frac{e^2}{4\pi mc^2R}\sim10^{-6}\frac{a_0}{R}, \tag{13}$$

where a_0 is the Bohr radius. This is a very small quantity, and therefore the magnetic energy is unimportant in the energy balance of the loop. The flux in the loop equals $f=f_{\rm ext}+2\eta j_f$, where $f_{\rm ext}$ is an external flux and $j_f=J(f)/J_0$. The correction for the externally applied flux is essential only at $f_{\rm ext}\sim\eta$; otherwise, we can ignore this contribution.

The property of nonzero persistent current thus demonstrated for the noninteracting electrons survives strong electron–electron coupling but collapses when the coupling to the lattice is included (see below). Nevertheless, when the loop is on a rigid background (say, a cyclic molecule on a substrate of a much more rigidly bound solid) the degeneracy may not be lifted, or may remain in a very narrow interval of externally applied fields. We will investigate this possibility in the tight binding approximation,[77,78] in which electrons are bound to certain atomic locations (traps) and make the loop conducting by resonant tunneling between these locations.

In the tight binding approximation, Hamiltonian of the loop in the second-quantized form reads

$$H=\sum_{j=1}^{N}(t_j a_{j\sigma}^{+}a_{j+1,\sigma}e^{i\alpha_j}+\text{h.c.})+U\sum_{i=1}^{N}n_{i\uparrow}n_{i\downarrow}+V\sum_{i=1,\sigma,\sigma'}^{N}n_{i\sigma}n_{i+1,\sigma'}+\frac{1}{2}K\sum_{j=1}^{N}(\theta_j-\theta_{j+1})^2, \tag{14}$$

where t_j is the hopping amplitude between two near configurational sites, j and $j+1$,

$$t_j=t_0+g(\theta_j-\theta_{j+1}), \quad n_{i\sigma}=a_{i\sigma}^{+}a_{i\sigma}, \tag{15}$$

and α_j is the Aharonov–Bohm phase (a Peierls substitution for the phase of hopping amplitude)

$$\alpha_j=\frac{2\pi f}{N}+(\theta_j-\theta_{j+1})f. \tag{16}$$

$a_{j\sigma}^{+}$ is the creation (and $a_{j\sigma}$, the annihilation) operator of an electron at site j with spin σ, θ_j, $j=1,2,\ldots,N$ are the angles of distortion of site locations from their equilibrium positions $\theta_j^0=2\pi j/N$ and satisfy the requirement $\Sigma_{j=1}^{N}\theta_j=0$, and g is the electron–phonon coupling constant. The interaction (15) reflects the fact that the hopping amplitude depends on the distance between the localization positions and assumes that the displacement $\theta_j-\theta_{j+1}$ is small in comparison to $2\pi/N$. U and V are Hubbard parameters of the on-site and intrasite interactions. The parameters are assumed such that system is not superconductive (e.g., $U>0$; and anyway, superconductivity is not allowed for a 1D system and is ruled out for a small system). The last term in Hamiltonian (14) is the elastic energy, and K is the stiffness parameter of the lattice.

In the smallest loop, the one with three sites ($N=3$), the only two free parameters of the lattice displacement, X_1 and X_2, are

$$\theta_1=X_1+X_2, \quad \theta_2=-X_1+X_2, \quad \theta_3=-2X_2 \tag{17}$$

which are decomposed to second-quantized Bose operators b_1 and b_2 according to

$$X_1=\left(\frac{3K}{\omega}\right)^{1/4}(b_1+b_1^{+}), \quad X_2=3\left(\frac{K}{3\omega}\right)^{1/4}(b_2+b_2^{+}). \tag{18}$$

The system (14) is solved numerically with the ABC compiler,[79] which includes the creation–annihilation operators as its parameter types. These are generated as compiler macros with sparse matrices

$$A_n=C_n^{(N_1)}\otimes1^{(N_2)} \ \text{ fermionic sector}$$

$$B_n=1^{(N_1)}\otimes C_n^{(N_2)} \ \text{ bosonic sector}, \tag{19}$$

where $1^{(N)}$ is a unit matrix of dimension 2^N and $C_n^{(N)}$, $n=1,\ldots,N$ are Fermi/Bose operators in a space of the same dimension,

$$C_n^{(N)}=(u\otimes)^{N-n}a(\otimes v)^{n-1}, \tag{20}$$

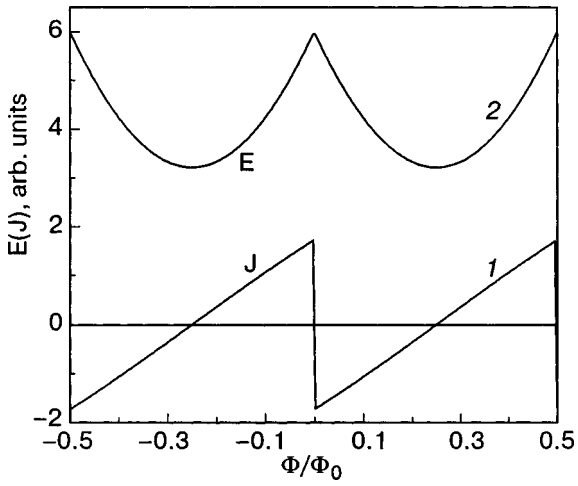

FIG. 6. Current versus magnetic flux in the 3-site loop with 3 noninteracting electrons (*1*). Energy versus flux for the $N=3$, $n=3$ loop at the value of the hopping parameter $t_0=-1$ (*2*). The energy is rescaled and arbitrarily shifted upward for clarity.

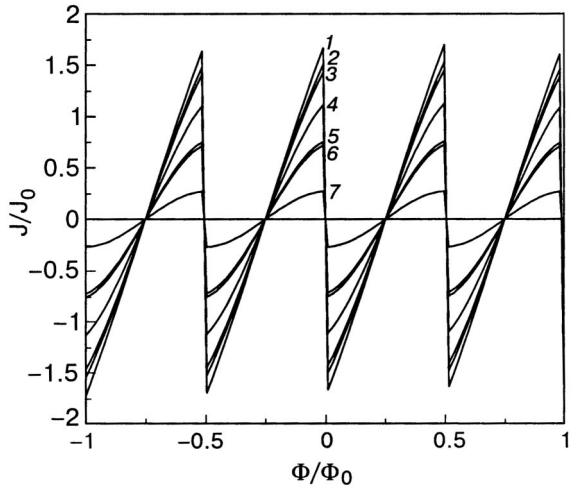

FIG. 7. Spontaneous persistent current versus flux for $t_0=-1$ and various values of the Hubbard parameter U:0 (*1*); −2 (*2*); 2 (*3*); −5 (*4*); 5 (*5*); −10 (*6*); 10 (*7*).

a, u, and v are the 2×2 matrices ($\otimes$ is the symbol of the Kronecker matrix product)

$$a=\begin{pmatrix}0 & 0\\ 1 & 0\end{pmatrix},\quad u=\begin{pmatrix}1 & 0\\ 0 & 1\end{pmatrix},\quad v=\begin{pmatrix}1 & 0\\ 0 & \eta\end{pmatrix}, \tag{21}$$

and η is a parameter

$$\eta=\begin{cases}-1 & \text{fermionic sector}\\ 1 & \text{bosonic sector.}\end{cases} \tag{22}$$

Bosons are considered as ''hard-core bosons,'' such that there are only two discrete states for each mode of displacement. We calculate the ground state of Hamiltonian (14) as a function of magnetic flux f (a classical variable). In application to real atomic (macromolecular) systems, we can consider X_1 and X_2 as classical variables, since the quantum uncertainties in the coordinates ($\Delta X_{1,2}\sim(\hbar/M\omega)^{1/2}$) are typically much smaller than the interatomic distances (M is the mass of an atom and $\omega\sim 10^{13}\ \mathrm{s}^{-1}$ is the characteristic vibration frequency). The energy of the loop is calculated as function of X_1, X_2 and further is minimized with respect to X_1, X_2 for each value of f. The nonzero values of X_1, X_2 will signify the ''lattice'' (the ionic core of the macromolecule) instability against the structural transformation which is analogous to the Peierls transition.

For the 3-site loop, the $E(f)$ dependence is shown in Fig. 6 together with the dependence of the current on f. The latter shows a discontinuity at $f=0$ of the same order of magnitude as the standard value of the persistent current. The current at $f=0$ is paramagnetic, since the energy versus flux has a maximum rather than a minimum at $f=0$. On-site interaction reduces the amplitude of the persistent current near zero flux (Fig. 7) but doesn't remove its discontinuity at $f=0$. Therefore, the strongest opponent of the Aharonov–Bohm effect, the electron–electron interaction, leaves it qualitatively unchanged.

On the other hand, the electron–phonon interaction flattens the $E(f)$ dependence near the peak value; see Fig. 8. At large stiffnesses K this flattening remains important only for small magnetic fluxes, much smaller than the flux quantization period $\Delta\Phi=\Phi_0$. Note that the persistent current peak is reduced in amplitude only slightly near $\Phi=0$. As is seen from Fig. 9, the electron–phonon interaction splits the singularity at $\Phi=0$ into two singularities at $\Phi=\pm\Phi_{\mathrm{sing}}$. Outside the interval $-\Phi_{\mathrm{sing}}<\Phi<\Phi_{\mathrm{sing}}$ the structural transformation is blocked by the Aharonov–Bohm flux. The range of magnetic fluxes between $-\Phi_{\mathrm{sing}}$ and Φ_{sing} determines the domain of the developing lattice transformation, which manifests itself in nonzero values of the lattice deformations X_1, X_2. The latter property allows us to suggest that the spontaneous persistent current state (a peak of dissipationless charge transport at, or near, zero flux) remains for nonzero flux when the electron–phonon coupling is not too strong or when the lattice stiffness is larger than certain critical value.

4. CONCLUSION

We have considered the Aharonov–Bohm effect in an angular-periodic macromolecular loop like, e.g., an aromatic cyclic molecule, and found that the Aharonov–Bohm flux applied to the loop arrests the lattice instability (rearrange-

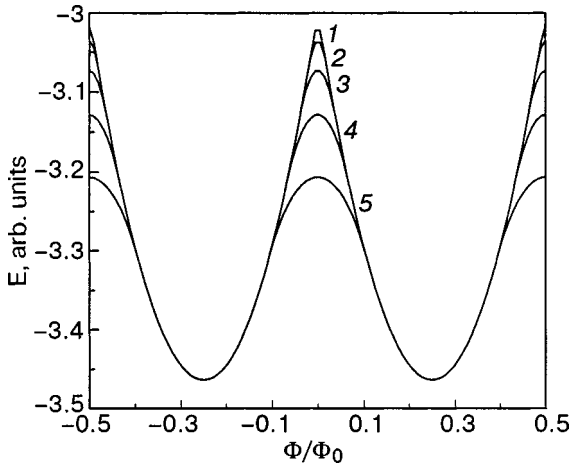

FIG. 8. Energy versus flux in a loop of noninteracting electrons coupled to the lattice with the value of the coupling parameter $g=1$ and various values of the stiffness parameter K:2 (*1*); 3 (*2*); 5 (*3*); 10 (*4*); 20 (*5*).

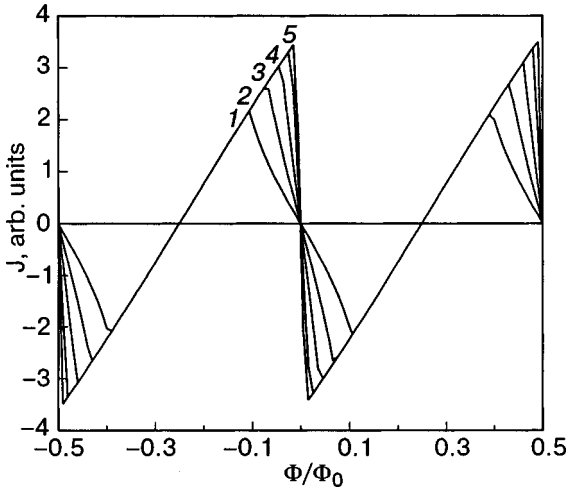

FIG. 9. Energy versus flux for a loop with coupling constant $g=1$ and various values of the stiffness K:2 (*1*); 3 (*2*); 5 (*3*); 10 (*4*); 20 (*5*).

ment of molecular atoms or blocks within the molecule). This is a consequence of the fact that the weak-coupling effect of electron hopping between sites of electron localization cannot provide enough energy for initiating a shift of the atoms from periodic locations except at quite small magnetic fields. As a result, the ground state of the system at a certain electron concentration becomes current-carrying at zero (or very small) magnetic flux—a state with ''spontaneous'' persistent current. This effect suggests the possibility of using appropriately engineered macromolecular structures as elementary qubits, the degenerate or near-degenerate states sought for processing of quantum information.[61] As was shown in Ref. 59, the three-site Aharonov–Bohm loop supports all logical operations (the quantum logic gates) required for quantum computation and quantum communication, which are effected by static voltages applied to the loop perpendicular to the magnetic flux and such that the loop is driven to a Λ-shaped energy configuration with the two degenerate ground states making elements of the qubit and the third, higher-energy state implementing radiation-free quantum logic gates. Very strong magnetic fields are required for the formation of such states (corresponding to a flux equal to half of the flux quantum). The spontaneous persistent currents discussed in the present paper allow one to reduce these fields by orders of magnitude.

*E-mail: iokulik@yahoo.com

[1] B. D. Josephson, Phys. Lett. **1**, 251 (1962).
[2] B. D. Josephson, in *Superconductivity*, Vol. 1, edited by R. D. Parks, Marcell Dekker, New York (1969), p. 423.
[3] F. Bloch, Phys. Rev. B **2**, 109 (1970) and references therein. This paper proved exact periodicity of the energy of a loop as a function of magnetic flux with a period hc/e but with an indefinite amplitude.
[4] I. O. Kulik, JETP Lett. **11**, 275 (1970).
[5] M. Buttiker, Y. Imry, and R. Landauer, Phys. Lett. A **96**, 365 (1983).
[6] Y. Aharonov and D. Bohm, Phys. Rev. B **115**, 485 (1959).
[7] V. Ambegaokar and A. Baratoff, Phys. Rev. Lett. **10**, 486 (1963); **11**, 104 (1963).
[8] O. Kulik and A. N. Omelyanchouk, Fiz. Nizk. Temp. **3**, 945 (1977) [Sov. J. Low Temp. Phys. **3**, 459 (1977)].
[9] O. Kulik, Zh. Éksp. Teor. Fiz. **57**, 1745 (1969) [Sov. Phys. JETP **30**, 944 (1970)].
[10] C. Ishii, Prog. Theor. Phys. **44**, 1525 (1970); J. Bardeen and J. L. Johnson, Phys. Rev. B **5**, 72 (1972); A. V. Swidzinsky, T. N. Antsygina, and E. N. Bratus, J. Low Temp. Phys. **10**, 131 (1973).
[11] O. Cakir and I. O. Kulik, Phys. Rev. B **67**, 174514 (2003).
[12] G. B. Arnold, J. Low Temp. Phys. **59**, 143 (1985).
[13] S. Kasiwaya and Y. Tanaka, Prog. Theor. Phys. **63**, 1641 (2000); A. Furusaki, H. Takayanagi, and M. Tsukada, Phys. Rev. B **45**, 10563 (1992).
[14] O. Kulik, in *Quantum Mesoscopic Phenomena and Mesoscopic Devices in Microelectronics*, edited by I. O. Kulik and R. Ellialtioglu, Kluwer, Dordrecht (2000), p. 259.
[15] E. Teller, Z. Phys. **67**, 311 (1931).
[16] L. D. Landau, Z. Phys. **64**, 629 (1930).
[17] N. B. Brandt, E. N. Bogachek, D. V. Gitsu, G. A. Gogadze, I. O. Kulik, A. A. Nikolaeva, and Ya. G. Ponomarev, Fiz. Nizk. Temp. **8**, 718 (1982) [Sov. J. Low Temp. Phys. **8**, 358 (1982)].
[18] L. P. Levy, G. Dolan, J. Dunsmuir, and H. Bouchiat, Phys. Rev. Lett. **64**, 2074 (1990).
[19] V. Chandrasekhar, R. A. Webb, M. J. Brady, M. B. Ketchen, W. J. Gallagher, and A. Kleinsasser, Phys. Rev. Lett. **67**, 3578 (1991).
[20] D. Mally, C. Chapelier, and A. Benoit, Phys. Rev. Lett. **70**, 2020 (1993).
[21] D. Gatteschi, A. Caneschi, L. Pardi, and R. Sessoli, Science **265**, 1054 (1994); K. L. Taft, C. D. Delfs, G. C. Papaefthymiou, S. Foner, D. Gatteschi, and S. J. Lippard, J. Am. Chem. Soc. **116**, 823 (1994).
[22] C. Schönenberger, A. Bachtold, and C. Strunk, J.-P. Salvetat, and L. Forro, Arrl. Phys. A **69**, 283 (1999).
[23] B. L. Altshuler, A. G. Aronov, and B. Z. Spivak, [JETP Lett. **33**, 94 (1981)].
[24] A. Ferretti, I. O. Kulik, and A. Lami, Phys. Rev. B **47**, 12235 (1993).
[25] F. V. Kusmartsev, J. Phys.: Condens. Matter **3**, 3199 (1991).
[26] M. V. Moskalets, Physica E **4**, 111 (1999).
[27] I. O. Kulik, Fiz. Nizk. Temp. **13**, 206 (1987) [Sov. J. Low Temp. Phys. **13**, 115 (1987)].
[28] G. Kirczenow, J. Phys.: Condens. Matter **7**, 2021 (1995).
[29] B. L. Altshuler, Y. Gefen, and Y. Imry, Phys. Rev. Lett. **66**, 88 (1991).
[30] G. Montambaux, H. Bouchiat, D. Sigeti, and F. Friesner, Phys. Rev. B **42**, 7647 (1990).
[31] J. F. Weisz, R. Kishore, and F. V. Kusmartsev, Phys. Rev. B **49**, 8126 (1994).
[32] Yi-Chang Zhou, Xin-E Yang, and Huo-Zhong Li, Phys. Lett. A **190**, 123 (1994).
[33] M. Bayindir and I. O. Kulik, in *Quantum Mesoscopic Phenomena and Mesoscopic Devices in Microelectronics*, edited by I. O. Kulik and R. Ellialtioglu, Kluwer, Dordrecht (2000), p. 283.
[34] D. Eliyahu, R. Berkovits, M. Abraham, and Y. Avishai, Phys. Rev. B **49**, 14448 (1994).
[35] I. O. Kulik, Physica B **284** (2000).
[36] Y. Lyanda-Geller, Phys. Rev. Lett. **80**, 4273 (1998).
[37] M. V. Moskalets, JETP Lett. **70**, 602 (1999).
[38] I. O. Kulik, A. S. Rozhavsky, and E. N. Bogachek, JETP Lett. **47**, 303 (1988).
[39] Yu. I. Latyshev, O. Laborde, P. Monceau, and S. Klaumunzer, Phys. Rev. Lett. **78**, 919 (1997).
[40] J. Yi, M. Y. Choi, K. Park, and E.-H. Lee, Phys. Rev. Lett. **78**, 3523 (1997).
[41] I. V. Krive, P. Sandstrom, R. I. Shekhter, S. M. Girvin, and M. Jonson, Phys. Rev. B **52**, 16451 (1995).
[42] M. V. Moskalets, Physica E **4**, 17 (1999).
[43] M. F. Lin and D. S. Chuu, Phys. Rev. B **57**, 6731 (1998).
[44] T. Swahn, E. N. Bogachek, Yu. M. Galperin, M. Jonson, and R. I. Shekhter, Phys. Rev. Lett. **73**, 162 (1994).
[45] E. N. Bogachek, Yu. M. Galperin, M. Jonson, R. I. Shekhter, and T. Swahn, J. Phys.: Condens. Matter **8**, 2603 (1996).
[46] I. O. Kulik, Physica B **218**, 252 (1996).
[47] O. Entin-Wohlman, A. Antony, Y. Imry, Y. Levinson, and A. Schiller, Phys. Rev. Lett. **88**, 166801 (2002).
[48] I. O. Kulik and A. S. Shumovsky, Appl. Phys. Lett. **69**, 2779 (1996).
[49] M. V. Moskalets, Physica E **5**, 124 (1999).
[50] E. N. Bogachek, I. V. Krive, I. O. Kulik, and A. S. Rozhavsky, Mod. Phys. Lett. B **5**, 1607 (1991).
[51] E. N. Bogachek, I. V. Krive, I. O. Kulik, and A. S. Rozhavsky, Phys. Rev. B **42**, 7614 (1990).
[52] E. N. Bogachek and U. Landman, Phys. Rev. B **50**, 2678 (1994).
[53] I. V. Krive and A. S. Rozhavsky, Int. J. Mod. Phys. B **6**, 1255 (1992).
[54] Y. Imry, in *Quantum Coherence in Mesoscopic Systems*, edited by B. Kramer, Plenum Press, New York (1991).

[55] S. Washburn, in *Mesoscopic Phenomena in Solids*, edited by B. L. Altshuler, P. A. Lee, and R. A. Webb, Elsevier (1991).
[56] S. Washburn and R. A. Webb, Adv. Phys. **35**, 375 (1986).
[57] I. O. Kulik, Doga: Turk. J. Phys. **27**, 395 (2003).
[58] A. Barone, T. Hakioglu, and I. O. Kulik, ''Quantum computation with Aharonov–Bohm qubits,'' E-print cond-mat/0203038 (2002).
[59] I. O. Kulik, T. Hakioglu, and A. Barone, Eur. Phys. J. B **30**, 219 (2002).
[60] I. O. Kulik, in *Towards the Controllable Quantum States: Mesoscopic Superconductivity and Spintronics*, edited by H. Takayanagi and J. Nitta, World Scientific (2002).
[61] M. A. Nielsen and I. L. Chuang, *Quantum Computation and Quantum Information*, Cambridge Univ. Press (2000).
[62] H. F. Cheung, E. K. Riedel, and Y. Gefen, Phys. Rev. Lett. **62**, 587 (1989).
[63] I. O. Kulik and I. K. Yanson, *The Josephson Effect in Superconductive Tunneling Structures*, Israel Program for Scientific Translations, Jerusalem (1972).
[64] Barone and G. Paterno, *Physics and Applications of the Josephson Effect*, Wiley, New York (1982).
[65] A. J. Leggett, in *Chance and Matter*, edited by J. Souletier, J. Vannimenus, and R. Stora, Elsevier, Amsterdam (1996), p. 395.
[66] K. K. Likharev, *Dynamics of Josephson Junctions and Circuits*, Gordon and Breach, Amsterdam (1996).
[67] Y. Makhlin, G. Schön, and A. Schnirman, Rev. Mod. Phys. **73**, 357 (2001).
[68] H.-F. Cheung, Y. Gefen, E. K. Riedel, and W.-H. Shih, Phys. Rev. B **37**, 6050 (1988).
[69] S. Latil, S. Roche, and A. Rubio, Phys. Rev. B **67**, 165420 (2003).
[70] M. I. Vischer, B. Rejaei, and G. E. W. Bauer, Europhys. Lett. **36**, 613 (1996).
[71] B. Nathanson, O. Entin-Wohlman, and B. Mülschlegel, Phys. Rev. Lett. **80**, 3416 (1998).
[72] G. Montambaux, Phys. Rev. Lett. **80**, 3417 (1998).
[73] R. E. Peierls, *Quantum Theory of Solids*, Clarendon Press, Oxford (1995).
[74] H. J. Jahn and E. Teller, Proc. R. Soc. London, Ser. A **161**, 220 (1937).
[75] C. Kittel, *Introduction to Solid State Physics*, Wiley, New York (1996).
[76] L. N. Bulaevskii, Usp. Fiz. Nauk [Sov. Phys. Usp. **115**, 261 (1975)].
[77] W. A. Harrison, *Electronic Structure and the Properties of Solids*, Cambridge (1972).
[78] J. M. Ziman, *Principles of the Theory of Solids*, Cambridge (1972).
[79] I. O. Kulik, in *Technical Proceedings of the 2003 Nanotechnology Conference and Trade Show*, edited by M. Laudon and B. Romanowicz, Computational Publications, Boston (2003), Vol. 2, p. 531.

This article was published in English in the original Russian journal. Reproduced here with stylistic changes by AIP.

Spontaneous currents in Josephson junctions between unconventional superconductors and *d*-wave qubits (Review)

Yu. A. Kolesnichenko* and A. N. Omelyanchouk

B. Verkin Institute for Low Temperature Physics and Engineering of the National Academy of Sciences of Ukraine, 47 Lenin Ave., Kharkov 61103, Ukraine

A. M. Zagoskin

D-Wave Systems Inc., 320-1985 West Broadway, Vancouver, B.C., V6J 4Y3, Canada;
The University of British Columbia, 6224, Agricultural Rd., Vancouver, B.C., V6T 1Z1, Canada
(Submitted January 29, 2004)
Fiz. Nizk. Temp. **30**, 714–737 (July–August 2004)

The modern physics of superconductivity can be called the physics of unconventional superconductivity. The discovery of the *d*-wave symmetry of the order parameter in high-temperature superconductors and the triplet superconductivity in compound Sr_2RuO_4 has caused a huge stream of theoretical and experimental investigations of unconventional superconductors. In this review we discuss some novel aspects of the Josephson effect which are related to the symmetry of the order parameter. The most intriguing of them is spontaneous current generation in an unconventional weak link. The example of a Josephson junction in the form of a grain boundary between two disorientated *d*-wave or *f*-wave superconductors is considered in detail. Josephson current–phase relations and the phase dependences of the spontaneous current that flows along the interface are analyzed. The spontaneous current and spontaneous phase difference are manifestations of the time-reversal symmetry ($\mathcal{T}$) breaking states in the system. We analyzed the region of appearance of $\mathcal{T}$-breaking states as function of temperature and mismatch angle. A review of the basics of superconducting qubits with emphasis on specific properties of *d*-wave qubits is given. Recent results in the problem of decoherence in *d*-wave qubits, which is the major concern for any qubit realization, are presented. © *2004 American Institute of Physics.* [DOI: 10.1063/1.1789112]

1. INTRODUCTION

The modern physics of superconductivity can be called the physics of unconventional superconductivity. It should be noted that right after the famous paper[1] of Bardeen, Cooper, and Schriffer (BCS) it became clear that (conventional) *s*-wave singlet pairing is not the only possibility,[2,3] and more-complex superconducting (superfluid) states may be realized, with nonzero orbital and spin momenta of the Cooper pairs. Because of the success of the BCS theory in describing properties of the known metallic superconductors, theoretical research on unconventional superconductivity was of purely academic interest and did not attract much attention. Interest in unconventional pairing symmetry has increased after the discovery of superfluidity in ^{3}He, with triplet spin symmetry and multiple superfluid phases.[4,5] Low-temperature experiments on complex compounds led to the discovery of unconventional superconductivity in heavy-fermion systems.[6] The heavy-fermion metal UPt_3, like ^{3}He, has a complex superconducting phase diagram, which shows the existence of several superconducting phases, while a weak temperature dependence of the paramagnetic susceptibility indicates triplet pairing. Another triplet superconductor is the recently discovered compound Sr_2RuO_4.

The real boom in investigations of unconventional superconductivity started after the discovery by Bednorz and Müller[7] of high-temperature (high-T_c) superconductivity in cuprates, because of its fundamental importance for both basic science and practical applications. Numerous experiments show that high-T_c cuprates are singlet superconductors with nontrivial orbital symmetry of the order parameter (a so-called *d*-wave state, with the orbital moment of pairs $l=2$).

The Josephson effect[8] is extremely sensitive to the dependence of the complex order parameter on the momentum direction on the Fermi surface. Thus the investigation of this effect in unconventional superconductors enables one to distinguish among different candidates for the symmetry of the superconducting state. This has stimulated numerous theoretical and experimental studies of unconventional Josephson weak links. One of the possibilities for forming a Josephson junction is to create a point contact between two massive superconductors. A microscopic theory of the stationary Josephson effect in ballistic point contacts between conventional superconductors was developed in Ref. 9. Later this theory was generalized for a pinhole model in ^{3}He,[10,11] for point contacts between *d*-wave high-T_c superconductors,[12–14] and for triplet superconductors.[15] A detailed theory of the Josephson properties of grain-boundary *d*-wave junctions was developed in Ref. 16. In those papers it was shown that the current–phase relations for the Josephson current in unconventional weak links are quite different from those of conventional superconductors. One of the most striking manifestations of a unconventional order-parameter symmetry is the appearance, together with the Josephson current, of a spontaneous current flowing along the contact

interface. The spontaneous current arises due to the breaking of the time-reversal symmetry ($\mathcal{T}$) in the system. Such a situation takes a place, for example, in a junction between two d-wave superconductors with different crystallographic orientations. The d-wave order parameter itself doesn't break the $\mathcal{T}$ symmetry. But the mixture of two differently oriented order parameters (proximity effect) forms a $\mathcal{T}$-breaking state near the interface.[17] Such spontaneous supercurrent $j_{\rm spon}$ (and corresponding spontaneous phase difference) exists even if the net Josephson current equals zero. The state of the junction with the spontaneous current is twofold degenerate, and in fact, two values $\pm j_{\rm spon}$ appear. An interesting possibility arises then to use these macroscopic quantum states for the design of d-wave quantum bits (qubits).

This review consists of three parts. In Sec. 2 the general features of unconventional superconductivity are presented. The different types of order parameters are described. We briefly outline the essence of $\mathcal{T}$-symmetry breaking in unconventional superconductors and experimental tests for order-parameter symmetry. In Sec. 3 (and Appendix II) the theory of coherent current states in Josephson junctions between d-wave superconductors and between triplet superconductors is considered. The current–phase relations for the Josephson and spontaneous currents, as well as the bistable states, are analyzed. Section 4 is devoted to Josephson phase qubits based on d-wave superconductors. It contains a review of the basics of superconducting qubits with emphasis on specific properties of d-wave qubits. Recent results in the problem of decoherence in d-wave qubits, which is the major concern for any qubit realization, are presented.

2. UNCONVENTIONAL SUPERCONDUCTIVITY

2.1. Order-parameter in unconventional superconductors. *s*-wave, *d*-wave, *p*-wave ... pairing

The classification and description of unconventional superconducting states can be found, for example, in the book[18] and review articles.[19–23] In our review we do not aim to discuss this problem in detail. We present only general information on the unconventional superconductors and their most likely model descriptions.

It is well known[1] that a Cooper pair has zero orbital momentum, and its spin can be either $S=0$ (singlet state) or $S=1$ (triplet state). It follows from the Pauli exclusion principle that the matrix order parameter of the superconductor $\Delta_{\alpha\beta}(\mathbf{k})$ (α,β are spin indices) changes sign under permutation of particles in the Cooper pair: $\Delta_{\alpha\beta}(\mathbf{k})=-\Delta_{\beta\alpha}(-\mathbf{k})$. Hence, the even parity state is a singlet state with zero spin moment, $S=0$:

$$\hat{\Delta}^{(\rm singlet)}(\mathbf{k})=g(\mathbf{k})i\hat{\sigma}_y;$$

$$g(\mathbf{k})=g(-\mathbf{k}). \tag{1}$$

The odd parity state is a triplet state with $S=1$, which is in general a linear superposition of three substates with different spin projection $S_z=-1,0,1$:

$$\hat{\Delta}^{(\rm triplet)}(\mathbf{k})=(\mathbf{d}(\mathbf{k})\sigma)\hat{\sigma}_y;$$

$$\mathbf{d}(-\mathbf{k})=-\mathbf{d}(\mathbf{k}). \tag{2}$$

Here the $\hat{\sigma}_i$ are Pauli matrices ($i=x,y,z$); $\mathbf{d}(\mathbf{k})$ and $\sigma=(\hat{\sigma}_x,\hat{\sigma}_y,\hat{\sigma}_z)$ are vectors in the spin space. The components of the vector $\mathbf{d}(\mathbf{k})$ are related with the amplitudes $g_{S_z}(k)$ of states with different spin projections $S_z=(-1,0,1)$ on the quantization axis:

$$g_1=-d_x+id_y;\ \ g_0=d_z;\ \ g_{-1}=d_x+id_y. \tag{3}$$

The functions $g(\mathbf{k})$ and $\mathbf{d}(\mathbf{k})$ are frequently referred to as an order parameter of the superconductor. For the isotropic model $g(\mathbf{k})=$const the paring state is singlet. In a triplet superconductor the order parameter $\mathbf{d}(\mathbf{k})$ is a vector (some authors call it the gap vector) in the spin space and in any case it depends on the direction on the Fermi surface. This vector defines the axis along which the Cooper pairs have zero spin projection.

The angular dependence of the order parameter is defined by the symmetry group $\mathcal{G}$ of the normal state and the symmetry of the electron interaction potential, which can break the symmetry $\mathcal{G}$. In a model of an isotropic conductor the quantum states of the electron pair can be described in terms of an orbital momentum l and its z projection m. The singlet (triplet) superconducting state is the state with an even (odd) orbital momentum l of Cooper pairs. The respective states are labeled by letters $s,p,d,\ldots$ (similar to the labeling of electron orbital states in atom) and are called s-wave, p-wave, d-wave, ... states. In the general case the superconducting state may be a mixture of states with different orbital momenta l.

The spherically symmetrical superconducting state, which now is frequently called the conventional one, corresponds to s-wave singlet pairing $l=m=S=0$. In this case of isotropic interaction, the order parameter is a single complex function $g=$const. Fortunately, this simple model satisfactorily describes the superconductivity in conventional metals, where the electron–phonon interactions leads to spin-singlet pairing with s-wave symmetry. The simplest triplet superconducting state is the state with p-wave pairing and orbital momentum of a Cooper pair $l=1$. In the case of p-wave pairing different superconducting phases with different $m=-1,0,1$ are possible. A Cooper pair in a p-wave superconductor has internal structure, because for $l=1$ it is intrinsically anisotropic. The next singlet d-wave state has the orbital momentum of Cooper pairs $l=2$.

In unconventional superconducting states the Cooper pairs may have a nonzero expectation value of the orbital $\mathbf{L}$ or (and) spin $\mathbf{S}$ momentum of a pair. States with $\mathbf{S}\neq 0$ ($\mathbf{S}=0$) are usually called nonunitary (unitary) triplet states.

The gap $\Delta(\mathbf{k})$

$$\Delta^2(\mathbf{k})=\tfrac{1}{2}\,\mathrm{Tr}\hat{\Delta}^{\dagger}(\mathbf{k})\hat{\Delta}(\mathbf{k}) \tag{4}$$

in the energy spectrum of elementary excitations is given by the relations

$$\Delta^{(\rm singlet)}(\mathbf{k})=|g(\mathbf{k})|; \tag{5}$$

$$\Delta^{(\rm triplet)}(\mathbf{k})=\sqrt{[|\mathbf{d}(\mathbf{k})|^2\pm|\mathbf{d}(\mathbf{k})\times\mathbf{d}^*(\mathbf{k})|]}. \tag{6}$$

In unconventional superconductors the gap can be equal to zero for some directions on the Fermi surface, and for nonunitary states ($\mathbf{S}\neq 0$, so-called magnetic superconductors) the energy spectrum has two branches.

In the absence of magnetic field the transition to a superconducting state is a second-order phase transition. According to the Landau theory[24] of second-order phase transitions, the order parameter of such a state must transform according to one of the irreducible representations of the point symmetry group $\mathcal{G}$ of the normal phase, i.e., the symmetry group of the superconducting state is a subgroup of the symmetry group of the normal state. The symmetry group $\mathcal{G}$ of the normal state contains the symmetry operations $G_{\text{spin-orbit}}$ in spin and orbital (coordinate) spaces, the operation of time reversal $\mathcal{T}$, and the gauge transformation $U(1)$:

$$\mathcal{G}=U(1)\times\mathcal{T}\times G_{\text{spin-orbit}}.$$

The transition to a superconducting state breaks the gauge symmetry $U(1)$, and states with different phases of the order parameter become distinguishable. The conventional superconducting state is described by the symmetry group $H=\mathcal{T}\times G_{\text{spin-orbit}}$. If another point symmetry property of the superconducting state is broken, such a superconductor is termed an unconventional one. The order parameter of different superconducting states can be expanded on basis functions of different irreducible representations of the point symmetry group G. For non-one-dimensional representations the order parameter is a sum of a few complex functions with different phases, and such an order parameter is called a multicomponent one.

In real crystalline superconductors there is no classification of Cooper pairing by angular momentum (s-wave, p-wave, d-wave, f-wave pairing, etc.). However, these terms are often used for unconventional superconductors, meaning that the point symmetry of the order parameter is the same as that for the corresponding representation of the $SO(3)$ symmetry group of an isotropic conductor. In this terminology conventional superconductors can be referred to as s-wave. If the symmetry of $\hat{\Delta}$ cannot be formally related to any irreducible representation of the $SO(3)$ group, these states are usually referred to as hybrid states.

2.2. Pairing symmetry in cuprate and triplet superconductors

Cuprate superconductors. All cuprate high-temperature superconductors ($La_{2-x}Sr_xCuO_4$, $Tl_2Ba_2CaCu_2O_8$, $HgBa_2CaCu_2O_6$, $YBa_2Cu_3O_7$, $YBa_2Cu_3O_{7-\delta}$, $Bi_2Sr_2CaCu_2O_8$ and others) have a layered structure with the common structural ingredient—the CuO_2 planes. In some approximation these compounds may be considered as quasi-two-dimensional metals having a cylindrical Fermi surface. It is generally agreed that superconductivity in cuprates basically originates from the CuO_2 layers. Knight shift measurements[25] below T_c indicate that in the cuprate superconductors pairs form spin singlets, and therefore even-parity orbital states.

The data of numerous experiments (see, for example, the review article[19]), in which the different properties of cuprate superconductors had been investigated, and the absence of multiple superconducting phases attests that the superconducting state in this compounds is most probably described by a one-component nontrivial order parameter of the form

$$g(\mathbf{k})=\Delta(T)(\hat{k}_x^2-\hat{k}_y^2), \tag{7}$$

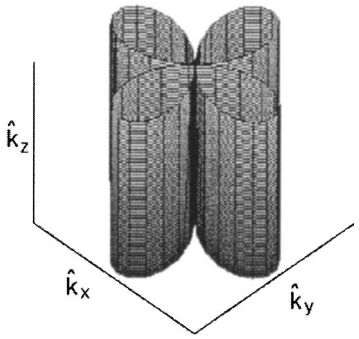

FIG. 1. The modulus of the order parameter $|g(\mathbf{k})|$ (7) in momentum space for a d-wave superconductor.

where $\Delta(T)$ is a real scalar function, which depends only on the temperature T, and $\hat{\mathbf{k}}=(\hat{k}_x,\hat{k}_y)$. This type of pairing is a two-dimensional analog of the singlet superconducting state with $l=2$ in an isotropic metal and usually is called "d-wave" (or $d_{x^2-y^2}$) pairing. The excitation gap $|g(\mathbf{k})|$ has four line nodes on the Fermi surface at $\varphi_n=(\pi/4)(2n+1)$, $n=0,1,2,3$ (Fig. 1), and the order parameter $g(\mathbf{k})$ changes sign in momentum space.

Triplet superconductivity, an analog of triplet superfluidity in ^{3}He, was first discovered in the heavy-fermion compound UPt_3 more than ten years ago.[26,27] Other triplet superconductors have been found recently: Sr_2RuO_4 (Refs. 28, 29) and $(TMTSF)_2PF_6$ (Ref. 30). In these compounds, the triplet pairing can be reliably determined, e.g., by Knight shift experiments.[31–33] It is, however, much harder to identify the symmetry of the order parameter. Apparently, in crystalline triplet superconductors the order parameter depends on the direction in momentum space, $\hat{\mathbf{k}}$, in a more complicated way than the well-known p-wave behavior of the superfluid phases of ^{3}He. While numerous experimental and theoretical works have investigated various thermodynamic and transport properties of UPt_3 and Sr_2RuO_4, the precise order-parameter symmetry is still to be determined (see, e.g., Refs. 34–37 and references therein). Symmetry considerations allow considerable freedom in the choice of irreducible representation and its basis. Therefore numerous authors (see, for example, Refs. 34–40) consider different models (so-called scenarios) of superconductivity in UPt_3 and Sr_2RuO_4, based on possible representations of crystallographic point groups. A conclusion as to the symmetry of the order parameter can be reached only after a comparison of the theoretical results with experimental data.

Pairing symmetry in Sr_2RuO_4. In experiment, Sr_2RuO_4 shows clear signs of triplet superconductivity below the critical temperature $T_c=1.5$ K. Investigation of the specific heat,[41] penetration depth,[42] thermal conductivity,[43] and ultrasound absorption[44] shows a power-law temperature dependence, which is evidence of line nodes in the energy gap in the spectrum of excitations. The combination of these results with the Knight shift experiment[32] led to the conclusion that Sr_2RuO_4 is an unconventional superconductor with spin-triplet pairing. A layered perovskite material, Sr_2RuO_4 has a quasi-two-dimensional Fermi surface.[45]

The first candidate for the superconducting state in Sr_2RuO_4 was the "p-wave" model[45–47]

$$\mathbf{d}(\mathbf{k}) = \Delta \hat{z}(\hat{k}_x \pm i\hat{k}_y). \tag{8}$$

The order parameter of the form (8) is a two-dimensional analog ($\hat{\mathbf{k}} = (\hat{k}_x, \hat{k}_y)$) of the order parameter in the A phase of ^{3}He. The **d** vector pointing along the z direction implies that the spin part of the Cooper pair wave function is the spin-triplet state with $S_z = 0$, i.e., in-plane equal-spin pairing (the z direction is along the c axis of Sr_2RuO_4). In a system with cylindrical symmetry the orbital part of the pair wave function is a state with finite angular momentum along the z axis, $L_z = \pm 1$.

However, the model (8) does not describe the whole corpus of the experimental data. Recently[36,37] it was shown that the pairing state in Sr_2RuO_4 most likely has lines of nodes, and some others models of the order parameter have been proposed:[36,37]

$$\mathbf{d}(\mathbf{k}) = \Delta \hat{z}\hat{k}_x\hat{k}_y(\hat{k}_x \pm \hat{k}_y). \tag{9}$$

$$\mathbf{d}(\mathbf{k}) = \Delta \hat{z}(\hat{k}_x^2 - \hat{k}_y^2)(\hat{k}_x \pm i\hat{k}_y). \tag{10}$$

In unitary states (8)–(10) the Cooper pairs have $L = \pm 1$ and $S = 0$.

Theoretical studies of specific heat, thermal conductivity, and ultrasound absorption for different models of triplet superconductivity show considerable quantitative differences between calculated dependences for "p-wave" and "f-wave" models.[34–36,40]

Heavy fermion superconductor UPt_3. One of the best-investigated heavy fermion superconductors is the heavy-fermion compound UPt_3 (Refs. 34 and 35). The weak temperature dependence of the Knight shift,[31] multiple superconducting phases,[26] unusual temperature dependence of the heat capacity,[48] thermal conductivity,[49,50] and sound absorption[51] in UPt_3 show that it is a triplet unconventional superconductor with a multicomponent order parameter.

The heavy-fermion superconductor UPt_3 belongs to the hexagonal crystallographic point group D_{6h}. The models which have been successful in explaining the properties of the superconducting phases in UPt_3 is based on the odd-parity two-dimensional representation E_{2u}. These models describe the hexagonal analog of spin-triplet f-wave pairing.

One of the models corresponds to the strong spin–orbital coupling with vector **d** locked along the lattice **c** axis ($\mathbf{c} \| \hat{z}$).[34,35] For this model $\mathbf{d} = \hat{z}[\eta_1 Y_1 \pm \eta_2 Y_2]$, where $Y_1 = k_z(k_x^2 - k_y^2)$ and $Y_2 = 2k_xk_yk_z$ are the basis functions of the representation. For the high-temperature polar phase ($\eta_1 = 1, \eta_2 = 0$)

$$\mathbf{d}(\mathbf{k}) = \Delta \hat{z}\hat{k}_z(\hat{k}_x^2 - \hat{k}_y^2), \tag{11}$$

and for the low-temperature axial phase ($\eta_1 = 1, \eta_2 = i$)

$$\mathbf{d}(\mathbf{k}) = \Delta \hat{z}\hat{k}_z(\hat{k}_x \pm \hat{k}_y)^2, \tag{12}$$

where $\hat{\mathbf{k}} = (\hat{k}_x, \hat{k}_y, \hat{k}_z)$.

Both are unitary states. The state (11) has zero expectation value of orbital momentum, while in the state (12) $\langle L \rangle = \pm 2$. For the polar phase (11) the gap in the energy spectrum of excitations $|\mathbf{d}(\mathbf{k})|$ has an equatorial nodal line at $\theta = \pi/2$ and longitudinal nodal lines at $\varphi_n = (\pi/4)(2n+1)$, $n = 0,2,3,4$ (Fig. 2). In the axial state (12) the longitudinal line nodes are closed and there is a pair of point nodes $\theta = 0, \pi$ (Fig. 3).

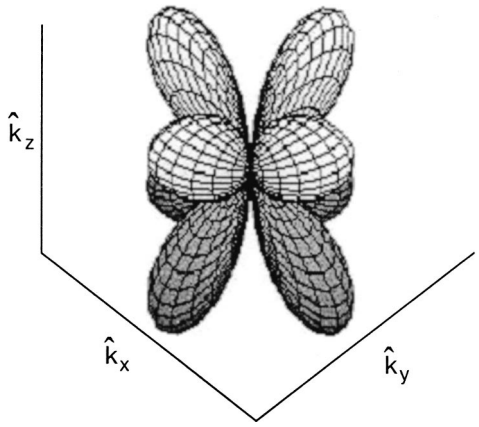

FIG. 2. The modulus of the order parameter $|\mathbf{d}(\mathbf{k})|$ (11) in momentum space for the polar phase in an f-wave superconductor.

Other orbital state candidates, which assume weak effective spin–orbital coupling in UPt_3, are the unitary planar state

$$\mathbf{d}(\mathbf{k}) = \Delta \hat{k}_z[\hat{x}(\hat{k}_x^2 - \hat{k}_y^2) + 2k_xk_y\hat{y}], \tag{13}$$

and the nonunitary bipolar state

$$\mathbf{d}(\mathbf{k}) = \Delta \hat{k}_z[\hat{x}(\hat{k}_x^2 - \hat{k}_y^2) + 2ik_xk_y\hat{y}]. \tag{14}$$

More models for the order parameter in UPt_3 are discussed in Refs. 21, 34 and 35. The models (8)–(10), (12), (14) are interesting in that they spontaneously break time-reversal symmetry ($\mathcal{T}$-breaking), which we discuss in the next Section.

2.3. Breaking of the time-reversal symmetry in unconventional superconductors. Spontaneous magnetic fields and currents

Time-reversal symmetry means that the Hamiltonian $\mathcal{H} = \mathcal{H}^*$, because if $\psi(\mathbf{r})$ is a solution of the Schrödinger equation, then $\psi^*(\mathbf{r})$ is also a solution of the same equation. The time-reversal operation $\mathcal{T}$ is equivalent to complex conjugation $\mathcal{T}\hat{\Psi} = \hat{\Psi}^*$. The simplest example, when both the time-

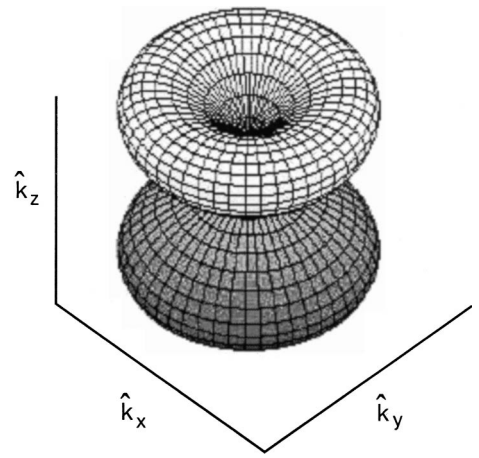

FIG. 3. The modulus of the order parameter $|\mathbf{d}(\mathbf{k})|$ (12) in momentum space for the axial phase in an f-wave superconductor.

reversal symmetry $\mathcal{T}$ and parity $\mathcal{P}$ are broken, is a charged particle in an external magnetic field $\mathbf{H}$, where $\psi(\mathbf{r},\mathbf{H})$ and $\psi^*(\mathbf{r},-\mathbf{H})$ are solutions of the Schrödinger equation, while $\psi(\mathbf{r},-\mathbf{H})$ and $\psi^*(\mathbf{r},\mathbf{H})$ describe different degenerate states of the system. This fact is crucial for understanding of the appearance of nondissipative (persistent) currents in mesoscopic rings, that reflects the broken clockwise–counterclockwise symmetry of electron motion along the ring, caused by the external vector potential.

Unconventional superconductivity allows for a large variety of possible phases. In some of them $\mathcal{T}$ and $\mathcal{P}$ are violated; such superconductors are frequently called *chiral* ones. (The word ''chiral,'' literally ''handed,'' was first introduced into science by Lord Kelvin (William Thomson) in 1884.) The time reversal (that is, complex conjugation) of a one-component order parameter is equivalent to its multiplication by a phase factor and does not change the observables. Therefore only in unconventional superconductors with a multicomponent order parameter can the $\mathcal{T}$-symmetry be broken. In particular, all superconducting states possessing nonzero orbital or/and spin momenta are chiral ones.

If the $\mathcal{T}$-symmetry is broken, the superconducting phase is determined not only by the symmetry of the order parameter but also by the topology of the ground state. The latter is characterized by the integer-valued topological invariant N in momentum space.[52–58] Among the various implications of chirality, perhaps the most striking is the set of chiral quasiparticle states, localized at the surface. These chiral states carry spontaneous dissipation-free currents along the surface. They are gapless, in contrast to bulk quasiparticles of the superconductor.[55]

Volovik and Gor'kov[52] have classified chiral superconducting states into two categories, the so-called ''ferromagnetic'' and ''antiferromagnetic'' states. They are distinguished by the internal angular moment of the Cooper pairs. In the ''ferromagnetic'' state the Cooper pairs possess a finite orbital or (for nonunitary states) spin moment, while in the ''antiferromagnetic'' state they have no net moments.

In high-temperature superconductors with the order parameter (7) the time reversal $\mathcal{T}$-symmetry is preserved in the bulk. However, it has been shown theoretically (see the review[22] and references therein) that the pure $d_{x^2-y^2}$ pair state is not stable against the $\mathcal{T}$-breaking states, such as $d_{x^2-y^2}+id_{xy}$ or $d_{x^2-y^2}+is$, at surfaces and interfaces, near impurities, or below a certain characteristic temperature (d_{xy} or s means an admixture of the d-wave state with $g(\mathbf{k}) \sim 2k_xk_y$ or the s-wave state with $g(\mathbf{k})=\text{const}$. It turns out that such states have larger condensation energy. The $d_{x^2-y^2}+id_{xy}$-wave state represents a ferromagnetic pairing state, while the $d_{x^2-y^2}+is$-wave state is antiferromagnetic.

Among the heavy-fermion superconductors there are two well-known systems which have $\mathcal{T}$-violating bulk superconducting phases: UPt_3 and $U_{1-x}Th_xBe_{13}$ $(0.017<x<0.45)$. These materials show double superconducting transitions on decreasing temperature, and $\mathcal{T}$-violation is associated with the second of them. The proposed models (12) and (14) of the order parameter in UPt_3 correspond to the $\mathcal{T}$-violating states. A more recent candidate for $\mathcal{T}$-violating superconductivity is Sr_2RuO_4. The ''p-wave'' and ''f-wave'' unitary models (8)–(10) describe the $\mathcal{T}$-violating bulk superconducting phases with finite orbital moments of the Cooper pairs.

$\mathcal{T}$-breaking leads to interesting macroscopic physics in a superconductor. Local currents generating orbital angular momenta flow in the bulk. In general, superconductivity and magnetism are antagonistic phenomena, but in this case, the superconducting state generates its own magnetism. The Meissner–Ochsenfeld effect, however, prevents uniform magnetization inside the superconductor, and magnetism is restricted to areas of inhomogeneities—that is, around impurities and domain walls or at interfaces and surfaces. In these regions, spontaneous supercurrents flow. The surface current generates a spontaneous magnetic moment.[59,60] In triplet superconductors all nonunitary models break time-reversal symmetry. For these states Cooper pairs have finite spins, while the magnetization in the bulk is negligible. It was demonstrated that chiral superconductors could show quantum Hall-like effects even in the absence of an external magnetic field:[61] a transverse potential difference would appear in response to the supercurrent.

2.4. Tests for order parameter in unconventional superconductors

The simplest way to test the unconventional superconducting state is to investigate the effect of impurity scattering on kinetic and thermodynamic characteristics. For s-wave superconductors, nonmagnetic impurities have no effects on T_c (Anderson's theorem). In superconductors with unconventional pairing the nonmagnetic impurities induce pair-breaking and suppress superconductivity. Increasing impurity concentration leads to the isotropization of the order parameter. In the state with broken spatial symmetry the only way to achieve it is make the order parameter to zero over entire Fermi surface. This happens if $\Delta_0\tau \sim 1$, where Δ_0 is of the order of the average gap magnitude in the absence of impurities at $T=0$, and τ is the quasiparticles' mean free time.[62–64]

The Knight shift $\delta\omega$ of the nuclear magnetic resonance (NMR) frequency (for details, see Ref. 65) is the most suitable instrument for determining the spin structure of the superconducting state. Because it results from electron interaction with nuclear magnetic moments, $\delta\omega$ is proportional to the Pauli paramagnetic susceptibility χ of normal electrons, the temperature dependence of $\delta\omega(T)$ depends strongly on whether the pairing is singlet or triplet. In singlet superconductors the Cooper pair spin $S=0$, and the density of normal electrons goes to zero at $T\to 0$. Therefore $\delta\omega \to 0$ as well. In triplet superconductors both Cooper pairs and excitations contribute to the susceptibility χ, which changes little with decreasing temperature.

The presence of point and line nodes of the order parameter in unconventional superconductors may be determined from the temperature dependence of thermodynamic quantities and transport coefficients. In fully gapped ($\Delta=\text{const}$) s-wave superconductors they display thermally activated behavior ($\sim \exp(-\Delta/T)$). In a superconductor with nodes in the gap of the elementary excitation spectrum the thermodynamic and kinetic quantities have power-law temperature dependence.

The most-detailed information on the order parameter can be obtained from phase-sensitive pairing symmetry tests.

These are based on Josephson tunneling and flux quantization: SQUID interferometry, tricrystal and tetracrystal magnetometry, magnetic flux imaging, and thin-film SQUID magnetometry (for review see Ref. 19 and references therein).

3. JOSEPHSON EFFECT AND SPONTANEOUS CURRENTS IN JUNCTIONS BETWEEN UNCONVENTIONAL SUPERCONDUCTORS

3.1. Superconducting weak links

The Josephson effect[8] arises in superconducting weak links—the junctions of two weakly coupled superconductors (massive banks) S_1 and S_2. The coupling (contacting) allows the exchange of electrons between the banks and establishes the superconducting phase coherence in the system as a whole. The weakness of the coupling means that the superconducting order parameters of the banks are essentially the same as for separate superconductors, and they are characterized by the phases of the order parameters χ_1 and χ_2. The Josephson weak link could be considered as the ''mixer'' of two superconducting macroscopic quantum states in the banks. The result of the mixing is a phase-dependent current-carrying state with current flowing from one bank to another. This current (Josephson current) is determined (parametrized) by the phase difference $\varphi=\chi_2-\chi_1$ across the weak link.

Classification. General properties. According to the type of coupling, Josephson junctions can be classified as follows. 1) Tunnel junctions (originally considered by Josephson), S–I–S (I is an insulator layer). Weak coupling is provided by quantum tunneling of electrons through a potential barrier. 2) Junctions with direct conductivity, S–c–S (c is a geometrical constriction). These are the microbridges or point contacts. To have the Josephson behavior the constriction size must be smaller than the superconducting coherence length $\xi \sim \hbar v_F/\Delta$. 3) Junctions based on the proximity effect, S–N–S (N is a normal metal layer), S–F–S (F is a ferromagnetic metal layer). The different combinations of these types of junctions are possible, e.g., S–I–N–I–S or S–I–c–S structures. Another type of Josephson weak links are the multiterminal Josephson microstructures, in which the several banks (more than two) are coupled simultaneously with each other.[66–69]

An important characteristic of a Josephson junction is the current–phase relation (CPR) $I_s(\varphi)$. It relates the dc supercurrent flowing from one bank to another with the difference of the phases of the superconducting order parameter in the banks. The maximum value of $I_s(\varphi)$ determines the critical current I_c in the system. The specific form of the CPR depends on the type of weak link. Only in a few cases does it reduce to the simple form $I_s(\varphi)=I_c\sin(\varphi)$ that was predicted by Josephson for the case of a S–I–S tunnel junction. In the general case the CPR is a 2π-periodic function. For conventional superconductors it also satisfies the relation $I_s(\varphi)=-I_s(-\varphi)$. The latter property of CPR is violated in superconductors with broken time-reversal symmetry.[70–73] For general properties of the CPR and its form for different types of weak links the reader is referred to the books and reviews.[66,74–76]

Unconventional Josephson weak links. The properties of the current-carrying states in the weak link depend not only on the manner of coupling but also on the properties of the banks states. For example, the S–c–S junction with the banks subjected to external transport current was considered in Ref. 77. In such a system the time-reversal symmetry is artificially broken, which leads to some interesting features in the junction properties (the appearance of vortex-like states and a surface current flowing opposite to the tangential transport current in the banks). In this review we consider the junctions formed by unconventional (d-wave and triplet) superconducting banks, which we call unconventional Josephson weak links. The most striking manifestation of the unconventional symmetry of the order parameter in the junction is the appearance of a spontaneous phase difference and spontaneous surface current in the absence of current flowing from one bank to the other.

3.2. Junctions between *d*-wave superconductors

Measurements of the characteristics of unconventional Josephson weak links give information about the symmetry of superconducting pairing (see the review[78]). There are several approaches to the calculation of coherent current states in unconventional Josephson junctions. These include the Ginzburg–Landau treatment,[22] description in the language of Andreev bound states,[79] and the numerical solution of the Bogoljubov–de Gennes equations on a tight binding lattice.[80] A powerful method of describing inhomogeneous superconducting states is based on the quasiclassical Eilenberger equations for the Green's functions integrated over energy.[81] It was first used in Ref. 9 to describe the dc Josephson effect in a ballistic point contact between conventional superconductors. The Eilenberger equations can be generalized to the cases of d-wave and triplet pairing (Appendix II). In this Section we present the results of quasiclassical calculations for the Josephson and spontaneous currents in the grain boundary junction between d-wave superconductors.[12,16,17]

3.2.1. Current–phase relations

We consider a Josephson weak link $S_1^{(d)}$–$S_2^{(d)}$ which is formed by the mismatching of the orientations of the lattice axes in the banks $S_1^{(d)}$ and $S_2^{(d)}$, as shown in Fig. 4. The x axis is perpendicular and the y axis is parallel to the interface between two superconducting 2D half-spaces with different

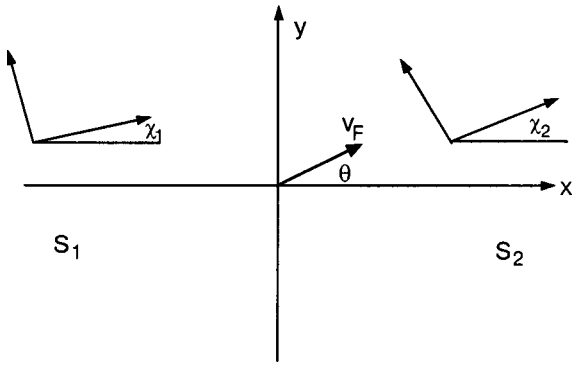

FIG. 4. Interface between two d-wave superconductors S_1 and S_2 with different orientations χ_1 and χ_2 of the lattice axes $a-b$.

$a-b$ axis orientations (angles χ_1 and χ_2 in Fig. 4). Far from the interface ($x\to\mp\infty$) the order parameter is equal to the bulk values $\Delta_{1,2}(\mathbf{v}_F)$. In the vicinity of the interface $x=0$, if the angles χ_1 and χ_2 do not coincide, the value of Δ deviates from $\Delta_{1,2}$. To describe the coherent current states in the system, the Eilenberger equations (A4) for the Green's functions must be solved simultaneously with the equation for Δ (A5). The equation of self-consistency (A5) determines the spatial distribution of $\Delta(\mathbf{r})$. The problem of solving the coupled equations (A4) and (A5) can be treated by numerical calculations. Analytical solutions can be obtained for the model (non-self-consistent) distribution of $\Delta(\mathbf{r})$:

$$\Delta(\mathbf{v}_F,\mathbf{r})=\begin{cases}\Delta_1(\mathbf{v}_F)\exp(-i\varphi/2), & x<0,\\ \Delta_2(\mathbf{v}_F)\exp(i\varphi/2), & x>0.\end{cases} \tag{15}$$

The phase φ is the global phase difference between superconductors S_1 and S_2. In the following we consider the case of an ideal interface with transparency $D=1$. For the influence of interface roughness and effect of surface reflectancy ($D\neq 1$) as well as the numerical self-consistent treatment of the problem, see Ref. 16.

Analytical solutions in the model with the non-self-consistent order-parameter distribution (15) are presented in Appendix II. Using the expressions (A9), (A12) and (A13), we obtain the current densities $j_x(x=0)\equiv j_J$ and $j_y(x=0)\equiv j_S$:

$$j_J=4\pi eN(0)v_FT\sum_{\omega>0}\left\langle\frac{\Delta_1\Delta_2|\cos\theta|}{\Omega_1\Omega_2+\omega^2+\Delta_1\Delta_2\cos\varphi}\right\rangle\sin\varphi, \tag{16}$$

$$j_S=4\pi eN(0)v_FT\sum_{\omega>0}\left\langle\frac{\Delta_1\Delta_2\sin\theta\,\mathrm{sign}(\cos\theta)}{\Omega_1\Omega_2+\omega^2+\Delta_1\Delta_2\cos\varphi}\right\rangle\sin\varphi. \tag{17}$$

We denote by j_J the Josephson current flowing from S_1 to S_2 and by j_S the surface current flowing along the interface boundary. Expressions (16) and (17) are valid (within the applicability of the model (15)) for arbitrary symmetry of the order parameters $\Delta_{1,2}$. In particular, for s-wave superconductors from Eq. (16) we have the current–phase relation for the Josephson current in a conventional (s-wave) 2D ballistic S–c–S contact:[9]

$$j_J=2eN(0)v_F\Delta_0(T)\sin\frac{\varphi}{2}\tanh\frac{\Delta_0(T)\cos(\varphi/2)}{2T}.$$

The surface current j_S (17) equals zero in this case.

For a $S_1^{(d)}-S_2^{(d)}$ interface (DD junction) between d-wave superconductors, the functions $\Delta_{1,2}(\mathbf{v}_F)$ in (16) and (17) are $\Delta_{1,2}=\Delta_0(T)\cos 2(\theta-\chi_{1,2})$. In Appendix I the temperature dependence of the maximum gap $\Delta_0(T)$ in d-wave superconductors is presented for reference. The results of the calculations of $j_J(\varphi)$ and $j_S(\varphi)$ for a DD junction are displayed in Fig. 5 for different mismatch angles $\delta\chi$ between the crystalline axes across the grain boundary and at temperature $T=0.1T_c$ (assuming the same transition temperature on both sides). The interface is between two d-wave superconductors S_1 and S_2 with different $a-b$ lattice axis orientations χ_1 and χ_2.

In these figures, the left superconductor is assumed to be aligned with the boundary, while the orientation of the right superconductor varies. The Josephson current–phase relation (Fig. 5a) demonstrates a continuous transition from a π-periodic (sawtooth-like) line shape at $\delta\chi=45°$ to a 2π-periodic one for small $\delta\chi$, as expected in the case of a clean DND junction.[82] The phase dependence of the surface current (Fig. 5b) is also in qualitative agreement with results for SND and DND junctions.[83]

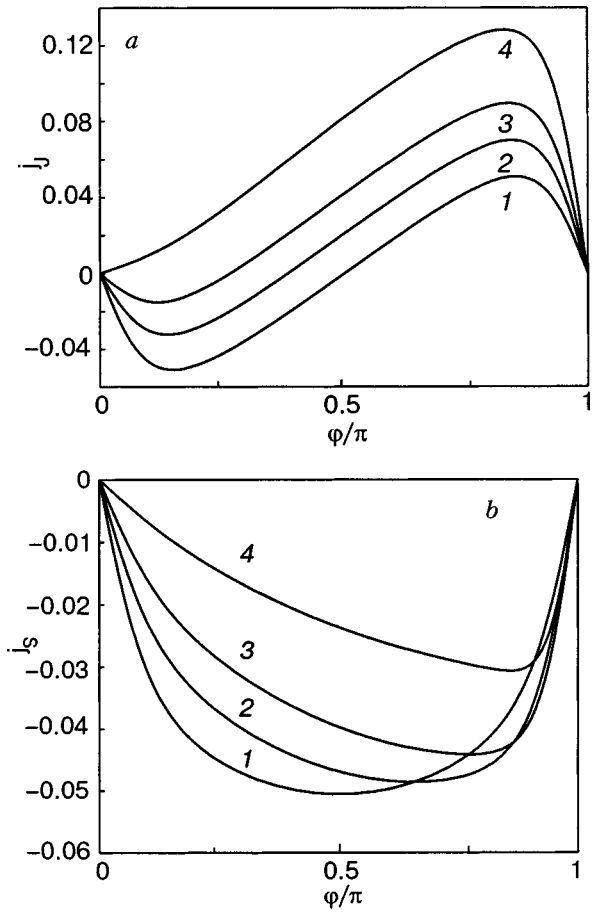

FIG. 5. Josephson current (a) and spontaneous current (b) versus the phase difference in a clean DD grain boundary junction calculated in a non-self-consistent approximation. Current densities are in units of $j_0=4\pi eN(0)v_FT$ and $T=0.1T_c$. The mismatch angles are $\chi_1=0$ and $\chi_2=45°$ (*1*), 40° (*2*), 34° (*3*), and 22.5° (*4*).

3.2.2. Spontaneous currents and bistable states

In contrast to the weak link between two conventional superconductors, the current j_S is not identically equal to zero. Moreover, in some region of angles χ_1 and χ_2 a value of the equilibrium phase difference $\varphi=\varphi_0$ exists at which $(dj_J(\varphi)/d\varphi)_{\varphi=\varphi_0}>0$ and $j_J(\varphi_0)=0$ but $j_S(\varphi_0)\neq 0$. These spontaneous phase difference φ_0 and spontaneous current $j_S(\varphi_0)\equiv j_{\mathrm{spon}}$ correspond to the appearance of time-reversal symmetry breaking states in the system (in fact, two values $\pm\varphi_0$ of the phase and corresponding spontaneous currents $\pm j_{\mathrm{spon}}$ appear). The region of $\mathcal{T}$-breaking states (as a function of temperature and mismatch angle) is shown in Fig. 6. In Figs. 6 and 7 we also present the self-consistent numerical result,[16] for comparison. Only in the asymmetric $\delta\chi=45°$ junction does the degeneracy (at $\varphi=\pm\pi/2$) survive at all temperatures, due to its special symmetry which leads to complete suppression of all odd harmonics of $I(\varphi)$; gener-

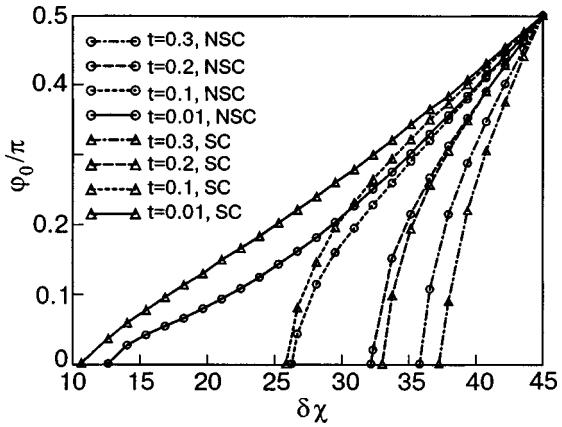

FIG. 6. Equilibrium phase difference in a clean DD grain boundary junction as a function of $\delta\chi=\chi_2-\chi_1$ (keeping $\chi_1=0$), at different values of $t=T/T_c$. The circles and triangles correspond to non-self-consistent (NSC) and self-consistent (SC) calculations, respectively. For nonzero φ_0 the ground state is twofold degenerate ($\varphi=\pm\varphi_0$).

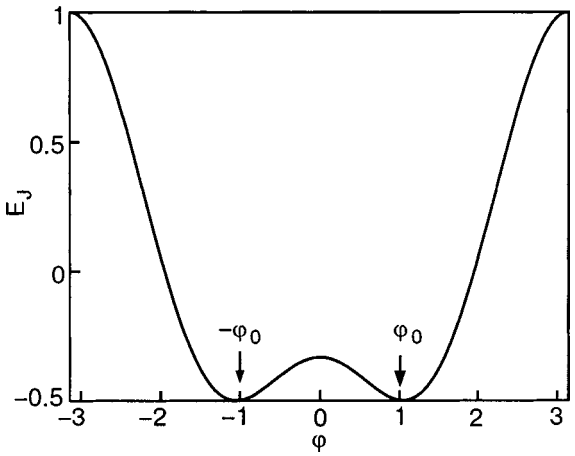

FIG. 8. Josephson energy of a DD junction.

ally, $\varphi_0\to 0$ at some temperature that depends on the orientation. The equilibrium value of the spontaneous current is nonzero in a certain region of angles and temperatures (Fig. 7), which is largest in the case of the asymmetric $\delta\chi=45°$ junction.

The Josephson current $I_J(\varphi)$ is related to the Josephson energy of the weak link $E_J(\varphi)$ through $I_J(\varphi)=(2e/\hbar)\times(\partial E_J(\varphi)/d\varphi)$. The Josephson energy for DD junction as function of phase difference is shown schematically in Fig. 8. The arrows indicate two stable states of the system. These are two macroscopic quantum states which can be used for *d*-wave qubit design (see Sec. 4 below).

3.3. Junctions between triplet superconductors

The Josephson effects in the case of triplet pairing was first discovered[84,85] in weak links in ^{3}He. It was found that at low temperatures the mass current–phase dependence $J(\varphi)$ can essentially differ from the case of a conventional superconductor, and a so-called "π-state" ($J'(\pi)>0$) is possible.[85,86] In several theoretical papers the Josephson effect has been considered for a pinhole in a thin wall separating two volumes of ^{3}He-B.[10,11,13,87–90] The discovery of metal superconducting compounds with triplet pairing of electrons has made topical the theoretical investigation of the Josephson effect in these superconductors. The Josephson effect is much more sensitive to dependence of $\Delta(\mathbf{k})$ on the momentum direction on the Fermi surface than are the thermodynamic and kinetic coefficients. In this Section the consideration of the Josephson effect in point contacts is based on the most favorable models of the order parameter in UPt_3 and Sr_2RuO_4, which were presented in Sec. 2.

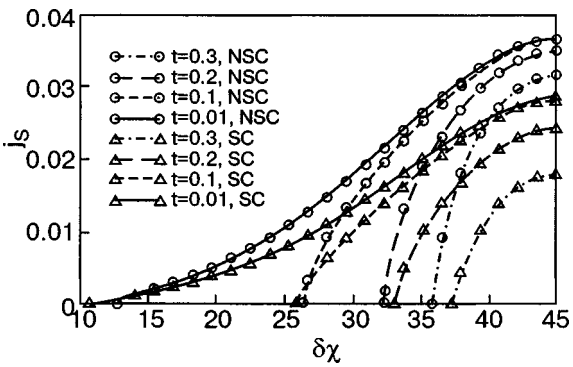

FIG. 7. Spontaneous current in the junction of Fig. 6.

3.3.1. Current density near an interface of misoriented triplet superconductors

Let us consider a model of the Josephson junction as a flat interface between two misoriented bulk triplet superconductors (Fig. 9). In this Section we follow the results of Ref. 15. In order to calculate the stationary Josephson current contact we use "transport-like" equations for ξ-integrated Green's functions[80] (see Appendix II.3). Here we consider the simple model of a constant order parameter up to the surface. The pair breaking and the electron scattering on the interface are ignored. For this non-self-consistent model the current–phase relation of a Josephson junction can be calculated analytically. This makes it possible to analyze the main features of the current–phase relations for different scenarios of "f-wave" superconductivity. We believe that under this strong assumption our results describe the real situation qualitatively, as was justified for point contacts between "d-wave" superconductors[12] and pinholes in ^{3}He.[91]

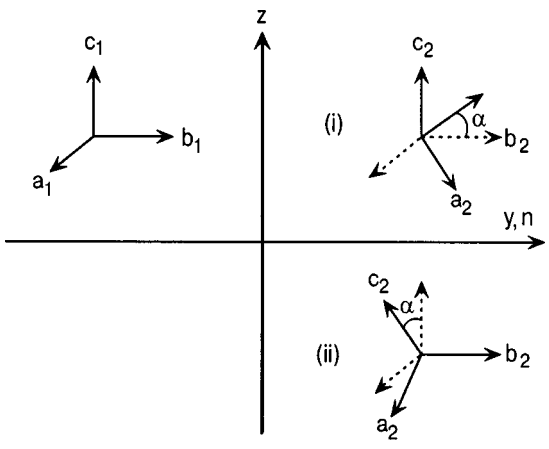

FIG. 9. Josephson junction as interface between two unconventional superconductors misorienated by an angle α and with order parameter $\mathbf{d}(\mathbf{k})$.

Knowing the component $\check{g}_1(0)$ (A29) of the Green's function $\check{g}(\hat{\mathbf{k}},\mathbf{r},\varepsilon_m)$, one can calculate the current density at the interface, $\mathbf{j}(0)$:

$$\mathbf{j}(0)=4\pi eN(0)v_F T\sum_{m=0}^{\infty} d\hat{\mathbf{k}}\hat{\mathbf{k}}\,\mathrm{Re}(\check{g}_1(0)), \tag{18}$$

where

$$\mathrm{Re}(\check{g}_1(0))=\frac{\Delta_1\Delta_2}{2}\sum_{\pm}\frac{\sin(\pm\theta)}{\frac{2}{m}+\Omega_1\Omega_2+\Delta_1\Delta_2\cos(\pm\theta)}. \tag{19}$$

The real vectors $\Delta_{1,2}$ are related to the gap vectors $\mathbf{d}_{1,2}(\hat{\mathbf{k}})$ in the banks by the relation

$$\mathbf{d}_n(\hat{\mathbf{k}})=\Delta_n(\hat{\mathbf{k}})\exp(i\psi_n). \tag{20}$$

The angle θ is defined by $\Delta_1(\hat{\mathbf{k}})\cdot\Delta_2(\hat{\mathbf{k}})=\Delta_1(\hat{\mathbf{k}})\Delta_2(\hat{\mathbf{k}})\cos\theta$, and $(\mathbf{k})=\psi_2(\hat{\mathbf{k}})-\psi_1(\hat{\mathbf{k}})+\varphi$.

Misorientation of the crystals would generally result in the appearance of a current along the interface,[17] as can be calculated by projecting the vector $\mathbf{j}$ on the corresponding direction.

We consider a rotation R in the right superconductor only (see Fig. 9), (i.e., $\mathbf{d}_2(\hat{\mathbf{k}})=R\mathbf{d}_1(R^{-1}\hat{\mathbf{k}})$). We choose the c axis in the left half-space along the partition between the superconductors (along the z axis in Fig. 9). To illustrate the results obtained by computing the formula (18), we plot the current–phase relation for different below-mentioned scenarios of "f-wave" superconductivity for two different geometries corresponding to different orientations of the crystals to the right and to the left at the interface (see Fig. 9): (i) The basal plane ab to the right is rotated about the c axis by the angle α; $\hat{\mathbf{c}}_1\|\hat{\mathbf{c}}_2$. (ii) The c axis to the right is rotated about the contact axis (y axis in Fig. 9) by the angle α; $\hat{\mathbf{b}}_1\|\hat{\mathbf{b}}_2$.

Further calculations require a definite model of the vector order parameter $\mathbf{d}$.

3.3.2. Current–phase relations and spontaneous surface currents for different scenarios of "f-wave" superconductivity

Let us consider the models of the order parameter in UPt_3 which are based on the odd-parity E_{2u} representation of the hexagonal point group D_{6h}. The first of them corresponds to the axial state (12) and assumes the strong spin–orbital coupling, with the vector $\mathbf{d}$ locked along the $\mathbf{c}$ axis of the lattice. The other candidate to describe the orbital states, which imply that the effective spin–orbital coupling in UPt_3 is weak, is the unitary planar state (13). The coordinate axes x,y,z here and below are chosen along the crystallographic axes $\hat{\mathbf{a}},\hat{\mathbf{b}},\hat{\mathbf{c}}$ as at the left in Fig. 9. These models describe the hexagonal analog of spin-triplet f-wave pairing.

In Fig. 10 we plot the Josephson current–phase relation $j_J(\varphi)=j_y(y=0)$ calculated from Eq. (18) for both the axial [with the order parameter given by Eq. (12)] and the planar [Eq. (13)] states for a particular value of α under the rotation of the basal plane ab to the right [the geometry (i)]. For simplicity we use a spherical model of the Fermi surface. For the axial state the current–phase relation is just a slanted sinusoid, and for the planar state it shows a "π-state." The

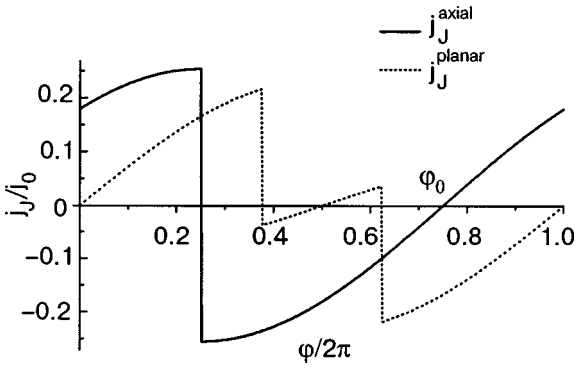

FIG. 10. Josephson current densities versus phase φ for axial (12) and planar (13) states in the geometry (i); misorientation angle $\alpha=\pi/4$; the current is given in units of $j_0=\pi/2\,eN(0)v_F\Delta_0(0)$.

appearance of the π-state at low temperatures is due to the fact that different quasiparticle trajectories contribute to the current with different effective phase differences $(\hat{\mathbf{k}})$ [see Eqs. (18) and (19)].[11] Such a different behavior can be a criterion for distinguishing between the axial and the planar states, taking advantage of the phase-sensitive Josephson effect. Note that for the axial model the Josephson current formally does not equal zero at $\varphi=0$. This state is unstable (does not correspond to a minimum of the Josephson energy), and the state with a spontaneous phase difference (value φ_0 in Fig. 10), which depends on the misorientation angle α, is realized.

The remarkable influence of the misorientation angle α on the current–phase relation is shown in Fig. 11 for the axial state in the geometry (ii). For some values of α (in Fig. 11 it is $\alpha=\pi/3$) there are more than one state which correspond to minima of the Josephson energy ($j_J=0$ and $dj_J/d\varphi>0$).

The calculated x and z components of the current, which are parallel to the surface, $\mathbf{j}_S(\varphi)$, are shown in Fig. 12 for the same axial state in the geometry (ii). Note that the current tangential to the surface as a function of φ is nonzero when the Josephson current (Fig. 11) is zero. This spontaneous tangential current is due to the specific "proximity effect," similar to spontaneous current in contacts between "d-wave" superconductors.[17] The total current is determined by the Green's function, which depends on the order parameters in both superconductors. As a result, for nonzero misorientation

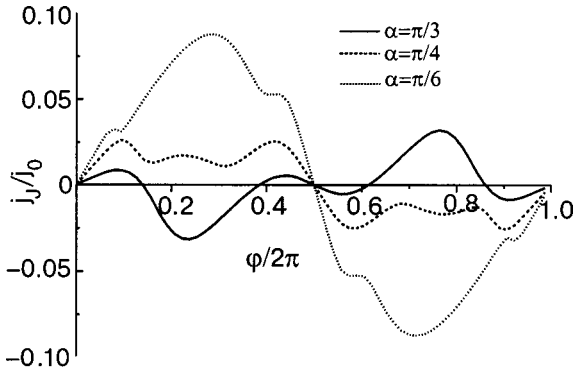

FIG. 11. Josephson current versus phase φ for the axial state (12) in the geometry (ii) for different α.

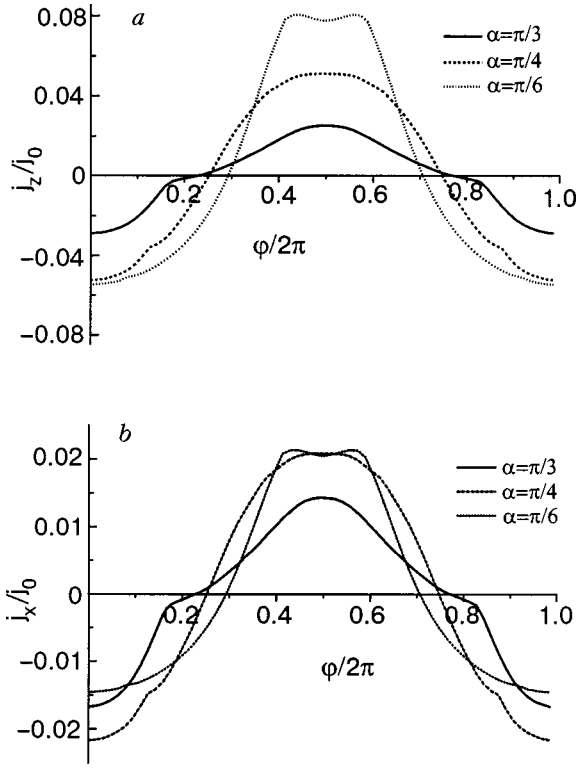

FIG. 12. z component (a) and x component (b) of the tangential current versus phase φ for the axial state (12) in the geometry (ii) for different α.

angles a current parallel to the surface can be generated. In the geometry (i) the tangential current for both the axial and planar states at $T=0$ is absent.

The candidates for the superconducting state in Sr_2RuO_4 are the "p-wave" model (8) and the "f-wave" hybrid model (10). Taking into account the quasi-two-dimensional electron energy spectrum in Sr_2RuO_4, we calculate the current (18) numerically using the model of a cylindrical Fermi surface. The Josephson current for the hybrid "f-wave" model of the order parameter (Eq. (10)) is compared to the p-wave model (Eq. (8)) in Fig. 13 (for $\alpha=\pi/4$). Note that the critical current for the "f-wave" model is several times smaller (for the same value of Δ_0) than for the "p-wave" model. This different character of the current–phase relation enables us to distinguish between the two states.

In Figs. 14 and 15 we present the Josephson current and the tangential current for the hybrid "f-wave" model for different misorientation angles α (for the "p-wave" model it

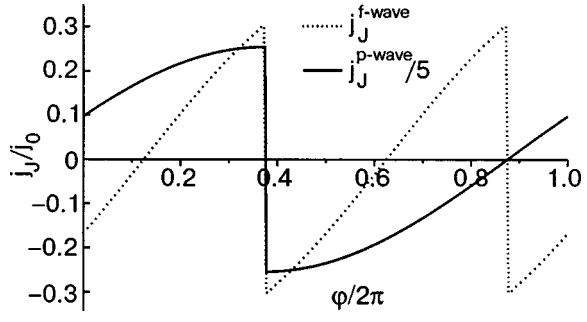

FIG. 13. Josephson current versus phase φ for hybrid "f-wave" (10) and "p-wave" (8) states in the geometry (i); $\alpha=\pi/4$.

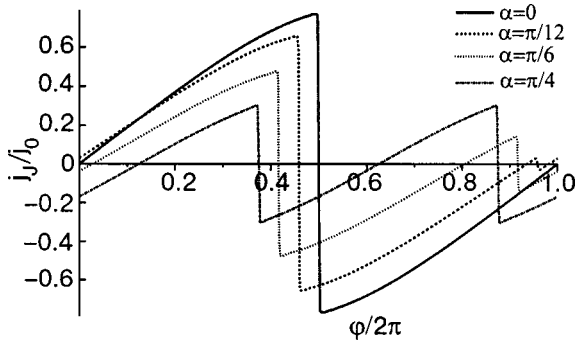

FIG. 14. Josephson current versus phase φ for the hybrid "f-wave" state (9) in the geometry (i) for different α.

equals zero). Just as in Fig. 10 for the "f-wave" order parameter (12), in Fig. 14 for the hybrid "f-wave" model (9) the steady state of the junction with zero Josephson current corresponds to a nonzero spontaneous phase difference if the misorientation angle $\alpha\neq 0$.

Thus, in this Section the stationary Josephson effect in a planar junction between triplet superconductors is considered. The analysis is based on models with "f-wave" symmetry of the order parameter belonging to the two-dimensional representations of the crystallographic symmetry groups. It is shown that the current–phase relations are quite different for different models of the order parameter. Because the order parameter phase depends on the momentum direction on the Fermi surface, the misorientation of the superconductors leads to a spontaneous phase difference that corresponds to zero Josephson current and to the minimum of the weak-link energy. This phase difference depends on the misorientation angle and can possess any value. It has been found that in contrast to the "p-wave" model, in the "f-wave" models the spontaneous current may be generated in a direction which is tangential to the orifice plane. Generally speaking this current is not equal to zero in the absence of the Josephson current. It is demonstrated that the study of the current–phase relation of a small Josephson junction for different crystallographic orientations of banks enables one to judge the applicability of different models to the triplet superconductors UPt_3 and Sr_2RuO_4.

It is clear that such experiments require very clean superconductors and perfect structures of the junction because of pair-breaking effects of nonmagnetic impurities and defects in triplet superconductors.

4. JOSEPHSON PHASE QUBITS BASED ON *d*-WAVE SUPERCONDUCTORS

4.1. Quantum computing basics

As we have seen, unconventional superconductors support time-reversal symmetry breaking states on a macroscopic, or at least, mesoscopic scale. An interesting possibility arises then to apply them in quantum bits (*qubits*), basic units of quantum computers (see, e.g., Refs. 92–94), using $\mathcal{T}$-related states of the system as basic qubit states.

A quantum computer is essentially a set of N two-level quantum systems which, without loss of generality, can be represented by spin operators $\hat{\sigma}^{(i)}$, $i=1...N$. The Hilbert space of the system is spanned by 2^N states $|s_1\rangle\otimes|s_2\rangle\otimes\ldots$

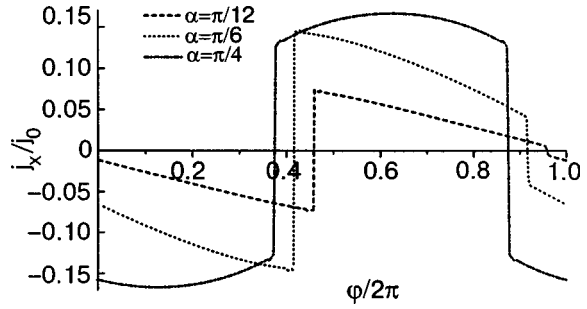

FIG. 15. Tangential current density versus phase φ for the hybrid "f-wave" state (9) in the geometry (i) for different α.

$\otimes|s_N\rangle$, $s_i=0,1$. The information to be processed is contained in complex coefficients $\{\alpha\}$ of the expansion of a given state in this basis:

$$|\Psi\rangle=\sum_{s_j=0,1}\alpha_{s_1s_2\ldots s_N}|s_1\rangle\otimes|s_2\rangle\otimes\ldots\otimes|s_N\rangle. \tag{21}$$

The unitary operations on states of the qubits are called gates, like in the classical case. Single qubit gates are $SU(2)$ rotations. An example of a two-qubit gate is a *conditional phase shift*, $CP(\gamma)$, which, being applied to a two-qubit wave function, shifts its phase by γ if and only if they are in the same ("up" or "down") state. In the basis $\{|0\rangle\otimes|0\rangle,|0\rangle\otimes|1\rangle,|1\rangle\otimes|0\rangle,|1\rangle\otimes|1\rangle\}$ it is

$$CP(\gamma)=\begin{pmatrix} e^{i\gamma} & 0 & 0 & 0\\ 0 & 1 & 0 & 0\\ 0 & 0 & 1 & 0\\ 0 & 0 & 0 & e^{i\gamma}\end{pmatrix}. \tag{22}$$

Obviously, if $CP(\gamma)$ is applied to a factorized state of two qubits, $|\Psi\rangle=(\alpha_1|0\rangle+\beta_1|1\rangle)\otimes(\alpha_2|0\rangle+\beta_2|1\rangle)$, in the general case we will obtain an *entangled* state. Up to an unimportant global phase factor, $CP(\gamma)$ results from the free evolution of two qubits, generated by the Hamiltonian $\mathcal{H}=J\hat{\sigma}_z^{(1)}\cdot\hat{\sigma}_z^{(2)}$, for a time $T=\hbar\gamma/(2J)$.

Another nontrivial example is the *controlled-not* gate CN_{12}, which, acting on $|s_1\rangle\otimes|s_2\rangle$, leaves s_1 intact and flips s_2 $(1\to0,0\to1)$ if and only if $s_1=1$. The combination $SW_{12}=CN_{12}CN_{21}CN_{12}$ *swaps* (exchanges) the states of two qubits.

It can be shown that a universal quantum computer (that is, one that can realize any possible quantum algorithm, the way a Turing machine can realize any possible classical algorithm) can be modeled by a chain of qubits with only nearest-neighbor interactions:

$$\mathcal{H}=\sum_{i=1}^{N}\{u_i\sigma_z^{(i)}+\Delta_i\sigma_x^{(i)}\}+\sum_{i=j+1}J_{ij}\sigma_z^{(i)}\cdot\sigma_z^{(j)}. \tag{23}$$

Further simplifications are possible,[95] but this would be irrelevant for our current discussion.

The operations of a quantum computer require that the parameters of the above Hamiltonian be controllable (more specifically, one must be able to *initialize*, *manipulate*, and *read out* qubits). For the unitary manipulations discussed above, at least some of the parameters u, Δ, J of the Hamiltonian must be controllable from the outside during the evolution. Initialization and readout explicitly require nonunitary operations (projections). Therefore any practical implementation of a quantum computer must satisfy contradictory requirements: qubits must be isolated from the outside world to allow coherent quantum evolution (characterized by a decoherence time τ_d) for long enough time to allow an algorithm to run, but they must be sufficiently coupled to each other and to the outside world to permit initialization, control, and readout.[94] Fortunately, quantum error correction allows one to translate a larger size of the system into a longer effective decoherence time by coding each logical qubit in several logical ones (currently it is accepted that a system with τ_d/τ_g in excess of 10^4 can run indefinitely, where τ_g is the time of a single gate application (e.g., the time T in the example of $CP(\gamma)$).

Note that the operation of a quantum computer based on consecutive application of quantum gates as described above is not the only possible, or necessarily the most efficient, way of its use. In particular, it requires a huge overhead for quantum error correction. Alternative approaches have been suggested (e.g., adiabatic quantum computing[96–98]) which may be more appropriate for the smaller-scale quantum registers likely to be built in the immediate future.

4.2. Superconducting qubits

The size of the system is crucial not only from the point of view of quantum error correction. It is mathematically proven that a quantum computer is exponentially faster than a classical one in factorizing large integers; the number of known quantum algorithms is still small, but an active search for more potential applications is under way (see the above reviews and, e.g., Refs. 96–98). Nevertheless the scale on which its qualitative advantages over classical computers begin to be realized is about a thousand qubits. This indicates that solid-state devices should be looked at for the solution. The use of some microsopic degrees of freedom as qubits, e.g., nuclear spins of ^{31}P in a Si matrix, as suggested by Kane,[99] is attractive due to both the large τ_d and well-defined basis states. The difficulties in fabrication (due to small scale) and control and readout (due to weak coupling to the external controls) have not allowed realization of the scheme so far.

Among mesoscopic qubit candidates, superconducting, more specifically Josephson systems have the advantage of a coherent ground state and the absence or suppression of low-energy excitations, which increases the decoherence time. Together with well-understood physics and developed experimental and fabrication techniques, this makes them a natural choice.

The degree of freedom which is coupled to the control and readout circuits determines the physics of a qubit. In the superconducting case, one can then distinguish *charge* and *phase* qubits, depending on whether the charge (number of particles) or phase (Josephson current) of the superconductor is well defined.

The simplest example of a Josephson qubit is an rf SQUID,[100] with the Hamiltonian

$$\mathcal{H}_q=\frac{\hat{Q}^2}{2C}+\frac{\Phi_0^2}{8\pi^2L}(\varphi-\varphi_x)^2-\frac{I_c\Phi_0}{2\pi}\cos(\varphi), \tag{24}$$

where L is the self-inductance of the loop, and I_c and C are the critical current and capacitance of the Josephson junction. The charge on the junction, $\hat{Q}=-2ie\partial_\varphi$, is conjugate to the phase difference φ across it. The external flux through the loop is $\Phi_x=\varphi_x\Phi_0/(2\pi)$. If it equals *exactly* $\Phi_0/2$ ($\varphi_x=\pi$) the $\mathcal{T}$-symmetry is broken. The potential part in (24) acquires a symmetric two-well structure, with tunneling between the wells possible due to the derivative term in (24), which reflects quantum phase uncertainty in a Josephson junction with finite capacitance. The tunneling rate is of the order of $\omega_p \exp(-U(0)/\omega_p)$, where the frequency of oscillations in one of the potential wells $\omega_p\sim\sqrt{E_JE_Q}$, and the height of the potential barrier between them $U(0)\sim E_J$.

The states in the right and left wells differ by the direction of the macroscopic persistent current and can be used as qubit states $|0\rangle$ and $|1\rangle$. The dynamics of the system is determined by the interplay of the charging energy $E_Q=2e^2/C$ and Josephson energy $E_J=hI_c/(2e)$. Here $E_J/E_Q\gg1$, and charging effects are responsible for the tunneling splitting of the levels. Coherent tunneling between them has actually been observed[100] in a Nb/AlO_x/Nb SQUID at 40 mK; the magnetic flux difference was approximately $\Phi_0/4$, which corresponded to currents of about 2 μA. (The actual design was a little more complicated than the simple rf SQUID.) Fine tuning of the external flux is essential to allow *resonant tunneling* through the potential barrier.

In the case of small loop inductance the phase will be fixed by flux quantization. For phase to tunnel, one has to introduce extra Josephson junctions in the loop. In the three-junction design,[101] two junctions are identical, each with a Josephson energy E_J, and the third one has a little smaller energy αE_J, $\alpha<1$. In the presence of external flux φ_x, the energy of the system as a function of phases on the identical junctions φ_1,φ_2 is

$$\frac{U(\varphi_1,\varphi_2)}{E_J}=-\cos\varphi_1-\cos\varphi_2-\alpha\cos(\varphi_x+\varphi_1-\varphi_2). \tag{25}$$

As before, if $\varphi_x=\pi$, the system has degenerate minima. Due to the two-dimensional potential landscape, tunneling between them does not require a large flux transfer of order $\Phi_0/2$, as in the previous case. Tunneling is again possible due to charging effects, which give the system an effective ''mass'' proportional to the Josephson junction capacitance C. Coherent tunneling between the minima has been observed.[102] The potential landscape (25) was recovered from measurements on a classical 3-junction loop (with C too large to allow tunneling).[103] Rabi oscillations were observed both indirectly, using the quantum noise spectroscopy[104] (the observed decay time of Rabi oscillation observed in these experiments $\tau_{\rm Rabi}=2.5$ μs), and directly, in time domain[105] ($\tau_{\rm Rabi}=150$ ns).

The above limit $E_J/E_Q\gg1$ can be reversed. Then the design must include a mesoscopic island separated from the rest of the system by two tunnel junctions (a superconducting single electron transistor, SSET). The Hamiltonian becomes

$$\mathcal{H}_q=\frac{(\hat{Q}-Q_x)^2}{2C}-\frac{I_c\Phi_0}{2\pi}\cos\varphi, \tag{26}$$

where this time the role of external $\mathcal{T}$-symmetry breaking parameter is played by the charge Q_x induced on the island by a gate electrode. The working states are eigenstates of charge on the island; at appropriate Q_x the states with $Q=2ne$ and $Q=2(n+1)e$ are degenerate due to a parity effect,[106] where n is the number of Cooper pairs in the SSET. Quantum coherence in an SSET has been observed not just through the observation of level anticrossing near the degeneracy point, as in Refs. 100 and 102, but also in the time domain.[107] The system was prepared in a superposition of states $|n\rangle,|n+1\rangle$, kept at a degeneracy point for a controlled time τ, and measured. The probability $P(\tau)$ of finding the system in state n exhibited quantum beats.

A ''hybrid'' system, with $E_J/E_Q\simeq1$, so-called ''quantronium,'' was fabricated and measured in the time domain at CEA-Saclay,[108] with an extraordinary ratio $\tau_d/\tau_t\approx8000$ (the tunneling time τ_t can be considered as the lower limit of the gate application time τ_g). Quantronium can be described as a charge qubit, which is read out through the phase variable, and is currently the best superconducting single qubit.

An interesting inversion of the quantronium design[109] is also a hybrid qubit, this time a flux qubit read out through the charge variable. It promises several advantages over other superconducting qubits, but has not yet been fabricated and tested.

Finally, a single current-biased Josephson junction can also be used as a qubit (phase qubit).[110,111] The role of basis states is played by the lowest and first excited states in the washboard potential. Rabi oscillations between them have been successfully observed.

The charge, hybrid, and phase qubits are mentioned here only for the sake of completeness, since unconventional superconductors are more naturally employed in flux qubits. Various Josephson qubits are reviewed in Ref. 112.

4.3. Application of *d*-wave superconductors to qubits

One of the main problems with the above flux qubit designs is the necessity of artificially breaking the $\mathcal{T}$-symmetry of the system by putting a flux $\Phi_0/2$ through it. Estimates show that the required accuracy is 10^{-5}–10^{-6}. The micron-size qubits must be positioned close enough to each other to make possible their coupling; the dispersion of their parameters means that applied fields must be locally calibrated; this is a formidable task given such sources of field fluctuations as fields generated by persistent currents in qubits themselves, which depend on the state of the qubit; field creep in the shielding; captured fluxes; magnetic impurities. Moreover, the circuitry which produces and tunes the bias fields is an additional source of decoherence in the system. (Similar problems arise in charge qubits, where the gate voltages must be accurately tuned.)

These problems are avoided if the qubit is *intrinsically bistable*. The most straightforward way to achieve this is to substitute the external flux by a static phase shifter, a Josephson junction with unconventional superconductors with nonzero equilibrium phase shift φ_0. From (25), one sees that, e.g., a three-junction qubit would require an extra π-junction ($\varphi_0=\pi$).[113] In the same way a π-junction can be added to a multiterminal phase qubit.[114] The only difference compared to the case of external magnetic field bias is in the decoher-

ence time: instead of noise from field generating circuits we will have to take into account decoherence from nodal quasiparticles (see below).

A more interesting possibility is opened up if the bistable d-wave system is employed dynamically, that is, if its phase is allowed to tunnel between the degenerate values. In a so-called ''quiet'' qubit[113] an SDS′ junction (effectively two SD junctions in the (110) direction) is put in a low-inductance SQUID loop in parallel with a conventional Josephson junction and large capacitor. One of the SD junctions plays the role of a $\pi/2$-phase shifter. The other junction's capacitance C is small enough to make possible tunneling between $\pi/2$ and $-\pi/2$ states due to the charging term $Q^2/2C$. Two consecutive SD junctions are effectively a single junction with equilibrium phases 0 and π (which are chosen as working states of the qubit). The control mechanisms suggested in Ref. 113 are based on switches c and s. Switch c connects the small S′D junction to a large capacitor, thus suppressing the tunneling. Connecting s for the duration Δt creates an energy difference ΔE between $|0\rangle$ and $|1\rangle$, because in the latter case we have a frustrated SQUID with 0- and π-junctions, which generates a spontaneous flux $\Phi_0/2$. This is a generalization of applying the operation σ_z to the qubit. Finally, if switch c is open, the phase of the small junction can tunnel between 0 and π. Entanglement between qubits is realized by connecting them through another Josephson junction in a bigger SQUID loop. The suggested implementation for switches is based on a low-inductance dc-SQUID design with a conventional and a π-junction in parallel, with $I_{c,0}=I_{c,\pi}$. In the absence of external magnetic field the Josephson current through it is zero, while at external flux $\Phi_0/2$ it equals $2I_c$. Instead of external flux, another SDS′ junction, which can be switched by a voltage pulse between the 0 (closed) and π (open) states, is put in series with the π-junction.

The above design is very interesting. Due to the absence of currents through the loop during tunneling between $|0\rangle$ and $|1\rangle$ the authors called it ''quiet,'' though, as we have seen, small currents and fluxes are still generated near the SD boundaries.

Another design based on the same bistability[115] only requires one SD or DD boundary. Here a small island contacts a massive superconductor, and the angle between the orientation of d-wave order parameter and the direction of the boundary can be arbitrary (as long as it is compatible with bistability). The advantage of such a design is that the potential barrier can to a certain extent be controlled and suppressed; moreover, in general there are two ''working'' minima $-\varphi_0, \varphi_0$; the phase of the bulk superconductor across the boundary is zero will be separated from each other by a smaller barrier than from the equivalent states differing by $2\pi n$. This allows us to disregard the ''leakage'' of the qubit state from the working space spanned by $(|0\rangle, |1\rangle)$, which cannot be done in a ''quiet'' design with exact π-periodicity of the potential profile. A convenient way of fabricating such qubits is to use grain-boundary DD junctions, where a two-well potential profile has indeed been observed.[104] Operations of such qubits are based on the tunable coupling of the islands to a large superconducting ''bus'' and would allow the realization of a universal set of quantum gates.[116]

A more advanced design was fabricated and tested in the classical regime in Ref. 117. Here two bistable d-wave grain-boundary junctions with a small superconducting island between them are set in a SQUID loop. (The junctions themselves are also small, so that the total capacitance of the system allows phase tunneling.) In the case when the two junctions have the same symmetry but different critical currents, in the absence of external magnetic field there is no current passing through the big loop, and therefore the qubit is decoupled from the electromagnetic environment (''silent''). The second-order degeneracy of the potential profile at the minimum drastically reduces the decoherence due to coupling to the external circuits.

4.4. Decoherence in *d*-wave qubits

Decoherence is the major concern for any qubit implementation, especially for solid-state qubits, due to the abundance of low-energy degrees of freedom. In superconductors, this problem is mitigated by the exclusion of quasiparticle excitations due to the superconducting gap. This also explains why the very fact of existence of gapless excitations in high-T_c superconductors long served as a deterrent against serious search for macroscopic quantum coherence in these systems. An additional source of trouble may be zero-energy states (ZES) in DD junctions.

Nevertheless, recent theoretical analysis of DD junctions,[118,119] all using quasiclassical Eilenberger equations, shows that the detrimental role of nodal quasiparticles and ZES could be exaggerated.

Before turning to these results, let us first do a simple estimate of dissipation due to nodal quasiparticles in bulk d-wave superconductors.[120]

Consider, for example, a three-junction (''Delft'') qubit with d-wave phase shifters. The $|0\rangle$ and $|1\rangle$ states support, respectively, clockwise and counterclockwise persistent currents around the loop, with superfluid velocity $\mathbf{v}_s$. Tunneling between these states leads to nonzero average $\langle \dot{\mathbf{v}}_s^2 \rangle$ in the bulk of the superconducting loop.

The time-dependent superfluid velocity produces a local electric field

$$\mathbf{E} = -\frac{1}{c}\dot{\mathbf{A}} = \frac{m}{e}\dot{\mathbf{v}}_s, \tag{27}$$

and quasiparticle current $\mathbf{j}_{\rm qp} = \sigma \mathbf{E}$. The resulting average energy dissipation rate per unit volume is

$$\dot{\mathcal{E}} = \sigma E^2 \approx m \tau_{\rm qp} \langle \overline{n}(v_s) \dot{v}_s^2 \rangle. \tag{28}$$

Here $\tau_{\rm qp}$ is the quasiparticle lifetime, and

$$\overline{n}(v_s) = \int_0^\infty d\varepsilon \overline{N}(\varepsilon)[n_F(\varepsilon - p_F v_s) + n_F(\varepsilon + p_F v_s)] \tag{29}$$

is the effective quasiparticle density. The angle-averaged density of states inside the d-wave gap is[121]

$$\overline{N}(\varepsilon) \approx N(0) \frac{2\varepsilon}{\mu \Delta_0}, \tag{30}$$

where $\mu=\Delta_0^{-1}d|\Delta(\theta)|/d\theta$, and Δ_0 is the maximal value of the superconducting order parameter. Substituting (30) in (29), we obtain

$$\overline{n}(v_s)\approx N(0)\frac{2}{\mu\Delta_0}(-T^2)[\mathrm{Li}_2(-\exp(-p_Fv_s/T)) + \mathrm{Li}_2(-\exp(p_Fv_s/T))], \tag{31}$$

where $\mathrm{Li}_2(z)$ is the dilogarithm. Expanding for small $p_Fv_s \ll T$, we obtain

$$\overline{n}(v_s)\approx\frac{N(0)}{\mu\Delta_0}\left(\frac{\pi^2T^2}{3}+(p_Fv_s)^2\right). \tag{32}$$

The two terms in parentheses correspond to thermal activation of quasiparticles and their generation by a current-carrying state. Note that a finite quasiparticle density by itself does not lead to any dissipation.

In the opposite limit ($T\ll p_Fv_s$) only the second contribution remains,

$$\overline{n}(v_s)\approx\frac{N(0)}{\mu\Delta_0}(p_Fv_s)^2. \tag{33}$$

The energy dissipation rate gives the upper limit τ_ε for the decoherence time (since dissipation is a sufficient but not necessary condition for decoherence). Denoting by I_c the amplitude of the persistent current in the loop, by L the inductance of the loop, and by Ω the effective volume of the d-wave superconductor in which persistent current flows, we can write

$$\tau_\varepsilon^{-1}=\frac{2\dot{\mathcal{E}}\Omega}{LI_c^2}\approx\frac{2m\tau_{\mathrm{qp}}N(0)\Omega\left(\frac{\pi^2T^2}{3}\langle\dot{v}_s^2\rangle+p_F^2\langle v_s^2\dot{v}_s^2\rangle\right)}{\mu\Delta_0LI_c^2}. \tag{34}$$

Note that the thermal contribution to τ_ε^{-1} is independent of the absolute value of the supercurrent in the loop ($\propto v_s$), while the other term scales as I_c^2. Both contributions are proportional to Ω and (via $\dot{v}_s$) to ω_t, the characteristic frequency of current oscillations (i.e., the tunneling rate between clockwise and counterclockwise current states).

It follows from the above analysis that the intrinsic decoherence in a d-wave superconductor due to nodal quasiparticles can be minimized by decreasing the amplitude of the supercurrent through it, and the volume of the material where *time-dependent* supercurrents flow.

Now let us estimate the dissipation in a DD junction. First, following Refs. 115 and 122, consider a DND model with ideally transmissive ND boundaries. Due to tunneling, the phase will fluctuate, creating a finite voltage on the junction, $V=(1/2e)\dot{\chi}$, and a normal current $I_n=GV$. The corresponding dissipative function and decay decrement are

$$\mathcal{F}=\frac{1}{2}\dot{\mathcal{E}}=\frac{1}{2}GV^2=\frac{G\dot{\chi}^2}{2}\left(\frac{1}{2e}\right)^2; \tag{35}$$

$$\gamma=\frac{2}{M_Q\dot{\chi}}\frac{\partial\mathcal{F}}{\partial\dot{\chi}}=\frac{G}{4e^2M_Q}=\frac{4N_\perp E_Q}{\pi}. \tag{36}$$

Here $E_Q=e^2/2C$, $M_Q=C/16e^2=1/32E_Q$, and $N_\perp$ are the Coulomb energy, effective "mass," and number of quantum channels in the junction, respectively. The last is related to the critical Josephson current I_0 and spacing between Andreev levels in the normal part of the system, $\overline{\epsilon}=v_F/2L$, via

$$I_0=N_\perp e\overline{\varepsilon}. \tag{37}$$

We require that $\gamma/\omega_0\ll 1$, where $\omega_0=\sqrt{32N_\perp E_Q\overline{\epsilon}}/\pi$ is the frequency of small phase oscillations about a local minimum. This means that

$$N_\perp\ll\frac{\overline{\varepsilon}}{E_Q}. \tag{38}$$

The above condition allows a straightforward physical interpretation. In the absence of thermal excitations, the only dissipation mechanism in the normal part of the system is through transitions between Andreev levels, induced by fluctuation voltage. These transitions become possible if $\overline{\epsilon}<2e\overline{V}\sim\sqrt{\overline{\dot{\chi}^2}}\sim\omega_0$, which brings us back to (38). Another interpretation of this criterion arises if we rewrite it as $\omega_0^{-1}\gg(v_F/L)^{-1}$ (Ref. 115). On the right-hand side we see the time for a quasiparticle to traverse the normal part of the junction. If it exceeds the period of phase oscillations (on the left-hand side), Andreev levels simply do not have time to form. Since they provide the only mechanism for coherent transport through the system, the latter is impossible, unless our "no dissipation" criterion holds.

For a normal-layer thickness $L\sim 1000$ Å and $v_F\sim 10^7$ cm/s this criterion limits $\omega_0<10^{-12}$ s^{-1}, which is a comfortable two orders of magnitude above the tunneling splitting usually obtained in such qubits (~ 1 GHz) and can be accommodated in the above designs. Nevertheless, while presenting a useful qualitative picture, the DND model is not adequate for the task of extracting quantitative predictions.

A calculation[123] using the model of a DD junction interacting with a bosonic thermal bath gave an optimistic estimate for the quality of the tricrystal qubit, $Q>10^8$.

The role of size quantization of quasiparticles in small DD and SND structures was suggested in Refs. 113 and 115. The importance of this effect is that it would exponentially suppress the quasiparticle density and therefore the dissipation below the temperature of the quantization gap, estimated as 1–10 K. Recently this problem was investigated for a finite-width DD junction. Contrary to expectations, the size quantization as such turned out to be effectively absent on a scale exceeding ξ_0 (that is, practically irrelevant). From the practical point of view this is a moot point, since the decoherence time due to the quasiparticles in the junction, estimated in Ref. 119, already corresponds to a quality factor $\tau_\varphi/\tau_g\sim 10^6$, which exceeds by two orders of magnitude the theoretical threshold allowing a quantum computer to run indefinitely.

The expression for the decoherence time obtained in Ref. 119,

$$\tau_\varphi=\frac{4e}{\delta\varphi_2 I(\Delta t/e)}, \tag{39}$$

where $\delta\varphi$ is the difference between equilibrium phases in degenerate minima of the junction (i.e., $\delta\varphi=2\chi_0$ in other notation), contains the expression for the quasiparticle current in the junction at finite voltage, Δ_t/e (where Δ_t is the tunneling rate between the minima). This agrees with our back-of-the-envelope analysis: phase tunneling leads to finite

voltage in the system through the second Josephson relation, and with finite voltage comes quasiparticle current and decoherence. The quality factor is defined as $Q=\tau_\varphi\Delta_t/2\hbar$, that is, we compare the decoherence time with the tunneling time. Strictly speaking, it is the quality factor with respect to the fastest quantum operation realized by the natural tunneling between the minima at the degeneracy point. For the Rabi transitions between the states of the qubit this number is much lower (10–20 versus 8000; Ref. 108) on account of the relatively low Rabi frequency.

A much bigger threat is posed by the contribution from zero-energy bound states, which can be at least two orders of magnitude larger. We can see this qualitatively from (39): a large density of quasiparticle states close to zero energy (i.e., at the Fermi level) means that even small voltages create large quasiparticle currents, which sit in the denominator of the expression for τ_φ. Fortunately, this contribution is suppressed in the case of ZES splitting, and such splitting is always present due, e.g., to the finite equilibrium phase difference across the junction.

A similar picture follows from the analysis presented in Ref. 124. A specific question addressed there is especially important: it is known that the RC constant measured in DD junctions is consistently 1 ps over a wide range of junction sizes,[125] and it is tempting to accept this value as the dissipation rate in the system. It would be a death knell for any quantum computing application of high-T_c structures, and nearly that for any hope to see some quantum effects there. Nevertheless, it is not quite that bad. Indeed, we saw that the ZES play a major role in dissipation in a DD junction but are sensitive to phase differences across it. Measurements of the RC constant are made in the resistive regime, when a finite voltage exists across the junction, so that the phase difference grows monotonically in time, forcing the ZES to approach the Fermi surface repeatedly. Therefore τ_{RC} reflects some averaged dissipation rate. On the other hand, in a free junction with not too high a tunneling rate the phase difference obviously tends to oscillate around χ_0 or $-\chi_0$, its equilibrium values, and does not spend much time near zero or π; therefore the ZES are usually shifted from the Fermi level, and their contribution to dissipation is suppressed.

This qualitative picture is confirmed by a detailed calculation. The decoherence time is related to the phase-dependent conductance via

$$\tau_\varphi=\frac{1}{\alpha F(\chi_0)^2\delta E}\tanh\frac{\delta E}{2T}. \tag{40}$$

Here α is the dissipation coefficient, δE is the interlevel spacing in the well, and

$$G(\chi)=4e^2\alpha[\partial_\chi F(\chi)]^2. \tag{41}$$

For a realistic choice of parameters Eq. (40) gives a conservative estimate $\tau_\varphi=1-100$ ns, and quality factor $Q\sim 1-100$. This is, of course, too little for quantum computing, but quite enough for observation of quantum tunneling and coherence in such junctions.

5. CONCLUSION

We have reviewed one of the most intriguing aspects of unconventional superconductivity, the generation of spontaneous currents in unconventional Josephson weak links. The mixing of the unconventional order parameters from the junction banks leads to the formation of a $\mathcal{T}$-breaking state in the weak link. A consequence of the time-reversal symmetry breaking is the appearance of a phase difference across the Josephson junction in the absence of current through the contact. This phenomenon, not present in conventional junctions between standard superconductors, radically changes the physics of weakly coupled superconductors. The current–phase relations for unconventional Josephson weak links, which we have discussed for $S^{(d)}-S^{(d)}$ and $S^{(\text{triplet})}-S^{(\text{triplet})}$ junctions, are quite different from the conventional one. Depending on the angle of misorientation of the d-wave order parameters in the banks, the current–phase relation $I_J(\varphi)$ is changed from a $\sin(\varphi)$-like curve to a $-\sin(2\varphi)$ dependence (Fig. 5). Clearly, it determines new features in the behavior of such a Josephson junction in applied voltage or magnetic field. We have discussed the simple case of an ideal interface between clean superconductors in which the spontaneous current generation effect is the most pronounced. Remaining beyond the scope of this review are a number of factors which complicate the simple models. They are the influence on the spontaneous current states of the interface roughness, potential barriers (dielectric layer), and scattering on impurities and defects in the banks. For the case of a diffusive junction see the article of Tanaka *et al.* in this issue. For the detailed theory of spontaneous currents in DD junctions see Ref. 16. The spatial distribution of spontaneous current, in particular, the effect of superscreening, is considered in Refs. 12 and 16. An important and interesting question concerns the possible induction of a subdominant order parameter near the junction interface and its influence on the value of spontaneous current. It was shown in Ref. 17 that the spontaneous currents decrease when there is interaction in the subdominant channel. This statement, which may seem paradoxical, can be explained in the language of current-carrying Andreev states (see Fig. 5 in Ref. 17). As a whole, the theory of unconventional Josephson weak links with breaking of $\mathcal{T}$ symmetry, in particular, the self-consistent consideration and nonstationary behavior, needs further development. The spontaneous bistable states in Josephson d-wave junctions attract considerable interest also from the standpoint of implementation of qubits, the basic units of quantum computers. In Sec. 4 we analyzed the application of d-wave superconductors to qubits. Unlike the Josephson charge and flux qubits based on conventional superconductors, the d-wave qubits have not yet been realized experimentally. Nevertheless, the important advantages of d-wave qubits, e.g., from the point of view of scalability, not to mention the fundamental significance of the $\mathcal{T}$-breaking phenomenon, demand future experimental investigations of unconventional weak links and devices based on them.

APPENDIX I. TEMPERATURE DEPENDENCE OF THE ORDER PARAMETER IN A *d*-WAVE SUPERCONDUCTOR

In a bulk homogeneous d-wave superconductor the BCS equation for the order parameter $\Delta(\mathbf{v}_F)$ takes the form

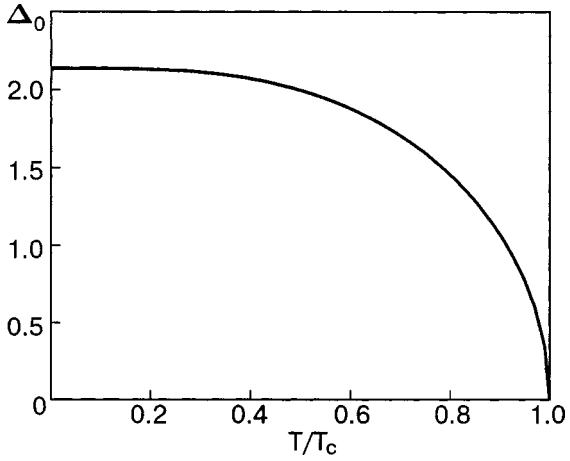

FIG. 16. Temperature dependence of the order parameter $\Delta_0(T)$ in a d-wave superconductor.

$$\Delta(\mathbf{v}_F)=2\pi N(0)T\sum_{\omega>0}\left\langle V(\mathbf{v}_F,\mathbf{v}_F')\frac{\Delta(\mathbf{v}_F')}{\sqrt{\omega^2+|\Delta(\mathbf{v}_F')|^2}}\right\rangle_{\mathbf{v}_F'} \tag{A1}$$

Or, writing $V(\mathbf{v}_F,\mathbf{v}_F')=V_d\cos 2\theta\cos 2\theta'$, $\lambda_d=N(0)V_d$, $\Delta=\Delta_0(T)\cos 2\theta$, we have for $\Delta_0(T)$

$$\Delta_0(T)=\lambda_d 2\pi T\sum_{\omega>0}^{\omega_c}\int_0^{2\pi}\frac{d\theta}{2\pi}\frac{\Delta_0(T)\cos^2 2\theta}{\sqrt{\omega^2+\Delta_0(T)^2\cos^2 2\theta}} \tag{A2}$$

($\omega=(2n+1)\pi T$, where ω_c is the cutoff frequency).

At zero temperature $T=0$, in the weak coupling limit $\lambda_d\ll 1$, for $\Delta_0(T=0)=\Delta_0(0)$ it follows from (A2) that

$$\Delta_0(0)=2\omega_c\beta\exp(-2/\lambda_d),\quad \ln\beta=\ln 2-1/2\approx 1.21.$$

The critical temperature T_c is

$$T_c=\frac{2}{\pi}\omega_c\gamma\exp(-2/\lambda_d),\quad \ln\gamma=C=0.577,\quad \gamma\approx 1.78.$$

Thus, $\Delta_0(0)/T_c=\pi\beta/\gamma\approx 2.14$.

In terms of T_c, Eq. (A2) can be presented in the form

$$\ln\frac{T}{T_c}=2\pi T\sum_{\omega>0}^{\infty}\left(2\int_0^{2\pi}\frac{d\theta}{2\pi}\frac{\cos^2 2\theta}{\sqrt{\omega^2+\Delta_0(T)^2\cos^2 2\theta}}-\frac{1}{\omega}\right). \tag{A3}$$

In the limiting cases, the solution of equation (A3) has the form

$$\Delta_0(T)=\begin{cases}\Delta_0(0)\left[1-3\varsigma(3)\left(\dfrac{T}{\Delta_0(0)}\right)^2\right], & T\ll T_c.\\ \left(\dfrac{32\pi^2}{21\varsigma(3)}\right)^{1/2}T_c\left(1-\dfrac{T}{T_c}\right)^{1/2}, & T\sim T_c.\end{cases}$$

For arbitrary temperatures $0\leqslant T\leqslant T_c$ the numerical solution of equation (A3) is shown in Fig. 16.

APPENDIX II. QUASICLASSICAL THEORY OF COHERENT CURRENT STATES IN MESOSCOPIC BALLISTIC JUNCTIONS

II.1. Basic equations

To describe the coherent current states in a superconducting ballistic microstructure we use the Eilenberger equations[80] for the ξ-integrated Green's functions

$$\mathbf{v}_F\cdot\frac{\partial}{\partial\mathbf{r}}\hat{G}_\omega(\mathbf{v}_F,\mathbf{r})+[\omega\hat{\tau}_3+\hat{\Delta}(\mathbf{v}_F,\mathbf{r}),\hat{G}_\omega(\mathbf{v}_F,\mathbf{r})]=0, \tag{A4}$$

where

$$\hat{G}_\omega(\mathbf{v}_F,\mathbf{r})=\begin{pmatrix}g_\omega & f_\omega\\ f_\omega^+ & -g_\omega\end{pmatrix}$$

is the matrix Green's function, which depends on the Matsubara frequency ω, the electron velocity on the Fermi surface $\mathbf{v}_F$, and the coordinate $\mathbf{r}$; here

$$\hat{\Delta}=\begin{pmatrix}0 & \Delta\\ \Delta^+ & 0\end{pmatrix}$$

is the superconducting order parameter. In the general case it depends on the direction of the vector $\mathbf{v}_F$ and is determined by the self-consistent equation

$$\Delta(\mathbf{v}_F,\mathbf{r})=2\pi N(0)T\sum_{\omega>0}\langle V(\mathbf{v}_F,\mathbf{v}_F')f_\omega(\mathbf{v}_F',\mathbf{r})\rangle_{\mathbf{v}_F'}. \tag{A5}$$

Solution of the matrix equation (A4) together with the self-consistent order parameter (A5) determines the current density $j(\mathbf{r})$ in the system:

$$\mathbf{j}(\mathbf{r})=-4\pi ieN(0)T\sum_{\omega>0}\langle\mathbf{v}_F g_\omega(\mathbf{v}_F,\mathbf{r})\rangle_{\mathbf{v}_F}. \tag{A6}$$

In the following we will consider the two-dimensional case; $N(0)=m/2\pi$ is the 2D density of states and $\langle\ldots\rangle=\int_0^{2\pi}d\theta/2\pi\ldots$ is the averaging over directions of the 2D vector $\mathbf{v}_F$.

Supposing the symmetry $\Delta(-\mathbf{v}_F)=\Delta(\mathbf{v}_F)$, from the equation of motion (A4) and equation (A5) we have the following symmetry relations:

$$f^*(-\omega)=f^+(\omega);\ \ g^*(-\omega)=-g(\omega);$$

$$f^*(\omega,-\mathbf{v}_F)=f^+(\omega,\mathbf{v}_F);\ \ g^*(\omega,-\mathbf{v}_F)=g(\omega,\mathbf{v}_F);$$

$$f(-\omega,-\mathbf{v}_F)=f(\omega,\mathbf{v}_F);\ \ g(-\omega,-\mathbf{v}_F)=-g(\omega,\mathbf{v}_F);$$

$$\Delta^+=\Delta^*.$$

On the phenomenological level the different types of symmetry of the superconducting pairing are determined by the symmetry of the pairing interaction $V(\mathbf{v}_F,\mathbf{v}_F')$ in Eq. (A5). For conventional (s-wave) pairing, the function $V(\mathbf{v}_F,\mathbf{v}_F')$ is constant, V_s, and the corresponding BCS interaction constant is $\lambda=N(0)V_s$. In the case of d-wave pairing $V(\mathbf{v}_F,\mathbf{v}_F')=V_d\cos 2\theta\cos 2\theta'$, $\lambda_d=N(0)V_d$. The angles θ and θ' determine the directions of vectors $\mathbf{v}_F$ and $\mathbf{v}_F'$ in the $a-b$ plane.

II.2. Analytical solutions of Eilenberger equations in the model with non-self-consistent order parameter distribution

The solutions of equation (A5) for the Green's function $\hat{G}_\omega(v_f,\mathbf{r})$ can be easily obtained for model distribution (15) of $\Delta(\mathbf{r})$. For $x\leqslant 0$:

$$f(x,\theta)=\frac{\Delta_1 e^{-i\varphi/2}}{\Omega_1}+\frac{e^{-i\varphi/2}}{\Delta_1}(\eta\Omega_1-\omega)e^{2x\Omega_1/|v_z|}C_1; \tag{A7}$$

$$f^+(x,\theta)=\frac{\Delta_1 e^{+i\varphi/2}}{\Omega_1}+\frac{e^{+i\varphi/2}}{\Delta_1}(-\eta\Omega_1-\omega)e^{2x\Omega_1/|v_z|}C_1; \tag{A8}$$

$$g(x,\theta)=\frac{\omega}{\Omega_1}+e^{2x\Omega_1/v_z}C_1. \tag{A9}$$

For $x\geqslant 0$:

$$f(x,\theta)=\frac{\Delta_2 e^{+i\varphi/2}}{\Omega_2}+\frac{e^{+i\varphi/2}}{\Delta_2}(-\eta\Omega_2-\omega)e^{-2x\Omega_2/|v_z|}C_2; \tag{A10}$$

$$f^+(x,\theta)=\frac{\Delta_2 e^{-i\varphi/2}}{\Omega_2}+\frac{e^{-i\varphi/2}}{\Delta_2}(\eta\Omega_2-\omega)e^{-2x\Omega_2/|v_z|}C_2; \tag{A11}$$

$$g(z,\theta)=\frac{\omega}{\Omega_2}+e^{-2z\Omega_2/|v_z|}C_2. \tag{A12}$$

Matching the solutions at $x=0$, we obtain

$$C_1=\frac{\Delta_1}{\Omega_1}\frac{\omega(\Delta_1-\Delta_2\cos\varphi)+i\eta\Delta_2\Omega_1\sin\varphi}{(\Omega_1\Omega_2+\omega^2+\Delta_1\Delta_2\cos\varphi)},$$

$$C_2=\frac{\Delta_2}{\Omega_2}\frac{\omega(\Delta_2-\Delta_1\cos\varphi)+i\eta\Delta_1\Omega_2\sin\varphi}{(\Omega_1\Omega_2+\omega^2+\Delta_1\Delta_2\cos\varphi)}. \tag{A13}$$

Here $\Omega_{1,2}=\sqrt{\omega^2+|\Delta_{1,2}|^2}$, $\eta=\mathrm{sign}(v_x)$.

II.3. Quasiclassical Eilenberger equations for triplet superconductors

The "transport-like" equations for the ξ-integrated Green's functions $\check{g}(\hat{\mathbf{k}},\mathbf{r},\varepsilon_m)$ can be obtained for triplet superconductors:

$$[i\varepsilon_m\check{\tau}_3-\check{\Delta},\check{g}]+iv_F\hat{k}\nabla\check{g}=0. \tag{A14}$$

The function $\check{g}$ satisfies the normalization condition

$$\check{g}\check{g}=-1. \tag{A15}$$

Here $\varepsilon_m=\pi T(2m+1)$ are discrete Matsubara energies, v_F is the Fermi velocity, and $\hat{\mathbf{k}}$ is a unit vector along the electron velocity, and $\check{\tau}_3=\tau_3\otimes\hat{I}$, and $\hat{\tau}_i$ $(i=1,2,3)$ are Pauli matrices in a particle–hole space.

The Matsubara propagator $\mathbf{g}$ can be written in the form:[96]

$$\check{g}=\begin{pmatrix} g_1+\mathbf{g}_1\hat{\sigma} & (g_2+\mathbf{g}_2\hat{\sigma})i\hat{\sigma} \\ i\hat{\sigma}_2(g_3+\mathbf{g}_3\hat{\sigma}) & g_4-\hat{\sigma}_2\mathbf{g}_4\hat{\sigma}\hat{\sigma}_2 \end{pmatrix}, \tag{A16}$$

as can be done for an arbitrary Nambu matrix. The matrix structure of the off-diagonal self-energy Δ in Nambu space is

$$\check{\Delta}=\begin{pmatrix} 0 & i\mathbf{d}\hat{\sigma}\hat{\sigma}_2 \\ i\hat{\sigma}_2\mathbf{d}^*\hat{\sigma} & 0 \end{pmatrix}. \tag{A17}$$

Below we consider so-called unitary states, for which $\mathbf{d}\times\mathbf{d}^*=0$.

The gap vector $\mathbf{d}$ has to be determined from the self-consistency equation:

$$\mathbf{d}(\hat{\mathbf{k}},\mathbf{r})=\pi TN(0)\sum_m\langle V(\hat{\mathbf{k}},\hat{\mathbf{k}}')\mathbf{g}_2(\hat{\mathbf{k}}',\mathbf{r},\varepsilon_m)\rangle, \tag{A18}$$

where $V(\hat{\mathbf{k}},\hat{\mathbf{k}}')$ is the pairing interaction potential; $\langle ...\rangle$ stands for averaging over directions of the electron momentum on the Fermi surface; $N(0)$ is the electron density of states.

Solutions of Eqs. (A14), (A18) must satisfy the conditions for the Greens's functions and the vector $\mathbf{d}$ in the banks of superconductors far from the orifice:

$$\check{g}(\mp\infty)=\frac{i\varepsilon_m\check{\tau}_3-\check{\Delta}_{1,2}}{\sqrt{\varepsilon_m^2+|\mathbf{d}_{1,2}|^2}}; \tag{A19}$$

$$\mathbf{d}(\mp\infty)=\mathbf{d}_{1,2}(\hat{\mathbf{k}})\exp\left(\mp\frac{i\varphi}{2}\right), \tag{A20}$$

where φ is the external phase difference. Equations (A14) and (A18) have to be supplemented by the boundary continuity conditions at the contact plane and conditions of reflection at the interface between superconductors. Below we assume that this interface is smooth and the electron scattering is negligible. In a ballistic case the system of 16 equations for the functions g_i and $\mathbf{g}_i$ can be decomposed into independent blocks of equations. The set of equations which enables us to find the Green's function g_1 is

$$iv_F\hat{\mathbf{k}}\nabla g_1+(\mathbf{g}_3\mathbf{d}-\mathbf{g}_2\mathbf{d}^*)=0; \tag{A21}$$

$$iv_F\hat{\mathbf{k}}\nabla\mathbf{g}_-+2i(\mathbf{d}\times\mathbf{g}_3+\mathbf{d}^*\times\mathbf{g}_2)=0; \tag{A22}$$

$$iv_F\hat{\mathbf{k}}\nabla\mathbf{g}_3-2i\varepsilon_m\mathbf{g}_3-2g_1\mathbf{d}^*-i\mathbf{d}^*\times\mathbf{g}_-=0; \tag{A23}$$

$$iv_F\hat{\mathbf{k}}\nabla\mathbf{g}_2+2i\varepsilon_m\mathbf{g}_2+2g_1\mathbf{d}-i\mathbf{d}\times\mathbf{g}_-=0, \tag{A24}$$

where $\mathbf{g}_-=\mathbf{g}_1-\mathbf{g}_4$. For the non-self-consistent model ($\Delta_{1,2}$ does not depend on the coordinates up to the interface), Eqs. (A21)–(A24) can be solved by integrating over ballistic trajectories of electrons in the right and left half-spaces. The general solution satisfying the boundary conditions (A19) at infinity is

$$g_1^{(n)}=\frac{i\varepsilon_m}{\Omega_n}+iC_n\exp(-2s\Omega_n t); \tag{A25}$$

$$\mathbf{g}_-^{(n)}=\mathbf{C}_n\exp(-2s\Omega_n t); \tag{A26}$$

$$g_2^{(n)}=\frac{-2C_n\mathbf{d}_n-\mathbf{d}_n\times\mathbf{C}_n}{-2s\eta\Omega_n+2\varepsilon_m}\exp(-2s\Omega_n t)-\frac{\mathbf{d}_n}{\Omega_n}; \tag{A27}$$

$$g_3^{(n)}=\frac{2C_n\mathbf{d}_n^*+\mathbf{d}_n^*\times\mathbf{C}_n}{-2s\eta\Omega_n-2\varepsilon_m}\exp(-2s\Omega_n t)-\frac{\mathbf{d}_n^*}{\Omega_n}, \tag{A28}$$

where t is the time of flight along the trajectory, $\mathrm{sign}(t)=\mathrm{sign}(z)=s$; $\eta=\mathrm{sign}(v_z)$; $\Omega_n=\sqrt{\varepsilon_m^2+|\mathbf{d}_n|^2}$. By matching the solutions (A25)–(A28) at the orifice plane ($t=0$), we find the constants C_n and $\mathbf{C}_n$. The index n numbers the left

$(n=1)$ and right $(n=2)$ half-spaces. The function $g_1(0) = g_1^{(1)}(-0) = g_1^{(2)}(+0)$, which determines the current density in the contact, is

$$g_1(0) = \frac{i\varepsilon_m(\Omega_1+\Omega_2)\cos\varsigma + \eta(\varepsilon_m^2+\Omega_1\Omega_2)\sin\varsigma}{\Delta_1\Delta_2+(\varepsilon_m^2+\Omega_1\Omega_2)\cos\varsigma - i\varepsilon_m\eta(\Omega_1+\Omega_2)\sin\varsigma}. \quad \text{(A29)}$$

In formula (A29) we have taken into account that for unitary states the vectors $\mathbf{d}_{1,2}$ can be written as

$$\mathbf{d}_n = \Delta_n \exp i\psi_n, \quad \text{(A30)}$$

where $\Delta_{1,2}$ are real vectors.

*E-mail: kolesnichenko@ilt.kharkov.ua

[1] J. Bardeen, L. Cooper, and J. Schriffer, Phys. Rev. **108**, 1175 (1957).
[2] P. W. Anderson and P. Morel, Phys. Rev. **123**, 1911 (1961).
[3] R. Balian and N. R. Werthamer, Phys. Rev. **131**, 1553 (1963).
[4] A. J. Leggett, Rev. Mod. Phys. **47**, 331 (1975).
[5] D. Vollhardt and P. Wöfle, *The Superfluid Phases of* ^{3}He, Taylor and Francis, New York (1990).
[6] G. Stewart, Rev. Mod. Phys. **56**, 755 (1984); G. Stewart, Z. Fisk, J. Willis, and J. L. Smith, Phys. Rev. Lett. **52**, 679 (1984).
[7] J. G. Bednorz and K. A. Muller, Z. Phys. B: Condens. Matter **64**, 189 (1986).
[8] B. D. Josephson, Phys. Lett. **1**, 251 (1962); B. D. Josephson, Adv. Phys. **14**, 419 (1965).
[9] I. O. Kulik and A. N. Omelyanchouk, Fiz. Nizk. Temp. **4**, 296 (1978) [Sov. J. Low Temp. Phys. **4**, 142 (1978)].
[10] J. Kurkijärvi, Phys. Rev. B **38**, 11184 (1988).
[11] S.-K. Yip, Phys. Rev. Lett. **83**, 3864 (1999).
[12] M. H. S. Amin, A. N. Omelyanchouk, and A. M. Zagoskin, in *New Trends in Superconductivity*, Kluwer, Dordrecht (2002), p. 95.
[13] M. Fogelstrom, S. Yip, and J. Kurkijärvi, Physica C **294**, 289 (1998).
[14] S. Yip, Phys. Rev. B **52**, 3087 (1995).
[15] R. Mahmoodi, S. N. Shevchenko, and Yu. A. Kolesnichenko, Fiz. Nizk. Temp. **28**, 262 (2002) [Low Temp. Phys. **28**, 184 (2002)].
[16] M. H. S. Amin, M. Coury, S. N. Rashkeev, A. N. Omelyanchouk, and A. M. Zagoskin, Physica B **318**, 162 (2002).
[17] M. H. S. Amin, A. N. Omelyanchouk, and A. M. Zagoskin, Phys. Rev. B **63**, 212502 (2001).
[18] V. P. Mineev and K. V. Samokhin, *Introduction to Unconventional Superconductivity*, Gordon and Breach, Amsterdam (1999).
[19] C. C. Tsuei and J. R. Kirtley, Rev. Mod. Phys. **72**, 969 (2000).
[20] J. Annett, N. Goldenfeld, and A. Leggett, *Physical Properties of High Temperature Superconductors*, Vol. 5, edited by D. M. Ginsberg, World Scientific, Singapore (1996).
[21] J. A. Sauls, Adv. Phys. **43**, 113 (1994).
[22] M. Sigrist, Prog. Theor. Phys. **99**, 899 (1998).
[23] R. Joynt and L. Taillefer, Rev. Mod. Phys. **74**, 235 (2002).
[24] L. D. Landau and E. M. Lifshitz, *Statistical Physics*, Part 1, Pergamon, New York (1979).
[25] M. Takigawa, P. C. Hammel, R. H. Heffer, and Z. Fisk, Phys. Rev. B **39**, 7371 (1989).
[26] V. Müller, Ch. Roth, E. W. Scheidt, K. Luders, E. Bucher, and N. E. Bommer, Phys. Rev. Lett. **58**, 1224 (1987).
[27] Y. J. Qian, M. F. Hu, A. Schedenstrom, H. P. Baum, J. B. Ketterson, D. Hinks, M. Levy, and B. K. Sarma, Solid State Commun. **63**, 599 (1987).
[28] Y. Maeno, H. Hashimoto, K. Yoshida, S. Nashizaki, T. Fujita, J. G. Bednorz, and F. Lichenberg, Nature (London) **372**, 532 (1994).
[29] Y. Maeno, Physica C **282–287**, 206 (1997).
[30] K. Kuroki, R. Arita, and H. Aoki, Phys. Rev. B **63**, 094509 (2001).
[31] H. Tou, Y. Kitaoka, K. Ishida, K. Asayama, N. Kimura, and Y. Onuki, Phys. Rev. Lett. **77**, 1374 (1996).
[32] K. Ishida, H. Mikuda, Y. Kitaoka, K. Asayama, Z. Q. Mao, Y. Mori, and Y. Maeno, Nature (London) **396**, 658 (1998).
[33] I. J. Lee *et al.*, cond-mat/0001332.
[34] K. Machida, T. Nishira, and T. Ohmi, J. Phys. Soc. Jpn. **68**, 3364 (1999).
[35] M. J. Graf, S.-K. Yip, and J. A. Sauls, Phys. Rev. B **62**, 14393 (2000).
[36] T. Dahm, H. Won, and K. Maki, preprint, cond-mat/0006301 (2000).
[37] M. J. Graf and A. V. Balatsky, Phys. Rev. B **62**, 9697 (2000).
[38] M. J. Graf, S.-K. Yip, and J. A. Sauls, J. Low Temp. Phys. **114**, 257 (1999).
[39] M. Sigrist, D. Agterberg, A. Furusaki, C. Honerkamp, K. K. Ng, T. M. Rice, and M. E. Zhitomirsky, Physica C **317–318**, 134 (1999).
[40] H. Won and K. Maki, Europhys. Lett. **52**, 427 (2000).
[41] Nishi Zaki *et al.*, J. Phys. Soc. Jpn. **69**, 572 (2000).
[42] I. Bonalde *et al.*, Phys. Rev. Lett. **85**, 4775 (2000).
[43] M. A. Tanatar *et al.*, Phys. Rev. B **63**, 64505 (2001).
[44] H. Matsui *et al.*, Phys. Rev. B **63**, 60505 (2001).
[45] Y. Maeno, T. M. Rice, and M. Sigrist, Phys. Today **54**, 42 (2001).
[46] T. M. Rice and M. Sigrist, J. Phys.: Condens. Matter **7**, L643 (1995).
[47] D. Agterberg, T. M. Rice, and M. Sigrist, Phys. Rev. Lett. **78**, 3374 (1997).
[48] L. Taillefer, B. Ellman, B. Lussier, and M. Poirier, Physica B **230**, 327 (1997).
[49] B. Lussier, B. Ellman, and L. Taillefer, Phys. Rev. B **53**, 5145 (1996).
[50] H. Suderow, J. P. Briston, A. Huxley, and J. Flouquet, J. Low Temp. Phys. **108**, 11 (1997).
[51] B. Ellman, L. Taillefer, and M. Porier, Phys. Rev. B **54**, 9043 (1996).
[52] G. E. Volovik and L. P. Gor'kov, Zh. Éksp. Teor. Fiz. **88**, 1412 (1985) [Sov. Phys. JETP **61**, 843 (1985)].
[53] A. Frusaki, M. Matsumoto, and M. Sigrist, Phys. Rev. B **64**, 054514 (2001).
[54] E. G. Volovik, JETP Lett. **55**, 368 (1992).
[55] E. G. Volovik, JETP Lett. **66**, 522 (1997).
[56] E. G. Volovik, and V. M. Yakovenko, J. Phys.: Condens. Matter **1**, 5263 (1980).
[57] V. M. Yakovenko, Phys. Rev. Lett. **65**, 251 (1990).
[58] V. M. Yakovenko, Phys. Rev. B **43**, 11353 (1991).
[59] E. G. Volovik and V. P. Mineev, Zh. Éksp. Teor. Fiz. **81**, 989 (1981) [Sov. Phys. JETP **54**, 524 (1981)].
[60] E. G. Volovik and V. P. Mineev, Zh. Éksp. Teor. Fiz. **86**, 1667 (1984) [Sov. Phys. JETP **59**, 972 (1984)].
[61] A. Furusaki, M. Matsumoto, and Manfred Sigrist, Phys. Rev. B **64**, 054514 (2001).
[62] A. I. Larkin, JETP Lett. **2**, 130 (1965).
[63] A. V. Balatsky *et al.*, Phys. Rev. B **51**, 15547 (1995).
[64] G. Preosti, H. Kim, and P. Muzikar, Phys. Rev. B **50**, 13638 (1994).
[65] G. A. Webb, *Nuclear Magnetic Resonance*, American Chemical Society (1997).
[66] K. K. Likharev, Rev. Mod. Phys. **51**, 101 (1979).
[67] I. O. Kulik, A. N. Omelyanchouk, and E. A. Kel'man, Fiz. Nizk. Temp. **3**, 1107 (1977) [Sov. J. Low Temp. Phys. **3**, 537 (1977)].
[68] R. de Bruyn Ouboter and A. N. Omelyanchouk, Superlattices Microstruct. **23**, 1005 (1999).
[69] M. H. S. Amin, A. N. Omelyanchouk, and A. M. Zagoskin, Fiz. Nizk. Temp. **27**, 835 (2001) [Low Temp. Phys. **27**, 616 (2002)].
[70] V. B. Geshkenbein, A. I. Larkin, and A. Barone, Phys. Rev. B **36**, 235 (1987).
[71] S. K. Yip, Phys. Rev. B **52**, 3087 (1995).
[72] Y. Tanaka and S. Kashiwaya, Phys. Rev. B **56**, 892 (1997).
[73] M. D. Fogelstrom, D. Rainer, and J. A. Sauls, Phys. Rev. Lett. **79**, 281 (1997).
[74] I. O. Kulik and I. K. Yanson, *The Josephson Effect in Superconductive Tunneling Structures*, Israel Program for Scientific Translation, Jerusalem (1972).
[75] A. Barone and G. Paterno, *Physics and Application of the Josephson Effect*, Wiley, New York (1982).
[76] A. A. Golubov, M. Yu. Kupriyanov, and E. Il'ichev, Rev. Mod. Phys. (2004) (in press).
[77] Yu. A. Kolesnichenko, A. N. Omelyanchouk, and S. N. Shevchenko, Phys. Rev. B **67**, 172504 (2004).
[78] R. Hlubina, M. Grajcar, and E. Il'ichev, cond-mat/0211255 (2002).
[79] T. Lofwander, V. S. Shumeiko, and G. Wendin, Phys. Rev. B **67**, R14653 (2000).
[80] Y. Tanuma, Y. Tanaka, M. Yamashiro, and S. Kashiwaya, Phys. Rev. B **57**, 7997 (1998).
[81] G. Eilenberger, Z. Phys. **214**, 195 (1968).
[82] A. M. Zagoskin, J. Phys.: Condens. Matter **9**, L419 (1997).
[83] A. Huck, A. van Otterlo, and M. Sigrist, Phys. Rev. B **56**, 14163 (1997).
[84] O. Avenet and E. Varoqaux, Phys. Rev. Lett. **60**, 416 (1988).
[85] S. Backhaus, S. Pereverzev, R. W. Simmond, A. Loshak, J. C. Davis, and R. E. Packard, Nature (London) **392**, 687 (1998).
[86] O. Avenet, Yu. Mukharsky, and E. Varoqaux, Physica B **280**, 130 (2000).
[87] E. V. Thuneberg, J. Kurkijärvi, and J. A. Sauls, Physica B **165&166**, 755 (1990).

[88]E. V. Thuneberg, M. Fogelström, and J. Kurkijärvi, Physica B **178**, 176 (1992).
[89]J. K. Vijas and E. V. Thuneberg, Phys. Rev. Lett. **83**, 3668 (1999).
[90]J. K. Vijas and E. V. Thuneberg, preprint, cond-mat/0107052 (2001).
[91]J. Viljas, preprint, cond-mat/0004246 (2000).
[92]A. Steane, Rep. Prog. Phys. **61**, 117 (1998).
[93]A. Kitaev, A. Shen', and M. Vialyj, *Classical and Quantum Calculations* [in Russian], Moscow MCNMO, CheRo (1999), p. 92.
[94]D. P. DiVincenzo, G. Burkard, D. Loss, and E. V. Sukhorukov, in *Quantum Mesoscopic Phenomena and Mesoscopic Devices in Microelectronics*, I. O. Kulik and R. Ellialtioglu (eds.), Vol. 559 of NATO Science Series C: Mathematical and Physical Sciences, Kluver (2000), p. 399.
[95]D. A. Lidar, L.-A. Wu, and A. Blais, Quant. Inf. Proc. **1**, 157 (2002).
[96]W. M. Kaminsky and S. Lloyd, quant-ph/0211152 (2002).
[97]E. Farhi, J. Goldstone, S. Gutmann, J. Lapan, A. Lundgren, and D. Preda, Science **292**, 472 (2001); quant-ph/0104129.
[98]W. Kaminsky, S. Lloyd, and T. P. Orlando, quant-ph/0403090.
[99]B. E. Kane, Nature (London) **393**, 133 (1999).
[100]J. R. Friedman, V. Patel, W. Chen, S. K. Tolpygo, and J. E. Lukens, Nature (London) **406**, 43 (2000).
[101]T. P. Orlando, J. E. Mooij, L. Tian, C. H. van der Wal, S. Levitov, S. Lloyd, and J. J. Mazo, Phys. Rev. B **60**, 15398 (1999).
[102]C. H. van der Wal, A. C. J. ter Haar, F. K. Wilhelm, R. N. Schouten, C. J. P. M. Harmans, T. P. Orlando, S. Lloyd, and J. E. Mooij, Science **290**, 773 (2000).
[103]E. Il'ichev, Th. Wagner, L. Fritzsch, J. Kunert, V. Schultze, T. May, H. E. Hoenig, H. G. Meyer, M. Grajcar, D. Born, W. Krech, M. V. Fistul, and A. M. Zagoskin, Appl. Phys. Lett. **80**, 4184 (2002).
[104]E. Il'ichev, N. Oukhanski, A. Izmalkov, Th. Wagner, M. Grajcar, H.-G. Meyer, A. Yu. Smirnov, A. Maassen van den Brink, M. H. S. Amin, and A. M. Zagoskin, Phys. Rev. Lett. **91**, 097906 (2003).
[105]I. Chiorescu, Y. Nakamura, C. J. P. M. Harmans, and J. E. Mooij, Science **299**, 1869 (2003).
[106]K. A. Matveev, M. Gisselfält, L. I. Glazman, M. Jonson, and R. I. Shekhter, Phys. Rev. Lett. **70**, 2940 (1993).
[107]Y. Nakamura, Yu. A. Pashkin, and J. S. Tsai, Nature (London) **398**, 786 (1999).
[108]D. Vion, A. Aassime, A. Cottet, P. Joyez, H. Pothier, C. Urbina, D. Esteve, and M. H. Devoret, Science **296**, 886 (2002).
[109]M. H. S. Amin, cond-mat/0311220.
[110]Y. Yu, S. Han, X. Chu, S.-I. Chu, and Z. Wang, Science **296**, 889 (2002).
[111]J. M. Martinis, S. Nam, and J. Aumentado, Phys. Rev. Lett. **89**, 117901 (2002).
[112]Y. G. Makhlin, G. Schoen, and A. Shnirman, Rev. Mod. Phys. **73**, 357 (2001).
[113]L. B. Ioffe, V. B. Geshkenbein, M. V. Feigel'man, A. L. Fauchere, and G. Blatter, Nature (London) **398**, 679 (1999).
[114]M. H. S. Amin, A. N. Omelyanchouk, A. Blais, A. Maassen van den Brink, G. Rose, T. Duty, and A. M. Zagoskin, Physica C **368**, 310 (2002).
[115]A. M. Zagoskin, cond-mat/9903170.
[116]A. Blais and A. M. Zagoskin, Phys. Rev. A **61**, 042308 (2000).
[117]M. H. S. Amin, A. Yu. Smirnov, A. M. Zagoskin, T. Lindstrom, S. Charlebois, T. Claeson, and A. Ya. Tzalenchuk, cond-mat/0310224.
[118]M. H. S. Amin, A. Yu. Smirnov, and A. Maassen van den Brink, Phys. Rev. B **67**, 100508(R) (2003).
[119]Ya. V. Fominov, A. A. Golubov, and M. Yu. Kupriyanov, cond-mat/0304383 (2003).
[120]A. M. Zagoskin, Doga: Turk. J. Phys. **27**, 491 (2003).
[121]D. Xu, D. K. Yip, and J. A. Sauls, Phys. Rev. B **51**, 16233 (1995).
[122]A. M. Zagoskin and M. Oshikawa, J. Phys.: Condens. Matter **10**, L105 (1998).
[123]D. M. Newns and C. C. Tsuei, US Patent No. US 6,495,854 B1 Dec. 17 (2002).
[124]M. H. S. Amin and A. Yu. Smirnov, Phys. Rev. Lett. **92**, 017001 (2004).
[125]A. Ya. Tzalenchuk, T. Lindstroöm, S. A. Charlebois, E. A. Sterantsov, Z. Ivanov, and A. M. Zagoskin, Phys. Rev. B **68**, 100501(R) (2003).

This article was published in English in the original Russian journal. Reproduced here with stylistic changed by AIP.

Charge and spin effects in mesoscopic Josephson junctions (Review)

I. V. Krive and S. I. Kulinich

Department of Applied Physics, Chalmers University of Technology, Göteborg University, SE-412 96 Göteborg, Sweden; B. Verkin Institute for Low Temperature Physics and Engineering of the National Academy of Sciences of Ukraine, 47 Lenin Ave., Kharkov 61103, Ukraine

R. I. Shekhter* and M. Jonson

Department of Applied Physics, Chalmers University of Technology, Göteborg University, SE-412 96 Göteborg, Sweden

(Submitted January 30, 2004)
Fiz. Nizk. Temp. **30**, 738–755 (July–August 2004)

We consider the charge and spin effects in low-dimensional superconducting weak links. The first part of the review deals with the effects of electron–electron interaction in Superconductor/Luttinger liquid/Superconductor junctions. The experimental realization of this mesoscopic hybrid system can be an individual single-wall carbon nanotube that bridges a gap between two bulk superconductors. The dc Josephson current through a Luttinger liquid is evaluated in the limits of perfectly and poorly transmitting junctions. The relationship between the Josephson effect in a long SNS junction and the Casimir effect is discussed. In the second part of the paper we review the recent results concerning the influence of the Zeeman and Rashba interactions on the thermodynamic properties of ballistic S–QW–S junction fabricated in a two-dimensional electron gas. It is shown that in a magnetically controlled junction there are conditions for a resonant Cooper pair transition which results in a giant supercurrent through a tunnel junction and a giant magnetic response of a multichannel SNS junction. The supercurrent induced by the joint action of the Zeeman and Rashba interactions in 1D quantum wires connected to bulk superconductors is predicted. [DOI: 10.1063/1.1789291]

1. INTRODUCTION

Since the discovery of superconductivity in 1911 this amazing macroscopic quantum phenomenon has influenced modern solid state physics more then any other fundamental discovery in the 20th century. The mere fact that five Nobel Prizes already have been awarded for discoveries directly connected to superconductivity indicates the worldwide recognition of the exceptional role superconductivity plays in physics.

Both at the early stages of the field development and later on, research in basic superconductivity brought surprises. One of the most fundamental discoveries made in superconductivity was the Josephson effect.[1] In 1962 Josephson predicted that when two superconductors are put into contact via an insulating layer (SIS junction) then (i) a dc supercurrent $J=J_c \sin\varphi$ (J_c is the critical current, φ is the superconducting phase difference) flows through the junction in equilibrium (dc Josephson effect) and (ii) an alternating current ($\varphi=\omega_J t$, $\omega_J=2eV/\hbar$, where V is the bias voltage) appears when a voltage is applied across the junction (ac Josephson effect). A year latter both the dc and the ac Josephson effect were observed in experiments.[2,3] An important contribution to the experimental proof of the Josephson effect was made by Yanson, Svistunov, and Dmitrenko,[4] who were the first to observe rf radiation from a voltage-biased contact and who measured the temperature dependence of the critical Josephson current $J_c(T)$.

As a matter of fact the discovery of the Josephson effect gave birth to a new and unexpected direction in superconductivity, namely, the superconductivity of weak links (weak superconductivity; see, e.g., Ref. 5). It soon became clear that any normal metal layer between superconductors (say, an SNS junction) will support a supercurrent as long as the phase coherence in the normal part of the device is preserved. Using the modern physical language one can say that the physics of superconducting weak links has turned out to be part of mesoscopic physics.

During the last decade the field of mesoscopic physics has been the subject of extraordinary growth and development. This has mainly been due to the recent advances in fabrication technology and to the discovery of fundamentally new types of mesoscopic systems such as carbon nanotubes (see, e.g., Ref. 6).

For our purposes metallic single-wall carbon nanotubes (SWNT) are of primary interest since they are strictly one-dimensional conductors. It has been demonstrated experimentally[7–9] (see also Ref. 10) that electron transport along an individual metallic SWNT at the low-bias-voltage regime is ballistic. At first glance this observation looks surprising. For a long time it was known (see Ref. 11) that 1D metals are unstable with respect to the Peierls phase transition, which opens up a gap in the electron spectrum at the Fermi level. In carbon nanotubes the electron–phonon coupling for conducting electrons is very weak while the Coulomb correlations are strong. The theory of metallic carbon nanotubes[12,13] shows that at temperatures outside the mK range the individual SWNT must exhibit the properties of a

two-channel spin-1/2 Luttinger liquid (LL). This theoretical prediction was soon confirmed by transport measurements on metal-SWNT and SWNT–SWNT junctions[14,15] (see also Ref. 16, where the photoemission measurements on a SWNT were interpreted as a direct observation of the LL state in carbon nanotubes). Both theory and experiments revealed strong electron–electron correlations in SWNTs.

An undoped individual SWNT is not intrinsically a superconducting material. Intrinsic superconductivity has been observed only in ropes of SWNTs (see Refs. 17 and 18). Here we consider the proximity-induced superconductivity in a LL wire coupled to superconductors (SLLS). The experimental realization of the SLLS junction could be an individual SWNT bridging a gap between two bulk superconductors.[19,20]

The dc Josephson current through a LL junction was evaluated for the first time in Ref. 21. In that paper a tunnel junction was considered in a geometry (see subsection 2.2) that is very suitable for theoretical calculations but probably difficult to realize in an experiment. It was shown that the Coulomb correlations in a LL wire strongly suppress the critical Josephson current. The opposite limit—a perfectly transmitting SLLS junction—was studied in Ref. 22, where it was demonstrated by a direct calculation of the dc Josephson current that the interaction does not renormalize the supercurrent in a fully transparent ($D=1$, where D is the junction transparency) junction. In subsection 2.2 we re-derive and explain these results using the boundary Hamiltonian method.[23]

The physics of quantum wires is not reduced to the investigations of SWNTs. Quantum wires can be fabricated in a two-dimensional electron gas (2DEG) by using various experimental methods. Some of them (e.g., the split-gate technique) originate from the end of the 1980s, when the first transport experiments with a quantum point contact (QPC) revealed unexpected properties of quantized electron ballistic transport (see, e.g., Ref. 24). In subsection 2.1 we briefly review the results concerning the quantization of the critical supercurrent in a QPC.

In quantum wires formed in a 2DEG the electron–electron interaction is less pronounced[25] than in SWNTs (presumably due to the screening effects of the nearby bulk metallic electrodes). The electron transport in these systems can in many cases be successfully described by Fermi liquid theory. For noninteracting quasiparticles the supercurrent in an SNS ballistic junction is carried by Andreev levels. For a long ($L \gg \xi_0 = \hbar v_F/\Delta$, where L is the junction length and Δ is the superconducting energy gap), perfectly transmitting junction the Andreev–Kulik spectrum[26] for quasiparticle energies $E \ll \Delta$ is a set of equidistant levels. In subsection 2.3 we show that this spectrum corresponds to twisted periodic boundary conditions for chiral (right- and left-moving) electron fields and calculate the thermodynamic potential of an SNS junction using field theoretical methods. In this approach there is a close connection between the Josephson effect and the Casimir effect.

In Section 3 of our review we consider the spin effects in ballistic Josephson junctions. As is well known, the electron spin does not influence the physics of standard SIS or SNS junctions. Spin effects become significant for SFS junctions (here "F" denotes a magnetic material) or when spin-dependent scattering on magnetic impurities is considered. As a rule, magnetic impurities tend to suppress the critical current in Josephson junction by inducing spin-flip processes.[27,28] Another system where spin effects play an important role is a quantum dot (QD). Intriguing new physics appears in normal and superconducting charge transport through a QD at very low temperatures when the Kondo physics starts to play a crucial role in the electron dynamics. Last year a vast literature was devoted to these problems.

Here we discuss the spin effects in a ballistic SNS junction in the presence of: (i) the Zeeman splitting due to a local magnetic field acting only on the normal part of the junction, and (ii) strong spin–orbit interaction, which is known to exist in quantum heterostructures due to the asymmetry of the electrical confining potential.[29] It is shown in subsection 3.1. that in a magnetically controlled single-barrier junction there are conditions when superconductivity in the leads strongly enhances electron transport, so that a giant critical Josephson current appears, $J_c \sim \sqrt{D}$. The effect is due to resonant electron transport through de Gennes–Saint-James energy levels split by tunneling.

The joint action of Zeeman splitting and superconductivity (see subsection 3.2.) results in yet another unexpected effect—a giant magnetic response, $M \sim N_\perp \mu_B$, (M is the magnetization, $N_\perp$ is the number of transverse channels of the wire, and μ_B is the Bohr magneton) of a multichannel quantum wire coupled to superconductors.[30] This effect can be understood in terms of the Andreev level structure which gives rise to an additional (superconductivity-induced) contribution to the magnetization of the junction. The magnetization has peaks at special values of the superconducting phase difference when the Andreev energy levels at $E_\pm = \pm \Delta_Z$ (ΔZ is the Zeeman energy splitting) become $2N_\perp$-fold degenerate.

The last two subsections of Sec. 3 deal with the influence of the Rashba effect on the transport properties of quasi-1D quantum wires. Strong spin–orbit (SO) interaction experienced by 2D electrons in heterostructures in the presence of additional lateral confinement results in a dispersion asymmetry of the electron spectrum in a quantum wire and in a strong correlation between the direction of electron motion along the wire (right/left) and the electron spin projection.[31,32]

The chiral properties of electrons in a quantum wire cause nontrivial effects when the wire is coupled to bulk superconductors. In particular, in subsection 3.4 we show that the Zeeman splitting in an S–QW–S junction induces an anomalous supercurrent, which is a Josephson current that persists even at zero phase difference between the superconducting banks.

In Conclusion we once more emphasize the new features of the Josephson current in ballistic mesoscopic structures and briefly discuss the novel effects that could appear in an ac Josephson current through an ultrasmall superconducting quantum dot.

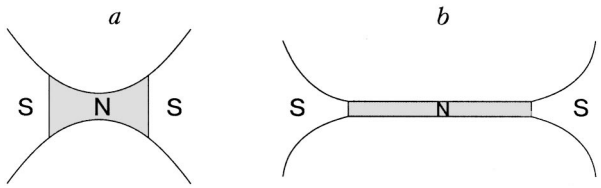

FIG. 1. A schematic picture of a superconducting point contact (a). Quantum wire adiabatically connected to bulk superconductors (b).

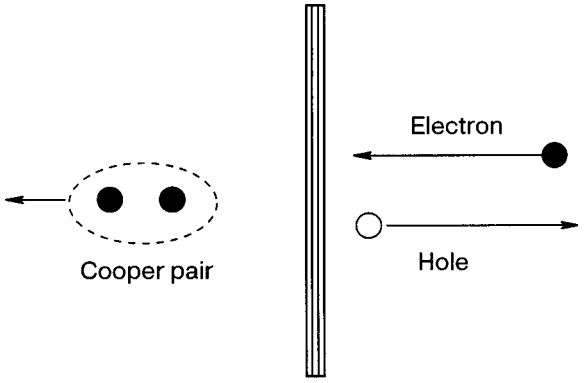

FIG. 2. A schematic illustration of Andreev reflection.

2. JOSEPHSON CURRENT THROUGH A SUPERCONDUCTOR–QUANTUM WIRE–SUPERCONDUCTOR JUNCTION

In this chapter we consider the Josephson current in a quantum wire coupled to bulk superconductors. One could expect that the conducting properties of this system depend strongly on the quality of the electrical contacts between the QW and the superconductors. The normal conductance of a QW coupled to electron reservoirs in Fermi liquid theory is determined by the transmission properties of the wire (see, e.g., Ref. 33). For the ballistic case the transmission coefficient of the system in the general situation of nonresonant electron transport depends only on the transparencies of the potential barriers which characterize the electrical contacts and does not depend on the length L of the wire. As already was mentioned in the Introduction, the Coulomb interaction in a long 1D (or few transverse channel) QW is strong enough to convert the conduction electrons in the wire into a Luttinger liquid. Then the barriers at the interfaces between the QW and electron reservoirs are strongly renormalized by electron–electron interaction, and the conductance of the N–QW–N junction at low temperature strongly depends on the wire length.[34] For a long junction and repulsive electron–electron interaction the current through the system is strongly suppressed. The only exception is the case of perfect (adiabatic) contacts when the backscattering of electrons at the interfaces is negligibly (exponentially) small. In the absence of electron backscattering the conductance G is not renormalized by interaction[35] and coincides with the conductance quantum $G=2e^2/h$ (per channel). From the theory of Luttinger liquids it is also known[36] that for a strong repulsive interaction the resonant transition of electrons through a double-barrier structure is absent even for symmetric barriers.

The well-known results listed above for the transport properties of a 1D Luttinger liquid (see, e.g., Ref. 37) allow us to consider two cases when studying ballistic S–QW–S junctions: (i) a transparent junction ($D=1$), and (ii) a tunnel junction ($D\ll 1$). These two limiting cases are sufficient to describe the most significant physical effects in S–QW–S junctions.

2.1. Quantization of the Josephson current in a short ballistic junction

At first we consider a short, $L\ll\xi_0$, ballistic S–QW–S junction. One of the realizations of this mesoscopic device is a quantum point contact (QPC) in a 2DEG (see Fig. 1a). For a QPC the screening of the Coulomb interaction is qualitatively the same as in a pure 2D geometry and one can evaluate the Josephson current through the constriction in a non-interacting electron model. Then due to Andreev backscattering of quasiparticles at the SN interfaces, a set of Andreev levels is formed in the normal part of the junction.[26] In a single-mode short junction the spectrum of bound states takes the form[38] ($L/\xi_0\to 0$)

$$E_{\pm}=\pm\Delta\sqrt{1-D\sin^2(\varphi/2)} \tag{1}$$

where φ is the superconducting phase difference. This spectrum does not depend on the Fermi velocity, and therefore the Andreev levels, Eq. (1), in a junction with $N_\perp$ transverse channels are $2N_\perp$ degenerate (the factor of 2 is due to spin degeneracy).

It is well known (see, e.g., Refs. 39 and 40) that the continuum spectrum in the limit $L/\xi_0\to 0$ does not contribute to the Josephson current,

$$J=\frac{e}{\hbar}\frac{\partial\Omega}{\partial\varphi}, \tag{2}$$

where Ω is the thermodynamic potential. It is evident from Eqs. (1) and (2) that the Josephson current through a QPC ($D=1$) is quantized.[39] At low temperatures ($T\ll\Delta$) we have[39]

$$J=N_\perp\frac{e\Delta}{\hbar}\sin\frac{\varphi}{2}. \tag{3}$$

This effect[1)] is the analog of the famous conductance quantization in QPCs (see Ref. 41).

Now let us imagine that the geometry of the constriction allows one to treat the QPC as a 1D quantum wire of finite length L smoothly connected to bulk superconductors (Fig. 1b). The 1D wire is still much shorter than the coherence length ξ_0. How does the weakly screened Coulomb interaction in a 1D QW influence the Josephson current in a fully transmitting ($D=1$) junction? Notice that the charge is freely transported through the junction, since the real electrons are not backscattered by the adiabatic constriction.[2] Thus it is reasonable to assume that the Coulomb interaction in this case does not influence the Josephson current at all. We will prove this assumption for the case of a long junction in the next Section. If the QW is separated from the leads by potential barriers (quite a natural situation in a real experiment) the charging effects have to be taken into account. As a rule, the Coulomb correlations, which tend to keep the number of electrons in the normal region (quantum dot in our case) constant, suppress the critical supercurrent due to

the Coulomb blockade effect (see, e.g., Ref. 43, where a consistent theory of the Coulomb blockade of Josephson tunneling was developed). They can also change the φ dependence of the Josephson current. One possible scenario for how charging effects influence the Josephson current in a short SNS junction is considered in Ref. 44.

2.2. Luttinger liquid wire coupled to superconductors

A consistent theory of electron–electron interaction effects in weak superconductivity has been developed for a long 1D or quasi-1D SNS junction, when the normal region can be modeled by a Luttinger liquid (LL). The standard approach to this problem (see, e.g., Ref. 23) is to use for the description of electron transport through the normal region the LL Hamiltonian with boundary conditions which take into account the Andreev[45] and normal backscattering of quasiparticles at the NS interfaces.

The LL Hamiltonian H_{LL} expressed in terms of charge density operators $\tilde{\rho}_{R/L,\uparrow/\downarrow}$ of right/left moving electrons with up/down spin projection takes the form (see, e.g., Ref. 46)

$$H_{LL}=\pi\hbar\int dx\,[u(\tilde{\rho}^2_{R\uparrow}+\tilde{\rho}^2_{L\uparrow}+\tilde{\rho}^2_{R\downarrow}+\tilde{\rho}^2_{L\downarrow}) + \frac{V_0}{\pi\hbar}(\tilde{\rho}_{R\uparrow}\tilde{\rho}_{R\downarrow}+\tilde{\rho}_{L\uparrow}\tilde{\rho}_{L\downarrow}+\tilde{\rho}_{R\uparrow}\tilde{\rho}_{L\uparrow}+\tilde{\rho}_{R\downarrow}\tilde{\rho}_{L\downarrow}+\tilde{\rho}_{R\uparrow}\tilde{\rho}_{L\downarrow}+\tilde{\rho}_{R\downarrow}\tilde{\rho}_{L\uparrow})], \tag{4}$$

where V_0 is the strength of electron–electron interaction ($V_0\sim e^2$) and the velocity $u=v_F+V_0/2\pi\hbar$. The charge density operators of the chiral (R/L) fields obey anomalous Kac–Moody commutation relations (see, e.g., Ref. 46):

$$[\tilde{\rho}_{R(L)j}(x),\tilde{\rho}_{R(L)k}(x')]=\pm\frac{\delta_{jk}}{2\pi i}\frac{\partial}{\partial x}\delta(x-x'),$$

$$j,k=\uparrow,\downarrow.$$

The Hamiltonian (4) is quadratic and can easily be diagonalized by a Bogoliubov transformation

$$H^{(d)}_{LL}=\pi\hbar\int dx[v_\rho(\rho^2_{R\rho}+\rho^2_{L\rho})+v_\sigma(\rho^2_{R\sigma}+\rho^2_{L\sigma})], \tag{5}$$

where $v_{\rho(\sigma)}$ are the velocities of noninteracting bosonic modes (plasmons), $v_{\rho(\sigma)}=v_F/g_{\rho(\sigma)}$, and

$$g_\rho=\left(1+\frac{2V_0}{\pi\hbar v_F}\right)^{-1/2},\quad g_\sigma=1. \tag{6}$$

Here g_ρ and g_σ are the correlation parameters of a spin-1/2 LL in the charge (ρ) and spin (σ) sectors. Notice that $g_\rho\ll 1$ for a strongly interacting ($V_0\gg\hbar v_F$) electron system.

The Andreev and normal backscattering of quasiparticles at the NS boundaries ($x=0$ and $x=L$) can be represented by the effective boundary Hamiltonian $H_B=H^{(A)}_B+H^{(N)}_B$, with

$$H^{(A)}_B=\Delta^{(l)}_B[\Psi_{R\uparrow}(0)\Psi_{L\downarrow}(0)+\Psi_{R\downarrow}(0)\Psi_{L\uparrow}(0)]+\Delta^{(r)}_B \times[\Psi_{R\uparrow}(L)\Psi_{L\downarrow}(L)+\Psi_{R\downarrow}(L)\Psi_{L\uparrow}(L)]+\text{h.c.}, \tag{7}$$

$$H^{(N)}_B=V^{(l)}_B\sum_{j,\sigma}\Psi^\dagger_{j\sigma}(0)\Psi_{j\sigma}(0)+V^{(r)}_B\sum_{j,\sigma}\Psi^\dagger_{j\sigma}(L)\Psi_{j\sigma}(L), \tag{8}$$

where $j=(L,R)$ and $\sigma=(\uparrow,\downarrow)$. Here $\Delta^{(l,r)}_B$ is the effective boundary pairing potential at the left (right) NS interface, and $V^{(l,r)}_B$ is the effective boundary scattering potential. The values of these potentials are related to the phase of the superconducting order parameters in the banks and to the normal scattering properties at the left and right interfaces. They can be considered either as input parameters (see, e.g., Ref. 47) or they can be calculated by using some particular model of the interfaces.[23] In what follows we will consider two limiting cases: (i) poorly transmitting interfaces $V^{(l,r)}_B\to\infty$ (tunnel junction) and (ii) perfectly transmitting interfaces $V^{(l,r)}_B\to 0$.

At first we relate the effective boundary pairing potentials $\Delta^{(l,r)}_B$ to the amplitudes $r^{(l,r)}_A$ of the Andreev backscattering process.[48,49] Let us consider for example the Andreev backscattering of an electron at the left interface. This process can be described as the annihilation of two electrons with opposite momenta and spin projections at $x=0$. The corresponding Hamiltonian is $h_A\sim r^{*(l)}_A a_{p,\uparrow}a_{-p,\downarrow}$, or equivalently in the coordinate representation $h_A\sim r^{*(l)}_A\Psi_{R\uparrow}(0)\Psi_{L\downarrow}(0)$. Here r_A is the amplitude of Andreev backscattering at the left interface,

$$r^{(l)}_A=\frac{|t^{(l)}|^2\exp[i(\varphi_l+\pi/2)]}{\sqrt{|t^{(l)}|^4+4|r^{(l)}|^2}}, \tag{9}$$

$t^{(l)}$ is the transmission amplitude ($|t^{(l)}|^2+|r^{(l)}|^2=1$), and φ_l is the phase of superconducting order parameter at the left bank. An analogous expression holds for the right interface. Notice that for a tunnel junction $|t^{(l,r)}|^2\ll 1$ the amplitude of Andreev backscattering is small—it is proportional to the transparency $D_{l,r}\equiv|t^{(l,r)}|^2\ll 1$ of the barrier at the right (left) interface. Thus in our model the effective boundary pairing potential is

$$\Delta^{(l)}_B=C\hbar v_F r^{*(l)}_A,\quad \Delta^{(r)}_B=-C\hbar v_F r^{*(r)}_A, \tag{10}$$

where C is a numerical factor which will be specified later.

2.2.1. Tunnel junction

For poorly transmitting interfaces $D_{r,l}\ll 1$ the amplitude of Andreev backscattering is small and we can use perturbation theory when evaluating the phase-dependent part of the ground state energy. In second-order perturbation theory the ground-state energy takes the form

$$\delta E^{(2)}(\varphi)=\sum_j \frac{|\langle j|H_B^{(A)}|0\rangle|^2}{E_0-E_j} = \frac{1}{\hbar}\int_0^\infty d\tau \langle 0|H_B^{(A)\dagger}(\tau)H_B^{(A)}(0)|0\rangle. \quad (11)$$

Here $H_B^{(A)}(\tau)$ is the boundary Hamiltonian (7) in the imaginary-time Heisenberg representation. After substituting Eq. (7) into Eq. (11) we get the following formula for $\delta E^{(2)}$ expressed in terms of electron correlation functions:

$$\delta E^{(2)}(\varphi) = -4C\hbar v_F^2 \,\mathrm{Re}(r_A^{*(l)} r_A^{(r)} \int_0^\infty d\tau \,[<\Psi_{R\uparrow}(\tau,0)\Psi_{L\downarrow}(\tau,0)\Psi_{L\downarrow}^\dagger(0,L)\Psi_{R\uparrow}^\dagger(0,L)> + <\uparrow \Leftrightarrow \downarrow>]. \quad (12)$$

We will calculate the electron correlation function by making use of the bosonization technique. The standard bosonization formula reads

$$\Psi_{\eta,\sigma}(x,t)=\frac{1}{\sqrt{2\pi a}}\exp[i\eta\sqrt{4\pi}\Phi_{\eta,\sigma}(x,t)], \quad (13)$$

where a is the cutoff parameter ($a\sim\lambda_F$), $\eta=(R,L)\equiv(1,-1)$, $\sigma=(\uparrow,\downarrow)\equiv(1,-1)$. The chiral bosonic fields in Eq. (13) are represented as follows (see, e.g., Ref. 51):

$$\Phi_{\eta,\sigma}(x,t)=\frac{1}{2}\hat{\varphi}_{\eta,\sigma}+\hat{\Pi}_\sigma\frac{x-\eta v t}{L}+\varphi_{\eta,\sigma}(x,t). \quad (14)$$

Here the zero mode operators $\hat{\varphi}_{\eta,\sigma}$ and $\hat{\Pi}_\sigma$ obey the standard commutation relations for ''coordinate'' and ''momentum,'' $[\hat{\varphi}_{\eta,\sigma},\hat{\Pi}_{\sigma'}]=-i\eta\delta_{\sigma,\sigma'}$. They are introduced for a finite length LL to restore correct canonical commutation relations for bosonic fields.[50,51] Notice that the topological modes associated with these operators fully determine the Josephson current in a transparent ($D=1$) SLLS junction.[22] The nontopological components $\varphi_{\eta,\sigma}(x,t)$ of the chiral scalar fields are represented by the series

$$\varphi_{\eta,\sigma}(x,t)=\sum_q \frac{1}{\sqrt{2qL}}\{\exp[iq(\eta x-vt)]\hat{b}_q+\text{h.c.}\}, \quad (15)$$

where $\hat{b}_q$ and $\hat{b}_q^\dagger$ are the standard bosonic annihilation and creation operators; L is the length of the junction, and v is the velocity.

It is convenient here to introduce[46] the charge (ρ) and spin (σ) bosonic fields $\varphi_\sigma,\theta_\rho$, which are related to the above-defined chiral fields $\varphi_{\eta,\sigma}$ by the simple linear equation

$$\begin{pmatrix}\varphi_\sigma\\ \theta_\rho\end{pmatrix}=\frac{1}{\sqrt{2}}(\varphi_{R\uparrow}\pm\varphi_{L\uparrow}\mp\varphi_{R\downarrow}-\varphi_{L\downarrow}) \quad (16)$$

(the upper sign corresponds to φ_σ and the lower sign denotes θ_ρ). After straightforward transformations Eq. (12) takes the form

$$\delta E^{(2)}(\varphi)=4C\hbar v_F^2 D\cos\varphi\int_0^\infty d\tau[\Pi_+(\tau)+\Pi_-(\tau)], \quad (17)$$

where $D=D_l D_r\ll 1$ is the junction transparency and

$$\Pi_\pm(\tau)=(2\pi a^2)^{-2}\exp\{2\pi[\langle\langle\varphi_\sigma(\tau,-L)\varphi_\sigma\rangle\rangle + \langle\langle\theta_\rho(\tau,-L)\theta_\rho\rangle\rangle\pm\langle\langle\theta_\rho(\tau,-L)\varphi_\sigma\rangle\rangle \pm\langle\langle\varphi_\sigma(\tau,-L)\theta_\rho\rangle\rangle]\}Q_\pm(\tau). \quad (18)$$

Here $\varphi_\sigma\equiv\varphi_\sigma(0,0)$, $\theta_\rho\equiv\theta_\rho(0,0)$, and the double brackets $\langle\langle\ldots\rangle\rangle$ denote the subtraction of the corresponding vacuum average at the points $(\tau,x)=(0,0)$. Note that the superconducting properties of a LL are determined by the correlators of the bosonic fields θ_ρ and φ_σ, unlike the normal conducting properties, where the fields θ_σ and φ_ρ play a dominant role. The factors $Q_\pm(\tau)$ originate from the contribution of zero modes,

$$Q_\pm(\tau)=\exp\left\{\frac{\pi}{2}<[\hat{\Pi}_\uparrow-\hat{\Pi}_\downarrow\pm\frac{iv_F\tau}{L}(\hat{\Pi}_\uparrow+\hat{\Pi}_\downarrow)]^2>\right\}\exp(\pi v_F\tau/L). \quad (19)$$

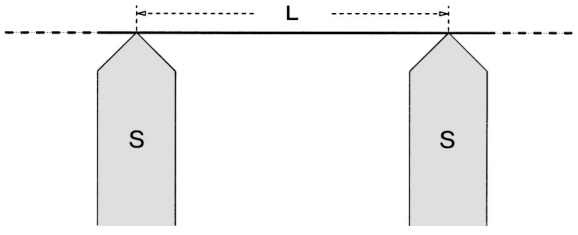

FIG. 3. A schematic picture of an SLLS junction formed by an effectively infinite Luttinger liquid coupled to bulk superconductors by side electrodes.

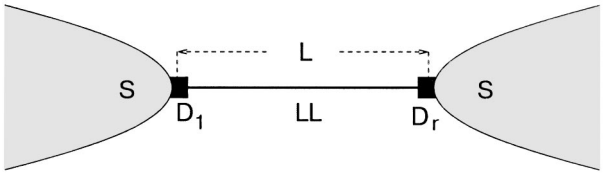

FIG. 4. A Luttinger liquid wire of length L coupled to bulk superconductors via tunnel barriers with transparencies $D_{l(r)}$.

With the help of a Bogoliubov transformation the chiral bosonic fields in Eq. (16) can be expressed in terms of noninteracting plasmonic modes with known propagators (see, e.g., Ref. 46). Two different geometries of SLLS junction have been considered in the literature, viz., an effectively infinite LL connected by side electrodes to bulk superconductors[21] (see Fig. 3) and a finite LL wire coupled via tunnel barriers to superconductors.[47,52] Notice that both model geometries can be related to realistic contacts of a single-wall carbon nanotube with metals (see, e.g., Ref. 53 and references therein). The geometry of Fig. 3 could model the junction when electron beam lithography is first used to define the leads and then ropes of SWSN are deposited on top of the leads. A tunnel junction of the type shown schematically in Fig. 4 is produced when the contacts are applied over the nanotube rope.

The topological excitations for an effectively infinite LL ($L\to\infty$) play no role, and the corresponding contributions can be omitted in Eqs. (15) and (18), $Q_{\pm}(\tau)\equiv 1$. The propagators of noninteracting chiral bosonic fields are (see, e.g., Refs. 46)

$$\langle\langle \varphi_{R/L,j}(t,x)\varphi_{R/L,k}\rangle\rangle = -\frac{\delta_{jk}}{4\pi}\ln\frac{a\mp x+s_k t}{a}, \tag{20}$$

where $j,k=1,2$ and the plasmonic velocities $s_1=v_\rho$, $s_2=v_\sigma=v_F$ (see Eq. (6)). Finally, the expression for the Josephson current through a ''side-contacted'' LL (Fig. 3) takes the form[21]

$$J_{LL}^{(i)}=J_c^{(0)}R_i(g_\rho)\sin\varphi, \tag{21}$$

where $J_c^{(0)}=(Dev_F/4L)(C/\pi)$ is the critical Josephson current for noninteracting electrons, and $R_i(g_\rho)$ is the interaction-induced renormalization factor ($R_i(g_\rho=1)=1$):

$$R_i(g_\rho)=\frac{g_\rho}{\sqrt{\pi}}\frac{\Gamma(1/2g_\rho)}{\Gamma(1/2+1/2g_\rho)}F\left(\frac{1}{2},\frac{1}{2};\frac{1}{2g_\rho}+\frac{1}{2};1-g_\rho^2\right)\times\left(\frac{a}{L}\right)^{g_\rho^{-1}-1}. \tag{22}$$

Here g_ρ is the correlation parameter of a spin-1/2 LL in the charge sector (Eq. (6)), $\Gamma(x)$ is the gamma function, and $F(\alpha,\beta;\gamma;z)$ is the hypergeometric function (see, e.g., Ref. 54). The expression for $R_i(g_\rho)$ in integral form was derived for the first time in Ref. 21. In the limit of strong interaction $V_0/\hbar v_F\gg 1$ the renormalization factor is small:

$$R_i(g_\rho\ll 1)\simeq\frac{\pi}{2}\left(\frac{\hbar v_F}{V_0}\right)^{3/2}\left(\frac{a}{L}\right)^{\sqrt{2V_0/\pi\hbar v_F}}\ll 1, \tag{23}$$

and the Josephson current through the SLLS junction is strongly suppressed. This is nothing but a manifestation of the Kane–Fisher effect[34] in the Josephson current.

To evaluate the correlation function, Eq. (18), for a LL wire of finite length coupled to bulk superconductors via tunnel barriers (Fig. 4), we must first formulate boundary conditions for the electron wave function:

$$\Psi_\sigma(x)=\exp(ik_Fx)\Psi_{R,\sigma}(x)+\exp(-ik_Fx)\Psi_{L,\sigma}(x),\quad \sigma=\uparrow\downarrow \tag{24}$$

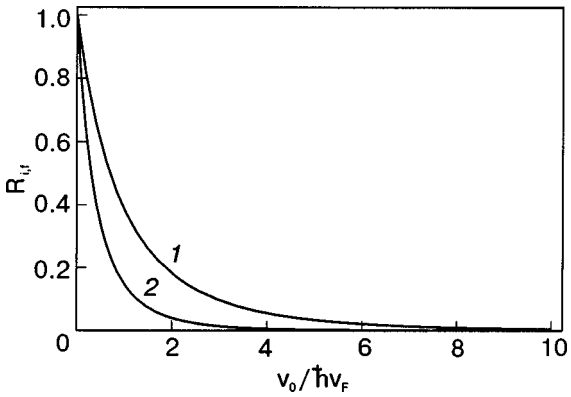

FIG. 5. Dependence of the renormalization factor $R_{i(f)}$ on the dimensionless electron–electron interaction strength $V_0/\hbar v_F$. Curve *1* corresponds to the case of a ''side-coupled'' LL wire (i), curve *2* to an ''end-coupled'' LL wire (f).

at the interfaces $x=0,L$. To zeroth order of perturbation theory in the barrier transparencies the electrons are confined to the normal region. Therefore the particle current $J_\sigma\sim\mathrm{Re}(i\Psi_\sigma^*\partial_x\Psi_\sigma)$ through the interfaces is zero. For a single-mode LL this requirement is equivalent to the following boundary condition for the chiral fermionic fields:[50,52]

$$\Psi_{R,\sigma}^*(x)\Psi_{R,\sigma}(x)\big|_{x=0,L}=\Psi_{L,\sigma}^*(x)\Psi_{L,\sigma}(x)\big|_{x=0,L}. \tag{25}$$

These boundary conditions (LL with open ends) result in zero eigenvalues of the ''momentum''-like zero mode operator $\hat{\Pi}_\sigma$ and in the quantization of nontopological modes on a ring with circumference $2L$ (see Ref. 50). In this case the plasmon propagators take the form

$$\langle\langle \varphi_{L,j}(t,x)\varphi_{RL,k}\rangle\rangle = -\frac{\delta_{jk}}{4\pi}\ln\frac{1-\exp[i\pi(\pm x-s_kt+ia)]}{\pi a/L}. \tag{26}$$

Using Eqs. (2), (17)–(19), and (26), one readily gets the expression, analogous to Eq. (21), for the Josephson current: $J_{LL}^{(f)}=J_c^{(0)}R_f(g_\rho)\sin\varphi$, where now the critical Josephson current of noninteracting electron is $J_c^{(0)}=(Dev_F/4L)(C/\pi)$ and the renormalization factor ($R_f(g_\rho=1)=1$) reads

$$R_f(g_\rho)=\frac{2g_\rho^2}{2-g_\rho^2}F\left(\frac{2}{g_\rho};\frac{2}{g_\rho}-g_\rho;\frac{2}{g_\rho}-g_\rho+1,-1\right)\times\left(\frac{\pi a}{L}\right)^{2(g_\rho^{-1}-1)}. \tag{27}$$

Comparing $J_c^{(0)}$ with the well-known formula for the critical Josephson current in a low-transparency SINIS junction (see, e.g., Ref. 40), we find the numerical constant $C=\pi$.

In the limit of strong interaction, $g_\rho\ll 1$, Eq. (27) is reduced to the simple formula

$$R_f(g_\rho\ll 1)\simeq\frac{\pi}{2}\frac{\hbar v_F}{V_0}\left(\frac{\pi a}{L}\right)^{2\sqrt{2V_0/\pi\hbar v_F}}\ll 1. \tag{28}$$

The dependence of the renormalization factor given by Eqs. (22), (27) on the strength of the electron–electron interaction $V_0/\hbar v_F$ is shown in Fig. 5. The behavior of the Josephson current as a function of the interaction strength is similar for

the two geometries considered. However we see that the interaction influences the supercurrent more strongly for the case of an ''end-coupled'' LL wire.

2.2.2. Transparent junction

This is the case of perfectly transmitting interfaces in terms of the boundary Hamiltonians (7), (8), which formally correspond to the limit $V_B \to 0$ and not small Δ_B. It cannot be treated perturbatively. Physically this means that charge is freely transported through the junction and only pure Andreev reflection takes place at the NS boundaries. It is well known that at energies much smaller than the superconducting gap ($E \ll \Delta$) the scattering amplitude of quasiparticles becomes energy independent (see Eq. (9)). This enables one to represent the Andreev scattering process as a boundary condition for a real-space fermion operator. It was shown in Ref. 22 that the corresponding boundary condition for chiral fermion fields takes the form of a twisted periodic boundary condition over the interval $2L$,

$$\Psi_{L/R,\pm\sigma}(x \pm 2L, t) = \exp(\pm i\vartheta)\Psi_{L/R,\pm\sigma}(x,t) \tag{29}$$

(the upper sign corresponds to the left-moving fermions, the lower sign—to right-moving particles), where $\vartheta = \pi + \varphi$, φ is the superconducting phase difference, and the phase π is acquired due to the Andreev reflection on two interfaces (see, e.g., Eq. (9)). Thus the problem can be mapped[22] to the one for the persistent current of chiral fermions on a ring of circumference $2L$. It is well known[51,55] (see also Ref. 56) that the persistent current in a perfect ring (without impurities) in the continuum model does not depend on the electron–electron interaction due to the translational invariance of the problem. This ''no-renormalization'' theorem allows us to conclude that the Josephson current in a perfectly transmitting SLLS junction coincides with the supercurrent in a long one-dimensional SNS ballistic junction:[26,57]

$$J_{LL} = J_{\text{nonint}} = \frac{4eT}{\hbar} \sum_{k=1}^{\infty} (-1)^{k+1} \frac{\sin k\varphi}{\sinh(2\pi kT/\Delta_L)}, \tag{30}$$

where T is the temperature and $\Delta_L = \hbar v_F / L$. The formal proof of this statement[22] consists in evaluating the partition function of the LL with the twisted boundary conditions, Eq. (29), supplemented by a connection between the $\Psi_{R,\sigma}$ and $\Psi_{L,\sigma}$ fields that follows from the chiral symmetry. The superconducting phase difference φ couples only to zero modes of the charge-current field θ_ρ. In a Galilelian invariant system zero modes are not renormalized by the interaction, and the partition function for an SLLS junction exactly coincides with that for a long SNS junction.

We notice here that Eq. (30) holds not only for perfectly transmitting interfaces. It also describes asymptotically at $T \ll \Delta$ the Josephson current through a tunnel junction when the interaction in the wire is assumed to be attractive. We have seen already in the previous subsection that the electron–electron interaction renormalizies the bare transparency of the junction due to the Kane–Fisher effect. The renormalization is known to suppress the electron current for a repulsive interaction and to enhance it for an attractive forces.[34] Thus one could expect that for an attractive interaction the electron interface scattering will be renormalized at low temperatures to perfect Andreev scattering.[23]

2.3. Josephson current and the Casimir effect

More then fifty years ago Casimir predicted[58] the existence of small quantum forces between grounded metallic plates in vacuum. This force (a kind of van der Waals force between neutral objects) arises due to a change of the vacuum energy (zero-point fluctuations) induced by the boundary conditions imposed by the metallic plates on the fluctuating electromagnetic fields (see Refs. 59 and 60). This force has been measured (see, e.g., one of the recent experiments[61] and the references therein), and in quantum field theory the Casimir effect is considered as the most spectacular manifestation of zero-point energy. In a general situation the shift of the vacuum energy of fluctuating fields in a constrained volume is usually called the Casimir energy E_C. For a field with zero rest mass dimensional considerations result in a simple behavior of the Casimir energy as a function of geometrical size. In 1D, $E_C \sim \hbar v/L$, where v is the velocity. Now we will show that the Josephson current in a long SNS junction from a field-theoretical point of view can be considered as a manifestation of the Casimir effect. Namely, the Andreev boundary condition changes the energy of the ''Fermi sea'' of quasiparticles in the normal region. This results in the appearance of: (i) an additional cohesive force between the superconducting banks,[30] and (ii) a supercurrent induced by the superconducting phase difference.

As a simple example we evaluate the Josephson current in a long, transparent, 1D SNS junction by using a field theoretical approach. Andreev scattering at the NS interfaces results in twisted periodic boundary conditions, Eq. (26), for the chiral fermion fields.[51] Thus the problem is reduced to the evaluation of the Casimir energy for chiral fermions on an S^1 manifold of circumference $2L$ with ''flux'' ϑ. Notice that the left- and right-moving quasiparticles feel opposite (in sign) ''flux'' (see Eq. (29)). The energy spectrum takes the form ($\Delta_L = \hbar v_F / L$)

$$E_{n,\eta}(L,\varphi) = \pi\Delta_L\left(n - \frac{1}{2} + \eta\frac{\varphi}{2\pi}\right),$$

$$n = 0, \pm 1, \pm 2, \ldots, \eta = \pm 1, \tag{31}$$

and coincides (as it should) with the electron and hole energies calculated by matching the quasiparticle wave functions at the NS boundaries.[26] The Casimir energy is defined as the shift of the vacuum energy induced by the boundary conditions

$$E_C(L,\varphi) = 2\left(-\frac{1}{2}\right)\left[\sum_{n,\eta} E_{n,\eta}(L,\varphi) - \sum_{n,\eta} E_{n,\eta}(L\to\infty)\right]. \tag{32}$$

Notice that the factor $(-1/2)$ in Eq. (32) is due to the zero-point energy of chiral fermions, and the additional factor of 2 is due to spin degeneracy. Both sums in Eq. (32) diverge, and one needs some regularization procedure to manipulate them. One of the most efficient regularization methods in the calculation of vacuum energies is the so-called generalized zeta-function regularization.[62] For the simple energy spectrum in Eq. (31), this procedure is reduced to the analytical continuation of the infinite sum over n in Eq. (32) to the complex plane,

$$E_C(\varphi) = -\pi\Delta_L \lim_{s\to -1} \sum_{n=-\infty,\,\eta=\pm 1}^{\infty} (n+a_\eta)^{-s}$$

$$= -\pi\Delta_L \sum_{\eta=\pm 1} [\zeta(-1,a_\eta)+\zeta(-1,-a_\eta)+a_\eta], \tag{33}$$

where $\zeta(s,a)$ is the generalized Riemann ζ function[54] and $a_\eta=(\pi+\eta\varphi)/2\pi$. Expressing $\zeta(-n,a)$ in terms of Bernoulli polynomials using a relation that is well known from textbooks (see Ref. 54), one gets the desired formula for the Casimir energy of a 1D SNS junction as

$$E_C = 2\pi\frac{\hbar v_F}{L}\left[\left(\frac{\varphi}{2\pi}\right)^2 - \frac{1}{12}\right], \quad |\varphi|\leqslant\pi. \tag{34}$$

The Casimir force F_C and the Josephson current J at $T=0$ are

$$F_C = -\frac{\partial E_C}{\partial\varphi} = \frac{E_C}{L}, \quad J = \frac{e}{\hbar}\frac{\partial E_C}{\partial\varphi} = \frac{ev_F}{L}\frac{\varphi}{\pi}, \quad |\varphi|\leqslant\pi. \tag{35}$$

The expression for the Josephson current coincides with the zero-temperature limit of Eq. (30). The generalization of the calculation method to finite temperatures is straightforward. The additional cohesive force between two bulk metals induced by superconductivity is discussed in Ref. 30. In that paper it was shown that for a multichannel SNS junction this force can be measured in modified AFM–STM experiments, where force oscillations in nanowires have been observed.

The calculation of the Casimir energy for a system of interacting electrons is a much more sophisticated problem. In Ref. 47 this energy and the corresponding Josephson current were calculated analytically for a special exactly solvable case of a double-boundary LL. Unfortunately the case considered there corresponds to the attractive regime of LLs ($g_\rho=2$ in our notation; see Eq. (6)), and the interesting results obtained in Ref. 47 cannot be applied for electron transport in quantum wires fabricated in a 2DEG or in individual SWNTs, where the electron–electron interaction is known to be repulsive.

3. THE EFFECTS OF ZEEMAN SPLITTING AND SPIN–ORBIT INTERACTION IN SNS JUNCTIONS

In the previous Section we considered the influence of electron–electron interactions on the Josephson current in an S–QW–S junction. Although all calculations were performed for a spin-1/2 Luttinger liquid model, it is readily seen that the spin degrees of freedom in the absence of a magnetic field are trivially involved in the quantum dynamics of our system. In essence, they do not change the results obtained for spinless particles. For noninteracting electrons spin only leads to an additional statistical factor of 2 (spin degeneracy) in the thermodynamic quantities. At the first glance spin effects could manifest themselves in SLLS junctions, since it is known that in a LL the phenomenon of spin–charge separation takes place.[46] One could naively expect some manifestations of this nontrivial spin dynamics in the Josephson current. Spin effects for interacting electrons indeed do not reduce to the appearance of statistical factor. However, as we have seen already in the previous Sections, the dependence of the critical Josephson current on the interaction strength is qualitatively the same for spin-1/2 and spinless Luttinger liquids. Thus for ease of calculations it is a common practice to investigate weak superconductivity in the model of a spinless Luttinger liquid.[47]

Spin effects in the Josephson current become important in the presence of a magnetic field, spin–orbit interactions, or spin-dependent scattering on impurities. At first we consider the effects induced by a magnetic field. Generally speaking a magnetic field influences both the normal part of the junction and the superconducting banks. It is the latter influence that determines the critical Josephson current in short and wide junctions. The corresponding problem was solved many years ago, and one can find analytical results for a short and wide junction in a magnetic field parallel to the NS interface (e.g., in Refs. 63 and 64).

In this review we are interested in the superconducting properties of junctions formed by a long ballistic quantum wire coupled to bulk superconductors. We will assume that a magnetic field is applied locally, i.e., only to the normal part of the junction (such an experiment could be realized for instance with the help of a magnetic tip and a scanning tunneling microscope). In this case the only influence of the magnetic field on the electron dynamics in a single channel (or few-channel) QW is due to the Zeeman interaction. For noninteracting electrons the Zeeman splitting lifts the double degeneracy of Andreev levels in an SNS junction and results in a periodic dependence of the critical Josephson current on magnetic field.[65]

Interaction effects can easily be taken into account for a 1D SLLS junction in a magnetic field by using bosonization techniques. The term in the Hamiltonian $\hat{H}_Z$, which describes the interaction of the magnetic field **B** with the electron spin $\mathbf{S}(x)$ is in bosonized form (see, e.g., Ref. 46)

$$\hat{H}_Z = -g_f\mu_B B_z \int dx S_z(x), S_z(x) = \frac{1}{\sqrt{2\pi}}\partial_x\varphi_\sigma, \tag{36}$$

where g_f is the g factor, μ_B is the Bohr magneton, and the scalar field φ_σ is defined in Eq. (16). As is easy to see, this interaction can be transformed away in the LL Hamiltonian by a coordinate-dependent shift of the spin bosonic field $\varphi_\sigma \Rightarrow \varphi_\sigma + \Delta_Z x/\hbar v_F\sqrt{2\pi}$, where $\Delta_Z = g_f\mu_B B$ is the Zeeman splitting. Thus the Zeeman splitting introduces an extra x-dependent phase factor in the chiral components of the fermion fields, and so the Zeeman interaction can be readily taken into account[66] by a slight change of the bosonization formula (13)

$$\psi^{(Z)}_{\eta,\sigma}(x,t) = \exp(iK_{\eta,\sigma}x)\,\psi_{\eta,\sigma}(x,t),$$

$$K_{\eta,\sigma} = \frac{\Delta_z}{4\hbar v_F}\eta\sigma, \quad \eta,\sigma=\pm 1. \tag{37}$$

The phase factor appearing in Eq. (37) results in a periodic dependence of the Josephson current on magnetic field. In the presence of Zeeman splitting the critical current, say, for an SLLS tunnel junction, Eq. (21), acquires an additional harmonic factor $\cos(\Delta_Z/\Delta_L)$, the same as for noninteracting particles.

3.1. Giant critical current in a magnetically controlled tunnel junction

Interesting physics for low-transparency junctions appears when resonant electron tunneling occurs. In this subsection we consider the special situation when the conditions for resonant tunneling through a junction are induced by superconductivity. The device we have in mind is an SNINS ballistic junction formed in a 2DEG with a tunable tunnel barrier (''I'') and a tunable Zeeman splitting which can be provided for instance with the help of a magnetic tip and a scanning tunneling microscope (STM). In quantum wires fabricated in 2DEG the effects of electron–electron interactions are not pronounced, and we will neglect them in what follows.

Resonant electron tunneling through a double-barrier mesoscopic structure is a well studied quantum phenomenon, which has numerous applications in solid state physics. The manifestations of resonant tunneling in the persistent current have recently been studied both in superconducting[67] and in normal systems.[68]

In these papers a double-barrier system was formed by the two tunnel barriers at the NS interfaces[67] or in a normal metal ring.[68] It was shown that for resonance conditions (realized for a special set of junction lengths[67] or interbarrier distances[68]) a giant persistent current appears which is of the same order of magnitude as the persistent current in a system with only a single barrier. In the case of the SINIS junction considered in Ref. 67 the critical supercurrent was found to be proportional to $\sqrt{D}$. Notice that the normal transmission coefficient for a symmetric double-barrier structure (i.e., the structure with normal leads) at resonance conditions does not depend on the barrier transparency at all. This means that for the hybrid structure considered in Ref. 67 the superconductivity actually suppresses electron transport.

Now we show[69] that in a magnetically controlled single-barrier SFIFS junction (''F'' denotes the region with nonzero Zeeman splitting) there are conditions when superconductivity in the leads strongly enhances electron transport. Namely, the proposed hybrid SFIFS structure is characterized by a giant critical current $J_c \sim \sqrt{D}$, while the normal conductance G is proportional to D.

For a single-barrier SFIFS junction of length L, where the barrier is located at a distance $l \ll L$ measured from the left bank, the spectrum of Andreev levels is determined from the transcendental equation[69]

$$\cos\frac{2E\pm\Delta_Z}{\Delta_L}+R\cos\frac{2E\pm\Delta_Z}{\Delta_{L-2l}}+D\cos\varphi=0, \tag{38}$$

where $\Delta_x=\hbar v_F/x$, $D+R=1$, and Δ_Z is the Zeeman splitting. In the limit $\Delta_Z=0$ Eq. (38) reduces to a well-known spectral equation for Andreev levels in a long ballistic SNS junction with a single barrier.[40,70]

At first we consider the symmetric single-barrier junction, i.e., the case when the scattering barrier is situated in the middle of the normal region, $l=L/2$. Then the second cosine term in the spectral equation is equal to 1, and Eq. (38) is reduced to a much simpler equation which is easily solved analytically. The evaluation of the Josephson current shows[69] that for $D \ll 1$ and for a discrete set of Zeeman splittings,

$$\Delta_Z^k=\pi(2k+1)\Delta_L, \quad k=0,1,2,..., \tag{39}$$

a resonance Josephson current (of order $\sqrt{D}$) is developed. At $T=0$ it takes the form

$$J_r(\varphi)=\frac{ev_F}{L}\sqrt{D}\frac{\sin\varphi}{|\sin(\varphi/2)|}. \tag{40}$$

This expression has the typical form of a resonant Josephson current associated with the contribution of a single Andreev level.[40] One can interpret this result as follows. Let us assume for a moment that the potential barrier in a symmetric SNINS junction is infinite. Then the system breaks up into two identical INS-hybrid structures. In each of the two systems de Gennes–Saint-James energy levels with spacing $2\pi\Delta_L$ are formed.[71] For a finite barrier these levels are split due to tunneling with characteristic splitting energy $\delta \sim \sqrt{D}\Delta_L$. The split levels, being already localized on the whole length L between the two superconductors, are nothing but the Andreev–Kulik energy levels, i.e., they depend on the superconducting phase difference. Although the partial current of a single level is large ($\sim\sqrt{D}$) (see Refs. 40 and 67), the current carried by a pair of split levels is small ($\sim D$) due to a partial cancellation. At $T=0$ all levels above the Fermi energy are empty and all levels below E_F are filled. Thus, in a system without Zeeman splitting the partial cancellation of currents carried by pairs of tunnel-split energy levels results in a small critical current ($\sim D$). The Zeeman splitting Δ_Z of order Δ_L (see Eq. (39)) shifts the two sets (''spin-up'' and ''spin-down'') of Andreev levels so that the Fermi energy lies in between the split levels. Now at $T=0$ only the lower state is occupied, and this results in an uncompensated large ($\sim\sqrt{D}$) Josephson current. Since the quantized electron–hole spectrum is formed by Andreev scattering at the NS interfaces, the resonance structure for a single-barrier junction disappears when the leads are in the normal (nonsuperconducting) state. Thus the electron transport through the normal region is enhanced by superconductivity. Electron spin effects (Zeeman splitting) are crucial for the generation of a giant Josephson current in a single-barrier junction.

The resonant transport described can occur not only in a symmetric junction. For a given value of the Zeeman splitting $\Delta_Z^{(k)}$ from Eq. (39) there is a set of points[69] (specified by their coordinates $x_m^{(k)}$ measured from the middle of the junction)

$$x_m^{(k)}=\pm\frac{m}{2k+1}L \tag{41}$$

(m is an integer in the interval $0\leqslant m\leqslant k+1/2$) at which a barrier still supports resonant transport. The temperature dependence of the giant Josephson current is determined by the energy scale $\delta\sim\sqrt{D}\Delta_L$ and therefore at temperatures $T\sim\delta$, which are much lower than Δ_L, all resonance effects are washed out.

3.2. Giant magnetic response of a quantum wire coupled to superconductors

It is known that the proximity effect produced in a wire by superconducting electrodes strongly enhances the normal conductance of the wire for certain value of the supercon-

ducting phase difference (giant conductance oscillations[72]). For ballistic electron transport this effect has a simple physical explanation[73] in terms of Andreev levels. Consider a multichannel ballistic wire perfectly (without normal electron backscattering) coupled to bulk superconductors. The wire is assumed to be connected to normal leads via tunnel contacts. In the first approximation one can neglect the electron leakage through the contacts, and then the normal part of the Andreev interferometer under consideration is described by a set of Andreev levels produced by superconducting mirrors. When the distance L between the mirrors is much longer than the superconducting coherence length $L \gg \xi_0 = \hbar v_F/\Delta$ (Δ is the superconducting gap), the spectrum takes a simple form:[26]

$$E^{(j)}_{n,\pm} = \frac{\hbar v^{(j)}_F}{2L}[\pi(2n+1) \pm \varphi], \quad n = 0, \pm 1, \pm 2, ..., \qquad (42)$$

where $v^{(j)}_F$ is the Fermi velocity of the jth transverse channel ($j = 1,2,\ldots,N_\perp$). It is evident from Eq. (42) that at special values of the phase difference $\varphi_n = \pi(2n+1)$ the energy levels belonging to different transverse channels j collapse to a single multi-degenerate ($N_\perp$-fold) level exactly at the Fermi energy. Thus resonant normal electron transport through a multichannel wire (the situation which is possible for symmetric barriers in the normal contacts) will be strongly enhanced at $\varphi = \varphi_n$. The finite transparency of the barriers results in a broadening and a shift of the Andreev levels. These effects lead to a broadening of the resonance peaks in giant conductance oscillations at low temperatures.[73]

The magnetic properties of a quantum wire coupled to superconductors can also demonstrate a behavior analogous to the giant conductance oscillations. We consider a long, perfectly transmitting SNS junction in a local (applied only to the normal region) magnetic field. In this case the only influence of the magnetic field on the Andreev level structure comes in through the Zeeman coupling. The thermodynamic potential $\Omega_A(\varphi, B)$ calculated for Zeeman-split Andreev levels is[30]

$$\Omega_A(\varphi, B) = 4T \sum_{\{j\}}^{N_\perp} \sum_{k=1}^{\infty} \frac{(-1)^k}{k} \frac{\cos k\varphi \cos k\chi_j}{\sinh(2\pi k T/\Delta^{(j)}_L)}. \qquad (43)$$

Here $\chi_j = \Delta_Z/\Delta^{(j)}_L$, where $\Delta_Z = g\mu_B B$ is the Zeeman energy splitting, $\Delta^{(j)}_L = \hbar v^{(j)}_f$, $v^{(j)}_F$ is the Fermi velocity in the jth transverse channel, and $\{j\}$ is the set of transverse quantum numbers. In Ref. 30 the normal part of the SNS junction was modeled by a cylinder of length L and cross-sectional area $S = V/L$. Hard-wall boundary conditions for the electron wave function on the cylinder surface were assumed. Then the set $\{j\}$ is determined by the quantum numbers (l,n) that label the zeroes $\gamma_{l,n}$ of the Bessel function $J_l(\gamma_{l,n}) = 0$, and the velocity $v^{(l,n)}_F$ takes the form

$$v^{(l,n)}_F = \sqrt{\frac{2}{m}\left(\varepsilon_F - \gamma^2_{ln}\frac{\pi\hbar^2 L}{2mV}\right)}. \qquad (44)$$

It is evident from Eq. (43) that the superconductivity-induced magnetization

$$M_A = -\frac{\partial \Omega_A(\varphi, B)}{\partial B} \qquad (45)$$

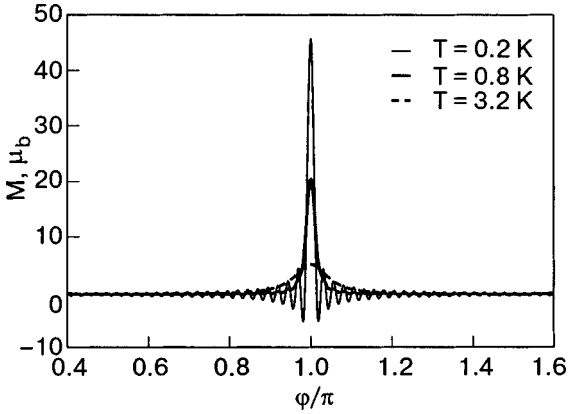

FIG. 6. Dependence of the magnetization M of an SNS junction on the superconducting phase difference for different temperatures.

at high temperatures ($T \gg \Delta_L$) is exponentially small and does not contribute to the total magnetization of the junction. At low temperatures T the magnetization has peaks at $M_A \sim N_\perp g\mu_B$, where the superconducting phase difference is an odd multiple of π (see Fig. 6, which is adapted from Ref. 30). A qualitative explanation for this resonance behavior of the magnetization is as follows. It is known[74] that for $\varphi = \varphi_n \equiv (2n+1)\pi$ (n is an integer) the two Andreev levels $E^{(\pm)}_A = \pm\Delta_Z/2$ become $2N_\perp$-fold degenerate.

At $T \to 0$ the filled state $E^{(-)}_A$ dominates in the magnetization at $\varphi = \varphi_n$, since at other values of superconducting phase the sets of Andreev levels corresponding to different transverse channels contribute to the magnetization [Eqs. (43), (45)] with different periods in "magnetic phase" χ_j (i.e., in general, incoherently), and their contributions partially cancel each other. Notice also that for a fixed volume V, the number of transverse channels $N_\perp$ has a steplike dependence on the wire diameter. Thus at resonance values of the phase difference $\varphi = \varphi_n$ one can expect a steplike behavior of the magnetization as a function of wire diameter.[30] This effect is a magnetic analog of the Josephson current quantization in a short SNS junction,[39] considered in Sec. 2.1.

3.3. Rashba effect and chiral electrons in quantum wires

Another type of system where spin is nontrivially involved in the quantum dynamics of electrons are conducting structures with strong spin–orbit (SO) interaction. It has long been known[29] that the SO interaction in the 2DEG formed in a GaAs/AlGaAs inversion layer is strong due to the structural inversion asymmetry of the heterostructure. The appearance in quantum heterostructures of a spin–orbit coupling linear in electron momentum is now called the Rashba effect. The Rashba interaction is described by the Hamiltonian

$$H^{(R)}_{\rm SO} = i\alpha_{\rm SO}\left(\sigma_y \frac{\partial}{\partial x} - \sigma_x \frac{\partial}{\partial y}\right), \qquad (46)$$

where $\sigma_{x(y)}$ are the Pauli matrices. The strength of the spin–orbit interaction is determined by the coupling constant $\alpha_{\rm SO}$, which ranges over a wide interval $(1-10)\times 10^{-10}$ eV·cm for different systems (see, e.g., Ref. 31 and references therein). Recently it was shown experimentally[75–77] that the strength of the Rashba interaction can be controlled by a gate

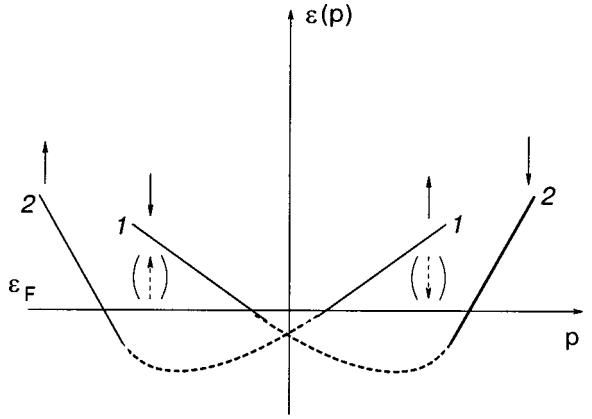

FIG. 7. Schematic energy spectrum of 1D electrons with dispersion asymmetry. Particles with energies close to the Fermi energy ε_F have an almost linear dependence on momentum and are classified by their Fermi velocities (v_{1F} subband *1*, v_{2F} subband *2*). The solid lines for spin projections correspond to the case of weak SO interaction; the arrows in parentheses indicate the spin projections in subband *1* for strong Rashba interaction.

voltage $\alpha_{\rm SO}(V_G)$. This observation makes the Rashba effect a very attractive and useful tool in spintronics. The best known proposal based on the Rashba effect is the spin-modulator device of Datta and Das.[78]

The spin–orbit interaction lifts the spin degeneracy of the 2DEG energy bands at $\mathbf{p}\neq 0$ ($\mathbf{p}$ is the electron momentum). The Rashba interaction [Eq. (46)] produces two separate branches for ''spin-up'' and ''spin-down'' electron states:

$$\varepsilon(\mathbf{p})=\frac{\mathbf{p}^2}{2m}\pm\frac{\alpha_{\rm SO}}{\hbar}|\mathbf{p}|. \tag{47}$$

Notice that under the conditions of the Rashba effect the electron spin lies in a 2D plane and is always perpendicular to the electron momentum. By the terms ''spin-up'' (''spin-down'') we imply two opposite spin projections at a given momentum. The spectrum (47) does not violate left–right symmetry; that is, the electrons with opposite momenta ($\pm\mathbf{p}$) have the same energy. Actually, the time reversal symmetry of the spin–orbit interaction [Eq. (46)] imposes less strict limitations on the electron energy spectrum, namely, $\varepsilon_\sigma(-\mathbf{p})=\varepsilon_{-\sigma}(\mathbf{p})$, and thus the Rashba interaction can in principle break the chiral symmetry. In Ref. 31 it was shown that in quasi-1D quantum wires formed in a 2DEG by a laterally confining potential the electron spectrum is characterized by a dispersion asymmetry $\varepsilon_\sigma(-\mathbf{p})\neq\varepsilon_\sigma(\mathbf{p})$, This means that the electron spectrum linearized near the Fermi energy is characterized by two different Fermi velocities $v_{1(2)F}$ and, what is more important, electrons with large (Fermi) momenta behave as chiral particles in the sense that in each subband (characterized by Fermi velocity $v_F^{(1)}$ or $v_F^{(2)}$) the direction of the electron motion is correlated with the spin projection[31,79] (see Fig. 7). It is natural in this case to characterize the spectrum by the asymmetry parameter

$$\lambda_a=\frac{v_{1F}-v_{2F}}{v_{1F}+v_{2F}}, \tag{48}$$

which depends on the strength of the Rashba interaction $\lambda_a(\alpha_{\rm SO}=0)=0$. The asymmetry parameter grows with increase of $\alpha_{\rm SO}$ and can be considered in this model as the effective dimensional strength of the Rashba interaction in a 1D quantum wire.[31] Notice that the spectrum proposed in Refs. 31 and 79 (Fig. 7, solid lines for spin projections) does not hold for strong SO interactions, when λ_a is not small. Spin is not conserved in the presence of the SO interaction, and the prevailing spin projection of electron states in quasi-1D wires has to be independently calculated. It was shown in Ref. 32 by a direct calculation of the average electron spin projection that for energies close to ε_F the electron spin projection for strong Rashba interaction (comparable with the band splitting in the confining potential) is strongly correlated with the direction of the electron motion. Namely, the right-moving (R) and left-moving (L) electrons always have opposite spin projections regardless of their velocities (see Fig. 7, where the parentheses indicate the spin projection for strong Rashba interaction). For our choice of Rashba SO Hamiltonian, Eq. (46), the R electrons ($k_x>0$) will be ''down-polarized'' ($\langle\sigma_y\rangle=-1$) and the L electrons ($k_x<0$) will be ''up-polarized'' ($\langle\sigma_y\rangle=+1$) to minimize the main part of electron energy $\sim(\hbar^2/2m)\langle k_x+\sigma_y m\alpha_{\rm SO}/\hbar\rangle^2$ in the presence of strong spin–orbit interaction.[32]

Chiral electrons in a 1D quantum wire result in such interesting predictions as ''spin accumulation'' in normal wires[32] or Zeeman-splitting-induced supercurrent in a S–QW–S junction.[69]

3.4. Zeeman-splitting-induced supercurrent

It was shown in the previous subsection that under the conditions of the Rashba effect in 1D quantum wires the spin degree of freedom is strongly correlated with the electron momentum. This observation opens up the possibility of magnetic control of an electric current. It is well known that in ring-shaped conductors a current can be induced by magnetic flux due to the momentum-dependent interaction of the electromagnetic potential $\mathbf{A}$ with a charged particle, $H_{\rm int}=(e/mc)\mathbf{p}\cdot\mathbf{A}$. Chiral properties of electrons in quasi-1D quantum wires allow one to induce a persistent current via a pure spin (momentum-independent) interaction $H=g\mu_B\mathbf{S}\cdot\mathbf{H}$. Below we consider the Josephson current in a ballistic S–QW–S junction in the presence of Rashba spin–orbit interaction and Zeeman splitting. We will assume at first that SO interactions exist both in the normal part of the junction and in the superconducting leads, so that one can neglect the spin rotation accompanied by electron backscattering induced by SO interactions at the NS interfaces. In other words the contacts are assumed to be fully adiabatic. This model can be justified at least for a weak SO interaction. The energy spectrum of electrons in a quantum wire is shown in Fig. 7 and the effect of the SO interaction in this approach is characterized by the dispersion asymmetry parameter λ_a, Eq. (48).

For a perfectly transparent junction ($D=1$) the two subbands *1* and *2* (see Fig. 7) contribute independently to the Andreev spectrum, which is described by two sets of levels[69]

$$E_{n,\eta}^{(1)}=\pi\Delta_L^{(1)}\left(n+\frac{1}{2}+\eta\frac{\varphi+\chi_1}{2\pi}\right),$$
$$E_{m,\eta}^{(2)}=\pi\Delta_L^{(2)}\left(m+\frac{1}{2}+\eta\frac{\varphi-\chi_2}{2\pi}\right), \tag{49}$$

where the integers $n,m=0,\pm1,\pm2,\ldots$ are ordinary quantum numbers which label the equidistant Andreev levels in a long SNS junction,[26] $\eta=\pm1$, $\Delta_L^{(j)}=\hbar v_{jF}/L$ $(j=1,2)$, and φ is the superconducting phase difference. The magnetic phases $\chi_j=\Delta_Z/\Delta_L^{(j)}$ characterize the shift of Andreev energy levels induced by the Zeeman interaction. Notice that the relative sign between the superconducting phase φ and the magnetic phase χ_j is different for channels *1* and *2*. This is a direct consequence of the chiral properties of the electrons in our model. In the absence of dispersion asymmetry ($v_{1F}=v_{2F}\equiv v_F$) the two sets of levels in Eq. (49) describe the ordinary spectrum of Andreev levels in a long, transparent SFS junction ("F" stands for a normal region with Zeeman splitting):

$$E_{n,\eta,\sigma}=\pi\Delta_L\left(n+\frac{1}{2}+\eta\frac{\varphi}{2\pi}+\sigma\frac{\chi}{2\pi}\right),\quad \eta,\sigma=\pm1. \tag{50}$$

Knowing the energy spectrum explicitly [Eq. (49)], it is straightforward to evaluate the Josephson current. It takes the form[69]

$$J(\varphi,T,\Delta_Z)=\frac{2eT}{\hbar}\sum_{k=1}^{\infty}(-1)^{k+1}\left[\frac{\sin k(\varphi+\chi_1)}{\sinh(2\pi kT/\Delta_L^{(1)})}+\frac{\sin k(\varphi-\chi_2)}{\sinh(2\pi kT/\Delta_L^{(2)})}\right]. \tag{51}$$

Here T is the temperature. The formal structure of Eq. (51) is obvious. The two sums in Eq. (51) correspond to the contributions of magnetically shifted sets of levels *1* and *2* in Eq. (49). In the absence of any SO interaction the Zeeman splitting results only in an additional factor of $\cos(k\Delta_Z/\Delta_L)$ in the standard formula for the supercurrent through a perfectly transmitting long SNS junction.[57] The most striking consequence of Eq. (51) is the appearance of an anomalous Josephson current $J_{\rm an}\equiv J(\varphi=0)$, when both the Zeeman splitting (Δ_Z) and dispersion asymmetry (λ_a) are nonzero. At high temperatures $T\geqslant\Delta_L^{(j)}$ the anomalous supercurrent is exponentially small. In the low-temperature regime $T\ll\Delta_L^{(j)}$ it is a piecewise-constant function of the Zeeman energy splitting Δ_Z,

$$J_{\rm an}(\Delta_Z)=\frac{e}{\pi L}\sum_{k=1}^{\infty}\frac{(-1)^{k+1}}{k}\left[v_{1F}\sin\left(k\frac{\Delta_Z}{\Delta_L^{(1)}}\right)-v_{2F}\sin\left(k\frac{\Delta_Z}{\Delta_L^{(2)}}\right)\right]. \tag{52}$$

For rational values $v_{1F}/v_{2F}=p/q$ ($p\leqslant q$ are integers) $J_{\rm an}$ is a periodic function of the Zeeman energy splitting with period $\delta\Delta_Z=2\pi q\Delta_L^{(1)}$; otherwise it is a quasiperiodic function. The dependence of the normalized supercurrent $J_{\rm an}/J_0$ (here $J_0=ev_F/L$, $v_F=(v_{1F}+v_{2F})/2$) on the dimensionless Zeeman splitting $\chi\equiv\Delta_Z/\Delta_L$ for $\lambda_a=0.1$ and for different temperatures is shown in Fig. 8. We see that at $T=0$ the Zeeman-splitting-induced supercurrent appears abruptly at finite values of Δ_Z of the order of the Andreev level spacing.

Let us now imagine the situation when the Zeeman splitting arises due to a local magnetic field (acting only on the normal part of the junction) applied in the 2D plane normal to the quantum wire. Then the vector product of that magnetic field with the electric field (normal to the plane) that induces the Rashba interaction determines the direction of the anomalous supercurrent. In other words the change of the sign of the SO interaction in Eq. (46) or the sign of Δ_Z makes the supercurrent Eq. (52) change sign as well.

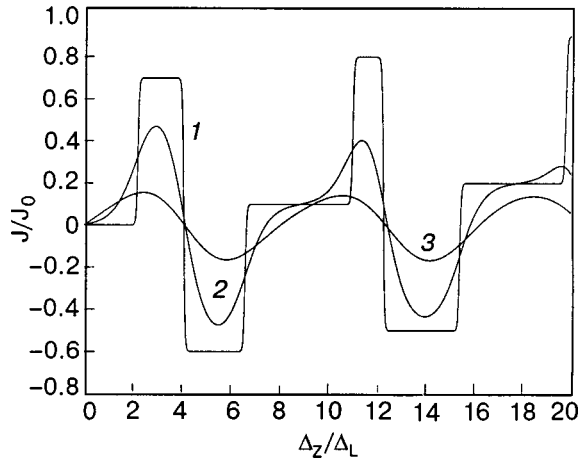

FIG. 8. Dependence of the normalized anomalous Josephson current $J_{\rm an}/J_0$ ($J_0=ev_F/L$) on the dimensionless Zeeman splitting Δ_Z/Δ_L ($\Delta_L=\hbar v_F/L$) for asymmetry parameter $\lambda_a=0.1$. The different plots correspond to different temperatures T: $0.1T^*$ (*1*); $1.5T^*$ (*2*); $3.5T^*$ (*3*), where $T^*=\Delta_L/2\pi$.

We now discuss briefly the case of a strong Rashba interaction (the characteristic momentum $k_{\rm SO}=m/\hbar\alpha_{\rm SO}(V_g)$ is of the order of the Fermi momentum). The electrons in a quantum wire with strong Rashba coupling are chiral particles; that is, the right- and left-moving particles have opposite spin projections.[32] There is no reason to assume a strong SO interaction in the 3D superconducting leads. We will follow the approach taken in Refs. 32 and 80, where the system was modeled by a quantum wire ($\alpha_{\rm SO}\neq0$) attached to semiinfinite leads with $\alpha_{\rm SO}=0$. In this model the SN interface acts as a special strong scatterer, where backscattering is accompanied by a spin-flip process. For a general nonresonant situation the dispersion asymmetry is not important in the limit of strong Rashba interaction, and we can put $v_{1F}\approx v_{2F}\approx v_F$. Then, up to a numerical factor, the Josephson current at $T=0$ takes the form

$$J(\varphi,\Delta_Z)\approx D_{\rm eff}(\alpha_{\rm SO})\frac{ev_F}{L}\sin\left(\varphi+\frac{\Delta_Z}{\Delta_L}\right). \tag{53}$$

Here $D_{\rm eff}(\alpha_{\rm SO})\ll1$ is the effective transparency of the junction. It can be calculated by solving the transition problem for the corresponding normal junction.[32] Anyway, in the NS-interface model considered (nonadiabatic switching on of the Rashba interaction) even in the limit of strong Rashba interaction the anomalous supercurrent $J_{\rm an}=J(\varphi=0,\Delta_Z)$ is small because of the smallness of the effective transparency of the junction. One could expect a large current only for the special case of a resonant transition. This problem has not yet been solved.

4. CONCLUSION

The objective of our review was to discuss the qualitatively new features of the Josephson effect that appear in

S–QW–S hybrid structures. Quantum wires are characterized by a 1D or quasi-1D character of the electron conductivity. Electron transport along QWs is ballistic, and due to the weak screening of the Coulomb interaction in 1D it is described by a Luttinger liquid theory. Thus the first question wanted to answer was, what is the Josephson effect in an SLLS junction? It was shown that although electrons do not propagate in a LL weak link the supercurrent in a perfectly transmitting SLLS junction coincides exactly with that in an SNS junction.[22] This ''no renormalization'' theorem is analogous to the result known for a LL adiabatically coupled to nonsuperconducting leads.[35] For a tunnel SILLIS junction the dc Josephson current is described by the famous Josephson current–phase relation, only now the effective transparency $D_{\rm eff} \ll 1$ defined by $J = J_0 D_{\rm eff} \sin\varphi$ (where $J_0 = ev_F/L$), depends strongly on the aspect ratio d/L of the LL wire ($d \sim \lambda_F$ is the width of the nanowire), temperature, and electron–electron interaction strength. This result[21] is a manifestation of the Kane–Fisher effect[34] in mesoscopic superconductivity. It was also interesting for us (and we hope for the reader as well) to find a close connection, rooted in the Andreev boundary conditions, between the physics of a long SNS junction and the Casimir effect (see Sec. 2.3.).

Qualitatively new behavior of the proximity-induced supercurrent in nanowires is predicted for systems with strong spin–orbit interactions. The Rashba effect in nanowires results in the appearance of chiral electrons,[31,32] for which the direction of particle motion along the wire (right or left) is strongly correlated with the electron spin projection. For chiral electrons the supercurrent can be magnetically induced via Zeeman splitting. The interplay of the Zeeman and Rashba interactions and proximity effects in quantum wires leads to effects that are qualitatively different from those predicted for 2D junctions.[81]

It is worthwhile to mention here another important trend in mesoscopic superconductivity, namely, the fabrication and investigation of superconductivity-based qubits. Among different suggestions and projects in this rapidly developing field, the creation of a so-called single-Cooper-pair box (SCPB) was a remarkable event.[82] The SCPB consists of an ultrasmall superconducting dot in tunneling contact with a bulk superconductor. A gate electrode, by lifting the Coulomb blockade of Cooper-pair tunneling, allows the delocalization of a single Cooper pair between the two superconductors. For a nanoscale grain the quantum fluctuations of the charge on the island are suppressed due to the strong charging energy associated with a small grain capacitance. By appropriately biasing the gate electrode it is possible to make the two states on the dot, differing by one Cooper pair, have the same energy. This twofold degeneracy of the ground state provides an opportunity to create a long-lived coherent mixture of two ground states (qubit).

A superconducting weak link which includes a SCPB as a tunnel element could be very sensitive to external ac fields. This problem was studied in Ref. 83, where the resonant microwave properties of a voltage-biased single-Cooper-pair transistor were considered. It was shown that the quantum dynamics of the system is strongly affected by interference between multiple microwave-induced interlevel transitions. As a result, the magnitude and the direction of the dc Josephson current are extremely sensitive to small variations of the bias voltage and to changes in the frequency of the microwave field. This picture, which differs qualitatively from the famous Shapiro effect,[3] is a direct manifestation of the role the strong Coulomb correlations play in the nonequilibrium superconducting dynamics of mesoscopic weak links.

The authors thank E. Bezuglyi, L. Gorelik, A. Kadigrobov, and V. Shumeiko for numerous fruitful discussions. Ilya V. Krive and Sergei I. Kulinich acknowledge the hospitality of the Department of Applied Physics at Chalmers University of Technology and Göteborg University. Financial support from the Royal Swedish Academy of Sciences (Sergei I. Kulinich), the Swedish Science Research Council (Robert I. Shekhter), and the Swedish Foundation for Strategic Research (Robert I. Shekhter and Mats Jonson) is gratefully acknowledged.

*E-mail: Shekhter@fy.chalmers.se

[1)]It was recently observed in: T. Bauch *et al.*, ''Supercurrent and conductance quantization in superconducting quantum point contact,'' cond-mat/0405205, May 11, 2004.

[1] B. D. Josephson, Phys. Lett. **1**, 251 (1962).
[2] P. W. Anderson and J. M. Rowell, Phys. Rev. Lett. **10**, 230 (1963).
[3] S. Shapiro, Phys. Rev. Lett. **11**, 80 (1963).
[4] I. K. Yanson, V. M. Svistunov, and I. M. Dmitrenko, Sov. Phys. JETP **48**, 976 (1965); I. K. Yanson, V. M. Svistunov, and I. M. Dmitrenko, Zh. Éksp. Teor. Fiz. **47**, 2091 (1964) [Sov. Phys. JETP **20**, 1404 (1965)].
[5] I. O. Kulik and I. K. Yanson, *Josephson Effect in Superconducting Tunnel Structures* [in Russian], Nauka, Moscow (1970).
[6] R. Saito, G. Dresselhaus, and M. S. Dresselhaus, *Physical Properties of Carbon Nanotubes*, Imperial College Press, London (1998).
[7] S. J. Tans *et al.*, Nature (London) **386**, 474 (1997).
[8] M. Bockrath *et al.*, Science **275**, 1922 (1997).
[9] A. Bachtold *et al.*, Phys. Rev. Lett. **84**, 6082 (2000).
[10] C. Dekker, Phys. Today, p. 22 (1999).
[11] R. E. Peierls, *Quantum Theory of Solids*, Oxford University Press, New York (1955).
[12] R. Egger and A. O. Gogolin, Phys. Rev. Lett. **79**, 5082 (1997), Eur. Phys. J. B **3**, 281 (1998).
[13] C. L. Kane, L. Balents, and M. P. A. Fisher, Phys. Rev. Lett. **79**, 5086 (1997).
[14] M. Bockrath *et al.*, Nature (London) **397**, 598 (1999).
[15] H. W. C. Postma *et al.*, Phys. Rev. B **62**, R10653 (2000).
[16] H. Ishii *et al.*, Nature (London) **402**, 540 (2003).
[17] M. Kociak *et al.*, Phys. Rev. Lett. **86**, 2416 (2001).
[18] A. Yu. Kasumov *et al.*, Physica B **329–333**, 1321 (2003).
[19] A. Yu. Kasumov *et al.*, Science **284**, 1508 (1999).
[20] A. F. Morpurgo *et al.*, Science **286**, 263 (1999).
[21] R. Fazio, F. W. J. Hekking, and A. A. Odintsov, Phys. Rev. Lett. **74**, 1843 (1995).
[22] D. L. Maslov *et al.*, Phys. Rev. B **53**, 1548 (1996).
[23] I. Affleck, J. S. Caux, and A. M. Zagoskin, Phys. Rev. B **62**, 1433 (2000).
[24] H. van Houten and C. Beenakker, Phys. Today **49**, 22 (1996).
[25] S. Tarucha *et al.*, Solid State Commun. **94**, 413 (1995); A. Yacoby *et al.*, Phys. Rev. Lett. **77**, 4612 (1996).
[26] I. O. Kulik, Zh. Éksp. Teor. Fiz. **57**, 1745 (1969) [Sov. Phys. JETP **30**, 944 (1970)].
[27] I. O. Kulik, Sov. Phys. JETP **22**, 841 (1966).
[28] B. I. Spivak and S. A. Kivelson, Phys. Rev. B **43** (1991).
[29] E. I. Rashba, Fiz. Tverd. Tela (Leningrad) **2**, 1224 (1960) [Sov. Phys. Solid State **2**, 1109 (1960)]; Yu. A. Bychkov and E. I. Rashba, J. Phys. C **17**, 6039 (1984).
[30] I. V. Krive, I. A. Romanovsky, E. N. Bogachek, and Uzi Landman, Phys. Rev. Lett. **92**, 126802 (2004).
[31] A. V. Moroz and C. H. W. Barnes, Phys. Rev. B **60**, 14272 (1999).
[32] M. Governale and U. Zulicke, Phys. Rev. B **66**, 073311 (2002).
[33] S. Datta, *Electronic Transport in Mesoscopic Systems*, Cambridge University Press, Cambridge (1995).
[34] C. L. Kane and M. P. A. Fisher, Phys. Rev. Lett. **68**, 1220 (1992).

[35] D. L. Maslov and M. Stone, Phys. Rev. B **52**, R5539 (1995); V. V. Ponomarenko, *ibid.* **52**, R8666 (1995); I. Safi and H. J. Schulz, *ibid.* **52**, R17040 (1995).
[36] C. L. Kane and M. P. A. Fisher, Phys. Rev. B **46**, 15233 (1992); A. Furusaki and N. Nagaosa, *ibid.* **47**, 3827 (1993).
[37] M. P. A. Fisher and L. I. Glazman, in *Mesoscopic Electron Transport*, Vol. 345 of NATO Advanced Study Institute, Series E: Applied Sciences, edited by L. L. Sohn, L. P. Kouwenhoven, and G. Schon, Kluwer, Dordrecht (1997).
[38] A. Furusaki and M. Tsukuda, Physica B **165–166**, 967 (1990); S. K. Kuplevakhskii and I. I. Fal'ko, Fiz. Nizk. Temp. **17**, 961 (1991) [Sov. J. Low Temp. Phys. **17**, 501 (1991)].
[39] C. W. J. Beenaker and H. van Houten, Phys. Rev. Lett. **66**, 3056 (1991).
[40] P. Samuelsson *et al.*, Phys. Rev. B **62**, 1319 (2000).
[41] B. J. van Wees *et al.*, Phys. Rev. Lett. **60**, 848 (1988); D. A. Wharam *et al.*, J. Phys. C **21**, L209 (1988).
[42] L. Glazman *et al.*, JETP Lett. **48**, 238 (1988).
[43] K. A. Matveev *et al.*, Phys. Rev. Lett. **70**, 2940 (1993).
[44] K. Engstom *et al.*, Low Temp. Phys. **29**, 546 (2003).
[45] A. F. Andreev, Zh. Éksp. Teor. Fiz. **46**, 1863 (1964); **49**, 655 (1965) [Sov. Phys. JETP **19**, 1228 (1964); **22**, 455 (1966)].
[46] A. O. Gogolin, A. A. Nersesyan, and A. M. Tsvelik, *Bosonization and Strongly Correlated Systems*, Cambridge University Press (1988).
[47] J. S. Caux, H. Saleur, and F. Siano, Phys. Rev. Lett. **88**, 106402 (2002).
[48] A. L. Shelankov, JETP Lett. **32**, 111 (1980).
[49] G. E. Blonder, M. Tinkham, and T. M. Klapwijk, Phys. Rev. B **25**, 4515 (1982).
[50] M. Fabrizio and A. O. Gogolin, Phys. Rev. B **51**, 17827 (1995).
[51] D. Loss, Phys. Rev. Lett. **69**, 343 (1992).
[52] J. S. Caux, A. Lopez, and D. Suppa, Nucl. Phys. B **651**, 413 (2003).
[53] R. Egger *et al.*, in *Interacting Electrons in Nanostructures*, R. Haug and H. Schoeller (eds.), Springer (2000); cond-mat/0008008 (2000).
[54] I. S. Gradshteyn and I. M. Ryzhik, *Tables of Integrals, Series and Products*, Academic Press, New York and London (1965).
[55] I. V. Krive *et al.*, Phys. Rev. B **52**, 16451 (1995).
[56] A. A. Zvyagin and I. V. Krive, Fiz. Nizk. Temp. **21**, 687 (1995) [Low Temp. Phys. **21**, 533 (1995)].
[57] C. Ishii, Prog. Theor. Phys. **44**, 1525 (1970); A. V. Svidzinsky, T. N. Antsygina, and E. N. Bratus, Zh. Éksp. Teor. Fiz. **61**, 1612 (1971) [Sov. Phys. JETP **34**, 860 (1972)].
[58] H. B. G. Casimir, Kon. Ned. Akad. Wetensch. Proc. **51**, 793 (1948).
[59] V. M. Mostepanenko and N. N. Trunov, *The Casimir Effect and its Application*, Clarendon Press, Oxford (1977).
[60] K. A. Milton, *The Casimir Effect: Physical Manifestation of Zero-Point Energy*, World Scientific (2001).
[61] G. Bressi *et al.*, Phys. Rev. Lett. **88**, 041804 (2002).
[62] S. W. Hawking, Commun. Math. Phys. **55**, 133 (1977).
[63] V. P. Galaiko and E. V. Bezuglyi, Zh. Éksp. Teor. Fiz. **60**, 1471 (1971) [Sov. Phys. JETP **33**, 796 (1971)]; G. A. Gogadze and I. O. Kulik, Zh. Éksp. Teor. Fiz. **60**, 1819 (1971). [Sov. Phys. JETP **33**, 984 (1971)].
[64] A. V. Svidzinsky, *Inhomogeneous Problems in the Theory of Superconductivity* [in Russian], Nauka, Moscow (1982).
[65] A. I. Buzdin, L. N. Bulayevskiĭ, and S. V. Panyukov, JETP Lett. **35**, 178 (1982).
[66] A. De Martino and R. Egger, Europhys. Lett. **56**, 570 (2001).
[67] G. Wendin and V. S. Shumeiko, Phys. Rev. B **53**, R6006 (1996); Superlattices Microstruct. **4**, 569 (1996).
[68] P. Sandstrom and I. V. Krive, Phys. Rev. B **56**, 9255 (1997).
[69] I. V. Krive, L. Y. Gorelik, R. I. Shekhter, and M. Jonson, Fiz. Nizk. Temp. **30**, 535 (2004) [Low Temp. Phys. **30**, 398 (2004)].
[70] P. F. Bagwell, Phys. Rev. B **46**, 12573 (1992).
[71] P. G. de Gennes and D. Saint-James, Phys. Lett. **4**, 151 (1963).
[72] V. T. Petrashov *et al.*, Phys. Rev. Lett. **70**, 347 (1993).
[73] A. Kadigrobov *et al.*, Phys. Rev. B **52**, R8662 (1995); H. A. Blom *et al.*, *ibid.* **57**, 9995 (1998).
[74] A. Kadigrobov *et al.*, Phys. Rev. B **60**, 14593 (1999).
[75] J. Nitta *et al.*, Phys. Rev. Lett. **78**, 1335 (1997).
[76] T. Schapers *et al.*, J. Appl. Phys. **83**, 4324 (1998).
[77] D. Grundler, Phys. Rev. Lett. **84**, 6074 (2000).
[78] S. Datta and B. Das, Appl. Phys. Lett. **56**, 665 (1990).
[79] A. V. Moroz, K. V. Samokhin, and C. H. W. Barnes, Phys. Rev. Lett. **84**, 4164 (2000); Phys. Rev. B **62**, 16900 (2000).
[80] F. Mireles and G. Kirczenow, Phys. Rev. B **64**, 024426 (2001).
[81] E. V. Bezuglyi *et al.*, Phys. Rev. B **66**, 052508 (2002).
[82] Y. Nakamura *et al.*, Nature (London) **398**, 786 (1999); A. Cottet *et al.*, Physica C **367**, 197 (2002).
[83] L. Y. Gorelik *et al.*, Phys. Rev. B **69**, 094516 (2004).

This article was published in English in the original Russian journal. Reproduced here with stylistic changes by AIP.

Some novel effects in superconducting nanojunctions

A. D. Zaikin*

Forshchungszentrum Karlsruhe, Institut für Nanotechnologie, 76021, Karlsruhe, Germany; I. E. Tamm Department of Theoretical Physics, P.N. Lebedev Physics Institute, Moscow 119991, Russia
(Submitted February 23, 2004)
Fiz. Nizk. Temp. **30**, 756–769 (July–August 2004)

In this paper we address several new developments in the theory of the dc Josephson effect in superconducting weak links. We analyze the interplay between quantum interference effects and Andreev reflection in SNS nanojunctions with insulating barriers and demonstrate that these effects may qualitatively modify the Josephson current in such structures. We also investigate the impact of the parity effect on persistent currents in superconducting nanorings interrupted by a quantum point contact (QPC). In the limit of zero temperature and for an odd number of electrons in the ring we predict complete suppression of the supercurrent across a QPC with one conducting mode. In nanorings with SNS junctions a π-state can occur for an odd number of electrons. Changing this number from even to odd yields *spontaneous* supercurrent in the ground state of such rings without any externally applied magnetic flux. [DOI: 10.1063/1.1789914]

In 1926 Albert Einstein posed a remarkable question:[1] ''Of particular interest is the question whether a link between two superconductors also turns superconducting.'' The answer to this question was provided by Brian Josephson in 1962.[2] It was predicted by Josephson that dissipativeless flow of Cooper pairs between two different superconductors separated by an insulating barrier is possible provided this supercurrent I_s does not exceed some critical value I_c. Furthermore, the dependence of this current on the phases of macroscopically coherent wave functions of Cooper pairs was established in a very simple form:[2]

$$I_s = I_c \sin \phi, \tag{1}$$

where ϕ is the difference between the phases of the BCS order parameters of two superconductors. Equation (1) represents the *dc Josephson effect*. Einstein's question[1] turned out to be answered in the affirmative.

What if the total current I flowing through the barrier is larger than I_c? In this case a part of the net current across the barrier is transferred by normal electrons (quasiparticles) and the rest of it is carried by Cooper pairs. While the second contribution, I_s, remains dissipativeless and is again described by Eq. (1), the first—quasiparticle—contribution to the current is dissipative and, hence, causes a nonzero voltage drop V across the insulating barrier. In the presence of this voltage the coherent phase difference ϕ acquires a time dependence described by another famous Josephson relation

$$\frac{\partial \phi}{\partial t} = \frac{2eV}{\hbar}. \tag{2}$$

Combining Eqs. (1) and (2), one immediately arrives at the conclusion that for any nonzero V the supercurrent I_s changes in time. In the case of time-independent voltages one has $\phi = 2eVt/\hbar$ and, hence, the Josephson current (1) will oscillate in time with a fundamental frequency proportional to the voltage V. Equation (2) and the related oscillations of the supercurrent represent the essence of the *ac Josephson effect*.

Soon after Josephson's predictions a microscopic theory of both the dc[3] and ac[4,5] Josephson effects was constructed, and these effects have been observed experimentally.[6,7] A huge number of publications and several monographs have been devoted to various aspects of these effects. It has turned out that the physics encoded in these phenomena is very rich and important for understanding the basic properties of superconductivity itself. More than forty years after its discovery the Josephson effect is still attracting the attention of many researchers and keeps providing us with new and interesting physics.

In this paper we will discuss several new phenomena for which a theoretical understanding has only very recently been achieved. In the next Section we very briefly review already well-known and established results which concern the dc Josephson effect in various types of superconducting weak links. Sections 2 and 3 are devoted to possible new effects[8,9] which emerge and gain importance as one decreases the size of a weak link, eventually turning it to a nanostructure with only few conducting channels. Fabrication of such quantum point contacts (QPCs)—unthinkable at the time of discovery of the Josephson effects—is now becoming a routine procedure. Hence, the new effects discussed here can be directly observed and investigated in a modern experiment.

1. INSTEAD OF INTRODUCTION

Relatively soon after Josephson's discovery it was understood that the nondissipative transport of Cooper pairs between two superconductors can take place not only through a (usually very thin) insulating barrier but also in various other situations. One of such situation is realized in the so-called SNS structures, i.e., if a piece of a normal metal is placed in-between two superconductors. In contrast to tun-

nel junctions, in SNS systems at sufficiently low temperatures appreciable supercurrent can flow even if the normal layer is as thick as few microns. This is because the wave function of Cooper pairs or, more precisely, the anomalous Green function, penetrates into the normal metal from a superconductor at the length $\sim v_F/T$ for ballistic and $\sim\sqrt{D/T}$ for diffusive metals (here and below $D=v_F l/3$ and l are the diffusion coefficient and the elastic mean free path, respectively). Clearly, at temperatures much lower than the critical temperature T_c of a superconductor this length becomes large (as compared, e.g., to the superconducting coherence length), and macroscopic quantum coherence is established between two superconducting banks separated by a normal metal.

Further studies revealed an interesting mechanism of Cooper pair transfer in such systems. It turned out that the supercurrent flow is directly related to another fundamentally important phenomenon: Andreev reflection.[10] Suffering Andreev reflections at both SN interfaces, quasiparticles with energies below the superconducting gap are effectively ''trapped'' inside the N layer and form a discrete set of levels.[10] It was demonstrated[11] that in the presence of a phase difference ϕ across the SNS junction these levels acquire a shift proportional to this phase difference. Thus, on the one hand, the position of the quasiparticle energy levels in such systems can be tuned by the passage of supercurrent, and, on the other hand, the magnitude of this supercurrent can be established by taking the derivative of the quasiparticle energy with respect to ϕ with subsequent summation over the whole energy spectrum. The microscopic theory[11,12] leads to the following expression for the current density through clean SNS systems:

$$j=\frac{e^2p_F^2v_F}{6\pi^2d}\phi, \quad -\pi<\phi<\pi. \tag{3}$$

This expression is valid at $T\to 0$ and for N-metal layers with thickness $d\gg\xi_0\sim v_F/\Delta$, where Δ is the superconducting order parameter. The most important features of this result are (i) the strongly nonsinusoidal current-phase relation, cf. Eqs. (1) and (3), and (ii) the linear dependence of the current on the gap in the quasiparticle spectrum $\epsilon_{qp}\sim v_F/d$ in the direction normal to the NS interfaces.

It is interesting that qualitatively both features (i) and (ii) survive not only for ballistic but also for diffusive SNS junctions, even though in the latter case the discrete Andreev levels are washed out due to elastic scattering of quasiparticles on impurities in the N metal. It has been demonstrated microscopically[13–15] that at low temperatures $T\ll D/d^2$ the current-phase relation in diffusive SNS junctions also deviates from the sinusoidal one[1)] and the critical Josephson current is again proportional to the gap in the quasiparticle spectrum, in this case the Thouless energy $\epsilon_{qp}=D/d^2$. The exact value of the critical Josephson current in long diffusive SNS junctions can be established only numerically. One finds[15]

$$I_c=10.82\frac{\epsilon_{qp}}{eR_N}, \tag{4}$$

where R_N is the junction normal state resistance.

The above results—both for the ballistic and diffusive limits—are valid for sufficiently long junctions. One can also decrease the thickness d of the normal metal and gradually cross over to the limit of short superconducting constrictions. A microscopic description of the dc Josephson effect in this type of weak links was developed by Kulik and Omel'yanchouk.[16] Also in such systems at low temperatures the current-phase dependence deviates from $\sin\phi$ and the critical current $I_c(T\to 0)$ is again proportional to the combination ϵ_{qp}/eR_N, where now $\epsilon_{qp}=\Delta$. A crossover between the two limits of long SNS junctions and short superconducting weak links can also be described microscopically. In the clean case this task can be accomplished trivially by solving the Eilenberger equations,[17–19] while in the dirty limit one must use the Usadel equations,[20] which can be solved only numerically. The latter task has recently been carried out in Ref. 15.

Let us also note that in all the above considerations the intermetallic interfaces were assumed to be perfectly transparent. It is also straightforward to generalize the analysis to include electron scattering at an insulating barrier that can be present inside a weak link. For short superconducting junctions containing an insulating barrier with an arbitrary energy-independent transmission the corresponding generalization has been worked out by Haberkorn *et al.*[21] This analysis yields a general formula for the Josephson current which matches with the Ambegaokar-Baratoff result[3] in the weak tunneling limit and crosses over to the Kulik-Omel'yanchouk expression[16] for clean constrictions at transmissions approaching unity. It is interesting that the result of Ref. 16 for diffusive constrictions can also be recovered from the formula of Ref. 21 after its slight generalization. In order to do so one should assume that the transmission is not the same for all conducting channels but rather obeys the Dorokhov distribution formula. Combining this formula with the expression from Ref. 21 and summing over all conducting channels, one arrives at the result of Ref. 16 for diffusive weak links.

One can also investigate the transport properties of more-complicated layered structures which contain both normal metal layers and insulating barriers. For instance, SNS systems with one insulating barrier, such as SINS and SNINS, have been analyzed by a number of authors.[22–28] For an extended review summarizing various features of the dc Josephson effect in different types of superconducting weak links and further references we refer the reader to Refs. 29–31.

Most of the results reviewed above were obtained a long time ago and are by now well established and well understood. One can think that considering dc Josephson effect in even more complicated structures like, for instance, SNS structures with two or three insulating barriers, may at most yield somewhat more cumbersome expressions but would not reveal any new physics beyond what has already been understood in simpler situations. Below we will show that that is not the case. On the contrary, in the next Section we will demonstrate that qualitatively new effects may occur in SNS junctions with more than one insulating barrier, in particular, provided the cross section of such junctions is reduced to where it is comparable to the square of the Fermi wavelength.

2. JOSEPHSON EFFECT AND QUANTUM INTERFERENCE OF QUASIPARTICLES

In this Section we will analyze the dc Josephson effect in SNS systems which contain several insulating barriers. In this case electrons scattered at different barriers can interfere inside the junction. We will demonstrate that such interference may lead to qualitatively new effects and cause severe modifications of the supercurrent across the junction. We will see that these modifications can go in both directions, i.e., the Josephson current can be dramatically decreased by *destructive interference* of quasiparticles or, on the contrary, increased as a result of their *constructive interference*.

The first situation is realized for sufficiently short junctions, while for longer ones the second effect might become more pronounced. The phenomenon of quantum interference of quasiparticles is of primary importance for SNS structures with few conducting channels. The interest in such structures has grown considerably after several experimental groups succeeded in connecting a carbon nanotube to two superconductors and performing transport measurements in such systems.[32–34] More-conventional SNS structures with many conducting channels and several insulating barriers are also of considerable interest, for instance in connection with possible applications (see, e.g., Ref. 35 and further references therein). We will demonstrate that for such systems quantum interference effects are also important provided there exist more than two scatterers inside the junction.

On the theoretical side, a significant difficulty is that the powerful formalism of quasiclassical energy-integrated Eilenberger Green functions[17–19,30] supplemented by the Zaitsev boundary conditions[36] cannot be directly applied to systems containing more than one insulating barrier. An important ingredient of the derivation[36] is the assumption that such barriers are located sufficiently far from each other, so that *interference effects* emerging from electron scattering can be totally neglected. It is also essential that Zaitsev boundary conditions do not depend on the scattering phases. Since here we are just interested in investigating the quantum interference of quasiparticles, we are not in a position to use the quasiclassical Eilenberger formalism for our purposes. One possible way of circumventing this problem is to apply the formalism[37,38] within which the presence of an arbitrary number of barriers in the system can be accounted for by linear boundary conditions. Another, even more straightforward, possibility for analyzing the dc Josephson effect in structures with several insulating barriers is to directly solve the exact Gor'kov equations.[39] Here we will follow the second approach.

The results presented in this Section were obtained in collaboration with Galaktionov.[8] A similar approach has also been used independently by Brinkman and Golubov.[40]

2.1. General formalism

In what follows we will assume that our system is uniform along the directions parallel to the interfaces (coordinates y and z). Performing the Fourier transformation of the normal G and anomalous F^+ Green function with respect to these coordinates,

$$G_{\omega_n}(\mathbf{r},\mathbf{r}')=\int \frac{d^2\mathbf{k}_\parallel}{(2\pi)^2} G_{\omega_n}(x,x',\mathbf{k}_\parallel)\mathrm{e}^{i\mathbf{k}_\parallel(\mathbf{r}_\parallel-\mathbf{r}'_\parallel)},$$

we express the Gor'kov equations in the following standard form:

$$\begin{pmatrix} i\omega_n-\hat{H} & \Delta(x) \\ \Delta^*(x) & i\omega_n+\hat{H}_c \end{pmatrix}\begin{pmatrix} G_{\omega_n}(x,x',\mathbf{k}_\parallel) \\ F^+_{\omega_n}(x,x',\mathbf{k}_\parallel)\end{pmatrix}=\begin{pmatrix}\delta(x-x') \\ 0\end{pmatrix}. \tag{5}$$

Here $\omega_n=(2n+1)\pi T$ is the Matsubara frequency, and $\Delta(x)$ is the superconducting order parameter. The Hamiltonian $\hat{H}$ in Eq. (5) reads

$$\hat{H}=-\frac{1}{2m}\frac{\partial^2}{\partial x^2}+\frac{\tilde{\mathbf{k}}_\parallel^2}{2m}-\varepsilon_F+V(x). \tag{6}$$

Here $\tilde{\mathbf{k}}_\parallel=\mathbf{k}_\parallel-e/c\,\mathbf{A}_\parallel(x)$, ε_F is the Fermi energy, the term $V(x)$ takes into account the external potentials (including the boundary potential), and $\mathbf{A}_\parallel$ is the vector potential. The Hamiltonian $\hat{H}_c$ is obtained from $\hat{H}$ (6) by inverting the sign of the electron charge e.

As usual, it is convenient to separate fast oscillations of the Green functions $\propto\exp(\pm ik_x x)$ from the envelope of these functions, which changes over distances much larger than atomic scales. Then one can construct a particular solution of the Gor'kov equations (5) in the following form:

$$\begin{pmatrix} G_{\omega_n}(x,x',\mathbf{k}_\parallel) \\ F^+_{\omega_n}(x,x',\mathbf{k}_\parallel)\end{pmatrix}=\overline{\phi}_{+1}(x)g_1(x')\mathrm{e}^{ik_x(x-x')} + \overline{\phi}_{-2}(x)g_2(x')\mathrm{e}^{-ik_x(x-x')} \quad \text{if } x>x' \tag{7}$$

and

$$\begin{pmatrix} G_{\omega_n}(x,x',\mathbf{k}_\parallel) \\ F^+_{\omega_n}(x,x',\mathbf{k}_\parallel)\end{pmatrix}=\overline{\phi}_{-1}(x)f_1(x')\mathrm{e}^{-ik_x(x-x')} + \overline{\phi}_{+2}(x)f_2(x')\mathrm{e}^{ik_x(x-x')} \quad \text{if } x<x'. \tag{8}$$

These functions satisfy Gor'kov equations at $x\neq x'$. Here $\overline{\phi}_\pm$ are two linearly independent solutions of the equation

$$\begin{pmatrix} i\omega_n-\hat{H}^a_\pm & \Delta(x) \\ \Delta^*(x) & i\omega_n+\hat{H}^a_{\pm c}\end{pmatrix}\overline{\phi}_\pm=0. \tag{9}$$

The solution $\overline{\phi}_{+1}$ does not diverge at $x\to+\infty$, while $\overline{\phi}_{+2}$ is well-behaved at $x\to-\infty$. Similarly, the two linearly independent solutions $\overline{\phi}_{-1,2}$ do not diverge, respectively, at $x\to-\infty$ and $x\to+\infty$.

In Eq. (9) we defined

$$\hat{H}^a_\pm=\mp iv_x\partial_x-\frac{e}{c}\mathbf{A}_\parallel(x)\mathbf{v}_\parallel+\frac{e^2}{2mc^2}\mathbf{A}^2_\parallel(x)+\tilde{V}(x). \tag{10}$$

Here $k_x=mv_x=\sqrt{k_F^2-k_\parallel^2}$, $\tilde{V}(x)$ represents a slowly varying part of the potential which does *not* include fast variations

possibly occuring at metallic interfaces. The latter will be taken into account by the boundary conditions to be considered below.

The functions $f_{1,2}(x)$ and $g_{1,2}(x)$ are determined with the aid of the continuity condition for the Green functions at $x=x'$ and the condition resulting from the integration of $\delta(x-x')$ in Eq. (5).

A general solution of the Gor'kov equations has the form

$$\begin{pmatrix} G_{\omega_n}(x,x') \\ F^+_{\omega_n}(x,x') \end{pmatrix} = \begin{pmatrix} G_{\omega_n}(x,x') \\ F^+_{\omega_n}(x,x') \end{pmatrix}_{\text{part}} + [l_1(x')\overline{\phi}_{+1}(x) + l_2(x')\overline{\phi}_{+2}(x)]e^{ik_x x} + [l_3(x')\overline{\phi}_{-1}(x) + l_4(x')\overline{\phi}_{-2}(x)]e^{-ik_x x}. \quad (11)$$

For systems which consist of several metallic layers the particular solution is obtained with the aid of the procedure outlined above, provided that both coordinates x and x' belong to the same layer. Should x and x' belong to different layers, the particular solution is zero because in that case the δ function in Eq. (5) fails. The functions $l_{1,2,3,4}(x')$ in each layer should be derived from the proper boundary conditions. These are just the matching conditions for the wave functions on the left and on the right side of a potential barrier, $A_1\exp(ik_{1x}x)+B_1\exp(-ik_{1x}x)$ and $A_2\exp(ik_{2x}x)+B_2\exp(-ik_{2x}x)$, respectively. These conditions have the standard form (see, e.g., Ref. 41):

$$A_2=\alpha A_1+\beta B_1,\quad B_2=\beta^* A_1+\alpha^* B_1,$$

$$|\alpha|^2-|\beta|^2=\frac{k_{1x}}{k_{2x}}. \quad (12)$$

The equations

$$R=\left|\frac{\beta}{\alpha}\right|^2,\quad D=1-R=\frac{k_{1x}}{k_{2x}|\alpha|^2} \quad (13)$$

define, respectively, the reflection and transmission coefficients of the barrier. Applying these boundary conditions at each insulating barrier, one uniquely determines all the unknown functions in Eq. (11) and thereby completes the construction of the Green functions for our problem. For further details we refer the reader to Ref. 8.

We are now in a position to specify the general expression for the Josephson current across ballistic SNS junctions which contain an arbitrary number of insulating barriers. In what follows we will assume that a thin specularly reflecting insulating barriers (I) are situated at both SN interfaces. Additional such barriers can also be present inside the N metal. Transmissions of these barriers may take any value from zero to one. We also assume that electrons propagate ballistically between any two adjacent barriers and that no electron-electron or electron-phonon interactions are present in the normal metal. For simplicity we will restrict our attention to the case of identical superconducting electrodes with singlet isotropic pairing and neglect suppression of the superconducting order parameter in the electrodes close to the SN interface. The phase of the order parameter is set to be $-\phi/2$ $(+\phi/2)$ in the left (right) electrode. As before, the thickness of the normal layer will be denoted by d.

Employing the standard formula for the current density

$$J=\frac{ie}{m}T\sum_{\omega_n}\int\frac{d^2k_\parallel}{(2\pi)^2}(\nabla_{x'}-\nabla_x)_{x'\to x}G_{\omega_n}(x,x',\mathbf{k}_\parallel) \quad (14)$$

and making use of the expressions for the Green functions, one arrives at the following result:

$$J=4eT\sum_{\omega_n>0}\int_0^{k_F}\frac{k_x dk_x}{2\pi}\frac{\sin\phi}{\cos\phi+W}, \quad (15)$$

where the function W depends on the number of insulating barriers. This function will be specified below for the case of two and three barriers.

Note that the integral over k_x in Eq. (15) can be replaced by a sum over independent conducting channels:

$$\frac{\mathcal{A}}{2\pi}\int_0^{k_F}k_x dk_x(\ldots)\to\sum_m^N(\ldots), \quad (16)$$

where $\mathcal{A}$ is the junction cross section. In this case $D_{1,2}$ and $R_{1,2}$ may also depend on the channel index m.

2.2. SINI′S junctions with few conducting channels

Let us first consider SNS junctions with two insulating barriers, one at each NS interface. In this case the function W in (15) takes the form

$$W=\frac{4\sqrt{R_1R_2}}{D_1D_2}\frac{\Omega_n^2}{\Delta^2}\cos\chi + \frac{\Omega_n^2(1+R_1)(1+R_2)+\omega_n^2D_1D_2}{D_1D_2\Delta^2}\cosh\frac{2\omega_n d}{v_x} + \frac{2(1-R_1R_2)}{D_1D_2}\frac{\Omega_n\omega_n}{\Delta^2}\sinh\frac{2\omega_n d}{v_x}. \quad (17)$$

Here $\chi=2k_x d+\varphi$ is the phase of the product $\alpha_2^*\beta_2\alpha_1^*\beta_1^*$. Equations (15), (17) provide a general expression for the dc Josephson current in SINI′S structures valid for arbitrary transmissions D_1 and D_2.

Let us first analyze the above result for the case of one conducting channel $N=1$. We observe that the first term in Eq. (17) contains $\cos(2k_x d+\varphi)$, which oscillates at distances of the order of the Fermi wavelength. Provided at least one of the barriers is highly transparent and/or (for sufficiently long junctions $d\gtrsim\xi_0$) the temperature is high $T\gg v_F/d$ this oscillating term is unimportant and can be neglected. However, at lower transmissions of both barriers and for relatively short junctions $d\lesssim v_F/T$ this term turns out to be of the same order as the other contributions to W (17). In this case the supercurrent is sensitive to the exact positions of the discrete energy levels inside the junction, which can in turn vary considerably if d changes at the atomic scales $\sim 1/k_F$. Hence, one can expect sufficiently strong sample-to-sample fluctuations of the Josephson current even for junctions with nearly identical parameters.

Let us first consider the limit of relatively short SINI′S junctions, in which case we obtain

$$I=\frac{e\Delta}{2}\frac{\mathcal{T}\sin\phi}{\mathcal{D}}\tanh\left[\frac{\mathcal{D}\Delta}{2T}\right], \quad (18)$$

where we have defined

$$\mathcal{D}(\phi)=\sqrt{1-\mathcal{T}\sin^2(\phi/2)} \quad (19)$$

and an effective normal transmission of the junction

$$\mathcal{T}=\frac{D_1D_2}{1-R_1R_2+2\sqrt{R_1R_2}\cos\chi}. \tag{20}$$

Equation (18) has exactly the same functional form as the result derived by Haberkorn *et al.*[21] for SIS junctions with an arbitrary transmission of the insulating barrier. This result is recovered from our Eqs. (18), (20) if we assume, e.g., $D_1 \ll D_2$, in which case the total transmission (20) reduces to $\mathcal{T}\simeq D_1$.

As we have already discussed, the total transmission $\mathcal{T}$ and, hence, the Josephson current fluctuate depending on the exact position of the bound states inside the junction. The resonant transmission is achieved for $2k_xd+\varphi=\pm\pi$, in which case we get

$$\mathcal{T}_{\rm res}=\frac{D_1D_2}{(1-\sqrt{R_1R_2})^2}. \tag{21}$$

This equation demonstrates that for symmetric junctions $D_1=D_2$ at resonance the Josephson current does not depend on the barrier transmission at all. In this case $\mathcal{T}_{\rm res}=1$, and our result (18) coincides with the formula derived by Kulik and Omel'yanchouk[16] for ballistic constrictions. In the limit of low transmissions $D_{1,2}\ll 1$ we recover the standard Breit-Wigner formula $\mathcal{T}_{\rm res}=4D_1D_2/(D_1+D_2)^2$ and reproduce the result obtained by Glazman and Matveev[42] for the problem of resonant tunneling through a single Anderson impurity between two superconductors.

Note that our results (18)–(20) also support the conclusion reached by Beenakker[43] that the Josephson current across sufficiently short junctions has a universal form and depends only on the total scattering matrix of the weak link, which can be evaluated in the normal state. Although this conclusion is certainly correct in the limit $d\to 0$, its applicability range depends significantly on the physical nature of the scattering region. From Eqs. (15), (17) we observe that the result (18), (19) applies at $d\ll\xi_0$ not very close to the resonance. On the other hand, at resonance the above result is valid only under the more stringent condition $d\ll\xi_0D_{\max}$, where we define $D_{\max}=\max(D_1,D_2)$.

Now let us briefly analyze the opposite limit of sufficiently long junctions $d\gg\xi_0$. Here we will restrict ourselves to the most interesting case $T=0$. From Eqs. (15), (17) we obtain

$$I=\frac{ev_x\sin\phi}{\pi dz_1}\left[\frac{\arctan\sqrt{z_2/z_1}}{\sqrt{z_2/z_1}}\right],$$

$$z_{1,2}=\cos^2\frac{\phi}{2}+\frac{1}{D_1D_2}(R_+\pm 2\sqrt{R_1R_2}\cos\chi), \tag{22}$$

where $R_+=R_1+R_2$. For a fully transparent channel $D_1=D_2=1$ the above expression reduces to the well known Ishii-Kulik result:[11,12]

$$I=\frac{ev_x\phi}{\pi d},\quad -\pi<\phi<\pi, \tag{23}$$

whereas if one transmission is small, $D_1\ll 1$, and $D_2\approx 1$, we reproduce the result[22]

$$I=\frac{ev_xD_1\sin\phi}{2d}. \tag{24}$$

Provided the transmissions of both NS interfaces are low, $D_{1,2}\ll 1$, we obtain in the off-resonance region

$$I=\frac{ev_x}{4\pi d}D_1D_2\sin\phi\,\Upsilon[\chi], \tag{25}$$

where $\Upsilon[\chi]$ is a 2π-periodic function defined as

$$\Upsilon[\chi]=\frac{\chi}{\sin\chi},\quad -\pi<\chi<\pi. \tag{26}$$

In the vicinity of the resonance, $||\chi|-\pi|\lesssim D_{\max}$, the above result no longer holds. Exactly at resonance, $\chi=\pm\pi$, we get

$$I=\frac{ev_x\sqrt{D_1D_2}\sin\phi}{4d\left\{\cos^2\dfrac{\phi}{2}+\dfrac{1}{4}\left(\sqrt{\dfrac{D_1}{D_2}}-\sqrt{\dfrac{D_2}{D_1}}\right)^2\right\}^{1/2}}. \tag{27}$$

For a symmetric junction, $D_{1,2}=D$, this formula yields

$$I=\frac{ev_xD\sin\phi/2}{2d},\quad -\pi<\phi<\pi, \tag{28}$$

while in the strongly asymmetric case, $D_1\ll D_2$, we again arrive at expression (24). This implies that at resonance the barrier with higher transmission D_2 becomes effectively transparent even if $D_2\ll 1$. We conclude that for $D_{1,2}\ll 1$ the maximum Josephson current is proportional to the product of transmissions D_1D_2 off resonance, whereas exactly at resonance it is proportional to the lower of the two transmissions D_1 or D_2.

We observe that both for short and long SINI′S junctions interference effects may enhance the Josephson effect or partially suppress it, depending on the exact positions of the bound states inside the junction. We also note that in order to evaluate the supercurrent across SINI′S junctions it is in general not sufficient to derive the transmission probability for the corresponding NINI′N structure. Although the normal transmission of the above structure is given by Eq. (20) for *all* values of d, the correct expression for the Josephson current can be recovered by combining Eq. (20) with the results[21,43] in the limit of short junctions $d\ll D\xi_0$ only. In this case one can neglect suppression of the anomalous Green functions inside the normal layer, and, hence, the information about the normal transmission turns out to be sufficient. On the contrary, for longer junctions the decay of Cooper pair amplitudes inside the N layer can no longer be disregarded. In this case the supercurrent will deviate from the form (18) even though the normal transmission of the junction (20) will remain unchanged. This deviation becomes particularly pronounced for long junctions, i.e., for $d\gg\xi_0$ off resonance and for $d\gg D\xi_0$ at resonance.

Generalization of the above results to the case of an arbitrary number of independent conducting channels $N>1$ is trivial: The supercurrent is simply given by the sum of the contributions from all the channels. These contributions are in general not equal because the phase factors $\chi=2k_xd+\varphi$ change randomly for different channels. Hence, mesoscopic

fluctuations of the supercurrent should become smaller with increasing number of channels and eventually disappear in the limit of large N.

In the latter limit the Josephson current is obtained by averaging over all values of the phase χ. This limit has already been studied in detail[8,40] and will not be considered here. We will only point out that, as was demonstrated in Ref. 8, in the limit $N\to\infty$ interference effects are effectively averaged out, and exactly the same result can be reproduced by means of the Eilenberger formalism supplemented by Zaitsev boundary conditions. It is also worthwhile to emphasize that the latter statement applies only to junctions with two insulating barriers. Below we will show that for systems with more than two barriers quasiparticle interference effects turn out to be even more significant, and the correct result for the current cannot be recovered with the aid of Zaitsev boundary conditions even in the limit $N\to\infty$.

2.3. Josephson current in SINI′NI″S junctions

Let us now turn to SNS structures with three insulating barriers. As before, two of them are located at SN interfaces, and the third barrier is inside the N layer at distances d_1 and d_2, respectively, from the left and right SN interfaces. The transmission and reflection coefficients of this intermediate barrier are denoted as D_0 and $R_0=1-D_0$, whereas the left and the right barriers are characterized by $D_1=1-R_1$ and $D_2=1-R_2$, respectively.

The supercurrent is calculated along the same lines as for the case of two barriers. The final result is again expressed by Eq. (15), where the function W is now defined by a substantially more cumbersome expression than for the case of two barriers. This expression was evaluated in Ref. 8 and will not be presented here. We will skip to the final results.

2.3.1. One-channel limit

Let us first discuss the case of one conducting channel. In the limit of short junctions $d\ll\xi_0 D_{\max}$ we again reproduce the result (18), where the total effective transmission of the normal structure with three barriers takes the form

$$\mathcal{T}=\frac{2t_1t_0t_2}{1+t_1t_0t_2+C(\phi_{1,2},t_{0,1,2})}, \tag{29}$$

where

$$C=\cos\chi_1\sqrt{(1-t_0^2)(1-t_1^2)}+\cos\chi_2\sqrt{(1-t_0^2)(1-t_2^2)} +(\cos\chi_1\cos\chi_2-t_0\sin\chi_1\sin\chi_2)\sqrt{(1-t_1^2)(1-t_2^2)}. \tag{30}$$

Here we define $t_{0,1,2}=D_{0,1,2}/(1+R_{0,1,2})$ and $\chi_{1,2}=2k_xd_{1,2}+\varphi_{1,2}$. For later purposes let us also perform averaging of this transmission over the phases $\chi_{1,2}$. We obtain

$$\langle\mathcal{T}\rangle=\frac{2t_1t_0t_2}{\sqrt{2t_1t_0t_2+t_1^2t_0^2+t_1^2t_2^2+t_0^2t_2^2-t_1^2t_0^2t_2^2}}. \tag{31}$$

In particular, in the case of similar barriers with small transparencies $D_{0,1,2}\approx D\ll 1$ the average normal transmission of our structure is $\langle\mathcal{T}\rangle\sim D^{3/2}$. Suppression of the average transmission below the value $\sim D$ is a result of destructive interference and indicates the tendency of the system towards localization.

Let us now proceed to the limit of a long junction $d_{1,2}\gg\xi_0$ and $T=0$. In the off-resonance region for $d_1=d_2$ we find

$$I=\frac{ev_xD_1D_0D_2\sin\phi}{8\pi d_1}\frac{\Upsilon[\chi_1]-\Upsilon[\chi_2]}{\cos\chi_2-\cos\chi_1}. \tag{32}$$

This expression diverges at resonance (i.e., at $\chi_1\simeq\pi$ or $\chi_2\simeq\pi$), where it becomes inapplicable. In the resonant region $\chi_2\simeq\pi$ we obtain

$$I=\frac{ev_x\sqrt{D_1D_0D_2}\sin\phi}{4d\sqrt{2(1+\cos\chi_1)[\mathcal{T}^{-1}-\sin^2(\phi/2)]}}. \tag{33}$$

2.3.2. Many-channel junctions

As was already discussed, in the many-channel limit it is appropriate to average the current over the scattering phases. Practically in any realistic physical realization the widths d_1 and d_2 fluctuate independently on the atomic scale. In this case averaging over χ_1 and χ_2 should also be performed independently. If d_1 and d_2 do not change on the atomic scale but are incommensurate, independent averaging over the two phases is to be performed as well. Independent averaging cannot be fulfilled only in the (physically irrelevant) case of strictly commensurate d_1 and d_2, which will not be considered below.

Technically, independent averaging over the scattering phases $\chi_1=x$ and $\chi_2=\lambda x$ amounts to evaluating the integral of the expression $1/[t+\cos x\cos(\lambda x)]$ from $x=0$ to some large value $x=L$. At $\lambda=1$ the result of this integration is $L/\sqrt{t(1+t)}$. However, if λ is irrational, the integral approaches the value $2LK(1/t^2)/\pi t$, where $K(h)=F(\pi/2,h)$ is the complete elliptic integral.

Let us assume that the transparencies of all three interfaces are small compared to unity. After averaging over the two scattering phases we arrive at the final expression for the current:

$$J=\frac{ek_F^2}{\pi^2}D_{\rm eff}\sin(\phi T)\sum_{\omega_n>0}\frac{\Delta^2}{\Omega_n^2}K\left[\frac{\Delta^2\sin^2(\phi/2)}{\Omega_n^2}\right], \tag{34}$$

where we define the effective transmission

$$D_{\rm eff}=\int_0^1 d_\mu\mu\sqrt{D_0D_1D_2}. \tag{35}$$

Hence, for similar barriers we obtain the dependence $J\propto D^{3/2}$ rather than $J\propto D$ (as would be the case for independent barriers). The latter dependence would follow from the calculation based on Zaitsev boundary conditions for the Eilenberger propagators. We observe, therefore, that quantum interference effects decrease the Josephson current in systems with three insulating barriers. This is an essentially quantum effect which cannot be recovered from Zaitsev boundary conditions even in the multichannel limit. This effect has exactly the same origin as a quantum suppression of the average normal transmission $\langle\mathcal{T}\rangle$ due to localization effects. Further limiting expressions for short junctions can be directly recovered from Eq. (31).

We also note that the current-phase relation (34) deviates from a pure sinusoidal dependence even though all three transmissions are small, $D_{0,1,2} \ll 1$. At $T=0$ the critical Josephson current is reached at $\phi \simeq 1.7$, which is slightly higher than $\pi/2$. Although this deviation is quantitatively not very significant, it is nevertheless important as yet one more indication of quantum interference of electrons inside the junction.

Finally, let us turn to the limit of long junctions $d_{1,2} \gg \xi_0$. We again restrict ourselves to the case of low-transparency interfaces. At high temperatures $T \gg v_F/2\pi d_{1,2}$ we get $J \propto D_0 D_1 D_2 \exp(-d/\xi(T))$, where $d = d_1 + d_2$ and $\xi(T) = v_F/(2\pi T)$. In this case the anomalous Green function decays strongly deep in the normal layer. Hence, interference effects are not important and the interfaces can be considered as independent from each other. In the opposite limit $T \ll D v_F/d$, however, interference effects become important, and the current becomes proportional to $D^{5/2}$ rather than to D^3. Explicitly, at $T \to 0$ we get to logarithmic accuracy

$$J = \frac{e k_F^2 v_F \sin\phi}{16\pi^2 \sqrt{d_1 d_2}} \int_0^1 d\mu \mu^2 D_1 D_2 \sqrt{D_0} \ln D_0^{-1}. \qquad (36)$$

We see that, in contrast to short junctions, in the limit of thick normal layers interference effects increase the Josephson current as compared to the case of independent barriers. The result (36), as well as one of Eqs. (34), (35), cannot be obtained from the Eilenberger approach supplemented by Zaitsev boundary conditions.

2.4. Some conclusions

By directly solving the Gor'kov equations we evaluated the dc Josephson current in SNS junctions containing two and three insulating barriers with arbitrary transmissions: SINI′S and SINI′NI″S junctions, respectively. Our results can be directly applied both to the junctions with few conducting channels (such as, e.g., superconductor–carbon nanotube–superconductor junctions[32–34]) and to more conventional SNS structures in the many-channel limit. We have demonstrated that an interplay between the proximity effect and quantum interference of quasiparticles may play a crucial role in such systems, causing strong modifications of the Josephson current.

For the system with two barriers and few conducting channels we found strong fluctuations of the Josephson critical current depending on the exact position of the resonant level inside the junction. For short junctions $d \ll \xi_0 D$ at resonance the Josephson current does not depend on the barrier transmission D and is given by the standard Kulik–Omel'yanchouk formula[16] derived for ballistic weak links. In the limit of long SNS junctions $d \gg \xi_0$ resonance effects may also lead to strong enhancement of the supercurrent, in this case at $T \to 0$ and at resonance the Josephson current is proportional to D and not to D^2, as it would be in the absence of interference effects.

While the above results for few conducting channels cannot be obtained by means of the approach employing Zaitsev boundary conditions, in the many-channel limit and for junctions with two barriers the latter approach does allow one to recover the correct results. This is because the contributions sensitive to the scattering phase are effectively averaged out during summation over conducting channels.

Quantum interference effects turn out to be even more important in the proximity systems which contain three insulating barriers. In this case the quasiclassical approach based on Zaitsev boundary conditions fails even in the limit of many conducting channels. In that limit the Josephson current is *decreased* for short junctions ($J \propto D^{3/2}$) as compared to the case of independent barriers ($J \propto D$). This effect is caused by destructive interference of electrons reflected from different barriers and indicates the tendency of the system towards localization. In contrast, for long SNS junctions with three barriers an interplay between quantum interference and the proximity effect leads to enhancement of the Josephson current at $T \to 0$: We obtained the dependence $J \propto D^{5/2}$ instead of $J \propto D^3$ for independent barriers.

3. PARITY-INFLUENCED JOSEPHSON CURRENT

Let us now turn to a different issue which, to the best of our knowledge, has not yet attracted much attention in the literature. Namely, we will discuss an interplay between the parity effect and the dc Josephson current in superconducting weak links. The results presented in this Section have been obtained in collaboration with Sharov.[9]

It is well known that the thermodynamic properties of isolated superconducting systems are sensitive to the parity of the total number of electrons[44,45] even though this number $\mathcal{N}$ is macroscopically large. This parity effect is a direct consequence of the fundamental property of a superconducting ground state described by the condensate of Cooper pairs. The number of electrons forming this condensate is necessarily even; hence, for odd $\mathcal{N}$ at least one electron always remains unpaired, having an extra energy equal to the superconducting energy gap Δ. At sufficiently low temperatures a clear difference between the superconducting states with even and odd $\mathcal{N}$ has been demonstrated experimentally.[45,46]

Can the supercurrent be affected by this parity effect? At the first sight the answer to this question should be negative because of the fundamental uncertainty relation $\delta\mathcal{N}\delta\phi \gtrsim 1$. Should the electron number $\mathcal{N}$ be fixed, fluctuations of the superconducting phase ϕ become large, disrupting the supercurrent in the system. On the other hand, suppressing fluctuations of the phase ϕ will destroy the parity effect because of large fluctuations of $\mathcal{N}$.

Despite that, we will demonstrate below that in certain superconducting structures the parity effect can coexist with nonvanishing supercurrent. Consider a superconducting system which can support circular persistent currents (PCs). An example is provided by an isolated superconducting ring pierced by a magnetic flux Φ, in which case a circulating PC is induced in the ring. In accordance with the number–phase uncertainty relation the global superconducting phase of the ring fluctuates strongly in this case; however, these fluctuations are decoupled from the supercurrent and therefore can be integrated out without any influence on the latter. In what follows we will show that the parity effect may substantially modify the PC in superconducting nanorings, in particular for an odd number of electrons.

3.1. Parity projection formalism

In order to investigate systematically the influence of the electron parity number on persistent currents in superconducting nanorings we will employ the well-known parity projection formalism.[48–50] Let us recapitulate the key points of this approach, closely following Ref. 49.

The grand canonical partition function $\mathcal{Z}(T,\mu) = \mathrm{Tr}\exp[-\beta(\mathcal{H}-\mu\mathcal{N})]$ is connected to the canonical one $\mathcal{Z}(T,\mathcal{N})$ by means of the following equation:

$$\mathcal{Z}(T,\mu)=\sum_{\mathcal{N}=0}^{\infty} Z(T,\mathcal{N})\exp\left(\frac{\mu\mathcal{N}}{T}\right). \tag{37}$$

Here and below $\mathcal{H}$ is the system Hamiltonian, $\mathcal{N}$ is the total number of electrons, and $\beta\equiv 1/T$. Inverting this relation and defining the canonical partition functions $\mathcal{Z}_e$ and $\mathcal{Z}_o$, respectively, for even ($\mathcal{N}\equiv\mathcal{N}_e$) and odd ($\mathcal{N}\equiv\mathcal{N}_o$) ensembles, one gets

$$Z_{e/o}(T)=\frac{1}{2\pi}\int_{-\pi}^{\pi} du\ \mathrm{e}^{-i\mathcal{N}_{e/o}u}\mathcal{Z}_{e/o}(T,iTu), \tag{38}$$

where

$$Z_{e/o}(T,\mu)=\frac{1}{2}\mathrm{Tr}\{[1\pm(-1)^{\mathcal{N}}]\mathrm{e}^{-\beta(\mathcal{H}-\mu\mathcal{N})}\}$$

$$=\frac{1}{2}[\mathcal{Z}(T,\mu)\pm\mathcal{Z}(T,\mu+i\pi T)] \tag{39}$$

are the parity projected grand canonical partition functions. For $\mathcal{N}\gg 1$ it is sufficient to evaluate the integral in (38) within the saddle-point approximation, which yields

$$Z_{e/o}(T)\sim\exp[-\beta(\Omega_{e/o}-\mu_{e/o}\mathcal{N}_{e/o})], \tag{40}$$

where $\Omega_{e/o}=-T\ln\mathcal{Z}_{e/o}(T,\mu)$ are the parity projected thermodynamic potentials. They can be presented in the form

$$\Omega_{e/o}=\Omega_f-T\ln\left[\frac{1}{2}(1\pm\mathrm{e}^{-\beta(\Omega_b-\Omega_f)})\right], \tag{41}$$

where

$$\Omega_{f/b}=-T\ln[\mathrm{Tr}\{(\pm 1)^{\mathcal{N}}\mathrm{e}^{-\beta(\mathcal{H}-\mu\mathcal{N})}\}]. \tag{42}$$

The chemical potentials $\mu_{e/o}$ are defined by the saddle-point condition $N_{e/o}=-\partial\Omega_{e/o}(T,\mu_{e/o})/\partial\mu_{e/o}$.

The main advantage of the above analysis is that it allows one to express the canonical partition functions and thermodynamic potentials in terms of the parity projected grand canonical ones, thereby enormously simplifying the whole calculation. We further note that Ω_f is just the standard grand canonical thermodynamic potential and Ω_b represents the corresponding potential linked to the partition function $\mathcal{Z}(T,\mu+i\pi T)$. It is easy to see[49] that in order to recover this function one can evaluate the true grand canonical partition function $\mathcal{Z}(T,\mu)$, express the result as a sum over the Fermi Matsubara frequencies $\omega_f=2\pi T(m+1/2)$ and then substitute the Bose Matsubara frequencies $\omega_b=2\pi Tm$ instead of the Fermi ones. This procedure will automatically yield the correct expression for $\mathcal{Z}(T,\mu+i\pi T)$ and, hence, for Ω_b.

Having found the thermodynamic potentials for the even and odd ensembles one can easily determine the equilibrium current I. Here we will be interested in describing the currents flowing in isolated superconducting rings pierced by the external magnetic flux Φ_x. Then in the case of even/odd total number of electrons one obtains

$$I_{e/o}=I_f\pm\frac{I_b-I_f}{\mathrm{e}^{\beta(\Omega_b-\Omega_f)}\pm 1}, \tag{43}$$

where the upper/lower sign corresponds to the even/odd ensemble and we have defined

$$I_{e/o}=-c\left(\frac{\partial\Omega_{e/o}}{\partial\Phi_x}\right)_{\mu(\Phi_x)},\quad I_{f/b}=-c\left(\frac{\partial\Omega_{f/b}}{\partial\Phi_x}\right)_{\mu(\Phi_x)}.$$

3.2. Parity effect in nanorings and blocking of the supercurrent

Let us now make use of the above general expressions and investigate the influence of the parity effect on the PC in superconducting nanorings with quantum point contacts (QPCs). Before turning to concrete calculations we shall specify the model for our system. We shall consider mesoscopic superconducting rings with cross section s and perimeter $L=2\pi R$. The rings will be assumed sufficiently thin, i.e., $\sqrt{s}\ll\lambda_L$, where λ_L is the London penetration length. Superconductivity will be described within the (parity projected) mean field BCS theory. At sufficiently low temperatures this description is justified provided that the quantum phase slips (QPS)[51–53] in the nanorings can be neglected. This requirement in turn implies that the ring cross section should be sufficiently large. With the aid of the results of Ref. 51 one concludes that the QPS tunneling amplitude remains exponentially small provided that the condition $s\gg\lambda_F^2\sqrt{\xi_0/l}$ is satisfied. Here λ_F is the Fermi wavelength, $\xi_0\sim v_F/\Delta$ is the coherence length, and l is the electron elastic mean free path, which is assumed to be shorter than ξ_0. For generic systems QPS effects can usually be neglected provided that the transverse size $\sqrt{s}$ of the wire/ring exceeds ~ 10 nm. Hence, the total number of conducting channels in the ring $N_r\sim s/\lambda_F^2$ must inevitably be large $N_r\gg 1$. In addition, the ring perimeter L should not be too large, so that one can disregard the QPS-induced reduction of the PC amplitude.[53] Finally, we will neglect the difference between the mean field values of the BCS order parameter for the even and odd ensembles.[48,49] This is legitimate provided the volume of the superconducting ring is large enough, $\mathcal{V}=Ls\gg 1/\nu\Delta$, where ν is the density of states at the Fermi level and Δ is the BCS order parameter for the bulk superconductor at $T=0$. All these requirements can easily be met in a modern experiment.

The task at hand is now to evaluate the thermodynamic potentials Ω_{fb}. Within the mean field treatment these quantities can be expressed in terms of the excitation energies ε_k and the superconducting order parameter $\Delta(\mathbf{r})$. One finds[49]

$$\Omega_f=\tilde{\Omega}-2T\sum_k\ \ln\left(2\cosh\frac{\varepsilon_k}{2T}\right), \tag{44}$$

$$\Omega_b=\tilde{\Omega}-2T\sum_k\ \ln\left(2\sinh\frac{\varepsilon_k}{2T}\right), \tag{45}$$

where $\tilde{\Omega}=\int d^3\mathbf{r}|\Delta(\mathbf{r})|^2/g+\mathrm{Tr}\{\hat{\xi}\}$, g is the BCS coupling constant, and $\hat{\xi}$ is the single-particle energy operator:

$$\hat{\xi}=\frac{1}{2m}\left(-i\hbar\frac{\partial}{\partial\mathbf{r}}-\frac{e}{c}\mathbf{A}(\mathbf{r})\right)^2+U(\mathbf{r})-\mu, \tag{46}$$

$\mathbf{A}(\mathbf{r})$ is the vector potential, and $U(\mathbf{r})$ describes the potential profile due to disorder and interfaces.

The excitation spectrum ε_k has the form

$$\varepsilon_k=\varepsilon(\mathbf{p})=\mathbf{p}\mathbf{v}_s+\sqrt{\xi^2+\Delta^2}, \tag{47}$$

where $\mathbf{p}$ is the quasiparticle momentum, $\xi=(p^2-\tilde{\mu})/2m$, and $\tilde{\mu}=\mu(\Phi_x)-mv_s^2/2$. The superconducting velocity vector $\mathbf{v}_s$ is oriented in the direction along the ring and is defined by the well-known expression

$$v_s=\frac{\hbar}{2mR}\min_n\left(n-\frac{\Phi_x}{\Phi_0}\right). \tag{48}$$

This expression and the excitation spectrum (47) are periodic functions of the flux Φ_x with period equal to the superconducting flux quantum $\Phi_0=hc/2e$.

Consider the most interesting case $T\to 0$. Making use of the above expressions, one easily finds

$$I_e=ev_s\rho_e s,\quad \mu_e=\mu(\rho_e)+mv_s^2/2 \tag{49}$$

for the even ensemble and

$$I_o=ev_s\rho_o s-e\frac{v_F}{L}\mathrm{sgn}(v_s),\quad \rho_o=\rho+\frac{1}{\mathcal{V}}\frac{|v_s|}{v_\mu} \tag{50}$$

for the odd one. Here $\rho_{e/o}=\mathcal{N}_{e/o}/\mathcal{V}$ are the electron densities for the even and odd ensembles, ρ is the grand canonical electron density at $T=0$, $v_\mu=\sqrt{2\mu/m}$, and v_s is assumed to be small as compared to the critical velocity $v_c=\Delta/p_F$. We also note that the second equation in (50) is an implicit equation for the chemical potential μ_o.

Equation (49), taken together with Eq. (48), coincides with that obtained for the grand canonical ensemble. In particular, the current I_e represents the well known ''saw-tooth'' dependence on magnetic flux. In contrast, for odd ensembles there exists an additional flux-dependent contribution to PC (50) which cannot be viewed as just a renormalization of ρ_o.

Unfortunately, this parity effect is rather small in multichannel rings, as we mentioned above. Estimating the leading contribution to $I_{e/o}$ as $I\sim ev_FN_r/L$, we find

$$(I_e-I_o)/I\sim 1/N_r\ll 1.$$

The results (49), (50) hold as long as $T\ll\hbar v_F/L$. At higher temperatures the parity effect gets even smaller and eventually disappears at temperatures exceeding the parameter[45] $T^*\approx\Delta/\ln(\nu\mathcal{V}\sqrt{\Delta T^*})$. The corresponding expressions are readily obtained within our formalism, but we will not consider them here.

Rather we turn to a somewhat different system—a superconducting ring interrupted by QPC—in which the parity effect turns out to play a much more important role. In this case the thermodynamic potential Ω of the system consists of two different contributions[2)]

$$\Omega=\Omega^{(r)}(\mu,T,\Phi_x,\phi)+\Omega^{(c)}(\mu,T,\phi) \tag{51}$$

from the bulk part of the ring and from the QPC, respectively.

The optimal value of the phase difference ϕ across the QPC is fixed by the condition $\partial\Omega/\partial\phi=0$, which reads

$$-c\frac{\partial\Omega^{(r)}}{\partial\Phi_x}=-\frac{2e}{\hbar}\frac{\partial\Omega^{(c)}}{\partial\phi}. \tag{52}$$

Here we have made use of the fact that the thermodynamic potentials of the ring depend both on Φ_x and ϕ only via the superfluid velocity $v_s=(1/4\pi mR)(\phi-2\pi\Phi_x/\Phi_0)$, in which case one can put $\partial/\partial\Phi_x=-(2e/\hbar c)(\partial/\partial\phi)$. The left-hand side of Eq. (52) represents the current flowing inside the superconducting ring $I^{(r)}=-c\partial\Omega^{(r)}/\partial\Phi_x\simeq(ev_FN_r/L)\times(\phi-2\pi\Phi_x/\Phi_0)$. This value should be equal to the current across the QPC, which is given by the right-hand side of Eq. (52). Estimating the maximum value of the latter for a single-channel QPC as $2e\mathcal{T}\Delta/\hbar$, we obtain

$$\phi\simeq 2\pi\frac{\Phi_x}{\Phi_0},\ \text{if}\ L\ll L^*, \tag{53}$$

$$\phi\simeq 2\pi n,\ \text{if}\ L\gg L^*, \tag{54}$$

where $L^*=\xi_0N_r/\mathcal{T}\gg\xi_0$. In a more general case of a QPC with N conducting channels, in the expression for L^* one should set

$$\mathcal{T}\to\sum_n^N\mathcal{T}_n.$$

In what follows we will consider the most interesting limit $N\ll N_r$ and $L\ll L^*$. Due to Eq. (53) in this case the dependence $I_{e/o}(\Phi_x)$ is fully determined by the current-phase relation for the QPC, which can be found by means of Eq. (43) with $I_{f/b}=-(2e/\hbar)\partial\Omega_{f/b}^{(c)}/\partial\phi$. It is convenient to employ the formula[8]

$$I_{f/b}=\frac{2e}{\hbar}\sum_{n=1}^N T\sum_{\omega_{f/b}}\frac{\sin\phi}{\cos\phi+W_n(\omega_{f/b})}. \tag{55}$$

In the case of short QPS one has

$$W_n(\omega)=(2/\mathcal{T}_n)(1+\omega^2/\Delta^2)-1,$$

where $\mathcal{T}_n$ is the transmission of the nth conducting channel. Substituting this function into (55) and summing over ω_f, one recovers the standard result[16,21]

$$I_f(\phi)=-\frac{2e}{\hbar}\sum_{n=1}^N\frac{\partial\varepsilon_n(\phi)}{\partial\phi}\tanh\frac{\varepsilon_n(\phi)}{2T}, \tag{56}$$

where

$$\varepsilon_n(\phi)=\Delta\sqrt{1-\mathcal{T}_n\sin^2(\phi/2)}. \tag{57}$$

The same summation over Bose Matsubara frequencies ω_b yields

$$I_b=-\frac{2e}{\hbar}\sum_{n=1}^N\frac{\partial\varepsilon_n(\phi)}{\partial\phi}\coth\frac{\varepsilon_n(\phi)}{2T}. \tag{58}$$

Finally, the difference $\Omega_b-\Omega_f\equiv\Omega_{bf}$ is evaluated as a sum of the ring ($\Omega_{bf}^{(r)}$) and QPS ($\Omega_{bf}^{(c)}$) contributions. The latter is found by integrating $I_{f/b}(\phi)$ over the phase difference ϕ:

$$\Omega_{bf}^{(c)}=2T\sum_{n=1}^N\ln\coth\left(\frac{\varepsilon_n(\phi)}{2T}\right), \tag{59}$$

while the former is defined by the standard expression[49]

$$\beta\Omega_{bf}^{(r)}=2\mathcal{V}\int\frac{d^3\mathbf{p}}{(2\pi\hbar)^3}\ln\left(\coth\frac{\varepsilon(\mathbf{p})}{2T}\right)\simeq v\mathcal{V}\sqrt{\Delta T}\mathrm{e}^{-\Delta T}.$$

Combining all these results with Eq. (43), we get

$$I_{e/o}=-\frac{2e}{\hbar}\sum_{n=1}^{N}\frac{\partial\varepsilon_n(\phi)}{\partial\phi}\tanh\frac{\varepsilon_n(\phi)}{2T}\times\left[1\pm\frac{\left(\coth\dfrac{\varepsilon_n(\phi)}{2T}\right)^2-1}{\mathrm{e}^{\beta\Omega_{bf}^{(r)}}\displaystyle\prod_{i=1}^{N}\left(\coth\dfrac{\varepsilon_i(\phi)}{2T}\right)^2\pm1}\right]. \tag{60}$$

Equation (60) represents the central result of this Section. Together with Eq. (53) it establishes the complete dependence of the PC on the magnetic flux Φ in isolated superconducting nanorings with QPCs.

Consider the most interesting limit $T\to0$. In this case for an even number of electrons in the ring the PC is given by expression (56), which coincides identically with that for grand canonical ensembles.[16,21] On the other hand, for an odd number of electrons the PC will acquire an additional contribution which turns out to be most important for the case of a single-channel QPC, $N=1$. In that case the expression in the square brackets of Eq. (60) reduces to zero, i.e., the PC will be totally blocked by the odd electron. Thus, we predict a novel mesoscopic effect—parity-influenced blocking of PC in superconducting nanorings with QPCs.

This result has a transparent physical interpretation. Indeed, it is well known[47] that the result (56) can be expressed via the contributions of discrete Andreev levels $E_{\pm}(\phi)=\pm\Delta\mathcal{D}(\phi)$ inside the QPC as

$$I(\phi)=\frac{2e}{\hbar}\left[\frac{\partial E_-}{\partial\phi}f_-(E_-)+\frac{\partial E_+}{\partial\phi}f_+(E_+)\right], \tag{61}$$

where $\mathcal{D}(\phi)$ is defined in Eq. (19). Using the Fermi filling factors for these levels $f_{\pm}(E_{\pm})=[1+\exp(E_{\pm}(\phi)/T)]^{-1}$ one arrives at Eq. (56). If we now fix the number of electrons inside the ring and consider the limit $T\to0$ the filling factors will be modified as follows. For even numbers $\mathcal{N}$ all of the electrons are paired, occupying states with energies below the Fermi level. In this case one has $f_-(E_-)=1$, $f_+(E_+)=0$, the current is entirely determined by the contribution of the quasiparticle state E_-, and Eq. (61) yields the same result as for the grand canonical ensemble. By contrast, in the case of an odd number of electrons, one electron always remains unpaired and occupies the lowest available energy state—in our case E_+—above the Fermi level. Hence, for odd $\mathcal{N}$ one has $f_{\pm}(E_{\pm})=1$, the contributions of two quasiparticle energy states in Eq. (61) exactly cancel each other, and the current across the QPC remains zero for any ϕ or magnetic flux Φ_x. This is just the blocking effect which we have already obtained above from a more formal consideration.

For $N>1$ and/or at nonzero temperatures this parity-influenced blocking of PC becomes incomplete. But also in this case the parity effect remains essential at temperatures $T<T^*$, substantially affecting, e.g., the current-phase relation for the QPC. For $T>0$ this relation will deviate from the grand canonical one both for even and odd ensembles.[9]

Finally, we consider superconducting rings containing a piece of a normal metal. Here we restrict our attention to transparent SNS junctions with lengths of the normal metal $d\gg\xi_0$. In this case for $\omega\ll\Delta$ one has $W_i(\omega)=\cosh(2\omega d/v_F)$. Substituting this function into (55) and repeating the whole calculation as above, in the limit $T\to0$ we obtain

$$I_e=\frac{ev_FN}{\pi d}\phi,\quad I_o=\frac{ev_FN}{\pi d}\left(\phi-\frac{\pi\,\mathrm{sgn}\,\phi}{N}\right). \tag{62}$$

These results apply for $-\pi<\phi<\pi$ and should be 2π-periodically continued otherwise. We observe that the current I_e again coincides with that for the grand canonical ensembles,[11] while for odd $\mathcal{N}$ the current-phase relation is shifted by the value π/N. This shift has a simple interpretation as being related to the odd-electron contribution $(2e/\hbar)\partial E_0/\partial\phi$ from the lowest (above the Fermi level) Andreev state $E_0(\phi)$ inside the SNS junction. Unlike in QPC, this contribution does not compensate for the current from other quasiparticle states. Rather it provides a possibility for a parity-induced π-junction state in our system. Indeed, according to Eq. (62) for single mode SNS junctions the ''sawtooth'' current-phase relation will be shifted exactly by π. For more than one conducting channel $N>1$ within the interval $-\pi<\phi<\pi$ there exists a twofold degenerate minimum energy (zero current) state occurring at $\phi=\pm\pi/N$.[54] In the special case $N=2$ the current-phase relation $I_o(\phi)$ turns π-periodic.

The well known feature of superconducting rings interrupted by a π-junction is the possibility of *spontaneous* supercurrent developing in the ground state.[55] Although this feature is inherent to any type of π-junctions, in the case of the standard sinusoidal current-phase relation, such spontaneous supercurrents can occur only for sufficiently large values of the ring inductance $\mathcal{L}$.[55] In contrast, in the situation studied here the spontaneous current state is realized for any inductance of the ring because of the nonsinusoidal dependence $I_o(\phi)$ (62).

In order to demonstrate that, let us assume that no external flux is applied to our system. Then at $T\to0$ the energy of an SNS ring with an odd number of electrons can be written in the form

$$E_o=\frac{\Phi^2}{2c\mathcal{L}}+\frac{\pi\hbar v_FN}{\Phi_0^2d}\left(\Phi-\frac{\Phi_0\,\mathrm{sgn}\,\Phi}{2N}\right)^2, \tag{63}$$

where Φ is the flux related to the circular current flowing in the ring. Minimizing this energy with respect to Φ, one easily observes that a nonzero spontaneous current

$$I=\pm\frac{ev_F}{d}\left[1+\frac{2ev_FN}{d}\frac{\mathcal{L}}{\Phi_0}\right]^{-1} \tag{64}$$

should flow in the ground state of our system. This is yet one more remarkable consequence of the parity effect: Just by changing $\mathcal{N}$ from even to odd, one can induce nonzero PC without any external flux Φ_x. In the limit of low inductances $\mathcal{L}\ll\Phi_0d/ev_fN$, which is easy to reach in the systems under consideration, the value of I does not depend on the number

of channels N and is given by the universal formula $I=\pm ev_F/d$. For generic parameters this value can easily be as large as $I\sim 10$ nA.

In summary, new physical effects emerge from an interplay between the electron parity number and persistent currents in superconducting nanorings. These effects can be directly tested in modern experiments and possibly used for engineering new types of superconducting flux–charge qubits.

The author gratefully acknowledges collaboration and numerous discussions with A. V. Galaktionov, D. S. Golubev, and S. V. Sharov. This work is part of the Kompetenznetz ''Funktionelle Nanostructuren'' supported by the Landestiftung Baden-Württemberg gGmbH. This work has also been supported by the European Community's Framework Program NMP4-CT-2003-505457 ULTRA-1D ''Experimental and theoretical investigation of electron transport in ultranarrow 1-dimensional nanostructures.''

*E-mail: zaikin@tfp.physik.uni-karlsruhe.de

[1)]This deviation is not as strong as in the ballistic case: The supercurrent in long diffusive junctions reaches its maximum at the value $\phi\simeq 1.27\pi/2$ (Ref. 15).

[2)]Relation (51) is strictly applicable only for grand canonical ensembles. However, at this point the difference between canonical and grand canonical ensembles is unimportant and can be disregarded.

[1] A. Einstein, Kuratoriumssitzung der Physikalisch-Technischen Reichsanstalt (Berlin Charlottenburg), March 1926: ''Von besonderem Interesse ist die Frage, ob die Verbindungsstelle zwischen zwei Supraleitern auch supraleitend wird.''
[2] B. Josephson, Phys. Lett. A **1**, 251 (1962).
[3] V. Ambegaokar and A. Baratoff, Phys. Rev. Lett. **10**, 486 (1963); **11**, 104 (1963).
[4] A. I. Larkin and Yu. N. Ovchinnikov, Zh. Éksp. Teor. Fiz. **51**, 1535 (1966) [Sov. Phys. JETP **24**, 1035 (1967)].
[5] N. R. Werthamer, Phys. Rev. **147**, 255 (1966).
[6] P. W. Anderson and J. M. Rowell, Phys. Rev. Lett. **10**, 230 (1963); J. M. Rowell, *ibid.* **11**, 200 (1963).
[7] I. K. Yanson, V. M. Svistunov, and I. M. Dmitrenko, Zh. Éksp. Teor. Fiz. **47**, 2091 (1964) [Sov. Phys. JETP **20**, 1404 (1965)].
[8] A. V. Galaktionov and A. D. Zaikin, Phys. Rev. B **65**, 184507 (2002).
[9] S. V. Sharov and A. D. Zaikin, cond-mat/0401338.
[10] A. F. Andreev, Zh. Éksp. Teor. Fiz. **46**, 1823 (1964) [Sov. Phys. JETP **19**, 1228 (1964)].
[11] I. O. Kulik, Zh. Éksp. Teor. Fiz. **57**, 1745 (1969) [Sov. Phys. JETP **30**, 944 (1970)].
[12] C. Ishii, Prog. Theor. Phys. **44**, 1525 (1970).
[13] K. K. Likharev, Pis'ma Zh. Tech. Phys. **2**, 29 (1976) [Sov. Tech. Phys. Lett. **2**, 12 (1976)].
[14] A. D. Zaikin and G. F. Zharkov, Fiz. Nizk. Temp. **7**, 375 (1981) [Sov. J. Low Temp. Phys. **7**, 184 (1981)].
[15] P. Dubos, H. Courtois, B. Pannetier, F. K. Wilhelm, A. D. Zaikin, and G. Schön, Phys. Rev. B **63**, 064502 (2001).
[16] I. O. Kulik and A. N. Omel'yanchouk, Fiz. Nizk. Temp. **4**, 296 (1978) [Sov. J. Low Temp. Phys. **4**, 142 (1978)].
[17] G. Eilenberger, Z. Phys. **214**, 195 (1968).
[18] A. I. Larkin and Yu. N. Ovchinnikov, in *Nonequilibrium Superconductivity*, edited by D. N. Langenberg and A. I. Larkin, North-Holland, Amsterdam (1986).
[19] A. Schmid, in *Nonequilibrium Superconductivity*, edited by K. E. Gray, Plenum, New York (1981).
[20] K. D. Usadel, Phys. Rev. Lett. **25**, 507 (1970).
[21] W. Haberkorn, H. Knauer, and J. Richter, Phys. Status Solidi A **47**, K161 (1978).
[22] A. D. Zaikin and G. F. Zharkov, Zh. Éksp. Teor. Fiz. **78**, 721 (1980) [Sov. Phys. JETP **51**, 364 (1980)].
[23] A. D. Zaikin and G. F. Zharkov, Zh. Éksp. Teor. Fiz. **81**, 1781 (1981) [Sov. Phys. JETP **57**, 944 (1981)].
[24] A. A. Svidzinskii, *Spatially Inhomogeneous Problems in the Theory of Superconductivity* [in Russian], Nauka, Moscow (1982).
[25] A. D. Zaikin and G. F. Zharkov, JETP Lett. **35**, 636 (1982).
[26] M. Yu. Kupriyanov and V. F. Lukichev, Zh. Éksp. Teor. Fiz. **94**, 139 (1988) [Sov. Phys. JETP **67**, 1163 (1988)].
[27] A. A. Golubov and M. Yu. Kupriyanov, J. Low Temp. Phys. **70**, 83 (1988).
[28] A. A. Golubov and M. Yu. Kupriyanov, Zh. Éksp. Teor. Fiz. **105**, 1442 (1994) [Sov. Phys. JETP **78**, 777 (1994)].
[29] C. J. Lambert and R. Raimondi, J. Phys.: Condens. Matter **10**, 901 (1998).
[30] W. Belzig, F. K. Wilhelm, C. Bruder, G. Schön, and A. D. Zaikin, Superlattices Microstruct. **25**, 1251 (1999).
[31] A. A. Golubov, M. Yu. Kupriyanov, and E. Il'ichev, Rev. Mod. Phys. **76**, 411 (2004).
[32] Yu. Kasumov *et al.*, Science **281**, 540 (1998).
[33] M. R. Buitelaar, T. Nussbaumer, and C. Schoenenberger, Phys. Rev. Lett. **89**, 256801 (2003).
[34] M. R. Buitelaar, W. Belzig, T. Nussbaumer, B. Babic, C. Bruder, and C. Schoenenberger, Phys. Rev. Lett. **91**, 057003 (2003).
[35] M. Yu. Kupriyanov, A. Brinkman, A. A. Golubov, M. Siegel, and H. Rogalla, Physica C **326–327**, 16 (1999).
[36] A. V. Zaitsev, Zh. Éksp. Teor. Fiz. **86**, 1742 (1984) [Sov. Phys. JETP **59**, 1015 (1984)].
[37] A. D. Zaikin and S. V. Panyukov, in *Nonequilibrium Superconductivity*, edited by V. L. Ginzburg, Nova Science Publ., New York (1988), p. 137.
[38] U. Gunsenheimer and A. D. Zaikin, Phys. Rev. B **50**, 6317 (1994).
[39] A. A. Abrikosov, L. P. Gor'kov, and I. Ye. Dzyaloshinkski, *Quantum Field Theoretical Methods in Statistical Physics*, 2nd ed., Pergamon, Oxford (1965).
[40] A. Brinkman and A. A. Golubov, Phys. Rev. B **61**, 11297 (2000).
[41] L. D. Landau and E. M. Lifshitz, *Quantum Mechanics*, Pergamon, Oxford (1962).
[42] L. I. Glazman and K. A. Matveev, JETP Lett. **49**, 659 (1989).
[43] C. W. J. Beenakker, Phys. Rev. Lett. **67**, 3836 (1991).
[44] D. V. Averin and Yu. V. Nazarov, Phys. Rev. Lett. **69**, 1993 (1992).
[45] M. T. Tuominen, J. M. Hergenrother, T. S. Tighe, and M. Tinkham, Phys. Rev. Lett. **69**, 1997 (1992).
[46] P. Lafarge, P. Joyes, D. Esteve, C. Urbina, and M. H. Devoret, Phys. Rev. Lett. **70**, 994 (1993).
[47] A. Furusaki and M. Tsukada, Physica B **165–166**, 967 (1990); C. W. J. Beenakker and H. van Houten, Phys. Rev. Lett. **66**, 3056 (1991).
[48] B. Janko, A. Smith, and V. Ambegaokar, Phys. Rev. B **50**, 1152 (1994).
[49] D. S. Golubev and A. D. Zaikin, Phys. Lett. B **195**, 380 (1994).
[50] D. V. Averin and Yu. V. Nazarov, Physica B **203**, 310 (1994).
[51] A. D. Zaikin, D. S. Golubev, A. van Otterlo, and G. T. Zimányi, Phys. Rev. Lett. **78**, 1552 (1997); D. S. Golubev and A. D. Zaikin, Phys. Rev. B **64**, 014504 (2001).
[52] A. Bezryadin, C. N. Lau, and M. Tinkham, Nature (London) **404**, 971 (2000); C. N. Lau *et al.*, Phys. Rev. Lett. **87**, 217003 (2001).
[53] K. A. Matveev, A. I. Larkin, and L. I. Glazman, Phys. Rev. Lett. **89**, 096802 (2002).
[54] A similar behavior is expected for SNS junctions formed by d-wave superconductors; for further discussion see Yu. S. Barash, A. V. Galaktionov, and A. D. Zaikin, Phys. Rev. B **52**, 665 (1995).
[55] L. N. Bulaevskii, V. V. Kuzii, and A. A. Sobyanin, JETP Lett. **25**, 290 (1977).

This article was published in English in the original Russian journal. Reproduced here with stylistic changes by AIP.

Impurity scattering effect on charge transport in high-T_c cuprate junctions

Y. Tanaka*

Department of Applied Physics, Nagoya University, Japan; CREST, Japan Science and Technology Corporation, Japan

Y. Asano

Department of Applied Physics, Hokkaido University, Sapporo 060-8628, Japan

S. Kashiwaya

NRI of AIST, Umezono, Tsukuba, Japan

(Submitted February 9, 2004)
Fiz. Nizk. Temp. **30**, 770–784 (July–August 2004)

It is known that the zero-bias conductance peak (ZBCP) is expected in tunneling spectra of normal-metal/high-T_c cuprate junctions because of the formation of the midgap Andreev resonant states (MARS) at junction interfaces. In the present review, we report the recent theoretical study of impurity scattering effects on the tunneling spectroscopy. In the former part of the present paper, we discuss impurity effects in the normal metal. We calculate tunneling conductance for diffusive normal metal (DN)/high-T_c cuprate junctions based on the Keldysh Green function technique. Besides the ZBCP due to the MARS, we can expect ZBCP of a different origin, i.e., caused by coherent Andreev reflection (CAR) assisted by the proximity effect in DN. Their relative importance depends on the angle α between the interface normal and the crystal axis of high-T_c superconductors. At $\alpha=0$ we find the ZBCP by the CAR for low-transparency junctions with small Thouless energies in DN; this is similar to the case of diffusive normal metal/insulator/s-wave superconductor junctions. Under increase of α from zero to $\pi/4$, the contribution of MARS to ZBCP becomes more prominent and the effect of the CAR is gradually suppressed. Such complex spectral features would be observable in conductance spectra of high-T_c junctions at very low temperatures. In the latter part of our paper, we study impurity effects in superconductors. We consider impurities near the junction interface on the superconductor side. The conductance is calculated from the Andreev and the normal reflection coefficients, which are estimated by using the single-site approximation in an analytic calculation and by the recursive Green function method in a numerical simulation. We find splitting of the ZBCP in the presence of the time reversal symmetry. Thus the zero-field splitting of ZBCP in the experiment does not perfectly prove the existence of a broken time reversal symmetry state. © *2004 American Institute of Physics.* [DOI: 10.1063/1.1789915]

1. INTRODUCTION

Nowadays, charge transport in unconventional superconductor junctions has become one of the most important topics in solid state physics. The most remarkable property is the so-called zero bias conductance peak (ZBCP) observed in tunneling experiments. The ZBCP arises from the formation of midgap Andreev bound states (MARS) at the interface.[1–5] The MARS, which are created by injected and reflected quasiparticles feeling different signs of the pair potential, can play an important role in determining the pairing symmetry of unconventional superconductors. The experimental observation of the ZBCP has been reported for various unconventional superconductors of anisotropic pairing symmetries.[5–20] A basic theory of the ballistic transport in the presence of MARS has been formulated in Refs. 3 and 5. Stimulated by this theory, extensive studies of MARS in unconventional superconductor junctions have been performed during the last decade: in the case of broken time reversal symmetry state,[21–28] in triplet superconductor junctions,[29–34] in quasi-one-dimensional organic superconductors,[35–38] MARS and the Doppler effect,[39–43] MARS in ferromagnetic junctions,[44–52] influence of MARS on the Josephson effect,[53–62] and other related problems.[63–71] However, the impurity scattering effect on the ZBCP in realistic normal metal/high-T_c cuprate junctions has not been clarified yet. The aim of the present paper is to review the important progress on this topic.

The organization of the paper is as follows. In Sec. 2, we discuss the impurity scattering effect in normal metal. We calculate the tunneling conductance for diffusive normal metal (DN)/high-T_c cuprate junctions based on the Keldysh Green function technique. Besides the ZBCP due to the MARS, we can expect ZBCP caused by a different mechanism, i.e., coherent Andreev reflection (CAR) assisted by proximity effect in DN. In Sec. 3, we discuss impurity effects in superconductors. The random potential near junction interfaces causes splitting of the ZBCP even in the presence of the time reversal symmetry.

2. THEORY OF CHARGE TRANSPORT IN DIFFUSIVE NORMAL METAL/HIGH-T_c CUPRATE SUPERCONDUCTOR CONTACTS

Before discussing charge transport in high-T_c cuprate junctions, we should review the progress of charge transport in mesoscopic superconducting systems. The low-energy transport in mesoscopic superconducting systems is governed by Andreev reflection,[72] a unique process specific to electron scattering at normal metal/superconductor interfaces. The phase coherence between incoming electrons and Andreev reflected holes persists at a mesoscopic length scale in the diffusive normal metal, which enhances interference effects on the probability of Andreev reflection.[73] The coherence plays an important role at sufficiently low temperatures and voltages when the energy broadening due to either voltages or temperatures becomes of the order of the Thouless energy E_{Th} in mesoscopic structures. As a result, the conductance spectra of mesoscopic junctions may be significantly modified by these interference effects. A remarkable experimental manifestation of the electron–hole phase coherence is the observation of the zero-bias conductance peak (ZBCP) in diffusive normal metal (N)/superconductor (S) tunneling junctions.[74–84]

Various theoretical models of charge transport in diffusive junctions extend the clean limit theories developed by Blonder, Tinkham, and Klapwijk[85] (BTK) and by Zaitsev.[86]. In Refs. 87–92, the scattering matrix approach was used. On the other hand, the quasiclassical Green function method in nonequilibrium superconductivity[93] is much more powerful and convenient for the actual calculations of the conductance at arbitrary bias voltages.[94] Using the Kuprianov and Lukichev (KL) boundary condition[95] for a diffusive SIN interface, Volkov, Zaitsev and Klapwijk (VZK) have obtained the conductance spectra with ZBCP, the origin of which was attributed to coherent Andreev reflection (CAR), which induces the proximity effect in the diffusive metal.[94] Several authors have studied the charge transport in mesoscopic junctions, combining this boundary condition with the Usadel[96] equation that describes superconducting correlations in the diffusive metal.[97–103] The modified boundary conditions were studied by several authors.[104,105] Important progress was achieved by Nazarov,[97,106] who developed a much more intuitive theory (the so-called ''circuit theory'') for matrix currents, which allows one to formulate boundary conditions for Usadel-like equations in the case of arbitrary transparencies.[107] Recently we have succeeded in extending this circuit theory for unconventional superconductors.[108–110] In order to resolve the charge transport in high-T_c cuprate junctions, we apply above theory for d-wave superconductors. We have shown that the formation of MARS strongly competes with the proximity effect that is an essential ingredient for CAR in diffusive conductor (DN). We consider a junction consisting of normal and superconducting reservoirs connected by a quasi-one-dimensional DN with a length L much larger than the elastic mean free path. The interface between the DN and the US (unconventional superconductor) electrode has a resistance R_b, while the DN/N interface has zero resistance. The positions of the DN/N interface and the DN/S interface are denoted as $x=-L$ and $x=0$, respectively. According to the circuit theory,[106] the constriction area between DN and US is considered as composed of a diffusive isotropization zone, a left side ballistic zone, a right side ballistic zone, and a scattering zone. The scattering zone is modeled as an insulating delta-function barrier with the transparency $T_n=4\cos^2\varphi/(4\cos^2\varphi+Z^2)$, where Z is a dimensionless constant, φ is the injection angle measured from the interface normal to the junction, and n is the channel index. We assume that the sizes of the ballistic and scattering zones along the x axis is much shorter than the superconducting coherence length.

Here, we express insulating barrier as a delta-function model $H\delta(x)$, where Z is given by $Z=2mH/(\hbar^2 k_F)$ with Fermi momentum k_F and effective mass m. In order to clarify the charge transport in DN/US junctions, we must obtain the Keldysh–Nambu Green function, which has indices of the transport channels and the direction of motion along the x axis, taking into account the proper boundary conditions. For this purpose it is necessary to extend a general theory of boundary conditions which covers the crossover from the ballistic to the diffusive case,[106] formulated for conventional junctions in the framework of the circuit theory.[97,106] However, the circuit theory cannot be directly applied to unconventional superconductors, since it requires isotropization. The latter is simply incompatible with the mere existence of unconventional superconductivity. To avoid this difficulty we restrict the discussion to the conventional model of a smooth interface by assuming momentum conservation in the plane of the interface. We apply the quasiclassical Keldysh formalism for calculation of the conductance. The spatial dependence of the 4×4 Green function $G_N(x)$ in DN, which is expressed in matrix form as

$$\check{G}_N(x)=\begin{pmatrix}\hat{R}_N(x) & \hat{K}_N(x)\\ 0 & \hat{A}_N(x)\end{pmatrix}, \tag{1}$$

must be determined. The Keldysh component $\hat{K}_N(x)$ is given by $\hat{K}_N(x)=\hat{R}_N(x)\hat{f}_1(x)-\hat{f}_1(x)\hat{A}_N(x)$ with retarded component $\hat{R}_N(x)$ and advanced component $\hat{A}_N(x)$ using distribution function $\hat{f}_1(x)$. We put the zero of electrical potential in the S electrode. In this case the spatial dependence of $\check{G}_N(x)$ in DN is determined by the static Usadel equation,[96]

$$D\frac{\partial}{\partial x}\left[\check{G}_N(x)\frac{\partial\check{G}_N(x)}{\partial x}\right]+i[\check{H},\check{G}_N(x)]=0, \tag{2}$$

with the diffusion constant D in DN, where $\check{H}$ is given by

$$\check{H}=\begin{pmatrix}\hat{H}_0 & 0\\ 0 & \hat{H}_0\end{pmatrix} \tag{3}$$

with $\hat{H}_0=\varepsilon\hat{\tau}_3$.

The boundary condition for $\check{G}_N(x)$ at the DN/S interface is given by

$$\frac{L}{R_d}\left[\check{G}_N(x)\frac{\partial\check{G}_N(x)}{\partial x}\right]\Bigg|_{x=0_-}=-\frac{h}{2e^2R_b}\langle\check{I}_{n0}\rangle. \tag{4}$$

$\check{I}$ is given by

$$\check{I}_{n0}=\frac{4e^2}{h}[\check{G}_1,\ \check{B}_n] \tag{5}$$

with

$$\check{B}_n=(-T_{1n}[\check{G}_1,\check{H}_-^{-1}]+\check{H}_-^{-1}\check{H}_+-T_{1n}^2\check{G}_1\check{H}_-^{-1}\check{H}_+\check{G}_1)^{-1}\times(T_{1n}(1-\check{H}_-^{-1})+T_{1n}^2\check{G}_1\check{H}_-^{-1}\check{H}_+). \quad (7)$$

Here $\check{H}_\pm=(\check{G}_{2+}\pm\check{G}_{2-})/2$. R_d and R_b denote the resistance in DN and that at the DN/S interface, respectively. The detailed derivation of the matrix current is shown in Ref. 109. The average over the various angles of injected particles at the interface is defined as

$$\langle\check{I}(\phi)\rangle=\int_{-\pi/2}^{\pi/2}d\phi\cos\phi\check{I}(\phi)\Big/\int_{-\pi/2}^{\pi/2}d\phi T(\phi)\cos\phi, \quad (8)$$

with $\check{I}(\phi)=\check{I}$ and $T(\phi)=T_n$. The resistance of the interface R_b is given by

$$R_b=\frac{h}{2e^2}\frac{2}{\int_{-\pi/2}^{\pi/2}d\phi T(\phi)\cos\phi}, \quad (9)$$

with Sharvin resistance R_0. $\check{G}_N(-L)$ coincides with that in the normal state. We denote the Keldysh–Nambu Green function $\check{G}_1$, $\check{G}_{2\pm}$,

$$\check{G}_1=\begin{pmatrix}\hat{R}_1 & \hat{K}_1\\ 0 & \hat{A}_1\end{pmatrix},\quad \check{G}_{2\pm}=\begin{pmatrix}\hat{R}_{2\pm} & \hat{K}_{2\pm}\\ 0 & \hat{A}_{2\pm}\end{pmatrix}, \quad (10)$$

where the Keldysh component $\hat{K}_{1,2\pm}$ is given by $\hat{K}_{1(2\pm)}=\hat{R}_{1(2\pm)}\hat{f}_{1(2)}(0)-\hat{f}_{1(2)}(0)\hat{A}_{1(2\pm)}$ with the retarded component $\hat{R}_{1,2\pm}$ and the advanced component $\hat{A}_{1,2\pm}$ using distribution function $\hat{f}_{1(2)}(0)$. In the above, $\hat{R}_{2\pm}$ is expressed by

$$\hat{R}_{2\pm}=(g_\pm\hat{\tau}_3+f_\pm\hat{\tau}_2) \quad (11)$$

with $g_\pm=\varepsilon/\sqrt{\varepsilon^2-\Delta_\pm^2}$, $f_\pm=\Delta_\pm/\sqrt{\Delta_\pm^2-\varepsilon^2}$, and $\hat{A}_{2\pm}=-\hat{\tau}_3\hat{R}_{2\pm}^\dagger\hat{\tau}_3$, where ε denotes the quasiparticle energy measured from the Fermi energy. $\hat{f}_2(0)=f_{0S}(0)=\tanh[\varepsilon/(2k_BT)]$ in thermal equilibrium with temperature T.

Using $\check{G}_N(x)$, one expresses the electric current as

$$I_{\rm cl}=\frac{-L}{4eR_d}\int_0^\infty d\varepsilon\,{\rm Tr}\left[\tau_3\left(\check{G}_N(x)\frac{\partial\check{G}_N(x)}{\partial x}\right)^K\right] \quad (12)$$

where $(\check{G}_N(x)\,\partial\check{G}_N(x)/\partial x)^K$ denotes the Keldysh component of $(\check{G}_N(x)\,\partial\check{G}_N(x)/\partial x)$. In the actual calculation, we introduce a parameter $\theta(x)$ which is a measure of the proximity effect in DN, where we have denoted $\theta(0)=\theta_0$. Using $\theta(x)$, $\hat{R}_N(x)$ can be written as

$$\hat{R}_N(x)=\hat{\tau}_3\cos(x)+\hat{\tau}_2\sin\theta(x). \quad (13)$$

$\hat{A}_N(x)$ and $\hat{K}_N(x)$ satisfy the following equations: $\hat{A}_N(x)=-\tau_3\hat{R}_N^\dagger(x)\hat{\tau}_3$, and $\hat{K}_N(x)=\hat{R}_N(x)\hat{f}_1(x)-\hat{f}_1(x)\hat{A}_N(x)$, with the distribution function $\hat{f}_1(x)$ given by $\hat{f}_1(x)=f_{0N}(x)+\hat{\tau}_3f_{3N}(x)$. In the above, $f_{3N}(x)$ is the relevant distribution function which determines the conductance of the junction we are now concentrating on. From the retarded or advanced component of the Usadel equation, the spatial dependence of $\theta(x)$ is determined by the following equation:

$$D\frac{\partial^2}{\partial x^2}\theta(x)+2i\varepsilon\sin[\theta(x)]=0, \quad (14)$$

while for the Keldysh component we obtain

$$D\frac{\partial}{\partial x}\left[\frac{\partial f_{3N}(x)}{\partial x}\cosh^2\theta_{\rm Im}(x)\right]=0 \quad (15)$$

with $\theta_{\rm Im}={\rm Im}[\theta(x)]$. At $x=-L$, since DN is attached to the normal electrode, $\theta(-L)=0$ and the condition $f_{3N}(-L)=f_{t0}$ is satisfied, with

$$f_{t0}=\frac{1}{2}\left\{\tanh\left(\frac{\varepsilon+eV}{2k_BT}\right)-\tanh\left(\frac{\varepsilon-eV}{2k_BT}\right)\right\}, \quad (16)$$

where V is the applied bias voltage. Next, we focus on the boundary condition at the DN/S interface. Taking the retarded part of Eq. (4), we obtain

$$\frac{L}{R_d}\frac{\partial\theta(x)}{\partial x}\bigg|_{x=0_-}=\frac{\langle F\rangle}{R_b}, \quad (17)$$

$$F=\frac{2T_n[\cos\theta_0(f_++f_-)-\sin\theta_0(g_++g_-)]}{(2-T_n)(1+g_+g_-+f_+f_-)+T_n[\cos\theta_0(g_++g_-)+\sin\theta_0(f_++f_-)]}. \quad (18)$$

On the other hand, from the Keldysh part of Eq. (4), we obtain

$$\frac{L}{R_d}\left(\frac{\partial f_{3N}}{\partial x}\right)\cosh^2[{\rm Im}(\theta_0)]\bigg|_{x=0_-}=-\frac{\langle I_{b0}\rangle f_{3N}(0_-)}{R_b}, \quad (19)$$

$$I_{b0}=\frac{T_n}{2}\frac{C_0f_{3N}(0_-)}{|(2-T_n)(1+g_+g_-+f_+f_-)+T_n[\cos\theta_0(g_++g_-)+\sin\theta_0(f_++f_-)]|^2}, \quad (20)$$

$$\begin{aligned}C_0 &= T_n(1+|\cos\theta_0|^2+|\sin\theta_0|^2)\,[|g_++g_-|^2+|f_++f_-|^2+|1+f_+f_-+g_+g_-|^2+|f_+g_--g_+f_-|^2]\\ &+2(2-T_n)\,{\rm Re}\,\{(1+g_+^*g_-^*+f_+^*f_-^*)\,[(\cos\theta_0+\cos\theta_0^*)(g_++g_-)+(\sin\theta_0+\sin\theta_0^*)(f_++f_-)]\}\\ &+4T_n\,{\rm Im}\,(\cos\theta_0\sin\theta_0^*)\,{\rm Im}\,[(f_++f_-)(g_+^*+g_-^*)].\end{aligned} \quad (21)$$

After a simple manipulation, we can obtain $f_{3N}(0_-)$:

$$f_{3N}(0_-)=\frac{R_b f_{t0}}{R_b+\dfrac{R_d\langle I_{b0}\rangle}{L}\displaystyle\int_{-L}^{0}\frac{dx}{\cosh^2\theta_{\rm Im}(x)}}. \tag{22}$$

Since the electric current $I_{\rm el}$ can be expressed via θ_0 in the form

$$I_{\rm el}=-\frac{L}{eR_d}\int_0^{\infty}\left\langle\frac{\partial f_{3N}}{\partial x}\right\rangle\Bigg|_{x=0_-}\cosh^2[{\rm Im}(\theta_0)]d\varepsilon, \tag{23}$$

we obtain the following final result for the current:

$$I_{\rm el}=\frac{1}{e}\int_0^{\infty}d\varepsilon\,\frac{f_{t0}}{\dfrac{R_b}{\langle I_{b0}\rangle}+\dfrac{R_d}{L}\displaystyle\int_{-L}^{0}\frac{dx}{\cosh^2\theta_{\rm Im}(x)}}. \tag{24}$$

Then the total resistance R at zero temperature is given by

$$R=\frac{R_b}{\langle I_{b0}\rangle}+\frac{R_d}{L}\int_{-L}^{0}\frac{dx}{\cosh^2\theta_{\rm Im}(x)}. \tag{25}$$

We will discuss the normalized conductance $\sigma_T(eV)=\sigma_S(eV)/\sigma_N(eV)$, where $\sigma_{S(N)}(eV)$ is the voltage-dependent conductance in the superconducting (normal) state given by $\sigma_S(eV)=1/R$ and $\sigma_N(eV)=\sigma_N=1/(R_d+R_b)$, respectively.

It should be remarked that in the present circuit theory, R_d/R_b can be varied independently of T_n, i.e., of Z, since we can change the magnitude of the constriction area independently. In other words, R_d/R_b is no longer proportional to $T_{\rm av}(L/l)$, where $T_{\rm av}$ is the averaged transmissivity and l is the mean free path in the diffusive region, respectively. Based on this fact, we can choose R_d/R_b and Z as independent parameters.

First, we focus on the line shapes of the conductance, where d-wave symmetry is chosen as the pairing symmetry of the unconventional superconductor. The pair potentials $\Delta_\pm$ are given by $\Delta_\pm=\Delta_0\cos[2(\varphi\mp\alpha)]$, where α denotes the angle between the normal to the interface and the crystal axis of the d-wave superconductors and Δ_0 is the maximum amplitude of the pair potential. In the above, φ denotes the injection angle of the quasiparticle measured from the x axis. It is known that quasiparticles with injection angle φ such that $\pi/4-|\alpha|<|\varphi|<\pi/4+|\alpha|$ feel the MARS at the interface, which induces ZBCP. In the following, we choose a relatively strong barrier $Z=10$. Results for the high-transparency cases are written in detail in Ref. 109.

Let us first choose $\alpha=0$, where ZBCP due to the MARS is absent. We calculate $\sigma_T(eV)$ for various R_d/R_b. For $E_{\rm Th}=\Delta_0$ [see Fig. 1*a*], the magnitude of $\sigma_T(eV)$ for $|eV|<\Delta_0$ increases with the increase of R_d/R_b. First, the line shape of the voltage-dependent conductance remains V-shaped, and only the height of the bottom value is enhanced (curves *2* and *3*). The V-shaped line shape originates from the existence of nodes of the d-wave pair potential. Then, with a further increase of R_d/R_b, a rounded bottom structure (curve *4*) appears, and finally it changes into a nearly flat line shape (curve *5*). For $E_{\rm Th}=0.01\Delta_0$ (Fig. 1*b*), the magnitude of $\sigma_T(eV)$ has a ZBCP once the magnitude of R_d/R_b deviates slightly from 0. The order of magnitude of the ZBCP width is given by $E_{\rm Th}$ as in the case of s-wave junctions.[107] When the magnitude of R_d/R_b exceeds unity, $\sigma_T(eV)$ acquires a zero bias conductance dip (ZBCD) (curve *5*). The qualitative features of the line shapes of $\sigma_T(eV)$ is different from those in s-wave junctions (see Figs. 1 and 2 in Ref. 37). It should be remarked that even in the case of d-wave junctions we can expect ZBCP by CAR as in the case of an s-wave junction for $\alpha=0$.

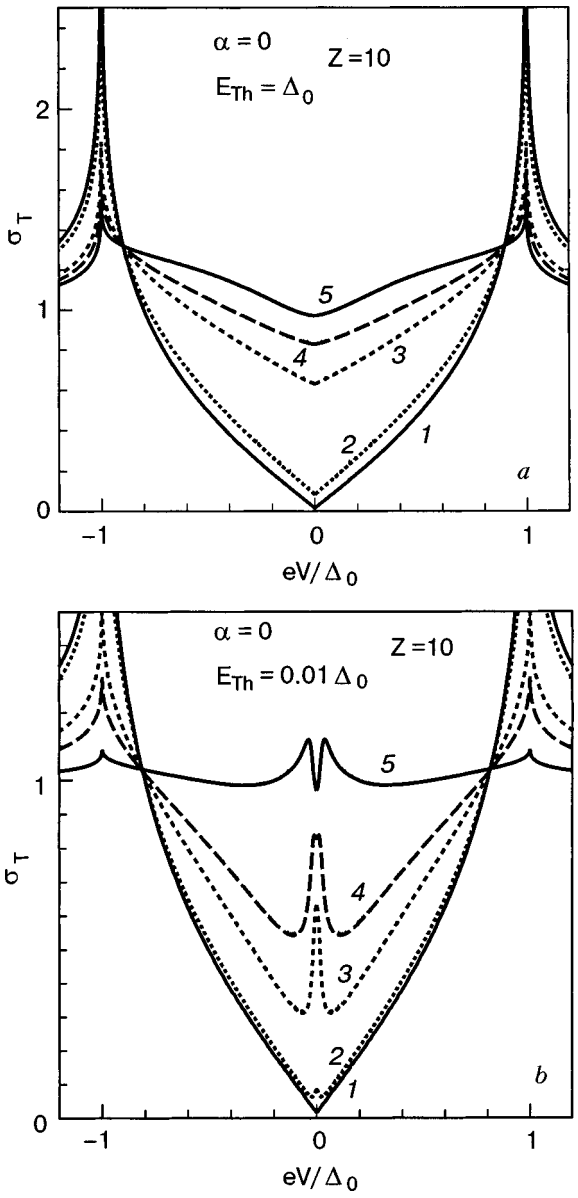

FIG. 1. Normalized conductance $\sigma_T(eV)$ for $Z=10$, $\alpha=0$, and $E_{\rm Th}=\Delta_0$ (*a*), $E_{\rm Th}=0.01\Delta_0$ (*b*) at different R_d/R_b: 0 (*1*), 0.1 (*2*), 1 (*3*), 2 (*4*), and 10 (*5*).

Next, we focus on $\sigma_T(eV)$ and θ_0 for $\alpha\neq0$ ($0<\alpha<\pi/4$). First we focus on $\alpha=\pi/8$, where MARS is formed for $\pi/8<|\varphi|<3\pi/8$. $\sigma_T(eV)$ has a ZBCP due to the formation of MARS at the DN/US interface. The height of ZBCP is reduced with the increase of R_d/R_b (see Fig. 2*a*). Contrary to the corresponding case of $\alpha=0$, $\sigma_T(eV)$ is almost independent of $E_{\rm Th}$ (see Fig. 2*b*). This is because the proximity effect is almost completely suppressed due to the competition of MARS, and the magnitude of $\theta(x)$ is reduced. In the extreme case $\alpha=\pi/4$, the $\sigma_T(eV)$ is completely independent

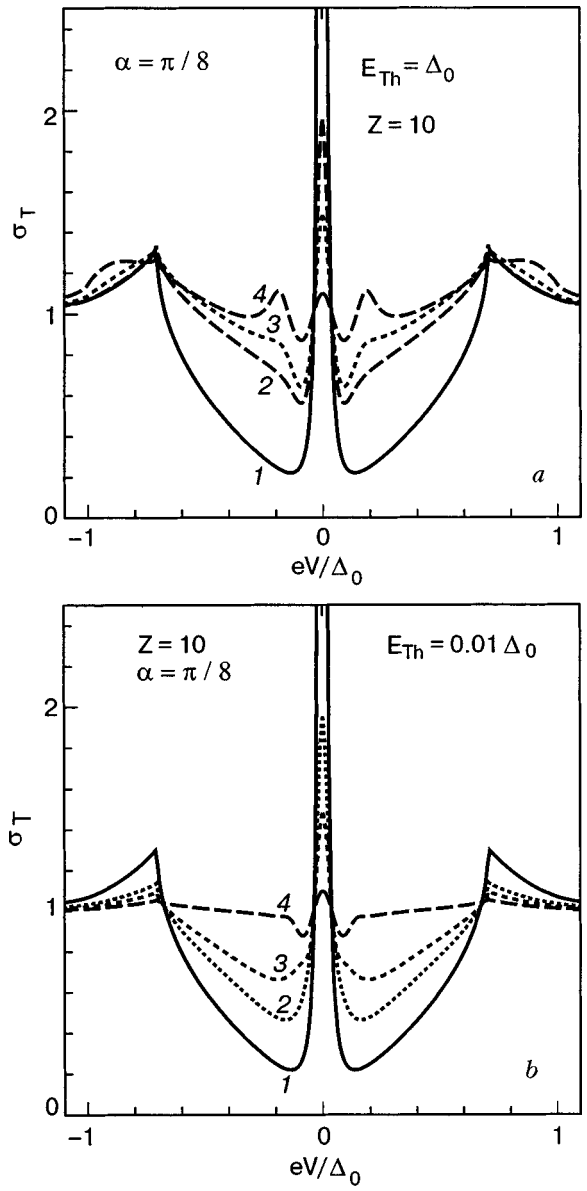

FIG. 2. Normalized conductance $\sigma_T(eV)$ for $\alpha=\pi/8$, $E_{\mathrm{Th}}=\Delta_0$ (*a*) and $E_{\mathrm{Th}}=0.01\Delta_0$ (*b*) at different R_d/R_b: 0 (*1*), 1 (*2*), 2 (*3*), and 10 (*4*).

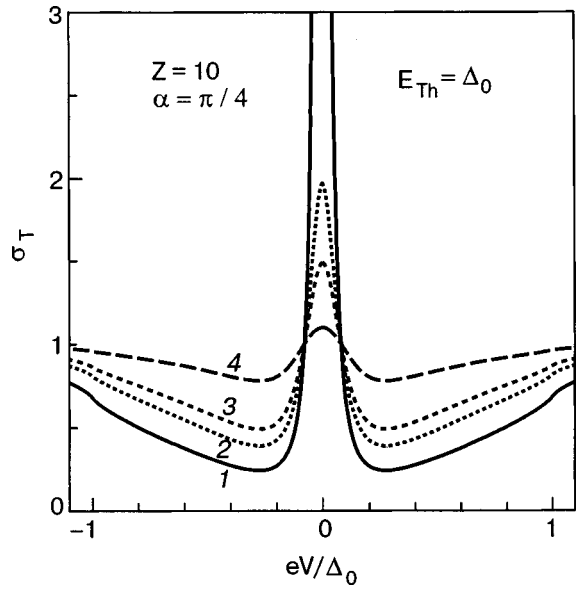

FIG. 3. Normalized conductance $\sigma_T(eV)$ for $\alpha=\pi/4$ at different R_d/R_b: 0 (*1*), 1 (*2*), 2 (*3*), and 10 (*4*).

of E_{Th}. The results obtained are plotted in Fig. 3.

In the present Section, a detailed theoretical investigation of the voltage-dependent conductance of diffusive normal metal/unconventional superconductor junctions is presented.

1. The ZBCP is frequently seen in the shape of $\sigma_T(eV)$. For $\alpha\neq 0$, the ZBCP is robust, being independent of the diffusive resistance R_d. For $\alpha=0$, the ZBCP is due to the CAR.

2. The appearance of the ZBCP is different for the MARS and CAR mechanisms. The first mechanism may lead to arbitrarily large $\sigma_T(0)$. The second mechanism cannot provide $\sigma_T(0)$ exceeding unity. While for the first mechanism the width of the ZBCP is determined by the transparency of the junction, for the second it is determined by the Thouless energy. These two mechanisms compete, since the proximity effect and the MARS in singlet junctions are generally incompatible.[108]

3. In the extreme case $\alpha=\pi/4$ the proximity effect and the CAR are absent. $\sigma_T(eV)$ is then given by a simple Ohm's law: $\sigma_T(eV)=(R_b+R_d)/(R_{R_d=0}+R_d)$, R_b being the resistance of the interface.

4. We have clarified various line shapes of the conductance including ZBCP. The results serve as an important guide to analyze the actual experimental data of the tunneling spectra of high-T_c cuprate junctions. We want to stress that the height of the ZBCP is strongly suppressed by the existence of DN, and the resulting $\sigma_T(0)$ is not so high as obtained in the ballistic regime.[3] In the actual fit of the experimental data, we strongly hope to take into account the effect of R_d. In such a case without solving the Usadel equation $\sigma_T(eV)$ can be simply approximated by

$$\sigma_T(eV)=\frac{R_d+R_b}{R_{R_d=0}+R_d}, \tag{26}$$

$$R_{R_d=0}=\frac{R_b}{\langle I_{b0}\rangle}, \tag{27}$$

$$\langle I_{b0}\rangle=\frac{\int_{-\pi/2}^{\pi/2}\cos\varphi I_{b0}d\varphi}{\int_{-\pi/2}^{\pi/2}\cos\varphi T(\varphi)d\varphi}, \tag{28}$$

$$I_{b0}=\frac{T(\varphi)\{1+T(\varphi)|\Gamma_+|^2+[T(\varphi)-1]|\Gamma_+\Gamma_-|^2\}}{|1+[T(\varphi)-1]\Gamma_+\Gamma_-|^2}, \tag{29}$$

$$\Gamma_\pm=\frac{\Delta_\pm}{\varepsilon+\sqrt{\varepsilon^2-\Delta_\pm^2}}, \tag{30}$$

$$R_b=\frac{2R_0}{\int_{-\pi/2}^{\pi/2}d\phi T(\phi)\cos\phi}, \tag{31}$$

with $\Delta_\pm=\Delta_0\cos[2(\varphi\mp\alpha)]$ and $\varepsilon=eV$. This expression is a convenient one for fitting of experimental data. However, for the quantitative discussions including much more general cases, one must solve the Usadel equation, as was done in

the present paper. Recently, mesoscopic interference effects have been observed in actual cuprate junctions.[111] We expect the present results will be observed in many experiments in the near future.

3. IMPURITY IN HIGH-T_c CUPRATE NEAR THE INTERFACE

The MARS is sensitive to the time reversal symmetry (TRS) of junctions because the retro-reflectivity of the Andreev reflection assists the constructive interference effect of a quasiparticle.[112] Actually, the ZBCP in NS junctions splits into two peaks under magnetic fields.[25,39–43] The peak splitting is also discussed[21–26,113,114] when a broken time reversal symmetry state (BTRSS) is formed at the interface. Theoretical studies showed that such BTRSSs are characterized by the $s+id_{xy}$ (Ref. 26) or $d_{xy}+id_{x^2+y^2}$ (Ref. 115) wave pairing symmetry. In the presence of the BTRSS, splitting of the ZBCP is expected in zero magnetic field. The experimental results, however, are still controversial.[116,117] Some experimental papers reported splitting of the ZBCP at zero magnetic field,[9,17,18,118–122] while in others the splitting was not observed.[8,10,11,15,20,123] In addition, a recent experiment has shown the near absence of BTRSS in high-T_c grain boundary junctions.[124]

In previous papers, we showed that random potentials at the NS interface cause the splitting of the ZBCP at the zero magnetic field by using the recursive Green function method in numerical simulations[55,125] and by the single-site approximation in an analytical calculation.[126] We also showed that the splitting due to the impurity scattering can be seen more clearly when realistic electronic structures of high-T_c materials are used.[127] Our conclusion, however, contradicts those of a number of theories[69–71,128,129] based on the quasiclassical Green function method.[2,86,130–132] While it is a common conclusion of all the theories that the ZBCP is drastically suppressed by interfacial randomness, the theories of the quasiclassical Green function method conclude that the random potentials do not split the ZBCP. Thus this issue has not been fixed yet. There are mainly two reasons for the disagreement in the two theoretical approaches (i.e., the recursive Green function method and the quasiclassical Green function method). One is the treatment of the random potentials, and the other is the effects of the rapidly oscillating wave functions on the conductance. In our simulations, we calculate the conductance without any approximation to the random potentials and the wave functions; this is an advantage of the recursive Green function method.[55,133] Our results indicate that the splitting of the ZBCP in experiments does not constitute direct evidence of the BTRSS at the interface of NS junctions.

Let us consider two-dimensional NS junctions as shown in Fig. 4*a*, where the normal metal ($x<0$) and d-wave superconductor ($x>0$) are separated by a potential barrier $V_B(\mathbf{r})=H\delta(x)$. We assume the periodic boundary condition in the y direction, and the width of the junction is W. The a axis of high-T_c superconductors is oriented at 45 degrees to the interface normal. The pair potential of a high-T_c superconductor is described by $\Delta_{\mathbf{k}}=2\Delta_0\overline{k_x}\overline{k_y}$ in momentum space, where $\overline{k_x}=k_x/k_F=\cos\varphi$ and $\overline{k_y}=k_y/k_F=\sin\varphi$ are the normalized wave number on the Fermi surface in the x and y directions, respectively. A schematic illustration of the

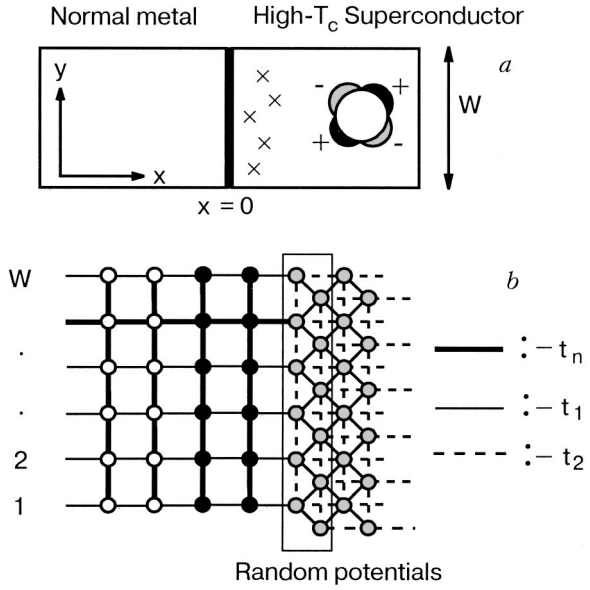

FIG. 4. The normal-metal/d-wave superconductor junction is schematically illustrated. In (a) the crosses represent impurities. In (b) the open, filled, and gray circles represent the normal metal, insulator, and superconductor, respectively.

pair potential is shown in Fig. 4. The NS junctions are described by the Bogoliubov–de Gennes equation,

$$\int d\mathbf{r}' \begin{pmatrix} \delta(\mathbf{r}-\mathbf{r}')h_0(\mathbf{r}') & \Delta(\mathbf{r},\mathbf{r}') \\ \Delta^*(\mathbf{r},\mathbf{r}') & -\delta(\mathbf{r}-\mathbf{r}')h_0(\mathbf{r}') \end{pmatrix} \begin{pmatrix} u(\mathbf{r}') \\ v(\mathbf{r}') \end{pmatrix} = E \begin{pmatrix} v(\mathbf{r}) \\ v(\mathbf{r}) \end{pmatrix}, \tag{32}$$

$$h_0(\mathbf{r}) = -\frac{\hbar^2\nabla^2}{2m} + V(\mathbf{r}) - \mu_F, \tag{33}$$

$$V(\mathbf{r}) = V_B(\mathbf{r}) + V_I(\mathbf{r}) \tag{34}$$

where

$$\Delta(\mathbf{r},\mathbf{r}') = \Theta(x)(1/V_{\mathrm{vol}})\sum_k \Delta_{\mathrm{k}} \exp[i\mathbf{k}\cdot(\mathbf{r}-\mathbf{r}')].$$

The normal conductance of clean junctions is given by $G_N=(2e^2/h)N_cT_B$ with T_B being the transmission probability of the junction, and $N_c=Wk_F/\pi$ is the number of propagating channels on the Fermi surface. In the low-transparency junctions (i.e., $Z\gg 1$), we find $T_B\propto 1/Z^2$. In what follows, we redefine $z_0=Z/2=Hm/\hbar^2k_F$. We consider impurities near the interface on the superconductor side as indicated by crosses in Fig. 4. The potential of the impurities is given by $V_I(\mathbf{r})=V_i\Sigma_{j=1}^{N_i}\delta(\mathbf{r}-\mathbf{r}_j)$, where N_i is the number of impurities. Effects of impurities on the wave functions are taken into account by using the Lippmann–Schwinger equation,

$$\psi^{(l)}(\mathbf{r}) = \psi_0^{(l)}(\mathbf{r}) + \sum_{j=1}^{N_i} \hat{G}_0(\mathbf{r},\mathbf{r}_j)V_i\hat{\sigma}_3\psi^{(l)}(\mathbf{r}_j), \tag{35}$$

where l indicates a propagating channel characterized by the transverse wave number $k_y^{(l)}$ and $\hat{G}_0(\mathbf{r},\mathbf{r}')$ are the real-space Green functions in the clean junctions and can be obtained analytically. Here $\psi_0^{(l)}(\mathbf{r})$ is the wave function in which an

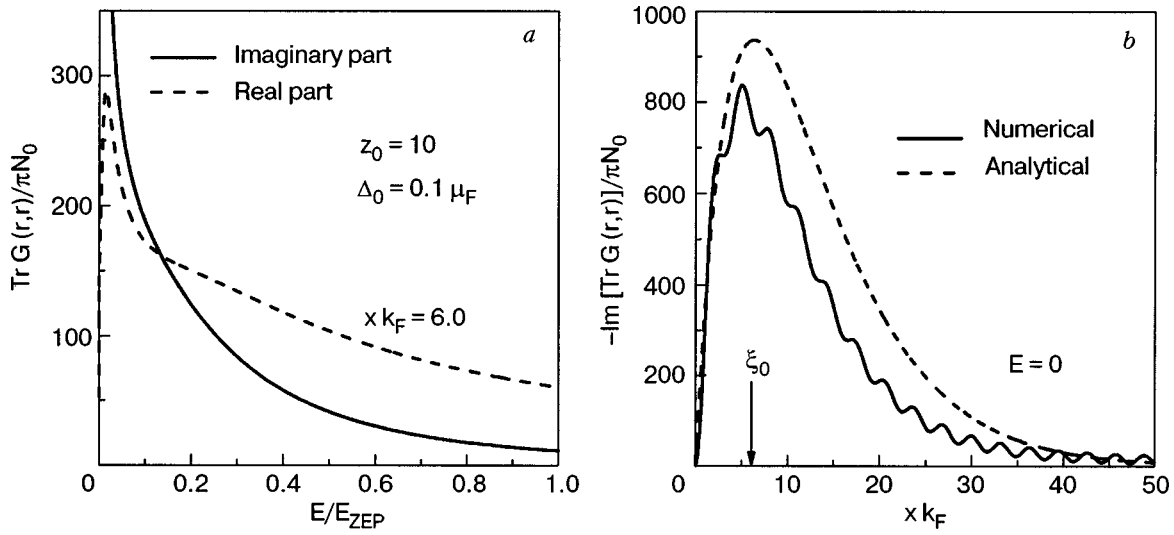

FIG. 5. In (a), the trace of the Green function in the superconductor is shown as a function of E. The peak width of the imaginary part is given by $E_{\mathrm{ZEP}}=\Delta_0/z_0^2$. In (b) the local density of states is shown as a function of xk_F, where $E=0$, $z_0=10$, and $\Delta_0=0.1\mu_F$. The numerical and analytical results are represented by the solid and broken lines, respectively.

electron like quasiparticle with $k_y^{(l)}$ is incident on the NS interface from the normal metal and is described as

$$\psi_0^{(l)}(\mathbf{r})=\chi_l(y)\left[\begin{pmatrix}1\\0\end{pmatrix}\exp(ik_lx)+\begin{pmatrix}0\\1\end{pmatrix}\exp(ik_lx)r_{NN}^{he}(l)+\begin{pmatrix}1\\0\end{pmatrix}\exp(-ik_lx)r_{NN}^{ee}(l)\right], \tag{36}$$

for $x<0$, where $\chi_l(y)=\exp[ik_y^{(l)}y]/\sqrt{W}$, k_l is the wave number of a quasiparticle in the normal metal and satisfies $k_l^2+k_y^{(l)^2}=k_F^2$, $r_{NN}^{ee}(l)$ and $r_{NN}^{he}(l)$ are the normal and the Andreev reflection coefficients, respectively, of the clean junctions. The wave function for $x>0$ is expressed in the same way. The wave function at an impurity $\psi^{(l)}(\mathbf{r}_{j'})$ can be obtained by letting $\mathbf{r}\to\mathbf{r}_{j'}$ in Eq. (35):

$$\psi_0^{(l)}(\mathbf{r}_{j'})=\sum_{j=1}^{N_i}[\hat{\sigma}_0\delta_{j,j'}-\hat{G}_0(\mathbf{r}_{j'},\mathbf{r}_j)V_i\hat{\sigma}_3]\psi^{(l)}(\mathbf{r}_j). \tag{37}$$

It is possible to calculate the exact conductance if we obtain $\psi^{(l)}(\mathbf{r}_j)$ for all impurities by solving Eq. (37). In this paper, we solve Eq. (37) within the single-site approximation, where the multiple scattering effects involving many impurities (Anderson localization) are neglected. However the multiple scattering by an impurity is taken into account to infinite order in the scattering events. In the summation of j in Eq. (37), only the contribution with $j=j'$ is taken into account in the single-site approximation.[134] In this way, the wave function at $\mathbf{r}_j$ is given approximately by

$$\psi^{(l)}(\mathbf{r}_j)\approx[\hat{\sigma}_0-\hat{G}_0(\mathbf{r}_j,\mathbf{r}_j)V_i\hat{\sigma}_3]^{-1}\psi_0^{(l)}(\mathbf{r}_j). \tag{38}$$

Substituting the wave function at impurities in Eq. (38) into Eq. (35), we obtain the wave function in the presence of impurities. The normal reflection coefficients $B_{l',l}$ and the Andreev reflection coefficients $A_{l,l'}$ are then calculated analytically from the expression for the wave function at $x\to-\infty$. The differential conductance in the NS junctions is calculated from the normal and the Andreev reflection coefficients,[85]

$$G_{NS}(eV)=\frac{2e^2}{h}\int_{-\infty}^{\infty}dE\left(\frac{\partial f_{FD}(E-eV)}{\partial(eV)}\right)\times\left[N_cg^{(0)}-4\sum_{j=1}^{N_i}\Gamma_j\right], \tag{39}$$

$$g^{(0)}=2\int_0^{\pi/2}d\varphi\,\frac{\Delta_0^2\cos^7\varphi\sin^2\varphi}{E^2z_0^4+\Delta_0^2\cos^6\varphi\sin^2\varphi}. \tag{40}$$

The first term of Eq. (39), $N_cg^{(0)}$, is the conductance in the clean junctions, $f_{FD}(E)$ is the Fermi–Dirac distribution function, and V is the bias voltage applied to the junctions. In Eq. (39), Γ_j represents effects of the impurity scattering on the conductance. An explicit expression for Γ_j is given in Ref. 126.

Before discussing the conductance, the local density of states (LDOS) near the junction interface should be clarified because the LDOS affects the scattering events of a quasiparticle. The LDOS is given by

$$N_s(E,x)=-\frac{1}{\pi}\mathrm{Im\,Tr}\,\hat{G}_0(\mathbf{r},\mathbf{r}), \tag{41}$$

$$=4N_0z_0^2\exp(-x/\xi_0)\times\frac{2}{\pi}\int_0^{\pi/2}d\varphi\,\frac{\Delta_0^2\cos^4\varphi\sin^2\varphi\sin^2(k_Fx\cos\varphi)}{E^2z_0^4+\Delta_0^2\cos^6\varphi\sin^2\varphi}. \tag{42}$$

In the second line, we use the condition $E\ll\Delta_0$ (Ref. 126). As shown in Fig. 5*a*, the imaginary part of the Green function has a large peak around $E=0$, reflecting the MARS formed at the junction interface, where $xk_F=6$, $z_0=10$, and $\Delta_0=0.1\mu_F$. The energy scale $E_{\mathrm{ZEP}}=\Delta_0/z_0^2$ characterizes the width of the peak of the LDOS. Since the self-energy of impurity scattering is roughly proportional to the LDOS, effects of scattering becomes strong for a quasiparticle with $E<E_{\mathrm{ZEP}}$. At $E=0$, we find

$$N_s(E=0,x)\simeq4N_0z_0^2\exp(-x/\xi_0)xk_F, \tag{43}$$

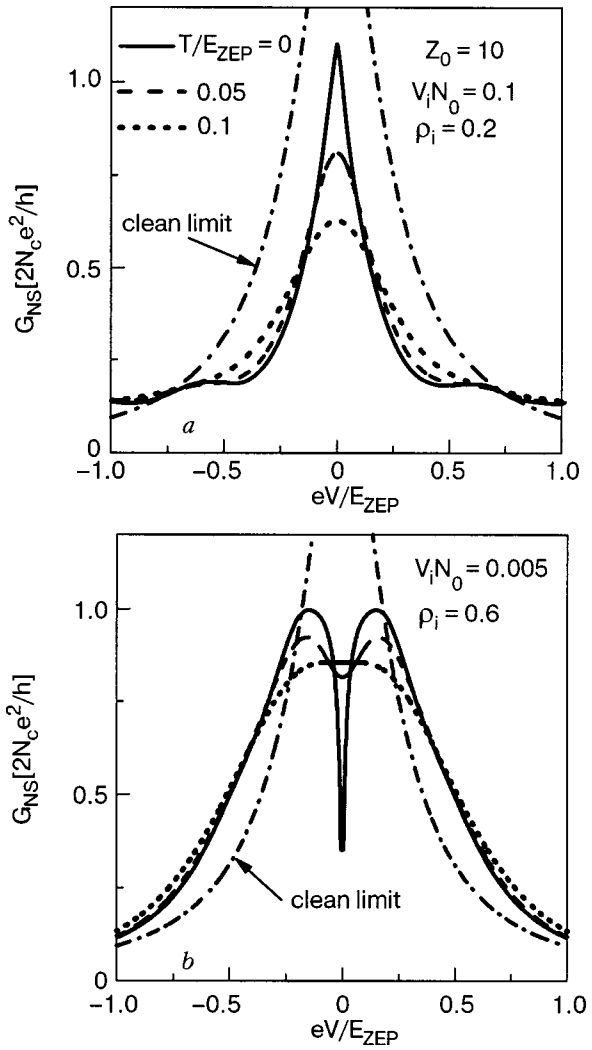

FIG. 6. The conductance in the presence of impurities distributed randomly in the range $1<x_jk_F<20$, where ρ_i is the dimensionless area density of impurities near the interface. The conductance for low-density strong impurities with $V_iN_0=0.1$ and $\rho_i=0.2$ is shown in (a). The conductance for high-density weak impurities with $V_iN_0=0.005$ and $\rho_i=0.6$ is shown in (b) for several choices of temperature. The conductance in the clean junction at the zero temperature is plotted with a dot-and-dash-line.

where $N_0=m/(\pi\hbar)^2$ is the normal density of states per unit area. In Fig. 5*b* we plot Eqs. (42) and (43) with the solid and broken lines, respectively. The results show the remarkable enhancement of the local density of states around $x\sim\xi_0$, where $\xi_0=(\hbar v_F/\pi\Delta_0)$ is the coherence length and is about $6/k_F$. This implies that the MARS is formed around $x\sim\xi_0$.

In the presence of impurities, the self-energy of the impurity scattering depends on the LDOS. Thus the impurities around $x\sim\xi_0$ are expected to be strong scatterers. At the same time, scattering effects become remarkably strong around $E\sim0$. The conductance in disordered junctions is shown in Fig. 6, where impurities are distributed randomly in the range $1<x_jk_F<L_sK_F$, $\rho_i=N_i\lambda_F^2/WL_s$ is the dimensionless area density of impurities, and $z_0=10$. The conductance is calculated from the expression

$$G_{NS}=\frac{2e^2}{h}N_c\int_{-\infty}^{\infty}dE\left(\frac{\partial f_{FD}(E-eV)}{\partial(eV)}\right)\times\left[g^{(0)}-\rho_i\frac{k_FL_s}{\pi}\langle\Gamma\rangle\right], \tag{44}$$

$$\langle\Gamma\rangle=\left\langle\frac{1}{N_i}\sum_{j=1}^{N_i}\Gamma_j\right\rangle, \tag{45}$$

where $\langle ...\rangle$ means the ensemble average. The broken line denotes the conductance in the clean limit. The width of the ZBCP in clean junctions is also characterized by E_{ZEP}. We choose $L_sk_F=20$ in Fig. 6 because we focus on the impurities near the interface and $\xi_0k_F\sim6$. In Fig. 6*a* we show the conductance of junctions in which low-density strong impurities are distributed (i.e., $V_iN_0=0.1$ and $\rho_i=0.2$). The conductance for high-density weak impurities (i.e., $V_iN_0=0.005$ and $\rho_i=0.6$) is shown in Fig. 6*b*. There is no peak splitting in Fig. 6*a*, whereas the conductance clearly splits into two peaks in Fig. 6*b* at zero temperature. The impurity scattering affects the ZBCP in two ways: (i) it decreases the conductance around zero bias, and (ii) it makes the ZBCP wider. Roughly speaking, the product of $V_iN_s(E=0,\xi_0)$ characterizes the strength of the impurity scattering. The suppression of the zero-bias conductance always happens irrespective of $V_iN_s(E=0,\xi_0)$. The widening, however, happens only if impurity scattering is sufficiently weak that $V_iN_s(E=0,\xi_0)\sim O(1)$ is satisfied.[126] Since $N_s(0,\xi_0)/N_0\gg1$, as shown in Fig. 6, the zero-bias conductance is drastically decreased by impurities. When $V_iN_s(E=0,\xi_0)\gg1$, as shown in Fig. 6*a*, the suppression of the zero-bias conductance dominates over the widening of the ZBCP. The conductance decreases from that in the clean junctions for almost the all bias region for $eV<E_{\mathrm{ZEP}}$, as is seen in Fig. 6*a*, which leads to no splitting. On the other hand, for weak scattering potentials, $V_iN_s(0,\xi_0)\sim O(1)$, impurities cause widening of the conductance peaks as well as the suppression of the zero-bias conductance. As a consequence, the conductance splits into two peaks, as shown in Fig. 6*b*. The splitting peaks merge into a single peak at finite temperatures such as $T=0.1E_{\mathrm{ZEP}}$, which is comparable to peak splitting width at zero temperature. The results obtained indicate that strong random potentials are not necessary for splitting of the ZBCP. High-density impurities with weak random potentials are responsible for the splitting of the ZBCP in low-transparency junctions.

The analytical results can be confirmed by numerical simulations based on the recursive Green function method on two-dimensional tight-binding lattice, as shown in Fig. 4*b*. The system consists of three regions: a perfect normal metal (open circles), an insulator (filled circles), and a superconductor (gray circles). The gray sites correspond to Cu atoms on CuO_2 layers. The Hamiltonian reads

$$\mathcal{H}=-\sum_{\mathbf{r},\mathbf{r}',\sigma}(t_{\mathbf{r},\mathbf{r}'}c^{\dagger}_{\mathbf{r},\sigma}c_{\mathbf{r}',\sigma}+\mathrm{h.c.})+\sum_{\mathbf{r},\sigma}(\varepsilon_{\mathbf{r}}-\mu)c^{\dagger}_{\mathbf{r},\sigma}c_{\mathbf{r},\sigma}-\sum_{\mathbf{r},\mathbf{r}'}(\Delta_{\mathbf{r}-\mathbf{r}'}c^{\dagger}_{\mathbf{r},\uparrow}c^{\dagger}_{\mathbf{r}',\downarrow}+\mathrm{h.c.}), \tag{46}$$

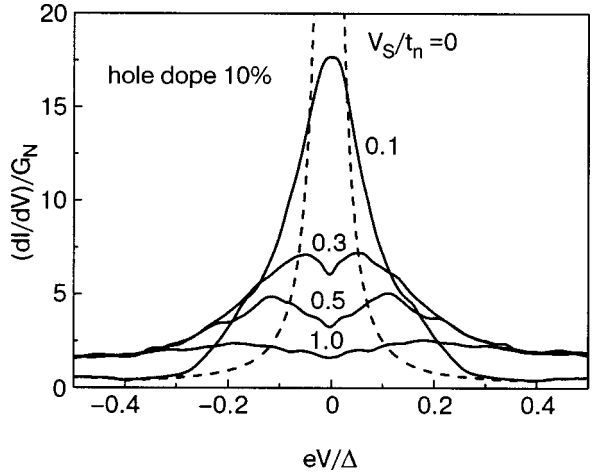

FIG. 7. The conductance calculated by the recursive Green function method. The degree of randomness is represented by V_S.

where $t_{r,r'}$ and $\Delta_{\mathbf{r}-\mathbf{r}'}$ are the hopping integral and the pair potential between $\mathbf{r}$ and $\mathbf{r}'$, respectively.

We consider the nearest-neighbor hopping, t_n, in normal metals and insulators. The on-site potential $\varepsilon_{\mathbf{r}}$ is fixed at zero in normal metals and is V_B in insulators. In superconductors, we consider nearest-neighbor hopping, t_1, and second-nearest-neighbor hopping, t_2. The random potential at the interface is taken into account through the on-site potential, given randomly in a range of $-V_S/2 \leqslant \varepsilon_{\mathbf{r}} \leqslant V_S/2$, as shown in Fig. 4*b*. The amplitude of the pair potential between the nearest-neighbor sites is Δ_0, and the sign of the pair potential is determined to satisfy a d-wave symmetry. The Bogoliubov–de Gennes equation derived from the Hamiltonian of Eq. (46) is solved numerically by using the recursive Green function method.[55] The transmission and reflection coefficients of the junction are computed exactly in the simulation. We obtain the differential conductance from these coefficients using the Blonder–Tinkham–Klapwijk formula.[85]

In Fig. 7 we show the conductance as a function of the bias voltage, where the Fermi energy in normal metals is $-2.0t_n$, $W=30$, and the conductance is divided by the normal conductance of the junction, G_N. The potential barrier at the insulators is $V_B/t_n=3.0$, and the transparency of the insulating layers is of the order of 0.01. The Fermi energy μ_S, Δ_0, t_1, and t_2 are determined from an analysis of the t–J model[135] for 10% hole doping. The degree of disorder is $V_S/t_n=0.0$ (broken lines), 0.1, 0.3, 0.5, and 1.0 from top to bottom. The conductance is averaged over a number of samples with different random configurations. The results show the drastic suppression of the ZBCP even for weak random potential at $V_S/t_n=0.1$. The split of the ZBCP can be seen for slightly stronger potentials such as $V_S/t_n=0.3$ and 0.5. For $V_S/t_n=1.0$, we find dip structures around $eV\sim 0$ instead of the ZBCP. These results may correspond to the dip structures observed in disordered NS junctions in an experiment.[136]

Several experiments[9,122] have shown a sensitivity of the conductance peaks to external magnetic fields. Here we discuss the conductance in the presence of magnetic fields. The

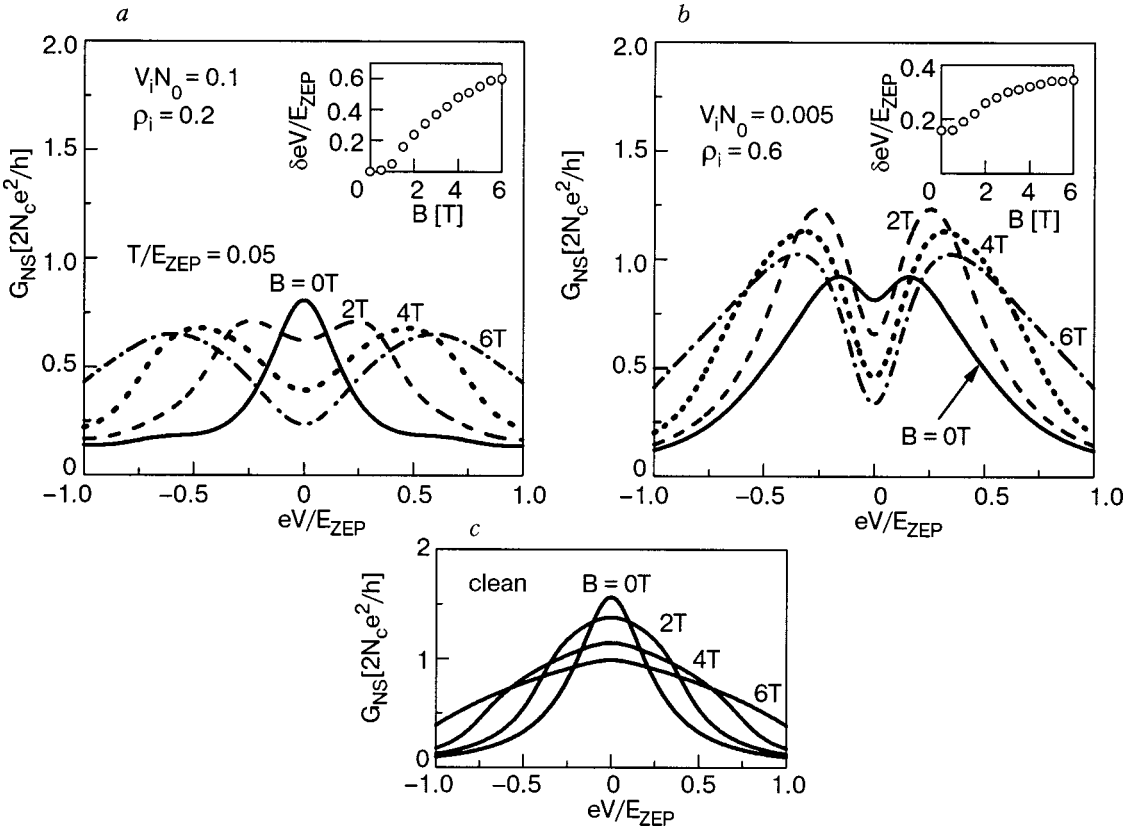

FIG. 8. The conductance in external magnetic fields for low-density strong impurities with $V_iN_0=0.1$ and $\rho_i=0.2$ are shown in (a), where T is fixed at $0.05E_{ZEP}$. Those for high-density weak impurities with $V_iN_0=0.005$ and $\rho_i=0.6$ are shown in (b). In the insets, the peak positions are plotted as a function of magnetic field. The conductance of clean junctions is shown in (c).

effects of magnetic fields are taken into account phenomenologically by using the Aharonov–Bohm-like phase shift[112,137] of a quasiparticle. Since the impurity scattering in magnetic fields is itself a difficult problem to solve analytically, we neglect the interplay between magnetic fields and impurity scattering. Within the phenomenological theory,[112] effects of magnetic fields are considered by replacing E in Eq. (40) by $E+|\Delta_0 \cos\varphi \sin\varphi|\varphi_B$:

$$g_B^{(0)}=\int_{-\pi/2}^{\pi/2} d\varphi \frac{\Delta_0^2 \cos^7\varphi \sin^2\varphi}{E_B^2 z_0^4+\Delta_0^2 \cos^6\varphi \sin^2\varphi}, \tag{47}$$

$$E_B=E+2\Delta_0|\cos\varphi \sin\varphi|\varphi_B, \tag{48}$$

$$\varphi_B=2\pi\frac{B\xi_0^2}{\varphi_0}\tan\varphi=B_0\tan\varphi, \tag{49}$$

where $\varphi_0=2\pi\hbar c/e$ and $B_0=0.001$ corresponds to $B=1$ T. A quasiparticle acquires the Aharonov–Bohm-like phase shift φ_B while moving near the NS interface.[112] In a previous paper, we found that ZBCP in clean junctions remains a single peak even in strong magnetic fields,[112] as is shown in Fig. 8*c*, where $z_0=10$ and $T=0.05E_{\mathrm{ZEP}}$. In Figs. 8*a* and 8*b* we show the conductance in the presence of low-density strong impurities and high-density weak impurities, respectively, where V_i and ρ_i are same as those in Figs. 6*a* and 6*b*, respectively. A temperature is fixed at $T=0.05E_{\mathrm{ZEP}}$. In contrast to clean junctions in Fig. 8*c*, the ZBCP in disordered junctions splits into two peaks in magnetic fields, as is shown in Fig. 8*a*. The results obtained within the phenomenological theory indicate that the sensitivity of the ZBCP to magnetic fields depends on the degree of impurity scattering. In the insets, the circlets show the peak positions (δeV) plotted as a function of magnetic field. For high-density weak impurities in Fig. 8*b*, we also found that the degree of peak splitting increases with increasing magnetic fields. In the limit of strong fields, δeV tends to be saturated, as shown in the inset. These characteristic behaviors have been found in experiment.[9]

In summary of this Section, we conclude that the impurity scattering causes the split of the ZBCP in normal-metal/high-T_c superconductor junctions. We consider impurities near the junction interface on the superconductor side. The conductance is calculated from the Andreev and the normal reflection coefficients, which are estimated by using the single-site approximation in an analytic calculation and by the recursive Green function method in a numerical simulation. The strength of the impurity scattering depends on the transparency of the junction, the position of impurities, and the energy of a quasiparticle, because the MARS are formed at the interface. We find splitting of the ZBCP in the presence of the time reversal symmetry. Thus the zero-field splitting of ZBCP in the experiment[9] does not perfectly prove the existence of BTRSS.

*E-mail: ytanaka@nuap.nagoya-u.ac.jp

[1]L. J. Buchholtz and G. Zwicknagl, Phys. Rev. B **23**, 5788 (1981); C. R. Hu, Phys. Rev. Lett. **72**, 1526 (1994).
[2]C. Bruder, Phys. Rev. B **41**, 4017 (1990).
[3]Y. Tanaka and S. Kashiwaya, Phys. Rev. Lett. **74**, 3451 (1995); S. Kashiwaya, Y. Tanaka, M. Koyanagi, and K. Kajimura, Phys. Rev. B **53**, 2667 (1996).
[4]Y. Tanaka and S. Kashiwaya, Phys. Rev. B **53**, 9371 (1996).
[5]S. Kashiwaya and Y. Tanaka, Rep. Prog. Phys. **63**, 1641 (2000) and references therein.
[6]J. Geerk, X. X. Xi, and G. Linker, Z. Phys. B **73**, 329 (1988).
[7]S. Kashiwaya, Y. Tanaka, M. Koyanagi, H. Takashima, and K. Kajimura, Phys. Rev. B **51**, 1350 (1995).
[8]L. Alff, H. Takashima, S. Kashiwaya, N. Terada, H. Ihara, Y. Tanaka, M. Koyanagi, and K. Kajimura, Phys. Rev. B **55**, 14757 (1997).
[9]M. Covington, M. Aprili, E. Paraoanu, L. H. Greene, F. Xu, J. Zhu, and C. A. Mirkin, Phys. Rev. Lett. **79**, 277 (1997).
[10]J. Y. T. Wei, N.-C. Yeh, D. F. Garrigus, and M. Strasik, Phys. Rev. Lett. **81**, 2542 (1998).
[11]I. Iguchi, W. Wang, M. Yamazaki, Y. Tanaka, and S. Kashiwaya, Phys. Rev. B **62**, R6131 (2000).
[12]F. Laube, G. Goll, H. v. Löhneysen, M. Fogelstrtsm, and F. Lichtenberg, Phys. Rev. Lett. **84**, 1595 (2000).
[13]Z. Q. Mao, K. D. Nelson, R. Jin, Y. Liu, and Y. Maeno, Phys. Rev. Lett. **87**, 037003 (2001).
[14]Ch. Wälti, H. R. Ott, Z. Fisk, and J. L. Smith, Phys. Rev. Lett. **84**, 5616 (2000).
[15]H. Aubin, L. H. Greene, Sha Jian, and D. G. Hinks, Phys. Rev. Lett. **89**, 177001 (2002).
[16]Z. Q. Mao, M. M. Rosario, K. D. Nelson, K. Wu, I. G. Deac, P. Schiffer, Y. Liu, T. He, K. A. Regan, and R. J. Cava, Phys. Rev. B **67**, 094502 (2003).
[17]A. Sharoni, O. Millo, A. Kohen, Y. Dagan, R. Beck, G. Deutscher, and G. Koren, Phys. Rev. B **65**, 134526 (2002).
[18]A. Kohen, G. Leibovitch, and G. Deutscher, Phys. Rev. Lett. **90**, 207005 (2003).
[19]M. M. Qazilbash, A. Biswas, Y. Dagan, R. A. Ott, and R. L. Greene, Phys. Rev. B **68**, 024502 (2003).
[20]J. W. Ekin, Y. Xu, S. Mao, T. Venkatesan, D. W. Face, M. Eddy, and S. A. Wolf, Phys. Rev. B **56**, 13746 (1997).
[21]Y. Tanuma, Y. Tanaka, M. Yamashiro, and S. Kashiwaya, Phys. Rev. B **57**, 7997 (1998).
[22]Y. Tanuma, Y. Tanaka, M. Ogata, and S. Kashiwaya, J. Phys. Soc. Jpn. **67**, 1118 (1998).
[23]Y. Tanuma, Y. Tanaka, M. Ogata, and S. Kashiwaya, Phys. Rev. B **60**, 9817 (1999).
[24]Y. Tanuma, Y. Tanaka, and S. Kashiwaya, Phys. Rev. B **64**, 214519 (2001).
[25]M. Fogelström, D. Rainer, and J. A. Sauls, Phys. Rev. Lett. **79**, 281 (1997); D. Rainer, H. Burkhardt, M. Fogelström, and J. A. Sauls, J. Phys. Chem. Solids **59**, 2040 (1998).
[26]M. Matsumoto and H. Shiba, J. Phys. Soc. Jpn. **64**, 1703 (1995); M. Matsumoto and H. Shiba, J. Phys. Soc. Jpn. **64**, 4867 (1995).
[27]L. J. Buchholtz, M. Palumbo, D. Rainer, and J. A. Sauls, J. Low Temp. Phys. **101**, 1097 (1995).
[28]Y. Tanaka and S. Kashiwaya, Phys. Rev. B **58**, 2948 (1998).
[29]M. Yamashiro, Y. Tanaka, and S. Kashiwaya, Phys. Rev. B **56**, 7847 (1997).
[30]M. Yamashiro, Y. Tanaka, Y. Tanuma, and S. Kashiwaya, J. Phys. Soc. Jpn. **67**, 3224 (1998).
[31]M. Yamashiro, Y. Tanaka, and S. Kashiwaya, J. Phys. Soc. Jpn. **67**, 3364 (1998).
[32]M. Yamashiro, Y. Tanaka, Y. Tanuma, and S. Kashiwaya, J. Phys. Soc. Jpn. **68**, 2019 (1999).
[33]C. Honerkamp and M. Sigrist, Prog. Theor. Phys. **100**, 53 (1998).
[34]Y. Asano, Y. Tanaka, Y. Matsuda, and S. Kashiwaya, Phys. Rev. B **68**, 184506 (2003).
[35]Y. Tanuma, K. Kuroki, Y. Tanaka, and S. Kashiwaya, Phys. Rev. B **64**, 214510 (2001).
[36]K. Sengupta, I. Žutić, and H.-J. Kwon, V. M. Yakovenko, and S. Das Sarma, Phys. Rev. B **63**, 144531 (2001).
[37]Y. Tanuma, K. Kuroki, Y. Tanaka, R. Arita, S. Kashiwaya, and H. Aoki, Phys. Rev. B **66**, 094507 (2002).
[38]Y. Tanuma, K. Kuroki, Y. Tanaka, and S. Kashiwaya, Phys. Rev. B **68**, 214513 (2003).
[39]Y. Tanuma, Y. Tanaka, K. Kuroki, and S. Kashiwaya, Phys. Rev. B **66**, 174502 (2002).
[40]Y. Tanaka, H. Tsuchiura, Y. Tanuma, and S. Kashiwaya, J. Phys. Soc. Jpn. **71**, 271 (2002).

[41]Y. Tanaka, Y. Tanuma, K. Kuroki, and S. Kashiwaya, J. Phys. Soc. Jpn. **71**, 2102 (2002).
[42]Y. Tanaka, H. Itoh, H. Tsuchiura, Y. Tanuma, J. Inoue, and S. Kashiwaya, J. Phys. Soc. Jpn. **71**, 2005 (2002).
[43]Yu. S. Barash, M. S. Kalenkov, and J. Kurkijarvi, Phys. Rev. B **62**, 6665 (2000).
[44]J.-X. Zhu, B. Friedman, and C. S. Ting, Phys. Rev. B **59**, 9558 (1999).
[45]S. Kashiwaya, Y. Tanaka, N. Yoshida, and M. R. Beasley, Phys. Rev. B **60**, 3572 (1999).
[46]I. Zutic and O. T. Valls, Phys. Rev. B **60**, 6320 (1999).
[47]N. Yoshida, Y. Tanaka, J. Inoue, and S. Kashiwaya, J. Phys. Soc. Jpn. **68**, 1071 (1999).
[48]T. Hirai, N. Yoshida, Y. Tanaka, J. Inoue, and S. Kashiwaya, J. Phys. Soc. Jpn. **70**, 1885 (2001).
[49]N. Yoshida, H. Itoh, T. Hirai, Y. Tanaka, J. Inoue, and S. Kashiwaya, Physica C **367**, 135 (2002).
[50]T. Hirai, Y. Tanaka, N. Yoshida, Y. Asano, J. Inoue, and S. Kashiwaya, Phys. Rev. B **67**, 174501 (2003).
[51]Y. Tanaka and S. Kashiwaya, J. Phys. Soc. Jpn. **68**, 3485 (1999).
[52]Y. Tanaka and S. Kashiwaya, J. Phys. Soc. Jpn. **69**, 1152 (2000).
[53]Y. Tanaka and S. Kashiwaya, Phys. Rev. B **53**, 11957 (1996); **56**, 892 (1997).
[54]E. Il'ichev, V. Zakosarenko, R. P. J. IJsselsteijn, V. Schultze, H.-G. Meyer, H. E. Hoenig, H. Hilgenkamp, and J. Mannhart, Phys. Rev. Lett. **81**, 894 (1998).
[55]Y. Asano, Phys. Rev. B **63**, 052512 (2001).
[56]Y. Asano, Phys. Rev. B **64**, 014511 (2001).
[57]Y. Asano, Phys. Rev. B **64**, 224515 (2001).
[58]Y. Asano, J. Phys. Soc. Jpn. **71**, 905 (2002).
[59]Y. Asano, Y. Tanaka, M. Sigrist, and S. Kashiwaya, Phys. Rev. B **67**, 184505 (2003).
[60]Y. S. Barash, H. Burkhardt, and D. Rainer, Phys. Rev. Lett. **77**, 4070 (1996).
[61]E. Ilichev, M. Grajcar, R. Hlubina, R. P. J. IJsselsteijn, H. E. Hoenig, H.-G. Meyer, A. Golubov, M. H. S. Amin, A. M. Zagoskin, A. N. Omelyanchouk, and M. Yu. Kuprianov, Phys. Rev. Lett. **86**, 5369 (2001).
[62]G. Testa, A. Monaco, E. Esposito, E. Sarnelli, D.-J. Kang, E. J. Tarte, S. H. Mennema, and M. G. Blamire, cond-mat/0310727.
[63]Y. Tanaka, T. Hirai, K. Kusakabe, and S. Kashiwaya, Phys. Rev. B **60**, 6308 (1999).
[64]T. Hirai, K. Kusakabe, and Y. Tanaka, Physica C **336**, 107 (2000); K. Kusakabe and Y. Tanaka, *ibid.* **367**, 123 (2002); K. Kusakabe and Y. Tanaka, J. Phys. Chem. Solids **63**, 1511 (2002).
[65]N. Stefanakis, Phys. Rev. B **64**, 224502 (2001).
[66]Z. C. Dong, D. Y. Xing, and Jinming Dong, Phys. Rev. B **65**, 214512 (2002); Z. C. Dong, D. Y. Xing, Z. D. Wang, Ziming Zheng, and Jinming Dong, *ibid.* **63**, 144520 (2001).
[67]M. H. S. Amin, A. N. Omelyanchouk, and A. M. Zagoskin, Phys. Rev. B **63**, 212502 (2001).
[68]Shin-Tza Wu and Chung-Yu Mou, Phys. Rev. B **66**, 012512 (2002).
[69]A. A. Golubov and M. Y. Kuprianov, JETP Lett. **69**, 262 (1999); *ibid.* **67**, 478 (1998); **67**, 501 (1998).
[70]A. Poenicke, Yu. S. Barash, C. Bruder, and V. Istyukov, Phys. Rev. B **59**, 7102 (1999); K. Yamada, Y. Nagato, S. Higashitani, and K. Nagai, J. Phys. Soc. Jpn. **65**, 1540 (1996).
[71]T. Lück, U. Eckern, and A. Shelankov, Phys. Rev. B **63**, 064510 (2002).
[72]A. F. Andreev, Sov. Phys. JETP **19**, 1228 (1964).
[73]F. W. J. Hekking and Yu. V. Nazarov, Phys. Rev. Lett. **71**, 1625 (1993).
[74]F. Giazotto, P. Pingue, F. Beltram, M. Lazzarino, D. Orani, S. Rubini, and A. Franciosi, Phys. Rev. Lett. **87**, 216808 (2001).
[75]T. M. Klapwijk, Physica B **197**, 481 (1994).
[76]A. Kastalsky, A. W. Kleinsasser, L. H. Greene, R. Bhat, F. P. Milliken, and J. P. Harbison, Phys. Rev. Lett. **67**, 3026 (1991).
[77]C. Nguyen, H. Kroemer, and E. L. Hu, Phys. Rev. Lett. **69**, 2847 (1992).
[78]B. J. van Wees, P. de Vries, P. Magnee, and T. M. Klapwijk, Phys. Rev. Lett. **69**, 510 (1992).
[79]J. Nitta, T. Akazaki, and H. Takayanagi, Phys. Rev. B **49**, 3659 (1994).
[80]S. J. M. Bakker, E. van der Drift, T. M. Klapwijk, H. M. Jaeger, and S. Radelaar, Phys. Rev. B **49**, 13275 (1994).
[81]P. Xiong, G. Xiao, and R. B. Laibowitz, Phys. Rev. Lett. **71**, 1907 (1993).
[82]P. H. C. Magnee, N. van der Post, P. H. M. Kooistra, B. J. van Wees, and T. M. Klapwijk, Phys. Rev. B **50**, 4594 (1994).
[83]J. Kutchinsky, R. Taboryski, T. Clausen, C. B. Sorensen, A. Kristensen, P. E. Lindelof, J. Bindslev Hansen, C. Schelde Jacobsen, and J. L. Skov, Phys. Rev. Lett. **78**, 931 (1997).
[84]W. Poirier, D. Mailly, and M. Sanquer, Phys. Rev. Lett. **79**, 2105 (1997).
[85]G. E. Blonder, M. Tinkham, and T. M. Klapwijk, Phys. Rev. B **25**, 4515 (1982).
[86]A. V. Zaitsev, Zh. Éksp. Teor. Fiz. **86**, 1742 (1984) [Sov. Phys. JETP **59**, 1015 (1984)].
[87]C. W. J. Beenakker, Rev. Mod. Phys. **69**, 731 (1997).
[88]C. J. Lambert, J. Phys. Cond. Matter **3**, 6579 (1991).
[89]Y. Takane and H. Ebisawa, J. Phys. Soc. Jpn. **61**, 2858 (1992).
[90]C. W. J. Beenakker, Phys. Rev. B **46**, 12841 (1992).
[91]C. W. J. Beenakker, B. Rejaei, and J. A. Melsen, Phys. Rev. Lett. **72**, 2470 (1994).
[92]G. B. Lesovik, A. L. Fauchere, and G. Blatter, Phys. Rev. B **55**, 3146 (1997).
[93]A. I. Larkin and Yu. V. Ovchinnikov, Sov. Phys. JETP **41**, 960 (1975).
[94]A. F. Volkov, A. V. Zaitsev, and T. M. Klapwijk, Physica C **210**, 21 (1993).
[95]M. Yu. Kuprianov and V. F. Lukichev, Zh. Exp. Teor. Fiz. **94**, 139 (1988) [Sov. Phys. JETP **67**, 1163 (1988)].
[96]K. D. Usadel, Phys. Rev. Lett. **25**, 507 (1970).
[97]Yu. V. Nazarov, Phys. Rev. Lett. **73**, 1420 (1994).
[98]S. Yip, Phys. Rev. B **52**, 3087 (1995).
[99]Yu. V. Nazarov and T. H. Stoof, Phys. Rev. Lett. **76**, 823 (1996); T. H. Stoof and Yu. V. Nazarov, Phys. Rev. B **53**, 14496 (1996).
[100]A. F. Volkov, N. Allsopp, and C. J. Lambert, J. Phys. Cond. Matter. **8**, L45 (1996); A. F. Volkov and H. Takayanagi, Phys. Rev. B **56**, 11184 (1997).
[101]A. A. Golubov, F. K. Wilhelm, and A. D. Zaikin, Phys. Rev. B **55**, 1123 (1997).
[102]R. Seviour and A. F. Volkov, Phys. Rev. B **61**, R9273 (2000).
[103]W. Belzig, F. K. Wilhelm, C. Bruder, *et al.*, Superlatt. Microstruct. **25**, 1251 (1999).
[104]C. J. Lambert, R. Raimondi, V. Sweeney, and A. F. Volkov, Phys. Rev. B **55**, 6015 (1997).
[105]E. V. Bezuglyi, E. N. Bratus', V. S. Shumeiko, G. Wendin, and H. Takayanagi, Phys. Rev. B **62**, 14439 (2000).
[106]Yu. V. Nazarov, Superlatt. Microstruct. 25 1221 (1999), cond-mat/9811155.
[107]Y. Tanaka, A. A. Golubov, and S. Kashiwaya, Phys. Rev. B **68**, 054513 (2003).
[108]Y. Tanaka, Y. V. Nazarov, and S. Kashiwaya, Phys. Rev. Lett. **90**, 167003 (2003).
[109]Y. Tanaka, Y. V. Nazarov, A. Golubov, and S. Kashiwaya, Phys. Rev. B **69**, 144519 (2004).
[110]Y. Tanaka and S. Kashiwaya, Phys. Rev. B **70**, 012507 (2004), cond-mat/0308123.
[111]H. Kashiwaya, A. Sawa, S. Kashiwaya, H. Yamasaki, M. Koyanagi, I. Kurosawa, Y. Tanaka, and I. Iguchi, Physica C **357–360**, 1610 (2001); H. Kashiwaya, I. Kurosawa, S. Kashiwaya, A. Sawa, and Y. Tanaka, Phys. Rev. B **68**, 054527 (2003).
[112]Y. Asano, Y. Tanaka, and S. Kashiwaya, Phys. Rev. B **69**, 134501 (2004).
[113]S. Kashiwaya, Y. Tanaka, M. Koyanagi, and K. Kajimura, J. Phys. Chem. **56**, 1721 (1995).
[114]N. Kitaura, H. Itoh, Y. Asano, Y. Tanaka, J. Inoue, Y. Tanuma, and S. Kashiwaya, J. Phys. Soc. Jpn. **72**, 1718 (2003).
[115]R. B. Laughlin, Phys. Rev. Lett. **80**, 5188 (1998).
[116]G. Koren and N. Levy, Europhys. Lett. **59**, 121 (2002).
[117]F. Tafuri and J. R. Kirtley, Phys. Rev. B **62**, 13934 (2000).
[118]M. Aprili, E. Badica, and L. H. Greene, Phys. Rev. Lett. **83**, 4630 (1999).
[119]R. Krupke and G. Deuscher, Phys. Rev. Lett. **83**, 4634 (1999).
[120]A. Biswas, P. Fournier, M. M. Qazilbash, V. N. Smolyaninova, H. Balci, and R. L. Greene, Phys. Rev. Lett. **88**, 207004 (2002).
[121]Y. Dagan and G. Deutscher, Phys. Rev. Lett. **87**, 177004 (2001).
[122]L. H. Greene, P. Hentges, H. Aubin, M. Aprili, E. Badica, M. Covington, M. M. Pafford, G. Westwood, W. G. Klempere, S. Jian, and D. G. Hinks, Physica C **387**, 162 (2003).
[123]A. Sawa, S. Kashiwaya, H. Obara, H. Yamasaki, M. Koyanagi, Y. Tanaka, and N. Yoshida, Physica C **339**, 107 (2000).
[124]W. K. Neils and D. J. Van Harlingen, Phys. Rev. Lett. **88**, 047001 (2002).
[125]Y. Asano and Y. Tanaka, Phys. Rev. B **65**, 064522 (2002).
[126]Y. Asano, Y. Tanaka, and S. Kashiwaya, Phys. Rev. B **69**, 214509 (2004), cond-mat/0302287.
[127]Y. Asano and Y. Tanaka, *Toward the Controllable Quantum State*, H. Takayanagi and J. Nitta (eds.), World Scientific, Singapole (2003).
[128]Y. S. Barash, A. A. Svidzinsky, and H. Burkhardt, Phys. Rev. B **55**, 15282 (1997).

[129]Y. Tanaka, Y. Tanuma, and S. Kashiwaya, Phys. Rev. B **64**, 054510 (2001).
[130]G. Eilenberger, Z. Phys. **214**, 195 (1968).
[131]A. I. Larkin and Yu. N. Ovchinnikov, Zh. Éksp. Teor. Fiz. **55**, 2262 (1986) [Sov. Phys. JETP **28**, 1200 (1968).]
[132]A. L. Schelankov, J. Low Temp. Phys. **60**, 29 (1985).
[133]P. A. Lee and D. S. Fisher, Phys. Rev. Lett. **47**, 882 (1981).
[134]Y. Asano and G. E. W. Bauer, Phys. Rev. B **54**, 11602 (1996); Erratum **56**, 9972 (1997).
[135]H. Tsuchiura, Y. Tanaka, M. Ogata, and S. Kashiwaya, Phys. Rev. Lett. **84**, 3165 (2000).
[136]M. Aprili, M. Covington, E. Paraoanu, B. Niedermeier, and L. H. Greene, Phys. Rev. B **57**, R8139 (1998).
[137]Y. Asano, Phys. Rev. B **61**, 1732 (2000); Y. Asano and T. Kato, J. Phys. Soc. Jpn. **69**, 1125 (2000); Y. Asano and T. Yuito, Phys. Rev. B **62**, 7477 (2000).

This article was published in English in the original Russian journal. Reproduced here with stylistic changes by AIP.

Advances in high-T_c grain-boundary junctions

F. Tafuri*

INFM-Coherentia, Dip. Ingegneria dell'Informazione Seconda Universitá di Napoli, Aversa (CE), Italy

J. R. Kirtley

IBM Watson Research Center, Route 134 Yorktown Heights, NY, USA

F. Lombardi

Department of Microelectronics and Nanoscience, MINA; Chalmers University of Technology and Göteborg University, S-41296 Göteborg, Sweden

P. G. Medaglia, P. Orgiani, and G. Balestrino

INFM-Coherentia, Dip. Ingegneria Meccanica, Universitá di Roma Tor Vergata, Roma, Italy
(Submitted February 9, 2004)
Fiz. Nizk. Temp. **30**, 785–794 (July–August 2004)

We review results on two novel types of grain-boundary Josephson junctions in the high-critical-temperature cuprate superconductors. The quality of $YBa_2Cu_3O_{7-\delta}$ biepitaxial grain-boundary Josephson junctions has been improved using a new growth geometry to the point that ''tunnel-like'' characteristics are reproducibly obtained. The consequent low barrier transmission probabilities are apparently favorable for isolating intrinsic *d*-wave induced effects. We also focus on peculiar aspects of spontaneous currents in HTS Josephson junctions, which are unique and reflect the intimate relation between vortex matter and the Josephson effect. Bicrystal grain-boundary Josephson junctions have also been fabricated using artificial superlattice films with as few as six superconducting copper–oxygen planes. Extrinsic and intrinsic *d*-wave effects in these junctions are discussed within the framework of novel designs for π-circuitry and qubits. [DOI: 10.1063/1.1789917]

INTRODUCTION

Ever since the discovery of high-critical-temperature superconductors (HTSs), the fabrication of high-quality junctions has presented a difficult materials science task. The goal of producing a trilayer structure, which could reproduce the very successful achievements of low-critical-temperature superconductor (S) junctions, with an insulating (I) barrier[1] (S–I–S), was always aimed at, but never really pursued in a systematic and reliable way. This situation reflected the structural complexity of HTSs, and the difficulty of finding a good material science recipe for growing a barrier on a highly nonuniform HTS electrode, which was also characterized by poor surface superconducting properties. Recently a significant step in the direction of the goal of an all-HTS trilayer with an insulating barrier was achieved through the structure composed of $La_{1.85}Sr_{0.15}CuO_4$ electrodes separated by a one-unit-cell-thick La_2CuO_4 barrier.[2] The conditions required to fabricate a trilayer structure are apparently critical and currently limited to a very few special HTS and barrier materials. Significant achievements have been also obtained by alternative junction techniques such as the YBCO–Au–Nb edge trilayer[3] and the engineered-interface[4] technique.

Despite the slow progress in material science issues related to the realization of HTS junctions, the new physical aspects which have been raised are particularly exciting. What has made the novel physics interesting is mostly related to the unconventional order parameter symmetry (OPS).[5–7] The OPS was made experimentally accessible by reproducible and good quality junctions, such as grain-boundary (GB) Josephson junctions (JJs).[8] The bicrystal technology was fundamental for the development of most of the pioneering experiments on fundamental issues, as well as for simple applications such as SQUIDs. On the other hand, the flexibility of the bicrystal technology, which can provide arbitrary GB orientation, is hindered by the fact that junctions have to be placed basically only on one line (three on a quite sophisticated tricrystal substrate). More recently the biepitaxial technique was revealed to be particularly suitable to study relevant issues of the physics of HTSs and HTS Josephson juncions.[9,10] The first biepitaxial technique provided 45° tilt GBs.[11] We extended the same biepitaxial concepts to novel configurations, in which one of the electrodes does not grow along the *c* axis orientation. Although this geometry appears to be complicated by the presence of an off-axis electrode, it gives major advantages in terms of junction flexibility and junction properties, as demonstrated in this paper.

In the present paper we will discuss some important insights into the debate of HTS weak links and *d*-wave induced effects, which have been achieved by using these double-angle CeO_2-based biepitaxial junctions, and mention novel approaches to HTS junctions based on ultrathin films. What will drive our approach to the problem is the prospect of exploiting the ''unique'' properties of HTS junctions for quantum circuitry, and the need for tunnel-like junctions.

This problem clearly involves the fundamental issue of transport in junctions. We will also focus on peculiar aspects of spontaneous currents in HTS JJs, which are unique and reflect the intimate relation between vortex matter and the Josephson effect.

THE QUBIT PROPOSALS: NEED FOR JUNCTIONS WITH TUNNEL-LIKE PROPERTIES

When considering new and exciting physical aspects associated with unconventional OPS and Josephson junctions, the idea of developing π-circuitry and, in particular, more novel designs of ''quiet qubits'' [12–15] is among the most fascinating. The ''quiet'' aspect of HTS proposals (no need to apply a constant magnetic bias, as opposed to systems based on low-temperature-superconductor Josephson junctions) probably represents the most relevant feature motivating the interest for HTS qubit systems. Furthermore, the concepts behind the various ''qubit'' proposals combine several other exciting physical aspects related to d-wave OPS, such as Andreev bound states,[16,17] time reversal symmetry breaking,[18] an imaginary component of the order parameter, and so on.

The ''qubit'' proposals involving high-T_c superconductors basically exploit the fact that JJs with an additional π shift in the phase between the electrodes can be produced in the absence of an externally applied supercurrent or field when using superconductors with a $d_{x^2-y^2}$-wave order parameter symmetry.[7] This may lead to intrinsically doubly degenerate systems, i.e., systems based on JJs with an energy–phase relation with two minima. Current versus the superconducting phase ($I_c-\varphi$) measurements on 45° asymmetric and 45° symmetric bicrystal GB JJs have demonstrated the prevalence of the 2φ component under some conditions.[19,20] On the other hand, the state of the art of HTS JJs and the actual understanding of transport mechanisms in GBs do not presently allow the reproducible determination of the conditions for observation of the 2φ component. Subsequent investigations have raised concerns about the quietness of these devices. It was argued that, while on the one hand a 45° misorientation of the OPS in one electrode is necessary to generate the π-behavior, it may on the other hand lead to spontaneous currents related to Andreev reflection and more precisely to Andreev bound states.[16,17] Such currents may cause additional noise[13] and enhance decoherence mechanisms. This analysis led to the development of alternative designs, in which a five-junction loop (with four ordinary junctions and a π-junction) takes the place of the original s-wave–d-wave superconductor junction. In this ''macroscopic analog'' of Ref. 12, the π-junction removes the need for a constant magnetic bias near $\Phi/2$.

Contributions to dissipation due to different transport processes, such as channels due to nodal quasiparticles or midgap states or their combination, have been identified and distinguished.[21] In particular cases, decoherence times and quality factors have been calculated. It has been also argued that problems in observing quantum effects due to the presence of gapless quasiparticle excitations can be overcome by choosing the proper working phase point.[22] In particular, decoherence mechanisms can be reduced by selecting appropriate tunneling directions because of the strong phase dependence of the quasiparticle conductance of a d-wave GB junction.

The Chalmers group has discussed the dynamics of the junctions in the zero-bias quantum regime and the dependence on junction parameters of the decoherence time in the system,[23] determining also the Josephson and Coulomb energies in submicron junctions. The same group has also studied experimentally the possibility of using size effects in submicron junctions to freeze out low-energy quasiparticles, and to induce a prevailing 2φ component in the $I_c-\varphi$ dependence.[20]

These are experimental and theoretical examples of innovative work towards a ''quantum'' treatment of HTS junctions, and are quite encouraging. Nevertheless a complete ''quantum'' approach to junction properties and parameters is still missing, and typical quantum effects, such as macroscopic quantum tunneling, have not been observed up to now. A lot of work has to be done in this respect, covering several different issues, but some ''trends'' and constraints on junction properties are becoming clear. It is reasonable to expect that for macroscopic quantum tunneling experiments, for instance, it is important to rely on junctions in the tunnel-like limit with relatively high values of the normal-state resistance. A favorable quantum regime may nevertheless be hindered by the lack of understanding of the junction transport processes and of the interplay between OPS effects and barrier/microstructure effects. It may be important to reach a regime in which ''intrinsic'' d-wave induced effects are isolated from ''extrinsic'' effects. Intrinsic effects are only due to the d-wave order parameter, while extrinsic effects are mostly due to the d-wave order parameter and occur only in junctions with particular morphologies and/or properties. Examples of extrinsic effects are the anomalous dependence of the critical current on the magnetic field[3,24] and the presence of specific spontaneous currents revealed through scanning SQUID microscopy (SSM).[25] Extrinsic effects may be undesirable and even mask the features of the intrinsic effects. We will discuss in the following Sections how it is possible to reach some regimes of HTS JJs in which intrinsic effects can be isolated.

NEW BIEPITAXIAL TECHNIQUE

Grain-boundary Josephson junctions are obtained at the interface between a (103) $YBa_2Cu_3O_{7-\delta}$ (YBCO) film grown on a (110) $SrTiO_3$ substrate and a c-axis film deposited on a (110) MgO (Fig. 1*a*) or CeO_2 (Fig. 1*b*) seed layer. The presence of the CeO_2 produces an additional 45° in-plane rotation of the YBCO axes with respect to the in-plane directions of the substrate.[10,26] As a consequence, the GBs are the product of two 45° rotations, a first one around the c axis, and a second one around the b axis. This configuration produces the desired 45° misorientation between the two electrodes to enhance d-wave OPS effects, as shown in Fig. 1*d* and as opposed to the MgO case of Fig. 1*c*, where no in-plane rotation occurs. MgO-based junctions have been proved to be of high quality and their properties to be very weakly influenced by OPS.[26] In this paper MgO based junctions will be discussed mostly for comparison with the CeO_2-based junctions.

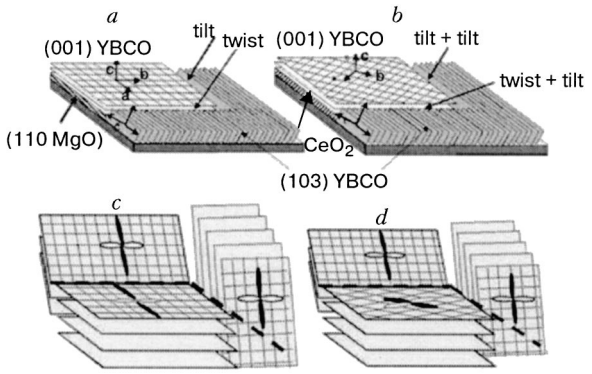

FIG. 1. Sketch of the grain-boundary structures. The two limit configurations, tilt and twist, are indicated for junctions based on the MgO or CeO_2 seed layer, respectively.

Furthermore, the degrees of freedom of the fabrication process allow the selection of any possible in-plane orientation for the GB interface. Details about the fabrication process can be found elsewhere.[9,10,26] We will define the GB interface angle θ with respect to the [001] in-plane $SrTiO_3$ direction. In the two limiting configurations, $\theta=0°$, $\theta=90°$, the GBs are characterized by a (100) 45° tilt or twist, respectively, of the c axis with respect to the interface, plus a 45° tilt around the c axis. In this paper they will be referred to as tilt–tilt and twist–tilt GBs. It is reasonable to assume that these MgO-based and CeO_2-based junctions can be considered complementary from the OPS point of view from a circuit design perspective.[26]

TRANSPORT PROPERTIES: GENERAL FEATURES

The analysis of current versus voltage ($I-V$) characteristics, while revealing basic properties of the junctions, is a broad topic that goes beyond the aims of this paper. We confine our attention to some specific properties, which are of relevance in our discussion of d-wave induced effects in HTS JJs. The general conclusion of different studies realized on the MgO-based and CeO_2-based junctions sketched above is that in our GBs, the crucial feature of relatively lower barrier transmission seems to be associated with a c-axis tilt. The normal-state resistances R_N and critical currents I_c are the relevant parameters. A direct comparison of the $I-V$ curves for MgO-based and CeO_2-based junctions in the extreme tilt and twist limit cases (see Fig. 2) reveals that the barrier transparency may be strongly connected to OPS configuration. In this case the 45° in-plane rotation of one of the electrodes produces π-contact behavior. For MgO-based junctions, higher critical current densities and lower normal-state resistances characterize the twist limit when compared with the tilt case, reflecting the different grain-boundary microstructures. On the other hand, for CeO_2-based junctions the influence of the resulting π-contacts cancels out any difference in critical current densities between the tilt and twist cases. Details will be given in the next Section.

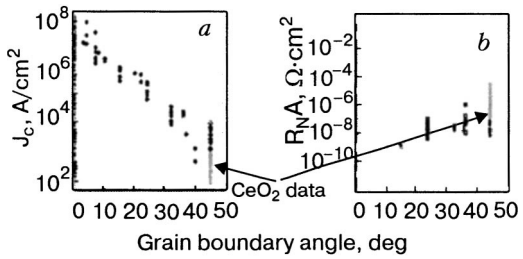

FIG. 3. (a) Critical current densities of CeO_2-based junctions of the present work (arrows) are compared with data published in Ref. 8. (b) Normal-state resistances of CeO_2-based junctions are compared with data published in Ref. 8.

The values of the critical current I_c and specific resistance R_NA (where A is the junction area) are compared with published data[8] in Figs. 3a and 3b. The data available in the literature mostly pertain to GB junctions for which the angle refers to an in-plane tilt. Our grain boundary is more complicated, as discussed in the previous subsection. As a matter of fact, our critical current density J_c and R_NA values are the lowest and the highest values, respectively, indicating a trend toward tunnel-like behavior. Values of R_NA typically range from 10^{-7} to 10^{-5} $\Omega\cdot cm^2$ at $T=4.2$ K, on average at least one order of magnitude higher than the values extracted from measurements on other (in particular, bicrystal) types of GB junctions.[8] The values of J_c typically range from 10^2 to 5×10^3 A/cm^2.

The tilt and twist configurations are the limiting cases, clearly different from each other (see Fig. 2). A fine tuning of the $I-V$ curves has been clearly observed by changing the interface angle orientations, as shown in Fig. 4a. The tuning of the junction properties follows a very peculiar behavior indicative of d-wave OPS (as discussed in the next subsection), while the junction parameters fall in the ranges given above. The $I-V$ curves are mostly described by the resistively shunted junction (RSJ) model. We also note the reproducible presence of hysteretic behavior (switching currents) in the $I-V$ characteristics in Figs. 4a,b. The hysteretic behavior is mostly observed in the angle range $\theta\geqslant45°$ (twist-

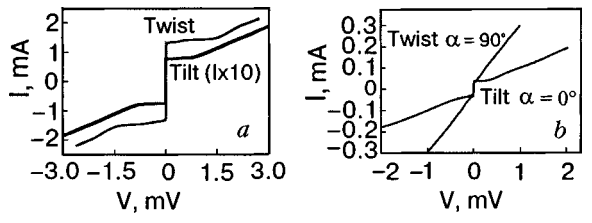

FIG. 2. Current versus voltage ($I-V$) characteristics of MgO and CeO_2 biepitaxial junctions are reported in the extreme cases of tilt and twist ($T=4.2$ K) for junctions of the same width (10 μm), respectively. In the MgO tilt case the current is multiplied by a factor of 10 for clarity.

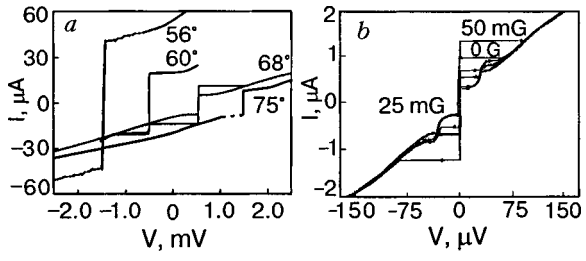

FIG. 4. Current versus voltage characteristics of biepitaxial junctions measured at $T=4.2$ K for various interface orientations (a) and of a twist junction (90°) at $T=0.8$ K for three different values of the magnetic field (b). In (a) the curves are shifted along the x axis for clarity.

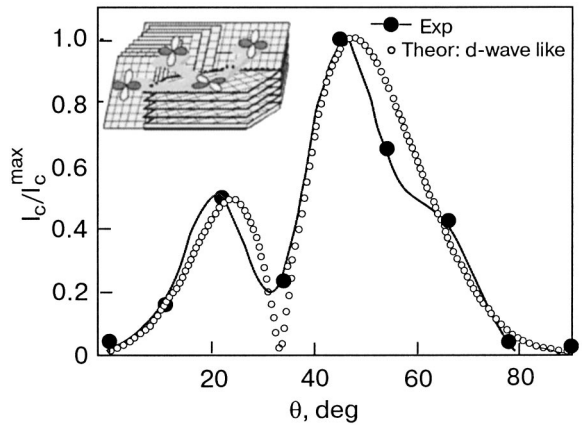

FIG. 5. Dependence of I_c on the angle θ; experimental data (filled circles) are compared with theoretical predictions based on $d_{x^2-y^2}$-wave pairing symmetry (open circles).[10] In the inset three different interface orientations are given as examples. The junction is 4 μm wide.

like regime) and for lower values of J_c, confirming a general trend towards tunnel-like behavior. The presence of such switching currents may be important for a series of different experiments, such as those aimed at detecting macroscopic quantum effects.

ANISOTROPY MEASUREMENTS: EVIDENCE FOR *d*-WAVE INDUCED EFFECTS

In Fig. 5 we report the dependence of I_c on the angle θ for junctions 4 μm wide. A clear oscillatory dependence of the critical current I_c on θ was observed[10] as expected in structures dominated by *d*-wave induced effects. This has been observed for various sets of junctions of different widths.

Minima in the critical current are observed for $\theta=0°$, 34°, and 90°, respectively. These values correspond to configurations in which the tunneling direction (the normal to the barrier) points towards a node of the OP on one of the two sides. The minima at $\theta=0°$ and 90° arise from the position of the nodes in the *c*-axis oriented side of the junction. The minimum at $\theta=34°$ occurs when the projection in the $a'b'$ planes of the normal to the barrier points towards a node of the OP on the (103) side. In the Sigrist–Rice (SR) phenomenological approach, the Josephson current density of an all *d*-wave junction is given by[5]

$$J_c=J_0(n_x^2-n_y^2)_L(n_x^2-n_y^2)_R \sin\varphi. \quad (1)$$

In this expression J_0 is the maximum Josephson current density, φ is the difference between the phase of the OP in the two electrodes, and n_x and n_y are the projections of the unit vector **n** onto the crystallographic axes *x* and *y* in the left (L) and right (R) electrode, respectively. Traditionally the SR formula has been applied to junctions where both electrodes are *c*-axis oriented. Specifying the expression above to our noncoplanar configuration ($J_c\sim\sin 2\theta(2-\cos^2\theta)(1-3\sin^2\theta)/(1+\sin^2\theta)$), and assuming a more efficient tunneling in the lobes directions,[10] we obtain the curve plotted as open circles in Fig. 5. The experimental behavior is well reproduced by the SR-like theoretical prediction. The $I_c(\theta)$ dependence in agreement with the SR formula apparently seems to be mostly determined by the OPS.

We believe that our junction configuration, with low barrier transmission probabilities, preserves the directionality of the Cooper pairs, whether the transport be by tunneling or some other mechanism. Therefore it is in principle more sensitive to the angular dependence of the order parameter symmetry and therefore reveals *d*-wave induced behavior. The anisotropy measurements have demonstrated for the first time that ''intrinsic'' *d*-wave effects are dominant in the phenomenology of the Josephson junctions themselves (not inserted in any loop) independently of the interface details.[10] The good agreement with the SR formula apparently suggests that the $I_c(\theta)$ dependence is mostly determined by the OPS. In this case the grain-boundary microstructure, which is the other main effect ruling the junctions' properties, does not significantly contribute to the qualitative behavior of $I_c(\theta)$. In other words, deviations from the Sigrist–Rice behavior may indicate a more significant contribution played by the actual GB microstructure to the angular dependence of I_c. The GB microstructure definitely contributes to form a ''tunnel-like'' barrier, characterized by higher values of the normal-state resistance.

SCANNING SQUID MICROSCOPY AND SPONTANEOUS CURRENTS

In this Section and the next we will deal with some aspects related to vortex matter and the Josephson effect, and in particular to the presence of spontaneous currents (i.e., spontaneous magnetization with random orientation and the half flux quantum effect) in CeO_2-based biepitaxial junctions. Phenomena related to spontaneous currents are peculiar to HTS Josephson junctions and π-contacts systems. Scanning SQUID microscopy[25] is an appropriate technique for the imaging and study of the magnetic response of different samples, and can be used in appropriate configurations to study phenomena in zero-field cooling, and therefore spontaneous currents. Spontaneous currents may have different origins depending on the system in which they are observed. The half flux quantum effect (such as observed in the tricrystal experiments) was the first remarkable example of spontaneous currents.[7] In this case the different flux distributions depend only on the intentionally introduced sample geometry and on the typical scaling lengths of the junctions involved. SSM has also demonstrated the presence of randomly distributed spontaneous currents along GBs.[24] These are determined by naturally occuring π-loops due to a combination of the *d*-wave OPS and the junction morphology (faceting).[24,27,28]

Spontaneous magnetization with random orientation

We first address spontaneous currents due to π-loops and how it is possible to prevent their formation.[28] To this aim we investigated through SSM the magnetic behavior of grain boundaries of biepitaxial samples cooled in zero field and characterized by different junction parameters.

In Fig. 6*a* we give evidence of the presence of spontaneous currents along the GBs in the tilt, twist, and intermediate situations represented, for instance, by the sides of the photolithographically defined triangles sketched in Fig. 6*b*. This behavior is consistent with the presence of π-loops along the GBs and with expectations based on faceted inter-

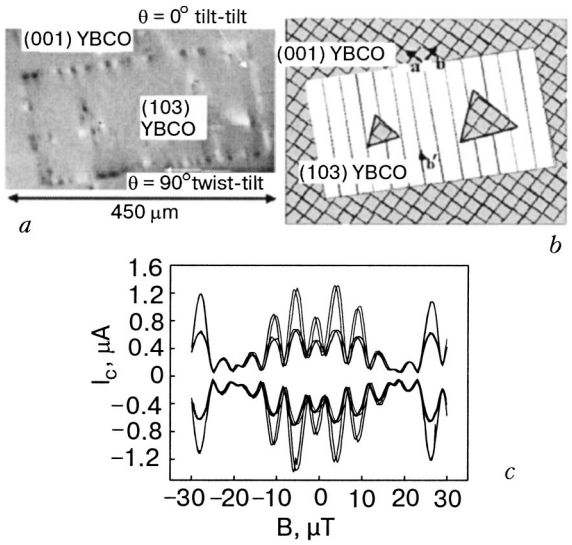

FIG. 6. (*a*) SSM image of a 600×400 μm area. The GBs are marked by the presence of spontaneous currents. The sample was cooled and imaged at $T=4.2$ K in nominally zero field. (*b*) Sketch of the grain boundaries imaged in (*a*). (*c*) Magnetic pattern of a hysteretic twist biepitaxial junction measured at $T=4.2$ K. The two different curves refer to the critical and the retrapping currents. The junction is 20 μm wide.

faces, in agreement with other experiments on bicrystal[24] and biepitaxial junctions.[27] The noise associated with such currents, due to π-loops along GBs, provide a simple example of how HTS JJs may be intrinsically noisy. Such a behavior is associated with samples characterized by higher critical current densities J_c.[29] In the literature it has been shown that the presence of π-loops is accompanied by an anomalous magnetic pattern[3,24] such as the one reported in Fig. 6*c*, measured on one of our junctions. In this case the $I-V$ characteristic is hysteretic, and we report both the critical escape and retrapping currents.

In Fig. 7, where a scanning SQUID microscope image of an 800×800 μm area is reported, no spontaneous magnetization was detected along any of the GB interfaces, which had arbitrary orientation.[28] Single-flux-quantum Josephson vortices are randomly present along the GBs. In this case we have changed J_c and, as a consequence, the Josephson penetration depth. This was done by reducing the thickness of the film in Fig. 7 to about one-third of the thickness of the sample reported in Fig. 6*a*. Differences in the J_c values correspond to the general feature in HTS JJs, that J_c does not perfectly scale with the film thickness.[8]

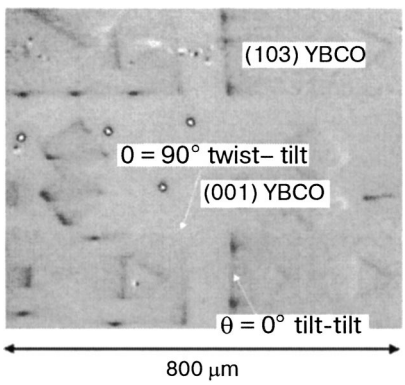

FIG. 7. SSM image of an 800×800 μm area, enclosing tilt–tilt and twist–tilt GBs. The sample was cooled in nominally zero field and imaged at $T=4.2$ K. No randomly oriented spontaneous magnetization was detected along the GB interfaces.

If we try to interpret these results, keeping in mind the *d*-wave nature of these junctions, as revealed by the anisotropy measurements, we attribute the absence of any spontaneous magnetization to the locally reduced J_c. This experimental conclusion is consistent with numerical solutions of the sine-Gordon equation for a $0-\pi$ Josephson junction.[30–32] In this modeling the spontaneous magnetization decreases when the ratio of the Josephson penetration depth λ_J to the facet spacing becomes large, as is discussed in detail in Refs. 28 and 31. We have modeled this for a regular array, varying the facet width L_π. For the faceted configuration there is a threshold for observation of spontaneous magnetization ($L_\pi \simeq \lambda_J$).[28] Sufficiently long penetration depths made the measurements of the Josephson critical currents as a function of the misorientation angle insensitive to faceting effects, and represent the crucial feature in preventing the formation of spontaneous currents due to π-loops in the systems analyzed.

We recall another interesting related configuration in which spontaneous currents with random orientation have been observed.[33] This case enriches possible scenarios of spontaneous currents. We refer to *c*-axis YBCO thin films grown on a MgO seed layer on a (110) $SrTiO_3$ substrate (which basically represents the *c*-axis electrode of the MgO based biepitaxial configuration). Spontaneous currents were observed to be spatially correlated with impurities due to the presence of the so-called green phase due to Y excess in *c*-axis films. The origin of such currents is unclear. It may be due to time reversal symmetry breaking (BTRS) or due to the spontaneous nucleation of topological defects in phase transitions (for instance, the pinning of a vortex tangle, produced near T_c in a Berezinskii–Kosterlitz–Thouless[34] type transition in the nearly two-dimensional superconductor YBCO). BTRS may be related to an imaginary component of the OPS near a surface facing the insulating green phase.[18] This would in principle be the only configuration able to prove the origin of BTRS as due to an imaginary component of the order parameter, since in junction interfaces the same effect could also be due simply to Andreev bound states.[35,36] The lack of an experiment showing reproducible, well-defined isolated spontaneous currents in controlled systems is a limitation for the former interpretation and for related arguments on fractional vortices. More recent studies on phase transitions on the amorphous superconductor Mo_3Si in ring geometry make the latter possibility feasible.[37] Further investigations are required for a definitive answer.

Half flux quantum

Once the conditions which lead to the absence of spontaneous currents due to π-loops along GBs were determined, we studied if and how the well-known half flux quantum effect occurs in our peculiar junction configurations.

Figure 8 is a three-dimensional SSM image of a large area of a biepitaxial sample containing different interfaces and types of grain boundary, cooled in presence of a small magnetic field. Various types of vortices and spread flux can be observed. We notice on the left, four standard in-plane

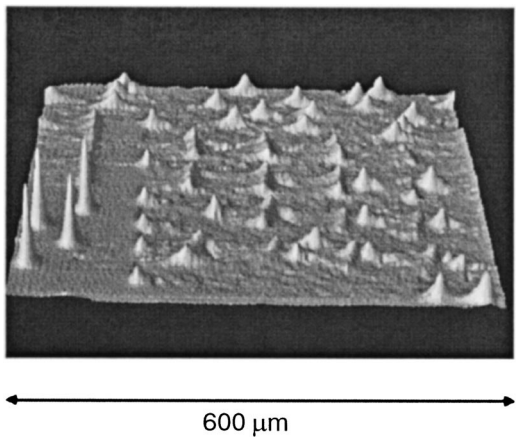

FIG. 8. SSM image of a 600×600 μm area, enclosing different types of Gbs. The sample was cooled in a small magnetic field and imaged at $T=4.2$ K. Flux tubes appear randomly localized in bulk material and along grain boundaries. Magnetic flux also appears along some grain-boundary lines.

Abrikosov vortices characterized by flux well localized in a narrow area. On the top anisotropic vortices in the (103) part of the YBCO film are also visible. These are more spread than the in-plane Abrikosov vortices. Both these types of vortices are a useful reference for determining the flux present in the center of the image along the lithographically pre-determined contours (triangles in particular). In contrast with the ordinary vortices, the flux along the triangles will not vanish even in zero-field cooling. This is due to the particular triangular shapes (defined by grain boundaries with different orientations) which were designed in order to observe the half flux quantum effect.

A schematic of a section of the sample imaged in Fig. 8, a set of 16 isosceles triangles (triangle side $L=50$ μm), is shown in Fig. 9*a*. Each triangle is rotated clockwise by 3° from the last in moving from bottom to top along the rows of triangles, and from left to right along the columns. Corners which have a sign change in the product of the normal components of the gap functions on opposite sides of the grain boundaries are expected to have spontaneously generated Josephson vortices with a flux localized at them equal to half of the superconducting flux quantum, if the Josephson depth is short relative to the length of a side of the triangle. In this design the half flux quantum vortices should systematically shift to different corners as the triangle orientation is changed. Figure 9*b* shows the corresponding SSM image of

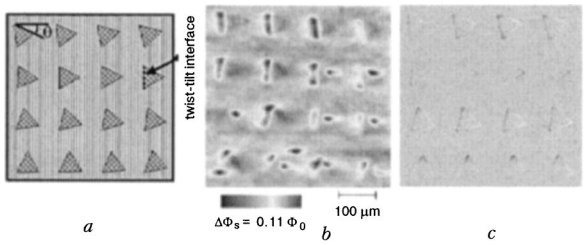

FIG. 9. (*a*) Schematic diagram of the sample geometry. (*b*) SSM image of a 450×450 μm area, enclosing a set of 16 triangles with various interface orientations. The image was taken at $T=4.2$ K. (*c*) Simulated spontaneous fluxes along the triangle interfaces, assuming *d*-wave momentum dependences of the pairing wave function.

the sample cooled and imaged in a magnetic field such that there is approximately 1 flux quantum (Φ_0) trapped per triangle. This image is the two-dimensional view of the central part of the image of Fig. 8. Spontaneous (since it was observed also when the sample was cooled in zero field) magnetization is visible along some interfaces and at some corners, and a systematic behavior clearly appears in moving from the top row, where the flux is spread along GBs, down to the bottom, where the flux is more localized in some corners.

The fact that under some circumstances the half flux quantum can be spread along the grain boundaries rather than being concentrated in the corner, is consistent with long Josephson penetration depths and low barrier transmissions,[38] occurring in our junctions. For comparison, simulations of the expected spontaneous currents in our triangular grain boundaries are shown in Fig. 9*c*. These simulations numerically solve the sine-Gordon equation for a faceted grain boundary,[31] with the sign and magnitude of the Josephson critical current density along the grain boundaries chosen using the Sigrist–Rice expressions,[5] assuming the standard $d_{x^2-y^2}$-like pairing symmetry.[28] It was assumed there was a total of one Φ_0 of magnetic flux in each triangle. The Josephson penetration depth λ_J was set equal to $\lambda_{J0}/\sqrt{|j_c(\theta)|}$, where $j_c(\theta)$ contains the dependence of the critical current on grain-boundary geometry. For the simulations $\lambda_J(0)$ was assumed to be 5 microns. Details about the simulations can be found in Ref. 28. Apart from minor local deviations, there is qualitative agreement between the experimental data and the modeling.

DISCUSSION: EXTRINSIC AND INTRINSIC *d*-WAVE EFFECTS IN GRAIN-BOUNDARY JUNCTIONS

The features discussed in the previous Section prove the existence of ''pure'' intrinsic *d*-wave effects in GB JJs, as indicated in anisotropy transport measurements and the half flux quantum effect, in agreement with theoretical expectations. Moreover experimental conditions can be chosen in which spontaneous extrinsic currents may be substantially reduced. It is possible therefore in the biepitaxial technology to observe the half flux quantum effect and to suppress spontaneous magnetization with random orientations. In other words there seems to be an accessible scaling range of junction parameters for reaching a favorable ''regime'' where *d*-wave induced intrinsic features are very robust, and extrinsic features such as noise from π-loops can be severely limited. The coherence related to the OPS seems to be preserved on a scale larger than the faceting and/or any interface impurity characteristic lengths. Both from anisotropy transport measurements and SSM analysis, results on junctions can be reasonably explained without invoking a significant imaginary component of the OPS.[18,35]

A study based on radio-frequency and SSM measurements[39] on the same tilt–tilt samples seemed to show the absence of the type of spontaneous magnetization reported, for instance, in Fig. 7, and Andreev bound states are effects which can co-exist. This also means that the possibility of preventing the spontaneous currents discussed above applies only to those generated by π-loops. However, a threshold of 0.01 of the flux quantum Φ_0 for other addi-

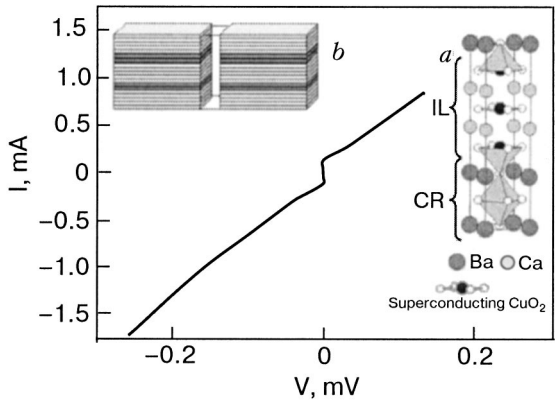

FIG. 10. $I-V$ curve in zero field for a bicrysal junction 1 mm wide. The misorientation angle in this case is 24°, and the configuration is asymmetric. The typical stacking sequence of the charge reservoir (CR) block and the infinite layer (IL) superconducting block characteristic of HTS compounds and of the CBCO compound used in this experiment is reported in inset (a). A schematic diagram of the grain boundary is shown in inset (b): only 6 superconducting CuO_2 planes are present on each electrode; Josephson phenomena should be associated only with such planes.

tional mechanisms generating noise in HTS JJs is set by SSM measurements. The tunnel-like behavior inferred from different experiments is the other crucial feature of these biepitaxial junctions; it favors a promising regime where junction quantum effects could manifest. The additional degree of freedom offered by the biepitaxial technique, to vary the interface orientation, can be crucial for finding more precise conditions in which to optimize specific performances and even to reduce decoherence mechanisms.[22] For instance, in the range $50° \leqslant \theta \leqslant 80°$ we could obtain a regime where the $I-V$ curves are hysteretic and the effect of midgap states should be reduced.

JOSEPHSON JUNCTIONS BASED ON ULTRATHIN CBCO FILMS

In this Section we discuss a ''novel'' type of HTS JJs. The philosophy is to develop controlled systems which may in the proper limit give more uniform barrier interfaces. This is realized by exploiting GB junctions and ultrathin films, i.e., artificially layered HTSs,[40] such as $[Ba_{0.9}Nd_{0.1}CuO_{2+x}]_m/[CaCuO_2]_n$ (CBCCO–$m\times n$). These films (similarly to all existing HTS cuprates) are composed by a stacking sequence of two structural subunits having different functions, namely the charge reservoir (CR) block and the infinite layer (IL) superconducting block (see inset (a) in Fig. 10). The IL block always consists of CuO_2 planes seperated by an alkaline earth (mostly Ca) plane, while the structure and the chemical composition of the CR block vary from compound to compound. The structural and transport properties of these compounds have been discussed elsewhere.[40,41] We have for the first time realized Josephson junctions composed of only a few superconducting CuO_2 planes (6 layers in particular). For this experiment we have focused in particular on ultrathin $[Ba_{0.9}Nd_{0.1}CuO_{2+x}]_5/[CaCuO_2]_2/[Ba_{0.9}Nd_{0.1}CuO_{2+x}]_5/[CaCuO_2]_n/[Ba_{0.9}Nd_{0.1}CuO_{2+x}]_5$ (5/2/5/2/5) structures and have employed the bicrystal technique. The junction schematic diagram is shown in inset (b) of Fig. 10, where the six superconducting CuO_2 planes are shown. The CBCO film is only 8 nm thick.

The current–voltage $I-V$ curves reported in Fig. 10 correspond to a $w=1$ mm wide bicrystal junction measured at $T=4.2$ K. The misorientation angle in this case is 24°, and the configuration is asymmetric. Similar behavior was observed for symmetric junctions up to 5 mm wide. The shape is RSJ-like and the $I-V$ curves are modulated by the magnetic field. Details will be discussed elsewhere.

The simple structure of the grain boundary composed by 6 superconducting CuO_2 layers (due to the highly controlled structure of the 5/2/5/2/5 artificial structure) also allows a reliable estimation of the coupling along the ab planes of two CuO_2 layers separated by a 24° asymmetric or symmetric GB: in particular, we calculate a critical current density per plane of about $(0.2-0.3)\times 10^2$ A/cm^2.

Additional evidence of the Josephson behavior comes from the observation through SSM of Josephson vortices, which will be discussed elsewhere. In this case the magnetic fields associated with the Josephson vortices are influenced by the extremely large Pearl lengths of these very thin films.

CONCLUSIONS

We have discussed different issues of grain-boundary HTS Josephson junctions. To produce high-quality junctions is a crucial step in pursuing quantum circuitry based on HTSs and to for investigating reliably all the exciting phenomenology occurring in HTS junctions. Good quality ''tunnel-like'' Josephson junctions can be fabricated by exploiting the biepitaxial technique. The anisotropic transport measurements and the half flux quantum effect, both in agreement with theoretical expectations, prove the existence of ''pure'' intrinsic d-wave effects in GB JJs. If this is combined with the absence of spontaneous magnetization in situations where faceting could be expected to be an issue, there seems to be an accessible scaling range of junction parameters to reach a favorable ''regime'' where d-wave induced intrinsic features are very robust and dominant over extrinsic features such as noise from π-loops. A remarkable feature is the presence of Josephson phenomena in nano-structured systems (ultrathin films) along macroscopic dimensions of the order of a few millimeters. More specifically we are able to identify Josephson phenomena in films with 6 superconducting layers in a nominally very uniform configuration. No analogous situation exists for other HTS junctions with thicker electrodes. This more controlled system could also open up some prospects for further understanding of the transport mechanisms in grain-boundary junctions.

This work has been partially supported by the ESF projects ''Π-Shift'' and ''QUACS.'' The authors would like to thank A. Barone, T. Bauch, S. Kubatkin, K. Moler, and C. Tsuei for helpful discussions.

*E-mail: tafuri@na.infn.it

[1] A. Barone and G. Paternó, *Physics and Applications of the Josephson Effect*, J. Wiley, New York (1982).
[2] I. Bozovic, G. Logvenov, M. A. J. Verhoeven, P. Caputo, E. Goldobin, and T. H. Geballe, Nature (London) **422**, 873 (2003).

[3] H. J. H. Smilde, Ariando, D. H. A. Blank, G. J. Gerritsma, H. Hilgenkamp, and H. Rogalla, Phys. Rev. Lett. **88**, 057004 (2002); H. Hilgenkamp, Ariando, H. J. H. Smilde, D. H. A. Blank, G. Rijnders, H. Rogalla, J. R. Kirtley, and C. C. Tsuei, Nature (London) **422**, 50 (2003).
[4] B. H. Moeckly and K. Char, Appl. Phys. Lett. **71**, 2526 (1997).
[5] M. Sigrist and T. M. Rice, J. Phys. Soc. Jpn. **61**, 4283 (1992); M. Sigrist and T. M. Rice, Rev. Mod. Phys. **67**, 503 (1995).
[6] D. J. van Harlingen, Rev. Mod. Phys. **67**, 515 (1995).
[7] C. C. Tsuei and J. R. Kirtley, Rev. Mod. Phys. **72**, 969 (2000) (and references therein).
[8] H. Hilgenkamp and J. Mannhart, Rev. Mod. Phys. **74**, 485 (2002) (and references therein).
[9] F. Tafuri, F. Miletto Granozio, F. Carillo, A. Di Chiara, K. Verbist, and G. Van Tendeloo, Phys. Rev. B **59**, 11523 (1999).
[10] F. Lombardi, F. Tafuri, F. Ricci, F. Miletto Granozio, A. Barone, G. Testa, E. Sarnelli, J. R. Kirtley, and C. C. Tsuei, Phys. Rev. Lett. **89**, 207001 (2002).
[11] K. Char, M. S. Colclough, S. M. Garrison, N. Newman, and G. Zaharchuk, Appl. Phys. Lett. **59**, 733 (1991).
[12] L. B. Ioffe, V. B. Geshkenbein, M. V. Feigel'man, A. L. Fauchere, and G. Blatter, Nature (London) **398**, 679 (1999).
[13] G. Blatter, V. B. Geshkenbein, and L. B. Ioffe, Phys. Rev. B **63**, 174511 (2001).
[14] A. Blais and A. M. Zagoskin, Phys. Rev. A **61**, 42308 (2000); A. M. Zagoskin, cond.-mat. 9903170.
[15] Y. Makhlin, G. Schon, and A. Shnirman, Rev. Mod. Phys. **73**, 357 (2001).
[16] C.-R. Hu, Phys. Rev. Lett. **72**, 1526 (1994).
[17] T. Lofwander, V. Shumeiko, and G. Wendin, Supercond. Sci. Tech. **14**, R53 (2001) (and references therein).
[18] M. Sigrist, Prog. Theor. Phys. **99**, 899 (1998).
[19] E. Ilichev, V. Zakosarenko, R. P. J. IJsselsteijn, H. E. Hoenig, V. Schultze, H. G. Meyer, M. Grajcar, and R. Hlubina, Phys. Rev. B **60**, 3096 (1999); E. Ilichev, M. Grajcar, R. Hlubina, R. P. J. IJsselsteijn, H. E. Hoenig, H. G. Meyer, A. Golubov, M. H. S. Amin, A. M. Zagoskin, A. N. Omelyanchuk, and M. Yu. Kupriyanov, Phys. Rev. Lett. **86**, 5369 (2001).
[20] T. Lindstrom, S. A. Charlebois, A. Ya. Tzalenchuk, Z. Ivanov, M. H. S. Amin, and A. M. Zagoskin, Phys. Rev. Lett. **90**, 117002 (2003).
[21] Ya. V. Fominov, A. A. Golubov, and M. Yu. Kypryanov, JETP Lett. **77**, 587 (2003).
[22] M. H. S. Amin and A. Smirnov, Phys. Rev. Lett. **92**, 17001 (2004).
[23] A. Ya. Tzalenchuk, T. Lindstrom, S. A. Charlebois, E. A. Stepantsov, Z. Ivanov, and A. M. Zagoskin, Phys. Rev. B **68**, 1005001 (2003).
[24] J. Mannhart, H. Hilgenkamp, B. Mayer, Ch. Gerber, J. R. Kirtley, K. A. Moler, and M. Sigrist, Phys. Rev. Lett. **77**, 2782 (1996); H. Hilgenkamp, J. Mannhart, and B. Mayer, Phys. Rev. B **53**, 14586 (1996).
[25] J. R. Kirtley, M. B. Ketchen, K. G. Stawiasz, J. Z. Sun, W. J. Gallagher, S. H. Blanton, and S. J. Wind, Appl. Phys. Lett. **66**, 113 (1995) (and references therein).
[26] F. Tafuri, F. Carillo, F. Lombardi, F. Miletto Granozio, F. Ricci, U. Scotti di Uccio, A. Barone, G. Testa, E. Sarnelli, and J. R. Kirtley, Phys. Rev. B **62**, 14431 (2000).
[27] J. R. Kirtley, P. Chaudhari, M. B. Ketchen, N. Khare, Shawn-Yu Lin, and T. Shaw, Phys. Rev. B **51**, R12057 (1995).
[28] F. Tafuri, J. R. Kirtley, F. Lombardi, and F. Miletto Granozio, Phys. Rev. B **67**, 174516 (2003).
[29] R. G. Mints, Ilya Papiashvili, J. R. Kirtley, H. Hilgenkamp, G. Hammerl, and J. Mannhart, Phys. Rev. Lett. **89**, 67004 (2002); R. G. Mints and Ilya Papiashvili, Phys. Rev. B **64**, 134501 (2001).
[30] C. S. Owen and D. J. Scalapino, Phys. Rev. **164**, 538 (1967).
[31] J. R. Kirtley, K. A. Moler, and D. J. Scalapino, Phys. Rev. B **56**, 886 (1997).
[32] E. Goldobin, D. Koelle, and R. Kleiner, Phys. Rev. B **67**, 224515 (2003).
[33] F. Tafuri and J. R. Kirtley, Phys. Rev. B **62**, 13934 (2000).
[34] J. M. Kosterlitz and D. J. Thouless, J. Phys. C **6**, 1181 (1973).
[35] M. H. S. Amin, A. N. Omelyanchouk, and A. M. Zagoskin, Phys. Rev. B **63**, 212502 (2001); M. H. S. Amin, S. N. Rashkeev, M. Coury, A. N. Omelyanchouk, and A. M. Zagoskin, *ibid.* **66**, 174515 (2002).
[36] T. Lofwander, V. S. Shumeiko, and G. Wendin, Phys. Rev. B **62**, R14653 (2003).
[37] J. R. Kirtley, C. C. Tsuei, and F. Tafuri, Phys. Rev. Lett. **90**, 257001 (2003).
[38] C. C. Tsuei and J. R. Kirtley, Phys. Rev. Lett. **85**, 182 (2000).
[39] E. Il'ichev, F. Tafuri, M. Grajcar, R. P. J. IJsselsteijn, J. Weber, F. Lombardi, and J. R. Kirtley, Phys. Rev. B **68**, 04510 (2003).
[40] G. Balestrino, S. Lavanga, P. G. Medaglia, S. Martellucci, A. Paoletti, G. Pasquini, G. Petrocelli, A. Tebano, A. A. Varlamov, L. Maritato, and M. Selvato, Phys. Rev. B **62**, 9835 (2000).
[41] G. Balestrino, S. Lavanga, P. G. Medaglia, P. Orgiani, and A. Tebano, Phys. Rev. B **64**, 020506 (2001).
[42] F. Tafuri, J. R. Kirtley, P. G. Medaglia, P. Orgiani, and G. Balestrino, Phys. Rev. Lett. **92**, 157006 (2004).
[43] J. Pearl, J. Appl. Phys. **37**, 4139 (1966).
[44] V. G. Kogan, V. V. Dobrovitski, and J. R. Clem, Phys. Rev. B **63**, 144501 (2001).

This article was published in English in the original Russian journal. Reproduced here with stylistic changes by AIP.

Electron transport in metal oxide superconducting heterojunctions

F. V. Komissinski

Institute of Radio Engineering and Electronics, Russian Academy of Sciences, Moscow 125009, Russia; Department of Microtechnology and Nanoscience, Chalmers University of Technology, Göteborg S412 96, Sweden*

K. I. Constantinian, Yu. Kislinskii, and G. A. Ovsyannikov

Institute of Radio Engineering and Electronics, Russian Academy of Sciences, Moscow 125009, Russia

(Submitted January 23, 2004)
Fiz. Nizk. Temp. **30**, 795–809 (July–August 2004)

Research results on electron transport in $Au/YBa_2Cu_3O_x$ and $Nb/Au/YBa_2Cu_3O_x$ thin-film heterojunctions are reviewed. The experimental current–phase relations of $Nb/Au/YBa_2Cu_3O_x$ heterojunctions on *c*-oriented YBCO films exhibit a second harmonic, temperature dependence, and a phase shift that is explained in terms of a combined symmetry $d_{x^2-y^2}+s$ of the superconducting order parameter of $YBa_2Cu_3O_x$. The current–voltage characteristics of $Au/YBa_2Cu_3O_x$ and $Nb/Au/YBa_2Cu_3O_x$ heterojunctions on $(1\,1\,20)YBa_2Cu_3O_x$ thin films with an inclined crystallographic *c* axis display an anomaly of the conductance at low voltages, the behavior of which is studied at various temperatures and magnetic fields. The experimental results are analyzed in the framework of a model for the appearance of bound states caused by multiple Andreev reflection in junctions containing a superconductor with $d_{x^2-y^2}$ symmetry of the superconducting order parameter. Studies of the noise characteristics of $Nb/Au/(1\,1\,20)YBa_2Cu_3O_x$ heterojunctions at $T=4.2$ K reveal the presence of thermal and shot components. However, enhancement of the shot noise due to multiple Andreev reflection is not observed in the experiment. © *2004 American Institute of Physics.*
[DOI: 10.1063/1.1789918]

1. INTRODUCTION

The results of various experiments indicate that in the majority of metal oxide superconductors a complex type of symmetry of the superconducting order parameter is realized, in which the $d_{x^2-y^2}$ component is dominant (*d*-superconductors).[1] Unlike superconductors with isotropic (having *s* symmetry) superconducting order parameters (*s*-superconductors), in *d*-superconductors the order parameter changes sign upon a 90° change in direction of the quasiparticle momentum in the *ab* plane. As a consequence, in Josephson junctions based on *d*-superconductors, when a transport current is flowing in the *ab* plane in a direction for which the magnitude of the superconducting order parameter equals zero, the shape of the current–phase relation (CPR) can differ from sinusoidal.[2] A nonsinusoidal CPR, containing components proportional to $\sin\varphi$ and $\sin 2\varphi$, has been observed in experiments[3] in symmetric 45° bicrystal Josephson junctions with a [001]-inclined bicrystal boundary.

A different situation is realized in d/s heterojunctions (the slash/denotes a potential barrier) for the direction perpendicular to the *ab* basal plane (along the crystallographic *c* axis). Because of the *d* symmetry of the order parameter, the superconducting current in such heterojunctions should be small (proportional to the second power of the boundary transparency $\overline{D^2}$) and should contain a $\sin 2\varphi$ component corresponding to the second harmonic of the CPR.[2] However, the experimentally observed[4–6] product of the critical current J_c times the normal resistance R_N of the Josephson junction depends weakly on the boundary transparency, but it decreases if an epitaxial film having twin boundaries is used instead of a single crystal.[5] The experimental data can be explained by assuming that in thin films both types of symmetry of the superconducting order parameter (*s* and *d*) are realized and that a change in sign of the *s* component (a change of its phase by π) occurs at a twin boundary, while the *d* component remains unchanged.[6] Studies of the CPR of $Pb/YBa_2Cu_3O_x$ junctions on *c*-oriented $YBa_2Cu_3O_x$ films (*c*-YBCO) from the appearance of fractional Shapiro steps under irradiation by millimeter waves have shown the absence of a second harmonic of the CPR.[5]

In tunnel junctions of a *d*-superconductor with a normal metal (N/d), with an *s*-superconductor (s/d), or with another *d*-superconductor (d/d') the change in sign of the superconducting order parameter of the *d*-superconductor for the incident and Andreev-reflected quasiparticle gives rise to an additional phase shift by π.[7] Such a process is realized, for example, in N/d junctions with a (110)-oriented *d*-superconductor. The sequence of specular and Andreev reflections of a quasiparticle in this case causes Andreev bound states to form at low energies on the (110) plane of a *d*-superconductor, localized near the interface[1)] at a distance of the order of the coherence length.[8] Low-energy Andreev bound states (LABSs) are manifested in the appearance of a conductance peak at zero bias (conductance anomaly) on the current–voltage (I–V) characteristic of an N/d junction.[9]

Tunneling spectroscopy of metal oxide superconductors, YBCO in particular, is difficult because of the short coherence length of the material (≈ 3 nm) and also the high sen-

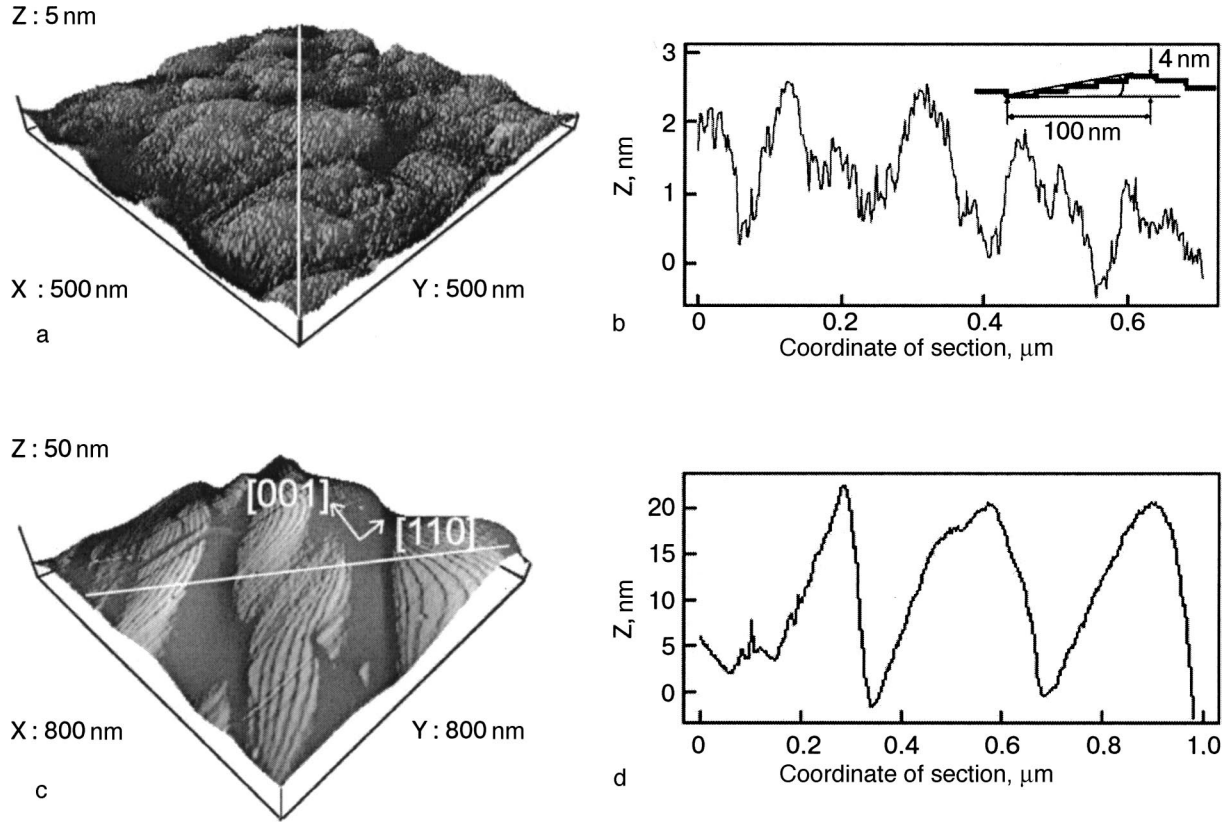

FIG. 1. Image of a portion of the surface, obtained with an atomic force microscope: *c*-oriented (*a*) and (1 1 20)-oriented (*c*) YBCO films. Profiles of the surface of the *c*-oriented (*b*) and (1 1 20)-oriented (*d*) YBCO films along the white lines in (*a*) and (*c*), respectively; the inset to panel *b* shows a schematic illustration of the structure of the surface of the *c*-oriented films.

sitivity to defects of the crystal lattice and to the presence of impurities. At the same time, as the experiment of Ref. 9 showed, the conductance anomaly has been observed in N/d and s/d heterojunctions, bicrystal junctions, end heterojunctions, and the point contacts of a scanning tunneling microscope. Therefore, of the two possible causes for the onset of the conductance anomaly, viz., the presence of magnetic impurities in the barrier[9] and LABSs in a *d*-superconductor,[8] a preference must be given to the latter. Theoretical studies have predicted the existence of LABSs on crystallographic planes of *d*-superconductors differing slightly from (110),[10] for example, on ''faceted'' surfaces,[11] and that prediction has been confirmed in experiments.[12] The experimentally observed splitting of the LABSs at high magnetic fields[12] was explained by a Doppler shift of the levels, caused by the flow of the screening current—the excitation of an imaginary *s* component of the superconducting order parameter in a surface layer of a *d*-superconductor.[12]

In this paper we review the results of experimental research on Au/YBCO and Nb/Au/YBCO heterojunctions based on *c*-oriented YBCO films on (001)$SrTiO_3$ substrates (*c* heterojunctions, *c*-HJs) and also single-domain films of (1 1 20)YBCO, which were prepared on specially oriented (7 10 2)$NdGaO_3$ substrates (inclined heterojunctions, IHJs).[13] We study the I–V characteristics of heterojunctions at low temperatures and low magnetic fields and also under irradiation by monochromatic millimeter-wave radiation. We analyze the current–phase relations of Nb/Au/YBCO heterojunctions of both types, obtained by the methods of rf superconducting quantum interference (SQUID)[14] and Shapiro steps.[15] We present the temperature dependence and magnetic-field dependence of the observed conductance anomaly on the I–V characteristic of the IHJ. In the Nb/Au/(1 1 20)YBCO IHJ at low temperatures we measured the noise characteristics and revealed the presence of thermal and shot components. The experimental results are discussed in the framework of a model for the onset of bound states due to Andreev reflection in superconductors with *d*-type symmetry of the superconducting order parameter.

2. PREPARATION OF THE HETEROJUNCTIONS AND THE MEASUREMENT TECHNIQUES

The *c*-oriented YBCO superconducting films were grown on (001)$SrTiO_3$ substrates. The *c* axis of the YBCO films grown on (7 10 2)NGO deviated from the normal to the plane of the substrate by an angle $\alpha \approx 11°$ of rotation in the (110)YBCO plane. As a result, the orientation of the YBCO film was close to (1 1 20)YBCO. YBCO epitaxial films 150 nm thick were laser deposited at a temperature of 770–790 °C in an oxygen atmosphere with a pressure of 0.6 mbar. The resulting YBCO films had a critical temperature $T_c = 85–90$ K and a critical current density $J_c \approx 2 \times 10^6$ and 5×10^4 A/cm^2 at 77 K for the *c*- and (1 1 20)-oriented YBCO films, respectively.[2)]

The morphology of our YBCO films was studied on an atomic force microscope. For the *c*-oriented YBCO films ($\alpha = 0$) the maximum surface roughness was 3–4 nm (Fig. 1*a*,*b*). With increasing angle α, growth steps appear on the surface, and at $\alpha = 11°$ [for (1 1 20)YBCO] their height is 20

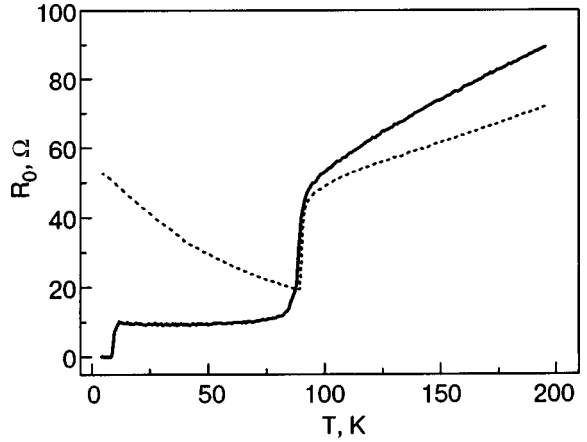

FIG. 2. Temperature dependence of the zero-bias resistance $R_0(T)$ for c-HJs Au/YBCO (dotted curve) and a Nb/Au/YBCO (solid curve) measured at a bias current of 1 μA.

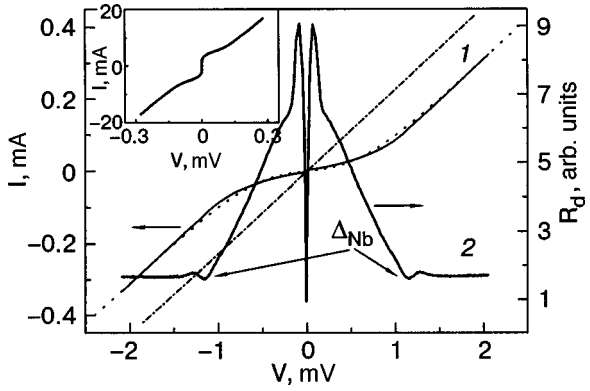

FIG. 3. I–V characteristic (*1*) and the voltage dependence of the differential resistance $R_d(V)$ of a Nb/Au/YBCO c-HJ at $T=4.2$ K (*2*). The dotted curve shows the dependence that follows from formula (1); the dot-and-dash line is Ohm's law $V=IR_N$. The inset shows the I–V characteristic in the range of voltages $V<0.3$ mV.

nm (Fig. 1*c*,*d*). The long and short sides of the growth steps are the (001) and (110) planes of YBCO, respectively. Therefore, in planar heterojunctions prepared on such YBCO films the total transport current is made up of the currents flowing through the contacts to the (001) and (110) crystallographic planes of YBCO. Because of the anisotropy of the conductivity of YBCO, a large part of the current flows through the (110)-oriented faces of the surface of the YBCO film.[16] We note that the surface roughness of (120)YBCO films on the (001)- and (110)-oriented faces is 1–2 lattice constants of the YBCO film.

For the formation of heterojunctions with areas A ranging from 5×5 to 30×30 μm we use the method of rf magnetron sputtering of Au and Nb, photolithography, and ion-beam etching in an argon atmosphere.[17] The eletrophysical parameters of the heterojunctions were measured in a four-point scheme in the fixed-current regime in the temperature range $T=4.2-300$ K, at magnetic fields up to 5 T, and under electromagnetic irradiation at frequencies of 40–100 GHz. The noise properties of the Nb/Au/(1 1 20)YBCO heterojunctions were investigated by two methods: direct measurement of the noise spectral density with a low-noise cooled amplifier working in the frequency range 1–2 GHz, and by the method of estimating the linewidth of the characteristic Josephson generation from the selective detector response to a weak external microwave signal.

3. HETEROJUNCTIONS ON *c*-ORIENTED YBCO FILMS AND THEIR PROPERTIES

3.1. Temperature dependence of the conductance of *c* heterojunctions

Figure 2 shows the temperature dependence of the resistance $R_0(T)$ at a low bias current (1 μA) for Au/YBCO and Nb/Au/YBCO c-HJs. At $T>T_c$ the resistance R_e of the YBCO leads is much larger than the resistance of the c-HJs, and therefore in this temperature region $R_0(T)$ characterizes the conductance of the leads in the ab basal plane of YBCO. It is seen in Fig. 2 that both curves correspond to a metallic type of conduction—the values of R_0 decrease with decreasing temperature. The value $T_c=84$ K of the YBCO leads for the Nb/Au/YBCO c-HJ is considerably lower than the analogous value $T_c=89.5$ K for the Au/YBCO c-HJ, probably because of the large number of technological operations in the fabrication of the Nb/Au/YBCO c-HJ and the resulting oxygen deficit in the surface layer of the YBCO film. At $T<T_c$ the behavior of $R_0(T)$ is fundamentally changed. For the Au/YBCO c-HJ at $T<T_c$ one observes the characteristic growth of R_0 for superconductor–insulator–normal metal tunnel junctions, while for the Nb/Au/YBCO c-HJ the resistance $R_0(T)\approx$const and remains unchanged down to the temperature of the transition of the niobium electrode to the superconducting state, $T_{cNb}\approx9.1$ K. Such behavior of $R(T)$ for the Nb/Au/YBCO c-HJ is apparently due to the presence in these c-HJs of a second interface, with a high transparency, between Nb and Au: in this regard the Au/Nb/YBCO c-HJ can be regarded as a highly asymmetric double-barrier structure $N/N'/s$, the conductance of which has a linear temperature dependence.[18]

3.2. I–V characteristics of Nb/Au/YBCO *c*-HJs

The I–V characteristics and the voltage dependence of the differential resistance $R_d(V)$ of the junction are shown in Fig. 3. The I–V characteristic of the c-HJ reveals the existence of a supercurrent with $J_c=1-10$ A/cm^2 and $I_cR_N=10-80$ μV in the c-HJ samples studied. Here R_N is the normal resistance of the junction, which is determined from the value of the differential resistance R_d of the junction at voltages $V\geqslant2$ mV. We also note that at $V>2$ mV the $R_d(V)$ curve is descending with increasing voltage, like that of the Au/YBCO c-HJ. The descending trend of $R_d(V)$ persists even at $V>\Delta_d=20$ mV, the value obtained in tunneling microscope experiments.[19]

At low voltages the I–V characteristic of the junction corresponds well to a resistive model of the Josephson junction, with low capacitance (see the inset in Fig. 3). When the voltage is increased to $V>2$ mV the I–V characteristic has the form $V=(I+I_e)R_N$, where $I_e<0$ is the excess current. $I_e>0$ is observed in superconducting junctions with direct (not tunneling) conduction.[20,21] Negative I_e (a current deficit) is typical of double-barrier superconducting heterostructures $s/N/s'$, in which with decreasing proximity effect in the N layer a change in sign of I_e is observed (a transition from a

current excess to a current deficit).[20] As we see in Fig. 3, the I–V characteristic of the junctions is well described by the relation typical for $s/N/s'$ structures:[22]

$$V = IR_N + I_e R_N \tanh(eV/kT). \quad (1)$$

From the experimentally measured I–V characteristic for this junction we have $I_e = -145$ μA at $T = 4.2$ K. According to Ref. 22, $I_e = (-\overline{D}\Delta_d - \Delta_{\rm Nb})/(eR_N) \approx -270$ μA, where $\Delta_{\rm Nb} = 1.2$ mV is the superconducting gap of Nb, and $\overline{D} \approx 7.6 \times 10^{-5}$ is the transparency, averaged over the area of the junction, of the Au/YBCO boundary, calculated according to the formula[20–22]

$$\overline{D} = 2\rho l/3r, \quad (2)$$

where $r = R_N A = 4.4 \times 10^{-6}$ $\Omega \cdot \text{cm}^2$ is the characteristic resistance of the contact ($R_N \equiv R_0(T_c)$), and $\rho = \rho_c \sim 5 \times 10^{-3}$ $\Omega \cdot$cm and $l = l_c \approx 1$ nm are, respectively, the resistivity and mean free path in the superconductor, the latter being equal to the distance between CuO_2 planes in the YBCO film (Ref. 16).[3)]

The $R_d(V)$ curve exhibits a feature in the form a local minimum at $V = 1.2$ mV, which coincides in value with $\Delta_{\rm Nb}$ and has a temperature dependence close to that given by BCS theory. This feature on the I–V characteristic vanishes together with the critical current at $T = 8.5$–9.1 K, and the temperature dependence of $I_c(T)$ is close to that of $\Delta_{\rm Nb}(T)$. We note that previously the gap structure of the *s*-superconductor Pb was observed in a Pb/YBCO *c*-HJ.[4]

To estimate the contribution to the measured resistance from the electron transport caused by the contact to the *ab* basal plane of the YBCO film, we used a parallel-resistor model for the resistances of the sharp boundaries between Au and YBCO along the *c* axis (r_c) and in the basal plane of YBCO (r_{ab}). Here r for the heterojunctions was determined from the condition

$$r = r_c r_{ab}/(r_{ab} + r_c \tan\gamma), \quad (3)$$

where $\tan\gamma \approx A_{ab}/A \approx 0.04$ and A_{ab} is the total area of the contacts to the *ab* plane of the YBCO film (see the inset to Fig. 1*b*). In Refs. 17 and 23 it was shown that for YBCO the experimentally observed values of r_c are an order of magnitude larger than r_{ab}. Consequently, for surface irregularities observed in experiment ($\gamma \approx 2°$), the contribution to the total current from the component of the contacts to the *ab* planes is small. This is confirmed by the absence of a conductance peak at low voltages—the conductance anomaly due to Andreev reflection in the *d*-superconductor—for the Nb/Au/YBCO junctions at $T > T_{c\rm Nb}$ (see also Sec. 4 of the present paper).[8] We recall that the theory predicts the appearance of such an anomaly for rough boundaries of N/d heterojunctions even in the case of an arbitrarily oriented *d*-superconductor.[11]

We note that superconducting shorts do not form in regions of possible punchthrough of the Au film (e.g., nonstoichiometric particles on the surface of the YBCO film). In particular, studies of Nb contacts to YBCO without the Au spacer layer on specially prepared samples revealed the absence of supercurrent and $r_c \sim 1$ $\Omega \cdot \text{cm}^2$, which is apparently a consequence of the active chemical interaction of Nb with oxygen from the YBCO film, with the formation of Nb_2O_5 and other oxides of Nb (see also Ref. 24).

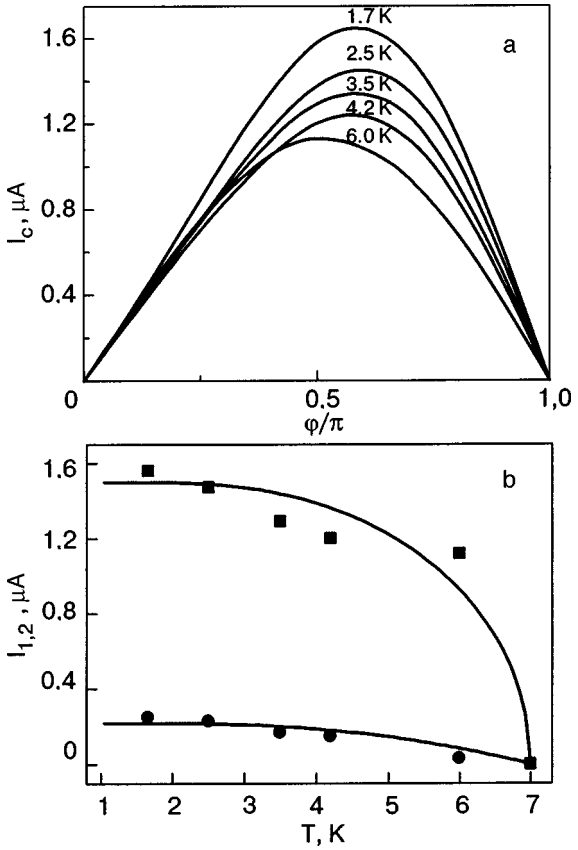

FIG. 4. Current–phase relation for a Nb/Au/YBCO *c*-HJ at temperatures of 1.7, 2.5, 3.5, 4.2, and 6.0 K (*a*). Temperature dependence of $I_1(T)$ (squares) and $I_2(T)$ (circles). The solid lines show the theoretical curves of $I_1(T)$ and $I_2(T)$ calculated according to formulas (6) and (7) (*b*).

3.3. Phase dependence of the supercurrent of a Nb/Au/YBCO *c*-HJ

For measurement of the dependence of the supercurrent on the phase different of the wave functions, $I_s(\varphi)$, we used a method in which a Nb/Au/YBCO *c*-HJ with dimensions of 10×10 μm was shorted by a ring of YBCO film with an inductance $L \approx 80$ pH and by another Nb/Au/YBCO *c*-HJ with a substantially larger area of 100×100 μm, forming a SQUID. The current–phase relation was calculated from the measurements of the amplitude–frequency characteristics of an rf resonator inductively coupled with this SQUID. This method is differential with respect to φ and gives high sensitivity in measurements of current–phase relations.[14]

In the temperature range $T = 1.7$–6.0 K in which the CPR was measured, the normalized critical current $\beta_L = 2\pi L I_c/\Phi_0$ ($\Phi_0 = 2.07 \times 10^{-15}$ Wb is the magnetic flux quantum) of the Nb/Au/YBCO *c*-HJ under study lay in the interval from 0.27 to 0.4, i.e., $\beta_L < 1$. Therefore the CPR could be determined for a whole period of variation of φ.[14] The CPR of a Nb/Au/YBCO *c*-HJ is shown in Fig. 4. It is seen that with decreasing temperature the shape of the current–phase relation begins to deviate from sinusoidal. A Fourier analysis of the measured CPR showed that its spectrum contains a finite number of first and second harmonics

and that the amplitudes of higher-order harmonics are small. Therefore, the superconducting component of the current can be written in the form

$$I_s(\varphi)=I_{c1}\sin\varphi+I_{c2}\sin(2\varphi+\varphi_0). \tag{4}$$

The experimentally observed sign of the I_{c2} term is always opposite to that of the I_{c1} term, i.e., $\varphi_0=\pi$. If $T\approx 1.7$ K, then $I_{c1}=1.57\ \mu$A, $I_{c2}=-0.25\ \mu$A, and $|I_{c2}/I_{c1}|\approx 0.16$. The temperature dependence of $I_{c1}(T)$ and $I_{c2}(T)$ is shown in Fig. 4*b*.[25]

After completion of the measurements of the CPRs the YBCO superconducting inductive ring of the SQUID was locally cut by a focused ion beam. In the resulting geometry we then measured the I–V characteristic and the $R_d(V)$ curve of the same Nb/Au/YBCO *c*-HJ for which the CPR had been measured. From the $R_d(V)$ curve we determined the value $R_N\approx 60\ \Omega$, which corresponds to $r_c=6\times10^{-5}\ \Omega\cdot\text{cm}^2$, and then, using Eq. (2), obtained the transparency of the given *c*-HJ: $\overline{D}\approx 5.6\times10^{-5}$.

The CPR of the *c*-HJ was also measured by a different method, based on measurement of the critical current and of the Shapiro steps on the I–V characteristic of a Nb/Au/YBCO *c*-HJ as functions of the amplitude of an external monochromatic electromagnetic wave irradiating the heterojunction.[15,26] Under external monochromatic electromagnetic irradiation at frequency $f_e\approx 40$ GHz Shapiro steps I_n corresponding to the fundamental frequency and a harmonic component appeared on the I–V characteristic at voltages of $n(hf/2e)$ (n is an integer). At a voltage of $\frac{1}{2}(hf/2e)$ ($n=1/2$) the first subharmonic Shapiro step was also observed, with an amplitude $I_{1/2}/I_c=0.08$ at $T=4.2$ K. Figure 5 shows I_c, I_1, and $I_{1/2}$ as functions of the amplitude of the rf current. The solid curves show the theoretical dependences $I_c(a)$, $I_1(a)$, and $I_{1/2}(a)$, where $a=I_{RF}/I_c$ is the experimental value of the normalized rf current, which was determined from a comparison of the experimental $I_1(a)$ curve with the theoretical one in respect to the first minimum of this quantity.[15] We note that for low amplitudes of the external radiation the first Shapiro step is symmetric with respect to the autonomous I–V characteristic, a circumstance that attests to the coherence of the Josephson generation in autonomous junctions.[26] Thus the subharmonic Shapiro steps observed on the experimental I–V characteristic may be indicative of a deviation of the dependence $I_s(\varphi)$ from sinusoidal. At $T=4.2$ K the ratios of the harmonics of the CPR determined by the rf SQUID method and also from the amplitudes of the Shapiro steps are $|I_{c2}/I_{c1}|\approx 0.12$ and $I_{1/2}/I_c=0.08$ for two *c*-HJs on one substrate.

The presence of the two harmonics $I_{c1}\propto\sin\varphi$ and $I_{c2}\propto\sin 2\varphi$ in the spectrum of the CPR of a Nb/Au/YBCO *c*-HJ can be explained by the existence of a combined $d+s$ symmetry of the superconducting order parameter in YBCO. For calculation of the supercurrent we use the expression[25]

$$I_s(\varphi)=\frac{2e}{\hbar}\sum_{k,\theta}k_BT\sum_{\omega}\times\frac{D(\theta)\Delta_R\Delta_k\sin\varphi}{2\Omega_R\Omega_k+D(\theta)(\omega^2+\Omega_R\Omega_k+\Delta_R\Delta_k\cos\varphi)}. \tag{5}$$

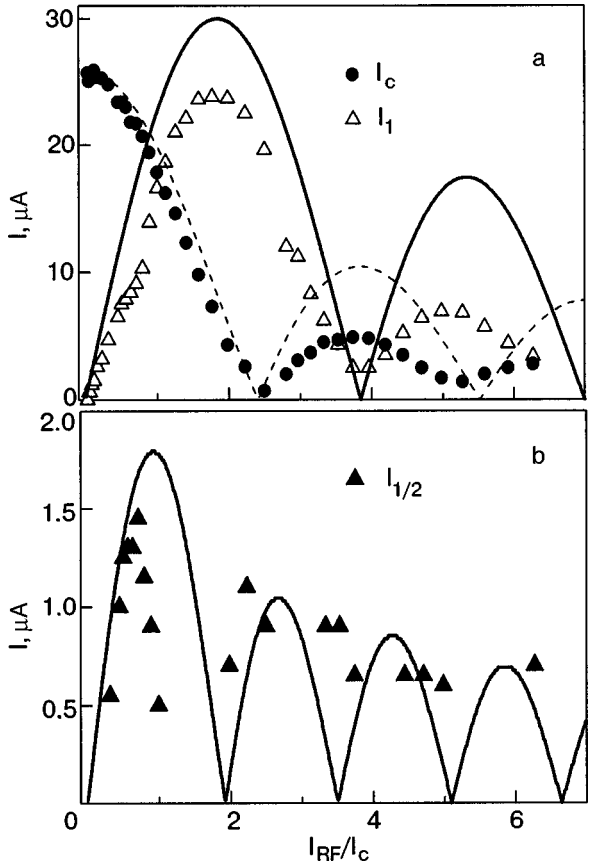

FIG. 5. Critical current I_c and the first Shapiro step I_1 (*a*) and the first subharmonic Shapiro step $I_{1/2}$ (*b*) on the experimental I–V characteristic of a Nb/Au/YBCO *c*-HJ as functions of the amplitude of 40-GHz electromagnetic radiation, normalized to I_c, at $T=4.2$ K. The solid and dashed curves show the corresponding dependences that follow from a resistive model of the Josephson junctions.

In formula (5) Δ_R and Δ_k denote the superconducting gaps of Nb and YBCO, respectively, and $\Omega_{R,k}=\sqrt{\omega^2+\Delta_{R,k}^2}$. Keeping in Eq. (5) terms up to second order in the small quantity $D(\theta)\ll 1$ inclusive, we obtain[25]

$$I_{c1}(T)R_N\approx\frac{\Delta_s}{\Delta_d^*}\frac{\Delta_R(T)}{e}, \tag{6}$$

$$I_{c2}(T)R_N\approx-\frac{\pi}{8}\overline{D}\frac{\Delta_R(T)}{e}\tanh\left(\frac{\Delta_R(T)}{2k_BT}\right), \tag{7}$$

where $\Delta_d^*=\pi\Delta_d[2\ln(3.56\Delta_d/k_BT_{cR})]^{-1}$. In deriving formulas (6) and (7) we have used an expression for the superconducting gap of YBCO of the form $\Delta(\theta)=\Delta_d\cos 2\theta+\Delta_s$, where Δ_d and Δ_s are the amplitude values of the *d* and *s* components of the superconducting order parameter of YBCO, where $\Delta_d\gg\Delta_s,\Delta_R$. There are differing estimates of the parameter Δ_s/Δ_d^* of YBCO in the literature. For example, in tunneling microscope experiments the values $\Delta_s\approx 1$ MeV and $\Delta_s/\Delta_d^*\approx 0.05$ were obtained,[19] while for a Pb/YBCO *c*-HJ a range $\Delta_s/\Delta_d^*\approx 0.3-1.1$ was found.[23]

An additional factor that influences the value of I_1 is the presence of twinning in the YBCO film. In this case the *s* component can enter the expression $\Delta(\theta)=\Delta_d\cos 2\theta+\Delta_s$ with a minus sign as well, which is a reflection of the change in sign of *s* on passage through a twin boundary in YBCO, although the sign of the *d* component remains unchanged

here.[6] Consequently, $I_{c1}=0$ in the limiting case of equal areas of the two twin domains. However, it has been shown[27] that the areas of the twinned domains can be different even when a YBCO thin film is deposited on a $SrTiO_3$ substrate, which has a cubic crystal lattice. Denoting the areas of two twin domains as $(1+\zeta)/2$ and $(1-\zeta)/2$, we find that the experimentally measured value $I_{c1}\propto\zeta$. Using the values $\Delta_s/\Delta_d^*\approx 0.3-1.1$ and $\Delta_R=1.2$ mV for $R_d(V)$ (see Fig. 3) and substituting the experimental value of I_{c1} into (6), we obtain $\zeta=0.07-0.21$, in qualitative agreement with the value $\zeta=0.14$ obtained for a YBCO film 100 nm thick.[25,27]

The maximum value $I_{c2}=-0.25$ μA for $T\approx 1.7$ K is obtained from (7) for $\overline{D}\approx 3.2\times 10^{-2}$, which strongly exceeds the value of the transparency $\overline{D}$ of the Au/YBCO barrier. This discrepancy can be explained by assuming that the transparency of the Nb/Au/YBCO c-HJ varies over the area of the junction. The transparency of a Nb/Au/YBCO c-HJ is determined by the transparency of the Au/YBCO boundary, the uniformity of which over the area of the c-HJ depends on the uniformity of the distribution of the oxygen content in the surface layer of the YBCO. The finite surface roughness of a YBCO film leads to local diffusion of oxygen from the coating contacts toward the ab planes of YBCO. This can lead to scatter in the values of ρ and l over the area of the junction, resulting in fluctuations of the value of the transparency of the Au/YBCO boundary.

It should be noted that the second harmonic of the CPR also arises in the model of $d+is$ type symmetry of the superconducting order parameter of YBCO, which was proposed in Ref. 28 ($i=\sqrt{-1}$). However, in the framework of that model a phase shift $\varphi_0=\pi/2$ between I_{c2} and I_{c1} should exist, in disagreement with the value $\varphi_0=\pi$ determined from experiment and also with the results of Ref. 6.

A possible alternative explanation of the experimentally observed CPR is the model proposed by Millis.[29] In that model one can represent the Nb/Au/YBCO c-HJ as a lattice of 0- and π-junctions connected in parallel, with a lattice constant equal to the characteristic size of a twin domain in a c-oriented YBCO film, 10 nm. Then, as was shown in Ref. 29, spontaneous currents arise in the ground state of a c-HJ, and the energy of the c-HJ is minimum for $\varphi=\pm\pi/2$. Estimates of the value of the amplitude of the second harmonic of the CPR (I_{c2m}) arising on account of this mechanism showed that $I_{c2m}/I_{c2}<0.03$.[25] Consequently, the contribution of this mechanism to the value of I_{c2} is small.

Another alternative cause for the appearance of the second harmonic in the CPR in Nb/Au/YBCO c-HJs may be the presence of the Nb/Au boundaries, which have high transparency ($\overline{D}_{\mathrm{Nb/Au}}\sim 10^{-1}$), which is reflected in the shape of the I–V characteristic (see Fig. 3). As we have said, a Nb/Au/YBCO c-HJ can be represented as a highly asymmetric double-barrier structure, in which the second harmonic of the CPR can appear.[18] On the other hand, simple estimates based on Eq. (9) of Ref. 18 show that in such a case $I_{c2}/I_{c1}\sim\overline{D}$, and consequently the amplitude of the second harmonic of the CPR is much smaller than that observed experimentally.

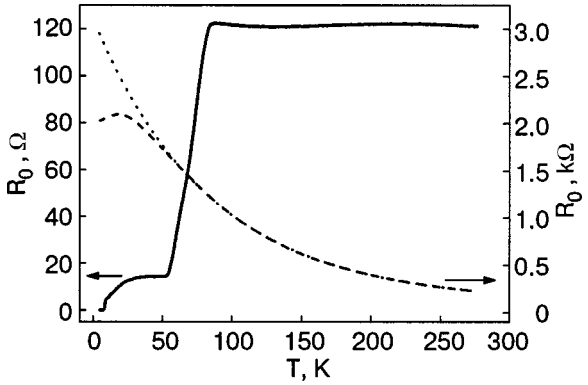

FIG. 6. Temperature dependence of the resistance R_0 of two types of inclined heterojunctions: Nb/Au/YBCO (solid curve) and Au/YBCO (dashed curve), measured at a bias current of 1 μA. The dotted curve shows the dependence $R[\mathrm{k}\Omega]=0.11+3\exp(-T[\mathrm{K}]/85)$, which is a good approximation for the experimental dependence of $R_0(T)$ of the Au/YBCO IHJ at $T>T_c=53$ K.

4. HETEROJUNCTIONS ON INCLINED FILMS (1 1 20)YBCO AND THEIR PROPERTIES

4.1. Temperature dependence of the resistance of inclined heterojunctions

Figure 6 shows the temperature dependence of the resistance R_0 measured at a current of 1 μA on inclined heterojunctions (IHJs) Au/YBCO (1 1 20) and Nb/Au/YBCO (1 1 20). It is seen that for $T\simeq 53$ K the resistance R_0 of the Au/YBCO IHJ increases exponentially with decreasing temperature, and for $T<53$ K a deviation of $R_0(T)$ from the exponential dependence is observed. In the case of the Au/YBCO IHJ one does not observe any significant change of R_0 at $T\approx T_c$, since the resistance R_N of the IHJ itself[4)] is substantially larger than the resistance of the YBCO(1 1 20) leads. This is the typical situation for Au/YBCO IHJs prepared by depositing the Au film on YBCO(1 1 20) *ex situ*. In this case the escape of oxygen atoms from the YBCO(1 1 20) surface layer decreases the transparency of the boundary. The characteristic boundary resistance r varied over wide limits, $10^{-2}-10^{-6}$ $\Omega\cdot\mathrm{cm}^2$, depending on the technique used to prepare theoretical IHJ. In particulate, for an IHJ for which the boundary between the Au and YBCO(1 1 20) was formed by depositing the Au film *ex situ*, r increased by 3–4 orders of magnitude as compared to IHJs for which the boundary between Au and YBCO(1 1 20) was formed *in situ*. Here one can speak of a decrease in $\overline{D}$ by the same factor by which r increases.

The behavior of $R_0(T)$ is completely different for $R_N \ll R_e$, which is the situation when the Au film has been deposited *in situ*. This is the case for the Nb/Au/YBCO IHJ whose $R_0(T)$ dependence is shown in Fig. 6. At $T\approx T_c=53$ K a sharp increase of R_0 is observed, due to the transition of the leads to the superconducting state. Upon further decrease of the temperature below T_c to $T_{c\mathrm{Nb}}\approx 9.2$ K the zero-bias resistance R_0 increases monotonically. The temperature at which $R_0(T)$ for the Au/YBCO IHJ deviates from the exponential dependence coincides with $T_c=53$ K.

In Au/YBCO and Nb/Au/YBCO IHJs the behavior of $R_0(T)$ for $T<T_c$ is due to the turning on of a current transport channel involving Andreev reflection as the temperature

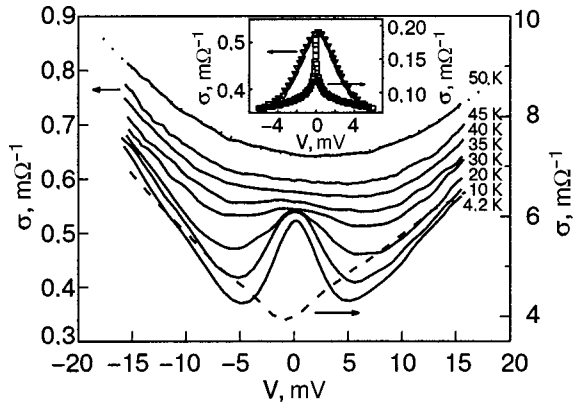

FIG. 7. Conductivity versus bias $\sigma(V)$ for an inclined Au/YBCO heterojunction at different temperatures (the solid curves from bottom to top): 4.2, 10, 20, 30, 35, 40, 45, and 50 K. The dotted curve shows the parabola approximating the dependence $\sigma(V)$ at $T=50$ K. The dashed curve corresponds to $\sigma(V)$ at $T=4.2$ K for the Au/YBCO *c*-HJ. The inset shows $\sigma(V)$ for IHJs Au/YBCO at $T=4.2$ K (inverted triangles) and Nb/Au/YBCO at $T=10$ K (squares) in the low-voltage region $|V|<6$ mV. The solid chamber is the approximation of $\sigma(V)$ for the Au/YBCO IHJ by a Lorentzian.

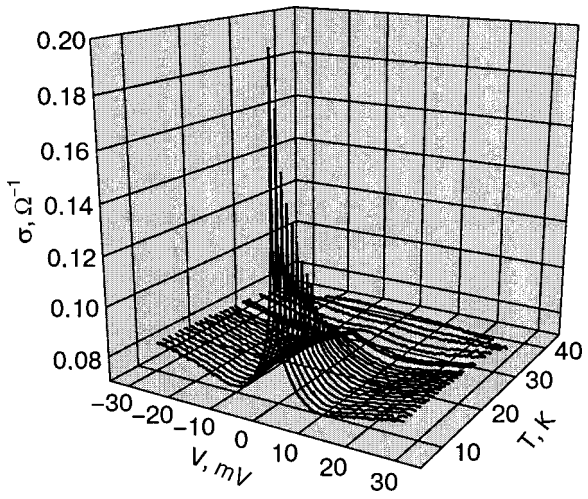

FIG. 8. $\sigma(V,T)$ for the Nb/Au/YBCO IHJ.

is lowered.[7] For IHJs on YBCO(1 1 20) films the influence of the LABSs should be manifested on the I–V characteristic in the form a conductance peak appearing at low voltages, i.e., the conductance anomaly that is observed experimentally.

4.2. Broadening of the Andreev states

Figure 7 shows the transformation of $\sigma(V)$ with decreasing temperature for a Au/YBCO IHJ. For $T>T_c$ the $\sigma(V)$ curve (the $T=50$ K curve in Fig. 7) can be approximated well by a parabola (the dashed curve in Fig. 7) in the framework of the tunneling theory of N/N' junctions with allowance for the influence of the voltage on the shape of the potential barrier.[30] For $T<T_c$ the $\sigma(V)$ curve at small V exhibits a deviation from the parabolic shape in the form of a conductance anomaly, increasing with decreasing T. The deviation of $R_0(T)$ for a Au/YBCO IHJ from the exponential growth corresponds to the onset of the conductance anomaly on the I–V characteristic. We note that the conductance anomaly is absent for the *c*-HJ Au/YBCO (dashed curve in Fig. 7).

Figure 8 shows $\sigma(V)$ for a Nb/Au/YBCO IHJ in the temperature region 9–40 K in which the conductance anomaly is most strongly expressed. We note that $\sigma(V)\approx$consts at $T=T_c$. This corresponds to the tunneling of quasiparticles through a delta-function-like barrier which is uniform over area, while for $T<T_c$ a conductance anomaly appears on the I–V characteristic of the Nb/Au/YBCO IHJ, just as for the Au/YBCO IHJ. For both types of IHJ one observes growth of the amplitude and a decrease of the half-width ΔV of the conductance anomaly as the temperature is lowered. Together with the thermal smearing of the conductance anomaly the LABS levels broaden on account of the finite lifetime of the states. For a quasiparticle with energy ε at $\varepsilon<\Delta_0$ (Δ_0 is the amplitude value of the energy gap $\Delta(\theta)=\Delta_0\cos 2\theta$ for the *d*-superconductor) one uses the following form of the density of states $N(\varepsilon,\theta)$:[8,12,31]

$$N(\varepsilon,\theta)=\frac{\pi^{-1}\Gamma^2(\theta)}{(\varepsilon-\varepsilon_b)^2+\Gamma(\theta)^2}, \tag{8}$$

where θ is the angle of incidence of the quasiparticle relative to the normal to the boundary, and ε_b describes the shift of the energy levels of the Andreev states, e.g., on account of the the flow of current along the N/d boundary. In formula (8) the level broadening is characterized by the parameter $\Gamma(\theta)\sim\hbar/\tau(\theta)$, where $\tau(\theta)$ is the lifetime of a quasiparticle in the LABS. In the general case $\Gamma(\theta)$ is determined by the tunneling of quasiparticles, $\Gamma_{\text{tunn}}(\theta)$, the diffusive scattering due to the rough surface of the YBCO film, $\Gamma_{\text{diff}}(\theta)$, umklapp processes of quasiparticle scattering with a change of the normal component of the momentum, $\Gamma_U(\theta)$, and scattering on lattice defects and impurities, Γ_{imp}:[31]

$$\Gamma(\theta)=\Gamma_{\text{tunn}}(\theta)+\Gamma_{\text{diff}}(\theta)+\Gamma_U(\theta)+\Gamma_{\text{imp}}. \tag{9}$$

If upon the formation of the LABSs the dominant contribution to their broadening comes from scattering on defects and impurities, Γ_{imp}, which is independent of the direction of the quasiparticle momentum, then, as follows from (8) and (9), the dependence of the conductance anomaly has the shape of a Lorentzian of width Γ. The inset in Fig. 7 shows the experimental dependence $\sigma(V)$ at low voltages ($V<6$ mV) for the Au/YBCO IHJ at $T=4.2$ K (inverted triangles) and the Nb/Au/YBCO IHJ at $T=10$ K (squares). The $\sigma(V)$ curve for the Au/YBCO IHJ is well approximated by a Lorentzian; consequently, it is scattering on defects and impurities that determines the half-width of the conductance anomaly in this case. It is also seen from the inset in Fig. 7 that the shape of $\sigma(V)$ for the Nb/Au/YBCO IHJ is not Lorentzian.

In the Au/YBCO IHJ the formation of the boundary was done with the vacuum broken (*ex situ*), and the (1 1 20)YBCO surface of the film was subjected to the atmosphere for about an hour prior to the deposition of Au. As a result of the interaction with the atmosphere, various impurities such as CO_2 and OH were precipitated on the surface of the YBCO film, and oxygen-deficient regions, which are lattice defects, also formed. The factors mentioned lead to the formation of a large number of scattering centers in the surface layer of the YBCO film and may give the governing contribution to the broadening of the conductance anomaly. The degree of diffuseness of the surface layer on the Au/YBCO boundary can be characterized with the aid of the parameter t/l, where t is the thickness of the disordered

layer.[2] Here $t/l=0$ corresponds to the ideal Au/YBCO (1 1 20) boundary, while $t/l=\infty$ corresponds to a completely diffuse boundary. Unfortunately, there are no data in Ref. 2 for the region $t/l>0.1$, which corresponds to the Au/YBCO IHJ under study here.

Among the LABS broadening mechanisms that depend on the direction of the momentum of the incident quasiparticles are tunneling, scattering on the YBCO surface roughness, and scattering with a change in direction of the quasiparticle momentum. With increasing transparency of the boundary the probability of escape of the quasiparticles by tunneling through the barrier increases, and that should lead to an increase of $\Gamma_{\text{tunn}}(\theta)$.[31,32] However, for the Nb/Au/YBCO IHJ the values of $\overline{D}$ are at least an order of magnitude larger than for the Au/YBCO IHJ, although ΔV at low temperatures is several times smaller for the Nb/Au/YBCO IHJ than for the Au/YBCO IHJ. For example, at $T=10$ K one has $\Delta V\approx 1$ mV for the Nb/Au/YBCO IHJ and 6.8 mV for the Au/YBCO IHJ. Thus ΔV in the IHJs falls off with increasing $\overline{D}$ and, hence, the tunneling of quasiparticles is not the governing factor for the broadening of the conductance anomaly.

The LABS broadening that leads to the non-Lorentzian shape of the conductance anomaly is apparently due to two processes: diffusive scattering due to the rough surface of the YBCO film, and umklapp processes of quasiparticle scattering with a change in the normal component of the momentum. The experimental study of the influence of each of these processes on the broadening of the conductance anomaly is difficult because of problems in determining the exact distribution of transparency over the area of the junction and over angles θ, and also of determining $\Gamma(\theta)$ for each process.

4.3. Magnetic-field dependence

When an N/d IHJ is placed in a perpendicular magnetic field a screening current arises in d, shifting the LABS levels (Doppler shift of the levels).[11] Analogously, spontaneous currents can also arise in the absence of external magnetic field if on the surface of d, e.g., when the temperature is lowered below a certain critical value T_s, a transition occurs to a mixed type of symmetry $d_{x^2-y^2}+is$ of the superconducting order parameter. In both cases this leads to splitting of the LABS levels. As a result, the peak of the conductance anomaly in an N/d IHJ is split into two peaks. In a perpendicular magnetic field H the LABS level splitting is[12]

$$\varepsilon_b=(e/c)v_F H\lambda_L \sin\theta, \tag{10}$$

where c is the speed of light in vacuum, v_F is the Fermi velocity in the ab plane of YBCO, and λ_L is the London penetration depth of the magnetic field in the c direction of YBCO. For studying a Au/YBCO IHJ in magnetic fields up to 5 T perpendicular to the plane of the substrate (making an angle of approximately 79° with the ab plane of YBCO), after subtraction of the analogous dependence for $H=0$ the presence of splitting of the conductance anomaly becomes obvious (Fig. 9). The inset in Fig. 9 shows the dependence of the splitting of the conductance anomaly on the value of the magnetic field, $\delta(H)$, in a Au/YBCO IHJ at $T=4.2$ K. In the high magnetic field region ($H>2$ T) the splitting $\delta(H)$ is practically constant and can be approximated well by the dependence $\delta(H)$ obtained in the framework of a Doppler shift model for the LABS levels owing to the generation of an additional s component of the superconducting order parameter at $T<T_s(\text{YBCO})\approx 7$ K (the solid curve in the inset of Fig. 9).[11,32] In this case the conductance anomaly should also be split at zero magnetic field, which has not been observed in experiment, even though the condition $T<T_s$ is met. It has been shown[32] that the splitting in zero magnetic field vanishes when the doping level of the d-superconductor goes from overdoping to underdoping. Apparently it is the underdoping by carriers due to the oxygen deficit that is realized in the YBCO films, as is indirectly confirmed by the low transition temperature to the superconducting state ($T_c=53$ K). In the low-magnetic-field region ($H<1$ T) the experimental data are insufficient for making a comparison of experiment with the theory.[11]

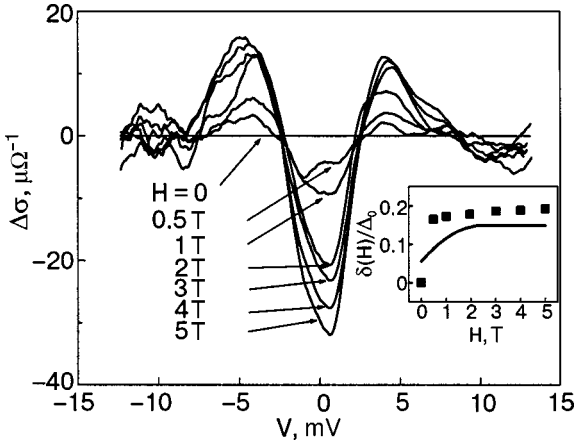

FIG. 9. $\Delta\sigma(V,H)=\sigma(V,H)-\sigma(V,0)$ at $T=4.2$ K for a Au/YBCO IHJ at various values, from 0 to 5 T, of the magnetic field applied perpendicular to the plane of the substrate. The curve for $H=0$ corresponds to a straight line passing through zero. In the inset the squares show the dependence of the splitting, calculated as half the distance between maxima of $\Delta\sigma(V,H)$ and normalized to $\Delta_0=20$ MeV, on the magnetic field strength. The solid curve corresponds to a calculation in a model in which an additional s component of the order parameter in YBCO is generated at temperatures below $T_s<7$ K, wherein $\Delta_{s-\text{YBCO}}=1.2$ meV, $\Delta_0=20$ MeV, $H_0=16$ T, and $H_c=1$ T.[12]

4.4. Influence of Andreev states on the supercurrent

The dependence of the energy of Andreev bound states on the phase difference φ of the superconducting order parameter of the electrodes forming the Josephson junction determines the supercurrent that flows through the Andreev bound states (see, e.g., Ref. 33):

$$I_s(\varphi)\propto \sum_{-\pi/2}^{\pi/2} \cos\theta_n \frac{dE_n(\theta,\varphi)}{d\varphi} f(E_n(\theta))\,d\theta, \tag{11}$$

where the summation over n goes over all the Andreev states with energies E_n, and $f(\varepsilon)$ is the Fermi distribution function. We note that for tunnel junctions made from s-superconductors ($\overline{D}\ll 1$) the energies of the Andreev states lie near the gap. For the Andreev states of a contact between an s-superconductor (Δ_R) with the (110) plane of a d-superconductor ($s/d_{(110)}$) there are also LABS levels for $\varepsilon\ll\Delta_d$:[8,33]

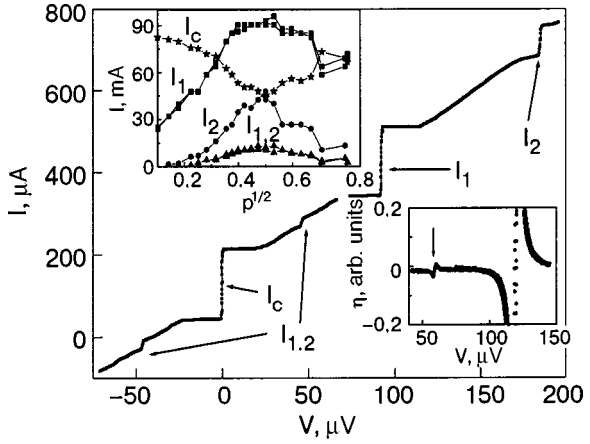

FIG. 10. I–V characteristic of a Nb/Au/YBCO IHJ of area 30×30 μm under irradiation by microwave radiation with a frequency of 46.4 GHz at $T=4.2$ K. The upper inset shows the critical current I_c and the first I_1 and second I_2 Shapiro steps as functions of the amplitude of the microwave radiation. The lower inset shows the selective detector response $\eta(V)$ obtained during irradiation by a low-power signal at $f=55.7$ GHz. The arrow indicates the subharmonic response.

$$E_n=\Delta_R\Delta_d\overline{D}\sin\varphi/[2\Delta_R+\overline{D}(\Delta_d-\Delta_R)]+O(\overline{D}^2). \quad (12)$$

It was shown in Ref. 33 that in $d/d_{(110)}$ junctions at low temperatures ($kT\ll\overline{D}\Delta_d/4\sqrt{2}$), just as in s/s junctions $I_c\propto\overline{D}$ and $I_cR_N\sim\pi\Delta_1/e$, but $I_s(\varphi)$ differs strongly from sinusoidal, $I_s(\varphi)\sim\cos\varphi$ $(0<\varphi<\pi)$ (case *a*). At higher temperatures ($\overline{D}\Delta_d/4\sqrt{2}\leqslant kT\leqslant\Delta_d/2$)$I_c\propto\overline{D}^2$, $I_cR_N\sim(\pi\Delta_d\overline{D}/4e)(\Delta_d/2kT-1)$ and $I_s(\varphi)\sim\sin2\varphi$ (case *b*). On the other hand, if $\Delta_d/2\leqslant kT\leqslant kT_c$, then $I_cR_N\approx0$.[33] Since $\overline{D}\sim10^{-4}-10^{-5}$ in the Nb/Au/YBCO iHJs studied here, we have $\overline{D}\Delta_d/4\sqrt{2}<0.01$ K, and at $T=4.2$ K case *b* is realized. For example, for a Nb/Au/YBCO IHJ with $\overline{D}\sim2.5\times10^{-5}$ one calculates $I_cR_N\approx10$ μV, which agrees in order of magnitude with the value observed in experiment. The $I_c(T)$ curve measured experimentally for the Nb/Au/YBCO IHJs falls off monotonically with increasing temperature. The nonmonotonicity of $I_c(T)$ predicted in Ref. 33 is not observed. At the same time, tunneling experiments in s/d *c*-HJs have revealed the presence of an additional *s* component of the superconducting order parameter of YBCO, with an energy gap $\Delta_{s-\mathrm{YBCO}}$. In that case the temperature dependence of the supercurrent, determined from formula (6) with allowance for the fact that, owing to the high transparency of the Nb/Au boundary and the proximity effect in the Au spacer layer, an order parameter with a critical temperature $T_c'\leqslant T_{c\mathrm{Nb}}$ can be manifested, in qualitative agreement with the experimental observations on Nb/Au/YBCO IHJs.

4.5. Phase dependence of the supercurrent of inclined Nb/Au/YBCO heterojunctions

Figure 10 shows the I–V characteristic of a 30×30 μm Nb/Au/YBCO IHJ under irradiation by monochromatic electromagnetic radiation with a frequency $f_e\approx46.4$ GHz. The I–V characteristic shows the critical current I_c, harmonic Shapiro steps I_1 and I_2, and also the first subharmonic step, with $I_{1/2}/I_1\approx0.1$ at 4.2 K.[5)] The upper inset in Fig. 10 shows the dependence of I_c, I_1, and I_2 on the normalized amplitude of the rf current for an IHJ of area 30×30 μm. The amplitudes of I_c, I_1, and I_2 oscillation with increasing amplitude of the external influence; this corresponds to a resistive model of Josephson junctions.[15] The subharmonic Shapiro steps observed experimentally on the I–V characteristic of both *c*-HJ and IHJ Nb/Au/YBCO at $V=\frac{1}{2}(hf/2e)$ are indicative of a deviation of the CPR from sinusoidal form. It should be noted that the high-amplitude irradiation of the heterojunctions under study from an external microwave source can alter the quasiparticle Fermi distribution function that appears in formula (11) for the phase dependence of the supercurrent.[34] We therefore made measurements of the selective detector response at a low amplitude of the external microwave signal relative to the value of the critical current of the Josephson junction under study, $I_{RF}\ll I_c$.

The lower inset in Fig. 10 shows the selective detector response $\eta(V)$ obtained under the influence of a low-power signal $I_{RF}\ll I_c$ with $f=55.7$ GHz. The arrow on the $\eta(V)$ curve indicates the feature at voltage $V=\frac{1}{2}(hf/2e)$, corresponding to the first subharmonic Shapiro step, the appearance of which in the given case cannot be explained by the onset of a nonequilibrium energy distribution function for the quasiparticles. For a Nb/Au/YBCO IHJ with $A=10\times10$ μm and $I_c<3$ μA we were unable to observe subharmonic Shapiro steps on the I–V characteristic, probably because of their small amplitudes.

4.6. Noise properties of inclined Nb/Au/YBCO heterojunctions

The noise properties of Nb/Au/YBCO IHJs were studied by two methods: direct measurement of the noise spectral density by a low-noise cooled amplifier working in the frequency range 1–2 GHz, and by the method of estimating the linewidth of the characteristic Josephson generation from the selective detector response to a weak external microwave signal. The I–V characteristic and the dependence of the noise power on the bias current for a Nb/Au/YBCO IHJ of area 10×10 μm are shown in Fig. 11*a*. Unlike the case of d/d contacts,[35] there is no increase in the noise on the resistive part at low values of the bias current. We note that the drop in the noise power upon the transition of the IHJ from the superconducting to the resistive state is caused by a change in the output impedance of the sample relative to the 50-Ω input impedance of the amplifier. Upon a significant increase in the bias voltage a growth of the noise spectral density $S(V)$ at the contact is observed; see Fig. 11*b*. The inset to Fig. 11*b* shows the part of the $S(V)$ curve for $|V|<9$ mV in greater detail. The dependence found is explained by growth of the shot-noise intensity $S_I=2eI$ as the current I_c through the heterojunction increases. We note that qualitatively similar $S(V)$ curves have been obtained previously[35] for d/d superconducting Josephson junctions with an averaged boundary transparency $\overline{D}\sim0.01$. The question of noise has been studied theoretically[36–38] for s/d junctions with relatively high transparency, $\overline{D}>0.1$, quite unlike the Nb/Au/YBCO IHJs studied experimentally, for which $\overline{D}\sim10^{-5}$.

It follows from Refs. 36–38 that suppression of the ex-

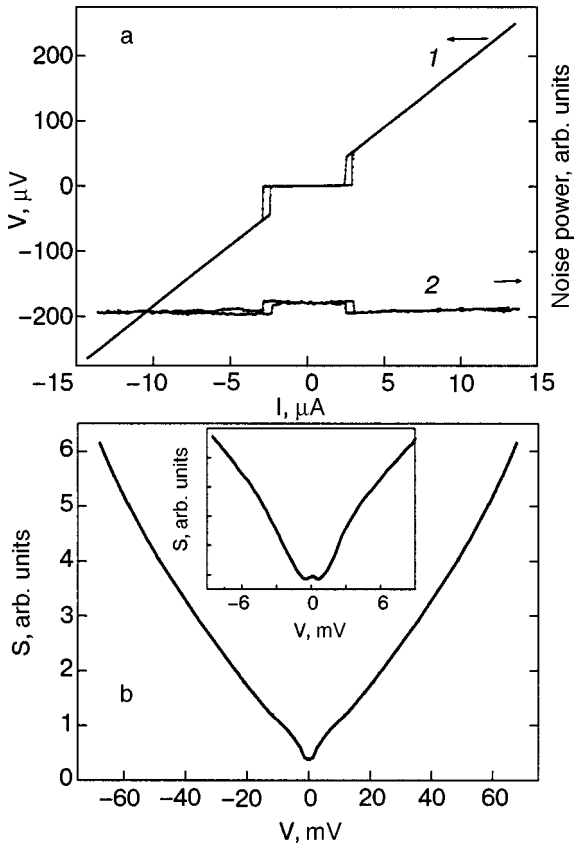

FIG. 11. I–V characteristic (*1*) and the dependence of the noise power on the bias current (*2*) for a Nb/Au/YBCO IHJ, obtained with the use of a low-noise cooled amplifier at $T=4.2$ K (*a*); dependence of the noise spectral density $S(V)$ on the voltage at $V\geqslant 50$ mV; the inset shows the part of $S(V)$ for $V<9$ mV (*b*).

cess shot noise occurs as the transparency decreases at low bias voltages for Josephson junctions with a *d*-superconductor as one or both electrodes. Most likely the absence of excess shot noise at low voltages $|V|<1$ mV in Nb/Au/YBCO IHJs can be explained by a decrease in the probability of Andreev reflection. The absence of excess noise is also shown by a second method of estimating the characteristic noise temperature of a heterojunction, which in the framework of the resistive model of Josephson junctions should be close to the physical temperature of the sample. An estimate of the linewidth Δf of the characteristic Josephson generation of a Nb/Au/YBCO IHJ based on the dependence $\eta(V)$ (the lower inset in Fig. 10) gives a value $\Delta f=4.4$ GHz, which is only 30% higher than the theoretical estimate made from the resistive model of Josephson junctions with only the contribution of the thermal fluctuations to the line broadening of the characteristic Josephson generation taken into accout. This fact again confirms the absence of excess noise in the Nb/Au/YBCO IHJs at low bias voltages.

CONCLUSION

We have investigated experimentally the superconducting and quasiparticle electron transport in thin-film HTSC heterojunctions Au/YBCO and Nb/Au/YBCO on the basis of *c*- and (1 1 20)-oriented YBCO films on (001)$SrTiO_3$ and (7 10 2)$NdGaO_3$ substrates, respectively. Studies of the dependence of the supercurrent on the phase difference of the superconducting electrodes revealed a deviation from sinusoidal form for both types of Nb/Au/YBCO heterojunctions.

A conductance peak on the I–V characteristics of the Au/(1 1 20)YBCO and Nb/Au/(1 1 20)YBCO at low voltages was found and investigated; this is the conductance anomaly due to multiple Andreev reflection in the junctions from superconductors with a $d_{x^2-y^2}$ type of order-parameter symmetry. The Lorentzian shape and the $\propto 1/T$ temperature dependence of the amplitude of the conductance anomaly in Au/YBCO heterojunctions indicate that its broadening is due to quasiparticle scattering on impurities and lattice defects, which is independent of the direction of the quasiparticle momentum, in the YBCO near the boundary. We have investigated the shot and thermal noise in Nb/Au/(1 1 20)YBCO heterojunctions, but we observed no excess noise due to the effect of Andreev reflection.

*E-mail: gena@hitech.cplire.ru

[1)] In the presence of the order-parameter suppression near the boundary in N/d junctions, bound states can also form at finite energies.[8]

[2)] X-ray diffraction experiments on (1 1 20)YBCO films have shown that such films are single-domain and have a single twin complex,[13] unlike, for example, YBCO films on (110)$SrTiO_3$ and (120)NGO substrates.[12]

[3)] Formula (2) is valid in the case of a spherical Fermi surface of the materials in contact. We note that even in the absence of an insulating layer the transparency $D\ll 1$ for the case of a large mismatch of the Fermi velocities of the metals in contact.

[4)] For the Nb/Au/YBCO IHJ one has $R_N\equiv R_0(T_c)$, while for the Au/YBCO IHJ the value of R_N was determined from the I–V characteristic as the maximum value of the resistance at 4.2 K. The low values of T_c for the Nb/Au/YBCO IHJ ($T_c\approx 53$ K) are apparently due to the escape of oxygen from the open *ab* planes of the YBCO(1 1 20) films during preparation of the samples.

[5)] We note that, as in the case of the Nb/Au/YBCO *c*-HJ, at low amplitudes of the external influence the first Shapiro step is symmetric with respect to the autonomous I–V characteristic; this attests to the coherence of the Josephson generation in autonomous junctions.[26]

[1] C. C. Tsuei and J. R. Kirtley, Rev. Mod. Phys. **72**, 969 (2000).
[2] Y. Tanaka, Phys. Rev. Lett. **72**, 3871 (1994); Y. Tanaka and S. Kashiwaya, Phys. Rev. B **53**, R11957 (1996); Yu. S. Barash, A. A. Svidzinsky, and H. Burkhardt, *ibid.* **55**, 15282 (1997).
[3] E. Il'ichev, V. Zakosarenko, R. P. J. Ijsselsteijn, V. Schultze, H.-G. Meyer, H. E. Hoenig, H. Hilgenkamp, and J. Mannhart, Phys. Rev. Lett. **81**, 894 (1998).
[4] H. Akoh, C. Camerlingo, and S. Takada, Appl. Phys. Lett. **56**, 1487 (1990); A. G. Sun, D. A. Gajewski, M. B. Maple, and R. C. Dynes, Phys. Rev. Lett. **72**, 2267 (1994); A. S. Katz, A. G. Sun, K. Char, and R. C. Dynes, Appl. Phys. Lett. **66**, 105 (1995).
[5] R. Kleiner, A. S. Katz, A. G. Sun, R. Summer, D. A. Gajewski, S. H. Han, S. I. Woods, E. Dantsker, B. Chen, K. Char, M. B. Maple, R. C. Dynes, and John Clarke, Phys. Rev. Lett. **76**, 2161 (1996).
[6] K. A. Kouznetsov, A. G. Sun, B. Chen, A. S. Katz, S. R. Bahcall, John Clarke, R. C. Dynes, D. A. Gajewski, S. H. Han, M. B. Maple, J. Giapintzakis, J.-T. Kim, and D. M. Ginsberg, Phys. Rev. Lett. **79**, 3050 (1997).
[7] A. F. Andreev, Zh. Éksp. Teor. Fiz. **46**, 1823 (1964) [Sov. Phys. JETP **19**, 1228 (1964)]; Zh. Éksp. Teor. Fiz. **49**, 655 (1965) [Sov. Phys. JETP **22**, 455 (1966)].
[8] T. Löfwander, V. S. Shumeiko, and G. Wendin, Semicond. Sci. Technol. **14**, R53 (2001).
[9] J. Lesueur, L. H. Greene, W. L. Feldmann, and A. Inam, Physica C **191**, 325 (1992).
[10] Yu. S. Barash, A. A. Svidzinsky, and H. Burkhardt, Phys. Rev. B **55**, 15282 (1997).
[11] M. Fogelström, D. Rainer, and J. A. Sauls, Phys. Rev. Lett. **79**, 281 (1997).
[12] M. Aprili, E. Badica, and L. H. Greene, Phys. Rev. Lett. **83**, 4630 (1999); R. Krupke and G. Deutscher, *ibid.* **83**, 4634 (1999); J. Lesueur, X. Grison, M. Aprili, and T. Kontos, J. Low Temp. Phys. **117**, 539 (1999).

[13] I. K. Bdikin, P. B. Mozhaev, G. A. Ovsyannikov, F. V. Komissinskiĭ, I. M. Kotelyanskiĭ, and E. I. Raksha, Fiz. Tverd. Tela (St. Petersburg) **43**, 1548 (2001) [Phys. Solid State **43**, 1161 (2001)].
[14] E. Il'ichev, V. Zakosarenko, L. Fritzsch, R. Stolz, H. E. Hoenig, H.-G. Meyer, M. Gotz, A. B. Zorin, V. V. Khanin, A. B. Pavolotsky, and J. Niemeyer, Rev. Sci. Instrum. **72**, 1882 (2001).
[15] K. K. Likharev and B. T. Ulrich, *Systems with Josephson Junctions: Basic Theory* [in Russian], MGU, Moscow (1978).
[16] M. Yu. Kupriyanov and K. K. Likharev, IEEE Trans. Magn. **MAG-27**, 2460 (1991).
[17] F. V. Komissinskiĭ, G. A. Ovsyannikov, Yu. V. Kislinskiĭ, I. M. Kotelyanskiĭ, and Z. G. Ivanov, Zh. Éksp. Teor. Fiz. **122**, 1247 (2002) [JETP **95**, 1074 (2002)].
[18] M. Yu. Kupriyanov, A. Brinkman, A. A. Golubov, M. Siegel, and H. Rogalla, Physica C **326–327**, 16 (1999).
[19] J. Y. T. Wei, N.-C. Yeh, D. F. Garrigus, and M. Strasik, Phys. Rev. Lett. **81**, 2542 (1998).
[20] V. Zaĭtsev, Zh. Éksp. Teor. Fiz. **86**, 1742 (1984) [Sov. Phys. JETP **59**, 1015 (1984)].
[21] M. Yu. Kuprianov and V. F. Lukichev, Zh. Éksp. Teor. Fiz. **94**(6), 139 (1988) [Sov. Phys. JETP **67**, 1164 (1988)].
[22] A. V. Zaĭtsev, JETP Lett. **51**, 41 (1990); A. F. Volkov, A. V. Zaitsev, and T. M Klapwijk, Physica C **210**, 21 (1993).
[23] G. Sun, A. Truscott, A. S. Katz, R. C. Dynes, B. W. Veal, and C. Gu, Phys. Rev. B **54**, 6734 (1996).
[24] H. J. H. Smilde, H. Hilgenkamp, G. J. Gerritsma, D. H. A. Blank, and H. Rogalla, IEEE Trans. Appl. Supercond. **11(2)**, 501 (2001).
[25] F. V. Komissinskiĭ, G. A. Ovsyannikov, E. Il'ichev, and Z. Ivanov, JETP Lett. **73**, 361 (2001); P. V. Komissinski, E. Il'ichev, G. A. Ovsyannikov, S. A. Kovtonyuk, M. Grajcar, R. Hlubina, Z. Ivanov, Y. Tanaka, N. Yoshida, and S. Kashiwaya, Europhys. Lett. **57**, 585 (2002).
[26] V. N Gubankov, V. P. Koshelets, and G. A. Ovsyannikov, Zh. Éksp. Teor. Fiz. **71**, 348 (1976) [Sov. Phys. JETP **44**, 181 (1976)].
[27] N. Didier, C. Dubourdieu, A. Rosova, B. Chenevier, V. Galindo, and O. Thomas, J. Alloys Compd. **251**, 322 (1997).
[28] M. Sigrist, K. Kuboki, P. A. Lee, A. J. Millis, and T. M. Rice, Phys. Rev. B **53**, 2835 (1996); R. Haslinger and R. Joynt, J. Phys.: Condens. Matter **12**, 8179 (2000).
[29] J. Millis, Phys. Rev. B **49**, 15408 (1994).
[30] J. G. Simmons, J. Appl. Phys. **34**, 1793 (1963).
[31] M. B. Walker and P. Pairor, Phys. Rev. B **60**, 10395 (1999); **59**, 1421 (1999); M. B. Walker and P. Pairor, Physica C **341–348**, 1523 (2000).
[32] G. Deutscher, Y. Dagan, A. Kohen, and R. Krupke, Physica C **341–348**, 1629 (2000); Y. Dagan and G. Deutscher, Phys. Rev. Lett. **87**, 177004 (2001).
[33] R. A. Riedel and P. F. Bagwell, Phys. Rev. B **57**, 6084 (1998).
[34] A. A. Golubov, M. Yu. Kupriyanov, and E. Il'ichev, Rev. Mod. Phys. **76**, 411 (2004).
[35] K. Y. Constantinian, G. A. Ovsyannikov, I. V. Borisenko, J. Mygind, and N. F. Pedersen, Physica C **367**, 276 (2002).
[36] Y. Tanaka, T. Asai, N. Yoshida, J. Inoue, and S. Kashiwaya, Phys. Rev. B **61**, R11902 (2000).
[37] T. Löfwander, V. S. Shumeiko, and G. Wendin, Physica C **377**, 86 (2002).
[38] J. C. Cuevas and M. Fogelström, Phys. Rev. B **64**, 104502 (2001); Phys. Rev. Lett. **89**, 227003 (2002).

Translated by Steve Torstveit

On the nonmonotonic temperature dependence of the magnetization of YBCO single crystals at low fields

V. P. Timofeev

B. Verkin Institute for Low Temperature Physics and Engineering of the National Academy of Sciences of Ukraine, 47 Lenin Ave., Kharkov 61103, Ukraine

A. V. Bondarenko*

V. N. Karazin Kharkov National University, 4 Svoboda Sq., Kharkov 61077, Ukraine

(Submitted March 11, 2004)
Fiz. Nizk. Temp. **30**, 810–813 (July–August 2004)

The results of experiments on the low-field dc magnetic response of $YBa_2Cu_3O_{7-x}$ single crystals having unidirectional twinning planes are presented. The nonmonotonicity observed in the temperature dependence of the magnetization of the samples is interpreted in the framework of a possible model for the existence of a system of Josephson weak links on the twinning planes and of anisotropy of the order parameter. © *2004 American Institute of Physics.*
[DOI: 10.1063/1.1789919]

Research on high-T_c superconductors (HTSCs) by magnetometric methods is topical both from the standpoint of understanding the nature of the formation of high-temperature superconductivity and for applied purposes. An advantage of such methods is their unique sensitivity in studies using SQUID magnetometry and the absence of contacts, which could alter the structure of the object near the surface. Despite numerous theoretical and experimental studies of metaloxide HTSCs,[1,2] a number of questions remain to be clarified, for example, in connection with the magnetic flux dynamics and the appearance of spontaneous currents in weak magnetic fields and at temperatures close to the critical point in the presence of various structural inhomogeneities.[3] In the design of rf SQUIDs and their input antenna elements (flux transformers) the solubility to these problems is urgently needed in order to reduce the inherent magnetic noise of sensors and to improve the sensitivity of equipment cooled at the nitrogen level.

Here we report the results of observations of nonmonotonic temperature dependence of the magnetization of YBCO single crystals at very low magnetic fields (0.01–0.2 Oe), possibly caused by a thermally activated transformation of a system of Josephson weak links on unidirectional twins in the region near the superconducting phase transition. As the object of study we chose impurity-free oriented single crystals of $YBa_2Cu_3O_{7-x}$ grown by flux-melt technology at a low longitudinal temperature gradient.[4] After annealing in an oxygen flow the single crystals had a superconducting transition temperature T_c of 93 K, which was measured by a resistive method at ''zero'' magnetic field, and the width of the superconducting transition was 0.3 K, which attests to the high quality of the samples. The annealing necessary for optimal doping in an oxygen flow at 400 °C leads to a transformation of the tetragonal structure of the crystals to orthorhombic and, as a consequence, to the formation of twinning planes. To study the influence of these planar defects on pinning processes we chose single crystals of $YBa_2Cu_3O_{7-x}$ with dimensions close to $1\times1\times0.02$ mm, having unidirectional twin boundaries oriented parallel to the c axis of the crystal.

The low-field measurements of the temperature dependence of the magnetization of $YBa_2Cu_3O_{7-x}$ near the phase transition temperature were made using a magnetic susceptibility meter based on a SQUID gradientometer (of the dB_z/dZ type) with cooling at the helium level. A standard technique of dc magnetization measurement by registering the response of an rf SQUID to motion of a sample along the axis of its antenna in the uniform magnetic field of a solenoid.[5] The residual level of Earth's magnetic field in the region of the experimental chamber was reduced to 0.5 mOe or less by the use of multilevel Permalloy shielding. Additional compensation of the residual field could be achieved with the use of an auxiliary solenoid. This permitted cooling of the sample and bringing it to the superconducting state in the zero-field cooling (ZFC) regime.

Figure 1 shows the typical temperature dependence of the output voltage of the susceptibility meter as the temperature of one of the samples was increased in the region around the superconducting phase transition. The coefficient of conversion of magnetic moment into the voltage response of the experimental apparatus was $k=5\times10^{-10}$ A·m^2/V in the working sensitivity range $\pm10\ \Phi_0$, where Φ_0 is the magnetic flux quantum. The magnetic field of the solenoid had a magnitude equal to 15.5 A/m ($\approx$0.2 Oe) and was directed along the c axis of the single crystal. In this orientation the magnetic field is parallel to the twinning planes, and the most effective pinning of Abrikosov vortices is achieved. To a high degree of accuracy similar curves were obtained for a number of YBCO single crystals with the optimum doping level. As can be seen in Fig. 1, the curve of the superconducting phase transition, unlike the data from resistive measurements on YBCO single crystals,[4] is nonmonotonic and occupies a significant temperature interval ($\Delta T=3-5$ K). The curves exhibited a smoothed step that cannot be explained by melting of a vortex lattice[1] at the low values of magnetic field used in the experiment.

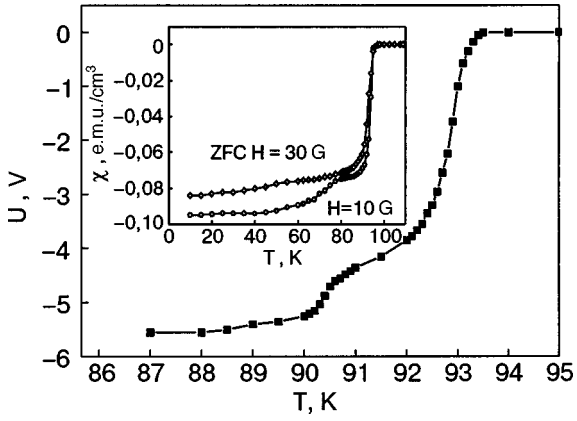

FIG. 1. Temperature dependence of the output voltage of the susceptibility meter with increasing temperature of the sample in the region of the superconducting phase transition. The inset shows the temperature dependence of the susceptibility of a ceramic HTSC from Ref. 6.

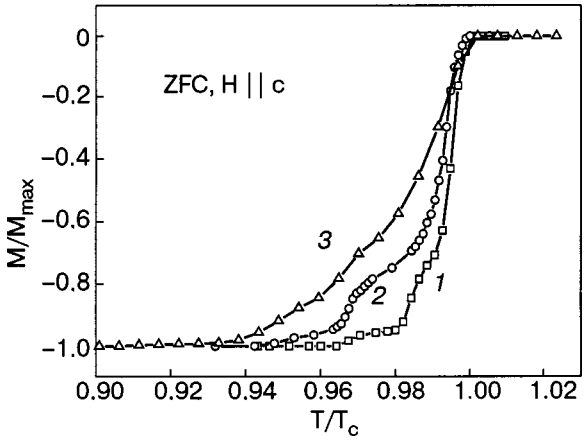

FIG. 2. Temperature dependence of the magnetization of a YBCO single crystal, normalized to the maximum value, for different values of the magnetic field H [A/m]: 8 (*1*), 15.5 (*2*), 65.9 (*3*).

Let us mention a few key points in this regard. In studying the magnetic susceptibility of polycrystalline cuprates of the YBCO and RBCO type (R=Nd, Eu, Gd) the authors of Ref. 6 found that some of the samples that had been subjected to annealing in oxygen had ZFC curves of the phase transition with a smoothed steplike kink. This form of the temperature dependence of the susceptibility of a HTSC is characteristic of the regime of the ''glass–liquid'' transition of the vortex matter, which occurs at a temperature $T_g<T_c$ in strong magnetic fields $H>H_{c1}$. Since in the experiment described in Ref. 6 the magnetic fields were weak ($H=10-30$ Oe), the observed stepped form of the phase characteristics was attributed to a transformation of a medium of Josephson weak links at low magnetic fields, which was predicted in the theoretical studies.[7]

The superconducting granules of a cuprate sample are coupled to each other in a random way by barriers of various transparency for Cooper pairs and thus form statistically distributed current networks. The parameters of this Josephson medium depend on the technology of preparation of the HTSC sample (pressures, degrees of oxygen saturation, etc.), the temperature of the sample, and the external magnetic field used in the measurements. By analogy with the spin glass this medium is sometimes called an ''orbital glass,'' since the orbital moments are identified with circulating induced or spontaneous superconducting currents. The latter can exist under certain conditions, e.g., in the presence of an odd number of Josephson π contacts in the random current loops. With increasing applied magnetic field the temperature T_g of this transition shifts to lower values, and the step vanishes completely at higher fields, where the susceptibility demonstrates typical diamagnetic behavior.

We have observed such effects in single-crystal samples of YBCO. Figure 2 shows the temperature dependence of the magnetization normalized to its maximum value for one of the YBCO single crystals at three values of the magnetic field $H\|c$, equal to 8 A/m ($\approx$0.1 Oe), 15.5 A/m ($\approx$0.2 Oe), and 65.9 A/m ($\approx$0.83 Oe). We see that with increasing field H the step shifts to lower temperatures and becomes smoother.

Because of the anisotropy of the grains, granular superconductors have a complex microstructure and are more favorable for the existence of an orbital glass. Abrikosov vortices can penetrate through the grains along the ab planes, and in that case supercurrents can flow through loops closing one or several granules. Similar plateaus on the phase transition curves have also been observed in high-quality epitaxial film samples of YBCO in studies of the current–voltage characteristics and magnetization at high fields ($B=0.3$ T).[8] This behavior was interpreted by the authors in the framework of a model based on the existence of a one-dimensional network of Josephson junctions with statistically distributed lengths and with magnetic field-dependent barrier thicknesses. There the transport current was treated as a tunneling current through this Josephson network. A given network consists of a number of current channels through the intergranular boundaries, and the pinning in this system is effected at interblock boundaries and/or correlated defects. In that case the sizes of the defects are comparable to the sizes of the current channels and also to the size of the vortex core. At high temperatures a significant fraction of these channels break up into individual superconducting granules, reducing the value of the critical current.

The results of our experiments with single-crystal samples of YBCO suggest that the twinning planes create conditions for the formation of similar Josephson networks with randomly distributed parameters. The twin boundaries include CuO_x layers containing oxygen vacancies and have a strong local influence on the suppression of the superconducting order parameter. The suppression of the superconducting order parameter at twins leads to a lowering of the energy of the vortex lines trapped by the twins. The density of vortex lines at twins is therefore higher than in the rest of the crystal. Experiments on the decorrelation of the vortex structure showed that in fields of 20–40 Oe the density of vortices at twins is twice as high as in the bulk of the crystal.[9] Since in a field of 0.2 Oe the intervortex distance $a_0=(\Phi_0/B)^{1/2}\approx 10^4$ nm exceeds the intertwin distance $d\approx 10^3$ nm and is comparable to the field penetration depth $\lambda\approx 10^4$ nm in the given temperature region, and since the interaction between vortices decays exponentially with the intervortex distance, it can be expected that all of the vortices are localized at twins.

Subsurface superconducting regions separated by twin

boundaries form chaotic loops and networks for circulating Meissner currents, which determine the resulting magnetization of a sample. As the temperature is raised the weakest links are broken, and a redistribution and attenuation of some of the induced supercurrents occur on account of the creep of individual vortices. The twinning planes, while being effective pinning centers, can simultaneously serve as directions of facilitated thermally activated entry of magnetic flux along them, providing regions where spontaneous currents appear.[2] To elucidate the contribution of these mechanisms to the behavior of the magnetization of $YBa_2Cu_3O_{7-x}$ single crystals the authors plan to continue our investigations on samples in which the twinning planes along the c axis change direction to the opposite, from (110) to $(1\bar{1}0)$, and also to compare the magnetic responses with untwinned single crystals.

Thus the nonmonotonic dependence of the magnetization of optimally doped $YBa_2Cu_3O_{7-x}$ single crystals in comparison with the published results of studies of ceramic and film samples permits the conclusion that a Josephson character of the behavior of the twin boundaries is possible in the presence of anisotropy of the order parameter.

The authors thank A. N. Omel'yancuk and M. A. Obolenskii for helpful discussions and assistance in organization of the research.

*E-mail: Aleksander.V.Bondarenko@univer.kharkov.ua

[1] G. Blatter, M. V. Feigel'man, V. B. Geshkenbein, A. I. Larkin, and V. M. Vinokur, Rev. Mod. Phys. **66**, 1125 (1994).
[2] E. Il'ichev, M. Grajcar, R. Hlubina, R. IJsselsteijn, H. Hoenig, H.-G. Meyer, A. Golubov, M. Amin, A. Zagoskin, A. Omel'yanchuk, and M. Kupriyanov, Phys. Rev. Lett. **86**, 5369 (2001); R. Hlubina, M. Grajcar, and E. Il'ichev, private communication.
[3] G. M. Tsoy, Z. Janu, and M. Novak, Physica B **284–288**, 811 (2000); A. L. Solovjov, V. M. Dmitriev, V. N. Svetlov, and V. B. Stepanov, Fiz. Nizk. Temp. **29**, 1281 (2003) [Low Temp. Phys. **29**, 973 (2003)].
[4] M. A. Obolenskii, A. V. Bondarenko, V. A. Shklovskiĭ, R. V. Vovk, and A. A. Prodan, Fiz. Nizk. Temp. **24**, 71 (1998) [Low Temp. Phys. **24**, 53 (1998)]; M. A. Obolenskii, A. V. Bondarenko, and M. O. Zubareva, Fiz. Nizk. Temp. **15**, 1152 (1989) [Low Temp. Phys. **15**, 635 (1989)].
[5] V. V. Khanin, J. N. Sotnikov, V. Y. Slobotchikov, and A. N. Matlashev, IEEE Trans. Appl. Supercond. **AS-5**, 2149 (1995).
[6] S. Glenis, T. Yuen, C. L. Lin, J. A. Zan, and T. Mihalishin, Physica C **317–318**, 624 (1999).
[7] F. V. Kusmartsev, Phys. Rev. Lett. **69**, 2268 (1992); D. Domínguez, E. A. Jagla, and C. A. Balseiro, *ibid.* **72**, 2773 (1994).
[8] G. Ghigo, A. Chiodoni, R. Gerbaldo, L. Gozzelino, F. Laviano, E. Mezzetti, B. Minetti, and C. Camerlingo, Physica C **341–348**, 1177 (2000).
[9] G. J. Dolan, G. V. Chandrashekhar, T. R. Dinger, C. Field, and F. Holtzberg, Phys. Rev. Lett. **62**, 827 (1989).

Translated by Steve Torstveit

Fractional ac Josephson effect in unconventional superconductors

H.-J. Kwon and V. M. Yakovenko*

Department of Physics, University of Maryland, College Park, Maryland 20742-4111, USA

K. Sengupta

Department of Physics, Yale University, New Haven, Connecticut 06520-8120, USA

(Submitted January 5, 2004)
Fiz. Nizk. Temp. **30**, 814–822 (July–August 2004)

For certain orientations of Josephson junctions between two p_x-wave or two d-wave superconductors, the subgap Andreev bound states produce a 4π-periodic relation between the Josephson current I and the phase difference φ: $I \propto \sin(\varphi/2)$. Consequently, the ac Josephson current has the fractional frequency $eV/\hbar$, where V is the dc voltage. In the tunneling limit, the Josephson current is proportional to the first power (and not the square) of the electron tunneling amplitude. Thus, the Josephson current between unconventional superconductors is carried by single electrons, rather than by Cooper pairs. The fractional ac Josephson effect can be observed experimentally by measuring the frequency spectrum of microwave radiation from the junction. © *2004 American Institute of Physics.* [DOI: 10.1063/1.1789931]

1. BRIEF HISTORY OF THE AC JOSEPHSON EFFECT

In 1962, Josephson[1] predicted theoretically that if a dc voltage V is applied to a junction between two superconductors, an ac supercurrent with the frequency $2eV/\hbar$ appears between the superconductors. The ac Josephson radiation was first observed experimentally 40 years ago in Kharkov by Yanson, Svistunov, and Dmitrenko.[2,3] In Ref. 3, the spectrum of microwave radiation from tin junctions was measured and a sharp peak in the frequency spectrum at $2eV/\hbar$ was found. It is amazing that without any attempt to match the impedances of the junction and waveguide, Dmitrenko and Yanson[3] found a signal several hundred times stronger than the noise and a ratio of linewidth to the Josephson frequency less than 10^{-3}. This discovery was followed by further work in the United States[4] and Ukraine.[5] The results of these investigations have been summarized in a classic book.[6] Since then, the ac Josephson radiation has been observed in many materials in various experimental setups. For example, a peak of Josephson radiation was found in Ref. 7 in indium junctions at a frequency of 9 GHz with a width of 36 MHz. In Ref. 8, a peak of Josephson radiation was observed around 11 GHz with a width of 50 MHz in $Bi_2Sr_2CaCu_2O_8$ single crystals with the current along the **c** axis perpendicular to the layers.

The theory of the Josephson effect was originally developed for conventional s-wave superconductors. In this paper, we study Josephson junctions between unconventional superconductors, such as d-wave cuprates or p_x-wave organic superconductors. We show that the midgap Andreev states in these materials produce a 4π-periodic relation between the Josephson current I and the phase difference φ: $I \propto \sin(\varphi/2)$. Consequently, the ac Josephson current has the fractional frequency $eV/\hbar$, half of the conventional value. We hope that this effect can be observed experimentally as a corresponding peak in the frequency spectrum of Josephson radiation from unconventional superconductors, such as d-wave cuprates, in a manner similar to the pioneering experiments[2,3] performed on conventional s-wave superconductors.

2. INTRODUCTION

In many materials, the symmetry of the superconducting order parameter is unconventional, i.e., not s-wave. In the high-T_c cuprates, it is the singlet $d_{x^2-y^2}$-wave.[9] There is experimental evidence that, in the quasi-one-dimensional (Q1D) organic superconductors $(TMTSF)_2X$,[10] the symmetry is triplet,[11] most likely the p_x-wave,[12] where the x axis is along the conducting chains. The unconventional pairing symmetry typically results in the formation of midgap Andreev bound states on the surfaces of these superconductors. For d-wave cuprate superconductors, the midgap Andreev states were predicted theoretically in Ref. 13 and discovered experimentally as a zero-bias conductance peak in tunneling between normal metals and superconductors (see Ref. 14). For the Q1D organic superconductors, the midgap states were theoretically predicted to exist at the edges perpendicular to the chains.[15,16] When two unconventional superconductors are joined together in a Josephson junction, their Andreev surface states hybridize to form Andreev bound states in the junction. These states are important for the Josephson current. Andreev bound states in high-T_c junctions were reviewed in Ref. 17. The Josephson effect between two Q1D p-wave superconductors was studied in Refs. 18 and 19.

In the present paper, we predict a new effect for Josephson junctions between unconventional (nonchiral) superconductors, which we call the fractional ac Josephson effect. Suppose both superconductors forming a Josephson junction have surface midgap states originally. This is the case for butt-to-butt junctions between two p_x-wave Q1D superconductors, as shown in Fig. 1*a*, and for 45°/45° in-plane junctions between two d-wave superconductors, as shown in Fig. 3*a*. (The two angles indicate the orientation of the junction line relative to the **b** axes of each $d_{x^2-y^2}$ superconductor.)

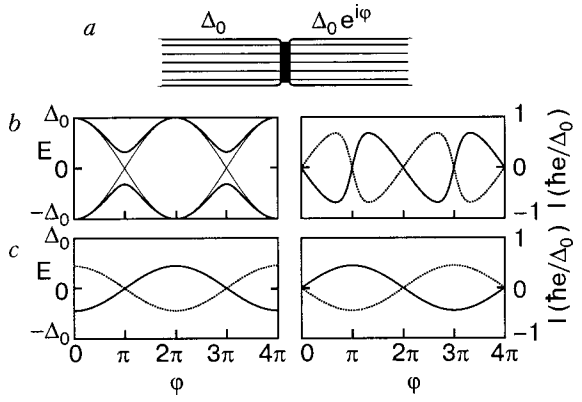

FIG. 1. Josephson junction between two Q1D p_x-wave superconductors (a). The energies (left panel) and the currents (right panel) of the subgap states in the $s-s$ junction as functions of the phase difference φ for $D=1$ (thin lines) and $D=0.9$ (thick lines) (b). The same as (b) for the p_x-p_x junction at $D=0.2$ (c).

We predict that the contribution of the hybridized Andreev bound states produces a 4π-periodic relation between the supercurrent I and the superconducting phase difference φ: $I\propto\sin(\varphi/2)$.[20] Consequently, the ac Josephson effect has the frequency $eV/\hbar$, where e is the electron charge, V is the applied dc voltage, and h is Planck's constant. The predicted frequency is one-half of the conventional Josephson frequency $2eV/\hbar$ originating from the conventional Josephson relation $I\propto\sin\varphi$ with period 2π. Qualitatively, the predicted effect can be understood as follows. The Josephson current across the two unconventional superconductors is carried by tunneling of single electrons (rather than Cooper pairs) between the two resonant midgap states. Thus, the Cooper pair charge $2e$ is replaced by the single charge e in the expression for the Josephson frequency. This interpretation is also supported by the finding that, in the tunneling limit, the Josephson current is proportional to the first power (not square) of the electron tunneling amplitude.[21–23] Possibilities for experimental observation of the fractional ac Josephson effect are discussed in Sec. 4.

The predicted current–phase relation $I\propto\sin(\varphi/2)$ is quite radical, because every textbook on superconductivity says that the Josephson current must be a 2π-periodic function of φ.[20] To our knowledge, the only paper that has discussed the 4π-periodic Josephson effect is that of Kitaev.[24] He considered a highly idealized model of spinless fermions on a one-dimensional (1D) lattice with superconducting pairing on the neighboring sites. The pairing potential in this case has the p_x-wave symmetry, and midgap states do exist at the ends of the chain. They are described by the Majorana fermions, which Kitaev proposed to use for nonvolatile memory in quantum computing. He found that, when two such superconductors are placed in contact, the system is 4π-periodic in the phase difference between the superconductors. Our results are in agreement with his work. However, we formulate the problem as an experimentally realistic Josephson effect between known superconducting materials.

3. THE BASICS

In this paper, we consider singlet pairing and triplet pairing with the spin polarization vector **n** having a uniform, momentum-independent orientation.[11,12] If the spin quantization axis z is selected along **n**, then the Cooper pairing takes a place between electrons with the opposite z-axis spin projections σ and $\overline{\sigma}$: $\langle\hat{c}_\sigma(\mathbf{k})\hat{c}_{\overline{\sigma}}(-\mathbf{k})\rangle\propto\Delta_\sigma(\mathbf{k})$, where $\hat{c}_\sigma(\mathbf{k})$ is the annihilation operator of an electron with momentum **k** and spin σ. The pairing potential has the symmetry $\Delta_\sigma(\mathbf{k})=\mp\Delta_{\overline{\sigma}}(\mathbf{k})=\pm\Delta_\sigma(-\mathbf{k})$, where the upper and lower signs correspond to the singlet and triplet cases.

We select the coordinate axis x perpendicular to the plane of the Josephson junction. We assume that the interface between the two superconductors is smooth enough, so that the electron momentum component k_y parallel to the junction plane is a conserved good quantum number.

Electron states in a superconductor are described by the Bogoliubov operators $\hat{\gamma}$, which are related to the electron operators $\hat{c}$ by the following equations[25]

$$\hat{\gamma}_{n\sigma k_y}=\int dx[u^*_{n\sigma k_y}(x)\hat{c}_{\sigma k_y}(x)+v^*_{n\sigma k_y}(x)\hat{c}^\dagger_{\overline{\sigma k_y}}(x)], \quad (1)$$

$$\hat{c}_{\sigma k_y}(x)=\sum_n [u_{n\sigma k_y}(x)\hat{\gamma}_{n\sigma k_y}+v^*_{n\overline{\sigma k_y}}(x)\hat{\gamma}^\dagger_{n\overline{\sigma k_y}}], \quad (2)$$

where $\overline{k_y}=-k_y$, and n is the quantum number of the Bogoliubov eigenstates. The two-component vectors $\psi_{n\sigma k_y}(x)=[u_{n\sigma k_y}(x),v_{n\sigma k_y}(x)]$ are the eigenstates of the Bogoliubov–de Gennes (BdG) equation with the eigenenergies $E_{n\sigma k_y}$:

$$\begin{pmatrix} \varepsilon_{k_y}(\hat{k}_x)+U(x) & \hat{\Delta}_{\sigma k_y}(x,\hat{k}_x) \\ \Delta^\dagger_{\sigma k_y}(x,\hat{k}_x) & -\varepsilon_{k_y}(\hat{k}_x)-U(x) \end{pmatrix}\psi_n=E_n\psi_n, \quad (3)$$

where $\hat{k}_x=-i\partial_x$ is the x component of the electron momentum operator, and $U(x)$ is a potential. In Eq. (3) and below, we often omit the indices σ and k_y to shorten the notation where this will not cause confusion.

4. JUNCTIONS BETWEEN QUASI-ONE-DIMENSIONAL SUPERCONDUCTORS

In this Section, we consider junctions between two Q1D superconductors, such as the organic superconductors $(TMTSF)_2X$, with the chains along the x axis, as shown in Fig. 1a. For a Q1D conductor, the electron energy dispersion in Eq. (3) can be written as $\varepsilon=\hbar^2k_x^2/2m-2t_b\cos(bk_y)-\mu$, where m is an effective mass, μ is the chemical potential, b and t_b are the distance and the tunneling amplitude between the chains. The superconducting pairing potentials in the s- and p_x-wave cases have the forms

$$\hat{\Delta}_{\sigma k_y}(x,\hat{k}_x)=\begin{cases} \sigma\Delta_\beta, & s\text{-wave}, \\ \Delta_\beta\hat{k}_x/k_F, & p_x\text{-wave}, \end{cases} \quad (4)$$

where $\hbar k_F=\sqrt{2m\mu}$ is the Fermi momentum, and σ is treated as $+$ for $\uparrow$ and $-$ for $\downarrow$. The index $\beta=R,L$ labels the right ($x>0$) and left ($x<0$) sides of the junction, and Δ_β acquires a phase difference φ across the junction:

$$\Delta_L=\Delta_0, \quad \Delta_R=\Delta_0 e^{i\varphi}. \quad (5)$$

The potential $U(x)=U_0\delta(x)$ in Eq. (3) represents the junction barrier located at $x=0$. Integrating Eq. (3) over x from -0 to $+0$, we find the boundary conditions at $x=0$:

$$\psi_L=\psi_R, \quad \partial_x\psi_R-\partial_x\psi_L=k_F Z\psi(0), \tag{6}$$

$$Z=2mU_0/\hbar^2k_F, \quad D=4/(Z^2+4), \tag{7}$$

where D is the transmission coefficient of the barrier.

4.1. Andreev bound states

The general solution of Eq. (3) is a superposition of terms with momenta close to αk_F, where the index $\alpha=\pm$ labels the right- and left-moving electrons:

$$\psi_{\beta\sigma}=e^{\beta\kappa x}\left[A_\beta\begin{pmatrix}u_{\beta\sigma+}\\ v_{\beta\sigma+}\end{pmatrix}e^{i\tilde{k}_F x}+B_\beta\begin{pmatrix}u_{\beta\sigma-}\\ v_{\beta\sigma-}\end{pmatrix}e^{-i\tilde{k}_F x}\right]. \tag{8}$$

Here $\beta=\mp$ for R and L. Equation (8) describes a subgap bound state with an energy $|E|<\Delta_0$, which is localized at the junction and decays exponentially in x within the length $1/\kappa$. The coefficients $(u_{\beta\sigma\alpha}, v_{\beta\sigma\alpha})$ in Eq. (8) are determined by substituting the right- and left-moving terms separately into Eq. (3) for $x\neq 0$, where $U(x)=0$. In the limit $k_F\gg\kappa$, we find

$$\frac{u_{\beta\sigma\alpha}}{v_{\beta\sigma\alpha}}=\frac{\Delta_{\beta\sigma\alpha}}{E+i\alpha\beta\hbar\kappa v_F}, \quad \kappa=\frac{\sqrt{\Delta_0^2-|E|^2}}{\hbar v_F}, \tag{9}$$

where $v_F=\hbar k_F/m$ is the Fermi velocity, and $\Delta_{\beta\sigma\alpha}$ is equal to $\sigma\Delta_\beta$ for the s-wave case and to $\alpha\Delta_\beta$ for the p_x-wave, with Δ_β given by Eq. (5). The k_y-dependent Fermi momentum $\hbar\tilde{k}_F=\hbar k_F+2t_b\cos(bk_y)/v_F$ in Eq. (8) eliminates the dispersion in k_y from the BdG equation.

Substituting Eq. (8) into the boundary conditions (6), we obtain linear homogeneous equations for the coefficients A_β and B_β. The compatibility condition for these equations gives an equation for the energies of the Andreev bound states. There are two subgap states, with the energies $E_a=aE_0(\varphi)$ labeled by the index $a=\pm$:

$$E_0^{(s)}(\varphi)=-\Delta_0\sqrt{1-D\sin^2(\varphi/2)}, \quad s-s\text{junction}, \tag{10}$$

$$E_0^{(p)}(\varphi)=-\Delta_0\sqrt{D}\cos(\varphi/2), \quad p_x-p_x\text{junction}. \tag{11}$$

The energies (10) and (11) are plotted as functions of φ in the left panels (b) and (c) of Fig. 1. Without the barrier $(D=1)$ the spectra of the $s-s$ and p_x-p_x junctions are the same and consist of two crossing curves $E=\mp\Delta_0\cos(\varphi/2)$, shown by the thin lines in the left panel of Fig. 1*b*. A nonzero barrier $(D<1)$ changes the energies of the Andreev bound states in the $s-s$ and p_x-p_x junctions in different ways. In the $s-s$ case, the two energy levels repel near $\varphi=\pi$ and form two separated 2π-periodic branches shown by the thick lines in the left panel of Fig. 1*b*.[25,26] In contrast, in the p_x-p_x case, the two energy levels continue to cross at $\varphi=\pi$, and they are separated from the continuum of states above $+\Delta_0$ and below $-\Delta_0$, as shown in the left panel of Fig. 1*c*. The absence of repulsion of the energy levels indicates that there is no matrix element between these levels at $\varphi=\pi$ in the p_x-p_x case, unlike the $s-s$ case.

As will be shown in Sec. 5, the 45°/45° junction between two d-wave superconductors is mathematically equivalent to the p_x-p_x junction. Equation (11) was derived for the 45°/45° junction in Refs. 22, 23, and 27.

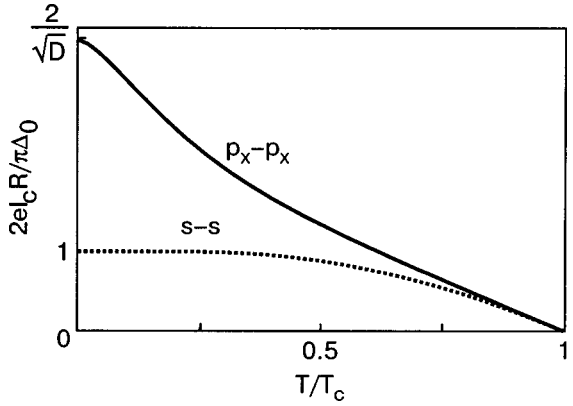

FIG. 2. Critical current of the $s-s$ (dashed line) and p_x-p_x (solid line) Josephson junctions as a function of temperature for $D=0.3$.

4.2. DC Josephson effect in thermodynamic equilibrium

It is well known[25,28] that the current carried by a quasiparticle state a is

$$I_a=\frac{2e}{\hbar}\frac{\partial E_a}{\partial\varphi}. \tag{12}$$

The two subgap states carry opposite currents, which are plotted versus φ in the right panels (b) and (c) of Fig. 1 for the $s-s$ and p_x-p_x junctions. In thermodynamic equilibrium, the total current is determined by the Fermi occupation numbers f_a of the states at temperature T:

$$I=\frac{2e}{\hbar}\sum_{a=\pm}\frac{\partial E_a}{\partial\varphi}f_a=-\frac{2e}{\hbar}\frac{\partial E_0}{\partial\varphi}\tanh\left(\frac{E_0}{2T}\right). \tag{13}$$

For the $s-s$ junction, substituting Eq. (10) into Eq. (13), we recover the Ambegaokar–Baratoff formula[29] in the tunneling limit $D\ll 1$:

$$I_s\approx D\sin\varphi\frac{e\Delta_0}{2\hbar}\tanh\left(\frac{\Delta_0}{2T}\right)=\sin\varphi\frac{\pi\Delta_0}{2eR}\tanh\left(\frac{\Delta_0}{2T}\right) \tag{14}$$

and the Kulik–Omelyanchuk formula[30] in the transparent limit $D\to 1$:

$$I_s\approx\sin\left(\frac{\varphi}{2}\right)\frac{e\Delta_0}{\hbar}\tanh\left(\frac{\Delta_0\cos(\varphi/2)}{2T}\right). \tag{15}$$

Taking into account that the total current is proportional to the number N of conducting channels in the junction (e.g., the number of chains), we have replaced the transmission coefficient D in Eq. (14) by the junction resistance $R=\hbar/2Ne^2D$ in the normal state.

Substituting Eq. (11) into Eq. (13), we find the Josephson current in a p_x-p_x junction in thermodynamic equilibrium:

$$I_p=\sqrt{D}\sin\left(\frac{\varphi}{2}\right)\frac{e\Delta_0}{\hbar}\tanh\left(\frac{\Delta_0\sqrt{D}\cos(\varphi/2)}{2T}\right)$$

$$=\sin\left(\frac{\varphi}{2}\right)\frac{\pi\Delta_0}{\sqrt{D}eR}\tanh\left(\frac{\Delta_0\sqrt{D}\cos(\varphi/2)}{2T}\right). \tag{16}$$

The temperature dependences of the critical currents for the $s-s$ and p_x-p_x junctions are shown in Fig. 2. They are obtained from Eqs. (14) and (16) assuming the BCS tem-

perature dependence for Δ_0. In the vicinity of T_c, I_p and I_s have the same behavior. With the decrease of temperature, I_s quickly saturates to a constant value, because, for $D \ll 1$, $E_a^{(s)} \approx \mp \Delta_0$ (10); thus for $T \lesssim \Delta_0$, the upper subgap state is empty and the lower one is completely filled. In contrast, I_p increases rapidly with decreasing temperature, as $1/T$, and saturates to a value enhanced by the factor $2/\sqrt{D}$ relative to the Ambegaokar–Baratoff formula (10) at $T=0$. This is a consequence of two effects. As Eqs. (14) and (16) show, $I_s \propto D$ and $I_p \propto \sqrt{D}$, and thus $I_p \gg I_s$ in the tunneling limit $D \ll 1$. At the same time, the energy splitting between the two subgap states in the p_x-p_x junction is small compared to the gap: $E_0^{(p)} \propto \sqrt{D}\Delta_0 \ll \Delta_0$. Thus, for $\sqrt{D}\Delta_0 \lesssim T \lesssim \Delta_0$, the two subgap states are almost equally populated, so the critical current has the $1/T$ temperature dependence analogous to the Curie spin susceptibility.

Equation (16) was derived analytically for the 45°/45° junction between two d-wave superconductors in Refs. 21 and 22, and a similar result was calculated numerically for the p_x-p_x junction in Refs. 18 and 19. Notice that Eq. (16) gives a Josephson current $I_p(\varphi)$ that is a 2π-periodic function of φ, both for $T=0$ and $T \neq 0$. This is a consequence of the thermodynamic equilibrium assumption. At $T=0$, this assumption implies that the subgap state with the lower energy is occupied, and the one with the higher energy is empty. As one can see in Fig. 1, the lower energy is always a 2π-periodic function of φ. The assumption of thermodynamic equilibrium was explicitly made in Ref. 22 and was implicitly invoked in Refs. 18, 19, and 21 in their use of the Matsubara diagram technique. In Ref. 31, the temperature dependence of the Josephson critical current was measured in YBCO ramp-edge junctions with different crystal angles and was found to be qualitatively consistent with the upper curve in Fig. 2.

4.3. Dynamical fractional ac Josephson effect

The calculations of the previous Section are applied in the static case, where a given phase difference φ is maintained for an infinitely long time, so the occupation numbers of the subgap states have enough time to relax to thermodynamic equilibrium. Now let us consider the opposite dynamical limit. Suppose a small voltage $eV \ll \Delta_0$ is applied to the junction, so the phase difference acquires dependence on time t: $\varphi(t) = 2eVt/\hbar$. In this case, the state of the system is determined dynamically starting from the initial conditions. Let us consider the p_x-p_x junction at $T=0$ in the initial state $\varphi=0$, where the two subgap states (11) with the energies $\pm E_0$ are, respectively, occupied and empty. If $\varphi(t)$ changes sufficiently slowly (adiabatically), the occupation numbers of the subgap states do not change. In other words, the states shown by the solid and dotted lines in Fig. 1*c* remain occupied and empty, respectively. The occupied state (11) produces the current (12):

$$I_p(t) = \frac{\sqrt{D}e\Delta_0}{\hbar} \sin\left(\frac{\varphi(t)}{2}\right) = \frac{\sqrt{D}e\Delta_0}{\hbar} \sin\left(\frac{eVt}{\hbar}\right). \qquad (17)$$

The frequency of the ac current (17) is $eV/\hbar$, a half of the conventional Josephson frequency $2eV/\hbar$. The fractional frequency can be traced to the fact that the energies of Eq. (11) and the corresponding wave functions have a period of 4π in φ, rather than conventional 2π. Although at $\varphi = 2\pi$ the spectrum in the left panel of Fig. 1*c* is the same as at $\varphi=0$, the occupation numbers are different. The lower state is empty and the upper state is occupied. Only at $\varphi = 4\pi$ are the occupation numbers the same as at $\varphi=0$.

The 4π periodicity is a consequence of the energy levels crossing at $\varphi=\pi$. In contrast, in the s-wave case, the levels repel at $\varphi=\pi$ in Fig. 1*b*, and so the energy curves are 2π-periodic. As discussed at the end of Sec. 4.1, there is no matrix element between the crossing energy levels at $\varphi = \pi$. Thus, there are no transitions between them, so the occupation numbers of the solid and dotted curves in Fig. 1*c* are conserved. In order to show this more formally, we can write a general solution of the time-dependent BdG equation as a superposition of the two subgap states with time-dependent $\varphi(t)$: $\psi(t) = \Sigma_a C_a(t)\psi_a[\varphi(t)]$. The matrix element of transitions between the states is proportional to $\dot{\varphi}\langle\psi_+|\partial_\phi\psi_-\rangle = \dot{\varphi}\langle\psi_+|\partial_\phi\hat{H}|\psi_-\rangle/(E_- - E_+)$. We found that it is zero in the p_x-wave case, and thus there are no transitions, and the initial occupation numbers of the subgap states at $\varphi=0$ are dynamically conserved.

As one can see in Fig. 1*c*, the system is not in the ground state when $\pi < \varphi < 3\pi$, because the upper energy level is occupied and the lower one is empty. In principle, the system might be able to relax to the ground state by emitting a phonon or a photon. At present time, we do not have an explicit estimate for such an inelastic relaxation time, but we expect that it is quite long. (The other papers[18,19,21,22] that assume thermodynamic equilibrium for each value of the phase φ do not have an estimate of the relaxation time either.) To observe the predicted ac Josephson effect with the fractional frequency $eV/\hbar$, the period of Josephson oscillations should be set shorter than the inelastic relaxation time, but not too short, so that the time evolution of the BdG equation can be treated adiabatically. Controlled nonequilibrium population of the upper Andreev bound state was recently achieved experimentally[32] in an s-wave Josephson junction.

Equation (17) can be generalized to the case where initially the two subgap states are populated thermally at $\varphi=0$, and these occupation numbers are conserved in the dynamical evolution:

$$I_p(t) = \frac{2e}{\hbar} \sum_a \frac{\partial E_a[\varphi(t)]}{\partial\varphi} f[E_a(\varphi=0)] \qquad (18)$$

$$= \sin\left(\frac{eVt}{\hbar}\right) \frac{\pi\Delta_0}{\sqrt{D}eR} \tanh\left(\frac{\Delta_0\sqrt{D}}{2T}\right). \qquad (19)$$

Note that the periodicities of the dynamical equation (16) and the thermodynamic equation (19) are different. The latter equation assumes that the occupation numbers of the subgap states are in instantaneous thermal equilibrium for each φ.

4.4. Tunneling Hamiltonian approach

In the infinite barrier limit $D \to 0$, the energies $\pm E_0^{(p)}$ of the two subgap states (11) degenerate to zero, i.e., they become midgap states. The wave functions (8) are simplified as follows:

$$\psi_{\pm 0}=\frac{\psi_{L0}(x)\mp\psi_{R0}(x)}{\sqrt{2}}, \tag{20}$$

$$\psi_{L0}=\sqrt{2\kappa}\sin(k_F x)e^{\kappa x}\begin{pmatrix}1\\ i\end{pmatrix}\theta(-x), \tag{21}$$

$$\psi_{R0}=\sqrt{2\kappa}\sin(k_F x)e^{-\kappa x}\begin{pmatrix}e^{i\varphi/2}\\ -ie^{-i\varphi/2}\end{pmatrix}\theta(x). \tag{22}$$

Since at $D=0$ the Josephson junction consists of two semi-infinite uncoupled p_x-wave superconductors, ψ_{L0} and ψ_{R0} are the wave functions of the surface midgap states[15] belonging to the left and right superconductors. Let us examine the properties of the midgap states in more detail.

If (u,v) is an eigenvector of Eq. (3) with eigenvalue E_n, then $(-v^*,u^*)$ for the s-wave case and (v^*,u^*) for the p-wave case are the eigenvectors with the energy $E_{\bar{n}}=-E_n$. It follows from these relations and Eq. (1) that $\hat{\gamma}_{\bar{n}\sigma\bar{k}_y}=C\hat{\gamma}^\dagger_{n\sigma k_y}$ with $|C|=1$. Notice that in the s-wave case, because (u,v) and $(-v^*,u^*)$ are orthogonal for any u and v, the states n and $\bar{n}$ are always different. However, in the p-wave case, the vectors (u,v) and (v^*,u^*) may be proportional, in which case they describe the same state with $E=0$. The states (21) and (22) indeed have this property:

$$v_{L0}=iu^*_{L0}, \quad v_{R0}=-iu^*_{R0}. \tag{23}$$

Substituting Eq. (23) into Eq. (1), we find the Bogoliubov operators of the left and right midgap states

$$\hat{\gamma}^\dagger_{L0\sigma k_y}=i\hat{\gamma}_{L0\bar{\sigma}\bar{k}_y}, \quad \hat{\gamma}^\dagger_{R0\sigma k_y}=-i\hat{\gamma}_{R0\bar{\sigma}\bar{k}_y}. \tag{24}$$

Operators (24) correspond to the Majorana fermions discussed in Ref. 24. In the presence of a midgap state, the sum over n in Eq. (2) should be understood as $\Sigma_{n>0}+\frac{1}{2}\Sigma_{n=0}$, where we identify the second term as the projection $\mathcal{P}\hat{c}$ of the electron operator onto the midgap state. Using Eqs. (23), (24), and (2), we find

$$\mathcal{P}\hat{c}_{\alpha k_y}(x)=u_0(x)\hat{\gamma}_{0\sigma k_y}=v_0^*(x)\hat{\gamma}^\dagger_{0\bar{\sigma}\bar{k}_y}. \tag{25}$$

Let us consider two semi-infinite p_x-wave superconductors on a 1D lattice with the spacing l, one occupying $x\leqslant\bar{l}=-l$ and the other $x\geqslant l$. They are coupled by the tunneling matrix element τ between the sites $\bar{l}$ and l:

$$\hat{H}_\tau=\tau\sum_{\sigma k_y}[\hat{c}^\dagger_{L\sigma k_y}(\bar{l})\hat{c}_{R\sigma k_y}(l)+\hat{c}^\dagger_{R\sigma k_y}(l)\hat{c}_{L\sigma k_y}(\bar{l})]. \tag{26}$$

In the absence of coupling ($\tau=0$), the subgap wave functions of each superconductor are given by Eqs. (21) and (22). Using Eqs. (25), (23), (21), and (22), we find that the tunneling Hamiltonian projected onto the basis of midgap states is

$$\begin{aligned}\mathcal{P}\hat{H}_\tau&=\tau[u^*_{L0}(\bar{l})u_{R0}(l)+\text{c.c.}](\hat{\gamma}^\dagger_{L0\uparrow}\hat{\gamma}_{R0\uparrow}+\text{H.c.})\\&=\Delta_0\sqrt{D}\cos(\varphi/2)(\hat{\gamma}^\dagger_{L0\uparrow}\hat{\gamma}_{R0\uparrow}+\hat{\gamma}^\dagger_{R0\uparrow}\hat{\gamma}_{L0\uparrow}),\end{aligned} \tag{27}$$

where $\sqrt{D}=4\tau\sin^2 k_F l/\hbar v_F$ is the transmission amplitude, and we have omitted summation over the diagonal index k_y. Notice that Eq. (27) is 4π-periodic in φ.[24]

Hamiltonian (27) operates between the two degenerate states of the system related by annihilation of the Bogoliubov quasiparticle in the right midgap state and its creation in the left midgap state. In this basis, Hamiltonian (27) can be written as a 2×2 matrix:

$$\mathcal{P}\hat{H}_\tau=\Delta_0\sqrt{D}\cos(\varphi/2)\begin{pmatrix}0&1\\1&0\end{pmatrix}. \tag{28}$$

The eigenvectors of Hamiltonian (28) are $(1,\mp 1)$, i.e., the antisymmetric and symmetric combinations of the right and left midgap states given in Eq. (20). Their eigenenergies are $E_\pm(\varphi)=\mp\Delta_0\sqrt{D}\cos(\varphi/2)$, in agreement with Eq. (11). The tunneling current operator is obtained by differentiating Eq. (27) or (28) with respect to φ. Because φ appears only in the prefactor, the operator structures of the current operator and the Hamiltonian are the same, so they are diagonal in the same basis. Thus, the energy eigenstates are simultaneously the eigenstates of the current operator, with the eigenvalues

$$I_\pm=\pm\sqrt{D}e\frac{\Delta_0}{\hbar}\sin\left(\frac{\varphi}{2}\right), \tag{29}$$

in agreement with Eq. (17). The same basis $(1,\mp 1)$ diagonalizes Hamiltonian (28) even when a voltage V is applied and the phase φ is time-dependent. Then the initially populated eigenstate with the lower energy produces the current $I_p=\sqrt{D}(e\Delta_0/\hbar)\sin(eVt/\hbar)$ with the fractional Josephson frequency $eV/\hbar$, in agreement with Eq. (17).

4.5. Josephson current carried by single electrons rather than Cooper pairs

In the tunneling limit, the transmission coefficient D is proportional to the square of the electron tunneling amplitude τ: $D\propto\tau^2$. Equations (17) and (29) show that the Josephson current in the p_x–p_x junction is proportional to the first power of the electron tunneling amplitude τ. This is in contrast to the s–s junction, where the Josephson current (14) is proportional to τ^2. This difference results in a large ratio $I_p/I_s=2/\sqrt{D}$ between the critical currents at $T=0$ in the p_x- and s-wave cases, as shown in Fig. 2 and discussed in Sec. 4.2. The reason for the different powers of τ is the following. In the p_x-wave case, the transfer of just one electron between the degenerate left and right midgap states is a real (nonvirtual) process. Thus, the eigenenergies are determined from the secular equation (28) already in the first order of τ. In the s-wave case, there are no midgap states, so the transferred electron is taken from below the gap and placed above the gap, at the energy cost $2\Delta_0$. Thus, the transfer of a single electron is a virtual (not real) process. It must be followed by the transfer of another electron, so that a pair of electrons is absorbed into the condensate. This implies that the current is proportional to τ^2.

This picture implies that the Josephson supercurrent across the interface is carried by single electrons in the p_x–p_x junction and by Cooper pairs in the s–s junction. Because the single-electron charge e is a half of the Cooper-pair charge $2e$, the frequency of the ac Josephson effect in the p_x–p_x junction is $eV/\hbar$, a half of the conventional Josephson frequency $2eV/\hbar$ for the s–s junction. These conclusions also apply to a junction between two cuprate

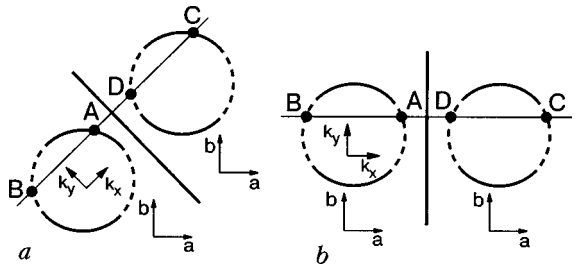

FIG. 3. Schematic drawing of the 45°/45° junction (*a*) and 0°/0° junction (*b*) between two *d*-wave superconductors. The thick line represents the junction line. The circles illustrate the Fermi surfaces, where positive and negative pairing potentials Δ are shown by the solid and dotted lines. The points A, B, C, and D in momentum space are connected by transmission and reflection from the barrier.

d-wave superconductors in such an orientation that both sides of the junction have surface midgap states, e.g., to the 45°/45° junction (see Sec. 5).

In both the p_x-p_x and $s-s$ junctions, electrons transferred across the interface are taken away into the bulk by the supercurrent of Cooper pairs. In the case of the p_x-p_x junction, a single transferred electron occupies a midgap state until another electron gets transferred. Then the pair of electrons becomes absorbed into the bulk condensate, the midgap state returns to the original configuration, and the cycle repeats. In the case of the $s-s$ junction, two electrons are simultaneously transferred across the interface and become absorbed into the condensate. Clearly, electric charge is transferred across the interface by single electrons at a rate proportional to τ in the first case and by Cooper pairs at a rate proportional to τ^2 in the second case, but the bulk supercurrent is carried by the Cooper pairs in both cases.

5. JOSEPHSON JUNCTIONS BETWEEN *d*-WAVE SUPERCONDUCTORS

In this Section we study Josephson junctions between two *d*-wave cuprate superconductors. As before, we select the coordinate x perpendicular to the junction line and assume that the electron momentum component k_y parallel to the junction line is a conserved good quantum number. Then the 2D problem separates into a set of 1D solutions (8) in the x direction labeled by the index k_y. Using an isotropic electron energy dispersion law $\varepsilon=\hbar^2(k_x^2+k_y^2)/2m-\mu$, we replace the Fermi momentum k_F and velocity v_F by their x components $k_{Fx}=\sqrt{k_F^2-k_y^2}$ and $v_{Fx}=\hbar k_{Fx}/m$. Thus, the transmission coefficient D in Eq. (7) becomes k_y-dependent. The total Josephson current is given by a sum over all occupied subgap states labeled by k_y.

For the cuprates, let us consider a junction parallel to the $[1,\bar{1}]$ crystal direction in the $a-b$ plane and select the x axis along the diagonal [1, 1], as shown in Fig. 3*a*. In these coordinates, the *d*-wave pairing potential is

$$\hat{\Delta}_{\sigma k_y}(x,\hat{k}_x)=\sigma 2\Delta_\beta k_y\hat{k}_x/k_F^2, \tag{30}$$

where the same notation as in Eq. (4) is used. Direct comparison of Eqs. (30) and (4) demonstrates that the *d*-wave superconductor with the 45° junction maps to the p_x-wave superconductor by the substitution $\Delta_0\to\sigma 2\Delta_0 k_y/k_F$. Thus, the results obtained in Sec. 4 for the p_x-p_x junction apply to the 45°/45° junction between two *d*-wave superconductors with the appropriate integration over k_y. The energies and the wave functions of the subgap Andreev states in the 45°/45° junction are 4π-periodic, as in Eqs. (11). Thus the ac Josephson current has the fractional frequency $eV/\hbar$, as in Eq. (17).

On the other hand, if the junction is parallel to the [0, 1] crystal direction, as shown in Fig. 3*b*, then $\hat{\Delta}_{\sigma k_y}(x,\hat{k}_x)=\sigma\Delta_\beta(\hat{k}_x^2-k_y^2)/k_F^2$. This pairing potential is an even function of k_x, and so it is analogous to the *s*-wave pairing potential in Eq. (4). Thus the 0°/0° junction between two *d*-wave superconductors is analogous to the $s-s$ junction. It should exhibit the conventional 2π-periodic Josephson effect with the frequency $2eV/\hbar$.

For a generic orientation of the junction line, the *d*-wave pairing potential acts like p_x-wave for some momenta k_y and like *s*-wave for other k_y. Thus, the total Josephson current is a sum of the unconventional and conventional terms:[20]

$$I=C_1\sin(\varphi/2)+C_2\sin(\varphi)+\ldots, \tag{31}$$

with some coefficients C_1 and C_2. We expect that both terms in Eq. (31) are present for any real junction between *d*-wave superconductors because of imperfections. However, the ratio C_1/C_2 should be maximal for the junction shown in Fig. 3*a* and minimal for the junction shown in Fig. 3*b*.

6. EXPERIMENTAL OBSERVATION OF THE FRACTIONAL AC JOSEPHSON EFFECT

Conceptually, the setup for experimental observation of the fractional ac Josephson effect is straightforward. One should apply a dc voltage V to the junction and measure the frequency spectrum of microwave radiation from the junction, expecting to detect a peak at the fractional frequency $eV/\hbar$. To observe the fractional ac Josephson effect predicted in this paper, it is necessary to perform this experiment with the 45°/45° cuprate junctions shown in Fig. 3*a*. For control purposes, it is also desirable to measure the frequency spectrum for the 0°/0° junction shown in Fig. 3*b*, where a peak at the frequency $eV/\hbar$ should be minimal. It should be absent completely in a conventional $s-s$ junction, unless the junction enters a chaotic regime with period doubling.[33] The high-T_c junctions of the required geometry can be manufactured using the step-edge technique. Bicrystal junctions are not appropriate, because the crystal axes **a** and **b** of the two superconductors are rotated relative to each other in such junctions. As shown in Fig. 3*a*, we need the junction where the crystal axes of the two superconductors have the same orientation. Unfortunately, attempts to manufacture Josephson junctions from the Q1D organic superconductors $(TMTSF)_2X$ thus far have failed.

The most common way of studying the ac Josephson effect is observation of the Shapiro steps.[34] In this setup, the Josephson junction is irradiated by microwaves with the frequency ω, and steps in the dc current are detected at the dc voltages $V_n=n\hbar\omega/2e$. Unfortunately, this method is not very useful for studying the effect that we predict. Indeed, our results are effectively obtained by the substitution $2e\to e$. Thus, we expect to see the Shapiro steps at the voltages $V_m=m\hbar\omega/e=2m\hbar\omega/2e$, i.e., we expect to see only even Shapiro steps. However, when both terms are present in Eq.

(31), they produce both even and odd Shapiro steps, so it would be difficult to differentiate the novel effect from the conventional Shapiro effect. Notice also that the so-called fractional Shapiro steps observed at the voltage $V_{1/2} = \hbar\omega/4e$ corresponding to $n = 1/2$ have nothing to do with the effect that we propose. They originate from the higher harmonics in the current–phase relation $I \propto \sin(2\varphi)$. The fractional Shapiro steps have been observed in cuprates[35] but also in conventional s-wave superconductors.[36] Another method of measuring the current–phase relation in cuprates was employed in Ref. 37, but the connection with our theoretical results is not clear at the moment.

7. CONCLUSIONS

In this paper, we have studied suitably oriented $p_x - p_x$ or $d - d$ Josephson junctions, where the superconductors on both sides of the junction originally have the surface Andreev midgap states. In such junctions, the Josephson current I, carried by the hybridized subgap Andreev bound states, is a 4π-periodic function of the phase difference φ: $I \propto \sin(\varphi/2)$, in agreement with Ref. 24. Thus the ac Josephson current should exhibit the fractional frequency $eV/\hbar$, a half of the conventional Josephson frequency $2eV/\hbar$. In the tunneling limit, the Josephson current is proportional to the first power of the electron tunneling amplitude and not to the square, as in the conventional case.[21–23] Thus, the Josephson current in the case considered is carried by single electrons with charge e rather than by Copper pairs with charge $2e$. The fractional ac Josephson effect can be observed experimentally by measuring the frequency spectrum of microwave radiation from the junction and detecting a peak at $eV/\hbar$.

This study was supported by NSF Grant DMR-0137726. K. Sengupta thanks S.M. Girvin for support.

*E-mail: yakovenk@physics.umd.edu

[1] B. D. Josephson, Phys. Lett. **1**, 251 (1962).
[2] I. K. Yanson, V. M. Svistunov, and I. M. Dmitrenko, Sov. Phys. JETP **21**, 650 (1965).
[3] I. M. Dmitrenko and I. K. Yanson, JETP Lett. **2**, 154 (1965).
[4] D. N. Langenberg, D. J. Scalapino, B. N. Taylor, and R. E. Eck, Phys. Rev. Lett. **15**, 294 (1965).
[5] I. M. Dmitrenko, I. K. Yanson, and I. I. Yurchenko, Sov. Phys. Solid State **9**, 2889 (1968).
[6] I. O. Kulik and I. K. Yanson, *The Josephson Effect in Superconducting Tunneling Structures*, Israel Program for Scientific Translations, Jerusalem (1972).
[7] A. K. Jain, K. K. Likharev, J. E. Lukens, and J. E. Savageau, Phys. Rep. **109**, 309 (1984).
[8] R. Kleiner, F. Steinmeyer, G. Kunkel, and P. Müller, Phys. Rev. Lett. **68**, 2394 (1992).
[9] D. J. Van Harlingen, Rev. Mod. Phys. **67**, 515 (1995); C. Tsuei and J. Kirtley, *ibid.* **72**, 969 (2000).
[10] TMTSF stands for tetramethyltetraselenafulvalene, and X represents inorganic anions such as ClO_4 or PF_6.
[11] I. J. Lee *et al.*, Phys. Rev. Lett. **88**, 017004 (2002); I. J. Lee, M. J. Naughton, G. M. Danner, and P. M. Chaikin, *ibid.* **78**, 3555 (1997); I. J. Lee, P. M. Chaikin, and M. J. Naughton, Phys. Rev. B **62**, R14669 (2000).
[12] A. G. Lebed, Phys. Rev. B **59**, R721 (1999); A. G. Lebed, K. Machida, and M. Ozaki, *ibid.* **62**, R795 (2000).
[13] C.-R. Hu, Phys. Rev. Lett. **72**, 1526 (1994).
[14] S. Kashiwaya and Y. Tanaka, Rep. Prog. Phys. **63**, 1641 (2000).
[15] K. Sengupta, I. Zutić, H.-J. Kwon, V. M. Yakovenko, and S. Das Sarma, Phys. Rev. B **63**, 144531 (2001).
[16] Y. Tanuma, K. Kuroki, Y. Tanaka, and S. Kashiwaya, Phys. Rev. B **64**, 214510 (2001); Y. Tanuma *et al.*, **66**, 094507 (2002).
[17] T. Löfwander, V. S. Shumeiko, and G. Wendin, Semicond. Sci. Technol. **14**, R53 (2001).
[18] Y. Tanaka, T. Hirai, K. Kusakabe, and S. Kashiwaya, Phys. Rev. B **60**, 6308 (1999).
[19] C. D. Vaccarella, R. D. Duncan, and C. A. R. Sá de Melo, Physica C **391**, 89 (2003).
[20] The current–phase relation $I \propto \sin(\varphi/2)$ that we propose should not be confused with another unconventional current–phase relation $I \propto \sin(2\varphi)$ with the period π, which has been predicted theoretically for junctions between s- and d-wave superconductors,[38,39] s- and p-wave superconductors,[38,40] and for 0°/45° junctions between two d-wave superconductors.[41]
[21] Y. Tanaka and S. Kashiwaya, Phys. Rev. B **56**, 892 (1997).
[22] R. A. Riedel and P. F. Bagwell, Phys. Rev. B **57**, 6084 (1998).
[23] Yu. S. Barash, Phys. Rev. B **61**, 678 (2000).
[24] A. Yu. Kitaev, cond-mat/0010440.
[25] A. M. Zagoskin, *Quantum Theory of Many-Body Systems*, Springer, New York (1998).
[26] A. Furusaki, Superlattices Microstruct. **25**, 809 (1999).
[27] Y. Tanaka and S. Kashiwaya, Phys. Rev. B **53**, 9371 (1996).
[28] Eq. (12) can be equivalently obtained as the difference between the right- and left-moving currents using the formulaI $I_a = ev_F(|A_a|^2 - |B_a|^2)$ with the normalization condition $\int dx|\psi^2| = 1$ (Ref. 26).
[29] V. Ambegaokar and A. Baratoff, Phys. Rev. Lett. **10**, 486 (1963); **11**, 104 (1963).
[30] I. O. Kulik and A. N. Omel'yanchuk, Fiz. Nizk. Temp. **4**, 296 (1978) [Sov. J. Low Temp. Phys. **4**, 142 (1978)].
[31] H. Arie, K. Yasuda, H. Kobayashi, I. Iguchi, Y. Tanaka, and S. Kashiwaya, Phys. Rev. B **62**, 11864 (2000).
[32] J. J. A. Baselmans, T. T. Heikkilä, B. J. van Wees, and T. M. Klarwijk, Phys. Rev. Lett. **89**, 207002 (2002).
[33] R. F. Miracky, J. Clarke, and R. H. Koch, Phys. Rev. Lett. **50**, 856 (1983); C. B. Whan, C. J. Lobb, and M. G. Forrester, J. Appl. Phys. **77**, 382 (1995).
[34] S. Shapiro, Phys. Rev. Lett. **11**, 80 (1963); S. Shapiro, A. R. Janus, and S. Holly, Rev. Mod. Phys. **36**, 223 (1964).
[35] E. A. Early, A. F. Clark, and K. Char, Appl. Phys. Lett. **62**, 3357 (1993); L. C. Ku *et al.*, Physica C **229**, 320 (1994); I. V. Borisenko *et al.*, **368**, 328 (2002).
[36] J. Clarke, Phys. Rev. Lett. **21**, 1566 (1968).
[37] E. Il'ichev *et al.*, Phys. Rev. Lett. **86**, 5369 (2001).
[38] S. Yip, J. Low Temp. Phys. **91**, 203 (1993).
[39] Y. Tanaka, Phys. Rev. Lett. **72**, 3871 (1994); A. M. Zagoskin, J. Phys.: Condens. Matter **9**, L419 (1997).
[40] N. Yoshida, Y. Tanaka, S. Kashiwaya, and J. Inoue, J. Low Temp. Phys. **117**, 563 (1999).
[41] T. Lösfwander, G. Johansson, M. Hurd, and G. Wendin, Phys. Rev. B **57**, R3225 (1998); M. Hurd, T. Löfwander, G. Johansson, and G. Wendin, *ibid.* **59**, 4412 (1999).

This article was published in English in the original Russian journal. Reproduced here with stylistic changes by AIP.

Radio-frequency method for investigation of quantum properties of superconducting structures

E. Il'ichev,* N. Oukhanski, Th. Wagner, and H.-G. Meyer

Institute for Physical High Technology, P.O. Box 100239, D-07702 Jena, Germany

A. Yu. Smirnov

D-Wave Systems Inc., 320-1985 W. Broadway, Vancouver, B.C., V6J 4Y3, Canada

M. Grajcar

Department of Solid State Physics, Comenius University, SK-84248 Bratislava, Slovakia

A. Izmalkov

Institute for Physical High Technology, P.O. Box 100239, D-07702 Jena, Germany; Moscow Engineering Physics Institute (State University), Kashirskoe sh. 31, Moscow, 115409, Russia

D. Born

Institute for Physical High Technology, P.O. Box 100239, D-07702 Jena, Germany; Friedrich Schiller University, Institute of Solid State Physics, D-07743 Jena, Germany

W. Krech

Friedrich Schiller University, Institute of Solid State Physics, D-07743 Jena, Germany

A. Zagoskin

D-Wave Systems Inc., 320-1985 W. Broadway, Vancouver, B.C., V6J 4Y3, Canada; Physics and Astronomy Dept., The University of British Columbia, 6224 Agricultural Rd., Vancouver, B.C., V6T 1Z1 Canada

(Submitted January 28, 2004)
Fiz. Nizk. Temp. **30**, 823–833 (July–August 2004)

We implement the impedance measurement technique (IMT) for characterization of interferometer-type superconducting qubits. In the framework of this method, the interferometer loop is inductively coupled to a high-quality tank circuit. We show that the IMT is a powerful tool for studying the response of an externally controlled two-level system to different types of excitations. Conclusive information about the qubits is obtained from a readout of the tank properties. © *2004 American Institute of Physics.* [DOI: 10.1063/1.1789933]

1. INTRODUCTION

Quantum effects in mesoscopic superconducting circuits of small Josephson junctions have attracted renewed attention. It was clearly demonstrated that Josephson devices can behave like single microscopic particles if they are sufficiently isolated from the environment. Therefore, ideas developed in atomic and molecular physics can be used for description of artificially fabricated circuits of macroscopic size. These concepts are stimulated further by the prospect of a promising way to realize quantum bits (qubits) for quantum information processing.

Qubits are two-level quantum systems with externally controlled parameters. Generally, two kinds of such devices with small-size Josephson junctions have been developed. One approach is based on the charge degree of freedom; basic states of this kind of qubit are distinguished by the number of Cooper pairs on a specially designed island. The alternative realization utilizes the phase of a Josephson junction (or the flux in a ring geometry), which is conjugate to the charge degree of freedom. Due to macroscopic the size of superconducting qubits, they are extremely sensitive to external disturbances. Thus the back-action of a detector should be as small as possible. Many different detectors have been suggested in the literature (see Ref. 1 and references therein).

In this paper we review our results obtained on superconducting qubits by the impedance measurement technique (IMT). Below we shall discuss several quantum effects including macroscopic quantum tunneling, Landau–Zener transitions, Rabi oscillations, and direct resonant spectroscopy of the qubit energy levels. Finally, we present our very recent results of investigation of two coupled qubits.

2. MACROSCOPIC QUANTUM TUNNELING

For the flux qubits the Josephson energy dominates over the charge energy, $E_J \gg E_C$. It was predicted that such systems should exhibit various quantum-mechanical effects, including macroscopic quantum tunneling (MQT) of the flux.[2] Indeed, the predicted effects have been observed experimentally.[3–6] In this Section we briefly discuss the main properties of the flux qubits and demonstrate that the IMT technique is a powerful tool for the investigation of the MQT.

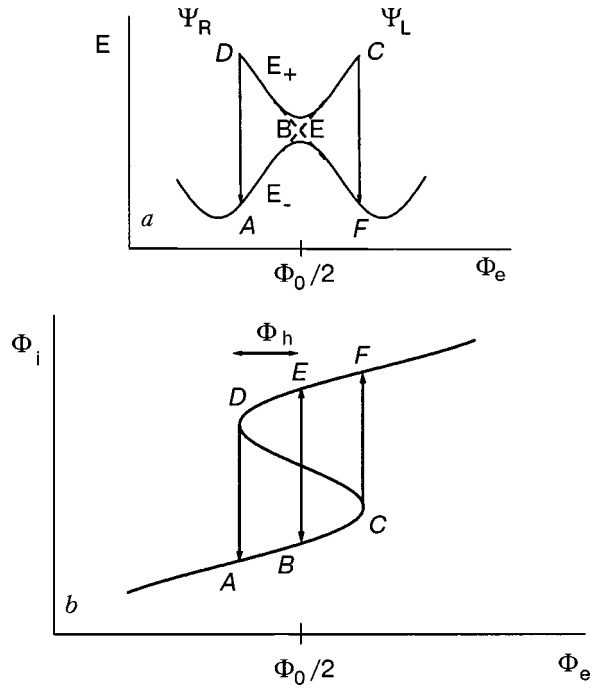

FIG. 1. *a*–Quantum energy levels of the 3JJ flux qubit versus external flux. The dashed lines correspond to the classical potential minima. In all graphs, the states *A*, *B*, *C* correspond to, say, Ψ_L with left-rotating supercurrent. As Φ_e is increased, these lose classical stability in favor of the corresponding states Ψ_R, denoted by *D*, *E*, and *F*. *b*—Internal versus external qubit flux.

One of the realizations of the flux qubit is a superconducting loop with low inductance L_q, including three Josephson junctions (a 3JJ qubit).[7] Its total Josephson energy is $E_J=\Sigma_{i=1}^{3}E_{Ji}(\varphi_i)$, where φ_i and $E_{Ji}=\hbar I_{ci}/2e$ are the phase difference and Josephson energy of the ith junction, respectively. Due to flux quantization, only $\varphi_{1,2}$ are independent, with $\varphi_3=-\varphi_1-\varphi_2-2\pi\Phi_e/\Phi_0$ (Φ_e is the external flux bias and $\Phi_0=h/2e$ is the flux quantum), for negligibly small L_q (though see Ref. 8).

At $\Phi_e=\Phi_0/2$ the potential $U(\varphi_1,\varphi_2)$ has two shallow minima. These two minima correspond to the qubit states ψ_L and ψ_R, carrying equal but opposite supercurrents around the loop. Therefore, according to the laws of quantum mechanics, near degeneracy the system can tunnel between the two potential minima.

In the basis $\{\psi_L,\psi_R\}$ and near $\Phi_e=\Phi_0/2$ the flux qubit can be described by the Hamiltonian

$$H=-\frac{\Delta}{2}\sigma_x-\frac{\varepsilon}{2}\sigma_z. \tag{1}$$

At bias $\varepsilon=0$, the two lowest levels of the qubit anticross (Fig. 1*a*), with an energy gap Δ. With ε changing sign, the qubit can either adiabatically transform from ψ_L to ψ_R staying in the ground state E_- or switch to the excited state E_+. The probability of the latter (called a Landau–Zener transition) for linear sweep $\varepsilon(t)=\nu t$ and ε changing from $-\infty$ to ∞ was calculated[9] to be $P_{LZ}=\exp(-\pi\Delta^2/2\hbar\nu)$.

In order to demonstrate the principle of the IMT measurements of this system, let us consider the internal flux representation (Fig. 1*b*) instead of the energy representation (Fig. 1*a*). A similar picture is usually used for explanation of the operation of the conventional radio-frequency (rf) SQUID. The main difference between rf-SQUID and qubit behavior is the existence of the adiabatic trajectory *BE* for latter one (see Fig. 1*a*,*b*). Let us assume that trajectory *BE* is forbidden and the "qubit" is inductively coupled to the high-quality resonant circuit. Then the system exhibits hysteretic behavior.[10] The tank circuit is simultaneously driven by a dc bias current I_{dc} and an ac current I_{rf} at a frequency ω close to the resonance frequency of the tank circuit. The two currents produce a total magnetic flux applied to the qubit $\Phi_e=\Phi_{dc}+\Phi_{rf}\cos\omega t$. If the amplitude $\Phi_{rf}>\Phi_h$, where Φ_h is the half-width of the hysteresis loop *ACFD* (Fig. 1*b*), the tank circuit will register energy losses proportional to the loop area, as long as $|\Phi_{dc}-\Phi_0/2|<\Phi_{rf}-\Phi_h$. These losses occur due to the jumps from E_+ to E_- at the ends of the loop. This idea was used by Silver and Zimmerman to build the first rf SQUID magnetometers.[11] If $\Phi_{rf}>\Phi_h$ the rf voltage across the tank circuit is a Φ_0-periodic function of applied dc flux $V_T(\Phi_{dc})$ with local minima at $\Phi_{dc}=\Phi_0/2+n\Phi_0$, where n is an integer.

Now, let us take into account the additional "quantum" trajectory *BE* (see Fig. 1*b*). If its probability $1-P_{LZ}$ is nonzero but less than 1, two new closed paths *ABED* and *BCFE* are possible. There are two contributing trajectories, adiabatic and Landau–Zener transition. Therefore the net dissipation is $P_{\rm loss}=2P_{LZ}(1-P_{LZ})$ and vanishes if P_{LZ} is either too small or too large.[13] Due to the exponential dependence of P_{LZ} on the sweep rate, in practice this makes the quantum losses observable only if the bias sweep narrowly overshoots the anticrossing, i.e., if

$$\left|\Phi_{dc}-\frac{1}{2}\Phi_0\right|\lesssim\Phi_{rf}, \tag{2}$$

when Φ_e changes slowly. Plotting $V_T(\Phi_{dc})$ for $\Phi_{rf}>\Phi_h/2$, a plateau flanked by two peaks is expected. The position of the dips depends on Φ_{rf} as follows from Eq. (2). Therefore in contrast to the $V_T(\Phi_{dc})$ dependence of an rf SQUID, the qubit should exhibit two local minima (in one period) which are symmetrical with respect to $\Phi_{dc}=\Phi_0/2$. For amplitudes $\Phi_{rf}>\Phi_h$ the *ACFD* hysteresis becomes closed as well. Here, as in the rf SQUID, a local minimum should appear on the $V_{rf}(\Phi_{dc})$ dependence exactly at $\Phi_{dc}=\Phi_0/2$. Note that Φ_e here plays the role of a bias ε for the Hamiltonian (1).

To test the ideas discussed above, square-shaped Nb pancake coils with inductance L_T were prepared lithographically on oxidized Si substrates for the tank circuits. An external capacitance C_T was used to permit changing the resonant frequency $\omega_T=1/\sqrt{L_TC_T}$. The linewidth of the 30 coil windings was 2 μm, with a 2 μm spacing. The quality factor of the tank was $Q_T\approx1500$ at $\omega_T\sim20$ MHz. The 3JJ qubit structure was fabricated out of Al in the middle of the coil by the conventional shadow evaporation technique. The Josephson junctions with critical current density $j_c\approx300$ A/cm^2 have areas $\approx130\times620$ nm, 120×600 nm, and 110×610 nm, respectively. The loop area was 90 μm^2, with $L_q=39$ pH. The fabricated structure is shown in Fig. 2.

We measured $V_T(\Phi_{dc})$ by a three-stage cryogenic amplifier placed at ≈2 K.[12] Results for small driving voltage are shown in Fig. 3. For the smallest voltages no dissipative response is observed; the two "quantum" peaks appear around 10.7 μV (Ref. 13) and subsequently move apart with-

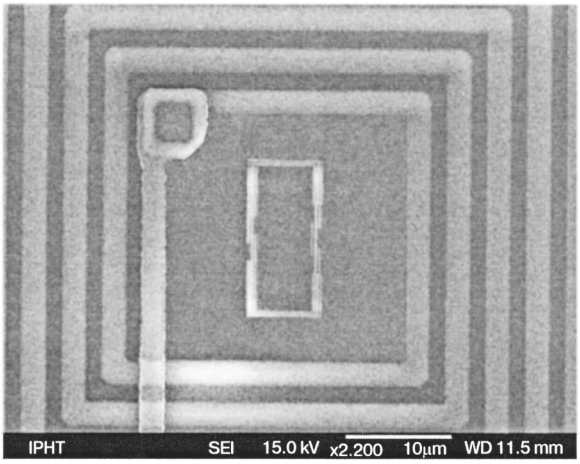

FIG. 2. Electron micrograph of the qubit at the center of the tank coil.

out significant broadening. The ''classical'' peak appears in the center, and with an ac bias threshold *double* that of the quantum peaks—both as predicted above.

Now assume that the probability of a Landau–Zener transition is small and the qubit changes adiabatically from ψ_L to ψ_R, always staying in the ground state E_-. This means that the hysteresis $ACFD$ is ''shunted'' by the BE trajectory. Therefore there are no losses caused by the flux jumps in the qubit. However, in the vicinity of B (see Fig. 1*b*) a small change of the external magnetic flux causes a considerable change of the flux inside the qubit. Due to coupling of the qubit to the tank, the effective inductance of the tank–qubit system is changed, which leads to a change of the resonant frequency. In this context a convenient measure of that change is the imaginary part of the total impedance[14] expressed in terms of the phase angle χ between the driving current $I_{\rm bias}(t)=I_{ac}\cos\omega t$ and the tank voltage $V_T(t)=V_T\cos(\omega t+\chi)$. For small L_q and if the amplitude of I_{rf} is negligible, the results are summarized by[15]

$$\tan\chi=k^2Q_TL_q\frac{d^2E_-(f_x)}{d\Phi_e^2}, \tag{3}$$

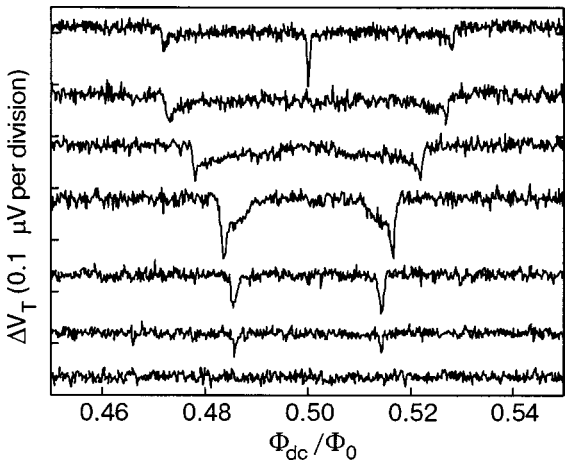

FIG. 3. Tank voltage versus magnetic flux bias near the degeneracy point of the qubit $\Phi_0/2$. From the lower to upper curve, the driving voltage is 10.2, 10.7, 11.2, 13.1, 17.2, 21.3, and 22.0 μV rms (the data have been shifted vertically for clarity).

where $k=M/\sqrt{L_qL_T}$ is the tank–qubit coupling coefficient, with M being the mutual inductance between them. The ground-state curvature is[15]

$$\frac{d^2E_-}{d\Phi_e^2}=-\frac{2E_J^2\Delta^2\lambda^2}{\Phi_0^2(4E_J^2\lambda^2f_x^2+\Delta^2)^{3/2}}, \tag{4}$$

where

$$f_x=\frac{\Phi_e}{\Phi_0}-\frac{1}{2}, \tag{5}$$

and λ is the normalized flux-to-energy conversion factor. Since all quantities in Eqs. (3)–(5) can be measured independently, experimental results can be compared with theoretical expectations.[16]

Strictly speaking, Eq. (3) describes a measurement of the quantum object with vanishing back-action. Therefore, its validity should be proved.[17] Taking into account the influence of the tank on the qubit, the Hamiltonian (1) should be rewritten as:

$$H=-\frac{\Delta}{2}\sigma_x-\frac{\varepsilon}{2}\sigma_z-\sigma_z(Q_0+f+\gamma\hat{I}_T)+H_T+H_{qB}, \tag{6}$$

where $\gamma=I_qM$ is the coupling coefficient between the qubit's current, $\hat{I}_q=I_q\sigma_z$ and the current in the tank $\hat{I}_T$. An infinitesimally small auxiliary force $f(t)$ is required for calculations of the qubit's magnetic susceptibility. A heat bath operator Q_0 and a Hamiltonian H_{qB} describe internal mechanisms of dissipation and fluctuations in the superconducting loop. The high-quality tank, treated here as a quantum cavity, is characterized by photon creation/annihilation operators a^+, a, which obey the Bose commutation rules $[a,a^+]_-=1$, etc. The quantum-mechanical operators of the current and voltage in the tank are defined as

$$\hat{I}_T=\sqrt{\hbar\omega_T/2L_T}(a+a^+),$$

$$\hat{V}_T=i\sqrt{\hbar\omega_T/2C_T}(a^+-a).$$

For the Hamiltonian of the tank driven by a bias current $I_{\rm bias}$ and coupled to its own heat bath Q_b we get the expression

$$H_T=\hbar\omega_T(a^+a+1/2)-(a+a^+)Q_b-L_T\hat{I}_TI_{\rm bias}+H_{TB}. \tag{7}$$

The internal heat bath of the tank Q_b, characterized by a free Hamiltonian H_{TB}, results in a finite lifetime of the photons, γ_T^{-1}, and, because of this, in a finite quality factor, $Q_T=\omega_T/\gamma_T$. Assuming that $\hbar=1$, $k_B=1$, we derive the Heisenberg equations for the tank operators: $\dot{\hat{I}}_T=\hat{V}_T/L_T$, and

$$\left(\frac{d^2}{dt^2}+\gamma_T\frac{d}{dt}+\omega_T^2\right)\hat{V}_T=\xi_b+\lambda\omega_T^2\dot{\sigma}_z+\frac{1}{C_T}\dot{I}_{\rm bias}, \tag{8}$$

where $\xi_T(t)$ is a fluctuation source with zero average value, $\langle\xi\rangle=0$, and with a correlator $\langle\xi_b(\omega)\xi_b\rangle$ that is proportional to the linewidth of the tank γ_T and the tank temperature T: $\langle\xi_b(\omega)\xi_b\rangle=(2\gamma_TT/C_T)\omega^2$. Because of inductive coupling, the current $\hat{I}_T$ and voltage $\hat{V}_T$ in the tank affect the qubit current: $\hat{I}_q=I_q\sigma_z$. Using linear response theory, we can present this influence as

$$\dot{\sigma}_z = \dot{\sigma}_{z,0} + \frac{\lambda}{L_T}\int dt_1 \left\langle \frac{\delta\sigma_z(t)}{\delta f(t_1)} \right\rangle \hat{V}_T(t_1), \tag{9}$$

where the operator $\sigma_{z,0}$ describes fluctuations of the qubit current caused by its internal heat bath, Q_0, which is not correlated with the heat bath of the tank, Q_b. We also take into account the relations $(\delta/\delta I_T) = \lambda(\delta/\delta f)$ and $\hat{\dot{I}}_T = \hat{V}_T/L_T$.

The function $\langle \delta\sigma_z(t)/\delta f(t_1)\rangle$ involved in Eq. (9) is proportional to the derivative of the qubit current $I_q(t) = \langle \hat{I}_q \rangle$ with respect to the flux $\Phi_T = L_T I_T$ created by the tank, $\delta I_q(t)/\delta\Phi(t_1)$, or to the second derivative of the qubit energy profile $E(\Phi)$ with respect to the flux, $\partial^2 E(\Phi)/\partial\Phi^2$ (compare with Eq. (3)). It is convenient to characterize the qubit response to the action of the tank by means of the magnetic susceptibility $\chi_{zz}(\omega)$, defined as[18]

$$\left\langle \frac{\delta\sigma_z(t)}{\delta f(t')} \right\rangle = \int \frac{d\omega}{2\pi} e^{-i\omega(t-t')}\chi_{zz}(\omega). \tag{10}$$

Then the voltage in the tank obeys the equation

$$\int dt_1 \left[\left(\frac{d^2}{dt^2} + \gamma_T \frac{d}{dt} + \omega_T^2 \right) \delta(t-t_1) - \frac{\lambda^2}{L_T}\omega_T^2 \left\langle \frac{\delta\sigma_z(t)}{\delta f(t_1)} \right\rangle \right] \hat{V}_T(t_1) = \xi_b + \lambda\omega_T^2 \dot{\sigma}_{z,0} + \lambda\omega_T^2 \frac{1}{C_T}\dot{I}_{\text{bias}}. \tag{11}$$

It is evident from this equation that the tank voltage contains information about the magnetic susceptibility $\chi_{zz}(\omega)$ of the qubit. Similarly to the classical case this information can be extracted from measurements of the phase angle χ. It follows from the averaged Eq. (11) that the amplitudes of harmonic oscillations of the tank voltage and the bias current are related through

$$V_T e^{-i\chi} = -i\omega \left\{ \omega_T^2 \left[1 - \frac{\lambda^2}{L_T}\chi'_{zz}(\omega) \right] - \omega^2 - i\omega \left[\gamma_T + \frac{\lambda^2\omega_T^2}{\omega L_T}\chi''_{zz}(\omega) \right] \right\}^{-1} \frac{I_{ac}}{C_T} \tag{12}$$

with $\chi'_{zz}(\omega)$ and $\chi''_{zz}(\omega)$ being the real and imaginary parts of the qubit magnetic susceptibility (10). In the case when the tank is driven exactly at the resonant frequency, $\omega = \omega_T$, the voltage amplitude V_T can be found from the equation

$$V_T = \frac{I_{ac}}{C_T}\{[k^2 L_q I_q^2 \omega_T \chi'_{zz}(\omega_T)]^2 + [\gamma_T + k^2 L_q I_q^2 \omega_T \chi''_{zz}(\omega_T)]^2\}^{-1/2}, \tag{13}$$

whereas for the voltage–current phase shift we obtain the expression

$$\tan\chi = -k^2 L_q I_q^2 \overline{Q}_T \chi'_{zz}(\omega_T). \tag{14}$$

Here $\overline{Q}_T = \omega_T/\overline{\gamma}_T$ is an effective quality factor of the tank wherein the broadening of the tank's linewidth due to the qubit,

$$\overline{\gamma}_T = \gamma_T + k^2 L_q I_q^2 \omega_T \chi''_{zz}(\omega_T), \tag{15}$$

is taken into account. The magnetic susceptibility of the qubit (Eq. (10)) is calculated from the Bloch equations written in the form

$$\begin{aligned} &\langle \dot{\sigma}_x \rangle + \Gamma_x(\langle \sigma_x \rangle - \sigma_x^0) = -\varepsilon\langle \sigma_y \rangle, \\ &\langle \dot{\sigma}_y \rangle + \Gamma_y\langle \sigma_y \rangle = -\Delta\langle \sigma_z \rangle + \varepsilon\langle \sigma_x \rangle - 2f\sigma_x^0, \\ &\langle \dot{\sigma}_z \rangle = \Delta\langle \sigma_y \rangle, \end{aligned} \tag{16}$$

where Γ_x and Γ_y are qubit's damping rates, and $\sigma_x^0 = -(\Delta/\omega_c)\tanh(\omega_c/2T)$ is the steady-state polarization of the qubit with energy splitting $\omega_c = \sqrt{\Delta^2+\varepsilon^2}$, which is much higher than the resonant frequency of the tank, $\omega_c \gg \omega_T$. Because of this the decoherence and relaxation rates drop out of the expression for the magnetic susceptibility:

$$\chi_{zz}(\omega_T) = \chi'_{zz}(\omega_T) = 2\frac{\Delta^2}{(\Delta^2+\varepsilon^2)^{3/2}}\tanh\frac{\sqrt{\Delta^2+\varepsilon^2}}{2T}. \tag{17}$$

As a result, the phase angle between the voltage in the tank and the bias current is given by the formula

$$\tan\chi = -2k^2\frac{L_q I_q^2}{\Delta}\overline{Q}_T\left(\frac{\Delta^2}{\Delta^2+\varepsilon^2}\right)^{3/2}\tanh\frac{\sqrt{\Delta^2+\varepsilon^2}}{2T}. \tag{18}$$

It can be shown by simple algebra that at $T=0$ Eqs. (3) and (18) are equivalent. Therefore, by measuring $\tan\chi$ as a function of the bias applied to the qubit one can indeed determine the qubit's tunneling rate Δ.

In order to realize the adiabatic response of the qubit experimentally, we fabricated a 3JJ Al qubit with the following parameters. Two of the junctions were nominally equivalent, each with an area of about 190×650 nm, while the third was smaller, so that $\alpha \equiv E_{J3}/E_{J1,2} \approx 0.8$. The value of the critical current for the larger junctions was determined to be $I_c \approx 380$ nA. The qubit inductance, tank parameters, and measurement setup were the same as in the case of the Landau–Zener transitions described above.

The measured $\chi(f_x)$ curve at a nominal mixing-chamber temperature $T=10$ mK is shown in Fig. 4. The curve was fitted by Eqs. (3) and (4) with Δ as a free parameter. The calculated curve for the best-fit parameter $\Delta/h = 650$ MHz is

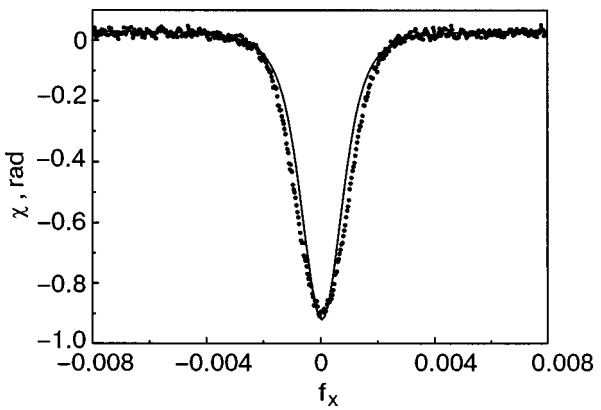

FIG. 4. Tank phase shift versus flux bias near degeneracy $f_x = 0$. The dots correspond to experimental data, and the solid line is the theoretical fit with $\Delta/h = 650$ MHz.

also shown Fig. 4. This value of the energy gap is in good agreement with that determined independently from temperature measurements.[16]

3. RABI SPECTROSCOPY

Quite generally, a two-level quantum system (including qubits), should exhibit coherent (Rabi) time oscillations in the presence of resonant irradiation. Microwaves in resonance with the spacing between the qubit's energy levels will cause their occupation probabilities to oscillate, with a frequency proportional to the microwave amplitude. Indeed, coherent oscillations between energy levels of the superconducting qubit have been detected.[19–22]

In this Section we show that the tank can be used for detection of Rabi oscillations as well. If a resonant microwave signal is applied, the phase-coherent oscillations of the level occupation will only last for a finite time, which is usually called the coherence time. The correlation between the occupations can be expressed by an autocorrelation function or its Fourier transform, the spectral density. For example for the IMT, when the flux qubit is coupled inductively to a tank circuit, the spectral density of the tank-voltage fluctuations rises above the background noise when the qubit's Rabi frequency Ω_R coincides with the tank's resonant frequency ω_T. This forms the basis for our measurement technique of *Rabi spectroscopy*. Rabi oscillations cause changes of the qubit's magnetic moment and, therefore, excite the tank. The tank circuit accumulates photons which were emitted by the qubit. This approach is similar to the one in entanglement experiments with Rydberg atoms and microwave photons in a cavity.[23]

Indeed, quantitative information can be extracted from the noise spectrum $S_V(\omega)$ of the voltage fluctuations (the Fourier transform of the correlator $M_V(t,t')=(1/2)\times\langle[\hat{V}_T(t),\hat{V}_T(t')]_+\rangle$ in the tank[17]), which incorporates the noise spectrum of the tank, S_{VT}, supplemented by the qubit's contribution S_{VQ}, i.e., $S_V=S_{VT}(\omega)+S_{VQ}(\omega)$, where

$$S_{VT}(\omega)=2\frac{\omega^2}{C_T}\frac{T\gamma_T}{(\overline{\omega_T^2}-\omega^2)^2+\omega^2\overline{\gamma_T^2}}. \tag{19}$$

The qubit's part of voltage noise can be found from the stochastic equation (11) for the tank voltage:

$$S_{VQ}(\omega)=\omega^2\frac{\omega_T}{C_T}\frac{k^2L_qI_q^2\omega_TS_{zz}(\omega)}{(\overline{\omega_T^2}-\omega^2)^2+\omega^2\overline{\gamma_T^2}}. \tag{20}$$

Here $S_{zz}(\omega)$ is the Fourier transform of the correlator $(1/2)\times\langle[\sigma_{z,0}(t),\sigma_{z,0}(t')]_+\rangle$, which describes internal fluctuations in the qubit (not related to the tank). Hand in hand with the tank's damping rate, $\overline{\gamma_T}$ (15), the resonance frequency of the tank, $\overline{\omega_T}$, is also shifted because of the qubit–tank interaction,

$$\overline{\omega_T}=\omega_T\sqrt{1-k^2L_qI_q^2\chi'_{zz}(\omega_T)}. \tag{21}$$

The spectrum of voltage fluctuations has a peak near the resonant frequency of the tank, ω_T, and it therefore contains information about the low-frequency component $S_{zz}(\omega_T)$ of the qubit spectrum. The equilibrium part of this spectrum peaks at the energy splitting $\omega_c=\sqrt{\Delta^2+\varepsilon^2}$ of the tunneling doublet, which differs significantly from the frequency of the tank, $\omega_c\gg\omega_T$. Because of this, the contribution of equilibrium qubit noise to the voltage spectrum of the tank is expected to be negligibly small. An external microwave source with a frequency ω_0 tuned to resonance with the energy splitting of the qubit ω_c induces periodic variations of the population difference between the excited and ground state of the qubit, which are characterized by a frequency $\Omega_R=\sqrt{(\Delta/\omega_c)^2F^2+\delta_0^2}$ that dependson the amplitude F of the microwave source as well as on the detuning $\delta_0=\omega_0-\omega_c$. With nonzero bias, $\varepsilon\neq0$, the left and right wells of the qubit potential have different energies. As a consequence, Rabi oscillations between the energy eigenstates will be accompanied by low-frequency transitions of the qubit from the left to the right well and back. The tank detects this kind of low-frequency noise, which is described by a Lorentzian spectrum centered at the Rabi frequency Ω_R with a linewidth dependent on the qubit decoherence rate Γ. Both the tank (Γ_T) and the internal heat bath (Γ_0) contribute to the decoherence rate: $\Gamma=\Gamma_0+\Gamma_T$. It should be emphasized that the external microwave field affects the qubit–bath coupling,[24] thus causing a distinction between the nonequlibrium decay rate Γ and its equilibrium counterparts Γ_x,Γ_y that enter the Bloch equations (16).

An informative part of the spectrum of voltage fluctuations, $S_{VQ}(\omega)$, incorporates the qubit Lorentzian multiplied by the transmission function of the tank, having a sharp peak at the frequency ω_T:

$$S_{VQ}(\omega)=2\frac{\varepsilon^2}{\omega_c^2}k^2\frac{L_qI_q^2}{C_T}\omega^2\Gamma_0\frac{\omega_T^2}{(\overline{\omega_T^2}-\omega^2)^2+\omega^2\overline{\gamma_T^2}}\times\frac{\Omega_R^2}{(\omega^2-\Omega_R^2)^2+\omega^2\Gamma^2}. \tag{22}$$

The linewidth of the tank is assumed to be much less than the qubit's damping rate, $\gamma_T\ll\Gamma$. Because of this, the spectrum of voltage noise (22) as a function of frequency ω represents a Lorentzian with a width γ_T and an amplitude which is given by a Lorentzian function of the Rabi frequency with its maximum near ω_T and a width Γ. Measurements of the noise spectrum amplitude at different values of the microwave power P allow one to extract information not only about the existence of Rabi oscillations but also about the nonequilibrium decoherence rate Γ of the qubit. We note that due to strong nonequilibrium conditions the populations of the qubit's levels are practically equal, and the noise spectrum amplitude does not depend on the temperature. The signal-to-noise ratio,

$$\frac{S_{VQ}(\omega)}{S_{VT}(\omega)}\Big|_{\omega=\omega_T}=\frac{\varepsilon^2}{\omega_c^2}k^2\frac{L_qI_q^2}{T}\frac{\Gamma_0}{\gamma_T}\frac{\omega_T^2\Omega_R^2}{(\omega_T^2-\Omega_R^2)+\omega_T^2\Gamma^2}, \tag{23}$$

peaks when $\Omega_R=\omega_T$. At the same point, the back-action of the measuring device (tank) on the quantum bit, which is described by the damping rate Γ_T,

$$\Gamma_T=4k^2L_qI_q^2\frac{\varepsilon^2}{\omega_c^2}\omega_T^2\frac{T\gamma_T}{(\omega_T^2-\Omega_R^2)^2+\Omega_R^2\gamma_T^2}, \tag{24}$$

reaches its maximum as well. However, the tank contribution to the qubit decoherence decreases drastically with small detuning of the Rabi frequency Ω_R from ω_T: $\gamma_T\ll|\Omega_R-\omega_T|$

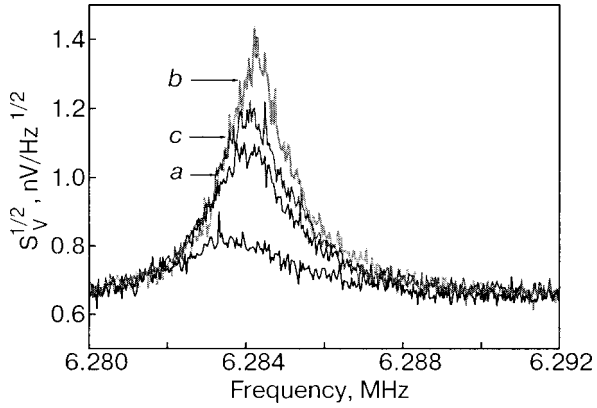

FIG. 5. The spectral noise amplitude of the tank voltage for UHF powers $P_a<P_b<p_c$ at 868 MHz. The bottom curve corresponds to the background noise without an HF signal.

$<\Gamma$. At the same time, the efficiency of measurements, $(S_{VQ}(\omega)/S_{VT}(\omega))_{|\omega=\omega_T}$, remains practically unchanged. Since $\Gamma \ll \Omega_R$, the spectroscopic monitoring of Rabi oscillations with the low-frequency tank circuit falls into the category of weak continuous quantum measurements.

The measurement setup and sample fabrication were similar to those described in the previous Section. Microwave irradiation (a UHF signal) was introduced to the sample through a commercial coaxial cable at temperatures between room and ~ 2 K and by a ThermoCoax resistive coaxial cable between ~ 2 K and 10 mK). In order to reduce external disturbances, a 20 dB commercial attenuator was installed at 2 K. To measure S_V, we tuned the UHF signal to resonance with the qubit level separation. We found noticeable output signal only when $\omega_{hf}/2\pi=(868\pm 2)$ MHz, in agreement with the estimated splitting $\Delta/h\sim 1$ GHz. Note that there is a difference of two orders of magnitude between ω_{hf} and the readout frequency ω_T. Together with the high Q_T, this ensures that the signal can only be due to resonant transitions in the qubit itself. This was verified by measuring S_V when biasing the qubit away from degeneracy. A signal exceeding the background, that is, emission of ~ 6 MHz photons by the qubit in response to a resonant UHF field in accordance with Eq. (24), was detected only when the qubit states were almost degenerate (cf. below Eq. (22)). The measurements were carried out at nominal temperature $T=10$ mK. No effect of radiation was observed above 40 mK (with 40 mK/$hk_B\approx 830$ MHz, i.e. close to Δ/h). We plotted $S_V(\omega)$ for different HF powers P in Fig. 5. As P is increased, ω_R grows and passes ω_T, leading to a nonmonotonic dependence of the maximum signal on P, in agreement with the above picture. This and the sharp dependence on the detuning of ω_{hf} from the qubit frequency confirm that the effect is due to Rabi oscillations.

For a quantitative comparison between theory and experiment, we subtracted the measured signal without an HF power from the observed S_V, yielding the qubit's contribution $S_{VQ}=S_V-S_{VT}(\omega)$. Subsequently, we extracted the peak values versus UHF amplitude, $S_{VQ,\max}(\sqrt{P/P_0})=\max_\omega S_{VQ}(\omega)\approx S_{VQ}(\omega_T)$, where P_0 is the power causing the maximum response; see Fig. 6*a*. In the same figure, we plot the theoretical curve for $S_{VQ,\max}$ normalized to its maximum S_0,

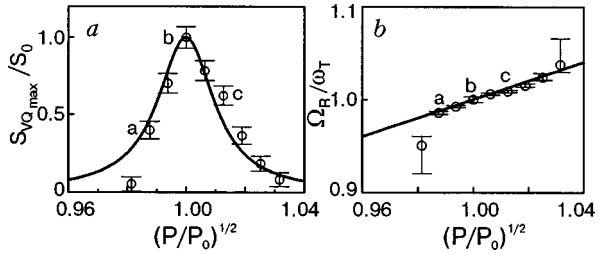

FIG. 6. *a*—Comparing the data to the theoretical Lorentzian. The fitting parameter is $g\approx 0.02$. The letters in the picture correspond to those in Fig. 5. *b*—The Rabi frequency extracted from (*a*) versus the applied UHF amplitude. The straight line is the predicted dependence $\omega_R/\omega_T=\sqrt{P/P_0}$. The good agreement provides strong evidence for Rabi oscillations.

$$\frac{S_{VQ,\max}(w)}{S_0}=\frac{w^2g^2}{(w^2-1)^2+g^2}\approx\frac{(g/2)^2}{(w-1)^2+(g/2)^2}; \quad (25)$$

$w\equiv\Omega_R/\omega_T$ ($=\sqrt{P/P_0}$ theoretically) and $g=\Gamma/\omega_T$. The best fit is found for $\Gamma\approx 0.02\omega_T\sim 8\times 10^5$ s^{-1}. Thus the lifetime of the Rabi oscillations is at least $\tau_{\text{Rabi}}=2/\Gamma\approx 2.5$ μs, leading to an effective quality factor $Q_{\text{Rabi}}=\Delta/(\hbar\Gamma)\sim 7000$. These values substantially exceed those obtained recently for a modified 3JJ qubit ($\tau_{\text{Rabi}}\sim 150$ ns),[22] which is not surprising. In our setup the qubit is read out not with a dissipative dc SQUID but with a high-quality resonant tank. The latter is weakly coupled to the qubit ($k^2\sim 10^{-3}$), suppressing the noise leakage to it.[25]

4. RESONANT SPECTROSCOPY

In this Section we show that the IMT can be also used for resonant spectroscopy, which is a well-known experimental method for investigation of quantum systems. As an example of such IMT application let us consider an interferometer-type charge qubit.[26–28] The device's core element is a single-Cooper-pair transistor—a small island, separated by two mesoscopic Josephson junctions, which is capacitively coupled to the gate. The transistor can be described by the Hamiltonian matrix[29,30]

$$H_{nm}=4E_C(N-n_g)^2\delta_{nm}-\frac{\varepsilon_J(\varphi)}{2}(\delta_{n,m+1}+\delta_{n,m-1}), \quad (26)$$

where N is the number of Cooper pairs on the island, $\delta_{n,m}$ is the Kronecker delta, and $E_C=e^2/2C_\Sigma$ is the single-electron charging energy expressed in terms of the total island capacitance C_Σ. The dimensionless parameter $n_g=C_gV_g/2e$ is continuously controllable by the gate voltage V_g via the capacitance C_g. The effective Josephson energy

$$\varepsilon_J(\varphi)=[E_{J1}^2+E_{J2}^2+2E_{J1}E_{J2}\cos\varphi]^{1/2} \quad (27)$$

is a function of the total phase difference across both junctions $\varphi=\phi_1-\phi_2$, where $E_{J1,J2}$ and $\phi_{1,2}$ are the Josephson coupling energies and phase differences of the first and second junction, respectively.

If the transistor is closed by a superconducting loop with low inductance L_q, the total phase difference is $\phi\approx 2\pi\Phi_e/\Phi_0$, and the ground-state curvature $d^2E_-/d\Phi_e^2$ can be obtained by finding the lowest eigenvalue of the Hamiltonian matrix (26) as a function of Φ_e. Using (3), we can calculate the phase shift of the tank inductively coupled

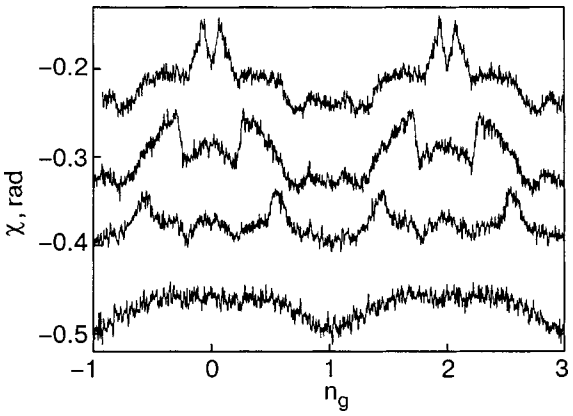

FIG. 7. Tank phase shift χ versus gate parameter n_g without microwave power (lowest curve) and with microwave power at different excitation frequencies. The data correspond to $\omega_{uhf}/2\pi=8.9$, 7.5, and 6.0 GHz (from top to bottom). The magnetic flux $\Phi_e=\Phi_0/2$ threading the interferometer loop provides a total phase difference $\delta=\pi$ across the single-Cooper-pair transistor. (The upper curves are shifted for clarity.)

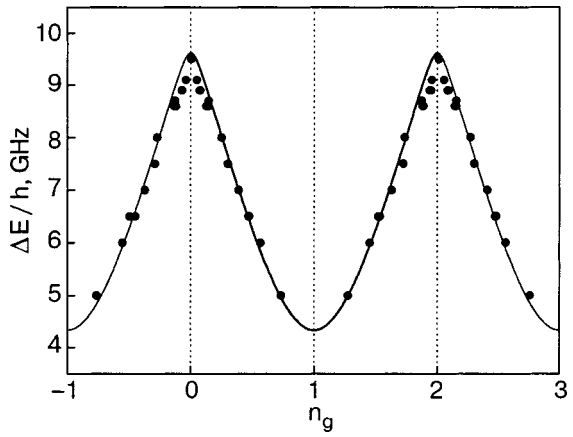

FIG. 8. Energy gap Δ between the ground and upper bands of the transistor determined from the experimental data for the case $\delta=\pi$. Some examples of these data are shown in Fig. 7. The dots represent the experimental data, and the solid line corresponds to the fit (cf. text).

to the charge qubit and compare it with experimental results obtained by IMT.[32] The principle of resonant spectroscopy is very simple. If the qubit is irradiated by microwaves with frequency corresponding to the energy gap between ground $(n=0)$ and upper level $(n=1)$, the latter level becomes populated also. In this sense the microwave irradiation acts like temperature, i.e., suppresses the tank phase shift (see Eq. (18)).

Similarly to the phase qubits, the interferometer-type charge qubit was fabricated out of Al by the conventional shadow evaporation technique and was placed in the middle of the Nb coil by making use of a flip-chip configuration. The geometric loop inductance of the interferometer was calculated to be $L_q=0.8$ nH. The layout size of the junctions was 140×180 nm. Deviations from the nominal dimensions caused by the fabrication process were estimated from the micrograph of the real structure and found to be less than 15%. The charging energy was overestimated within the framework of the plate capacitor model from the junctions delivering $E_C\simeq7$ GHz. In fact and also in accordance with the experimental results below, this value is reduced due to the strong tunneling regime.[31] The measurements were performed at a mixing chamber temperature of 10 mK.

The presence of the microwave power significantly changes the obtained dependence, namely, peaks appear in the $\chi(n_g)$ curve (see the upper curves in Fig. 7). The peak position depends on the microwave frequency and does not depend on the amplitude (the shape depends slightly). These peaks disappear when the phase bias is far from π as well as at higher temperatures. Therefore, we believe that they correspond to the excitation of the system from the ground to the upper state.

The microwave-induced transition (both the frequency of the microwave and the phase difference across the transistor, $\varphi=\pi$, are fixed) from the ground to the upper state occurs only at certain value of the gate charge. From the position of the peaks on the $\chi(n_g)$ curves at different frequencies of the microwave, we have reconstructed the energy difference between ground and upper states as a function of the quasicharge on the island. The obtained dependence is shown in Fig. 8. We fitted the experimental data by using the numerical solution of the energy spectrum of the Hamiltonian matrix (26). The best fitting parameters were found to be $\varepsilon_J(\pi)=4.4$ GHz and $E_C=2.2$ GHz. This value of the Josephson coupling energy is in very good agreement with the estimated value, and, as expected, the charging energy is smaller than estimated.

5. NONRESONANT SPECTROSCOPY OF TWO COUPLED QUBITS

After the successful demonstration of quantum coherence in many types of superconducting qubits, an observation of entangled states in two coupled qubits presents the next step on the road to the quantum processor. Entangled states were recently observed in both the charge[33] and the current-biased Josephson junction[34] qubits. In this Section we demonstrate that entangled states in a system of two inductively coupled flux qubits[35] can be detected by the IMT.[36]

The system of two Al flux qubits inductively coupled to each other and to the Nb tank is shown in Fig. 9. The area of each qubit and the self-inductance and critical current were $S_q=80\ \mu\text{m}^2$, $L_q=39$ pH, and $I_c\approx400$ nA, respectively, and $E_C\approx3.2$ GHz. The mutual inductance between the qubits

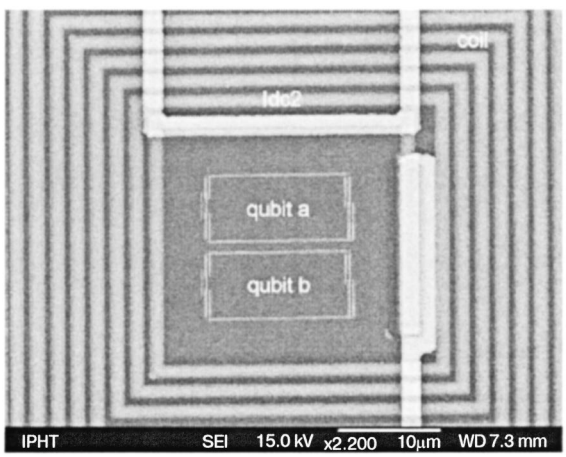

FIG. 9. Micrograph of the two-qubit system coupled to a resonant tank circuit.

$M_{ab}=2.7$ pH was estimated numerically from the electron micrograph. The magnetic flux through the qubits was created by the dc component of the current in the coil I_{dc1} and by the bias current I_{dc2} through a wire close to one of the qubits. This allowed independent control of the bias in each qubit. The system of Fig. 9 is described by the Hamiltonian $H=H_0+H_T+H_{\rm int}+H_{\rm diss}$, where the two-qubit Hamiltonian in the two-state approximation is expressed as[8]

$$H_0=-\Delta_a\sigma_x^{(a)}-\Delta_b\sigma_x^{(b)}+\varepsilon_a\sigma_z^{(a)}+\varepsilon_b\sigma_z^{(b)}+J\sigma_z^{(a)}\sigma_z^{(b)}, \tag{28}$$

H_T is the tank Hamiltonian (a harmonic oscillator), the qubit–tank interaction is

$$H_{\rm int}=-(\lambda_a\sigma_z^{(a)}+\lambda_b\sigma_z^{(b)})I_T, \tag{29}$$

and $H_{\rm diss}$ describes the standard weak coupling of the qubits to a dissipative bath.[37]

Here the coefficients are $\lambda_{a/b}=M_{a/b,T}I_{a/b}$, where $M_{a/b,T}$ is the qubit–tank mutual inductance, $L_{a/b}$ is the self-inductance, and $I_{a/b}$ is the amplitude of the persistent current in the corresponding qubit. In the standard two-state approximation, the qubit current operators are $\hat{I}_{a/b}=I_{a/b}\sigma_z^{(a/b)}$. The qubit biases are given by $\epsilon_a=I_a\Phi_0(f_x-0.5+f_{\rm shift})$, $\epsilon_b=I_b\Phi_0(f_x-0.5+\eta f_{\rm shift})$, where the dimensionless flux $f_x\sim I_{dc1}$ describes the field created by the niobium coil in both qubits, while the parameters $f_{\rm shift}\sim I_{dc2}$ and $\eta=M_{bw}/M_{aw}<1$ give the bias difference between the qubits created by the additional wire. Here M_{aw} (M_{bw}) are the mutual inductances between the a (b) qubit and the additional dc wire (for our sample, M_{aw} and M_{bw} were calculated numerically, yielding $\eta=0.32$). The qubit–qubit coupling constant $J=M_{ab}I_aI_b$ is positive because the two qubits are in the same plane side to side, leading to antiferromagnetic coupling (according to the north-to-south attraction law).

The application of the IMT for spectroscopy of two coupled qubits, similar to the single-qubit problem (see Sec. 2), can be conveniently discussed in terms of their magnetic susceptibility χ_{zz}. In the linear-response approximation the magnetic susceptibility $\chi_{zz}(\omega)$ of the two-qubit system is expressed in terms of retarded Green's functions of the qubit operators $\sigma_z^{(a/b)}$, calculated with the equilibrium density matrix $\rho=e^{(F-H_0)/T}$, with H_0 as in Eq. (28). It can be generally assumed that the latter's eigenvalues E_μ, $\mu=1,2,3,4$ are nondegenerate and its eigenstates orthonormalized, $\langle\nu|\mu\rangle=\delta_{\mu\nu}$. Taking into account the qubits' interaction with a dissipative environment,[17,38] we derive

$$\chi_{zz}(\omega)=-\sum_{\mu\neq\nu}\frac{\rho_\mu-\rho_\nu}{\omega+E_\mu-E_\nu+i\Gamma_{\mu\nu}}P_{\mu\nu}, \tag{30}$$

$$\tan\chi=-2\frac{Q_T}{L_T}\sum_{\mu<\nu}\frac{\rho_\mu-\rho_\nu}{E_\nu-E_\mu}P_{\mu\nu}, \tag{31}$$

where $\rho_\mu=\exp(-E_\mu/T)/Z$ is the thermal population of the μth energy level, $Z=\Sigma_\nu\exp(-E_\nu/T)$, $\Gamma_{\mu\nu}$ are the decoherence rates of the double-qubit system, and

$$\begin{aligned}P_{\mu\nu}=&\lambda_a^2\langle\mu|\sigma_z^{(a)}|\nu\rangle\langle\nu|\sigma_z^{(a)}|\mu\rangle+\lambda_b^2\langle\mu|\sigma_z^{(b)}|\nu\rangle\\&\times\langle\nu|\sigma_z^{(b)}|\mu\rangle+\lambda_a\lambda_b\langle\mu|\sigma_z^{(a)}|\nu\rangle\langle\nu|\sigma_z^{(b)}|\mu\rangle\\&+\lambda_a\lambda_b\langle\mu|\sigma_z^{(b)}|\nu\rangle\langle\nu|\sigma_z^{(a)}|\mu\rangle.\end{aligned} \tag{32}$$

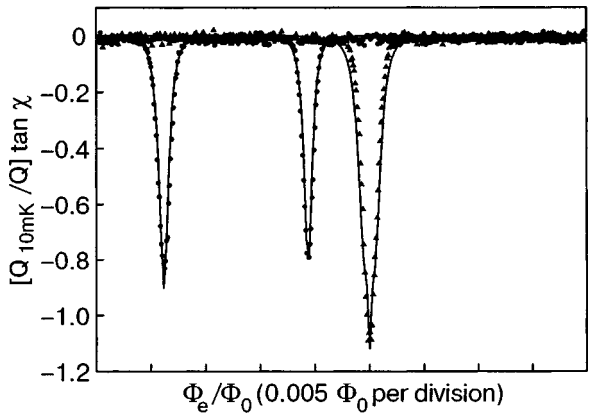

FIG. 10. Normalized tangent of the current–voltage angle χ in the tank versus external flux bias Φ_e at 50 mK. A relative flux bias $f_{\rm shift}$ between the qubits is created by changing the current I_{dc2} in the additional wire. The shifted curves correspond to $I_{dc2}=27.3$ μA, while the central curve is for $I_{dc2}=-2.7$ μA. The experimental data are denoted by the dots ($I_{dc2}=27.3$ μA) and triangles ($I_{dc2}=-2.7$ μA). The solid curves correspond to the theoretical fit.

At low frequencies $\omega=\omega_T\ll|E_\mu-E_\nu|$ and in a weak damping regime, $\Gamma_{\mu\nu}\ll|E_\mu-E_\nu|$, the decoherence rates $\Gamma_{\mu\nu}$ have no effect on $\tan\chi$ but are responsible for an equilibrium distribution in the system.

The first two terms in Eq. (32) are nonzero even if the two-qubit states are factorized. The first (second) term corresponds to the contribution of qubit a (b) and is nonzero near the qubit's degeneracy point. These contributions are practically independent of whether the qubits' degeneracy points coincide or not.

The second line in Eq. (32) describes coherent flipping of both qubits, which is only possible for nonfactorizable (entangled) eigenstates $|\mu\rangle,|\nu\rangle$. Therefore the difference between the coinciding IMT dip of the two qubits and the sum of two single-qubit IMT dips provides a measure of how coherent is the two-qubit dynamics (that is, whether entangled eigenstates of the two-qubit Hamiltonian Eq. (32) are formed). This is a necessary condition for the system to be in an entangled (pure or mixed) state.

The measurement results are shown in Fig. 10. Comparison of the single-qubit dips with the coincident IMT dip shows clearly that the contribution to $\tan\chi$ from the entangled eigenstates is significant. Indeed, the amplitude of the central dip in Fig. 10 at $T=50$ mK is 1.12, compared to a value of 1.69 for the sum of the single-qubit dips. This means that the entangled terms (the second line in Eq. (32)) are responsible for a negative contribution of ≈-0.57 to $\tan\chi$.

At 50 mK the temperature is comparable to the characteristic energies in the two-qubit system (at the two-qubit degeneracy point the gap between the ground state and top excited state is $\sim$100 mK). Since the characteristic measurement time in our approach is dictated by the much smaller tank frequency, ω_T, the system will have time to equilibrate. Indeed, the excellent quantitative agreement between the experiment (Fig. 10) and the theory Eq. (31) confirms that the system is described by the equilibrium density matrix with the Hamiltonian Eq. (28) (all the parameters of which we determined from the experiment). In other words, our system is an equilibrium mixture of entangled two-qubit states.

SUMMARY

We have shown that interferometer-type superconducting qubits can be characterized by making use of the impedance measurement technique. Moreover, weak continuous quantum measurements can be performed with this method.

We are grateful to our colleagues M. H. S. Amin, Ya. S. Greenberg, H. E. Hoenig, U. Hübner, A. Maassen van den Brink, T. May, V. I. Shnyrkov, and I. N. Zhilyaev for their help and contribution to this work at different stages.

Helpful discussions with D. V. Averin, G. Blatter, M. Feigel'man, M. V. Fistul, V. B. Geshkenbein, A. J. Leggett, Yu. Makhlin, A. N. Omelyanchouk, A. Shnirman, P. C. E. Stamp, S. Uchaikin, A. V. Ustinov, A. D. Zaikin, and A. B. Zorin are gratefully acknowledged.

*E-mail: ilichev@ipht-jena.de

[1] D. V. Averin, in *Quantum Noise in Mesoscopic Physics*, Yu. V. Nazarov (ed.), Kluwer (2003).
[2] A. O. Caldeira and A. J. Leggett, Ann. Phys. (N.Y.) **149**, 374 (1983).
[3] J. Clarke, A. N. Cleland, M. H. Devoret, D. Estive, and J. M. Martinis, Science **239**, 992 (1988).
[4] R. Rouse, S. Han, and J. E. Lukens, Phys. Rev. Lett. **75**, 1614 (1995).
[5] J. R. Friedman, V. Patel, W. Chen, S. K. Tolpygo, and J. E. Lukens, Nature (London) **406**, 43 (2000).
[6] C. H. van der Wal, A. C. J. ter Haar, F. K. Wilhelm, R. N. Schouten, C. J. P. M. Harmans, T. P. Orlando, S. Lloyd, and J. E. Mooij, Science **290**, 773 (2000).
[7] J. E. Mooij, T. P. Orlando, L. Levitov, L. Tian, C. H. van der Wal, and S. Lloyd, Science **285**, 1036 (1999).
[8] A. Maassen van den Brink, cond-mat/0310425.
[9] L. D. Landau, Z. Phys. **2**, 46 (1932); C. Zener, Proc. R. Soc. London, Ser. A **137**, 696 (1932).
[10] E. Il'ichev, Th. Wagner, L. Fritzsch, J. Kunert, V. Schultze, T. May, H. E. Hoenig, H.-G. Meyer, M. Grajcar, D. Born, W. Krech, M. V. Fistul, and A. M. Zagoskin, Appl. Phys. Lett. **80**, 4184 (2002).
[11] A. H. Silver and J. E. Zimmerman, Phys. Rev. B **157**, 317 (1967).
[12] N. Oukhanski, M. Grajcar, E. Il'ichev, and H.-G. Meyer, Rev. Sci. Instrum. **74**, 1145 (2003).
[13] A. Izmalkov, M. Grajcar, E. Il'ichev, N. Oukhanski, Th. Wagner, H.-G. Meyer, W. Krech, M. H. S. Amin, A. Maassen van den Brink, and A. M. Zagoskin, Europhys. Lett. **65**, 844 (2004).
[14] E. Il'ichev, V. Zakosarenko, L. Fritsch, R. Stolz, H. E. Hoenig, H.-G. Meyer, M. Götz, A. B. Zorin, V. V. Khanin, and A. B. Pavolotsky, and J. Niemeyer, Rev. Sci. Instrum. **72**, 1882 (2001).
[15] Ya. S. Greenberg, A. Izmalkov, M. Grajcar, E. Il'ichev, W. Krech, H.-G. Meyer, M. H. S. Amin, and A. Maassen van den Brink, Phys. Rev. B **66**, 214525 (2002).
[16] M. Grajcar, A. Izmalkov, E. Il'ichev, Th. Wagner, N. Oukhanski, U. Hübner, T. May, I. Zhilyaev, H. E. Hoenig, Ya. S. Greenberg, V. I. Shnyrkov, D. Born, W. Krech, H.-G. Meyer, and A. Maassen van den Brink, and M. H. S. Amin, Phys. Rev. B **69**, 060501 (R) (2004).
[17] A. Yu. Smirnov, Phys. Rev. B **68**, 134514 (2003).
[18] The fact that tan χ is proportional to the magnetic susceptibility has been used previously for investigation of the magnetic responce of ''classical'' Josephson samples—see E. Il'ichev, F. Tafuri, M. Grajcar, R. P. J. IJsselsteijn, J. Weber, F. Lombardi, and J. R. Kirtley, Phys. Rev. B **68**, 014510 (2003).
[19] Y. Nakamura, Yu. A. Pashkin, and J. S. Tsai, Phys. Rev. Lett. **87**, 246601 (2001).
[20] D. Vion, A. Aassime, A. Cottet, P. Joyez, H. Pothier, C. Urbina, D. Esteve, and M. H. Devoret, Science **296**, 886 (2002).
[21] J. M. Martinis, S. Nam, J. Aumentado, and C. Urbina, Phys. Rev. Lett. **89**, 117901 (2002).
[22] I. Chiorescu, Y. Nakamura, C. J. P. M. Harmans, and J. E. Mooij, Science **299**, 1869 (2003).
[23] J. M. Raimond, M. Brune, and S. Haroche, Rev. Mod. Phys. **73**, 565 (2001).
[24] A. Yu. Smirnov, Phys. Rev. B **67**, 155104 (2003).
[25] E. Il'ichev, N. Oukhanski, A. Izmalkov, Th. Wagner, M. Grajcar, H.-G. Meyer, A. Yu. Smirnov, A. Maassen van den Brink, M. H. S. Amin, and A. M. Zagoskin, Phys. Rev. Lett. **91**, 097906 (2003).
[26] J. R. Freedman and D. V. Averin, Phys. Rev. Lett. **88**, 050403 (2002).
[27] A. B. Zorin, Physica C **368**, 284 (2002).
[28] W. Krech, M. Grajcar, D. Born, I. Zhilyaev, Th. Wagner, E. Il'ichev, and Ya. Greenberg, Phys. Lett. A **303**, 352 (2002).
[29] D. V. Averin and K. K. Likharev, in *Mesoscopic Phenomena in Solids*, B. L. Altshuler, P. A. Lee, and A. Webb (eds.), Elsevier, Amsterdam (1991), p. 173.
[30] M. Tinkham, *Introduction to Superconductivity*, McGraw-Hill, New York (1996), p. 276.
[31] A. I. Larkin and Yu. N. Ovchinnikov, Phys. Rev. B **28**, 6281 (1983); G. Schön and A. D. Zaikin, Phys. Rep. **198**, 237 (1990).
[32] D. Born, V. I. Shnyrkov, W. Krech, Th. Wagner, E. Il'ichev, U. Hübner, and H.-G. Meyer, cond-mat/0312696.
[33] Yu. A. Pashkin, T. Yamamoto, O. Astafiev, Y. Nakamura, D. V. Averin, and J. S. Tsai, Nature (London) **421**, 823 (2003).
[34] A. J. Berkley, H. Xu, R. C. Ramos, M. A. Gubrid, F. W. Strauch, P. R. Johnson, J. R. Anderson, A. J. Dragt, C. J. Lobb, and F. C. Wellstood, Science **300**, 1548 (2003).
[35] J. B. Majer, F. G. Paauw, A. C. J. ter Haar, C. J. P. M. Harmans, and J. E. Mooij, cond-mat/0308192.
[36] A. Izmalkov, M. Grajcar, E. Il'ichev, Th. Wagner, H.-G. Meyer, A. Yu. Smirnov, M. H. S. Amin, A. Maassen van den Brink, and A. M. Zagoskin, cond-mat/0312332.
[37] U. Weiss, *Quantum Dissipative Systems*, 2nd ed., World Scientific, Singapore (1999).
[38] A. Yu. Smirnov, cond-mat/0312635.

This article was published in English in the original Russian journal. Reproduced here with stylistic changes by AIP.

Spin and current variations in Josephson junctions

A. Shnirman*

Institut für Theoretische Festkörperphysik, Universität Karlsruhe, D-76128 Karlsruhe, Germany

Z. Nussinov, Jian-Xin Zhu, and A. V. Balatsky

Theoretical Division, Los Alamos National Laboratory, Los Alamos, New Mexico 87545, USA

Yu. Makhlin

Institut für Theoretische Festkörperphysik, Universität Karlsruhe, D-76128 Karlsruhe, Germany; Landau Institute for Theoretical Physics, Kosygin Str. 2, 117940 Moscow, Russia

(Submitted February 2, 2004)
Fiz. Nizk. Temp. **30**, 834–840 (July–August 2004)

We study the dynamics of a single spin embedded in the tunneling barrier between two superconductors. As a consequence of pair correlations in the superconducting state, the spin displays rich and unusual dynamics. To properly describe the time evolution of the spin we derive the effective Keldysh action for the spin. The superconducting correlations lead to an effective spin action, which is nonlocal in time, leading to unconventional precession. We further illustrate how the current is modulated by this novel spin dynamics. © *2004 American Institute of Physics.* [DOI: 10.1063/1.1789934]

INTRODUCTION

The analysis of spins embedded in Josephson junctions has had a long and rich history. Early on, Kulik[1] argued that spin flip processes in tunnel barriers reduce the critical Josephson current as compared to the Ambegaokar—Baratoff limit.[2] More than a decade later, Bulaevskii *et al.*[3] conjectured that π-junctions may be formed if spin flip processes dominate. The competition between the Kondo effect and the superconductivity was elucidated in Ref. 4. Transport properties formed the central core of these and many other pioneering works, while spin dynamics was relegated to a relatively trivial secondary role. In the present article, we report on new nonstationary spin dynamics and illustrate that the spin is affected by the Josephson current. As a consequence of the Josephson current, spins exhibit novel nonplanar precessions while subject to the external magnetic field. A spin in a magnetic field exhibits circular Larmor precession about the direction of the field. As we report here, when the spin is further embedded between two superconducting leads, new out-of-plane longitudinal motion, much like that displayed by a mechanical top, will arise. We term this new effect the Josephson nutation. We further outline how transport is, in turn, modulated by this rather unusual spin dynamics. Our predictions are within experimental reach, and we propose a detection scheme.

THE SYSTEM

The system under consideration is illustrated in Fig. 1. It consists of two identical ideal s-wave superconducting leads coupled each to a single spin; the entire system is further subject to a weak external magnetic field. In Fig. 1, $\mu_{L,R}$ denote the chemical potentials of the left and right leads, **B** is a weak external magnetic field along the z axis, and $\mathbf{S}=(S_x,S_y,S_z)$ is the operator of the localized spin.

The Hamiltonian of the system reads

$$\mathcal{H}=\mathcal{H}_0+\mathcal{H}_T, \quad \mathcal{H}_0=\mathcal{H}_L+\mathcal{H}_R-\mu B_z S_z, \tag{1}$$

$$\mathcal{H}_T=\sum_{\mathbf{k},\mathbf{p},\alpha,\alpha'} e^{i\varphi/2} c^{\dagger}_{R\mathbf{k}\alpha}[T_0\delta_{\alpha\alpha'}+T_1\boldsymbol{\sigma}_{\alpha\alpha'}\cdot\mathbf{S}]c_{L\mathbf{p}\alpha'}+\text{h.c.}, \tag{2}$$

where $\mathcal{H}_L$ and $\mathcal{H}_R$ are the Hamiltonians in the left and right superconducting leads, while $c^{\dagger}_{ik\alpha}$ ($c_{ik\alpha}$) creates (annihilates) an electron in the lead in the state $\mathbf{k}$ with spin α in the right (left) lead for $i=L(R)$. The vector $\boldsymbol{\sigma}$ represents the three Pauli matrices and μ is the magnetic moment of the spin. When a spin is embedded in the tunneling barrier, the conduction electron tunneling matrix, not too surprisingly, becomes spin-dependent: $\hat{T}=[T_0\hat{1}+T_1\mathbf{S}\cdot\hat{\boldsymbol{\sigma}}]$.[5,6] Here T_0 is a spin-independent tunneling matrix element and T_1 is a spin-dependent matrix element originating from the direct exchange coupling J of the conduction electron to the localized spin **S**. We take both tunneling matrix elements to be momentum independent. This is not a crucial assumption and is merely introduced to simplify the notation. Typically, from the expansion of the work function for tunneling, $T_1/T_0 \sim J/U$, where U is the height of a spin-independent tunneling barrier.[7] A weak external magnetic field $B_z \sim 100$ G does not influence the superconductors, and we may ignore its

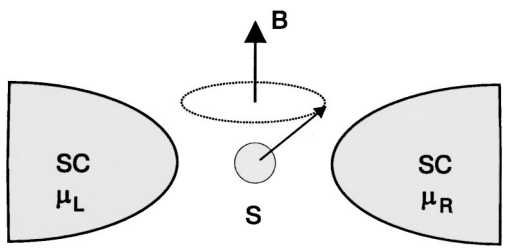

FIG. 1. Magnetic spin coupled to two superconducting leads.

effect on the leads. In what follows, we abbreviate μB_z by B. The operator $e^{i\varphi/2}$ is the single electron number operator. When the junction is linked to an external environment, the coupling between the junction and the environment induces fluctuation of the superconducting phase φ.

THE EFFECTIVE ACTION

Josephson junctions are necessarily embedded into external electrical circuits. This implies that the dynamics will explicitly depend on the superconducting phase φ. The evolution operator is given by the real-time path integral

$$Z=\int D\varphi D\mathbf{S}\exp[iS_{\text{circuit}}(\varphi)+iS_{\text{spin}}(\mathbf{S}) +iS_{\text{tunnel}}(\varphi,\mathbf{S})]. \tag{3}$$

The effective action S_{tunnel} describes the junction itself. We generalize the formerly known effective tunneling action for a spinless junction[8–10] to the spin-dependent arena to obtain

$$S_{\text{tunnel}}=-2\oint_K dt\oint_K dt'\alpha(t,t')[T_0^2+T_1^2\mathbf{S}(t)\cdot\mathbf{S}(t')] \times\cos\frac{\varphi(t)-\varphi(t')}{2}-2\oint_K dt\oint_K dt'\beta(t,t') \times[T_0^2-T_1^2\mathbf{S}(t)\cdot\mathbf{S}(t')]\cos\frac{\varphi(t)+\varphi(t')}{2}, \tag{4}$$

where

$$i\alpha(t,t')\equiv G(t,t')G(t',t),\quad i\beta(t,t')\equiv F(t,t')F^\dagger(t,t')$$

and the Green functions are

$$G(t,t')\equiv -i\sum_{\mathbf{k}}\langle T_K c_{\mathbf{k}\sigma}(t)c^\dagger_{\mathbf{k}\sigma}(t')\rangle, \tag{5}$$

$$F(t,t')\equiv -i\sum_{\mathbf{k}}\langle T_K c_{\mathbf{k}\uparrow}(t)c_{-\mathbf{k}\downarrow}(t')\rangle, \tag{6}$$

$$F^\dagger(t,t')\equiv -i\sum_{\mathbf{k}}\langle T_K c^\dagger_{\mathbf{k}\uparrow}(t)c^\dagger_{-\mathbf{k}\downarrow}(t')\rangle. \tag{7}$$

In Eq. (4) $\oint_K$ denotes integration along the Keldysh contour. We now express the spin action on the Keldysh contour in the basis of coherent states

$$S_{\text{spin}}=\oint_K dt\mathbf{B}\cdot\mathbf{S}+S_{WZNW}. \tag{8}$$

Here S denotes the magnitude of the spin $\mathbf{S}$. The second, Wess—Zumino—Novikov—Witten (WZNW), term in Eq. (8) depicts the Berry phase accumulated by the spin as a result of motion of the spin on a sphere of radius S.[11,12] Explicitly,

$$S_{WZNW}=\frac{1}{S^2}\int_0^1 d\tau\oint_K dt[\mathbf{S}(t,\tau)\cdot(\partial_\tau\mathbf{S}(t,\tau)\times\partial_t\mathbf{S}(t,\tau))]. \tag{9}$$

The additional integral over τ allows us to express the action in a local form. At $\tau=0$ the spin is set along the z direction at all times, $\mathbf{S}(t,0)=\text{const}$; at $\tau=1$ the spin field corresponds to the physical configurations, $\mathbf{S}(t,1)=\mathbf{S}(t)$.

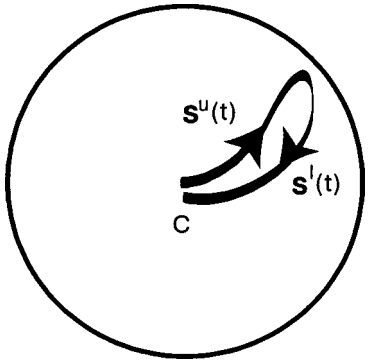

FIG. 2. The sphere of radius S for the vectors $\mathbf{S}^{u,l}(t)$ is shown. The path C describes the evolution of the spin along the upper (u) and lower (l) branches of the Keldysh contour. To properly describe the spin dynamics on this closed contour, we analyze the WZNW action; see Eq. (9). For clarity, we have drawn a small piece of the closed trajectories.

DYNAMICS

We now perform the Keldysh rotation, defining the values of the spin and the phase variables on the forward/backward branches of the Keldysh contour (see Fig. 2, $\mathbf{S}^{u,l}$ for the upper and lower branches) and rewriting all the expressions in terms of their average (classical component $\mathbf{S}$) and difference (quantum component $\mathbf{l}$):

$$\mathbf{S}\equiv(\mathbf{S}^u+\mathbf{S}^l)/2,\quad \mathbf{l}\equiv\mathbf{S}^u-\mathbf{S}^l,\quad \mathbf{S}\cdot\mathbf{l}=0. \tag{10}$$

After the Keldysh rotation we obtain[13,14]

$$S_{WZNW}=\frac{1}{S^2}\int_0^1 d\tau\int dt[\mathbf{S}^u(t,\tau)\cdot(\partial_\tau\mathbf{S}^u(t,\tau) \times(\partial_t\mathbf{S}^u(t,\tau))-(u\to l)]. \tag{11}$$

The relative minus sign stems from the backward time ordering on the return part of C. The individual WZNW phases for the upper (u) and lower (l) branches are given by the areas spanned by the trajectories $\mathbf{S}^{u,l}(t)$ on the sphere of radius S divided by the spin magnitude (S). The WZNW term contains odd powers of $\mathbf{l}$. Insofar as the WZNW term of Eq. (11) is concerned, the standard Keldysh transformation to the two classical and quantum fields, $\mathbf{S}$ and $\mathbf{l}$, mirrors the decomposition of the spin in an antiferromagnet (AF) to the two orthogonal slow and fast fields.[1)] The difference between the two individual WZNW terms in Eq. (11) is the area spanned between the forward and backward trajectories. For close forward and backward trajectories the WZNW action on the Keldysh loop may be expressed as

$$S_{WZNW}=\frac{1}{S^2}\int dt\mathbf{l}\cdot(\mathbf{S}\times\partial_t\mathbf{S}). \tag{12}$$

For the spin part of the (semiclassical) action we then obtain

$$S_{\text{spin}}=\int dt\mathbf{B}\cdot\mathbf{l}+\frac{1}{S^2}\int dt\mathbf{l}\cdot(\mathbf{S}\times\partial_t\mathbf{S}). \tag{13}$$

Next, we perform the Keldysh rotation to the classical and quantum components with respect to both the phase and spin variables in the tunneling part of the effective action. Towards this end, we introduce (with notation following Refs. 8 and 10)

$$\varphi=(\varphi^u+\varphi^d)/2,\quad \chi=\varphi^u-\varphi^d. \tag{14}$$

With these definitions in hand, the tunneling part of the action reads

$$S_{\text{tunnel}}=S_\alpha+S_\beta, \tag{15}$$

where the normal (quasi-particle) tunneling part S_α is expressed via the Green functions

$$\alpha^R\equiv\theta(t-t')(\alpha^>-\alpha^<);\quad \alpha^K(\omega)\equiv\alpha^>+\alpha^<,$$

where

$$i\alpha^>(t,t')\equiv G^>(t,t')G^<(t',t);$$

$$i\alpha^<(t,t')\equiv G^<(t,t')G^>(t',t).$$

Similarly the Josephson-tunneling part S_β is expressed via the off-diagonal Green's functions

$$\beta^R\equiv\theta(t-t')(\beta^>-\beta^<);\quad \beta^K(\omega)\equiv\beta^>+\beta^<,$$

where

$$i\beta^>(t,t')\equiv F^>(t,t')F^{\dagger>}(t,t');$$

$$i\beta^<(t,t')\equiv F^<(t,t')F^{\dagger<}(t,t').$$

In this paper we are interested in the interaction between the supercurrent and the spin. Thus we provide the expression for the Josephson part:

$$\begin{aligned}
S_\beta=&\int dt\int dt' 4\beta^R(t,t')\Bigg[\Bigg\{[2T_0^2-2T_1^2\mathbf{S}(t)\\
&\cdot\mathbf{S}(t')]\sin\frac{\chi(t)}{4}\cos\frac{\chi(t')}{4}-\frac{1}{2}T_1^2\mathbf{l}(t)\\
&\cdot\mathbf{l}(t')\cos\frac{\chi(t)}{4}\sin\frac{\chi(t')}{4}\Bigg\}\times\sin\frac{\varphi(t)+\varphi(t')}{2}\\
&+\Bigg\{T_1^2\mathbf{l}(t)\cdot\mathbf{S}(t')\cos\frac{\chi(t)}{4}\cos\frac{\chi(t')}{4}-T_1^2\mathbf{S}(t)\\
&\cdot\mathbf{l}(t')\sin\frac{\chi(t)}{4}\sin\frac{\chi(t')}{4}\Bigg\}\cos\frac{\varphi(t)+\varphi(t')}{2}\Bigg]\\
&+\int dt\int dt\beta^K(t,t')\Bigg[\Bigg\{[4T_0^2-4T_1^2\mathbf{S}(t)\\
&\cdot\mathbf{S}(t')]\sin\frac{\chi(t)}{4}\sin\frac{\chi(t')}{4}+T_1^2\mathbf{l}(t)\\
&\cdot\mathbf{l}(t')\cos\frac{\chi(t)}{4}\cos\frac{\chi(t')}{4}\Bigg\}\cos\frac{\varphi(t)+\varphi(t')}{2}\\
&-\Bigg\{2T_1^2\mathbf{l}(t)\cdot\mathbf{S}(t')\cos\frac{\chi(t)}{4}\sin\frac{\chi(t')}{4}+2T_1^2\mathbf{S}(t)\\
&\cdot\mathbf{l}(t')\sin\frac{\chi(t)}{4}\cos\frac{\chi(t')}{4}\Bigg\}\sin\frac{\varphi(t)+\varphi(t')}{2}\Bigg].
\end{aligned}\tag{16}$$

The normal-tunneling part S_α is obtained from S_β by the following substitution: $\beta^{R/K}(t,t')\to\alpha^{R/K}(t,t')$, $\varphi(t')\to-\varphi(t')$, and $\chi(t')\to-\chi(t')$. The Keldysh terms (those including β^K and α^K), which normally give rise to random Langevin terms (see, e.g., Ref. 10) are, in our case, suppressed at temperatures much lower than the superconducting gap ($T\ll\Delta$), due to the exponential suppression of the correlators $\beta^K(\omega)$ and $\alpha^K(\omega)$ at $\omega<\Delta$.

To obtain β^R, we start from the Gorkov Green functions

$$F^>(t,t')=-i\sum_k\frac{\Delta}{2E_k}e^{-iE_k(t-t')},$$

$$F^{>\dagger}(t,t')=i\sum_k\frac{\Delta}{2E_k}e^{-iE_k(t-t')}, \tag{17}$$

where the quasiparticle energy $E_k\equiv\sqrt{\Delta^2+\epsilon_k^2}$, ϵ_k being the free-conduction-electron dispersion in the leads. Putting all of the pieces together, we find that

$$\beta^R(t-t')=\theta(t-t')\sum_{k,p}\frac{\Delta^2}{2E_kE_p}\sin[(E_k+E_p)(t-t')]. \tag{18}$$

The kernel $\beta^R(t-t')$ decays on short time scales of order $O(\hbar/\Delta)$. Varying the total action with respect to the quantum components $\mathbf{l}$ and χ and setting these to zero, we obtain coupled equations of motion for both the spin and phase:

$$\begin{aligned}
\frac{d\mathbf{S}(t)}{dt}=&\mathbf{S}(t)\times\mathbf{B}+T_1^2\int dt' 4\beta^R(t-t')\mathbf{S}(t)\times\mathbf{S}(t')\\
&\times\cos\frac{\varphi(t)+\varphi(t')}{2},
\end{aligned}\tag{19}$$

$$\begin{aligned}
\left.\frac{\delta S_{\text{circuit}}}{\delta_\chi(t)}\right|_{\chi\to0}=&-\int dt' 2\beta^R(t-t')(T_0^2-T_1^2\mathbf{S}(t)\cdot\mathbf{S}(t'))\\
&\times\sin\frac{\varphi(t)+\varphi(t')}{2}.
\end{aligned}\tag{20}$$

Note that if the rest of the circuit contains dissipative elements, e.g., resistors, then S_{circuit} will contain the nonvanishing Keldysh components, the corresponding Langevin terms should be included in Eq. (20). The rather complicated equations of motion (19) and (20) are very general. To make headway, we now adopt a perturbative strategy. In Eq. (19), we first assume an ideal voltage bias, i.e., an imposed phase $\varphi(t)=\omega_J t$, where the "Josephson frequency" $\omega_J=2eV/\hbar$. To this lowest order, we neglect the influence of the spin on the phase. Next, we use the separation of characteristic time scales to our advantage. To this end, we note that the spin dynamics is much slower as compared to electronic processes, i.e., ω_J, $B\ll\Delta$. This separation of scales allows us to set $\mathbf{S}(t')\simeq\mathbf{S}(t)+(t-t')d\mathbf{S}/dt$ in the integrand of Eq. (19), whereby we obtain

$$\frac{d\mathbf{S}}{dt}=\lambda\mathbf{S}\times\frac{d\mathbf{S}}{dt}\sin\omega_J t+\mathbf{S}\times\mathbf{B}. \tag{21}$$

Here

$$\lambda = -4T_1^2\int_0^\infty dt\, t\beta^R(t)\sin\frac{\omega_J t}{2} \approx -2T_1^2\omega_J\int_0^\infty dt\; t^2\beta^R(t)$$
$$= 2\omega_J\sum_{k,p}\frac{|\Delta|^2|T_1|^2}{E_kE_p(E_k+E_p)^3}$$
$$= 2T_1^2\rho^2\frac{\omega_J}{\Delta}\int\int\frac{dz_1dz_2}{(\cosh z_1+\cosh z_2)^3}$$
$$= \frac{\pi^2}{8}T_1^2\rho^2\frac{\omega_J}{\Delta} = \frac{g_1}{32}\frac{\omega_J}{\Delta} \tag{22}$$

with $g_1 \equiv (2\pi T_1\rho)^2$ being the spin channel conductance. In Eq. (22) we employ the separation of time scales ($\omega_J \ll \Delta$) again. When expressed in the spherical coordinates (in the semiclassical limit) $\mathbf{S} = S(\sin\theta\cos\varphi, \sin\theta\sin\varphi, \cos\theta)$, Eq. (21) transforms into two simple first-order differential equations:

$$\frac{d\varphi}{dt} = -\frac{B}{1+S^2\lambda^2\sin^2(\omega_J t)}, \tag{23}$$

$$\frac{d\theta}{dt} = -S\lambda\frac{d\varphi}{dt}\sin\theta\sin\omega_J t. \tag{24}$$

These equations can be solved exactly. For a spin oriented at time $t=0$ at an angle θ_0 relative to $\mathbf{B}$,

$$\varphi(t) = -\frac{B}{\omega_J\sqrt{1+S^2\lambda^2}}\tan^{-1}[\sqrt{1+S^2\lambda^2}\tan(\omega_J t)],$$

$$\theta(t) = 2\tan^{-1}\left(\left[\frac{(1-c\cos(\omega_J t))(1+c)}{(1+c\cos(\omega_J t))(1-c)}\right]^\gamma\tan\frac{\theta_0}{2}\right),$$

with $c = S\lambda/\sqrt{1+S^2\lambda^2}$ and $\gamma = -S\lambda B/2\omega_J c$. For $S\lambda \ll 1$ we have $\varphi \simeq -Bt$ and $\theta \simeq \theta_0 - S\lambda(B/\omega_J)\sin\theta_0\cos\omega_J t$. Typically, whenever a spin is subjected to a uniform magnetic field, the spin precesses azimuthally with the Larmor frequency $\omega_L = B$. In a Josephson junction, however, the spin exhibits additional polar (θ) displacements. The resulting dynamics may be likened to that of a rotating rigid top. The Josephson current leads to a nonplanar gyroscopic motion (Josephson nutations) of the spin much like that generated by torques applied to a mechanical top. For small λ we find nutations (see Fig. 3) of amplitude

$$\theta_1 - \theta_2 \propto S\lambda\frac{B}{\omega_J}\sin\theta \propto Sg_1\frac{B}{\Delta}\sin\theta.$$

The origin of the first term on the right-hand side of Eq. (21) can be understood as follows (this origin can be also traced in the calculations): the spin is subject to the electron-induced fluctuating field $\mathbf{h} = T_1\Sigma e^{i\varphi/2}c^\dagger\boldsymbol{\sigma}c + \text{h.c.}$ The same coupling may be thought of as an influence of the spin on the leads, which results in a nonzero low-frequency contribution $\delta\mathbf{h}$ to $\mathbf{h}$. Since the response function of the electron liquid is isotropic but retarded, $\delta\mathbf{h}(t)$ is not aligned with $\mathbf{S}(t)$ but contains information about the values of $\mathbf{S}(t')$ at earlier times. The response function decays on a time scale $\sim\hbar/\Delta$, much shorter than the period of the spin precession, $\sim 1/B$.

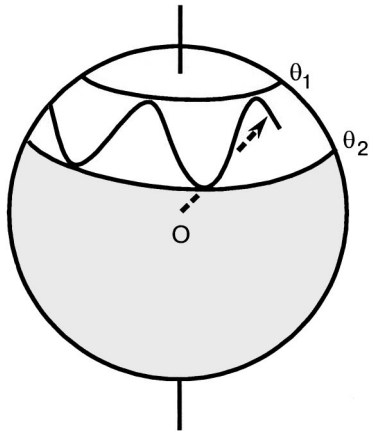

FIG. 3. The resulting spin motion on the unit sphere in the general case. As in the motion of classical spinning top, the spin exhibits undulations along the polar direction.

As a consequence, in addition to a contribution $\propto\mathbf{S}$ the field $\mathbf{h}$ acquires a component $\propto\dot{\mathbf{S}}/\Delta$, which leads to the first term on the right-hand side of Eq. (21).

The right-hand side of the second equation of motion (20) clearly corresponds to the Josephson current. Indeed, in the Keldysh formalism one has $I = (2\pi/\Phi_0)\partial S/\partial\chi$ (instead of $I = (2\pi/\Phi_0)\partial S/\partial\varphi$). Thus we obtain for the Josephson current

$$I_J(t) = \frac{2\pi}{\Phi_0}\int dt'\,2\beta^R(t-t')(T_0^2 - T_1^2\mathbf{S}(t)\cdot\mathbf{S}(t'))$$
$$\times\sin\frac{\varphi(t)+\varphi(t')}{2}. \tag{25}$$

We start from the lowest-order (local in time) adiabatic approximation, i.e., we set $\mathbf{S}(t) = \mathbf{S}(t')$ and $\varphi(t) = \varphi(t')$. This yields

$$I_J(t) = \frac{2\pi}{\Phi_0}E_{J,0}\left(1 - \frac{T_1^2}{T_0^2}\mathbf{S}^2\right)\sin\varphi(t), \tag{26}$$

where $E_{J,0} \equiv 2T_0^2\int dt\beta^R(t) = \pi^2\rho^2T_0^2\Delta = (1/4)g_0\Delta$ is the spin-independent Josephson energy[2] (g_0 being the conductance of the spin-independent channel). The second term of Eq. (26) gives the spin-related reduction of the Josephson critical current studied in Ref. 1. We now evaluate the lowest-order correction to this equation due to deviations from locality in time and spin precessions. Expanding $\mathbf{S}(t')$ in Eq. (25) in $(t'-t)$ and using the fact that for the Larmor precession we have $\mathbf{S}\cdot\dot{\mathbf{S}} = 0$ and $\mathbf{S}\cdot\ddot{\mathbf{S}} = B^2(S_z^2 - \mathbf{S}^2)$, we find a correction to the Josephson current which depends on S_z^2:

$$I_J(t) = \frac{2\pi}{\Phi_0}\left[E_{J,0}\left(1 - \frac{T_1^2}{T_0^2}\mathbf{S}^2\right) + \delta E_J(S_z^2 - \mathbf{S})\right]\sin\varphi(t), \tag{27}$$

where

$$\delta E_J \equiv -T_1^2B^2\int dt\beta^R(t)t^2 = \frac{\pi^2}{16}T_1^2\rho^2(B^2/\Delta).$$

Here we have clearly elucidated the manner in which the spin dynamics alters the Josephson current.

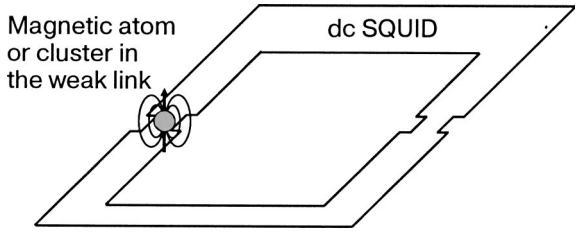

FIG. 4. A SQUID-based detection scheme. The SQUID monitors the magnetic field produced by the magnetic cluster in one of the junctions.

For $S=1/2$ the semiclassical approximation is insufficient. In this case it is easier to perform a calculation with spin operators,[13] rather than a path integral. One then obtains[13] an expression for the Josephson current identical to Eq. (25) but with $\mathbf{S}(t)$ being the spin operator in the interaction representation. Using the commutation relations of the spin operators, one obtains an extra contribution to the Josephson current proportional to S_z. This permits reading out of the spin state via the Josephson current. This extra contribution scales as S while the spin-dependent contributions in Eq. (27) scale as S^2.

DETECTION

We now briefly discuss a detection scheme for the Josephson nutations for $S\gg 1$, e.g., in the semiclassical limit. In principle the nutations should affect the Josephson current. The level of approximation employed in this paper was, however, insufficient to describe this effect. Indeed, one has to substitute $\mathbf{S}(t)$ containing the nutations into Eq. (25). As the amplitude of the nutations is of the order g_1, the correction to the current will be of the order g_1^2. We will study this correction elsewhere. Here we discuss a more direct detection strategy. The spin motion generates a time-dependent magnetic field,

$$\delta\mathbf{B}(\mathbf{r},t)=\frac{\mu_0}{4\pi r^5}[3\mathbf{r}(\mathbf{r}\cdot\mathbf{m}(t))-r^2\mathbf{m}(t)],$$

superimposed on the constant external field $\mathbf{B}$. Here $\mathbf{r}$ is the position relative to the spin, with magnetic moment $\mathbf{m}(t)=\mu\mathbf{S}(t)$. A ferromagnetic cluster of spin $S=100$ generates a detectable field $\delta B\sim 10^{-10}$ T which appears a micron away from the spin. For a SQUID loop of micron dimensions located at that position, the corresponding flux variation $\delta\Phi\sim 10^{-7}\Phi_0$ (Φ_0 is the flux quantum) are within reach of modern SQUIDs. For such a setup with $T_1/T_0\sim 0.1$, the typical critical Josephson current is $J_S^{(0)}\sim 10\ \mu$A, $|\Delta|=1$ MeV, and $eV\sim 10^{-3}|\Delta|$. We find that $\lambda S\sim 0.1$. Since $S_x=S\sin\theta\cos\varphi$, $S_y=S\sin\theta\sin\varphi$, the spin components orthogonal to $\mathbf{B}$ vary, to first order in (λS), with Fourier components at frequencies $|\omega_L\pm\omega_J|$ ($\omega_L=B$), leading to a discernible signal in the magnetic field $\mathbf{B}+\delta\mathbf{B}$. For a field $B\sim 200$ G one has $\omega_L\sim 560$ MHz, and a new side band will appear at $|\omega_L-\omega_J|$, whose magnitude may be tuned to 10–100 MHz. This measurable frequency is markedly different from the Larmor frequency ω_L.

The efficiency of the detector may be further improved by embedding the spin in one of the Josephson junctions of the SQUID itself. The setup is sketched in Fig. 4. The Josephson junction containing the spin is used both for driving the nutations and, together with the second junction of the SQUID, for detecting them.

CONCLUSION

In this article we have illustrated that the dynamics of a spin embedded in a Josephson junction is richer than appreciated hitherto. We have reported unusual nonplanar spin motion (in a static field), which might be probed directly and which was further shown to influence the current in the Josephson junction. Using a path-integral formalism, we described this nonplanar spin dynamics and the ensuing current variations that it triggers. To describe the time evolution we derived the effective action for a spin of arbitrary amplitude S on the Keldysh contour. In passing, we noted a similarity between the resultant effective action and that encountered in quantum antiferromagnetic spin chains. Our central results are encapsulated in the effective action (16).

In the semiclassical limit of large S, relevant to ferromagnetic spin clusters,[14] we obtained two coupled equations of motion (Eqs. (19) and (20)). These equations may be solved perturbatively, as outlined above, or numerically. We presented an exact limiting-case solution and illustrated how the new spin dynamics may be experimentally probed.

The formalism developed can also be applied to the minimal $S=1/2$ system. In this case, however, it is simpler to perform a calculation with spin operators[13] rather than a path integral.

This work was supported by the US Department of Energy under LDRD X1WX, the CFN of the DFG, and the S. Kovalevskaya Award (Y. M.). We thank L. N. Bulaevskii and G. Schön for discussions.

*E-mail: shnirman@tfp.uni-karlsruhe.de

[1)] These two orthogonal AF fields represent (i) the slowly varying staggered spin field (the antiferromagnetic staggered moment **m** taking on the role of **S** and (ii) the rapidly oscillating uniform spin field **l** (paralleling our **l**). In the antiferromagnetic correspondence, the two forward time spin trajectories at two nearest neighbor AF sites become the two forward (u) and backward (l) single spin trajectories of the nonequilibrium problem. This staggered doubling correspondence is general.

[1] I. O. Kulik, Sov. Phys. JETP **22**, 841 (1966).
[2] V. Ambegaokar and A. Baratoff, Phys. Rev. Lett. **10**, 486 (1963).
[3] L. N. Bulaevskii, V. V. Kuzii, and A. A. Sobyanin, JETP Lett. **25**, 290 (1977).
[4] L. I. Glazman and K. A. Matveev, JETP Lett. **49**, 659 (1989).
[5] A. V. Balatsky and I. Martin, Quan. Inform. Process. **1**, 53 (2002).
[6] A. V. Balatsky, Y. Manassen, and R. Salem, Phys. Rev. B **66**, 195416 (2002).
[7] J. X. Zhu and A. V. Balatsky, Phys. Rev. B **67**, 174505 (2003).
[8] V. Ambegaokar, U. Eckern, and G. Schön, Phys. Rev. Lett. **48**, 1745 (1982).
[9] A. I. Larkin and Y. N. Ovchinnikov, Phys. Rev. B **28**, 6281 (1983).
[10] U. Eckern, G. Schön, and V. Ambegaokar, Phys. Rev. B **30**, 64191 (1984).
[11] E. Fradkin, *Field Theories of Condensed Matter Systems*, Addison-Wesley, Redwood City (1991).
[12] S. Sachdev, *Quantum Phase Transitions*, Cambridge University Press, London (1999).
[13] L. N. Bulaevskii, M. Hruška, A. Shnirman, D. Smith, and Y. Makhlin, Phys. Rev. Lett. **92**, 177001 (2004).
[14] J. X. Zhu, Z. Nussinov, A. Shnirman, and A. V. Balatsky, Phys. Rev. Lett. **92**, 107001 (2004).

This article was published in English in the original Russian journal. Reproduced here with stylistic changes by AIP.

Topologically protected quantum states and quantum computing in Josephson junctions arrays

L. B. Ioffe

Center for Materials Theory, Department of Physics and Astronomy, Rutgers University 136 Frelinghuysen Rd., Piscataway NJ 08854, USA; Landau Institute for Theoretical Physics, 2 Kosygina Str., Moscow 117940, Russia

M. V. Feigel'man*

Landau Institute for Theoretical Physics, 2 Kosygina Str., Moscow 117940, Russia

B. Douçot

Laboratoire de Physique Théorique et Hautes' Energies, CNRS UMR 7589, Universités Paris 6 et 7, 4 Place Jussieu, Paris 75252 Cedex 05, France

(Submitted January 5, 2004)
Fiz. Nizk. Temp. **30**, 841–855 (July–August 2004)

We review recent results on a new class of Josephson arrays which have nontrivial topology and exhibit novel quantum states at low temperatures. One of these states is characterized by long-range order in a two-Cooper-pair condensate and by a discrete topological order parameter. The second state is insulating and can be considered as being the result of an evolution of the former state due to Bose-condensation of usual superconductive vortices with a flux quantum Φ_0. The quantum phase transition between these two states is controlled by variation of the external magnetic field. Both the superconductive and insulating states are characterized by the presence of 2^K-degenerate ground states, with K being the number of topologically different cycles existing in the plane of the array. This degeneracy is ''protected'' from the external perturbations (and noise) by the topological order parameter and spectral gap. We show that under ideal conditions the low-order effect of the external perturbations on this degeneracy is exactly zero and that deviations from ideality lead to only exponentially small effects of perturbations. We argue that this system provides a physical implementation of an ideal quantum computer with a built-in error correction. A number of relatively simple ''echo-like'' experiments possible on small-size arrays are discussed. © *2004 American Institute of Physics.* [DOI: 10.1063/1.1789936]

1. INTRODUCTION

Quantum computing[1,2] is in principle a very powerful technique for solving classic ''hard'' problems such as factorizing large numbers[3] or sorting large lists.[4] The remarkable discovery of quantum error correction algorithms[5] shows that there is no problem of principle involved in building a functioning quantum computer. However, implementation still seems dauntingly difficult: the essential ingredient of a quantum computer is a quantum system with 2^K (with $K \gg 100$) quantum states which are degenerate (or nearly so) in the absence of external perturbations and are insensitive to the ''random'' fluctuations which exist in every real system, but which may be manipulated by controlled external fields with errors less than 10^{-6}. Moreover, the standard schemes of error correction (assuming an error rate of order 10^{-6}) require very big system sizes, $K \sim 10^4 - 10^6$, to correct the errors (i.e., the total number of all qubits is a factor of 100–1000 larger than the number of qubits needed to perform the computational algorithm under the ''ideal'' conditions of no errors). If the frequency of errors could be reduced by orders of magnitude, the conditions for residual-error correction would becomes much less stringent, and the total size K of the system would be much smaller.[6]

Insensitivity to random fluctuations means that any coupling to the external environment neither induces transitions among these 2^K states nor changes the phase of one state with respect another. Mathematically, this means that one requires a system whose Hilbert space contains a 2^K-dimensional subspace (called ''the protected subspace'' [7–9]) within which any local operator $\hat{O}$ has (to a high accuracy) only state-independent diagonal matrix elements:

$$\langle n|\hat{O}|m\rangle = O_0 \delta_{mn} + o(\exp(-L)),$$

where L is a parameter such as the system size that can be made as large as desired. It has been very difficult to design a system which meets these criteria. Many physical systems (for example, spin glasses[10]) exhibit exponentially many distinct states, so that the off-diagonal matrix elements of all physical operators between these states are exponentially small. In such systems the longitudinal relaxation of a superposition of these states is very slow. The absence of the transverse relaxation which is due to the different diagonal matrix elements $O_{mm} - O_{nn}$ is a different matter: it is a

highly nontrivial requirement that is not satisfied by usual physical systems (such as spin glasses) and which puts systems satisfying it in a completely new class.

One very attractive possibility, proposed in an important paper by Kitaev[7] and developed further in Ref. 11, involves a protected subspace[8,9] created by a topological degeneracy of the ground state. Typically such degeneracy happens if the system has a conservation law such as conservation of the parity of the number of ''particles'' along some long contour, and the absence of any local order parameter. Physically, it is clear that two states that differ only by the parity of some big number that cannot be obtained from any local measurement are very similar to each other. A ''cartoon'' example of this idea can be presented as follows. Consider two locally flat surfaces, one with the topology of a simple cylinder and the other a Möbius strip, and imagine an observer moving on one of these surfaces. Clearly, the only way to decide on which surface the observer is located is to walk the whole loop around the strip and find himself either at the same point (in which case the surface is a cylinder) or on the other side of the surface (a Möbius strip).

The model proposed in Ref. 7 has been shown to exhibit many properties of the ideal quantum computer; however before now no robust and practical implementation was known. In a recent paper we and others proposed a Josephson junction network which is an implementation of a similar model with protected degeneracy and which is possible (although difficult) to build in the laboratory.[12]

In this paper we review our recent results on the further development of the ideas of Ref. 12. We propose a new Josephson junction network that has a number of practical advantages (a shorter account of this approach can be found in Refs. 13 and 14). This network operates in a phase regime (i.e., when Josephson energy is larger than the charging energy), which reduces undesired effects of parasitic stray charges. All Josephson junctions in this array are similar, which should simplify the fabrication process. This system has 2^K-degenerate ground states ''protected'' to even a higher extent than in Ref. 12: the matrix elements of local operators scale as ε^L, where $\varepsilon \leqslant 0.1$ is a measure of nonideality of the system's fabrication (e.g., the spread of critical currents of different Josephson junctions and geometrical areas of different elementary cells in the network). The new array does not require a fine tuning of its parameters into a narrow region. The relevant degrees of freedom of this new array are described by a model analogous to the one proposed in Ref. 7.

In physical terms, the array we propose may exist in two different phases: i) topological superconductor, which is a superfluid of $4e$ composite objects, and ii) topological insulator, which is a superfluid of superconductive vortices with a flux quantum $\Phi_0 = hc/2e$. The topological degeneracy of the ground state i) arises because $2e$ excitations have a gap. Indeed, in such system with the geometry of an annulus, one extra Cooper pair injected at the inner boundary can never escape it; on the other hand, it is clear that two states differing by the parity of the number of Cooper pairs at the boundary are practically indistinguishable by a local measurement. In the ground state ii) the lowest excitation is a ''half-vortex'' (i.e., vortex with a flux $\Phi_0/2$), and topological double-degeneracy appears due to the possibility of putting a half-vortex inside the opening, without paying any energy.

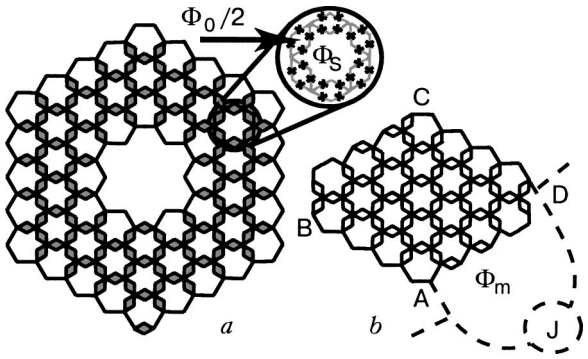

FIG. 1. Examples of the proposed Josephson junction array. The thick lines show superconductive wires, each wire containing one Josephson junction as shown in the detailed view of one hexagon. The width of each rhombus is such that the ratio of the area of the Star of David to the area of one rhombus is an odd integer. The array is put in a magnetic field such that the flux through each elementary rhombus and through each Star of David (inscribed in each hexagon) is half-integer. The thiin lines show the effective bonds formed by the elementary rhombi. The Josephson coupling provided by these bonds is π-periodic. An array with one opening; generally the effective number of qubits, K is equal to the number of openings. The choice of boundary condition shown here makes the superconducting phase unique along the entire length of the outer (inner) boundary; the state of the entire boundary is described by a single degree of freedom. The topological order parameter controls the phase difference between the inner and outer boundaries. Each boundary includes one rhombus to allow experiments with flux penetration; the magnetic flux through the opening is assumed to be $(1/2+m)\Phi_0/2$ with any integer m (a). With this choice of boundary circuits the phase is unique only inside the sectors AB and CD of the boundary; the topological degree of freedom controls the difference between the phases of these boundaries. This allows a simpler setup of the experimental test for the signatures of the ground state described in the text, e.g., by the SQUID interference experiment sketched here, which involves a measuring loop with flux Φ_m and a very weak junction J balancing the array (b).

Below we first describe the physical array, with the ''topological superconductor'' state, and identify its relevant low-energy degrees of freedom and the mathematical model that describes their dynamics. We then show how the protected states appear in this model, derive the parameters of the model, and identify various corrections appearing in a real physical system and their effects. Then we discuss the generalization of this array that is needed to obtain in a controllable way a second ''topological insulator'' phase. Finally, we discuss how one can manipulate quantum states in a putative quantum computer based upon those arrays, and the physical properties expected in a small arrays of this type. We remark that the properties of the excitations and topological order parameter exhibited by the system we propose here are in many respects similar to the properties of the ring exchange and frustrated magnet models discussed recently in Refs. 8, 9, and 15–25.

2. ARRAY 1: TOPOLOGICAL SUPERCONDUCTOR

The basic building block of the lattice is a rhombus made of four Josephson junctions with each side of the rhombus containing one Josephson contact; these rhombi form a hexagonal lattice as shown in Fig. 1. We denote the centers of the hexagons by letters $a,b,\ldots$ and the individual rhombi by $(ab),(cd),\ldots$, because each rhombus is in one-to-one correspondence with the link (ab) between the sites

of the triangular lattice dual to the hexagonal lattice. The lattice is placed in a uniform magnetic field so that the flux through each rhombus is $\Phi_0/2$. The geometry is chosen in such a way that the flux Φ_s through each Star of David is a half-integer multiple of Φ_0: $\Phi_s=(n_s+1/2)\Phi_0$.[1)] Finally, globally the lattice contains a number K of big openings (the size of the opening is much larger than the lattice constant; a lattice with $K=1$ is shown in Fig. 1*a*). The dimension of the protected space will be shown to be equal 2^K. The system is characterized by the Josephson energy, $E_J=(\hbar/2e)I_c$, of each contact and by the capacitance matrix of the islands (vertices of the lattice). We shall assume (as is usually the case) that the capacitance matrix is dominated by the capacitances of individual junctions; we write the charging energy as $E_C=e^2/2C$. The "phase regime" of the network mentioned above implies that $E_J>E_C$. The whole system is described by the Lagrangian

$$\mathcal{L}=\sum_{(ij)}\frac{1}{16E_C}(\dot{\varphi}_i-\dot{\varphi}_j)^2+E_J\cos(\varphi_i-\varphi_j-a_{ij}), \qquad (1)$$

where φ_i are the phases of individual islands and a_{ij} are chosen to produce the correct magnetic fluxes. The Lagrangian (1) contains only gauge invariant phase differences, $\varphi_{ij}=\varphi_i-\varphi_j-a_{ij}$, so it will be convenient sometimes to treat them as independent variables satisfying the constraint $\Sigma_\Gamma\varphi_{ij}=2\pi\Phi_\Gamma/\Phi_0+2\pi n$, where the sum is taken over closed loop Γ and n is an arbitrary integer.

As will become clear below, it is crucial that the degrees of freedom at the boundary have dynamics identical to those in the bulk. To ensure this one needs to add additional superconducting wires and Josephson junctions at the boundary. There are a few ways to do this; two examples are shown in Fig. 1*a* and Fig. 1*b*: type I boundary (the entire length of the boundaries in Fig. 1*a*, parts AB and CD of Fig. 1*b*), and type II boundary (BC,AD). For both types of boundaries one needs to include in each boundary loop a flux equal to $\frac{1}{4}Z_b\Phi_0$, where Z_b is the coordination number of the dual triangular lattice site. For instance, for the four-coordinated boundary sites one needs to enclose an integer flux in these contours. In the type I boundary the entire boundary corresponds to one degree of freedom (the phase at some point), while the type II boundary includes many rhombi so it contains many degrees of freedom.

Note that each (inner and outer) boundary shown in Fig. 1*a* contains one rhombus; we included it to allow flux to enter and exit through the boundary when that is energetically favorable.

3. GROUND STATE, EXCITATIONS AND TOPOLOGICAL ORDER

In order to identify the relevant degrees of freedom in this highly frustrated system we consider first an individual rhombus. As a function of the gauge invariant phase difference between the far ends of the rhombus the potential energy is

$$U(\varphi_{ij})=-2E_J(|\cos(\varphi_{ij}/2)|+|\sin(\varphi_{ij}/2)|). \qquad (2)$$

This energy has two equivalent minima, at $\varphi_{ij}=\pm\pi/2$, which can be used to construct an elementary unprotected qubit; see Ref. 26. In each of these states the phase changes by $\pm\pi/4$ in each junction clockwise around the rhombus. We denote these states as $|\uparrow\rangle$ and $|\downarrow\rangle$, respectively. In the limit of large Josephson energy the space of low-energy states of the full lattice is described by these binary degrees of freedom, and the set of operators acting on these states is given by Pauli matrices $\sigma_{ab}^{x,y,z}$. We now combine these rhombi into hexagons forming the lattice shown in Fig. 1. This gives another condition: the sum of phase differences around the hexagon should be equal to the flux Φ_s through each Star of David inscribed in this hexagon. The choice $\varphi_{ij}=\pi/2$ is consistent with the flux Φ_s being equal to a half-integer number of flux quanta. This state minimizes the potential energy (2) of the system. This is, however, not the only choice. Although flipping the phase of one rhombus changes the phase flux around the star by π and thus is prohibited, flipping two, four and six rhombi is allowed; generally the low-energy configurations of $U(\varphi)$ satisfy the constraint

$$\hat{P}_a=\prod_b\sigma_{ab}^z=1, \qquad (3)$$

where the product runs over all neighbors b of site a. The number of (classical) states satisfying the constraint (3) is still huge: the corresponding configurational entropy is extensive (proportional to the number of sites). We now consider the charging energy of the contacts, which results in the quantum dynamics of the system. We show that it reduces this degeneracy to a much smaller number, 2^K. The dynamics of the individual rhombus is described by a simple Hamiltonian $H=\tilde{t}\sigma_x$, but the dynamics of a rhombus embedded in the array is different because individual flips are not compatible with the constraint (3). The simplest dynamics compatible with (3) contains flips of three rhombi belonging to the elementary triangle, (a,b,c), $\hat{Q}_{(abc)}=\sigma_{ab}^x\sigma_{bc}^x\sigma_{ca}^x$ and therefore the simplest quantum Hamiltonian operating on the subspace defined by (3) is

$$H=-r\sum_{(abc)}Q_{(abc)}. \qquad (4)$$

We discuss the derivation of the coefficient r in this Hamiltonian and the correction terms and their effects below, but first we solve the simplified model (3), (4) and show that its ground state is "protected" in the sense described above and that excitations are separated by a gap.[2)]

Clearly, it is very important that the constraint is imposed on all sites, including boundaries. Evidently, some boundary hexagons are only partially complete but the constraint should be still imposed on the corresponding sites of the corresponding triangular lattice. This is ensured by additional superconducting wires that close the boundary hexagons in Fig. 1.

We note that constraint operators commute not only with the full Hamiltonian but also with individual $\hat{Q}_{(abc)}$: $[\hat{P},\hat{Q}_{(abc)}]=0$. The Hamiltonian (4) without constraint has an obvious ground state, $|0\rangle$, in which $\sigma_{ab}^x=1$ for all rhombi. This ground state, however, violates the constraint. This can be fixed, noting that since operators $\hat{P}_a$ commute with the Hamiltonian, any state obtained from $|0\rangle$ by acting on it by $\hat{P}_a$ is also a ground state. We can now construct a true ground state satisfying the constraint by

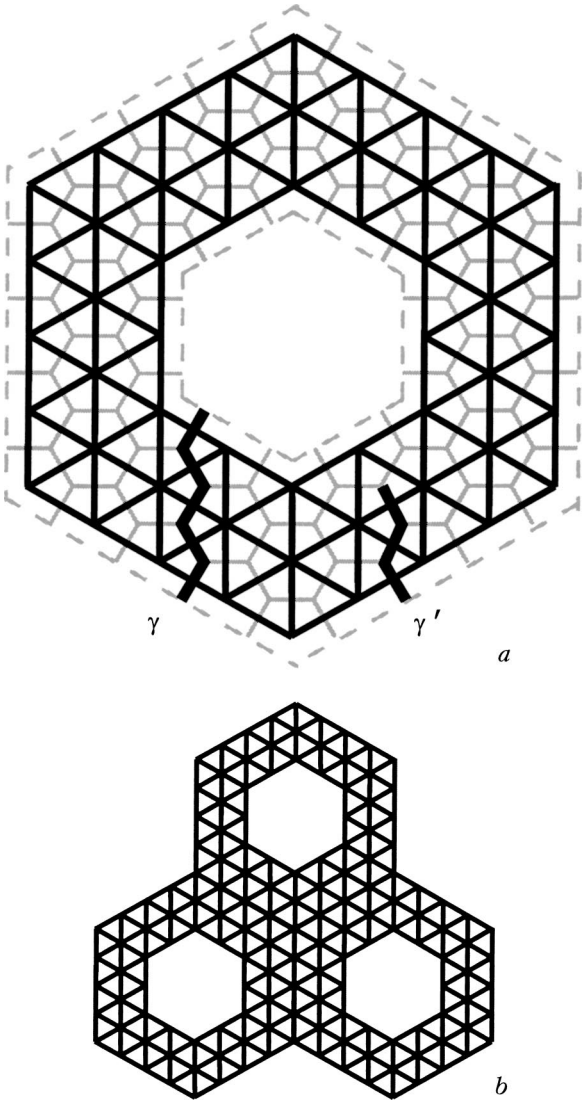

FIG. 2. Location of the discrete degrees of freedom responsible for the dynamics of the Josephson junction array shown in Fig. 1. The spin degrees of freedom describing the state of the elementary rhombi are located on the bonds of the triangular lattice (shown by thick lines), while the constraints are defined on the sites of this lattice. The dashed line indicates the boundary condition imposed by the physical circuitry shown in Fig. 1*a*. Contours γ and γ' are used in the construction of the topological order parameter and excitations (a). The lattice with $K=3$ openings; the ground state of the Josephson junction array on this lattice is $2^k=8$-fold degenerate (b).

$$|G\rangle=\prod_a \frac{1+\hat{P}_a}{\sqrt{2}}|0\rangle. \tag{5}$$

Here $(1+\hat{P}_a)/\sqrt{2}$ is a projector onto the subspace satisfying the constraint at site a and preserving the normalization.

Obviously, the Hamiltonian (4) commutes with any product of $\hat{P}_a$ which is equal to the product of σ^z_{ab} operators around a set of closed loops. These integrals of motion are fixed by the constraint. However, for a topologically nontrivial system there appear a number of other integrals of motion. For a system with K openings a product of σ^z_{ab} operators along a contour γ that begins at one opening and ends at another (or at the outer boundary; see Fig. 2),

$$\hat{T}_q=\prod_{(\gamma_q)} \sigma^z_{ab}, \tag{6}$$

commutes with the Hamiltonian and is not fixed by the constraint. Physically these operators count the parity of "up" rhombi along such contour. The presence of these operators results in degeneracy of the ground state. Note that multiplying such an operator by an appropriate $\hat{P}_a$ gives a similar operator defined on the shifted contour, so all topologically equivalent contours give one new integral of motion. Further, multiplying two operators defined along the contours beginning at the same (e.g., outer) boundary and ending in different openings, A, B is equivalent to the operator defined on the contour leading from A to B, so the independent operators can be defined (e.g.) by the set of contours that begin at one opening and end at the outer boundary. The state $|G\rangle$ constructed above is not an eigenstate of these operators, but this can be fixed by defining

$$|G_f\rangle=\prod_q \frac{1+c_q\hat{T}_q}{\sqrt{2}}|G\rangle, \tag{7}$$

where $c_q=\pm 1$ is the eigenvalue of the operator $\hat{T}_q$ defined on the contour γ_q. Equation (7) is the final expression for the ground-state eigenfunctions.

Construction of the excitations is similar to the construction of the ground state. First, one notices that since all operators $\hat{Q}_{abc}$ commute with each other and with the constraints, any state of the system can be characterized by the eigenvalues $(Q_{abc}=\pm 1)$ of $\hat{Q}_{abc}$. The lowest excited state correspond to only one Q_{abc} being -1. Notice that a simple flip of one rhombus (by the operator $\sigma^z_{(ab)}$) somewhere in the system changes the sign of the two eigenvalues Q_{abc} corresponding to the two triangles to which it belongs. To change only one Q_{abc} one needs to consider a continuous string of these flip operators starting from the boundary: $|(abc)\rangle = v_{abc}|0\rangle$ with $v_{abc}=\Pi_{\gamma'}\sigma^z_{(cd)}$, where the product is over all rhombi (cd) that belong to the path γ' that begins at the boundary and ends at (abc) (see Fig. 2, which shows one such path). This operator changes the sign of only one Q_{abc}, the one that corresponds to the "last" triangle. This construction does not satisfy the constraint, so we have to apply the same "fix" as for the ground-state construction above

$$|v_{(abc)}\rangle=\prod_q \frac{1+c_q\hat{T}_q}{\sqrt{2}}\prod_a \frac{1+\hat{P}_a}{\sqrt{2}}v_{(abc)}|0\rangle \tag{8}$$

to get the final expression for the lowest-energy excitations. The energy of each excitation is $2r$. Note that a single flip excitation at a rhombus (ab) can be viewed as a combination of two elementary excitations located at the centers of the triangles to which rhombus (ab) belongs and has twice their energy. Generally, all excited states of the model (4) can be characterized as a number of elementary excitations (8), so they give an exact quasiparticle basis. Note that creation of a quasiparticle at one boundary and moving it to another is equivalent to the operator $\hat{T}_q$, so this process acts as τ^z_q in the space of the 2^K degenerate ground states. As will be shown below, in the physical system of Josephson junctions these excitations carry charge $2e$, so that the process τ^z_q is equivalent to the transfer of charge $2e$ from one boundary to another.

Consider now the matrix elements, $O_{\alpha\beta}=\langle G_\alpha|\hat{O}|G_\beta\rangle$ of a local operator, $\hat{O}$, between two ground states, e.g., of an operator that is composed of a small number of σ_{ab}. To evaluate this matrix element we first project a general operator onto the space that satisfies the constraint: $\hat{O}\to\mathcal{P}\hat{O}\mathcal{P}$, where $\mathcal{P}=\Pi_a(1+\hat{P}_a)/2$. The new (projected) operator is also local; it has the same matrix elements between ground states but it commutes with all $\hat{P}_a$. Since it is local, it can be represented as a product of σ_z and $\hat{Q}$ operators, and this implies that it also commutes with all $\hat{T}_q$. Thus, its matrix elements between different states are exactly zero. Further, using the fact that it commutes with $\hat{P}_a$ and $\hat{T}_q$ we write the difference between its diagonal elements evaluated between the states that differ by parity over contour q as

$$O_+-O_-=\left\langle 0\left|\prod_i\frac{1+\hat{P}_i}{\sqrt{2}}\hat{T}_q\hat{O}\right|0\right\rangle. \tag{9}$$

This equation can be viewed as a sum of products of σ_z operators. Clearly to get a nonzero contribution each σ^z should enter even number of times. Each $\hat{P}$ contains a closed loop of six σ^z operators, so any product of these terms is also a collection of closed loops of σ^z. In contrast to it, the operator $\hat{T}_q$ contains a product of σ^z operators along the loop γ, so the product of them contains a string of σ^z operators along a contour that is topologically equivalent to γ. Thus one gets a nonzero O_+-O_- only for the operators $\hat{O}$ which contain a string of σ^z operators along a loop that is topologically equivalent to γ, which is impossible for a local operator. Thus we conclude that for this model all off-diagonal matrix elements of a local operator are exactly zero, and all the diagonal elements are exactly equal.

4. EFFECT OF PHYSICAL PERTURBATIONS

We now come back to the original physical system described by the Lagrangian (1) and derive the parameters of the model (4) and discuss the most important corrections to it and their effect. We begin with the derivation. In the limit of small charging energy the flip of three rhombi occurs by a virtual process in which the phase φ_i at one (6-coordinated) island i changes by π. In the quasiclassical limit the phase differences on the individual junctions are $\varphi_{\rm ind}=\pm\pi/4$; the leading quantum process changes the phase on one junction by $3\pi/2$ and on others by $-\pi/2$, changing the phase across the rhombus: $\varphi\to\varphi+\pi$. The phase differences φ satisfy the constraint that the sum of them over the closed loops remains equal to $2\pi(n+\Phi_s/\Phi_0)$. The simplest such process preserves the symmetry of the lattice, and changes simultaneously the phase differences on the three rhombi containing island i while leaving all other phases constant. The action for such process is three times the action of elementary transitions of individual rhombi, S_0:

$$r\approx E_J^{3/4}E_C^{1/4}\exp(-3S_0),\quad S_0=1.61\sqrt{E_J/E_C}. \tag{10}$$

In the alternative process the phase differences between i and other islands change in turn, via a high-energy intermediate state in which one phase difference has changed while others remain close to their original values. The estimate for this action shows that it is larger than $3S_0$, so (10) gives the dominant contribution. There are in fact many processes that contribute to this transition: the phase of island i can change by $\pm\pi$ and, in addition, in each rombus one can choose arbitrarily the junction at which the phase changes by $\pm3\pi/2$; the amplitude of all these processes should be added. This does not change the result qualitatively unless these amplitudes exactly cancel each other, which happens only if the charge of the island is exactly half-integer (because phase and charge are conjugate, the amplitude difference of processes that are different by 2π is $\exp(2\pi iq)$). We assume that in a generic case this cancellation does not occur. External electrical fields (created by stray charges, for example) might induce noninteger charges on each island, which would lead to a randomness in the phase and amplitude of r. The phase of r can be eliminated by a suitable gauge transformation $|\uparrow\rangle_{ab}\to\exp(i\alpha_{ab})|\uparrow\rangle_{ab}$ and has no effect at all. The amplitude variations result in a position-dependent quasiparticle energy.

We now consider the corrections to the model (4). One important source of corrections is the difference of the actual magnetic flux through each rhombus from the ideal value $\Phi_0/2$. If this difference is small, it leads to a bias of ''up'' versus ''down'' states; their energy difference becomes

$$2\epsilon=2\pi\sqrt{2}\,\frac{\delta\Phi_d}{\Phi_0}E_J. \tag{11}$$

Similarly, the difference of the actual flux through Star of David and the difference in the Josephson energies of individual contacts leads to the interaction between ''up'' states:

$$\delta H_1=\sum_{(ab)}V_{ab}\sigma^z_{ab}+\sum_{(ab),(cd)}V_{(ab),(cd)}\sigma^z_{ab}\sigma^z_{cd}, \tag{12}$$

where $V_{ab}=\epsilon$ for a uniform field deviating slightly from the ideal value and $V_{(ab),(cd)}\neq0$ for rhombi belonging to the same hexagon. Consider now the effect of perturbations described by δH_1, Eq. (12). These terms commute with the constraint but do not commute with the main term, H, so the ground state is no longer $|G_\pm\rangle$. In other words, these terms create excitations (8) and give them kinetic energy. In the leading order of the perturbation theory the ground state becomes $|G_\pm\rangle+(\epsilon/4r)\Sigma_{(ab)}\sigma^z_{(ab)}|G_{i\pm}\rangle$. Qualitatively, this corresponds to the appearance of virtual pairs of quasiparticles in the ground state. The density of these quasiparticles is ϵ/r. As long as these quasiparticles do not form a topologically nontrivial string, all of our previous conclusions remain valid. However, there is a nonzero amplitude for forming such a string; it is now exponential in the system size. With exponential accuracy this amplitude is $(\epsilon/2r)^L$, which leads to an energy splitting of the same order for the two ground-state levels and for the matrix elements of typical local operators:

$$E_+-E_-\sim O_+-O_-\sim(\epsilon/2r)^L.$$

The physical meaning of the $v_{(abc)}$ excitations becomes clearer if one consider the effect of the addition of one σ^z operator to the end of the string defining the quasiparticle: it results in a charge transfer of $2e$ across this last rhombus. To prove this, note that the wave function of a superconductor corresponding to the state that is a symmetric combination of

$|\uparrow\rangle$ and $|\downarrow\rangle$ is periodic with period π and thus corresponds to charge which is multiple of $4e$, while the antisymmetric combination corresponds to charge $(2n+1)2e$. The action of one σ^z induces a transition between these states and thus transfers a charge $2e$. Thus, these excitations carry charge $2e$. Note that continuous degrees of freedom are characterized by long-range order in $\cos(2\varphi)$ and thus correspond to the condensation of pairs of Cooper pairs. In other words, this system superconducts with elementary charge $4e$ and has a gap $2r$ to the excitations carrying charge $2e$. It was shown in a recent paper[29] that a similar pairing of Cooper pairs occurs in a chain of rhombi, and in Ref. 30 it was predicted that a classical superconductive state with effective charge $6e$ is formed in a frustrated Kagome wire network.

The model (4) completely ignores the processes that violate the constraint at each hexagon. Such processes might violate the conservation of the topological invariants $\hat{T}_q$ and thus are important for the long-time dynamics of the ground-state manifold. In order to consider these processes we need to go back to the full description involving the continuous superconducting phases φ_i. Since potential energy (2) is periodic in π it is convenient to separate the degrees of freedom into a continuous part (defined modulo π) and discrete parts. The continuous parts have a long-range order: $\langle\cos(2\varphi_0-2\varphi_r)\rangle\sim 1$. The elementary excitations of the continuous degrees of freedom are harmonic oscillations and vortices. The harmonic oscillations interact with discrete degrees of freedom only through the local currents that they generate. Further the potential (2) is very close to quadratic, so we conclude that they are practically decoupled from the rest of the system. In contrast to this, vortices have an important effect. By construction, the elementary vortex carries flux π in this problem. Consider the structure of these vortices in greater detail. The superconducting phase should change by 0 or 2π when one moves around a closed loop. In a half-vortex this is achieved if the gradual change by π is compensated (or augmented) by a discrete change by π on a string of rhombi, which costs no energy. Thus, from the viewpoint of discrete degrees of freedom, the position of the vortex is the hexagon where constraint (3) is violated. The energy of the vortex is found from the usual arguments,

$$E_v(R)=\frac{\pi E_J}{4\sqrt{6}}(\ln R+c),\quad c\approx 1.2; \tag{13}$$

it is logarithmic in the vortex size R. The process that changes the topological invariant $\hat{T}_q$ is the one in which one half-vortex completes a circle around an opening. The amplitude of such a process is exponentially small: $(\tilde{t}/E_v(D))^{\Lambda}$, where $\tilde{t}$ is the amplitude for the flipping of one rhombus and Λ is the length of the shortest path around the opening. In the quasiclassical limit the amplitude $\tilde{t}$ can be estimated analogously to (10): $\tilde{t}\sim\sqrt{E_J E_Q}\exp(-S_0)$. The half-vortices would appear in a realistic system if the flux through each hexagon is systematically different from the ideal half-integer value. The presence of free vortices destroys topological invariants, so a realistic system should either be not too large (so that deviations of the total flux do not induce free vortices) or these vortices should be localized in prepared traps (e.g., Stars of David with fluxes slightly larger or smaller than Φ_s). In the absence of half-vortices the model is equivalent to the Kitaev model[7] placed on triangular lattice in the limit of the infinite energy of the excitation violating the constraints.

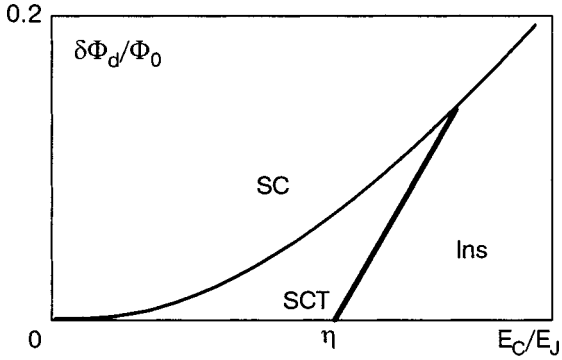

FIG. 3. Schematic of the phase diagram for half-integer Φ_s at low temperatures: $\delta\Phi_d$ is the deviation of the magnetic flux through each rhombus from its ideal value. SC stands for the usual superconducting phase, SCT for the phase with $\cos(2\varphi)$ long-range order of the continuous degrees of freedom and a discrete topological order parameter, discussed extensively in the text. The SCT phase and SC phase are separated by a 2D quantum Ising phase transition.

Quantitatively, the expression for the parameters of the model (4) becomes exact only if $E_J\gg E_C$. One expects, however, that the qualitative conclusions remain the same and the formulas derived above provide reliable estimates of the scales even for $E_J\sim E_C$, provided that the charging energy is not so large as to result in a phase transition to a different phase. One expects this transition to occur at $E_C^*=\eta E_J$, with $\eta\sim 1$, its exact value being reliably determinable only from numerical simulations.

Practically, since the perturbations induced by flux deviations from Φ_0 are proportional to $(\delta\Phi/\Phi_0)(E_J/r)$ and r becomes exponentially small at small E_C, the optimal choice of the parameters for the physical system is $E_C\approx E_C^*$. We show the schematics of the phase diagram in Fig. 3. We assume here that the transition to the insulating phase is direct; another alternative is an intermediate phase in which the energy of the vortex becomes finite instead of being logarithmic. If this phase indeed exists it is likely to have properties more similar to the one discussed in Ref. 7 (in the next Section we consider a generalized JJ array, where such an intermediate phase does exist). The ''topological'' phase is stable in a significant part of the phase diagram. The phase transition between ''topological superconductor '' and usual superconductor belongs to the class of quantum spin-1/2 2D Ising model on a hexagonal lattice, placed in a transverse field:

$$H_{\text{Ising}}=-\epsilon\sum_{(ij)} s_j^x s_i^x - r\sum_i s_i^z. \tag{14}$$

Here i, j denote sites of the hexagonal lattice, the eigenvalue of operator s_i^z measures the parity of the number n_i of Cooper pairs on the ith island: $n_i(\text{mod }2)=\frac{1}{2}(1-s_i^z)$; the parameters r and ϵ are defined in Eqs. (10) and (11). As long as the ratio $\lambda=r/\epsilon$ is larger than some critical value λ_c, the ground state is one with an even number of Cooper pairs on each island, which corresponds to our ''topological superconductor'' phase. The values of λ_c for square, triangular, and cubic

lattices was found via quantum Monte–Carlo simulations;[31] in particular, $\lambda_c^{\text{triang}} \approx 4.6 \pm 0.3$, and $\lambda_c^{\text{square}} \approx 2.7 \pm 0.3$. There are no available data for a hexagonal lattice; based upon the results cited above, one could estimate $\lambda_c^{\text{hex}} \approx 2 \pm 0.5$.

Furthermore, since the vortex excitations have logarithmic energy, we expect that this phase survives at finite temperatures as well. In the thermodynamic limit, at $T \neq 0$ one gets a finite density of $2e$-carrying excitations ($n_v \sim \exp(-2r/T)$), but vortices remain absent as long as the temperature is below the BKT-like depairing transition for half-vortices.

5. ARRAY 2: TOPOLOGICAL INSULATOR

Generally, increasing the charging energy in a Josephson junction array makes it an insulator. This transition is due to an increase of phase fluctuations in the original array and the resulting appearance of free vortices that form a superfluid of their own. The new situation arises in a topological superconductor because it allows half-vortices. Two scenarios are now possible. The ''conventional'' scenario would involve condensation of half-vortices since they are conjugate to charges $4e$. In this case we get an insulator with elementary excitations carrying charge $4e$. An alternative is condensation of full vortices (pairs of half-vortices) with a finite gap to half-vortices. In this case the elementary excitations are charge-$2e$ objects. Similar fractionalization was discussed in the context of high-T_c superconductors in Refs. 19 and 32 and in the context of spin or quantum dimer systems in Refs. 22 and 33–36. Such an insulator acquires interesting topological properties on a lattice with holes, because each hole leads to a new binary degree of freedom which describes the presence or absence of a half-vortex. The energies of these states are equal up to corrections which vanish exponentially with the size of the holes. These states cannot be distinguished by local measurements and have all the properties expected for a topological insulator. They can be measured, however, if the system is adiabatically brought into the superconductive state by changing some control parameter. Here we propose a modification of the ''topologically superconductive'' array that provides such a control parameter and, at the same time, allows us to solve the model and compute the properties of the topological insulator. The key idea of this modification is to allow full vortices (of flux Φ_0) to move with large amplitude between plackets of the hexagonal lattice, so that they lower their energy due to delocalization and eventually Bose-condense, while half-vortices remain (almost) localized.

Consider the array shown in Fig. 4, which contains rhombi with junctions characterized by Josephson and charging energies $E_J > E_C$ and weak junctions with $\epsilon_J \ll \epsilon_C \ll E_C$. Each rhombus encloses half of a flux quantum, leading to an exact degeneracy between the two states of opposite chirality of the circulating current.[13,29] This degeneracy is a consequence of the symmetry operation which combines the reflection about the long diagonal of the rhombus and a gauge transformation needed to compensate the change of the flux $\Phi_0/2 \to -\Phi_0/2$. This gauge transformation changes the phase difference along the diagonal by π. This $\mathcal{Z}_2$ symmetry implies conservation of the parity of the number of pairs at each site of the hexagonal lattice and is the origin of the

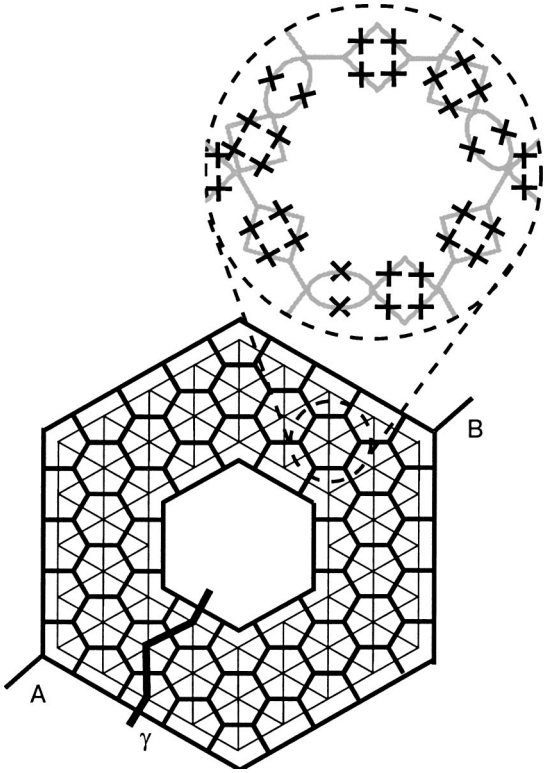

FIG. 4. Schematics of the array. The main figure: Global structure of the array. Discrete variables controlling the low energy properties are defined on the links of the hexagonal lattice. Generally, the lattice might have K big holes; here we show the example $K=1$. Zoom in: Each inner bond of the lattice contains a rhombus made out of four Josephson junctions; some bonds also contain an effective weaker link made of two Josephson junctions so that each hexagon of the lattice contains $k=3$ such links. The flux through each rhombus is a half flux quantum, $\Phi_0/2$; the flux through a loop constituting a weak link is close to a half flux quantum $\phi = \Phi_0/2 + \delta\Phi$. The boundary of the lattice contains rhombi and weak links so that each boundary plaquette has the same number, k, of weak links as the bulk hexagon.

Cooper pair binding. We assume that each elementary hexagon contains exactly k such junctions: in the case where each link contains one weak junction $k=6$, but generally it can take any value $k \geqslant 1$. As will be shown below, the important condition is the number of weak junctions that one needs to cross in the elementary loop. Qualitatively, a value $k \geqslant 1$ ensures that it costs a little to put a vortex in any hexagon.

For the general arguments that follow below, the actual construction of the weak links is not important; however, practically it is difficult to vary the ratio of the capacitance to the Josephson energy, so weaker Josephson contact usually implies larger Coulomb energy. This can be avoided if weak contact is made from a Josephson junction loop frustrated by magnetic field. The charging energy of this system is half the charging energy of an individual junction, while the effective Josephson junction strength is $\epsilon_J = 2\pi(\delta\Phi/\Phi_0)E_0$, where E_0 is the Josephson energy of each contact and $\delta\Phi = \Phi - \Phi_0/2$ is the difference of the flux from the half flux quantum. This construction also allows one to control the system by varying the magnetic field.

Under these conditions the whole array is insulating. Assume that ϵ_J sets the lowest energy scale in this problem (the exact condition will be discussed below). The state of the array is controlled by discrete variables $u_{ij} = 0,1$, which describe the chiral state of each rhombus, and by continuous

phases φ_{ij} that specify the state of each weak link (here and below i, j denote the sites of the hexagonal lattice). If the Josephson coupling $\epsilon_J \equiv 0$, different islands are completely decoupled and the potential energy does not depend on the discrete variables u_{ij}. For small ϵ_J we can evaluate its effect using perturbation theory:

$$V(u) = -W\cos\left(\pi \sum_{\text{hex}} u_{ij}\right), \quad W = \frac{k^k}{k!}\epsilon_J\left(\frac{\epsilon_J}{8\epsilon_C}\right)^{k-1}. \tag{15}$$

This potential energy lowers the relative energy of classical configurations of u_{ij} that satisfy the constraint $\Sigma_{\text{hex}} u \equiv 0$ (mod 2) but it does not prohibit configurations with $\Sigma_{\text{hex}} u \equiv 1$ (mod 2).

Now consider the dynamics of discrete variables. Generally, two types of tunneling processes are possible. In the first type the phase changes by π across each of the three rhombi that have a common site. This is the same process that gives the leading contribution to the dynamics of the superconducting array;[13] its amplitude is given (in the quasiclassical approximation) by Eq. (10) above. In the second type of process the phase changes across one rhombus and across one weak junction. Because the potential energy of the weak junction is assumed to be very small, the main effect of the weak junction is to change the kinetic energy. The total kinetic energy for this process is the sum of the terms due to the phase across the rhombi and across the weak link. Assuming that these phase variations are equal and opposite in sign, the former is about $E_C^{-1}\varphi^2$ and the latter $\epsilon_C^{-1}\varphi^2$, so the effective charging energy of this process is $\tilde{E}_C = (E_C^{-1} + \varepsilon_C^{-1})^{-1}$. For $\epsilon_C \ll E_C$ this charging energy is small, and the process is suppressed. Thus, under these conditions the dominating process is the simultaneous flip of three rhombi, as in the superconducting case. In the following we restrict ourselves to this case. Further, we shall assume that $r \gg W$, so that in the leading order one can neglect the potential energy compared to the kinetic energy corresponding to the flip of three rhombi. As W is increased by turning on ϵ_J the continuous phase φ_{ij} orders, and the transition to the superconducting state happens at $\epsilon_J \sim \epsilon_C$. At larger ϵ_J, W becomes equal to ϵ_J and with a further increase of ϵ_J, for $\epsilon_J \gg r$ vortices completely disappear from the low-energy spectrum, and the array becomes equivalent to the one studied in Ref. 13.

The low-energy states are the ones that minimize the kinetic energy corresponding to simultaneous flip processes:

$$H_T = -r\sum_i \prod_{j(i)} \tau_{ij}^x. \tag{16}$$

Here $j(i)$ denote the nearest neighbors of site i, τ_{ij}^x is the operator that flips discrete variables u_{ij}, and r is given by (10). The states minimizing this energy satisfy the gauge invariance condition

$$\prod_{j(i)} \tau_{ij}^x |\Psi\rangle = |\Psi\rangle. \tag{17}$$

The Hilbert space of states that satisfy the condition (17) is still huge. If all weaker terms in the Hamiltonian are neglected, all states that satisfy (17) are degenerate. These states can be visualized in terms of half-vortices positioned on the sites of the dual lattice, a, b. Indeed, a convenient way to describe different states that satisfy (17) is to note that operator $\Pi_{j(i)}\tau_{ij}^x$ does not change the value of $\Sigma_{\text{hex}} u_{ij}$ for the second type of tunneling processes. Thus, one can fix the values of $\Sigma_{\text{hex}} u_{ij} = v_a$ on all hexagonal plaquettes a and impose the constraint (17). In physical terms the binary values $v_i = 0,1$ describe the positions of half-vortices on the dual (triangular) lattice. This degeneracy between different states is lifted when the subdominant terms are taken into account. The main contribution to the potential energy of these half-vortices comes from (15), it is simply proportional to their number. The dynamics of these vortices is due to the processes in which only one rhombus changes its state, with a corresponding flip of the phase across the weak junction. The amplitude of this process is

$$\tilde{r} \approx E_J^{3/4} E_C^{1/4} \exp(-\tilde{S}_0), \quad \tilde{S}_0 = 1.61\sqrt{\frac{E_J}{\tilde{E}_C}}.$$

In this approximation the effective Hamiltonian controlling these vortices becomes (cf. Eq. (14)):

$$H_v = -\tilde{r}\sum_{(ab)} \sigma_a^x \sigma_b^x - W\sum_a \sigma_a^z, \tag{18}$$

where the operators σ_a act in the usual way on the states with/without half-vortices at plaquette a and the first sum runs over adjacent plaquettes (ab). This Hamiltonian describes an Ising model in a transverse field. For small $W/\tilde{r} < \lambda_c \sim 1$ its ground state is "disordered": $\langle \sigma^z \rangle = 0$ but $\langle \sigma_x \rangle \neq 0$ while for $W/\tilde{r} > \lambda_c$ it is "ordered": $\langle \sigma^z \rangle \neq 0$, $\langle \sigma^x \rangle = 0$. The critical value of the transverse field is known from extensive numerical simulations:[31] $\lambda_c \approx 4.6 \pm 0.3$ for the triangular lattice. The "disordered" state corresponds to a liquid of half-vortices, while in the "ordered" state the density of free half-vortices vanishes, i.e., the ground state contains an even number of half-vortices, so the total vorticity of the system is zero. To prove this we start from the state $|\uparrow\rangle$, which is the ground state at $\tilde{r}/W = 0$, and consider the effect of $\tilde{r}\Sigma_{(ab)}\sigma_b^x\sigma_a^x$ in perturbation theory. Higher energy states are separated from the ground state by the gap W, so each order is finite. Further, in each order the operator $\sigma_a^x\sigma_b^x$ creates two more half-vortices, proving that the total number of half-vortices remains even in each order. The states with odd numbers of half-vortices have a gap $\Delta(\tilde{r}/W)$ which remains nonzero for $W/\tilde{r} > \lambda_c$.

In terms of the original discrete variable defined on the rhombi the Hamiltonian (18) becomes

$$H_u = -\tilde{r}\sum_{(ij)} \tau_{ij}^x - W\sum_i \prod_{j(i)} \tau_{ij}^z, \tag{19}$$

where the τ operators act on the state of each rhombus. This Hamiltonian commutes with the constraint (17) and is in fact the simplest Hamiltonian of the lattice $\mathcal{Z}_2$ gauge theory. The disordered regime corresponds to a confined phase of this $\mathcal{Z}_2$ gauge theory, leading to elementary $4e$ charge excitations, while the ordered regime corresponds to the deconfined phase.

Now consider a system with nontrivial topology, e.g., a hole. In this case the set of variables v_a is not sufficient to determine uniquely the state of the system, one has to

TABLE I. The typical properties of topological superconductor and insulator.

State	Topological superconductor	Topological insulator
Ground state	Condensate of $4e$ charges	Condensate of 2π phase vortices
Fluxons	Gapful, charge $2e$	Gapful, π phase vortices
Pseudocharges	Half fluxes with energy $\epsilon \sim E_J \log L$	Charge $2e$ with $\epsilon = 2r + \beta\epsilon_C \min[\log L, \log(c/c_0)]$[a]
Ground-state degeneracy	Charge on the inner boundary mod $4e$	Number of π vortices inside the hole mod 2
Ground-state splitting	$(\delta\Phi/\Phi_0)(E_J/r)^L$	$(\tilde{r}/W)^L$

[a]Comment: Here β is a number ~ 1, c is the capacitance of a weak link, and c_0 is the self-capacitance of an island.

supplement it by the variable $v_0 = \Sigma_L u_{ab}$, where the sum is taken over a closed contour L that goes around the hole. Physically, it describes the presence/absence of a half-vortex in the hole. The effective Hamiltonian of this additional variable has only a kinetic part because the presence or absence of a half-vortex in a hole which has l weak links in its perimeter gives a potential energy $W_0 = c\epsilon_J(\epsilon_J/\epsilon_C)^l$ which is exponentially small for $l \gg 1$. The kinetic part is similar to other variables: $H_0 = -\tilde{r}\Sigma_{a\in I}\sigma_a^x\sigma_0^x$; it describes a process in which a half-vortex jumps from the hole into the inner boundary I of the system. In the state with $\langle\sigma^z\rangle \neq 0$ this process increases the energy of the system by $\tilde{W}(\tilde{r}/W)$ ($\tilde{W}(0) = W$ and $\tilde{W}(\lambda_c) = 0$). In the state with $\langle\sigma^x\rangle \neq 0$ it costs nothing. Thus, the process in which a half-vortex jumps from the hole into the system and another half-vortex exits into the outside region appears in second order of perturbation theory, and the amplitude of this process is $t_v = \tilde{r}^2\Sigma_{i\in I, j\in O} g_{ab}$, where the summation is performed over all sites of the inner (I) and outer (O) boundaries, and

$$g_{ab} = \left\langle \sigma_a^x \frac{1}{H - E_0} \sigma_b^x \right\rangle$$

has the physical meaning of the half-vortex tunneling amplitude from the inner to outer boundaries. At small $\tilde{r}/W$, deep in the insulating phase, we can estimate g_{ab} using the perturbation expansion in $\tilde{r}/W$: the leading contribution appears in $|a-b|$th order of perturbation theory, and thus $g_{ab} \propto (\tilde{r}/W)^{|a-b|}$. Thus for small $\tilde{r}/W$ the tunneling amplitude of the half-vortex is exponentially small in the distance L from the outer to the inner boundary; we expect that it remains exponentially small for all $\tilde{r}/W < \lambda_c$. For $\tilde{r}/W > \lambda_c$ this amplitude is of the order of $\tilde{r}^2/W$ and is therefore significant.

In different language, in the system with a hole we can construct a topological invariant $\mathcal{P} = \Pi_\gamma \tau_{ij}^x$ (contour γ is shown in Fig. 4) which can take values ± 1. Note that now the contour goes via triangular lattice sites (where vortices are defined), whereas in the first (superconductive array) version the corresponding path was drawn via sites of the basic hexagonal lattice. The same arguments as used for the superconducting array show that any dynamics consistent with constraint (17) preserves $\mathcal{P}$. Thus, formally, the properties of the topological insulator are very similar to the properties of the topological superconductor discussed in Ref. 12, if one replaces the words Cooper pair by half-vortex and vice versa. We summarize this duality in Table I.

Note that at small $\tilde{r}/W \to 0$ the ground state of the Hamiltonian (19) satisfies the condition (17) and minimizes the second term in (19), i.e., satisfies the condition $\Pi_{j(i)}\tau_{ij}^z|\Psi\rangle = |\Psi\rangle$; it can be explicitly written as

$$|0\rangle_{\text{ins}} = \prod_i \frac{1}{2}\left(1 + \prod_{j(i)} \tau_{ij}^z\right) \prod_{kl} |{\to}\rangle_{kl}. \tag{20}$$

This state is a linear superposition of the degenerate states with $\mathcal{P} = 1$ and $\mathcal{P} = -1$:

$$|0\rangle_{\text{ins}} = \frac{1}{\sqrt{2}}(|+\rangle_{\text{ins}} + |-\rangle_{\text{ins}}) \tag{21}$$

and it coincides with the ground state $|G\rangle$ of discrete variables in the superconducting array (cf. Eq. (5)). The orthogonal superposition of $\mathcal{P} = \pm 1$ states,

$$|1\rangle_{\text{ins}} = \frac{1}{\sqrt{2}}(|+\rangle_{\text{ins}} - |-\rangle_{\text{ins}}), \tag{22}$$

corresponds to a half-vortex inside the hole. The energy difference between the above two states $E_1 - E_0$ is exponentially small in the insulating state of the array, whereas it is large in the superconductive state.

6. QUANTUM MANIPULATIONS

We now discuss the manipulation of the protected states formed in this system. We start from a *superconductive* version of the array.

First, we note that here the topological invariant $\hat{T}_q$ has a simple physical meaning—it measures the total phase difference (modulo 2π) between the inner and outer boundaries. In an array with even number of rhombi between internal and outer boundaries, the state with eigenvalue $c_q = 1$ has a phase difference of 0, whereas the state with eigenvalue $c_q = -1$ has a phase difference of π. This means that measuring this phase difference measures the state of the qubit in the same basis in which $\hat{T}_q$ is diagonal. For the following discussion we define a set of Pauli matrices $\Sigma_q^{x,y,z}$ acting in the 2×2 qubit space, such that $\Sigma_q^x \equiv T_q$.

Introducing a weak coupling between these boundaries by a very weak Josephson circuit (characterized by a small energy e_J) would change the phase of these states in a controllable manner, e.g., in a unitary transformation

$$U^z = \exp(ie_J t\Sigma_q^z). \tag{23}$$

The transformation coupling two qubits can be obtained if one introduces a weak Josephson circuit that connects two different inner boundaries (corresponding to different qubits). Namely, it will produce the operation

$$U^z_{p,q} = \exp(ie_J t \Sigma^z_q \Sigma^z_p). \quad (24)$$

Analogously, the virtual process involving half-vortex motion around the opening gives the tunneling amplitude, ϵ_t between topological sectors, e.g., the unitary transformation $U^x = \exp(it\epsilon_t \Sigma^x_q)$. This tunneling can be controlled by magnetic field if the system is prepared with some number of vortices that are pinned in the idle state in a special plaquette, where the flux is integer. The slow (adiabatic) change of this flux towards a normal (half-integer) value would release the vortex and result in the transitions between topological sectors with $\epsilon_t \sim \tilde{t}/D^2$.

These operations are analogous to usual operations on a qubit and are prone to usual sources of errors. This system, however, allows another type of operations that are naturally discrete. As we show above, the transmission of the elementary quasiparticle across the system changes its state by Σ^z_q. This implies that a discrete process of one-pair transfer across the system is equivalent to the Σ^z_q transformation. Similarly, a controlled process in which a vortex is moved around a hole results in a discrete Σ^x_q transformation. Moreover, this system allows one to make discrete transformations such as $\sqrt{\Sigma^{x,y}}$. Consider, for instance, a process in which, by changing the total magnetic flux through the system, one half-vortex is placed at the center of the system shown in Fig. 1*b* and then released. It can escape through the left or through the right boundary; in one case the state does not change, in the other it changes by Σ^x. The amplitudes add, resulting in the operation $(1+i\Sigma^x)/\sqrt{2}$. Analogously, using the electrostatic gate(s) to pump one charge $2e$ from one boundary to the island in the center of the system and then releasing it results in a $(1+i\Sigma^x)/\sqrt{2}$ transformation. This type of processes admits a straightforward generalization to an array with many holes: there an extra half-vortex or charge should be placed at equal distances from the inner and outer boundaries.

The degenerate ground states in the *insulating* array can be manipulated in the same way as in the superconductor, up to duality (half-vortex→Cooper pair and *vice versa*). As mentioned above, these states $|0\rangle_{\rm ins}$ and $|1\rangle_{\rm ins}$ correspond to the absence or presence of a half-vortex inside the hole. We define by $\tilde{\Sigma}^{x,y,z}$ the Pauli operators acting in the space spanned by $|0\rangle_{\rm ins}$ and $|1\rangle_{\rm ins}$. An adiabatic change of local magnetic field that drags one half-vortex across the system will flip the state of the system, providing us with the implementation of the operator $\tilde{\Sigma}^x$ acting on the state of the qubit. Analogously, the motion of elementary charge $2e$ around the hole will change the relative phase of the states $|0\rangle_{\rm ins}$ and $|1\rangle_{\rm ins}$ by π, providing us with the operator $\tilde{\Sigma}^z$. The operators $\sqrt{\tilde{\Sigma}^{x,z}}$ can be realized in a way similar to that described for a superconductive array. Rotation by an arbitrary angle $U^x = \exp(i\alpha\tilde{\Sigma}^x)$, which is an analog of the operator (23), can be achieved by modifying (during time t) the parameter r in such a way as to produce a non-negligible amplitude A of half-vortex tunneling across the system: $\alpha = At$. In the same way, a two-qubit entanglement operation can be realized which is an analog of operator (24):

$$\tilde{U}^x_{p,q} = \exp(itA_{pq}\tilde{\Sigma}^x_p \tilde{\Sigma}^x_q); \quad (25)$$

in this case A_{pq} is the half-vortex tunneling amplitude between holes p and q.

7. PHYSICAL PROPERTIES OF SMALL ARRAYS

7.1. Superconducting array

Even without these applications for quantum computation the physical properties of this array are remarkable: it exhibits a long-range order in the square of the usual superconducting order parameter: $\langle\cos(2(\varphi_0-\varphi_r))\rangle \sim 1$ without the usual order: $\langle\cos(\varphi_0-\varphi_r)\rangle = 0$; the charge transferred through the system is quantized in the units of $4e$. This can be tested in the interference experiment sketched in Fig. 1*b*; as a function of external flux Φ_m, the supercurrent through the loop should be periodic with half the usual period. This simpler array can be also used for a kind of ''spin-echo'' experiment: applying two consecutive operations $(1+i\Sigma_x)/\sqrt{2}$ described above should again give a unique classical state, while applying only one of them should result in a quantum superposition of two states with equal weight.

The echo experiment can be used to measure the decoherence time in this system. Generally one distinguishes processes that flip the classical states and processes that change their relative phases. In the NMR literature the former are referred to as longitudinal relaxation and the latter as transverse. The transverse relaxation occurs when a vortex is created and then moved around the opening by an external noise. Assuming a thermal noise, we estimate the rate of this process $\tau_\perp^{-1} \sim \tilde{t}\exp(-E_V(L)/T)$. Similarly, the transfer of a quasiparticle from the outer to the inner boundary changes the relative phase of the two states, leading to longitudinal relaxation. The rate of this is proportional to the density of quasiparticles, $\tau_\parallel^{-1} = R\exp(-2r/T)$. The coefficient R depends on the details of the physical system. In an ideal system with some nonzero uniform value of ϵ (defined above (12) the quasiparticles are delocalized and $R \sim \epsilon/L^2$. Random deviations of the fluxes Φ_r from a half-integer value produce randomness in ϵ, in which case one expects Anderson localization of quasiparticles due to off-diagonal disorder, with a localization length of the order of the lattice spacing; thus $R \sim \overline{\epsilon}\exp(-cL)$ with $c \sim 1$, and $\overline{\epsilon}$ is a typical value of ϵ. Stray charges induce randomness in the values of r, i.e., add some *diagonal* disorder. When the random part of r, denoted δr, becomes larger than $\overline{\epsilon}$ the localization becomes stronger: $R \sim \overline{\epsilon}(\overline{\epsilon}/\overline{\delta r})^L$, where $\overline{\delta r}$ is a typical value of δr. Upon a further increase of stray charge field there appear rare sites where r_i is much smaller than the average value. Such sites act as additional openings in the system. If the density of these sites is significant, the effective length that controls the decoherence becomes the distance between these sites. For typical $E_V(L) \approx E_J \approx 2$ K the transverse relaxation time reaches seconds for $T \sim 0.1$ K, while realistic $\epsilon/r \sim 0.1$ imply that due to a quasiparticle localization in a random case the longitudinal relaxation reaches the same scale for systems of size $L \sim 10$; note that the temperature T has to be only somewhat lower than the excitation gap $2r$ in order to make the longitudinal rate low.

Most properties of the array are only weakly sensitive to the effect of stray charges: as discussed above, they result in a position-dependent quasiparticle potential energy which

has very little effect because these quasiparticles had no kinetic energy and were localized anyway. A direct effect of stray charges on the topologically protected subspace can also be described physically as a effect of the electrostatic potential on states with even and odd charges at the inner boundary; since the absolute value of the charge fluctuates strongly, this effect is exponentially weak.

7.2. Insulating array

The signature of the topological insulator is the persistence of trapped half flux inside the central hole (see Fig. 4), which can be observed by cycling the magnetic field so as to drive the system back and forth between insulating and superconducting states. This trapping is especially striking in the insulator. Experimentally, this can be revealed by driving slowly the array into a superconducting state and then measuring the phase difference between opposite points such as A and B in Fig. 4. In the state with a half-vortex the phase difference is $\pi/2+\pi n$ while it is πn in the other state. The πn contribution is due to the usual vortices that get trapped in a big hole. This slow transformation can be achieved by changing the strength of weak links using the external magnetic field as a control parameter. The precise nature of the superconductive state is not essential because a phase difference π between points A and B can be interpreted as due to a full vortex trapped in a hole in a conventional superconductor or due to π-periodicity in a topological one, which makes no essential difference. These flux trapping experiments are similar to the ones proposed for high-T_c cuprates[18,19] with a number of important differences: the trapped flux is half of Φ_0, the cycling does not involve temperature (avoiding problems with excitations) and the final state can be either a conventional or topological superconductor.

8. CONCLUSION

We have shown that a Josephson junction array of a special types (shown in Fig. 1 and Fig. 4) have degenerate ground states described by a topological order parameter. The manifold of these states is protected in the sense that local perturbations have exponentially weak effect on their relative phases and transition amplitudes. The simpler array of Fig. 1 possesses a superconductive state with topological order.

Its minor modification shown in Fig. 4 may be brought into both superconductive and insulating ''topological'' phases in a controllable manner.[3)] Both versions of the array are expected to demonstrate very long coherence time in ''spin-echo'' type experiments and to be promising basic elements for scalable quantum computers.

The main building block of the array is a rhombus which has two (almost) degenerate states; in the array discussed here these rhombi are assembled into hexagons, but we expect that lattices in which these rhombi form other structures would have similar properties.

However, the dynamics of these arrays is described by spin exchange terms of quartic (or higher) order, which have a larger barrier in a quasiclassical regime, implying that their parameter r is much smaller than for the array considered here. This makes them more difficult to build in the interesting regime.

We are grateful to G. Blatter, D. Ivanov, S. Korshunov, A. Larkin, A. Millis, B. Pannetier, E. Serret, and L. Shchur for discussions and helpful comments, and to ENS (Paris), to LPTMS, Orsay, and to LSI, Ecole Polytechnique for their hospitality which allowed this work to be completed.

We acknowledge the support by NSF Grant 4-21262. M. F. was supported by the SCOPES program of Switzerland, the Dutch Organization for Fundamental Research (NWO), RFBR Grant 01-02-17759, the program ''Quantum Macrophysics'' of the Russian Academy of Sciences, and the program ''Physics of Quantum Computing'' of the Russian Ministry of Industry, Science and Technology.

*E-mail: feigel@landau.ac.ru

1) The flux Φ_s can be also chosen so that it is an integer multiple of Φ_0: this would not change significantly the final results but would change the intermediate arguments and make them longer, so for clarity we discuss in detail only the half-integer case here. Note, however, that the main quantitative effect of this alternative choice of the flux is beneficial: it would push upward the phase transition line separating the topological and superconducting phases shown for the half-integer case in Fig. 3.

2) In a rotated basis $\sigma^x \to \sigma^z$, $\sigma^z \to \sigma^x$ this model is reduced to a special case of Z_2 lattice gauge theory,[27,28] which contains only a magnetic term in the Hamiltonian, with the constraint (3) playing the role of a gauge invariance condition.

3) It is possible that the array shown in Fig. 1 also has a topological insulator phase, but we cannot prove it.

[1] A. Steane, Rep. Prog. Phys. **61**, 117 (1998).
[2] A. Ekert and R. Jozsa, Rev. Mod. Phys. **68**, 733 (1996).
[3] P. W. Shor, in *Proceedings of the 35th Symposium on the Foundations of Computer Science*, IEEE Press, Los Alamitos, CA (1994).
[4] L. Grover, in *Proceedings of the Annual ACM Symposium on the Theory of Computing*, ACM Press, New York (1996).
[5] P. W. Shor, Phys. Rev. A **52**, 2493 (1995).
[6] J. Preskill, Proc. R. Soc. London, Ser. A **454**, 385 (1998).
[7] A. Yu. Kitaev, Preprint, http://xxx.lanl.gov/abs/quant-ph/9707021 (1997); I. Kant, *Critique of Pure Reason* (1781).
[8] X.-G. Wen and Q. Niu, Phys. Rev. B **41**, 9377 (1990).
[9] X.-G. Wen, Phys. Rev. B **44**, 2664 (1991).
[10] M. Mezard, G. Parisi, and M. Virasoro, *Spin Glass Theory and Beyond*, Word Scientific, Singapore (1997).
[11] S. B. Bravyi and A. Kitaev, Preprint, http://xxx. lanl.gov/abs/quant-ph/0003137; M. H. Freedman, A. Kitaev, and Z. Wang, Preprint, http://xxx.lanl.gov/abs/quant-ph/0001071.
[12] L. B. Ioffe, M. V. Feigel'man, A. Ioselevich, D. Ivanov, M. Troyer, and G. Blatter, Nature (London) **415**, 503 (2002).
[13] L. B. Ioffe and M. V. Feigel'man, Phys. Rev. B **66**, 224503 (2002).
[14] B. Douçot M. V. Feigel'man, and L. B. Ioffe, Phys. Rev. Lett. **90**, 107003 (2003).
[15] N. Read and B. Chakraborty, Phys. Rev. B **40**, 7133 (1989).
[16] N. Read and S. Sachdev, Phys. Rev. Lett. **66**, 1773 (1991).
[17] S. Kivelson, Phys. Rev. B **39**, 259 (1989).
[18] T. Senthil and M. P. A. Fisher, Phys. Rev. Lett. **86**, 292 (2001).
[19] T. Senthil and M. P. A. Fisher, Phys. Rev. B **63**, 134521 (2001).
[20] L. Balents, S. M. Girvin, and M. P. A. Fisher, Preprint, http://xxx.lanl.gov/abs/cond-mat/0110005.
[21] A. Paramekanti, L. Balents, and M. P. A. Fisher, Preprint, http://xxx.lanl.gov/abs/cond-mat/0203171.
[22] G. Misguich, D. Serban, and V. Pasquier, Preprint, http://xxx.lanl.gov/abs/cond-mat/0204428.
[23] O. Motrunich and T. Senthil, Preprint, http://xxx. lanl.gov/abs/cond-mat/0205170.
[24] P. Fendley, R. Moessner, and S. L. Sondhi, Preprint, http://xxx.lanl.gov/abs/cond-mat/0206159.
[25] A. S. Ioselevich, D. A. Ivanov, and M. V. Feigel'man, Preprint, http://xxx.lanl.gov/abs/cond-mat/0206451.

[26] G. Blatter, V. B. Geshkenbein, and L. B. Ioffe, Phys. Rev. B **63**, 174511 (2001).
[27] F. Wegner, J. Math. Phys. **12**, 2259 (1971).
[28] R. Balian, J. M. Droufle, and C. Itzykson, Phys. Rev. D **11**, 2098 (1975).
[29] B. Douçzot and J. Vidal, Preprint, http://xxx. lanl.gov/abs/cond-mat/0202115.
[30] K. Park and D. A. Huse, Phys. Rev. B **64**, 134522 (2001).
[31] R. F. Bishop, D. J. J. Farrel, and M. L. Ristig, Int. J. Mod. Phys. B **14**, 1517 (2000).
[32] T. Senthil and M. P. A. Fisher, Phys. Rev. B **62**, 7850 (2000).
[33] N. Read and S. Sachdev, Phys. Rev. Lett. **66**, 1773 (1991).
[34] L. Balents, M. P. A. Fisher, and S. M. Girvin, Phys. Rev. B **65**, 224412 (2002).
[35] T. Senthil and O. Motrunich, Preprint, http://xxx. lanl.gov/abs/cond-mat/0201320.
[36] R. Moessner, S. L. Sondhi, and E. Fradkin, Phys. Rev. B **65**, 24504 (2002).

Note added in proof

The approach to the construction of topologically stable superconductive qubits and anomalous superconducting states with Cooper-pair pairing that is reviewed in the present article has been further developed in two very recent papers: B. Douçot, M. V. Feigel'man, L. B. Ioffe, and A. S. Ioselevich, ''Protected qubits and Chern Simons theories in Josephson-junction arrays,'' cond-mat/0403712, and I. V. Protopopov and M. V. Feigel'man, ''Theory of $4e$ versus $2e$ supercurrent in frustrated Josephson-junction rhombi chain,'' cond-mat/0405170.

This article was published in English in the original Russian journal. Reproduced here with stylistic changes by AIP.

Topological solitons of the Lawrence–Doniach model as equilibrium Josephson vortices in layered superconductors

S. V. Kuplevakhsky*

B. Verkin Institute for Low Temperature Physics and Engineering of the National Academy of Science of Ukraine, 47 Lenin Ave., Kharkov 61103, Ukraine

(Submitted January 22, 2004)
Fiz. Nizk. Temp. **30**, 856–873 (July–August 2004)

We present a complete, exact solution of the problem of the magnetic properties of layered superconductors with an infinite number of superconducting layers in parallel fields $H>0$. Based on a new exact variational method, we determine the type of all stationary points of both the Gibbs and Helmholtz free-energy functionals. For the Gibbs free-energy functional, they are either points of strict, strong minima or saddle points. All stationary points of the Helmholtz free-energy functional are those of strict, strong minima. The only minimizers of both the functionals are the Meissner (0-soliton) solution and soliton solutions. The latter represent equilibrium Josephson vortices. In contrast, nonsoliton configurations (interpreted in some previous publications as ''isolated fluxons'' and ''fluxon lattices'') are shown to be saddle points of the Gibbs free-energy functional: They violate the conservation law for the flux and the stationarity condition for the Helmholtz free-energy functional. For stable solutions, we give a topological classification and establish a one-to-one correspondence with Abrikosov vortices in type-II superconductors. In the limit of weak interlayer coupling, exact, closed-form expressions for all stable solutions are derived: They are nothing but the ''vacuum state'' and topological solitons of the coupled static sine-Gordon equations for the phase differences. The stable solutions cover the whole field range $0\leqslant H<\infty$ and their stability regions overlap. Soliton solutions exist for arbitrary small transverse dimensions of the system, provided the field H is sufficiently high. Aside from their importance for weak superconductivity, the new soliton solutions can find applications in different fields of nonlinear physics and applied mathematics. © *2004 American Institute of Physics.* [DOI: 10.1063/1.1789938]

1. INTRODUCTION

In Ref. 1, concerned with a microscopic model, and Ref. 2, concerned with the phenomenological Lawrence–Doniach (LD) model 3, we have shown that the problem of the minimization of the Gibbs free-energy functional of layered superconductors with an infinite number of superconducting (S) layers ($N=\infty$) in parallel magnetic fields $H>0$ admits an exact solution. Advanced mathematical methods, employed in Refs. 1 and 2, allowed us to overcome the complications related to mutual dependence of the phases φ_n of the S layers. (Unfortunately, these complications were not noticed in previous publications on the LD model,[4–9] which led to a loss of minimizers.) The main results of Refs. 1 and 2 are worth recalling: The set of minimizers derived in Refs. 1 and 2 comprises the topologically trivial Meissner configuration and true soliton (vortex) configurations. As in the case of the Meissner state and Abrikosov vortices (i.e., the topological solitons[10–13] of the Ginzburg–Landau equations) in continuum type-II superconductors, all these configurations are characterized by the conserved topological index $N_v=0,1,2,\ldots$ (the vortex number; $N_v=0$ for the Meissner state) and the conserved magnetic flux. For this reason, the topologically nontrivial solution with $N_v=1$ has been identified as an elementary Josephson vortex in layered superconductors at $H>0$. Physically, such a solution can be regarded as a bound state of interlayer flux quanta (one flux quantum per insulating layer). We have termed this solution ''a vortex plane'' because its field distribution has symmetry typical of plane defects.

The present paper complements and completes the investigation of Refs. 1 and 2 in two major respects. First, we determine the type of *all* stationary points of the Gibbs free-energy functional, which allows us to classify all of the solutions available in the literature with regard to their stability. In particular, we show that, except for the Meissner solution, all nonsoliton solutions (such as, e.g., ''vortex lattices'' [6,7,14]) correspond to saddle points. Second, in the limit of weak interlayer coupling, we derive *exact, closed-form* analytical expressions for the full set of stable solutions with $N_v=0,1,2,\ldots$. These solutions cover the whole field range $0\leqslant H<\infty$, as they should, and include the results of Refs. 1 and 2 as particular cases. They illustrate all the features of the Meissner state and vortex structure in weakly coupled superconductors (such as, e.g., overlap of the stability regions and the soliton nature of Josephson vortices) and establish true isomorphism with Abrikosov vortices in type-II superconductors. Moreover, they refute the erroneous belief[15,16] that Josephson vortices ''do not exist'' in small (along the S layers) structures.

Although the issue of stability is crucial for the determination of the equilibrium vortex structure in layered superconductors, it has not been addressed in any previous publications.[1] Mathematically, a classification of stable solu-

tions amounts to the determination of all points of local minima of the energy functionals. A local minimum of the Gibbs free-energy functional of layered superconductors is determined by the relations[18,19]

$$\delta\Omega\left[\delta f_n, \frac{d\delta f_n}{dy}, \delta\varphi_n, \frac{d\delta\varphi_n}{dy}, \delta\mathbf{A}; H\right]_{\{\bar{f}_n, \bar{\varphi}_n, \bar{A}\}} = 0, \tag{1}$$

$$\Omega\left[\bar{f}_n + \delta f_n, \frac{d\bar{f}_n}{dy} + \frac{d\delta f_n}{dy}, \bar{\varphi}_n + \delta\varphi_n, \frac{d\bar{\varphi}_n}{dy} + \frac{d\delta\varphi_n}{dy}, \bar{\mathbf{A}} + \delta\mathbf{A}; H\right] \geqslant \Omega\left[\bar{f}_n, \frac{d\bar{f}_n}{dy}, \bar{\varphi}_n, \frac{d\bar{\varphi}_n}{dy}, \bar{\mathbf{A}}; H\right], \tag{2}$$

where $\delta\Omega$ is the first variation of the Gibbs free-energy functional, induced by small variations δf_n, $\delta\varphi_n$, $\delta\mathbf{A}$ of the modulus of the order parameter ($\bar{f}_n$), phase ($\bar{\varphi}_n$), and vector potential ($\bar{\mathbf{A}}$), respectively.[1,2] [For example, the numerical nonsoliton solutions of Ref. 16 satisfy the stationarity condition (1) but do not meet the condition of the minimum (2).] The value of Ω on the right-hand side of (2) is associated with the thermodynamic (observable) Gibbs free energy. The true equilibrium state corresponds to the minimum of the thermodynamic Gibbs free energy (i.e., the absolute minimum of the Gibbs free-energy functional) at a given $H>0$. The rest of the states, satisfying (1), (2) at a given $H>0$, are thermodynamically metastable: As an illustration, we refer to the Meissner state of the semi-infinite (along the layers) layered superconductor near the superheating field H_s.[1,2]

To eliminate any questions about the actual equilibrium field configurations in layered superconductors at $H>0$, we present an explicit mathematical proof that the Meissner (0-soliton) and vortex-plane (soliton) configurations are *unique* solutions that satisfy the conditions of the minimum (1), (2). Moreover, we show that all the minima are *strict* and *strong*.[19] For the sake of diversification, we employ a new method of exact minimization of the Gibbs free-energy functional that, in contrast to Refs. 1 and 2, does not involve variation with respect to the phases φ_n: The new method starts directly from the definition (1), (2) and automatically yields the conservation law for the flux and a full set of soliton boundary conditions. For definitiveness, we restrict ourselves to consideration of the popular LD model: Owing to the relationship[2] between the LD model and the true microscopic model of Ref. 1, all the results hold for the latter model as well. The present paper is mostly concerned with mathematical aspects of the problem; all major derivations are given in full detail. As regards a comparison with experiment, the reader is referred to Refs. 1 and 2.

Section 2 of this paper is devoted to exact minimization of the Gibbs free-energy functional. In Sec. 2.1 we specify the geometry of the problem, introduce the Gibbs free-energy functional of the LD model, Ω_{LD}, and discuss some of its properties. Using the conditions of the minimum, in Sec. 2.2 we reduce the problem of the minimization of Ω_{LD} to that of a simpler functional, Ω, that possesses the same set of minimizers as Ω_{LD}. In Sec. 2.3 we prove that the stationary points of Ω belong to two types: minima and saddle points. From the conditions of the minimum of Ω we derive the conservation law for the flux, which yields the Meissner and soliton (vortex-plane) solutions. The uniqueness of these solutions as minimizers of both Ω and Ω_{LD} is verified by consideration of the exact lower bounds of the related Helmholz free-energy functional Ω_H, which depend explicitly on the conserved topological index N_v. In Sec. 2.4 we present a topological classification of the stable solutions and establish isomorphism between vortex planes in layered superconductors at $H>0$ and Abrikosov vortices in type-II superconductors.

In Sec. 3, in the limit of weak interlayer coupling, we derive exact, closed-form expressions for all stable solutions of the LD model (the Meissner and the soliton, or vortex, ones). The properties of these solutions are thoroughly investigated; all major limiting cases are considered. Isomorphism between vortex planes and ordinary Josephson vortices in the single junction is established.

The results obtained are summarized and discussed in Sec. 4. In particular, we explain where unstable nonsoliton solutions come from. We also draw a comparison between our approach to layered superconductors and those of other authors. Mathematical flaws of these latter approaches are explicitly pointed out.

In Appendix A we discuss analytical properties and the solution of coupled static sine-Gordon (SG) equations for the phase differences, considered in some previous publications. We prove that the Meissner and vortex-plane solutions, derived in Sec. 3, are the unique stable solutions to the SG equations at $H>0$. We also establish a relationship to the exact variational principle of Refs. 1 and 2. In Appendix B we verify the fulfillment of the Jacobi–Weierstrass–Hilbert sufficient condition for a strong minimum for the exact, closed-form solutions of Sec. 3. In Appendix C we draw a comparison between the soliton solutions of Sec. 3 and the nonsoliton (''lattice'') solutions of Refs. 6, 7 and 14; this comparison serves as a good illustration of the general results of the main text.

2. EXACT MINIMIZATION OF THE LD FUNCTIONAL

2.1. Formulation of the problem

The geometry of the problem is that of Refs. 1 and 2: The layering axis is x, with p being the period; the y axis is directed along the S layers, with $-L\leqslant y\leqslant +L$ being the region occupied by the system [or $-\infty<y<+\infty$, if $L=\infty$]. A static, uniform external field is applied along the z axis: $\mathbf{H}=(0,0,H\geqslant 0)$. The case of external current is not considered, i.e., $I=0$.

Under the assumption of homogeneity along the z axis, we can write the Gibbs free-energy functional of the LD model as

$$\Omega_{LD}\left[f_n, \frac{df_n}{dy}, \varphi_n, \frac{d\varphi_n}{dy}, \mathbf{A}; H\right] = \frac{pH_c^2(T)}{4\pi} W_z \times \int_{-L}^{L} dy \sum_n \left\{ -f_n^2(y) + 12 f_n^4(y) + \zeta^2(T) \times \left[\frac{df_n(y)}{dy}\right]^2 + \zeta^2(T)\left[\frac{d\varphi_n(y)}{dy}\right.\right.$$

$$-2eA_y(np,y)\Big]^2 f_n^2(y)+\frac{r(T)}{2}[f_{n-1}^2(y)+f_n^2(y)$$
$$-2\,f_n(y)f_{n-1}(y)\cos\Phi_{n,n-1}(y)]$$
$$+\frac{4e^2\zeta^2(T)\lambda^2(T)}{p}\int_{(n-1)p}^{np}dx\Big[\frac{\partial A_y(x,y)}{\partial x}$$
$$-\frac{\partial A_x(x,y)}{\partial y}-H\Big]^2\Big\}, \tag{3}$$

$$\Phi_{n,n-1}(y)=\varphi_n(y)-\varphi_{n-1}(y)-2e\int_{(n-1)p}^{np}dxA_x(x,y)$$
$$=\phi_n(y)-2e\int_{(n-1)p}^{np}dxA_x(x,y). \tag{4}$$

Here $\hbar=c=1$; $\mathbf{A}=(A_x,A_y,0)$ is the vector potential; W_z is the length of the system in the z direction ($W_z\to\infty$); $f_n(y)\times[0\leqslant \mathrm{fn}(y)\leqslant 1]$ and $\varphi_n(y)$ are, respectively, the reduced modulus and the phase of the pair potential $\Delta_n(y)$ in the nth superconducting layer: $\Delta_n(y)=\Delta(T)f_n(y)\exp i\phi_n(y)$; $\phi_n\equiv\varphi_n-\varphi_{n-1}$; $H_c(T)$ is the thermodynamic critical field; $r(T)$ is a dimensionless phenomenological parameter of the Josephson interlayer coupling; $\zeta(T)$ and $\lambda(T)$ are the Ginzburg–Landau coherence length and the penetration depth, respectively. The local magnetic field $\mathbf{h}=(0,0,h)$ obeys the Maxwell equation

$$h(x,y)=\frac{\partial A_y(x,y)}{dx}-\frac{\partial A_x(x,y)}{\partial y}. \tag{5}$$

The variables f_n, φ_n, and $\mathbf{A}$ are subject to standard requirements:[19] f_n and φ_n are supposed to be smooth in the whole interval $-L\leqslant y\leqslant L$, whereas $\mathbf{A}$ is piecewise smooth on the domain of definition, because at $x=np$ only the continuity of $\mathbf{A}$ can be required. The summation in Eq. (3) runs over all the S layer indices n. To avoid mathematical complications related to the appearance of infinite sums while retaining the property of the periodicity of the barrier potential and the absence of outer boundaries in the x direction, it is reasonable to compactify the model[20] by imposing periodic boundary conditions on observable quantities,

$$f_{n+N}=f_n,\quad \Phi_{n+N,n+N-1}(y)=\Phi_{n,n-1}(y),$$
$$h(x+Np,y)=h(x,y), \tag{6}$$
$$\frac{d\varphi_{n+N}(y)}{dy}-2eA_y[(n+N)p,y]=\frac{d\varphi_n(y)}{dy}$$
$$-2eA_y(np,y),$$

and proceed to the thermodynamic $\lim_{N\to\infty}\Omega_{LD}/N=\omega_{LD}<\infty$ in the final expressions. (The existence of this limit will be proved in Sec. 2.3.). Using (6), we can write the total flux through the system as

$$\Phi=\int_{-L}^{L}dy\sum_n\int_{(n-1)p}^{np}dxh(x,y)$$
$$=\int_{-L}^{L}dy\sum_{i=1}^{N}\int_{(n-1+i)p}^{(n+i)p}dxh(x,y)$$
$$=\int_{-L}^{L}dy[A_y[(n+N)p,y]-A_y(np,y)]$$
$$+\sum_{i=1}^{N}\int_{(n-1+i)p}^{(n+i)p}dx[A_x(x,-L)-A_x(x,L)]$$
$$=\frac{1}{2e}\sum_{i=1}^{N}[\Phi_{n+i,n-1+i}(L)-\Phi_{n+i,n-1+i}(-L)]. \tag{7}$$

What we are going to do now is to find all sets of allowed field configurations $\{\overline{f_n},\overline{\varphi_n},\overline{\mathbf{A}}\}$ that at a given H satisfy the condition of the minimum (2), i.e.,

$$\Omega_{LD}\Big[f_n,\frac{df_n}{dy},\varphi_n,\frac{d\varphi_n}{dy},\mathbf{A};H\Big]$$
$$\geqslant\Omega_{LD}\Big[\overline{f_n},\frac{d\overline{f_n}}{dy},\overline{\varphi_n},\frac{d\overline{\varphi_n}}{dy},\overline{\mathbf{A}};H\Big]$$
$$\equiv\min\Omega_{LD}\Big[f_n,\frac{df_n}{dy},\varphi_n,\frac{d\varphi_n}{dy},\mathbf{A};H\Big], \tag{8}$$

where $\{f_n,\varphi_n,\mathbf{A}\}$ belong to a sufficiently small neighborhood of $\{\overline{f_n},\overline{\varphi_n},\overline{\mathbf{A}}\}$.

2.2. A new minimization method

Our approach is standard[19] and consists in the determination of an exact lower bound of (3) at a given H and finding the field configuration $\{\overline{f_n},\overline{\varphi_n},\overline{\mathbf{A}}\}$ that makes (3) equal to this lower bound. We begin with the stationarity condition (1) for Ω_{LD}.

Variation with respect to f_n immediately yields a set of equations

$$f_n(y)-f_n^3(y)+\zeta^2(T)\frac{d^2f_n(y)}{dy^2}=\frac{r(T)}{2}[2\,f_n(y)$$
$$-f_{n+1}(y)\cos\Phi_{n+1,n}(y)-f_{n-1}(y)\cos\Phi_{n,n-1}(y)]$$
$$+\zeta^2(T)\Big[\frac{d\phi_n(y)}{dy}-2eA_y(np,y)\Big]^2 f_n(y) \tag{9}$$

and boundary conditions

$$\frac{df_n}{dy}(\pm L)=0. \tag{10}$$

Variation with respect to A_x leads to the Maxwell equation

$$\frac{\partial h(x,y)}{\partial y}=4\pi j_{n,n-1}(y)$$
$$\equiv 4\pi j_0 f_n(y)f_{n-1}(y)\sin\Phi_{n,n-1}(y), \tag{11}$$

in the regions $(n-1)p<x<np$, and the boundary conditions

$$h(x,\pm L)=H. \tag{12}$$

In Eq. (11) the quantity $j_{n,n-1}(y)$ is the density of the Josephson current between the $(n-1)$th and the nth layers, and $j_0 = r(T)p/16\pi e\zeta^2(T)\lambda^2(T)$.

By variation with respect to A_y, we obtain the Maxwell equation

$$\frac{\partial h(x,y)}{\partial x} = 0 \tag{13}$$

in the regions $(n-1)p < x < np$, and the boundary conditions at the S layers

$$h(hp-0,y) - h(np+0,y) = \frac{p f_n^2(y)}{2e\lambda^2(T)}\left[\frac{d\varphi_n(y)}{dy} - 2eA_y(np,y)\right]. \tag{14}$$

At this point, it is convenient to partially fix the gauge by the condition[2)]

$$A_x(x,y) = 0, \quad A_y(x,y) \equiv A(x,y), \tag{15}$$

which turns Eqs. (5), (11) and (13) into a system of linear inhomogeneous differential equations for $A(x,y)$:

$$\frac{\partial^2 A(x,y)}{\partial y \partial x} = 4\pi j_0 f_n(y) f_{n-1}(y) \sin\phi_n(y), \tag{16}$$

$$\frac{\partial^2 A(x,y)}{\partial x^2} = 0. \tag{17}$$

with the boundary conditions

$$A(np-0,y) = A(np+0,y), \tag{18}$$

$$\frac{\partial A}{\partial x}(np-0,y) - \frac{\partial A}{\partial x}(np+0,y) = \frac{p f_n^2(y)}{2e\lambda^2(T)}\left[\frac{d\varphi_n(y)}{dy} - 2eA(np,y)\right], \tag{19}$$

$$\frac{\partial A}{\partial x}(x,\pm L) = H. \tag{20}$$

From (19), (20), we get the conditions for the vanishing of the intralayer currents at the outer boundaries

$$\frac{d\varphi_n}{dy}(\pm L) - 2eA(np,\pm L) = 0 \tag{21}$$

and the conservation law for the total intralayer current

$$\sum_n f_n^2(y)\left[\frac{d\varphi_n(y)}{dy} - 2eA(np,y)\right] = 0. \tag{22}$$

In Refs. 1 and 2, relation (22) was employed for the minimization of (3) with respect to the phases φ_n.

The solution of (16), (17) under the conditions (18)–(20) is straightforward and has the form[2]

$$A(x,y) = \left[4\pi j_0 \int_{-L}^{y} du f_n(u) f_{n-1}(u) \sin\phi_n(u) + H\right] \times (x - np) + \frac{1}{2e}\frac{d\varphi_n(y)}{dy} - \frac{r(T)}{4e\zeta^2(T)}\frac{1}{f_n^2(y)}\int_{-L}^{y} du f_n(u) \times [f_{n-1}(u)\sin\phi_n(u) - f_{n+1}(u)\sin\phi_{n+1}(u)], \tag{23}$$

$$(n-1)p < x \leqslant np,$$

where

$$f_n(-y) = f_n(y), \tag{24}$$

$$\phi_n(-y) = -\phi_n(y) + 2\pi Z_n, \quad Z_n = 0, \pm 1, \pm 2, ..., \tag{25}$$

and the phase differences $\phi_n \equiv \varphi_n - \varphi_{n-1}$ obey the solvability conditions

$$\frac{d\phi_{n+1}(y)}{dy} = \frac{1}{\lambda_J^2}\int_{-L}^{y} du f_{n+1}(u) f_n(u) \sin\phi_{n+1}(u) + 2epH + \frac{\varepsilon^2}{\lambda_J^2}\left[\frac{1}{f_{n+1}^2(y)}\int_{-L}^{y} du f_{n+1}(u) \times [f_n(u)\sin\phi_{n+1}(u) - f_{n+2}(u)\sin\phi_{n+2}(u)] - \frac{1}{f_n^2(y)}\int_{-L}^{y} du f_n(u)[f_{n-1}(u)\sin\phi_n(u) - f_{n+1}(u)\sin\phi_{n+1}(u)]\right]. \tag{26}$$

In Eqs. (26), we have introduced the Josephson penetration depth $\lambda_J = (8\pi e j_0 p)^{-1/2}$ and a dimensionless parameter $\varepsilon = p/\lambda$ (Ref. 2). By virtue of (24), (25), equations (26) yield

$$\frac{d\phi_{n+1}}{dy}(\pm L) = \frac{d\phi_n}{dy}(\pm L) \equiv \frac{d\phi}{dy}(\pm L), \tag{27}$$

$$\frac{d\phi}{dy}(\pm L) = 2epH. \tag{28}$$

For given f_n obeying relations (24), equations (26) constitute a system of nonlinear integro-differential equations for ϕ_n, of first order with respect to differentiation. The formulation of the boundary value problem for these equations requires imposition of boundary conditions on ϕ_n. Appropriate boundary conditions at $y = 0$ are provided by the symmetry relations (25), i.e., the boundary conditions are

$$\phi_n(0) = nZ_n, \quad Z_n = 0, \pm 1, \pm 2, \ldots. \tag{29}$$

The main issue now is to find all solutions to (26), (29) that actually make (3) a minimum. As was shown in Refs. 1 and 2, this issue is equivalent to exact minimization of (3) with respect to the phases φ_n. (See also Appendix A.) Below, we present an alternative, simpler method of exact minimization.

Instead of minimizing with respect to φ_n, we introduce a new functional Ω via the relation

$$\Omega_{LD}\left[f_n,\frac{df_n}{dy},\varphi_n,\frac{d\varphi_n}{dy},\mathbf{A};H\right]=\Omega\left[f_n,\frac{df_n}{dy},\varphi_n,\mathbf{A};H\right]+\Omega_0+\frac{pH_c^2(T)\zeta^2(T)W_z}{4\pi}\times\int_{-L}^{L}dy\sum_n\left[\frac{d\varphi_n(y)}{dy}-2eA_y(np,y)\right]^2 f_n^2(y), \tag{30}$$

where

$$\Omega_0\equiv\Omega_{LD}(0)=-\frac{H_c^2(T)pNLW_z}{4\pi} \tag{31}$$

is the LD free energy for $H=0$. The functional Ω will be considered on the same class of functions f_n, φ_n, $\mathbf{A}$ as the functional Ω_{LD}: In particular, these functions are supposed to satisfy conditions (14) at the internal boundaries and natural conditions at the outer boundaries $y=\pm L$.

The advantage of the new functional

$$\Omega\left[f_n,\frac{df_n}{dy},\varphi_n,\mathbf{A};H\right]=\frac{pH_c^2(T)}{4\pi}W_z\int_{-L}^{L}dy\sum_n\left[\frac{1}{2}[1-f_n^2(y)]^2+\zeta^2(T)\left[\frac{df_n(y)}{dy}\right]^2+\frac{r(T)}{2}[f_{n-1}^2(y)+f_n^2(y)-2f_n(y)f_{n-1}(y)\cos\Phi_{n,n-1}(y)]+\frac{4e^2\zeta^2(T)\lambda^2(T)}{p}\int_{(n-1)p}^{np}\times dx\left[\frac{\partial A_y(x,y)}{\partial x}-\frac{\partial A_x(x,y)}{\partial y}-H\right]^2\right] \tag{32}$$

is that it has simple properties: Minimization of (32) does not require variation with respect to φ_n.

Moreover, a local minimum of Ω at a given H, $\min\Omega$, provides a lower bound for Ω_{LD}.

Indeed, the functional Ω is positive, i.e.,

$$\Omega\left[f_n,\frac{df_n}{dy},\varphi_n,\mathbf{A};H\right]\geqslant 0, \tag{33}$$

and its exact lower bound at $H=0$, $\inf\Omega=0$, is achieved on the field configurations

$$\overline{f_n}(y)\equiv 1,\quad \overline{\varphi_n}(y)\equiv\psi(y),\quad \overline{A_x}\equiv 0,\quad \overline{A_y}=\frac{d\psi}{dy}, \tag{34}$$

where $\psi(y)$ is an arbitrary smooth function. [Note that the exact lower bound of (3) at $H=0$, $\inf\Omega_{LD}=\Omega_0$, is achieved on the same field configurations (34).] Because of (33), the continuous functional (32) necessarily has a minimum at any $H>0$ in the allowed class of functions, specified above.[19] By virtue of (30) and the definition of the minimum,

$$\Omega_{LD}\left[f_n,\frac{df_n}{dy},\varphi_n,\frac{d\varphi_n}{dy},\mathbf{A};H\right]\geqslant\Omega\left[f_n,\frac{df_n}{dy},\varphi_n,\mathbf{A};H\right]+\Omega_0\geqslant\min\Omega\left[f_n,\frac{df_n}{dy},\varphi_n,\mathbf{A};H\right]+\Omega_0, \tag{35}$$

where the right-hand side of the second inequality provides the desired lower bound for Ω_{LD} at a given H.

To determine $\min\Omega$, we first find all field configurations $\{f_n,\varphi_n,\mathbf{A}\}$ that satisfy the stationarity condition (1). Variation with respect to f_n yields the equations

$$f_n(y)-f_n^3(y)+\zeta^2(T)\frac{d^2f_n(y)}{dy^2}=\frac{r(T)}{2}[2f_n(y)-f_{n+1}(y)\cos\Phi_{n+1,n}(y)-f_{n-1}(y)\cos\Phi_{n,n-1}(y)] \tag{36}$$

and boundary conditions (10). Variation with respect to A_x leads to the Maxwell equation (11) in the regions $(n-1)p<x<np$ and the boundary conditions (12). By variation with respect to A_y, we obtain the Maxwell equation (13) in the regions $(n-1)p<x<np$ and new boundary conditions at the S layers,

$$h(np-0,y)=k(np+0,y). \tag{37}$$

Application of (37) to (14), in turn, yields

$$\frac{d\varphi_n(y)}{dy}-2eA(np,y)=0. \tag{38}$$

Combining (14) with (13), we get

$$h(x,y)\equiv h(y), \tag{39}$$

which, upon substitution into (11), results in

$$f_{n-1}(y)\sin\Phi_{n,n-1}(y)=f_{n+1}(y)\sin\Phi_{n+1,n}(y). \tag{40}$$

Relations (40) reflect the continuity of the Josephson currents at $x=np$ and constitute a consequence of $U(1)$ gauge symmetry: They can be obtained directly, by varying (32) with respect to φ_n.[1,2] In view of (39), the solution of these relations is straightforward:

$$f_n(y)\equiv f(y),\quad \Phi_{n,n-1}(y)\equiv\phi(y)-2e\int_0^p dxA_x(x,y). \tag{41}$$

Note that relations (39), (41) identically satisfy the periodic boundary conditions (6). According to (41), the phases φ_n obey the finite difference equation $\varphi_{n+1}-2\varphi_n+\varphi_{n-1}=0$ with the boundary condition $\varphi_n-\varphi_{n-1}=\phi$, whose solution is[21]

$$\varphi_n(y)=n\phi(y)+\psi(y), \tag{42}$$

where $\psi(y)$ is an arbitrary smooth function.

Our next course of action follows the steps leading to Eqs. (23)–(29): We fix the gauge by (15) and solve the resulting equations for $A(x,y)$. As a consequence, in addition to (42), we arrive at coupled equations for f and ϕ,

$$f(y)-f^3(y)+\zeta^2(T)\frac{d^2f(y)}{dy^2}+r(T)[1-\cos\phi(y)]f(y)=0,$$

$$\frac{df}{dy}(\pm L)=0, \tag{43}$$

$$\frac{d\phi(y)}{dy}=\frac{1}{\lambda_J^2}\int_{-L}^{y}du f^2(u)\sin\phi(u)+2epH, \tag{44}$$

$$\phi(-y)=-\phi(y)+2\pi Z, \quad Z=0,\pm1,\pm2,... \tag{45}$$

and explicit expressions

$$A(x,y)=\frac{1}{2ep}\frac{d\phi(y)}{dy}x+\frac{1}{2ep}\frac{d\psi(y)}{dy}, \tag{46}$$

$$h(y)=\frac{1}{2ep}\frac{d\phi(y)}{dy}. \tag{47}$$

Any minimizer $\{\overline{f}_n,\overline{\varphi}_n,\overline{\mathbf{A}}\}$ of (32), at a given H, necessarily satisfies (15) and (41)–(47). At the same time, this minimizer automatically satisfies (9)–(14) and (16)–(28). Moreover, as can be easily verified by direct substitution,

$$\Omega_{LD}\left[\overline{f},\frac{d\overline{f}}{dy},\overline{\varphi}_n,\overline{\mathbf{A}};H\right]=\Omega\left[\overline{f},\frac{d\overline{f}}{dy},\overline{\varphi}_n,\overline{\mathbf{A}};H\right]+\Omega_0$$
$$=\min\Omega\left[f_n,\frac{df_n}{dy},\varphi_n,\mathbf{A};H\right]+\Omega_0. \tag{48}$$

According to (35) and the definition of the minimum (8), this means that

$$\Omega_{LD}\left[\overline{f},\frac{d\overline{f}}{dy},\overline{\varphi}_n,\overline{\mathbf{A}};H\right]=\inf\Omega_{LD}\left[f_n,\frac{df_n}{dy},\varphi_n,\frac{d\varphi_n}{dy},\mathbf{A};H\right]$$
$$=\min\Omega_{LD}\left[f_n,\frac{df_n}{dy},\varphi_n,\frac{d\varphi_n}{dy},\mathbf{A};H\right], \tag{49}$$

i.e., any set $\{\overline{f}_n,\overline{\varphi}_n,\overline{\mathbf{A}}\}$ that in the gauge (15) satisfies (41)–(47) and minimizes (32) is a minimizer of (3). On the other hand, for any set $\{f_n,\varphi_n,\mathbf{A}\}$ that in the gauge (15) does not satisfy (41)–(47) we have

$$\Omega_{LD}\left[f_n,\frac{df_n}{dy},\varphi_n,\frac{d\varphi_n}{dy},\mathbf{A};H\right]>\Omega\left[f_n,\frac{df_n}{dy},\varphi_n,\mathbf{A};H\right]$$
$$+\Omega_0\geqslant\min\Omega\left[f_n,\frac{df_n}{dy},\varphi_n,\mathbf{A};H\right]+\Omega_0$$
$$=\Omega\left[\overline{f},\frac{d\overline{f}}{dy},\overline{\varphi}_n,\mathbf{A};H\right]+\Omega_0=\Omega_{LD}\left[\overline{f},\frac{d\overline{f}}{dy},\overline{\varphi}_n,\overline{\mathbf{A}};H\right]$$
$$=\min\Omega_{LD}\left[f_n,\frac{df_n}{dy},\varphi_n,\frac{d\varphi_n}{dy},\mathbf{A};H\right]. \tag{50}$$

A strict inequality in the first line of (50) means that the minimizer $\{\overline{f}_n,\overline{\varphi}_n,\overline{\mathbf{A}}\}$ makes (3) a *strict* minimum.[19] [Note that the gauge (15) was employed here for the sake of convenience only: It allowed us to obtain an explicit solution for $\mathbf{A}$ by simple means.]

Summarizing, we have proved the following: A set $\{\overline{f}_n,\overline{\varphi}_n,\overline{\mathbf{A}}\}$ minimizes the LD functional (3) if and only if it is a minimizer of the functional (32) and, hence, necessarily satisfies the symmetry relations (41), with the resulting local magnetic field obeying (39). In the next subsection, we will show that a full set of the minimizers of (32), and, respectively, of (3), comprises the soliton (vortex-plane) solutions and the Meissner (0-soliton) solution.[1,2]

2.3. The conservation law for the flux and soliton boundary conditions

To determine all the minimizers of (32), we first rewrite this functional as follows:

$$\Omega\left[f,\frac{df}{dy},\phi,\frac{d\phi}{dy};H\right]=\frac{NpWW_zH^2}{8\pi}+\Omega_H\left[f,\phi,\frac{d\phi}{dy}\right]$$
$$-\frac{H\Phi W_z}{4\pi}, \tag{51}$$

where

$$\Omega_H\left[f,\frac{df}{dy},\phi,\frac{d\phi}{dy}\right]=\frac{NpH_c^2(T)}{4\pi}W_z\int_{-L}^{L}dy\left[\frac{1}{2}[1-f^2(y)]^2\right.$$
$$+\zeta^2(T)\left[\frac{df(y)}{dy}\right]^2+r(T)\left[[1-\cos\phi(y)]\right.$$
$$\left.\left.\times f^2(y)+\frac{\lambda_J^2}{2}\left[\frac{d\phi(y)}{dy}\right]^2\right]\right]. \tag{52}$$

and the total flux (7), in view of (15) and (41), is given by

$$\Phi=\frac{N}{2e}[\phi(L)-\phi(-L)]\equiv N\Phi_0\frac{1}{2\pi}\int_{-L}^{L}dy\frac{d\phi(y)}{dy}, \tag{53}$$

with $\Phi_0=\pi/e$ being the flux quantum. Note that the first term on the right-hand side of (51) is merely the energy of the magnetic field in the absence of Josephson coupling.

Note that both Ω and Ω_H explicitly satisfy Legendre's necessary condition of the *strong minimum*:[19]

$$\frac{\delta^2\Omega(H)}{[\delta(df/dy)]^2}\equiv\frac{NpH_c^2(T)W_z}{2\pi}\zeta^2(T)>0,$$

$$\frac{\delta^2\Omega_{(H)}}{[\delta(d\phi/dy)]^2}\equiv\frac{NpH_c^2(T)W_z}{4\pi}r(T)\lambda_J^2(T)>0,$$

$$\frac{\delta^2\Omega_{(H)}}{\delta(df/dy)\,\delta(d\phi/dy)}=\frac{\delta^2\Omega_{(H)}}{\delta(d\phi/dy)\,\delta(df/dy)}\equiv0. \tag{54}$$

Therefore, all stationary points of Ω,Ω_H are either *strong minima* or *saddle points*.

The stationarity condition for both Ω and Ω_H requires that first variations with respect to f and ϕ vanish [compare with (1)]. Variation with respect to f yields Eqs. (43), as expected. Consider now the first variation of Ω and Ω_H with respect to ϕ:

$$\delta\Omega\left[\delta f,\frac{d\delta f}{dy},\delta\phi,\frac{d\delta\phi}{dy};H\right]=\delta\Omega_H\left[\delta f,\frac{d\delta f}{dy},\delta\phi,\frac{d\delta\phi}{dy}\right]$$
$$-\frac{HW_z}{4\pi}\delta\Phi, \tag{55}$$

$$\delta\Omega_H\left[\delta f, \frac{d\delta f}{dy}, \delta\phi, \frac{d\delta\phi}{dy}\right] = \frac{NpH_c^2(T)W_z r(T)}{4\pi} \times \int_{-L}^{L} dy\left[f^2(y)\sin\phi(y) - \lambda_J^2\frac{d^2\phi(y)}{dy^2}\right]\delta\phi(y) + \frac{1}{ep}\frac{d\phi}{dy} \times(-L)\frac{W_z}{8\pi}\delta\Phi, \tag{56}$$

where the variation of the flux is

$$\delta\Phi = \frac{N}{2e}[\delta\phi(L) - \delta\phi(-L)] \equiv N\Phi_0\delta\left(\frac{1}{2\pi}\int_{-L}^{L} dy\frac{d\phi(y)}{dy}\right). \tag{57}$$

The requirement of the vanishing of the volume variation in both (55) and (56) yields

$$\frac{d^2\phi(y)}{dy^2} = \frac{f^2(y)}{\lambda_J^2}\sin\phi(y), \tag{58}$$

which is a mere consequence of (44). However, the requirement of stationarity with respect to surface variation [which is proportional to the variation of the flux (57)] is stronger for (56) than for (55). The surface variation in (55) cancels out owing to the boundary conditions (28). In contrast, conditions (28) do not ensure the vanishing of the surface variation in (56), and the stationarity of Ω_H at $H>0$ requires

$$\delta\Phi = 0, \tag{59}$$

or, equivalently,

$$\Phi = N\Phi_0\frac{1}{2\pi}\int_{-L}^{L} dy\frac{d\phi(y)}{dy} = \text{const} \geqslant 0, \tag{60}$$

where the inequality sign corresponds to $H \geqslant 0$.

Note that higher variations of Ω and Ω_H are equal to each other: $\delta^k\Omega = \delta^k\Omega_H$ $(k \geqslant 2)$. Thus, all the minimizers of Ω_H also minimize Ω. On the other hand, the functional Ω has no minimizers other than those that simultaneously minimize Ω_H. Indeed, let $\{\overline{f}, \overline{\phi}\}$ be a minimizer of Ω in a class of trial functions that admit arbitrary variations $\delta\Phi$. Then $\{\overline{f}, \overline{\phi}\}$ is necessarily a minimizer of Ω in a subclass of trial functions that satisfy (59). From the condition for the minimum of Ω

$$\Omega\left[\widetilde{f} + \delta f, \frac{d\overline{f}}{dy} + \frac{d\delta f}{dy}, \overline{\phi} + \delta\phi, \frac{d\overline{\phi}}{dy} + \frac{d\delta\phi}{dy}; H\right] \geqslant \Omega\left[\overline{f}, \frac{d\overline{f}}{dy}, \overline{\phi}, \frac{d\overline{\phi}}{dy}; H\right] \tag{61}$$

[compare with (2)] on this subclass of trial functions, we have

$$\Omega_H\left[\overline{f} + \delta f, \frac{d\overline{f}}{dy} + \frac{d\delta f}{dy}, \overline{\phi} + \delta\phi, \frac{d\overline{\phi}}{dy} + \frac{d\delta\phi}{dy}\right] - \Omega_H\left[\overline{f}, \frac{d\overline{f}}{dy}, \overline{\phi}, \frac{d\overline{\phi}}{dy}\right] - \frac{HW_z}{4\pi}\delta\Phi = \Omega_H\left[\overline{f} + \delta f, \frac{d\overline{f}}{dy} + \frac{d\delta f}{dy}, \overline{\phi} + \delta\phi, \frac{d\overline{\phi}}{dy} + \frac{d\delta\phi}{dy}\right] - \Omega_H\left[\overline{f}, \frac{d\overline{f}}{dy}, \overline{\phi}, \frac{d\overline{\phi}}{dy}\right] \geqslant 0, \tag{62}$$

which is the condition for the minimum of Ω_H. For this reason, it is sufficient to find all the minimizers of Ω_H.

Physically, conditions (59), (60) ensure the stability of the flux Φ against any small perturbations, represented by the variations $\overline{\phi} \to \overline{\phi} + \delta\phi$, which is a manifestation of the Meissner effect.[22] Conditions (59), (60) also imply that Φ plays the role of a thermodynamic variable in (51), which, in turn, allows us to identify Ω_H as the Helmholz free-energy functional.

Now we will derive the Meissner (0-soliton) and vortex-plane (soliton) boundary conditions[1,2] from the conservation law for the flux (59), (60). As a starting point, we note that all the extremals of Ω_H that satisfy (58), (28) possess the symmetry properties (45). Since trial functions of this type take on only discrete values at $y=0$, $\phi(0) = \pi Z$, the requirement of continuity of variations $\delta\phi$ imposes the constraint

$$\delta\phi(0) = \pi\delta Z = 0. \tag{63}$$

Equations (57), (59), in turn, yield

$$\delta\phi(L) = \delta\phi(-L). \tag{64}$$

On the other hand, relations (45), applied at $y=L$, by virtue of (63) yield

$$\delta\phi(L) = -\delta\phi(-L). \tag{65}$$

Combining (64) with (65), we arrive at the conditions

$$\delta\phi(\pm L) = 0. \tag{66}$$

Using (60), we write:

$$\frac{\phi(L) - \phi(-L)}{2\pi} = \frac{1}{2\pi}\int_{-L}^{L} dy\frac{d\phi(y)}{dy} = \left[\frac{1}{2\pi}\int_{-L}^{L} dy\frac{d\phi(y)}{dy}\right] + \left\{\frac{1}{2\pi}\int_{-L}^{L} dy\frac{d\phi(y)}{dy}\right\} = \text{const} \geqslant 0, \tag{67}$$

where $[x]$ and $\{x\}$ are, respectively, the integer and fractional parts of x $[0 \leqslant \{x\} < 1]$. On the other hand, taking account of (45) and (63), (66), we have

$$\frac{\phi(L) - \phi(-L)}{2\pi} = Z - \frac{\phi(-L)}{\pi} = \text{const} \geqslant 0. \tag{68}$$

A comparison of (67) with (68) leads to the identification

$$\frac{\phi(0)}{\pi} = Z = N_v \equiv \left[\frac{1}{2\pi}\int_{-L}^{L} dy\frac{d\phi(y)}{dy}\right] \geqslant 0, \tag{69}$$

$$-\frac{\phi(-L)}{\pi}\equiv\left\{\frac{1}{2\pi}\int_{-L}^{L}dy\,\frac{d\phi(y)}{dy}\right\},\ -\pi<\phi(-L)\leqslant 0. \tag{70}$$

Relations (69), (70) are exactly the Meissner ($N_v=0$) and vortex-plane ($N_v=1,2,\ldots$) boundary conditions employed in Refs. 1 and 2. The conserved topological index $N_v=0,1,2\ldots$ has a clear meaning of the number of solitons (i.e., vortex planes or the *Josephson vortices*) at $H>0$. The conserved flux (60), rewritten via the conserved quantities N_v and $\phi(-L)$, takes the form

$$\Phi=N\Phi_0\left[N_v+\frac{|\phi(-L)|}{\pi}\right]. \tag{71}$$

As follows from (71), the solution with given N_v appears when

$$\phi(-L)=0,\quad \phi(0)=\pi N_v,\quad \phi(-L)=2\pi N_v, \tag{72}$$

which corresponds to the minimum of the Josephson energy density [the third term on the right-hand side of (52)] at the boundaries $y=\pm L$. This solution vanishes when

$$\phi(\pm L)=\pm\pi,\quad \phi_n(0)=\pi N_v, \tag{73}$$

which corresponds to the maximum of the Josephson energy density at $y=\pm L$ and saddle-point instability. By (28), conditions (72), (73) determine, respectively, the exact lower and upper bounds of the stability regions of the Meissner ($N_v=0$) and vortex ($N_v=1,2,\ldots$) configurations in the external field $H\geqslant 0$.

We will show now that conditions (69), (70) for the SG equations (58) together with (44) actually specify all the minimizers of (52) [and, accordingly, of (51)]. Indeed, let $\overline{f}(y)$ be an arbitrary smooth function that for $y\in[-L,L]$ satisfies the conditions $0<\overline{f}\leqslant 1$, $(d\overline{f}/dy)(\pm L)=0$, and $\overline{f}_0\equiv\min\overline{f}(y)$. Using the elementary inequalities $a+b\geqslant 2\sqrt{ab}$ $(a,b>0)$ and $-|q|\leqslant q\leqslant|q|$, we derive a sequence of inequalities for (52) with $f=\overline{f}$:

$$\begin{aligned}\Omega_H\left[\overline{f},\frac{d\overline{f}}{dy},\phi,\frac{d\phi}{dy}\right]&\geqslant C+\frac{NpH_c^2(T)W_z r(T)}{4\pi}\times\int_{-L}^{L}dy\left[\overline{f}_0^2[1-\cos\phi(y)]+\frac{\lambda_J^2}{2}\left[\frac{d\phi(y)}{dy}\right]^2\right]\\&\geqslant C+\frac{NpH_c^2(T)W_z r(T)\lambda_J\overline{f}_0}{4\pi}\times\int_{-L}^{L}dy\left|\sin\frac{\phi(y)}{2}\right|\left|\frac{d\phi(y)}{dy}\right|\\&\geqslant C+\frac{2NpH_c^2(T)W_z r(T)\lambda_J\overline{f}_0}{\pi}\times\left[N_v+1-\cos\frac{\phi(-L)}{2}\right],\end{aligned} \tag{74}$$

where

$$C\equiv\frac{NpH_c^2(T)W_z}{4\pi}\times\int_{-L}^{L}dy\left[\frac{1}{2}[1-\overline{f}^2(y)]^2+\zeta^2(T)\times\left[\frac{d\overline{f}(y)}{dy}\right]^2\right]\geqslant 0.$$

Inequalities of the type (74) are employed in soliton theory to prove the existence and stability of soliton solutions.[10–12,23] In our case, inequality (74) shows that (52) has an exact lower bound in the class of functions $\{f,\phi\}$ parameterized by the conserved quantities N_v and $\phi(-L)$:

$$\inf\Omega_H\left[f,\frac{df}{dy},\phi,\frac{d\phi}{dy}\right]=\mu[N_v,\phi(-L)],$$

$$\mu[N_v,\phi(-L)]\geqslant\frac{2NpH_c^2(T)W_z r(T)\lambda_J f_*}{\pi}\left[N_v+1-\cos\frac{\phi(-L)}{2}\right], \tag{75}$$

where $f_*>0$ is the same for all the sets $\{N_v,\phi(-L)\}$.

In view of the continuity of Ω_H,[19] the exact lower bound (75) is achieved on the corresponding solution $\{\overline{f},\overline{\phi}\}$ to (43), (58), (69), and (70). According to Sec. 2.2, this solution represents the desired minimizer of (3). Given that for any minimizer

$$\Omega_{LD}\left[\overline{f},\frac{d\overline{f}}{dy},\overline{\varphi}_n,\overline{\mathbf{A}};H\right]=N\omega_{LD}\left[\overline{f},\frac{d\overline{f}}{dy},\overline{\varphi}_n,\overline{\mathbf{A}};H\right],$$

where $\omega_{LD}<\infty$, we have thus proved the existence of the thermodynamic limit for $N\to\infty$.

For practical applications, we note the first integral of Eqs. (43), (58) that immediately follows from (52):

$$\zeta^2(T)\left[\frac{df}{dy}\right]^2+\frac{r(T)\lambda_J^2}{2}\left[\frac{d\phi}{dy}\right]^2+f^2-\frac{1}{2}f^4-r(T)[1-\cos\phi]f^2=C, \tag{76}$$

where the constant of integration can be determined from the boundary conditions at $y=-L$:

$$C=2e^2p^2\lambda_J^2H^2+f^2(-L)-\frac{1}{2}f^4(-L)-r(T)[1-\cos\phi(-L)]f^2(-L). \tag{77}$$

2.4. A topological classification and isomorphism to Abrikosov vortices in type-II superconductors

The above results can be given a very clear interpretation within the framework of the theory of topological defects in continuous media.[10–12,24] Consider the thermodynamic LD free energy, obtained by the substitution of a minimizer $\{\overline{f}_n,\overline{\varphi}_n,\overline{\mathbf{A}}\}$ into (3):

$$\Omega_{LD}(H)=\Omega_0+\frac{NpWW_zH^2}{8\pi}-\frac{H\Phi W_z}{4\pi}+\frac{NpH_c^2(T)W_z}{4\pi}\int_{-L}^{L}dy\left[\frac{1}{2}[1-\overline{f}^2(y)]^2+\zeta^2(T)\left[\frac{d\overline{f}(y)}{dy}\right]^2+r(T)\left[\overline{f}^2(y)[1-\cos\overline{\phi}(y)]+\frac{\lambda_J^2}{2}\left[\frac{d\overline{\phi}(y)}{dy}\right]^2\right]\right]. \tag{78}$$

Owing to the symmetry relations (24), (41), (45) and the boundary conditions (10), (28), the density of $\Omega_{LD}(H)$ is equal at $y=-L$ and $y=+L$ and thus corresponds to the degenerate equilibrium (''vacuum'') state, unperturbed by topological defects (solitons). Mathematically, the boundary of the interval $-L\leqslant y\leqslant L$ can be considered as a 0-dimensional sphere: $S^0=\{-L,+L\}$. Given that configurations $\overline{\phi}$ and $\overline{\phi}+2\pi Z$ $(Z=0,\pm1,\pm2,\ldots)$ are physically indistinguishable, we can fix the values $\overline{\phi}(-L)$ as in (70) and regard the functions

$$\psi(+L)\equiv\frac{\overline{\phi}(+L)+\overline{\phi}(-L)}{2\pi}=Z_n\equiv\left[\frac{1}{2\pi}\int_{-L}^{L}dy\,\frac{d\overline{\phi}(y)}{dy}\right] \tag{79}$$

as continuous maps of the boundary into the additive group of the integers, $\mathbf{Z}$: $S^0\overset{\psi}{\rightarrow}\mathbf{Z}$. ($\mathbf{Z}$ is the group of the degeneracy of the equilibrium state, or the order-parameter space.) The fact of the existence of topologically nontrivial maps of this type, realized by soliton solutions, can be expressed in terms of the zeroth homotopy group[10–13,24] $\pi_0(M)$, where the index ''0'' stands for the boundary S^0 and M is the order-parameter space:

$$\pi_0(\mathbf{Z})=\mathbf{Z}. \tag{80}$$

The external field $H>0$ breaks the symmetry $\overline{\phi}\rightarrow-\overline{\phi}$ [see the third term on the right-hand side of (78)]. Therefore, only the values $Z\equiv N_v=0,1,2,\ldots$ are allowed, with $N_v=0$ being the ''vacuum'' Meissner state. In this way, we arrive at a natural classification of the minimizers of (3) with respect to the conserved topological (vortex) number N_v.

Note that in the case of Abrikosov vortices in continuum type-II superconductors the boundary is topologically equivalent to the circle S^1, the order-parameter space is also the circle: $M\equiv S^1$ (Refs. 10–13). Thus, the pertinent homotopy group is the fundamental group of the circle:

$$\pi_1(S^1)=\mathbf{Z}. \tag{81}$$

Since in the presence of an external field $H>0$ the topological indices for Abrikosov vortices take on the values $Z\equiv N_v=0,1,2,\ldots$, relations (80) and (81) establish an isomorphism between the vortex structure in type-II superconductors and that in layered superconductors at $H>0$, with $N_v=0$ for the Meissner state and a single Abrikosov vortex $(N_v=1)$ standing in a one-to-one correspondence with a single vortex plane (not an ''isolated fluxon'' as is claimed in previous publications[41]).

3. THE EXACT, CLOSED-FORM SOLUTION FOR $r(T)\ll1$ AND ISOMORPHISM TO JOSEPHSON VORTICES IN THE SINGLE JUNCTION

Equations (43) and (58) with the soliton boundary conditions (69) and (70) can be solved by perturbation methods for arbitrary values of the interlayer coupling $r(T)$. Of particular interest, however, is the limit of weak coupling, $r(T)\ll1$.

In the case $r(T)\ll1$ the zeroth-order solution to (43) has the form $f_0\equiv1$. Upon substitution into (58), we obtain the well-known static sine-Gordon equation:

$$\frac{d^2\phi(y)}{dy^2}=\frac{1}{\lambda_J^2}\sin\phi(y). \tag{82}$$

Under the conditions (69), (70), the exact solution to (82) is

$$\phi(y)=\pi(N_v-1)+2\ \mathrm{am}\left(\frac{y}{k\lambda_J}+K(k^2),k\right), \tag{83}$$

$$\mathrm{dn}\left(\frac{L}{k\lambda_J},k\right)=\frac{\sqrt{1-k^2}}{k}\,\frac{H_s}{H},\quad N_v=2m,\quad m=0,1,\ldots; \tag{84}$$

$$\phi(y)=\pi N_v+2\ \mathrm{am}\left(\frac{y}{k\lambda_J},k\right), \tag{85}$$

$$\mathrm{dn}\left(\frac{L}{k\lambda_J},k\right)=k\,\frac{H}{H_s},\quad N_v=2m+1,\quad m=0,1,\ldots, \tag{86}$$

where $\mathrm{am}(u)$ and $\mathrm{dn}(u)=(d/du)\mathrm{am}(u)$ are the Jacobian elliptic functions, and $K(k^2)$ is the elliptic integral of the first kind.[25]

The stability ranges for the solution (83)–(86) are determined from (28), (72) and (73). They are given by

$$0\leqslant H<H_0,\quad N_v=0; \tag{87}$$

$$\sqrt{H_{N_v-1}^2-H_s^2}\leqslant H<H_{N_v},\quad N_v=1,2,\ldots. \tag{88}$$

The upper bounds in (87) and (88), H_{N_v} $(N_v=0,1,2,\ldots)$, are determined by the implicit equation

$$\frac{L}{\lambda_J}=(N_v+1)\,\frac{H_s}{H_{N_v}}K\left(\frac{H_s^2}{H_{N_v}^2}\right),\quad N_v=0,1,2,\ldots, \tag{89}$$

where $H_s=(ep\lambda_J)^{-1}$ is the superheating field of the Meissner state in a semi-infinite $(0\leqslant y<\infty)$ layered superconductor,[1,2] and $H_0\equiv H_{sL}>H_s$ is the superheating field of the Meissner state for $L<\infty$. Upon substitution of (83)–(86) into (78) (with $\overline{f}\equiv1$, $\overline{\phi}\equiv\phi$), one can verify the lower-bound estimates (74), (75). In Appendix B, we show that the solution (83)–(89) satisfies the Jacobi–Weierstrass–Hilbert sufficient condition for a strong minimum[19] of (51) [and hence of (3)].

Note that equation (82) was first analyzed in the context of a single Josephson junction a long time ago.[26,27] It has been discussed in numerous subsequent publications.[28] Unfortunately, the complete, exact, closed-form solution (83)–(89), valid for arbitrary values of $L>0$ and $H\geqslant0$, has not been obtained until now. This situation was reflected in the absence of any clear mathematical definition of the Josephson vortex at $H>0$ and gave rise to the erroneous belief[15,16] that Josephson vortices ''do not exist'' for $L\ll\lambda_J$.

Equations (83)–(89) provide an explicit form for the complete set of minimizers of the LD model (3) with $r(T) \ll 1$ and generalize the results of Refs. 1 and 2. For $N_v = 1,2,\ldots$ they provide a complete set of soliton solutions to the coupled static SG equations (A1) and establish a one-to-one correspondence between vortex planes in layered superconductors and ordinary Josephson vortices in the single junction. (The only difference lies in the definition of the Josephson length λ_J.) For these reasons, the properties of (83)–(89) are of crucial importance.

Equations (83)–(86) reflect a general soliton feature: Solutions (83), (84) with even N_v cannot be continuously transformed into solutions (85), (86) with odd N_v by changing H and *vice versa*. Solutions with $N_v \geqslant 1$ are pure solitons (vortex planes) only at $H = \sqrt{H^2_{N_v-1} - H_s^2}$, which corresponds to the boundary conditions (72). In the rest of the regions (88), we have solitons "dressed" by the Meissner field. (The Meissner and the vortex fields cannot be separated from each other, because the principle of superposition does not apply to the nonlinear equations (A1). Unfortunately, this important issue was not understood in previous publications.[29])

Of special interest is the overlap of the regions (87), (88) for $N_v = \overline{N}_v$ and $N_v = \overline{N}_v + 1$. Owing to this property, the solutions obtained cover the whole field range $0 \leqslant H < \infty$, as they should. The overlap practically vanishes for $H_{N_v} \gg H_s$. Given that all H_{N_v} decrease when $W = 2L$ increases, the overlap is stronger for large W and can involve several neighboring states. As explained in the Introduction, the actual equilibrium state is the one that corresponds to the minimum of the thermodynamic Gibbs free energy for given H. A transition from the state with $N_v = \overline{N}_v$ to the state $N_v = \overline{N}_v + 1$ with lower Gibbs free energy is a phase transition of the first-order type.[1,2] In particular, the lower critical field H_{c1} is determined from the requirement that the Gibbs free energy of the state $N_v = 1$ be equal to that of the Meissner state ($N_v = 0$) and satisfy the relation $\sqrt{H^2_{sL} - H_s^2} < H_{c1} < H_{sL}$. In the case $\lambda_J \ll L < \infty$, it is given by $H_{c1} = 2H_s/\pi$.[1,2]

Equations (83)–(89) contain the corresponding results of Refs. 1 and 2 as limiting cases. For example, by making the change of variable $y \to y - L$ and proceeding to the limit $L \to \infty$ in Eqs. (83), (84) with $N_v = 0$, we obtain the exact Meissner solution in the semi-infinite interval $y \in [0, +\infty)$:

$$\phi(y) = -4 \arctan \frac{H \exp[-y/\lambda_J]}{H_s + \sqrt{H_s^2 - H^2}}. \tag{90}$$

By proceeding to the limit $L \to \infty$ in Eqs. (85), (86) with $N_v = 1$, we arrive at the vortex-plane solution in the infinite interval $y \in (-\infty, +\infty)$:

$$\phi(y) = 4 \arctan \exp[y/\lambda_J]. \tag{91}$$

When the screening by Josephson currents is negligibly small, i.e., (i) for $L \ll \lambda_J$ and arbitrary H, or (ii) for $H_s \ll H$ and arbitrary L, equations (83)–(89) become

$$\phi(y) = \pi N_v + 2epHy - \frac{(-1)^{N_v}}{4e^2p^2\lambda_J^2H^2}[\sin(2epHy) - 2epHy \cos(epHW)], \tag{92}$$

where $N_v = [epHW/\pi]$ [see (69)]. The overlap of states with different N_v now practically vanishes, and the period of the vortex structure for $N_v \geqslant 1$ is $P = \pi/epH$, which refutes the claims[15,16] that Josephson vortices "do not exist" in the limit $L \ll \lambda_J$.

The substitution of (92) into (78) gives the equilibrium value of the LD free-energy functional (the thermodynamic free energy):

$$\Omega_{LD}(H) = \frac{H_c^2(T) pNLW_z}{4\pi} \times \left[-1 + r(T) \left[1 - \frac{|\sin(epHW)|}{epHW} + \frac{\cos^2(epHW)}{8(ep\lambda_J H)^2} \right] \right]. \tag{93}$$

4. DISCUSSION

We have obtained a complete, exact solution of the problem of the magnetic properties of layered superconductors with an infinite number of superconducting layers ($N = \infty$) in parallel fields $H > 0$, in the absence of transport currents. Based on a new exact variational method (Secs. 2.2 and 2.3 and Appendix A), we have determined the type of all stationary points of the Gibbs free-energy functional (3) and the related Helmholtz free-energy functional [derived from (3) by setting $H = 0$]: For the Gibbs free-energy functional, they are either points of *strict, strong minima* or *saddle points*. All stationary points of the Helmholtz free-energy functional are those of *strict, strong minima*.

By evaluating the surface variation of the Helmholtz free-energy functional, we have found a complete set of stable, equilibrium field configurations: Namely, the Meissner (0-soliton or "vacuum") solution and soliton (vortex-plane) solutions. These solutions conserve the flux and realize exact lower bounds of the Helmholtz free-energy functional in the corresponding topological sectors. As is shown in Appendix A, the absence of soliton solutions of the "fluxon" and "lattice" types at $H > 0$ is due to the boundary conditions on the derivatives of the phase differences [Eqs. (27), (28)] that require the continuity of the local field at the outer interfaces. Physically, the fact that a vortex plane locally minimizes the free-energy functionals means that, contrary to a widespread belief,[4] the effective interaction between flux quanta positioned in *different* insulating layers is *attractive*. The topological methods of Sec. 2.4 establish the true mathematical analogy between the vortex structure in continuum type-II superconductors and that in layered superconductors at $H > 0$: It consists in an isomorphism between a single Abrikosov vortex and a single *vortex plane*. (Note the role of the conservation law for the flux in the derivation of these results: Such conservation laws in nonlinear field theories always yield soliton solutions that minimize the energy functionals.[10–13])

In the limit of weak interlayer coupling, $r(T) \ll 1$, we have derived exact, closed-form analytical expressions for all stable solutions [Eqs. (83)–(89)]. Solutions (83)–(89) explicitly satisfy the SG equations (A1) with a full set of boundary conditions. They meet the Legendre necessary and Jacobi–Weierstrass–Hilbert sufficient conditions for a strong minimum[19] and contain the exact results of Refs. 1 and 2 as particular limiting cases. Expressions (83)–(89) provide an

adequate description of real physical systems with $N \gg [\varepsilon^{-1}]$, $\varepsilon \ll 1$ (see Appendix A), when boundary effects along the layering axis can be neglected.

We can now answer the question what kind of configurations correspond to saddle points of (3). As is shown in Sec. 2.3 and Appendix A, all saddle-point configurations are nonsoliton and violate the conservation law for the flux. Saddle points of the first type appear if one increases the external field H beyond the stability regions (87), (88). (Saddle points of this type exist already in the case of a single Josephson junction.) Saddle points of the second type appear as solutions to the boundary value problem (27), (28), (A18) for (A1), where the Z_n violate (A22). Nonsoliton solutions of this type, interpreted as ''vortex lattices,'' have been considered in some previous publications on the LD model:[6,7,14] As is shown in Appendix C, they are just perturbations of the soliton solutions (83)–(86) with $N_v > 0$. Note that nonsoliton numerical solutions[16,17] for finite ($N < \infty$) Josephson-junction stacks, interpreted as ''isolated fluxons,'' belong to the same type: They are characterized by the condition

$$\left[\frac{1}{2\pi}\int_{-L}^{L} dy\,\frac{d\phi_n(y)}{dy}\right] = 0$$

for all n and thus constitute perturbations of the Meissner solution (83), (84) with $N_v = 0$.

It is instructive to compare our mathematical approach with previous approaches. Both in Refs. 1 and 2 and in the present paper, we start by exact minimization of the Gibbs free-energy functional. By determining a complete set of minimizers, we arrive at a natural physical interpretation of all relevant mathematical relations and the identification of equilibrium Josephson vortices as topological solitons (vortex planes). [In the weak-coupling limit, they are just the soliton solutions to the SG equations (A1).] In contrast, previous publications on the LD model started with the *a priori* assumption that the vortex structure in layered superconductors resembled that in continuum type-II superconductors.[4–9] Unfortunately, similarities in the spatial distribution of field configurations were erroneously sought. However, unlike the true analogy in terms of homotopy theory (Sec. 2.4), any analogy in the configurational space is precluded by fundamental differences between the Gibbs free-energy functional (3) and that of continuum type-II superconductors.

We have already pointed out (Refs. 1 and 2 and the Introduction) the inadequacy of mathematical methods of previous publications. It should be added that the necessity of ensuring the vanishing of the surface variation in the stationarity condition for the Helmholtz free-energy functional was not taken into account:[4,7–9] As a result, the conservation law for the flux and soliton solutions were lost. Since the exact solvability and soliton solutions of the SG equations (A1) were not noticed, no mathematical definition of the Josephson vortex could be given. This situation has led to confusion as to what might be called the Josephson vortex at $H > 0$ even in the simplest case of the single junction: Hence the erroneous claims[15,16] that Josephson vortices ''do not exist'' for $L \ll \lambda_J$.

The problem of the stability of the proposed nonsoliton configurations (i.e., whether they correspond to any points of minima of the Gibbs free-energy functional) has never been posed in previous theoretical publications. [This fact is not surprising in view of the neglect of the conservation law for the flux and accompanying uncontrolled mathematical approximations.[3)]] Unfortunately, the issue of stability was disregarded in numerical simulations[16] for finite ($N < \infty$) Josephson-junction stacks as well: hence the misunderstanding[17] of the profound physical and mathematical difference between soliton and nonsoliton solutions.

In summary, the central result of this paper is that equilibrium Josephson vortices in layered superconductors with $N = \infty$ are topological solitons of the static SG equations for the phase differences. This result should be viewed in the general context of vortex solutions in nonlinear field theories.[10–13] (For example, Abrikosov vortices in continuum type-II superconductors are topological solitons of the GL equations.) Mathematically, the exact, closed-form expressions (83)–(89) represent a new class of soliton solutions. Aside from their importance for weak superconductivity, they can find applications in different fields of nonlinear physics and applied mathematics where the SG equations are involved.[11]

APPENDIX A

The solution of coupled static SG equations

In the limit of weak coupling, considered in Sec. 3, the zeroth-order [with respect to $r(T) \ll 1$] solution to (9), (10) has the form $f_n \equiv 1$. Upon substitution into Eqs. (26) and subsequent differentiation with respect to y, the latter equations are reduced to coupled static SG equations

$$\lambda_J^2 \frac{d^2\phi_n(y)}{dy^2} = \frac{1}{\varepsilon^2}\sum_m G^{-1}(n,m)\sin\phi_m(y), n = 1,...,N, \tag{A1}$$

where $G^{-1}(n,m)$ is a Jacobian matrix[31] with elements $G^{-1}(n,n) = 2 + \varepsilon^2$ $(n = 1,...,N)$, $G^{-1}(n+1,n) = G^{-1}(n,n+1) = -1$ $(n = 1,...,N-1)$, and $G^{-1}(n,m) = 0$ for $|n-m| > 1$. Owing to the periodic boundary conditions

$$\phi_{n+N}(y) = \phi_n(y) \tag{A2}$$

[see (6)], the matrix $G^{-1}(n,m)$ is cyclic. Equations (A1) are subject to conditions (27), (28), and their solutions obey the symmetry relations (25).

In the limit $N \to \infty$, equations (A1) were derived by a different method in a number of publications.[6,7] Unfortunately, their analytical properties have not been studied. The main property can be formulated as the following proposition:

Proposition. Consider Eqs. (A1) on the whole axis $-\infty < y < +\infty$. The initial value problem for Eqs. (A1) with arbitrary initial conditions

$$\phi_n(y_0) = \alpha_n, \quad \frac{d\phi_n}{dy}(y_0) = \beta_n \quad (|y_0| < \infty)$$

has a unique solution in the whole interval $-\infty < y < +\infty$. This solution has continuous derivatives with respect to y of arbitrary order and depends continuously on the initial data.

To prove the Proposition, we note that Eqs. (A1) satisfy the conditions of Picard's theorem on the existence and

uniqueness of a *global* solution.[32] This property is rather unusual for nonlinear differential equations: A global character of the solution and its infinite differentiability are ensured by the fact that the ϕ_n enter the right-hand side of Eqs. (A1) only as arguments of the sine.

Equations (A1) can be rewritten in an equivalent form:

$$\sin\phi_n(y)=\varepsilon^2\lambda_J^2\sum_m G(n,m)\frac{d^2\phi_m(y)}{dy^2},\quad n=1,...,N. \tag{A3}$$

The matrix $G(n,m)$, being the inverse of $G^{-1}(n,m)$, has the form

$$G(n,m)=\frac{\mu^{|n-m|}}{2\varepsilon\sqrt{1+\varepsilon^2/4}},\quad \mu=1+\frac{\varepsilon^2}{2}-\varepsilon\sqrt{1+\varepsilon^2/4}, \tag{A4}$$

and obeys the summation rule

$$\sum_m G(n,m)=\frac{1}{\varepsilon^2}. \tag{A5}$$

The matrix $G(n,m)$ is positive definite, because all its eigenvalues e_k are positive:

$$e_k=\frac{\lambda_k^2}{\varepsilon^2\lambda_J^2},\quad \lambda_k=\frac{\varepsilon\lambda_J}{\sqrt{2+\varepsilon^2-2\cos(2\pi k/N)}},$$
$$k=0,\pm1,...,\left[\frac{N}{2}\right]. \tag{A6}$$

The quantities λ_k in (A6) are the characteristic length scales of Eqs. (A1). [Note that (A1) is characterized by a distribution of length scales, not just two length scales, as is claimed in some previous publications.] The distribution of the length scales becomes quasicontinuous under the condition

$$N\gg[\varepsilon^{-1}], \tag{A7}$$

which can be regarded as a criterion of applicability of the LD model to layered superconductors.

The fact that equilibrium solutions (83)–(89) correspond to the largest length scale $\lambda_{\max}\equiv\lambda_0\equiv\lambda_J$ is by no means surprising: In equilibrium, the system tends to minimize the diamagnetic response to the external field H. Note that for $N\to\infty$, $H=0$, $L=\infty$, equations (A1) admit an exact soliton–antisoliton solution

$$\phi_n(y)=(-1)^n\phi(y),\quad \phi(y)=4\arctan\exp\left(\frac{y}{\lambda_{\min}}\right), \tag{A8}$$

$$\lambda_{\min}\equiv\lambda_{[N/2]}=\frac{\varepsilon\lambda_J}{\sqrt{4+\varepsilon^2}}. \tag{A9}$$

However, solution (A8), (A9) vanishes for any $H>0$, $L<\infty$.

Note the first integral of (A1):

$$\sum_n\cos\phi_n(y)+\frac{\varepsilon^2\lambda_J^2}{2}\sum_n\sum_m G(n,m)\frac{d\phi_n(y)}{dy}\frac{d\phi_m(y)}{dy}=C. \tag{A10}$$

In the case of a finite interval $y\in[-L,L]$ the constant of integration C can be determined from the conditions (27), (28):

$$C=\frac{2NH^2}{H_s^2}+\sum_n\cos\phi_n(-L). \tag{A11}$$

$C=N$ in the infinite interval $y\in(-\infty,+\infty)$.

Now, we will prove that Eqs. (83)–(89) provide a complete set of stable solutions to (A1) at $H>0$. Using equations of Secs. 2.1, 2.2 with $f_n\equiv1$ and introducing the "local magnetic field" in the regions $(n-1)p\leqslant x<np$ via

$$h_n(y)=\frac{\varepsilon^2}{2ep}\sum_m G(n,m)\frac{d\phi_m(y)}{dy}, \tag{A12}$$

we rewrite (3) as follows:

$$\Omega_{LD}\left[\phi_n,\frac{d\phi_n}{dy};H\right]=\Omega_0+\Omega^*\left[\phi_n,\frac{d\phi_n}{dy};H\right], \tag{A13}$$

$$\begin{aligned}\Omega^*\left[\phi_n,\frac{d\phi_n}{dy};H\right]&=\frac{pW_z}{8\pi}\sum_n\int_{-L}^{L}dy\left[\frac{H_s^2}{2}[1-\cos\phi_n(y)]+\frac{1}{\varepsilon^2}[h_{n+1}(y)-h_n(y)]^2+[h_n(y)-H]^2\right]\\&=\frac{NpWW_z^2H}{8\pi}+\Omega_H^*\left[\phi_n,\frac{d\phi_n}{dy}\right]-\frac{H\Phi W_z}{4\pi}\geqslant0,\end{aligned} \tag{A14}$$

where

$$\begin{aligned}\Omega_H^*\left[\phi_n,\frac{d\phi_n}{dy}\right]&=\frac{H_s^2pW_z}{16\pi}\int_{-L}^{L}dy\left[\sum_n[1-\cos\phi_n(y)]+\frac{\varepsilon^2\lambda_J^2}{2}\sum_n\sum_m G(n,m)\times\frac{d\phi_n(y)}{dy}\frac{d\phi_m(y)}{dy}\right]\geqslant0\end{aligned} \tag{A15}$$

is the Helmholtz free-energy functional, and the total flux is given by

$$\Phi=\frac{1}{2e}\sum_n[\phi_n(L)-\phi_n(-L)]. \tag{A16}$$

The treatment of the functionals Ω^*, Ω_H^* is fully analogous to that of Ω,Ω_H in Sec. 2.3. Thus, by virtue of positive definitiveness of (A4), the Legendre necessary condition for a *strong minimum*,[19]

$$\sum_n\sum_m G(n,m)\rho_n\rho_m>0,\quad \sum_n\rho_n^2\neq0, \tag{A17}$$

where ρ_n are arbitrary real numbers, is explicitly fulfilled. The functionals Ω^*, Ω_H^* have a common set of minimizers. The stationarity condition for Ω_H^* involves the vanishing of the volume variation, which yields Eqs. (A3), and of the

surface variation, which leads, by (27) and (A16), to the conservation law for the flux $\delta\Phi=0$. By analogy with (69), (70), we arrive at soliton boundary conditions

$$\frac{\phi_n(0)}{\pi}=Z_n\equiv\left[\frac{1}{2\pi}\int_{-L}^{L}dy\,\frac{d\phi_n(y)}{dy}\right]\geqslant 0\,(n=1,...,N), \tag{A18}$$

$$-\frac{\phi_n(-L)}{\pi}\equiv\left\{\frac{1}{2\pi}\int_{-L}^{L}dy\,\frac{d\phi_n(y)}{dy}\right\},\quad -\pi < \phi_n(-L)\leqslant 0. \tag{A19}$$

The soliton solution in the sector $\{Z_1,\ldots,Z_N\}$ first appears under the N conditions

$$\phi_1(-L)=\ldots=\phi_N(-L)=0 \tag{A20}$$

[see (A19)] and the $N-1$ conditions

$$\frac{d\phi_1}{dy}(-L)=\ldots=\frac{d\phi_N}{dy}(-L)=2epH^*\geqslant 0, \tag{A21}$$

where the field H^* is as yet undetermined [compare with (27), (28)]. Given that the general solution to (A1) contains $2N$ constants of integration, conditions (A20), (A21) leave only one undetermined constant to satisfy the boundary conditions (A18). For this reason, we have to set

$$Z_1=\ldots Z_N=Z\equiv N_v=0,1,\ldots. \tag{A22}$$

For $H^*=0$, by the Proposition, the unique solution to the initial value problem (A20), (A21) in the interval $y\in[-L,L]$ is the trivial Meissner configuration $\phi_1=\ldots\phi_N\approx 0$, $N_v=0$. For arbitrary $H^*>0$, by the Proposition, the initial-value problem (A20), (A21) also admits a unique solution in the interval $y\in[-L,L]$, and its explicit form is

$$\phi_1(y)=\ldots=\phi_N(y)\equiv\phi(y)=-\pi+2\ \mathrm{am}\left(\frac{y+L}{k\lambda_J}+K(k^2),k\right), \tag{A23}$$

$$k=\frac{H_s}{H^{*2}+H_s^2}. \tag{A24}$$

Upon substitution of (A23) and (27) into (A18), with (A22) and $N_v=1,2,\ldots$, we determine $H^*=\sqrt{H_{N_v-1}-H_s^2}$, where the H_{N_v} are given by (41). In this way, we arrive at the solutions (83)–(89), which proves their uniqueness as minimizers of (A13)–(A15). This proof clearly demonstrates that the absence of soliton solutions of any other types is a result of the physical boundary conditions (A21) [or (27), (28)].

To establish a connection to the exact variational method of Refs. 1 and 2, we note that (83)–(89) can also be obtained by the minimization of (A13)–(A15) with respect to the phases φ_n. (We recall that $\phi\equiv\varphi_n-\varphi_{n-1}$). However, as was first noticed in Refs. 1 and 2, we must take into account that not all the φ_n are independent: The conservation law for the current (22) constitutes a constraint on $d\varphi_n/dy$. This problem can be easily circumvented by making use of the first integral (A10), (A11). The substitution of (A10), (A11) into (A15) yields

$$\Omega_H^*\left[\phi_n;\phi_n(-L),\frac{d\phi}{dy}(-L)\right]=\frac{NWW_z}{32\pi e^2 p}\left[\frac{d\phi}{dy}(-L)\right]^2+\frac{H_s^2 pW_z}{16\pi}\int_{-L}^{L}dy\sum_n\,[1-2\cos\phi_n(y)+\cos\phi_n\times(-L)]. \tag{A25}$$

Taking the variation of (A25) with respect to φ_n, we immediately arrive at the relations

$$\sin\phi_n(y)=\sin\phi_{n+1}(y) \tag{A26}$$

[compare with (40)], and hence the condition (A22) and Eqs. (83)–(89).

APPENDIX B

Verification of the Jacobi–Weierstrass–Hilbert sufficient condition for a strong minimum

In the weak-coupling limit $r(T)\ll 1$, when $f(y)\equiv 1$, the Legendre necessary condition for a strong minimum of Ω_H reduces to the second relation in (54). Complemented by the requirement that the explicit solution (83)–(89) can be embedded into a field of extremals, this condition becomes the Jacobi–Weierstrass–Hilbert *sufficient* condition for a strong minimum.[19]

In view of the symmetry relation $\phi(y)=-\phi(-y)+2\pi N_v$ the conditions on variations $\delta\phi(\pm L)=0$, $\delta\phi(0)=0$, it suffices to verify the Jacobi–Weierstrass–Hilbert condition for $y\in[-L,0]$. At $H>0$, the desired field is given by the one-parameter family

$$\phi(y,\beta)=\pi(N_v-1)+2\ \mathrm{am}\left(\frac{y\sqrt{4+\beta^2}}{2\lambda_J}+K\left(\frac{4}{4+\beta^2}\right),\frac{2}{\sqrt{4+\beta^2}}\right), \tag{B1}$$

$N_v=2m,\quad m=0,1,\ldots;$

$$\phi(y,\beta)=\pi N_v+2\ \mathrm{am}\left(\frac{y\beta}{2\lambda_J},2\beta\right),$$

$N_v=2m+1,\quad m=0,1,\ldots,$ (B2)

where $\beta>0$. The family $\phi(y,\beta)$ explicitly satisfies (82) and the initial conditions

$$\phi(0,\beta)=\pi N_v\frac{d\phi}{dy}(0,\beta)=\frac{\beta}{\lambda_J}. \tag{B3}$$

For $\beta=\overline{\beta}$, where $\overline{\beta}=2\sqrt{1-k^2}/k$ in the case (B1), and $\overline{\beta}=2/k$ in the case (B2), we have $\phi(y,\overline{\beta})=\phi(y)$, i.e., relations (B1) and (B2) yield the solutions (83), (84) and (85), (86), respectively. To prove that the family $\phi(y,\beta)$ indeed forms a field of extremals, we have to show that any two representatives $\phi_1\equiv\phi(y,\beta_1)$ and $\phi_2\equiv\phi(y,\beta_2)$, where 0

$<\beta_1<\beta_2$, do not intersect in the interval $[-L,0)$. From the first integral of (82) [equation (76) with $f\equiv 1$] and (B3), we have

$$\frac{\lambda_J^2}{2}\left(\frac{d\phi_1}{dy}\right)^2+\cos\phi_1=\frac{\beta_1^2}{2}+(-1)^{N_v},$$

$$\frac{\lambda_J^2}{2}\left(\frac{d\phi_2}{dy}\right)^2+\cos\phi_2=\frac{\beta_2^2}{2}+(-1)^{N_v}. \tag{B4}$$

We will prove the absence of points of intersection of ϕ_1 and ϕ_2 by contradiction.

Consider $\psi(y)\equiv\phi_2(y)-\phi_1(y)$. As Eq. (82) yields

$$\frac{d^2\phi_1}{dy^2}(0)=\frac{d^2\phi_2}{dy^2}(0)=0,$$

for $y\in(-\delta_1,0)$, where δ_1 is sufficiently small, we have

$$\psi(y)=(\beta_1-\beta_2)|y|+o(y^2)>0.$$

By continuity of $\psi(y)$, relation (B5) implies the existence of a finite interval $y\in(y_0,0)$ where $\psi(y)>0$. Let $y=y_0\in\times[-L,0)$ be a point of intersection, i.e.,

$$\phi_1(y_0)=\phi_2(y_0),\quad \frac{d^2\phi_1}{dy^2}(y_0)=\frac{d^2\phi_2}{dy^2}(y_0).$$

For $y\in(y_0,y_0+\delta)$, where $\delta>0$ is sufficiently small, we have

$$\psi(y)=\left[\frac{d\phi_2}{dy}(y_0)-\frac{d\phi_1}{dy}(y_0)\right](|y_0|-|y|)+o[(y-y_0)^2]>0 \tag{B5}$$

which, in view of the arbitrariness of δ, implies

$$\frac{d\phi_2}{dy}(y_0)\geqslant\frac{d\phi_1}{dy}(y_0). \tag{B6}$$

However, equations (B4), by virtue of $d\phi_1/dy$, $d\phi_2/dy>0$, yield

$$\frac{d\phi_2}{dy}(y_0)<\frac{d\phi_1}{dy}(y_0). \tag{B7}$$

The contradiction between (B6) and (B7) proves the absence of points of intersection in the whole interval $[-L,0)$, as expected. Thus, the solution (83)–(89), for any $H>0$, can be embedded into a field of extremals and, as such, satisfies the Jacobi–Weierstrass–Hilbert sufficient condition for a strong minimum.

APPENDIX C

Comparison between soliton and nonsoliton ("lattice") configurations

At fields

$$H\gg\varepsilon^{-1}H_s\equiv(\varepsilon ep\lambda_J)^{-1}, \tag{C1}$$

the SG equations (A1) with $N=2m\to\infty$ admit an exact, closed-form analytical nonsoliton solution under the conditions

$$\frac{d\phi_n}{dy}(\pm L)=2epH,\quad \phi_n(0)=\pi n. \tag{C2}$$

A solution of this type was proposed, e.g., in Refs. 7 and 14, where it was erroneously interpreted as a "dense triangular lattice of Josephson vortices." As an illustration of the general results of this paper, it is instructive to compare this solution with the exact closed-form analytical soliton solution (92), valid in a wider field range $H\gg H_s$.

By introducing a dimensionless variable $u\approx 2epHy$ and new functions $\psi_n(u)\equiv\Phi_n(u/2epH)$, we rewrite Eqs. (A1) as

$$\frac{d^2\psi_n(u)}{du^2}=\frac{1}{(2\varepsilon ep\lambda_J H)^2}\sum_m G^{-1}(n,m)\sin\psi_m(u),$$

$$n=1,\ldots,N. \tag{C3}$$

The boundary conditions, Eqs. (C2), become

$$\frac{d\psi_n}{du}(\pm 2epHL)=1,\quad \phi_n(0)=\pi n. \tag{C4}$$

Taking into account (C1), we seek the solution to (C3), (C4) as an asymptotic expansion in powers of $1/(2ep\lambda_J H)^2$:

$$\psi_n(u)=\sum_{k\geqslant 0}\psi_n^{(k)}(u), \tag{C5}$$

where $\psi_n^{(k)}(u)$ is of order $1/(2\varepsilon ep\lambda_J H)^{2k}$ $(k=0,1,\ldots)$. Retaining only the first two terms in (C5), we obtain

$$\phi_n(y)=\pi n+2epHy-\frac{4+\varepsilon^2}{\varepsilon^2}\frac{(-1)^n}{4(ep\lambda_J H)^2}\sin(2epHy)+\frac{4+\varepsilon^2}{\varepsilon^2}\frac{(-1)^n}{2ep\lambda_J^2 H}\cos(epHW)y. \tag{C6}$$

The sum of the first three terms on the right-hand side of (C6) in the limit $\varepsilon\ll 1$ gives the solution of Refs. 7 and 14. The presence of the last term on the right-hand side of (C6), resulting from the boundary conditions (C2) at $y=\pm L$, was not noticed in Refs. 7 and 14, and therefore the solution of Refs. 7 and 14 does not meet the boundary conditions at $y=\pm L$ in required order. In contrast to the exact closed-form analytical soliton solution (92), valid in the same field range and minimizing the LD functional (3), the nonsoliton solution (C6) is just a saddle point of (3): see Secs. 2.3 and 4 and Appendix A. This is illustrated below.

The substitution of (C6) into (A13), (A14) yields a nonequilibrium value of the LD functional:

$$\tilde{\Omega}_{LD}(H)=\frac{H_c^2(T)pNLW_z}{4\pi}\times\left[-1+r(T)\left[1+\frac{[1+2/\varepsilon^2]\cos^2(epHW)}{8(ep\lambda_J H)^2}\right]\right]. \tag{C7}$$

Expression (C7) is to be compared with the thermodynamic free energy (93) of the soliton solution (92). Their difference is

$$\Delta\tilde{\Omega}_{LD}(H)\equiv\tilde{\Omega}_{LD}(H)-\Omega_{LD}(H)=\frac{H_c^2(T)pNLW_z r(T)}{4\pi}\times\left[\frac{|\sin(epHW)|}{epHW}+\frac{\cos^2(epHW)}{4(ep\lambda_J H)^2\varepsilon^2}\right]>0. \tag{C8}$$

Thus the saddle-point, nonsoliton solution (C6) is nothing but an unstable perturbation of the soliton solution (92).

*E-mail: kuplevakhsky@ilt.kharkov.ua

[1)]Contrary to what is claimed in Ref. 17, for example, this issue cannot be resolved by comparing ''characteristic length scales'' or values of the energy functionals for distinct field configurations. The main problem is to establish whether the configurations under comparison *locally minimize* the energy functionals.

[2)]This can be done by the gauge transformation $\mathbf{A}'(x,y)=\mathbf{A}(x,y)+\nabla\psi(x,y)$, $\varphi_n'(y)=\varphi_n(y)+2e\psi(np,y)$, where $\psi(x,y)=-\int_C^x dt\, A_x(t,y)$.

[3)]For example, as was shown by Farid,[30] field configurations of the type in Refs. 4 and 5 do not constitute solutions in a true mathematical sense. We add that equations (A1) for the phase differences [let alone the more general equations (9), (10), and (26)–(28)] were not derived in Refs. 4 and 5.

---

[1] S. V. Kuplevakhsky, Phys. Rev. B **60**, 7496 (1999).
[2] S. V. Kuplevakhsky, Phys. Rev. B **63**, 054508 (2001).
[3] W. E. Lawrence and S. Doniach, *Proceedings of the Twelfth Conference on Low Temperature Physics, Kyoto, 1970*, E. Kanda (ed.), Keigaku, Tokyo (1970), p. 361.
[4] L. N. Bulaevskii, Zh. Éksp. Teor. Fiz. **64**, 2241 (1973) [Sov. Phys. JETP **37**, 1133 (1973)].
[5] J. R. Clem and M. W. Coffey, Phys. Rev. B **42**, 6209 (1990).
[6] J. P. Carton, J. Phys. I (France) **1**, 113 (1991).
[7] L. N. Bulaevskii and J. R. Clem, Phys. Rev. B **44**, 10234 (1991).
[8] L. N. Bulaevskii, M. Ledvij, and V. G. Kogan, Phys. Rev. B **46**, 366 (1992).
[9] A. E. Koshelev, Phys. Rev. B **48**, 1180 (1993).
[10] R. Rajaraman, *Solitons and Instantons*, North-Holland, Amsterdam (1982).
[11] R. K. Dodd, J. C. Eilbeck, J. D. Gibbon, and H. C. Morris, *Solitons and Nonlinear Wave Equations*, Academic Press, London (1982).
[12] P. Goddard and P. Mansfield, Rep. Prog. Phys. **49**, 725 (1986).
[13] A. S. Schwarz, *Quantum Field Theory and Topology* [in Russian], Nauka, Moscow (1989).
[14] L. N. Bulaevskii, M. Maley, H. Safar, and D. Dominguez, Phys. Rev. B **53**, 6634 (1996).
[15] L. N. Bulaevskii, J. R. Clem, and L. I. Glazman, Phys. Rev. B **46**, 350 (1992).
[16] V. M. Krasnov, Phys. Rev. B **63**, 064519 (2001).
[17] V. M. Krasnov, Phys. Rev. B **65**, 096503 (2002).
[18] C. Lancsos, *The Variational Principles of Mechanics*, University of Toronto Press, Toronto (1962).
[19] N. I. Akhiezer, *The Calculus of Variations*, Blaisdell Publishing, New York (1962).
[20] N. W. Ashcroft and N. D. Mermin, *Solid State Physics*, Holt, Rinehart and Winston, New York (1976).
[21] A. O. Gelfond, *The Calculus of Finite Difference* [in Russian], GIFML, Moscow (1959).
[22] A. A. Abrikosov, *Fundamentals of the Theory of Metals*, North-Holland, Amsterdam (1988).
[23] V. E. Zakharov and E. A. Kuznetsov, Zh. Éksp. Teor. Fiz. **66**, 594 (1974).
[24] N. D. Mermin, Rev. Mod. Phys. **51**, 591 (1979).
[25] M. Abramowitz and I. A. Stegun, *Handbook of Mathematical Functions*, Dover, New York (1965).
[26] I. O. Kulik, Zh. Éksp. Teor. Fiz. **51**, 1953 (1966) [Sov. Phys. JETP **24**, 1307 (1967)].
[27] C. S. Owen and D. J. Scalapino, Phys. Rev. **164**, 538 (1967).
[28] A. Barone and G. Paterno, *Physics and Applications of the Josephson Effect*, Wiley, New York (1982).
[29] A. Buzdin and D. Feinberg, Phys. Lett. A **165**, 281 (1992).
[30] B. Farid, J. Phys.: Condens. Matter **10**, L589 (1998).
[31] R. Bellman, *Introduction to Matrix Analysis*, McGraw-Hill, New York (1960).
[32] V. C. L. Hutson and J. S. Pym, *Applications of Functional Analysis and Operator Theory*, Academic Press, London (1980).

This article was published in English in the original Russian journal. Reproduced here with stylistic changes by AIP.

Wigner distribution function formalism for superconductors and collisionless dynamics of the superconducting order parameter

M. H. S. Amin

D-Wave Systems Inc., 320-1985 W. Broadway, Vancouver, B.C., V6J 4Y3 Canada

E. V. Bezuglyi,* A. S. Kijko, and A. N. Omelyanchouk

B. Verkin Institute for Low Temperature Physics and Engineering of the National Academy of Science of Ukraine, 47 Lenin Ave., Kharkov 61103, Ukraine

(Submitted April 16, 2004)
Fiz. Nizk. Temp. **30**, 874–880 (July–August 2004)

A technique for studying collisionless dynamics of a homogeneous superconducting system is developed which is based on Riccati parametrization of the Wigner distribution function. The quantum evolution of the superconducting order parameter, initially deviating from the equilibrium value, is calculated using this technique. The effect of a time-dependent BCS paring interaction on the dynamics of the order parameter is also studied. © *2004 American Institute of Physics.* [DOI: 10.1063/1.1789939]

1. INTRODUCTION

In this paper we study the dynamics of the superconducting order parameter within the Wigner distribution function approach. The problem of nonstationary phenomena in superconductors has been attracting attention for a long time.[1,2] The general method for description of nonstationary and nonequilibrium processes is the Keldysh technique for nonequilibrium real-time Green's functions.[3] The equations for superconducting Keldysh Green's functions[4,5] are a set of quite complicated nonlinear integro-differential equations, which are nonlocal in the time and space domains. These equations can be simplified considerably in the quasiclassical approximation by integrating the Green's functions over $\xi_p = p^2/2m - \mu$ (μ is the chemical potential).[6] The quasiclassical Larkin–Ovchinnikov equations are still nonlocal in time, but are local in space. In the stationary case, these equations transform into Eilenberger's equations,[7] which are effective tools for solving stationary inhomogeneous problems.

When the time-dependent processes in superconductors are considered, three time scales are most essential. The time $t_p \sim \omega_p^{-1}$ (ω_p is the plasma frequency) characterizes the scale at which the self-consistent scheme for the electromagnetic fields $\mathbf{A}(\mathbf{r},t)$, $\phi(\mathbf{r},t)$, and for the BCS pairing field $\Delta(\mathbf{r},t)$ is established. The time $t_0 \sim \Delta^{-1}$ (Δ is the modulus of the order parameter) is an intrinsic time for superconductors, during which quasiparticles with the energy spectrum $\sqrt{\Delta^2+\xi_p^2}$ are formed in the superconductor. The stage of the relaxation of a nonequilibrium disturbance in the quasiparticle distribution is determined by the energy relaxation time τ_ε due to inelastic processes. For conventional superconductors, at temperature T not too close to the critical temperature T_c, the hierarchy of the characteristic times is $t_p \ll t_0 \ll \tau_\varepsilon$. In the time interval $t \sim \tau_\varepsilon \gg t_0$ the superconductor's dynamics is described by the quasiclassical Boltzman kinetic equation for the quasiparticle distribution function together with a self-consistent equation for $\Delta(\mathbf{r},t)$ (Aronov–Gurevich equations[8]). In the opposite case $t \ll \tau_\varepsilon$, the dynamics of the superconducting order parameter should be described by the quantum kinetic equation. Considering the collisionless evolution of the superconducting order parameter ($t \ll \tau_\varepsilon$), the equations for the Keldysh Green's functions are reduced to simpler equations for the Green's functions at coinciding times. The latter can be transformed to the quantum kinetic equation for the Wigner distribution function (WDF). The collisionless kinetic equation for superconducting WDF can also be obtained directly from the generalized Hartree–Fock approach to the BCS pairing model[9] (see also Refs. 10 and 11).

Wigner[12] has introduced a distribution function in the phase space as a quantum analog of the classical Boltzman distributions. In studying the quantum transport, the Wigner-function formalism has many advantages. It is extensively used for the description of normal metal and semiconducting electron devices whose behavior is dominated by quantum interference effects, e.g., for self-consistent treatment of transient response to a change in the applied voltage.[13] In recent years, Wigner functions have been widely used in the field of quantum optics to describe the effects of quantum coherence and superposition in optical systems.[14] Such effects are of great interest in qubit (quantum bit for quantum computation) investigations.[15]

The collisionless dynamics of the superconducting order parameter has gained renewed attention after the discovery of the BCS-like paired state in dilute fermionic gases.[16] The ability to control and change the strength of the pairing interaction in these systems opens up possibilities for new experimental investigations of the dynamics of the order parameter. Recently, time-dependent BCS pairing was studied theoretically in Ref. 17. The WDF technique developed in our paper provides a useful tool for studying such problems.

In Sec. 2, following Kulik's approach,[9] we derive a quantum kinetic equation for the superconducting WDF in $(\mathbf{r},t)$ space. This equation is simplified for the case of a homogeneous state (Sec. 3) and then used to study the collisionless dynamics of the order parameter in small superconducting systems (Sec. 4). We consider the problem of the

time evolution of the order parameter after an initial deviation from the equilibrium value and found that on a time scale much shorter than τ_ε the time dependence of Δ has an oscillatory character. Earlier, such a problem was studied by other authors using a linear response approach,[18] assuming small deviation from equilibrium. In the present paper, the time dependences were obtained under arbitrary initial perturbations (not only small). The time dependent response of the order parameter to a time-varying pairing potential is also studied. A numerical method for solving the equation for the WDF, which is based on the Maki–Schopohl transformation,[19] is developed.

2. WIGNER DISTRIBUTION FUNCTION FORMALISM FOR THE SUPERCONDUCTING STATE

We write the Hamiltonian of the superconductor as $H=H_0+H_1$, where H_0 includes electron interactions with external fields, the vector potential $\mathbf{A}(\mathbf{r})$ and the scalar potential $\phi(\mathbf{r})$, as well as with the pairing field $\Delta(\mathbf{r})$,

$$H_0=\sum_{\sigma=\uparrow,\downarrow}\int d\mathbf{r}\,\psi_\sigma^\dagger(\mathbf{r})[\varepsilon-\mu+e\phi(\mathbf{r})]\psi_\sigma(\mathbf{r}) - \int d\mathbf{r}[\Delta(\mathbf{r})\psi_\uparrow^\dagger(\mathbf{r})\psi_\downarrow^\dagger(\mathbf{r})+\Delta^*(\mathbf{r})\psi_\downarrow(\mathbf{r})\psi_\uparrow(\mathbf{r})], \tag{1}$$

$$\varepsilon=\frac{1}{2m}\left[\frac{\nabla}{i}-\frac{e}{c}\mathbf{A}(\mathbf{r})\right]^2 \tag{2}$$

(we use a system of units in which $\hbar=k_B=1$). Here

$$\psi_\sigma(\mathbf{r})=\frac{1}{\sqrt{V}}\sum_{\mathbf{p}} a_{\mathbf{p}\sigma}(t)e^{i\mathbf{p}\cdot\mathbf{r}}$$

is the annihilation operator of an electron with spin σ. The Hamiltonian H_1 describes the impurity, electron–phonon, electron–electron, etc. scattering processes that provide the relaxation.

The pairing field $\Delta(\mathbf{r})$ is to be determined from the self-consistency equation

$$\Delta^*(\mathbf{r})=V_0\langle\psi_\uparrow^\dagger(\mathbf{r})\psi_\downarrow^\dagger(\mathbf{r})\rangle, \tag{3}$$

where V_0 is the pairing potential. The electromagnetic potentials obey Maxwell's equations,

$$\nabla\times\mathbf{A}(\mathbf{r})=\frac{4\pi}{c}\mathbf{j}(\mathbf{r}), \tag{4}$$

$$\nabla^2\phi+\frac{1}{c}\frac{\partial}{\partial t}\nabla\cdot\mathbf{A}=-4\pi\rho(\mathbf{r}), \tag{5}$$

where $\rho(\mathbf{r})$ and $\mathbf{j}(\mathbf{r})$ are the charge and current densities, respectively:

$$\rho(\mathbf{r})=e\sum_\sigma\langle\psi_\sigma^\dagger(\mathbf{r})\psi_\sigma(\mathbf{r})\rangle, \tag{6}$$

$$\mathbf{j}(\mathbf{r})=-\frac{ie}{m}\sum_\sigma\langle\psi_\sigma^\dagger(\mathbf{r})\nabla\psi_\sigma(\mathbf{r})-(\nabla\psi_\sigma^\dagger(\mathbf{r}))\psi_\sigma(\mathbf{r})\rangle - \frac{2e^2}{mc}\mathbf{A}(\mathbf{r})\sum_\sigma\langle\psi_\sigma^\dagger(\mathbf{r})\psi_\sigma(\mathbf{r})\rangle, \tag{7}$$

and the angle brackets denote statistical averaging.

By introducing the "particle–hole" (Gor'kov–Nambu) representation of the electron creation and annihilation operators in terms of 2-vectors,

$$A_{\mathbf{p}}=\begin{pmatrix} a_{\mathbf{p}\uparrow}\\ a_{-\mathbf{p}\downarrow}^\dagger\end{pmatrix},\quad A_{\mathbf{p}}^\dagger=(a_{\mathbf{p}\uparrow}^\dagger\quad a_{-\mathbf{p}\downarrow}), \tag{8}$$

$$\Psi(\mathbf{r})=\begin{pmatrix}\psi_\uparrow(\mathbf{r})\\ \psi_\downarrow^\dagger(\mathbf{r})\end{pmatrix},\quad \Psi^\dagger(\mathbf{r})=(\psi_\uparrow^\dagger(\mathbf{r})\psi_\downarrow(\mathbf{r})), \tag{9}$$

we define the matrix $\hat f_{\mathbf{pq}}$ in the "particle–hole" space,

$$f_{\mathbf{pq}}^{\alpha\beta}(t)=\langle A^\dagger_{\mathbf{p}-\frac{\mathbf{q}}{2},\beta}(t)A_{\mathbf{p}+\frac{\mathbf{q}}{2}\alpha}(t)\rangle,$$

where $\alpha,\beta=1,2$ are the indices of the vectors $A_{\mathbf{p}}$. The function $f_{pq}^{\alpha\beta}$ is the Fourier transform of the Wigner distribution function $f_{\alpha\beta}(\mathbf{p},\mathbf{r},t)$ generalized to the superconducting case,

$$f_{\alpha\beta}(\mathbf{p},\mathbf{r},t)=\sum_{\mathbf{q}} e^{i\mathbf{q}\mathbf{r}}\langle A^\dagger_{\mathbf{p}-\frac{\mathbf{q}}{2},\alpha}(t)A_{\mathbf{p}+\frac{\mathbf{q}}{2},\beta}(t)\rangle. \tag{10}$$

Correspondingly, the components of the matrix $\hat f(\mathbf{p},\mathbf{r},t)$ are expressed in terms of the Nambu operators $\Psi_\alpha(\mathbf{r},t)$ in the Heisenberg representation as

$$f_{\alpha\beta}=\int d\mathbf{r}'\,e^{-i\mathbf{p}\mathbf{r}'}\langle\Psi_\alpha^\dagger(\mathbf{r}+\mathbf{r}'/2,t)\Psi_\beta(\mathbf{r}-\mathbf{r}'/2,t)\rangle. \tag{11}$$

It follows from Eq. (11) that f_{11} and f_{22} are real functions, and $f_{12}=f_{21}^*$. The self-consistency relations, Eqs. (3), (6), and (7), can be written in terms of $\hat f$ as

$$\Delta=V_0\int\frac{d\mathbf{p}}{(2\pi)^3}\mathrm{Tr}\,\tau_-\hat f(\mathbf{p}), \tag{12}$$

$$\rho=e\int\frac{d\mathbf{p}}{(2\pi)^3}\mathrm{Tr}\,\tau_3\hat f(\mathbf{p}), \tag{13}$$

$$\mathbf{j}=\int\frac{d\mathbf{p}}{(2\pi)^3}\mathrm{Tr}\,\tilde{\mathbf{p}}\,\hat f(\mathbf{p}), \tag{14}$$

where $\tilde{\mathbf{p}}=\mathbf{p}-e\tau_3\mathbf{A}/c$, $\tau_-=(1/2)(\tau_1-i\tau_2)$, and τ_i are the Pauli matrices.

The evolution equation for the WDF can be derived from the equation of motion for the electron field operators $\psi=\psi_\sigma(\mathbf{r},t)$:

$$i\frac{\partial\psi}{\partial t}=[\psi,H]. \tag{15}$$

Restricting our consideration to the collisionless stage of the evolution, we neglect the interaction part $\hat H_1$ of the Hamiltonian and obtain, from Eq. (15), the equations of motion for the Nambu operators $\Psi(\mathbf{r},t)$:

$$\left[i\frac{\partial}{\partial t}-\tau_3(\hat\xi+e\phi)+\hat\Delta\right]\Psi=0,\quad \hat\Delta=\begin{pmatrix}0&\Delta\\ \Delta^*&0\end{pmatrix}, \tag{16}$$

where $\hat\xi=-(\nabla+ie\tau_3\mathbf{A}/c)^2/2m-\mu$. By making use of the definition of the WDF in Eq. (11), we arrive, after some algebra, at the following dynamic equation for $\hat f(\mathbf{p},\mathbf{r},t)$:

$$\frac{\partial\hat f}{\partial t}+i\left[\frac{(\tilde{\mathbf{p}}-i\tilde\nabla/2)^2}{2m}\tau_3,\hat f\right]+i[e\phi\tau_3-\hat\Delta,\hat f]_\otimes=0, \tag{17}$$

where [...] denotes the usual commutator, in which we consider $\tilde{\nabla}$ as an integral operator with the kernel $\nabla_{\mathbf{r}}\delta(\mathbf{r}-\mathbf{r}')$, and thus $(\tilde{\nabla}\hat{f})=-(\hat{f}\tilde{\nabla})=\nabla\hat{f}$. The quantity $[\ldots]_{\otimes}$ is defined as $[A,B]_{\otimes}\equiv A\otimes B-B\otimes A$, where $(A\otimes B)(\mathbf{p},\mathbf{r},t)$ is the Fourier transform of the spatial convolution $(AB)(\mathbf{r}_1,\mathbf{r}_2)=\int d\mathbf{r}\,A(\mathbf{r}_1,\mathbf{r})B(\mathbf{r},\mathbf{r}_2)$:

$$(A\otimes B)(\mathbf{p},\mathbf{r})=\int d\mathbf{r}'\,\mathrm{e}^{-i\mathbf{p}\mathbf{r}'}(AB)(\mathbf{r}+\mathbf{r}'/2,\mathbf{r}-\mathbf{r}'/2)$$
$$=\exp\left\{\frac{i}{2}[\partial^A_{\mathbf{r}}\partial^B_{\mathbf{p}}-\partial^A_{\mathbf{p}}\partial^B_{\mathbf{r}}]\right\}A(\mathbf{p},\mathbf{r})B(\mathbf{p},\mathbf{r}). \tag{18}$$

By making use of the transformation $\hat{f}\rightarrow\exp(i\tau_3\chi/2)\hat{f}\exp(-i\tau_3\chi/2)$, we can exclude the phase χ of the superconducting order parameter and proceed to gauge-invariant quantities, i.e., the momentum of the superfluid condensate $\mathbf{p}_s$ and the potential Φ defined by

$$\mathbf{p}_s=m\mathbf{v}_s=\frac{1}{2}\left(\nabla\chi-\frac{2e}{c}\mathbf{A}\right),\quad \Phi=\frac{1}{2}\left(\frac{\partial\chi}{\partial t}+2e\phi\right). \tag{19}$$

The electromagnetic fields are related to $\mathbf{p}_s$ and Φ through

$$e\mathbf{E}=\frac{\partial\mathbf{p}_s}{\partial t}-\nabla\Phi,\quad e\mathbf{H}=-\nabla\times\mathbf{p}_s. \tag{20}$$

This results in the substitutions $\tilde{\mathbf{p}}\rightarrow\mathbf{p}+\tau_3\mathbf{p}_s$ and $e\phi\rightarrow\Phi$ in the dynamical equation (17), as well as in the definition of the current in Eq. (14). Note that the anisotropic term $\mathbf{p}\cdot\mathbf{v}_s$ arising from $\tilde{\mathbf{p}}$ in Eq. (17) commutes with $\hat{f}$ and thus drops out from this equation.

While the physical sense of $\mathbf{p}_s$ is obvious, the interpretation of the gauge-invariant potential Φ is less evident. Within the framework of the two-fluid model, it can be interpreted as the difference $\Phi=\mu_s-\mu_n$ between the electrochemical potentials of the condensate of Cooper pairs, $\mu_s=\mu+(1/2)\partial\chi/\partial t$, and quasiparticles, $\mu_n=\mu-e\phi$; thus a nonzero value of Φ means nonequilibrium of the electrons in the superconductor. In bulk superconductors, Φ and $\mathbf{p}_s$ decay within their corresponding lengths: the London (skin) depth δ in the case of $\mathbf{p}_s$, and the electric field penetration depth λ_E for Φ.

3. WIGNER DISTRIBUTION FUNCTION FOR HOMOGENEOUS SUPERCONDUCTING SYSTEMS

In what follows, we focus on homogeneous superconducting systems in the clean limit, assuming the scattering rate is much smaller than Δ. To be more specific, we assume the magnitude of the order parameter Δ and the gradient of its phase, $\nabla\chi$, to be uniform inside the superconductor. The spatially varying part of the phase of Δ is included in the homogeneous $\mathbf{p}_s$ by means of an appropriate gauge transformation. A ''residual'' spatially uniform phase is kept to describe the dynamics of the phase of the order parameter. It can be related to, e.g., possible (time-dependent) phase on either side of a Josephson junction. In this case, the equation for the WDF takes the form

$$\frac{\partial\hat{f}}{\partial t}+i[\tilde{\xi}_p\tau_3-\hat{\Delta},\hat{f}]+\nu(\hat{f}-\hat{f}_0)=0, \tag{21}$$

where $\tilde{\xi}_p=\xi_p+\Phi+mv_s^2/2$. The phenomenological collision term $\nu(\hat{f}-\hat{f}_0)$ qualitatively describes slow relaxation of the WDF to its equilibrium value $\hat{f}_0$ which is associated with the interaction Hamiltonian H_1. In the collisionless limit considered below, we will assume $\nu\rightarrow+0$, in order to provide correct analytical behavior of the WDF at $t\rightarrow+\infty$.

Equation (21) has several important properties which can be derived from the equations for the matrix elements of $\hat{f}$,

$$i\frac{\partial f_{11}}{\partial t}=-i\frac{\partial f_{22}}{\partial t}=-(\Delta f_{21}-\Delta^* f_{12}), \tag{22}$$

$$i\frac{\partial f_{12}}{\partial t}=2\tilde{\xi}_p f_{12}+\Delta(f_{11}-f_{22}), \tag{23}$$

$$-i\frac{\partial f_{21}}{\partial t}=2\tilde{\xi}_p f_{21}+\Delta^*(f_{11}-f_{22}). \tag{24}$$

First, we note that only the difference $f_{11}-f_{22}$ of the diagonal components of the matrix $\hat{f}$ enters the equations for the off-diagonal components f_{12} and f_{21}. Furthermore, from Eq. (22), one finds that the sum of the diagonal components $f_{11}+f_{22}=\text{const}$. This allows us to present the function $\hat{f}$ in the following form:

$$\hat{f}=\frac{1}{2}[\hat{1}(1-\mathcal{F}_-)-\hat{\tilde{f}}\mathcal{F}_+],\quad \hat{\tilde{f}}=\begin{pmatrix}-g & f\\ f^* & g\end{pmatrix}, \tag{25}$$

where f and g are isotropic functions, and the time-independent quantities $\mathcal{F}_\pm$ have the meaning of quasiparticle distribution functions which are conserved during the stage of the collisionless evolution. Assuming the system to be initially in equilibrium and comparing Eq. (25) with the equilibrium form of the WDF, which can be directly obtained from the definition in Eq. (10):

$$\hat{f}_0=\frac{1}{2}\left\{\hat{1}(1-\mathcal{F}_-)-\frac{1}{\tilde{\varepsilon}_p}(\tilde{\xi}_p\hat{\tau}_3-\hat{\Delta})\mathcal{F}_+\right\}, \tag{26}$$

we find the distribution functions

$$\mathcal{F}_\pm=\frac{1}{2}\left[\tanh\frac{\tilde{\varepsilon}_p+\mathbf{p}\cdot\mathbf{v}_s(0)}{2T}\pm\tanh\frac{\tilde{\varepsilon}_p-\mathbf{p}\cdot\mathbf{v}_s(0)}{2T}\right],$$
$$\tilde{\varepsilon}_p=\sqrt{\tilde{\xi}_p^2+|\Delta|^2}, \tag{27}$$

and the equilibrium values of the functions f and g

$$f_0=\frac{\Delta}{\tilde{\varepsilon}_p},\quad g_0=\frac{\tilde{\xi}_p}{\tilde{\varepsilon}_p}. \tag{28}$$

In this representation the dynamic equation (21) for the WDF reduces to the following system of scalar equations for the functions g and f:

$$\frac{\partial g}{\partial t}=i(\Delta^* f-\Delta f^*),\quad \frac{\partial f}{\partial t}=2i(\Delta g-\tilde{\xi}_p f), \tag{29}$$

which, together with Eq. (28), lead to the normalization condition $\hat{\tilde{f}}^2=1$ or

$$g^2+ff^*=1. \tag{30}$$

The self-consistency equation has the form

$$\Delta(t)=\frac{\lambda}{2}\int\frac{d\Omega_p}{4\pi}\int_{-\omega_D}^{\omega_D}d\xi_p f(\xi_p,t)\mathcal{F}_+, \tag{31}$$

where ω_D is the Debye frequency, $\lambda=N(0)V_0$ is the dimensionless pairing constant, $N(0)$ is the electron density of states per spin at the Fermi level, and Ω_p denotes angle variables associated with the momentum vector. The charge and current densities are given by

$$\rho(t)=-eN(0)\int\frac{d\Omega_p}{4\pi}\int d\xi_p g(\xi_p,t)\mathcal{F}_+, \tag{32}$$

$$\mathbf{j}(t)=en\mathbf{v}_s(t)-eN(0)\int\frac{d\Omega_p}{4\pi}\mathbf{p}\int d\xi_p\mathcal{F}_-, \tag{33}$$

where n is the net electron density. Equation (33) shows that the electric current is governed directly by the superfluid velocity and has nothing to do with the evolution of the WDF,

$$\begin{aligned}\mathbf{j}(t)&=en\mathbf{v}_s(t)+e(n_s-n)\mathbf{v}_s(0)\\&=\mathbf{j}(0)+en[\mathbf{v}_s(t)-\mathbf{v}_s(0)],\end{aligned} \tag{34}$$

where n_s is the condensate density calculated for the initial superfluid velocity $\mathbf{v}_s(0)$. This property reflects the specifics of the collisionless regime, in which the normal component of the current flow is not affected by scattering, and therefore the velocities of both the superfluid and normal components of the electron fluid undergo equal changes $\mathbf{v}_s(t)-\mathbf{v}_s(0)$: $\mathbf{v}_s(0)\to\mathbf{v}_s(t)$, $\mathbf{v}_n(0)=0\to\mathbf{v}_s(t)-\mathbf{v}_s(0)$: From this we conclude that at nonzero temperature, when the density of the normal component, $n_n\equiv n-n_s$, is nonzero, the current reverses its direction with respect to $\mathbf{v}_s(t)$ if the latter becomes smaller than $\mathbf{v}_s(0)n_n/n$.

4. COLLISIONLESS EVOLUTION OF THE ORDER PARAMETER IN SUPERCONDUCTORS

In the paper by Volkov and Kogan,[18] the problem of evolution of the order parameter $\Delta(t)$ at a given initial value of the WDF (and the corresponding initial self-consistent value of $\Delta=\Delta(0)$) was analyzed within a linear approximation, assuming small deviations of $\Delta(t)$ and $\hat{f}(\xi,t)$ from their equilibrium values. It was shown that the time variations of Δ have the form of harmonic oscillations with a period of the order of Δ^{-1} and an amplitude decreasing slowly as $t^{-1/2}$. At large $t\gg t_0=\Delta^{-1}(0)$, the order parameter approaches a constant value $\Delta_\infty\equiv\Delta(t\to\infty)$, which is determined by the initial conditions and coincides neither with $\Delta(0)$ nor with the equilibrium value Δ_0.

In this paper, we address a more general nonlinear problem, with arbitrary initial conditions, which may differ substantially from the equilibrium state. In particular, this allows us to consider the formation of the superconducting state from the initial normal state at low enough temperatures, or destruction of the initial superconducting state at high temperatures. To this end, we apply a numerical procedure, by making use of the so-called Riccati parametrization of the functions f and g. Due to the normalization condition (30), these functions can be expressed in terms of a single function $a(\xi_p,t)$,

$$g=\frac{1-aa^*}{1+aa^*},\quad f=\frac{2a}{1+aa^*}, \tag{35}$$

which satisfies a nonlinear Riccati-type equation,

$$\frac{\partial a}{\partial t}=i(-2\tilde{\xi}_p a-\Delta^* a^2+\Delta). \tag{36}$$

In the stationary limit ($\Delta=$const), the solution of Eq. (36) is

$$a_0=\frac{\Delta}{\tilde{\xi}_p+\tilde{\varepsilon}_p}. \tag{37}$$

In the general nonstationary case, one needs to integrate Eq. (36) together with the self-consistency equation (31). Thus, proceeding to the discrete time variable, $t=n\delta t$, $n=0,1,\ldots$, one has to calculate the new value of Δ from Eq. (31) after each time step δt and then use it for the next step. For sufficiently small δt, Δ can be approximately considered as constant between t and $t+\delta t$, which allows us to apply an analytical solution of Eq. (36) within this time interval,

$$a(t+\delta t)=a(t)+\frac{\Delta(t)-2\tilde{\xi}_p a(t)-\Delta^*(t)a^2(t)}{\Delta^*(t)a(t)+\tilde{\xi}_p-i\tilde{\varepsilon}_p\cot(\tilde{\varepsilon}_p\delta t)}, \tag{38}$$

and thus to calculate $a(t+\delta t)$ explicitly. As a result, the numerical procedure reduces to the numerical solution of the self-consistency equation at each step of the calculations.

In our calculations, we use time steps $\delta t=0.02t_0$. After each step, the values of the modulus and the phase of $\Delta(t)$ were recalculated by means of the self-consistency equation (31). In Fig. 1, we present time variations of the order parameter modulus for initial values $\Delta(0)$ substantially different from the equilibrium value Δ_0 at $T=0$. It is obvious that equal values of $\Delta(0)$ may be obtained for different forms of the initial Wigner distribution function $\hat{f}(0)$. In our evaluation, we use the equilibrium form of $\hat{f}(0)$ given by Eq. (26) at $T=0$, with a formal parameter Δ_{in}, which, however, appears to be slightly different from the initial self-consistent value $\Delta(0)$. This difference depends weakly on the value of the pairing constant λ, for which in the following we put $\lambda=0.5$. The initial value of $\Delta_{\text{in}}=1.5\Delta_0$ leads to $\Delta(0)\approx1.3\Delta_0$ (Fig. 1*a*), whereas $\Delta_{\text{in}}=0.5\Delta_0$ yields a self-consistent $\Delta(0)\approx0.67\Delta_0$ (Fig. 1*b*).

Another type of perturbation in the system is the switching of λ from one value to another, or, more generally, the case of time-dependent BCS pairing. We have used the equations (35), (36), (38), and (31) with time-dependent $\lambda=\lambda(t)$ to study this problem numerically. The collisionless evolution of the order parameter as λ changes in time is shown in Fig. 2.

It is interesting to note that the initial BCS form of the WDF automatically leads to conservation of arbitrary initial values of the order parameter phase χ. Actually, this property is associated with the definite symmetry of the initial WDF with respect to ξ_p, $f(\xi_p,t)=f(-\xi_p,t)$, $g(\xi_p,t)=-g(-\xi_p,t)$, which holds during the time evolution and manifests equality of the populations of the electron- and hole-

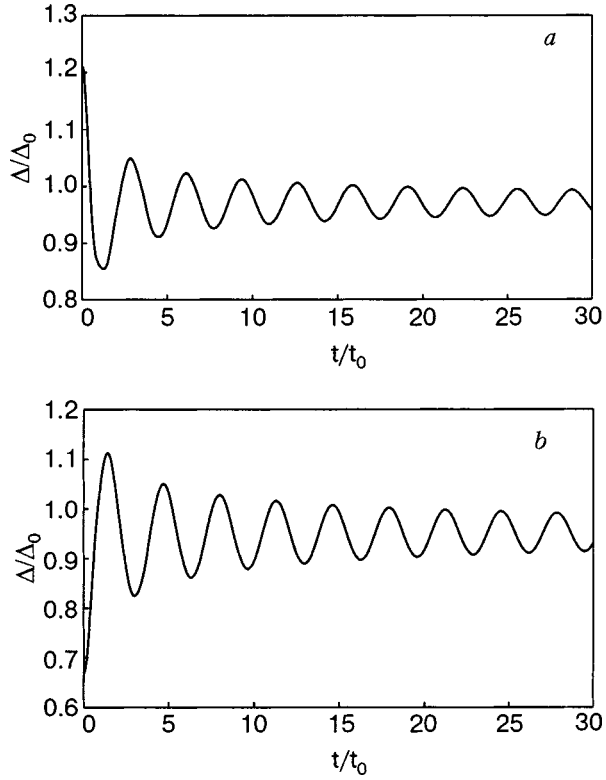

FIG. 1. Collisionless time evolution of the order parameter for an initial value $\Delta(0)$ larger (a) or smaller (b) than the equilibrium value Δ_0 at $T=0$. In all figures the time is normalized to $t_0=1/\Delta_0$.

like excitations with equal energies $\tilde{\varepsilon}_p$. The introduction of an imbalance between the electron and hole branches of the excitation spectrum (i.e., violation of the above-mentioned symmetry) produces an excess charge in the quasiparticle subsystem which, due to electroneutrality of the metal, should be compensated by the opposite charge of the superfluid condensate. This means the appearance of the difference $\delta\mu$ between the electrochemical potentials μ_n and μ_s of excitations and the condensate, respectively, which produces time variations of the order parameter phase according to the relationship $d\chi/dt=2\delta\mu$. For a given constant $\delta\mu$, we find continuous variation of the phase with a constant rate.

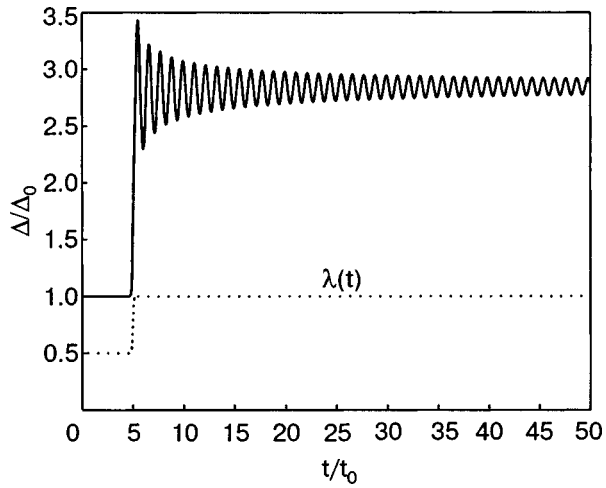

FIG. 2. Collisionless time evolution of the order parameter as the coupling constant λ changes from the value 0.5 to 1.0.

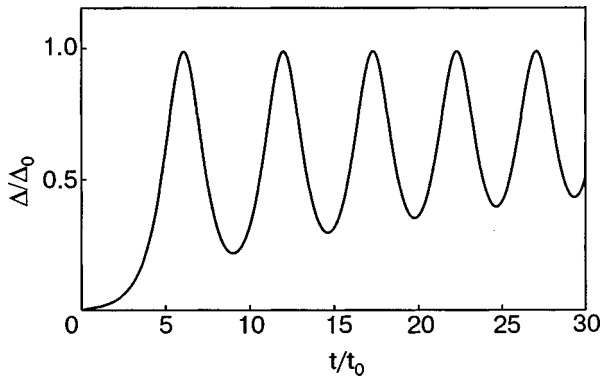

FIG. 3. Instability of the equilibrium normal state at $T=0$. We start from $\Delta(0)=0.001\Delta_0$.

The processes of formation and destruction of the superconducting state can be also analyzed within the nonlinear collisionless approach. By starting evaluations from a very small value of Δ_{in} ($\sim 10^{-3}\Delta_0$) in Eq. (28) at $T=0$, which approximately represents an initial normal state, we observe a rapid increase in $\Delta(t)$ at the time $t\sim t_0$ up to $\Delta\sim\Delta_0$, followed by an oscillatory approach to a stable superconducting state (see Fig. 3). We note that the asymptotic value Δ_∞ appears to be noticeably lower than Δ_0, which means that the real equilibrium value of Δ at the superconducting transition is formed via relaxation processes.

Strictly speaking, at any temperature, including the region $T<T_c$, the self-consistency equation (3) always has a trivial solution $\Delta=0$, which corresponds to the normal state. However, at $T<T_c$ the normal state is associated with a maximum of the free energy, and therefore Fig. 3 actually illustrates the thermodynamic instability of the normal state with respect to an infinitesimal Δ, which develops through the quantum kinetic process described by Eqs. (3) and (29). It is interesting to note that, despite the strong nonlinearity of the process, the oscillations of $\Delta(t)$ have an almost purely harmonic shape.

The instability of the superconducting state at temperatures $T>T_c$ is illustrated by Fig. 4, which was obtained by starting evaluations from the initial superconducting state in Eq. (28) at the rather high temperature $T=2.5\Delta_0$. The order parameter decreases approximately exponentially with the

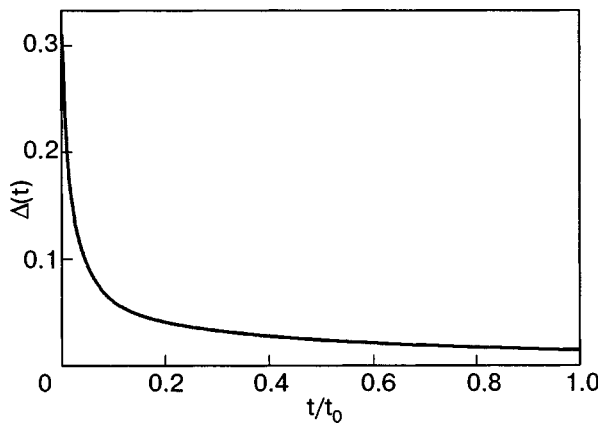

FIG. 4. Instability of the superconducting state at $T=2.5\Delta_0>T_c$, with the initial condition $\Delta(0)=0.31\Delta_0$.

characteristic decay time $0.42t_0$ without any oscillations. In the final stage of the evolution, the order parameter enters the fluctuation regime, which is outside of the framework of our self-consistent approach.

In closing, the authors express their gratitude to B. Z. Spivak and A. M. Zagoskin for discussing problems encountered in this work.

*E-mail: bezugly@ilt.kharkov.ua

[1] D. N. Langenberg and A. I. Larkin (eds.), *Nonequilibrium Superconductivity*, Elsevier (1986).
[2] M. Tinkham, *Introduction to Superconductivity*, McGraw-Hill, New York (1996).
[3] L. V. Keldysh, Zh. Éksp. Teor. Fiz. **47**, 1515 (1964) [Sov. Phys. JETP **20**, 1018 (1965)].
[4] G. M. Eliashberg, Sov. Phys. JETP **34**, 668 (1972).
[5] A. I. Larkin and Yu. N. Ovchinnikov, J. Low Temp. Phys. **10**, 407 (1973).
[6] A. I. Larkin and Yu. N. Ovchinnikov, Sov. Phys. JETP **46**, 155 (1978).
[7] G. Eilenberger, Z. Phys. **214**, 195 (1968).
[8] A. G. Aronov and V. L. Gurevich, Sov. Phys. Solid State **16**, 1722 (1974).
[9] I. O. Kulik, Fiz. Nizk. Temp. **2**, 962 (1976) [Sov. J. Low Temp. Phys. **2**, 471 (1976)].
[10] V. P. Galaiko, Sov. Phys. JETP **61**, 382 (1971).
[11] V. P. Galaiko, Sov. Phys. JETP **65**, 2039 (1973).
[12] E. Wigner, Phys. Rev. **40**, 749 (1932).
[13] W. R. Frensley, Rev. Mod. Phys. **62**, 745 (1990).
[14] W. Mecklenbrauker and F. Hlawatsch (eds.), *The Wigner Distribution—Theory and Applications in Signal Processing*, Elsevier (1997).
[15] Yu. Makhlin, G. Schön, and A. Shnirman, Rev. Mod. Phys. **73**, 357 (2001).
[16] M. Greiner, C. A. Regal, and D. S. Jin, Nature (London) **426**, 537 (2003); C. A. Regal, M. Greiner, and D. S. Jin, Phys. Rev. Lett. **92**, 040403 (2004).
[17] R. A. Barankov, L. S. Levitov, and B. Z. Spivak, cond-mat/0312053.
[18] A. F. Volkov and S. M. Kogan, Sov. Phys. JETP **38**, 1018 (1974).
[19] N. Schopohl and K. Maki, Phys. Rev. B **54**, 490 (1995).

This article was published in English in the original Russian journal. Reproduced here with stylistic changes by AIP.